PDR Advance Copy
- FILE IN NUREGS!

NUREG/CR-0000

Seismic Analysis of Piping

Prepared by W. P. Chen, K. R. Jaquay

Energy Technology Engineering Center

Prepared for
U. S. Nuclear Regulatory Commission

DF02 1/1

Dedication

This report is dedicated to the memory of Dr. Wellington Paul Chen, the principle investigator and program manager of the Seismic Analysis of Piping program up to the time of his tragic death. Dr. Chen planned and directed all of the research in this report and wrote the initial draft of Part I. Paul will be greatly missed.

Acknowledgments

The Seismic Analysis of Piping program created an informal Peer Review Group (PRG) of Professor W. D. Iwan, Everett C. Rodabaugh, Dr. Edward A. Wais and Larry Shipley, and later Dr. Gery M. Wilkowski and Dr. Robert P. Kennedy to review findings of the program studies and provide program technical oversight. PRG members were also contracted to conduct several special program research studies described in this report. Their invaluable expert insights, advice, reviews, studies and commentaries are greatly appreciated. Frank Naugle provided expert help with the early issue identifications and margin tables. A special acknowledgment goes to Dr. Ching-Tung Huang whose comprehensive and revealing margin evaluations published in this report provide the primary basis for many of the program conclusions. The programmatic direction and continued support of Dr. Nilesh C. Chokshi is also gratefully acknowledged as are the many helpful technical insights provided by John Fair.

Contents

Dedication i
Acknowledgments iii
Contents v
List of Tables ix
List of Figures xi
Commonly Used Acronyms xiii
PART I BACKGROUND, OVERVIEW AND ISSUE IDENTIFICATION I-1
1 Introduction I-3
1.1 Overview I-3
1.2 Background I-4
1.3 References I-6
2 Status of Initiatives I-7
2.1 Identification and Status of Initiatives I-7
2.2 References I-8
3 Overview of PFDR Program Test Results I-9
3.1 Pipe Component Tests I-9
3.1.1 Component Test Description I-9
3.1.2 Data Correlations I-11
3.1.2.1 Evaluation of Critical Damping I-11
3.1.2.2 Fatigue Analysis of Test Components I-12
3.1.3 Observed Trends in Component Response I-13
3.1.3.1 Ratchet Buckling and the Effect of Pressure I-13
3.1.3.2 Component Cyclic Strains I-13
3.1.3.3 Component Cumulative Ratchet Strain I-13
3.2 Pipe System Tests I-13
3.3 Specimen Fatigue-Ratchet Testing I-14
3.3.1 Simulated 2-Bar Tests I-14
3.3.2 Axially Preloaded Rectangular Beam Tests I-15
3.3.3 Pressurized Pipe Tests I-15
3.3.4 Conclusions I-15
3.4 References I-15
4 New Rules and Bases I-17
4.1 Summary of New Rules I-17
4.2 Technical Bases for New Rules I-18
4.2.1 Margin Definitions I-18
4.2.2 TCG Margin Assessment I-19
4.2.2.1 Test Based Broadened Spectrum Load Margins I-19
4.2.2.2 Load Margin Extrapolations I-20
4.2.2.2.1 Load Margin Extrapolations for Off-Resonance Tests I-21
4.2.2.2.2 Load Margin Adjustments for Temperature Effects I-23
4.3 References I-23
5 Results of ETEC Review I-25
5.1 Identified General Issues I-25
5.1.1 Collapse Failure Mode I-25
5.1.2 Inelastic Analysis Criterion I-26
5.1.3 Margin Basis I-27
5.1.4 Acceptable Margin Level I-27
5.1.5 Predicted Loads for Design I-28
5.1.6 Limited Test Data I-28
5.1.7 Semi-Empirical Basis for New Rules I-29
5.1.8 Component versus System Behavior I-29
5.1.9 Concurrent SAM Loadings I-30

5.1.10 Evaluation of Flaws Greater Than Code Workmanship Flaws I-30
5.1.11 Applicability Limits and Exclusions I-31
5.1.12 Variation in Seismic Margins Predicted for PFDRP Component Testing I-31
5.2 Identified Specific Rule Issues I-31
5.2.1 Deletion of S_y-based Allowable Stress I-31
5.2.2 6 S_m Allowable Stress for Seismic Anchor Motion I-32
5.2.3 S_m-based Allowable Stress for Code Safety Class 2 and 3 Systems I-32
5.3 References I-32
6 ETEC Minimum Fatigue Margin Evaluation I-35
6.1 Overview I-35
6.2 Assumptions and Details I-36
6.2.1 B_2 Indices Selection I-36
6.2.1.1 Elbow Indices I-36
6.2.1.2 Reducer Indices I-36
6.2.1.3 Straight Pipe Indices I-37
6.2.1.4 Tee Indices I-37
6.2.2 Calculated Moments I-38
6.2.3 Actual Geometry I-38
6.2.4 Event Count I-39
6.2.5 Concurrent Loads I-39
6.2.6 Test Margin Calculation I-39
6.2.7 Actual Material I-39
6.2.8 Elevated Temperature Adjustments I-40
6.2.8.1 Carbon Steel I-40
6.2.8.2 Stainless Steel I-40
6.2.9 Frequency Adjustments I-40
6.3 Margin Study Results I-41
6.4 References I-41
Appendix I-A: New Rules I-A-1
Appendix I-B: Data Collection from ANCO Quick Look Test Reports I-B-1
Appendix I-C: Predicted Maximum Moments for Selected PFDR Component Tests I-C-1
PART II SEISMIC MARGIN ASSESSMENTS II-1
1 Introduction II-3
Appendix II-A: Analytical Study of Frequency Effects on Margins II-A-1
Appendix II-B: PFDR Component Tests Seismic Ratchet-Fatigue Margins II-B-1
PART III PEER REVIEW GROUP MEMBER INPUTS III-1
1 Introduction III-3
Appendix III-A: W. Iwan Inputs III-A-1
Appendix III-B: R. Kennedy Inputs III-B-1
Appendix III-C: E. Rodabaugh Inputs III-C-1
Appendix III-D: L. Shipley Inputs III-D-1
Appendix III-E: E. Wais Inputs III-E-1
Appendix III-F: G. Wilkowski Inputs III-F-1
PART IV CONCLUSIONS AND RECOMMENDATIONS IV-1

List of Tables

Table 1: PFDRP Component Test Basic Data and Failure Information I-42
Table 2: Moment Data from PFDRP Component Testing I-44
Table 3: ARC-TCG Seismic Margin Evaluations for PFDRP Component Tests I-46
Table 4: Minimum Strength, 650F, Hard Side REMS Test 36 MRF, Upper-Bound (Fatigue Only) Ratchet-Fatigue Margins I-47

List of Figures

Figure 1: PFDRP Test 11 Configuration I-52
Figure 2: Other Key PFDRP Test Configurations I-53
Figure 3: Typical Targeted PFDRP Sled Acceleration Time History I-54
Figure 4: Response Spectra of PFDRP Targeted Sled Acceleration Time History I-55
Figure 5: Response Spectra of Measured PFDRP Sled Acceleration Time History I-56
Figure 6: Instrumentation Layout for PFDRP Elbow Tests I-57
Figure 7: Instrumentation Layout for PFDRP Tee Tests I-58
Figure 8: Instrumentation Layout for PFDRP Reducer Tests I-59
Figure 9: Comparison of Moments Versus Strain, PFDRP Elbow Tests 3 and 37 .... I-60
Figure 10: Strain Versus Sled Acceleration, PFDRP Elbow Test 3 .... I-61
Figure 11: PFDRP Scratch Mark Based Strain Accumulation I-62
Figure 12: PFDRP Piping System 1, Photo I-63
Figure 13: PFDRP Piping System 1, Isometric I-64
Figure 14: PFDRP Piping System 2, Photo I-65
Figure 15: PFDRP Piping System 2, Isometric I-66
Figure 16: PFDRP System 1 Instrumentation Layout I-67
Figure 17: PFDRP System 2 Instrumentation Layout I-68
Figure 18: Typical PFDRP 2-Bar Failure Map, Room Temperature I-69
Figure 19: Typical PFDRP 2-Bar Failure Map, 550°F I-70
Figure 20: Dynamic Amplification for Elastic and Elastic-Plastic Systems I-71
Figure 21: Initial REMS Based Test 36 Frequency Dependent Margins I-72
Figure 22: 9/93 Revised REMS Based Test 36 frequency Dependent Margins I-73
Figure 23: 9/93 Revised REMS Based Test 36 Normalized Frequency Dependent Margins I-74
Figure 24: Beaney 1-inch Diameter Pipe Test Data I-75
Figure 25: Beaney Yield Correction of Figure 24 Data I-76
Figure 26: Derivation of Stainless Steel Fatigue Strength Reduction I-77

COMMONLY USED ACRONYMS

ABB	Asea Brown Boveri
ABWR	Advanced Boiling Water Reactor
ALWR	Advanced Light Water Reactor
ANCO	ANCO Engineers, Inc.
ARC	Advanced Reactor Corporation
ASME	American Society of Mechanical Engineers
BNL	Brookhaven National Laboratory
BWR	Boiling Water Reactor
CE	Combustion Engineering
CIT	California Institute of Technology (Caltech)
CS	Carbon Steel
DOE	US Department of Energy
EPRI	Electrical Power Research Institute
ETEC	DOE Energy Technology Engineering Center (operated by Boeing)
FOAKE	First-of-a-Kind Engineering (Task E-1, NPOC Strategic Plan)
GE	General Electric Company, Nuclear Energy Division
ISM	Independent Support Motion
LCF	Low Cycle Fatigue
MDOF	Multiple Degrees of Freedom
MOV	Motor Operated Valve
MRF	Margin Reduction Factor
NEI	Nuclear Energy Institute
NPOC	Nuclear Power Oversight Committee (NEI)
NPS	Nominal Pipe Size
NRC	US Nuclear Regulatory Commission
NUMARC	Nuclear Management Resources Council
OBE	Operating Basis Earthquake
PFDRP	Piping and Fitting Dynamic Reliability Program
PRA	Probabilistic Risk Assessment
PRC	NRC Piping Review Committee
PRG	ETEC Seismic Analysis of Piping Program Peer Review Group
PVRC	Pressure Vessel Research Council (WRC)
QL	ANCO "Quick Look" (test report)
REMS	REMS3/REMSFATI (computer code)
SAM	Seismic Anchor Motion
SDOF	Single Degree of Freedom
SGD	ASME Section III Subgroup on Design (III)
SRSS	Square Root of the Sum of the Squares
SS	Stainless Steel
SSE	Safe Shutdown Earthquake
STGIPC	ASME Special Task Group on Integrated Piping Criteria (III-SGD)
TAM	Thermal Anchor Motion
TCG	ARC Technical Core Group
TE	Thermal Expansion
W	Westinghouse
WGPD	ASME Working Group on Piping Design (III-SGD)

PART I : BACKGROUND, OVERVIEW AND ISSUE IDENTIFICATION

1 Introduction

1.1 Overview

The US Department of Energy (DOE) Energy Technology Engineering Center (ETEC) is assisting the US Nuclear Regulatory Commission (NRC) in developing regulatory changes relating to seismic analysis of piping systems in nuclear plants and in evaluating the cumulative impact of recent changes in design criteria on overall safety margins of these piping systems. This assistance is being provided under the Seismic Analysis of Piping program.

The initiation of this program was due to the major revision of the ASME Boiler and Pressure Vessel Code (Code), Section III dynamic load design criteria for nuclear plant piping under consideration in the late 1980's and early 1990's. Revised dynamic load design criteria (the "new rules") were eventually passed by the ASME Code Main Committee in February 1994 and published in the 1994 Code Addenda. The ETEC program was focused on the treatment of seismic loading, although the revised criteria affected other dynamic load considerations as well.

The new rules are the culmination of a series of industry efforts, including the joint Electrical Power Research Institute (EPRI)/NRC Piping and Fitting Dynamic Reliability Program (PFDRP), References 1-1 through 1-5[1], which was initiated in response to reviews conducted in the early 1980's by the NRC and the Pressure Vessel Research Council (PVRC). These criteria were developed and promoted by the Technical Core Group (TCG) of the Advanced Reactor Corporation (ARC)[2] and were based on earlier EPRI/General Electric, Nuclear Energy (GE) proposed dynamic load design criteria developed from the PFDRP. The development of the TCG criteria is documented in the ARC FOAKE Task E-1 report (Reference 1-11).

The technical bases for the TCG criteria were reviewed by the ASME Special Task Group on Integrated Piping Criteria (STGIPC) which was to provide the ASME Section III Subgroup on Design (SGD) an integrated plan for the consideration of proposed changes to the design criteria for piping systems. The plan and its endorsement by a majority (essentially, the non-NRC members) of the STGIPC are documented in the STGIPC preliminary report (Reference 1-12).

The support provided by ETEC to the NRC is documented in this four part report of which this is the first part:

Part I Background, Overview and Issue Identifications

Part II Seismic Margin Assessments

Part III Peer Review Group Member Inputs

Part IV Conclusions and Recommendations

Part I documents the results of the initial ETEC evaluations of the new rules conducted in the 1993-1994 time frame. Commentary is added, and noted as such, when more recent evaluations have led to a significant deviation from, or refinement to, the initial evaluations. Specifically, Part I of the report includes:

(1) A background section on the developments leading to the new rules and the Seismic Analysis of Piping program at ETEC.

(2) An assessment of the status of recent seismic design criteria initiatives.

(3) An overview of the PFDRP, particularly the piping component, piping system, and material specimen testing.

(4) A summary of the new rules and the technical bases offered to justify the new rules.

(5) The results of ETEC's assessment of the technical bases for the new rules, specifically, the draft STGIPC and the TCG reports.

(6) A compilation of test data from the PFDRP test reports and plots of hysteretic moment-rotation behavior for selected test runs.

(7) The results of the initial ETEC evaluation of the potential minimum seismic fatigue margins associated with the new rules, based on an extension of the TCG margin studies for Test 36.

[1] References 1-1 through 1-5 replace the earlier draft GE reports References 1-6 through 1-10. The reviews in this report were based primarily on these earlier GE reports. The EPRI and GE reports are not identical, however, for convenience, only the EPRI reports are referenced.

[2] ARC is a dedicated project organization established to manage the implementation of the Nuclear Energy Institute (NEI), formerly Nuclear Management Resources Council (NUMARC), Nuclear Power Oversight Committee (NPOC) Strategic Plan. The TCG was formed by ARC in part to enhance approval of new piping and pipe support rules which were to be developed under Task E-1 of the First-of-a-Kind Engineering (FOAKE) technical element of the NPOC Strategic Plan.

Part II of this report includes a comprehensive assessment by researchers affiliated with the California Institute of Technology (CIT) of frequency, P-delta, temperature, load eccentricity and worst case combined effects on seismic margins undertaken in response to issues identified in Part I of this report. Margin results for Tests 11, 14, 36, and 40 are presented. These results are used to develop nominal seismic fatigue margins consistent with recent definitions of acceptable margin level, including consideration of revised stress indices.

Part III of this report contains commentaries and contributions by members of the Seismic Analysis of Piping Peer Review Group (PRG). Included are:

(1) Individual PRG member commentaries on the adequacy of the technical basis provided for the new rules.

(2) An approach for defining acceptable margin levels based on piping not impacting plant Probabilistic Risk Assessment (PRA) evaluations.

(3) A study of the impact of the new rules on flaw tolerance and Section XI flaw evaluation rules for continued operation.

(4) "Strawman" rule revisions that may provide acceptable margin levels and the remaining issues that need resolution in order to justify these rules.

Part IV of this report contains the final program conclusions and recommendations to the NRC staff.

1.2 Background

The majority of the initiatives reviewed in this report have their genesis in the results of reviews and investigations by the NRC and the PVRC in the early 1980's.

In 1983, the NRC Piping Review Committee (PRC) was formed to perform a comprehensive review of NRC requirements for nuclear power plant piping. Regulatory changes and research recommended by the PRC are contained in NUREG-1061 (References 1-13 through 1-17).

On the issue of overall design margins in piping systems, the PRC recognized that a key element in the development of optimized design criteria was the proper balance among the margins associated with various individual effects such as seismic and thermal loads. This balance was to be achieved relative to actual failure rather than code defined limits. However, this balance was difficult to define in view of the lack of real failure information for piping, particularly for seismic loads.

Accordingly, the PRC recommended that: 1) test programs for verifying piping seismic design margins and identifying failure modes be supported, and 2) studies be conducted to establish and justify the level of earthquake piping systems can safely withstand with sufficient confidence to not require seismic design analyses.

In addition, as a result of the overall industry concern regarding the perceived unduly restrictive ASME Boiler & Pressure Vessel Code (Code), Section III, piping seismic design rules, the PVRC formed a Steering Committee and Technical Committee on Piping in the early 1980's to investigate alternatives that might improve overall piping system safety and reliability. The committees were to conduct critical evaluations of nuclear reactor piping systems with regard to overlapping and excessive conservatism in seismic and other dynamic loading design rules, and to support piping design rule modifications by the ASME.

The PVRC Technical Committee on Piping formed four Task Groups with the purpose of recommending improvements in industry practice, damping values, spectral broadening, and dynamic stress allowables. Of these, the PVRC Task Group on Dynamic Stress Allowables was given the responsibility of making recommendations for changes to the current criteria for evaluation of dynamic loads. The Task Group concluded that: 1) the use of ductility ratios and inelastic response spectra was difficult to justify on a technical basis, since they rely on elastic analysis to account for inelastic behavior; and 2) changes should be made to better predict the response of piping systems to dynamic loads. However, the Task Group found that the available data on the analytical and experimental behavior of piping systems subjected to dynamic loads were not sufficient to justify changes in the methodology of dynamic load evaluation.

Subsequently, in response to the second conclusion, EPRI formulated a broad plan to develop a larger data base and address the needs identified by the PVRC Task Group on Dynamic Stress Allowables. The plan was implemented by GE under the extensive EPRI/NRC sponsored PFDRP.

The PFDRP included simulated seismic, hydrodynamic and water-hammer testing (i.e. low-, mid- and high-frequency dynamic testing, respectively) of piping components and systems. Seismic tests were performed on 33 simple cantilever configurations of piping components and 2 prototypic piping systems. Material specimen testing was also performed and proposed EPRI/GE rules for the design of ASME Code, Section III, Class 1, 2 and 3 piping systems were developed.

Subsequently, a number of other rule changes were proposed to the ASME SGD and considered by the ASME Working Group on Piping Design (WGPD). NRC staff members participated in these considerations and documented their concerns (Reference 1-18). In mid-1991, as previously described, the SGD formed the STGIPC to develop an integrated strategy for considering these numerous rule changes.

Concurrent with the formation of the STGIPC, the ARC was investigating modifications to piping design criteria for application to standardized advanced light water reactor (ALWR) designs. Development of these criteria was assigned to the TCG under FOAKE Task E-1 relating to ASME Piping. All but one of the TCG members were also members of the STGIPC.

The draft TCG and STGIPC reports, issued in early 1993, together were intended to provide the following:

(1) An assessment of margins present in the previous, (i.e., ASME Code, 1989 and 1992 Editions) design rules.

(2) An assessment of the impact of methods of dynamic analysis on margins.

(3) An assessment of the impact of frequency ratio, design temperature, and non-linear force-deflection on margins.

(4) An assessment of the degree of acceptance of the report by industry and regulatory personnel.

(5) A recommended process for evaluating margins.

(6) A discussion of the impact on other sections of the ASME Code.

The STGIPC report was supported by a majority of the STGIPC but opposed by a minority consisting of NRC representatives. The bases for the minority position were documented in the STGIPC report. Some of the issues identified by the NRC representatives such as the effect of test frequency on demonstrated test margins were evaluated by the TCG and documented in both the TCG and STGIPC reports. The need for, evaluation of, and significance of the results of these and other evaluations were controversial issues.

Subsequently, the rules contained in Appendix I-A to this report were passed by the ASME Code Main Committee in February, 1994. These rules are similar to, but not identical to, those published in the Code 1994 Addenda, nor identical to those in the 1993 TCG draft report which in turn are also not identical to the earlier EPRI/GE rules: nevertheless, all of these rules will be referred to in this report as the "new rules"

The new rules are based on the premise that the results of the PFDRP demonstrate that:

(1) Seismic inertia loads do not cause collapse failure of piping systems.

(2) The primary failure mode in piping due to seismic inertia loading is a combination of fatigue and ratcheting.

(3) Piping can withstand seismic inertia loadings on the order of 10 to 15 times the input levels permitted by current ASME Code acceptance criteria.

The TCG introduced a definition of failure load margin for a given seismic event, given piping system, and a given set of design rules (and implicitly, a given method of design analysis) as the ratio of the level of the seismic event required to produce a through-wall crack in the piping system during one application of the seismic event to the maximum level of the seismic event permitted under the set of rules. The TCG represent that the minimum failure load margin obtained in the PFDRP testing was 10.6 for the previous ASME Code rules and 4.2 for the new rules. This minimum failure load margin was obtained in Test 36. Failure load margins were based on analytical extrapolations which were required to determine the seismic event level to induce failure in one application since typically, a number of high-level simulated seismic events were required to induce failure during testing.

Further analytical extrapolations were required to account for effects not considered in the PFDRP testing. These effects include "frequency effects" to account for the fact that the PFDRP tests were conducted near resonance. The corrected failure load margin for Test 36 was presented as approximately 2 which was judged by the TCG to be acceptable.

Concurrent with these industry initiatives, the NRC was assessing modifications to the regulations to decouple the Operating Basis Earthquake (OBE) from the Safe Shutdown Earthquake (SSE). An ETEC review of early criteria modifications to support design certification commitments for standard ALWR designs was documented in Reference 1-19. Eventually, earthquake engineering criteria were placed in a new Appendix S to 10 CFR Part 50 that permits the applicant to select whether or not an OBE response analysis is to be performed. With the OBE level set at one-third or less of the SSE, only the SSE is used for design (the OBE only serves the function of an inspection and shutdown level).

However, if an applicant selects an OBE value at a fraction of the SSE higher than one-third, a suitable analysis must be performed to demonstrate that the requirements associated with the OBE are satisfied. The new rules contain modified requirements for the OBE. The current ETEC review of the new rules only considers design requirements for the SSE..

The current ETEC review of the new rules is a continuation of an earlier review by ETEC, sponsored by NRC/NRR, of the PFDRP system testing in an effort to develop seismic criteria for ALWRs. This earlier effort was not completed and interim findings were documented in Reference 1-20. The current ETEC review was initiated by NRC/RES in response to the Reference 1-21 User Need memorandum issued subsequent to this earlier ETEC effort.

1.3 References

1-1 EPRI TR-102792-V1, "Piping and Fitting Dynamic Reliability Program, Volume 1 - Project Summary," EPRI, 1994

1-2 EPRI TR-102792-V2, "Piping and Fitting Dynamic Reliability Program, Volume 2 - Component Tests," EPRI, 1994

1-3 EPRI TR-102792-V3, "Piping and Fitting Dynamic Reliability Program, Volume 3 - System Tests," EPRI, 1994

1-4 EPRI TR-102792-V4, "Piping and Fitting Dynamic Reliability Program, Volume 4 - Fatigue-Ratchet Tests," EPRI, 1994

1-5 EPRI TR-102792-V5, "Piping and Fitting Dynamic Reliability Program, Volume 5 - Piping Design Rules Revisions," EPRI, 1994

1-6 Draft GE report, "Piping and Fitting Dynamic Reliability Program, Volume 1 - Project Summary," November 1989

1-7 Draft GE report, "Piping and Fitting Dynamic Reliability Program, Volume 2 - Component Test Report," December 1989

1-8 Draft GE report, "Piping and Fitting Dynamic Reliability Program, Volume 3 - System Test Report," December 1989

1-9 Draft GE Report, "Piping and Fitting Dynamic Reliability Program, Volume 4 - Specimen Fatigue-Ratcheting Test Report," January 1990

1-10 Draft GE Report, 'Piping and Fitting Dynamic Reliability Program, Volume 5 - Piping Design Rules Revisions," January 1990.

1-11 "Technical Core Group Report on FOAKE Task E1: ASME Piping," Advanced Reactor Corporation report, April 1993

1-12 Preliminary Report for ASME SCIII, SGD from Special Task Group on Integrated Piping Criteria, April 16, 1993

1-13 NUREG 1061, Volume 1, "US NRC Piping Review Committee, Investigation and Evaluation of Stress Corrosion Cracking in Piping of Boiling Water Reactor," August 1984

1-14 NUREG 1061, Volume 2, "US NRC Piping Review Committee, Evaluation of Seismic Designs - A Review of Seismic Design Requirements for Nuclear Plant Piping," April 1985

1-15 NUREG 1061, Volume 3, "US NRC Piping Review Committee, Evaluation of Potential for Pipe Breaks," November 1984

1-16 NUREG 1061, Volume 4, "US NRC Piping Review Committee, Evaluation of Other Dynamic Loads and Load Combinations," December 1984

1-17 NUREG 1061, Volume 5, "US NRC Piping Review Committee, Summary - Piping Review Committee Conclusions and Recommendations," April 1985

1-18 ASME Committee Correspondence, Subgroup on Design, SC-III, Hartzman, M. to Barnes, R.W., "Basis for the Negative Vote on the EPRI/GE Proposed Changes of the ASME Section III Piping Design Criteria", September 11, 1992, revised March 20, 1993.

1-19 ETEC Document, "Draft Safety Evaluation on the Use of Simple Earthquake Design for ASME Code Piping Systems in the ABWR Standard Plant," July 1993

1-20 ETEC Document, "Task Status Report, Advanced Reactor Review, Piping Seismic Criteria," July 10, 1992

1-21 NRC Memorandum, T. Murley to E.S. Beckjord, "User Needs for Engineering Research on Advanced Light Water Reactors," September 23, 1992

2 Status of Initiatives

During STGIPC deliberations, significant industry and regulatory piping design initiatives were identified and their status evaluated (References 2-1 and 2-2). The following is based on and updates this prior identification effort. For convenience, the ordering of the initiatives in the following is identical to that in the STGIPC listing. More detailed descriptions of the initiatives than provided in the following are available in References 2-1 and 2-2.

2.1 Identification and Status of Initiatives

(1) Code Case N-411

This code case was developed by PVRC to address one feature of dynamic analysis believed to contribute unnecessary conservatism to seismic design of piping. This code case has been conditionally endorsed by the NRC: limitations on application of the code case have been prescribed. Subsequent PVRC reviews of the code case have resulted in recommendations to change ASME Code Appendix N to require one value of damping for all frequencies, with 5% recommended for the OBE and 6% for the SSE. The new rules may make these recommendations moot.

(2) New Rules for Reversing Dynamic Loads

These rules were passed by the ASME Code Main Committee in February 1994. Results of ETEC reviews of these rules are provided in this report.

(3) Code Case ABC

This code case provides a simplified method of seismic dynamic analysis of plastically loaded piping systems. This code case has been passed by the ASME WGPD, but not voted on by the ASME SGD.

(4) Code Cases N-451 and N-462

These code cases were interim steps towards the new rules. Code Case N-451 has been annulled. Code Case N-462 is now moot since the criteria have been revised.

(5) 10 CFR Part 50 Appendix S

Depending on applicant selection of the OBE level, these new regulations can eliminate the OBE loading from the design of piping systems. Nevertheless, the contribution of lessor seismic loadings than the SSE to cumulative fatigue damage needs to be considered along with all other cyclic service loadings when evaluating the adequacy of design criteria for an SSE fatigue or ratchet-fatigue failure mode.

(6) NCIG-14 Procedure for Small Bore Piping

These design by rule procedures were reviewed by the NRC (Reference 2-3). NEI, formerly NUMARC, has decided to withdraw these procedures from consideration.

(7) Regulatory Guide 1.60, 1.61, and 1.92

ASME Code Appendix N reflects Regulatory Guides 1.60 and 1.61 requirements but not those of Regulatory Guide 1.92. Industry is concerned that the NRC has not endorsed Appendix N.

(8) As-built tolerances and WRC 316

Industry is considering incorporation of these tolerance requirements into the ASME Code.

(9) Code Cases N-122, N-318, N-391, N-392, Welded Attachments

These active code cases prescribe stress indices for components not covered by the present Code. At issue is whether the new rules apply to these code cases.

(10) Code Case N-468, Class 2 and 3 Low Seismic Zones

Incorporation of this code case into ASME Code Appendix N was under consideration. However, this code case has been annulled.

(11) Code Case N-196

Incorporation of this code case into ASME Code Appendix N was under consideration. However, this code case has been annulled.

(12) Code Case N-319, Stresses in Elbows

This active code cases prescribes alternate stress indices for elbows. At issue is whether the new rules apply to this code case.

(13) Code Case N-420, Energy Absorbers

This code case is now being incorporated into the Code. At issue is whether the new rules apply to piping systems incorporating these devices.

(14) SRP 3.9.3, Functional Capability

NUREG-1367 (Reference 2-4) specifies functional capability limits equal to ASME Code, 1989 Edition, Service Level D allowables. These limits are more conservative that those in the new rules.

(15) SRP 3.6 and ANSI/ANS-58.2 Break and Crack Locations

These issues have been addressed in Reference 2-5.

(16) Seismic Design-by-Rule for Large Bore Piping

This design approach is contrary to current: a) 10CFR50, Appendix A General Design Criteria, and b) 10CFR100, Appendix A criteria which require: i.) in part, that effects of natural phenomena be combined appropriately with normal and accident conditions and, ii) specify that the method used to insure that systems and components maintain their safety function during and after an SSE involve the use of suitabie dynamic analyses and qualification tests or conservative static load method, respectively.

(17) Independent Support Motion (ISM)

The NRC has not endorsed the PVRC ISM procedure in WRC-352 (Reference 2-6). Although not pending, the PVRC procedure could be included in ASME Code Appendix N.

Based on the preceding it appears that some of the initiatives identified by the STGIPC are now moot since the new rules have been approved by the ASME Code. Others related to the incorporation of code cases into ASME Code Appendix N and the lack of endorsement of Appendix N by the NRC have not changed. Others involving the applicability of the new rules to stress indices not previously contained in the ASME Code need to be assessed on a case-by-case basis.

2.2 References

2-1 "Integration of Issues and Changes for ASME Nuclear Piping", S.W. Tagart, Jr., July 8, 1991

2-2 Preliminary Report for ASME SCIII, SGD by Special Task Group on Integrated Piping Criteria, April 16, 1993

2-3 NRC letter to NUMARC, J.A. Norberg to W. Rasin, "Procedure for Seismic Evaluation and Design of Small Bone Piping (NCIG-14), EPRI Report NP-6628", June 1, 1992

2-4 NUREG-1367, "Functional Capability of Piping Systems," Terao, D. and Rodabaugh, E.C., November 1992

2-5 ETEC Document, "Draft Safety Evaluation on the Use of Simple Earthquake Design for ASME Code Piping Systems in the ABWR Standard Plant," July 1993

2-6 WRC Bulletin 352, "Independent Support Motion (ISM) Method of Modal Spectra Seismic Analysis," April 1990.

3 Overview of PFDRP Test Results

The objectives of the PFDRP (Reference 3-1) were:

(1) To identify failure modes and failure levels of piping components and systems under dynamic loadings.

(2) To provide a data base that will improve the prediction of piping system response and failure due to high-level dynamic loads.

(3) To develop an improved, realistic and defensible set of piping design rules for inclusion into the ASME Code.

Tests performed in the PFDRP included piping component, piping system, and simple specimen fatigue-ratchet tests.

Test data and evaluations were documented in GE semi-annual progress reports (References 3-2 through 3-5), and the EPRI final program summary reports (References 3-6 through 3-10).

3.1 Piping Component Tests

The PFDRP piping component tests were conducted by ANCO Engineers, Inc. (ANCO). ANCO was responsible for the fabrication and testing of the piping components. ANCO also prepared "Quick Look" test (QL) reports which summarized the basic features and results of the tests including measured and computed time-history plots. Measured time-history plots included acceleration, deflection, strain, and internal pressure. Computed time-history plots included rotation of and moments in the test articles. Computed rotations were based on measured displacements at several locations on the test configuration. Rotations across the test article were rarely provided, rather rotations of the adjacent straight pipe nipple or rotations of the inertia load arm were provided. Computed moments in the test articles were based on strain gage measurements on the inertia load arm combined with accelerometer measurements at the connection flanges below the inertia load arm (see Section 3.1.1). The moment computations assumed linearly elastic behavior of the inertia load arm, classical beam behavior, a single predominant mode of response and ignored rotational inertial effects.

GE performed test data reductions and analytical evaluations. Discussions with GE researchers indicate the small differences between the Reference 3-7 listed-maximum measured moment data and QL plot data is due to an uncorrected error in the lower inertia arm connecting flange accelerometer (Y_2) sign convention used for the QL plots.

Analytical evaluations included linearly elastic predicted moments in the test articles. The predicted moments were based on response spectrum analyses using unpublished ±15% peak-broadened acceleration spectra developed from the measured sled accelerations. Various damping values were used for different data correlations. Comparative analyses using unbroadened spectra were also performed for Test 36 and Test 41.

During testing, various piping components including straight runs, long-radius and short-radius elbows, tees, fabricated branch connections, concentric reducers, nozzles and integral lug supports were subjected to simulated seismic, hydrodynamic and water-hammer (low-, mid- and high-frequency, respectively) loadings. Pressure boundary failures occurred during the simulated seismic and water-hammer tests but not during the simulated hydrodynamic tests. ETEC's review was limited to the simulated seismic tests only.

Components ranged between 4- and 8-inch nominal pipe size; were between Schedule 10 and 80 thickness, and were fabricated from either carbon steel or wrought stainless steel.

3.1.1 Component Test Description

A total of 41 piping components were tested during the PFDRP. Of these 41 tests, 33 included test runs with simulated high-level seismic loading, 2 tests were quasi-static tests on elbows, and the remaining 6 tests were predominately mid- and high-frequency tests. Results from these last 8 tests were not included in the ETEC review.

Data for 27 of the 33 tests containing simulated high-level seismic loading are provided in Tables 1 and 2. Table 1 provides basic test configuration data, dimensional and material properties data at the failure location, and failure mode information. Table 2 provides pressure stresses, weight moments, calculated and measured dynamic moments, and comparative moment ratios The notes to the tables define the entries. Several general observations will be offered here while later sections of the report will use specific data contained in the tables.

The Table 1 Column entry F_N is the QL report test measured natural frequency determined in preliminary low-level tests. These values do not always agree with the Reference 3-7 Appendix B reported values "Natural Freq".

The FI values in Table 1 are the frequencies of the peak acceleration on the acceleration response spectra developed in the QL report for the test measured sled acceleration time history. These can vary slightly from test run to test run, and the Table 1 values are for the test run with the Reference 3-7 Appendix B reported highest moments calculated by the response spectrum method. For selected tests, Appendix I-B to this report contains FI values for all the high-level test runs for which the QL report provides a sled acceleration response spectrum. The Table 1 FI values seldom agree with the targeted sled peak input frequency values which Reference 3-7 derives from test duration - the targeted sled peak input frequency equals 143 divided by the full test duration. In a few tests, noted in this report's Appendix I-B, the FI values were not available in the QL report and other test run values, or the targeted values, had to be used.

The Table 1 entry "TEST T" is the pre-test measured thickness closest to the location of failure based on the QL report listings of measured wall thickness. The Table 1 value is the average of the four thickness readings at every 90° around the circumference.

The Table 2 B_1 and B_2 entries are Code stress indices for the piping component that contained the failure location except for Tests 11 and 36, where, as discussed in Section 6.2.1.4, an alternative value of 1.0 was used in Table 2.

The Table 2 M_{CODE} and M_{LIMIT} entries , calculated as stated in the heading, and their associated moment ratios F_S and F_{S2}, respectively, were provided for Kennedy's PRG member commentary presented in Appendix III-B of this report.

The Table 2 GE MM and QL MM entries are failure location maximum single cycle moment half-range values derived from test data for the highest level test run. In principle they should be identical, but their ratio in the Table 2 QL/GE column is not always unity. The GE MM entries are from Reference 3-7 Appendix B and the QL MM entries are from the QL report plots.

The Table 2 M_{UD} entries are "dynamic ultimate moments" derived from the calculated test moment plots in Appendix I-C of this report when the plot is for the highest level test run. The Appendix I-C plots were developed by CIT researchers using the test setup information in Reference 3-7, QL test data, and a closed form solution of the equations of motion. When the Appendix I-C plots were not for the highest level test run, the M_{UD} values were extrapolated using the average ratios of Appendix I-C moments to the QL and GE measured moments. Appendix I-B to this report contains these extrapolations. The M_{UD} moments are based on the closing moment amplitudes for elbows and the half-range moments for non-elbows.

The ratio M_{UD} / MM entry for Test 11 is shaded to indicate the test is suspect. Review of the test video indicates the attached weight may not have been the full amount listed in Reference 3-7 Table 7-2 and the M_{UD} value would then be in error. The QL and GE measured moment values do not use the attached weight in the calculation. On the other hand, the measured natural frequency of the test setup agrees well with predictions when the full weight is assumed.

The following six seismic tests are not included in Tables 1 and 2 for reasons discussed below:

Test 17:	Elbow torsional test
Test 18:	Fabricated branch test
Test 20:	Nozzle test
Test 21:	Integral-lug pipe support test
Test 22:	Integral-lug pipe support test
Test 23:	Elbow-axial-strut pipe support test

Test 17 was not included because measured moments were not available. Test 18 was not a standard piping component and no Code stress indices were available. Test 20 failed in a region that is covered by ASME Code vessel rules, not piping rules. Tests 21 and 22 were support load tests and not pressure boundary moment capacity tests. Test 23 was not an inertial mass driven test.

Tests 31, 34 and 36 had mixtures of high-level sinesweep and seismic loadings that introduced uncertainty into margin evaluation. Nevertheless, Test 36 was used in the ETEC margin evaluation for comparison to the TCG margins. Tests 1, 2 and 41 had inadequate test records of the data needed for the ETEC margin evaluations. Tests 3, 5, 6, 7, 8, 12, 13 and 30 had missing data in the test records that had to be assumed or extrapolated from existing data to perform the ETEC margin evaluations.

Figure 1 shows two views of the Test 11 configuration illustrating the sled, base fixture and inertia load arm common to all the component tests. Figure 2 provides views perpendicular to the sled motion for other key tests.

Figure 3 shows a typical targeted seismic sled acceleration time-history used in the PFDRP tests. This time-history is scaled from a baseline (Reference 3-11) boiling water reactor (BWR) seismic acceleration time-history. The baseline time-history was generated using the Taft earthquake and 7% building damping and is the predicted BWR reactor pressure vessel horizontal acceleration time-history at the attachment point of the main steam line. The amplitude of the sled input time-history was uniformly scaled up or down to adjust the sled load levels, and the time scale of the sled input time-history was stretched and compressed to adjust the sled peak acceleration response frequency.

Figure 4 shows the acceleration response spectrum for a typical targeted sled acceleration time-history. Figure 5 shows acceleration response spectra for several high-level test runs based on acceleration measurements on the sled. The additional high frequency content in the tests are not unusual for dynamic test fixtures driven by hydraulic actuators, and is usually attributed to fluid column vibration created by servo-valve closures.

Each test configuration was instrumented with approximately two dozen strain gages, three or four displacement transducers, one pressure transducer, and several accelerometers. Figures 6, 7 and 8 show test instrumentation layouts for typical elbow, tee, and reducer tests, respectively.

Standardized test run sequences were developed for most of the component tests. All tests were conducted at room temperature. Up to sixteen test runs were conducted on each of the components tested. Four low-level inputs (two random and two step displacement) were used to identify test configuration response characteristics (natural frequency and damping) and to checkout the instrumentation. One low-level seismic time-history was usually applied to establish test configuration response at nominally elastic stress levels. The remaining test runs were mid-level and high-level seismic runs. The highest level test runs were repeated up to ten times until either a through-wall crack developed in the test configuration or until the rotation of the inertia load arm became excessive. Internal pressure was monitored and adjusted where necessary to accommodate test specimen expansion. Selected configurations had test run sequences with step-wise increasing input level until the high-level input was reached. Other configurations were tested unpressurized for some test runs and pressurized in other test runs. Still other configurations were tested with different frequency content time histories in different test runs. And a few configurations were subjected to high-level sinesweep loadings in addition to the seismic loadings.

Most tests required several test runs at the highest level to induce failure, and the number of those high-level runs were reported in the PFDRP summary volume (Reference 3-6). In some cases, failure occurred before the end of the first high-level run, and in those cases, a fractional number was reported for the "number of earthquakes for failure." For example, in Test 36, failure occurred slightly more than half way through the first high-level test run (Run 8) and the number of earthquakes to cause failure was reported in Reference 3-6 as 0.5 even though seven prior test runs had been conducted, starting at low input levels and increasing in magnitude. Runs 5 and 6 were high-level sinesweeps and Run 7 was a mid level seismic test run.

Pre-test, during-test (after each test run) and post-test dimensional measurements were recorded. One set of measurements was the distances between pairs of scratch marks initially 2 inches apart at key locations on the outside surface of the test articles. Other measurements were the thickness and diameter at various sections along the test articles and adjacent pipe nipples. In some tests with significant distortion, the flow restriction due to the deformed geometry at the end of testing was calculated in the QL reports.

Video tape and photograph records were made. In addition, test articles were archived. ETEC eventually acquired a full set of QL reports, video tapes and floppy diskettes of the test data.

3.1.2 Data Correlations

Data correlations by GE reported in Reference 3-7 included:

(1) Evaluation of critical damping.

(2) Fatigue analysis of test components.

3.1.2.1 Evaluation of Critical Damping

Two kinds of damping ratio were estimated for the various loading conditions during testing: equivalent damping ratio and the so-called "true" damping ratio.

The equivalent damping ratios were obtained by performing a linear elastic response spectrum analysis using the acceleration response spectrum of the measured sled acceleration time-history with ±15% peak broadening and adjusting the damping until the calculated moment in the test component was equal to the measured moment. This damping is, in effect, a "calibration factor" chosen such that the calculations match the measurements. By using the equivalent damping ratio for the analysis, calculated and measured piping forces and moments, flange moments, and nozzle loads can be matched, but the displacements and the acceleration will be under-predicted.

Values of equivalent damping obtained for five elastic level elbow tests ranged between 0.40% and 0.77%. Values of equivalent damping for six high-level elbow tests centered near 35% with one Schedule 80 test having a value near 45%.

The "true" damping ratios were obtained from a Fourier transformation of the input and output data to obtain power spectrum density and transfer functions. Analyses based on true damping with peak broadened acceleration response spectra will result in the over-prediction of forces, moments, and acceleration but provide good agreement between calculated and measured displacements. Values of true damping obtained ranged between 1.5% for a low-level elbow test and 33.6% for a high-level tee test.

GE concludes that the measured damping below 2% of critical at elastic levels is not inconsistent with the Code use of 5% of critical for design levels since in the PFDRP tests there is no insulation, no supports and no gaps to influence damping ratios. GE also observes that the increase in damping at higher excitation levels is more pronounced for the same surface strain levels in the thicker wall test articles apparently due to the greater volume of material being deformed plastically.

GE's damping study reported two important observations related to the issue of margins demonstrated in the component tests versus margins in piping systems. The first observation was:

"In a piping system undergoing forced vibration, a time-history plot of the response of the system will have an apparent response frequency at the predominant frequency of the input forcing function. This will occur even in a system where a high amplitude input has caused the natural frequency of the system to decrease because of the occurrence of plastic deformation. However, in the component tests, the actual transfer function of the test records illustrates that the reduced system natural frequency does reflect the effects of plastic action. . . . It can be seen that in some tests the frequencies were shifted 30% lower."

The second observation was:

"An important distinction that deserves emphasis is the fact that the damping values determined here are for component tests, which are essentially single degree of freedom systems. In more realistic piping configurations (which are multiple degree of freedom systems), the plasticity effects are likely to be localized. Thus, the equivalent damping in a realistic piping system is expected to be lower."

3.1.2.2 Fatigue Analysis of Test Components

Based on fatigue failure data obtained during testing, three fatigue analyses were conducted by GE using different fatigue curves: 1) Markl's equation, 2) the Code Appendix I-9.0 design fatigue curves, and 3) the fatigue equation in the background document to the Code Section III criteria. In addition, two cycle counting methods were investigated: 1) the standard ASME Code NB-3222.4 method of minimum-maximum pair elimination, and 2) a sequential cycle counting method pairing cycle reversals along a time line. Three mean stress correction methods were also considered: 1) the modified Goodman, 2) the Gerber, and 3) the Soderberg methods.

Fatigue analyses were performed in the following three stages:

1) The first stage utilized the measured moment time histories and strain time histories from uniaxial strain gage measurements. Three methods were used to obtain the alternating stress ranges: 1) measured strains, 2) calculated strain amplitude based on measured moment and results of plastic analysis, and 3) measured moment and the ASME Code NB-3653 K_e procedure. Strain time histories for elbow Test 1 Run 8, elbow Test 3 Run 9, elbow Test 3 Run 10, elbow Test 4 Run 6, and moment time histories for elbow Test 4 Run 8 and tee Test 9 Run 6 were identified for evaluation.

2) The second stage utilized data from the rosette gages to obtain principal strain time histories and included consideration of ratchet strain effects. Rosette gage time histories for elbow Test 4 Runs 6, 7, and 8 were evaluated.

3) The third stage utilized linear elastic response spectrum analysis based on the measured inputs, PVRC damping values, ±15% peak broadening and ASME Code NB-3653 K_e procedures. 31 of the 41 component tests were evaluated.

In the first stage, the third method (i.e., measured moment and Code K_e procedure) provided reasonable results for elbows. When applied to tees, this method also closely predicted the runs to failure when body stress indices were used, however this was inconsistent with the failures occurring in the adjacent straight pipe or at the tee to straight pipe butt welds where lower stress indices would be permitted by the current rules. In all of the tees evaluated, both run ends were attached to the sled and out-of-plane inertia loads applied through the branch.

In the second stage, the method was unconservative.

In the third stage, use of the Code K_e values resulted in conservative results. However, if K_e was assumed to be 2, this conservatism was reduced.

3.1.3 Observed Trends in Component Response

A listing of the more important test observations from the component tests was provided in Reference 3-7, Section 10. These observations included the following:

3.1.3.1 Ratchet Buckling and the Effect of Pressure

Ratchet buckling (defined as inelastic buckling under high stress/strains experienced during component ratcheting) was observed in Tests 37 and 40. Both of these tests involved unpressurized components. Reference 3-7 suggested that pressure reduces the compressive wall stresses and therefore reduces the likelihood of ratchet buckling.

3.1.3.2 Component Cyclic Strains

Based on a comparison of the results of Schedule 10 elbow Tests 3 and 37 in Figure 9, Reference 3-7 speculated that reducing the test frequency will lead to higher strain ranges. One other difference between Tests 3 and 37, not shown in the figure, was that the weight stress in Test 37 was ten times that in Test 3. Reference 3-7 offered that the lower the frequency of dynamic testing at resonance, the closer the loading condition approaches the quasi-static condition and higher strains are to be expected.

However, there may be a low-frequency threshold suggested by GE's observation that Schedule 40 straight pipe sine Test 33 (at 5 Hz resonant testing) and Test 34 (at 15 Hz resonant testing) did not exhibit any differences in strain range for the same measured moment range.

Another interesting observation was offered on cyclic strain versus input acceleration. Figure 10 is a plot of these parameters for Test 3. Reference 3-7 stated that the cyclic strain is "tending to approach an asymptotic value."

3.1.3.3 Component Cumulative Ratchet Strain

These are observations using measurements of the change in distances between parallel scratch marks on the test articles, and the change of thickness during testing. The "ratcheting strain" based on scratch mark distance measurement after each test run was plotted in Reference 3-7 against the number of high-level inputs, and is presented in Figure 11. Figure 11 indicates generally greater strain accumulation per test run in the higher pressure tests. Generally greater increments of strain accumulation are also observed in the initial high-level test run versus subsequent test runs. Figure 11 also indicates there is no definite relationship between accumulated strain and the number of test ~~runs~~ to failure.

Cross-plots of scratch mark based ratchet strain versus pressure, and, wall thickness reduction versus pressure, were developed that confirmed that pressure was the driving force for the ratchet mechanism.

3.2 Piping System Tests

The piping system tests also consisted of seismic, hydrodynamic and water-hammer (low-, mid-, and high-frequency) tests.

The low-frequency and mid-frequency tests were conducted at ETEC and the high frequency tests at ANCO. However, only the piping system low frequency tests were considered in the current review. ETEC prepared engineering data packages for each test which consisted of time-history plots of all the data channels and a magnetic tape containing all the data in engineering units. GE was responsible for test data reduction and evaluation.

Two representative welded piping systems were instrumented and tested under time-history dynamic loads while subjected to sustained primary loads (weight and pressure). Testing was conducted at ambient temperature without any preloading other than these sustained primary loads. The loads were applied at discrete points on the piping systems using hydraulically actuated sleds operating in a single horizontal direction. The two piping systems were significantly different.

The configuration of the System 1 piping system is shown in Figures 12 and 13. The A106 Gr B carbon steel piping system consisted of six-inch diameter Schedule 40 piping, a three-inch diameter Schedule 40 bypass line and an 18-inch diameter Schedule 30 pressure vessel. All piping and fittings were uninsulated. The piping system was filled with hydraulic oil that was pressurized during testing to 1000 psig. The bypass line contained an unsupported motor operated valve (MOV) and three offset masses were distributed throughout the piping system to simulate additional valves. The MOV was functional and was operated during the testing. A spring hanger was included in the test configuration.

The MOV and spring hanger were representative of those used in nuclear power plant service.

System 1 was "tuned and seismically balanced." "Tuned" indicates that the frequency of the piping system's fundamental and predominant response mode was near (5% greater than) the frequency of the peak of the input acceleration response spectrum. "Seismically balanced" indicates that under the input loading, several locations of maximum calculated stresses were distributed throughout the piping system, specifically, at three elbows in the piping system.

The test configuration of the System 2 piping system is shown in Figures 14 and 15. The Type 316L stainless steel piping system consisted of six-inch and four-inch diameter Schedule 40 piping and a 12-inch diameter Schedule 40 pressure vessel. All welds were full penetration butt welds except at the four-inch pipe connection to the 12-inch pressure vessel. This connection was a "stub-in" weld. The piping system was filled with hydraulic oil pressurized during testing to 1000 psig. The bypass line contained two offset masses to simulate valves and the sled loading at one location was transferred through a snubber. An undersized snubber for the high-level test run was intentionally used to study the effect of support failure. After damage to the snubber, a larger snubber was used.

System 2 was "detuned and seismically unbalanced." "Detuned" indicates that the frequency of the piping system's predominant response mode (the second mode) without snubber failure, was 30% greater than the frequency of the peak of the input acceleration response spectrum. The input acceleration was tuned to the fundamental mode, but the direction of sled motion was perpendicular to the plane of the mode shape and the fundamental mode response was low. "Seismically unbalanced" indicated that there was a single location of high plasticity, the vessel nozzle area.

The instrumentation for the System 1 and System 2 tests consisted of strain gages, displacement transducers, accelerometers, load cells and scratch marks as shown in Figures 16 and 17, respectively.

A variety of time histories were applied to the two piping systems to obtain dynamic response behavior. These included low-level step displacement and sinesweeps, synchronous and non-synchronous seismic inputs and mid-frequency inputs. The highest level tests that introduced the most significant damage and eventually failure were synchronous seismic inputs of the same signature as that used in the component tests.

3.3 Specimen Fatigue-Ratchet Testing

The PFDRP materials tests of Reference 3-9 was conducted at Materials Testing Characterization Laboratory to assess reductions in fatigue life due to the effects of significant ratcheting or excessive deformation. Specifically, a test program was performed to quantitatively evaluate low cycle fatigue (LCF) in the presence of ratcheting. In these tests, sustained mean stresses were combined with alternating strains to induce ratcheting that resulted principally from the stress bias due to the sustained mean stress.

Six materials were tested: A333 Gr.6 carbon steel pipe material, A358 Type 304 stainless steel pipe material, A387 2 ¼ Cr-1 Mo pressure vessel plate material, A533 Mn-1/2 Mo-1/2 Ni pressure vessel material, and CF-8 & CF-3 cast stainless steels materials, with two to seven tests per material. All of these materials are ASME Code Section II P Nos. 1 through 8 materials except for A533 material which is P No. 11 A.

Baseline low cycle fatigue tests (zero mean stress) were performed at room temperature and at 550°F. In addition, three types of fatigue-ratchet tests were also performed:

(1) Simulated 2-bar tests

(2) Axially preloaded rectangular beam tests

(3) Pressurized pipe tests

3.3.1 Simulated 2-Bar Tests

Simulated 2-bar tests were performed at room temperature and at 550°F on single cylindrical tensile specimens (bars) in which the specimens were subjected to displacements based on computer analysis of the response of the classic 2-bar ratcheting model to strain cycling. These data were intended to provide the primary basis for developing material fatigue-ratchet damage models.

Two distinct types of response were observed during strain cycling, one termed "fatigue ratchet" in which a stable hysteresis loop was attained with subsequent failure by fatigue cracking characterized as "flat fracture with no necking" and another termed "sustained ratchet" in which continued ratcheting occurred with failure by ductility exhaustion characterized by "ductile fracture with significant necking." Unfortunately, there was no response involving a mix of continued ratcheting and fatigue, i.e., cracking characterized by a flat fracture with necking.

During testing, following saturation to a stable condition during initial strain cycling, the cyclic loading was changed to load-controlled cycling until failure occurred.

Typical test results for the fatigue-ratchet failure mode, where the results are reported as strain range versus cycles to failure for 0, 10, and 20 ksi mean stress, are shown in Figure 18. Likewise, typical test results for the sustained ratchet failure mode, where the results are reported as incremental ratchet strain per cycle versus strain range for 10 and 20 ksi mean stress, are shown in Figure 19. "Because of limited test data, the curves are at best estimates" but as expected, ratchet strain increases rapidly with mean stress. Ratchet data are compared with a Miller-based model (Reference 3-12) predictions and an exponential relationship.

3.3.2 Axially Preloaded Rectangular Beam Tests

Three preloaded beam tests were conducted on each of the A333 carbon steel and A358 stainless steel materials at room temperature. During these tests, axially preloaded rectangular beams were subjected to displacement-controlled alternating bending stresses. The tests were performed as a check on the 2-bar simulation tests. Five of the six tests failed by fatigue crack propagation and only the 13.3 ksi mean stress test of the A333 carbon steel failed by sustained ratcheting. It is noted in these tests that to the extent tested, "mean stress had very little effect on the fatigue life of the material" and that "cycles to failure of both A333 and A358 steels showed no detrimental effect of mean stress and fell within the data scatter of the baseline uniaxial results."

3.3.3 Pressurized Pipe Tests

Two room temperature tests were conducted on pressurized pipes, one on a ¾ inch diameter galvanized steel pipe and one on a 1 inch diameter 304 stainless steel tube. Pressures were selected to produce approximately 10 ksi hoop stress. The intent of these tests was to provide multiaxial stress response under comparable loading conditions at room temperature. Stress cycles were mechanically applied in the axial direction. Ratcheting occurred in both axial and circumferential directions and "failure occurred well before the expected life in fatigue." The radial force exerted by rubber bands used to attach an extensometer "constrained the ratcheting."

3.3.4 Conclusions

The GE Reference 3-9 report concluded that for low values of strain range, the failure is essentially fatigue that correlates with ASME fatigue data and little if any effect of ratcheting damage is noted. Shakedown occurred and the failure did not involve substantial plastic deformation.

For larger strain ranges Reference 3-9 observed that while the Miller type model predicted shakedown for hardening materials, test observations showed sustained ratchet failure occurred for the materials tested. No shakedown occurred for larger strain ranges and a uniform increment of plastic deformation was accumulated with each cycle.

The Miller type model predictions using a flow stress equal to the average of the measured yield and ultimate strengths were found to follow a curved line that lies above the experimental data which GE trended as straight lines on semi-log plots.

3.4 References

3-1 Guzy, D., "Piping Design Criteria and Research Current NRC Activities in Dynamic Design", Nuclear Engineering and Design, Vol. 107, pp. 161-167, 1988

3-2 English, W.F, "Piping and Fitting Dynamic Reliability Program First Semi-Annual Progress Report, May 1985 - October 1985," General Electric Company, NEC-31272, November 1985

3-3 English, W.F, "Piping and Fitting Dynamic Reliability Program Second Semi-Annual Progress Report, November 1985 - April 1986," General Electric Company, NEC-31364, November 1986

3-4 English, W.F, "Piping and Fitting Dynamic Reliability Program Third Semi-Annual Progress Report," May - October 1986," General Electric Company, NEC-31450, June 1987

3-5 English, W.F, "Piping and Fitting Dynamic Reliability Program Fourth Semi-Annual Progress Report, November 1986 - April 1987," General Electric Company, NEC-31542, January 1988

3-6 EPRI TR-102792-V1, "Piping and Fitting Dynamic Reliability Program, Volume 1 - Project Summary," EPRI 1994

3-7 EPRI TR-102792-V2, "Piping and Fitting Dynamic Reliability Program, Volume 2 - Component Tests," EPRI, 1994

3-8 EPRI TR-102792-V3, "Piping and Fitting Dynamic Reliability Program, Volume 3 - System Tests," EPRI, 1994

3-9 EPRI TR-102792-V4, "Piping and Fitting Dynamic Reliability Program, Volume 4 - Fatigue-Ratchet Tests," EPRI, 1994

3-10 EPRI TR-102792-V5, "Piping and Fitting Dynamic Reliability Program, Volume 5 - Piping Design Rules Revisions," EPRI, 1994

3-11 GE Letter to ANCO, Kaul, A.K. and English, W.F. to ANCO Engineers, "Input Seismic Acceleration Data for EPRI-PFDR Component Tests", WFE059.85, September 4, 1985

3-12 D.R. Miller, "Thermal-Stress Ratchet-Mechanism in Pressure Vessels," Transactions of the ASME, Journal of Basic Engineering, Vol. 81, No: 2, 1959, pp. 190-196

4 New Rules and Bases

At the February, 1994 meeting of the ASME Code Main Committee, the rules contained in Appendix I-A to this report were passed. The following is a summary of these new rules.

4.1 Summary of New Rules

The new rules provide modifications to the design criteria for ASME Code Section III, Class 1, 2, and 3 piping systems in Code Subsections NB/NC/ND-3600, respectively. The new rules also provide alternate Class 1 criteria in Code Subsection NB-3200.

The new rules maintain the previous criteria for "non-reversing" dynamic loads and "reversing" dynamic loads in combination with non-reversing dynamic loads. However, conditionally higher allowable stresses are provided for reversing dynamic loads not required to be combined with non-reversing dynamic loads. Typically these conditionally higher allowables are applicable to earthquake loadings.

The new rules apply to both ASME Code Service Level B OBE and Service Level D SSE loadings. For the Service Level B OBE loading, the new Subsection NB-3600 rules do not require that seismic inertia effects be included in the Equation (9) primary membrane plus bending stress load combination for Section III Class 1, 2 and 3 piping systems. However, both OBE seismic inertia and anchor motion effects are included in the Equation (10) shakedown load combination and the Equation (11) fatigue load combination for Section III Class 1 piping systems and in the Equation (10) thermal expansion load combination with an increased allowable stress of 2 S_A for Section III Class 2 and 3 piping systems.

For the Service Level D SSE loading, the new Subsections NB/NC/ND-3600 rules are the same for Section III Class 1, 2 and 3 piping systems and require that:

$$B_1 \frac{PD_o}{2t} + B_2 \frac{D_o}{2I} M_i \leq 4.5 S_m \qquad (1)$$

where:

P = Pressure coincident with SSE loading

M_i = Resultant moment amplitude due to weight, SSE inertia effects and other mechanical loads

B_1, B_2 = ASME Code stress indices

S_m = ASME Code material allowable stress

Other terms = Geometry based constants

Equation (1) is similar to the previous Service Level D rules except: 1) the system analysis used to calculate M_i is specified as discussed below, 2) the allowable S_m-based limit has been increased by 50% from the current limit of $3S_m$, and 3) the allowable S_y-based limit has been eliminated (previous rules included a $2S_y$ limit).

Conditions for application of the higher allowable stress are as follows:

(1) The analysis is based on a linearly elastic response spectrum solution, with spectrum peak broadening of no less than 15% and a damping value of 5% of critical. Currently, the ASME Code does not specify analysis methodology, but in Appendix N are non-mandatory dynamic analysis methods that specifies procedures for dynamic seismic analysis. The new rules require that certain procedures of Appendix N be followed. Currently, Appendix N has not been endorsed by the NRC.

(2) The ground motion input for the structural analysis that results in the floor response spectra to be used for the piping system analysis meets the requirements of ASME Code Appendix N.

(3) Alternatively, another methodology (e.g., time-history or static analysis) may be used if the methodology "is demonstrated to produce" forces and moments which envelop those using the methodology in 1) and 2).

(4) The piping components must be fabricated from material designated P No. 1 through 9 in Table 2A of the ASME Code, Section II, Part D. This Table 2A restriction essentially permits only ferrous materials.

(5) The maximum pressure during the SSE must be less than or equal to the Design Pressure (NCA-2142.1(a)). The current Service Level D pressure limit is twice the Design Pressure.

(6) The resultant moment amplitude due to weight loading, M_W, is limited to:

$$B_2 \frac{D_o}{2I} M_W \leq 0.5 S_m \tag{2}$$

There is no equivalent to Equation (2) in the previous rules.

(7) The range of the resultant moment due to SSE seismic anchor motion (SAM) loading, M_{AM}, is limited to:

$$C_2 \frac{D_o}{2I} M_{AM} \leq 6 S_m \tag{3}$$

The previous rules did not provide limits on Service Level D SAM loading.

(8) The ratio of the outside diameter, D_O, to nominal thickness, t, is limited as follows:

$$\frac{D_o}{t} \leq 50 \tag{4}$$

The previous rules contained the same limitation on the use of B stress indices in Table NB-3681(a)-1.

(9) The longitudinal force amplitude due to SSE relative anchor motions, F_{AM}, is limited to:

$$\frac{F_{AM}}{A_M} \leq S_m \tag{5}$$

where:

A_M = Cross-sectional area of metal in the piping component wall

The previous rules did not address longitudinal forces.

(10) The ratio of the dominant dynamic load driving frequency to the lowest piping system natural frequency is equal to or greater than 0.5.

The new rules also provide alternate Subsection NB-3200 criteria for plastic dynamic analysis, effectively requiring the consideration of nonlinear path dependent cyclic plasticity effects. These NB-3200 criteria impose a 5% limit on accumulated plastic strain averaged through the wall and a 10 cycle based limit on effective peak strain ranges.

4.2 Technical Bases for New Rules

The technical bases for the new rules are provided primarily in Reference 4-1. Additional studies performed by the TCG in response to issues raised by NRC STGIPC members during STGIPC deliberations are documented in the STGIPC and TCG reports (References 4-2 and 4-3). Results of ETEC reviews of these three reports to determine the technical bases being offered for the new rules are provided in the following.

From an overview perspective the ETEC review found that References 4-1 through 4-3 assert that results of the PFDRP component and system tests and analytical studies provide justification for removal of reversing dynamic loads from the ASME Code collapse analysis. However, stresses due to these loads need to be limited to prevent failures due to ratcheting and/or fatigue and other effects as observed in the PFDRP component and system tests. In addition, specific dynamic analysis methods are prescribed. References 4-1 through 4-3 expect that these linear analysis methods will adequately predict elastic-plastic dynamic response in the presence of limited plasticity.

4.2.1 Margin Definitions

For this review the following refinements to the TCG and STGIPC definitions of margins were adopted. These margins are defined with respect to a given seismic input load, a given piping system and a given set of ASME Code design rules and, consequently, also a given method of analysis.

- FM_{FL} = margin on level of seismic loading to cause fatigue failure for a given duration of seismic loading, pressure and temperature.

This is the minimum level of the given input that will produce a through-wall crack in the piping system during one application of this level of the input divided by the maximum level of input permitted under a given set of ASME Code piping design rules. The pressure and temperature in the piping system are at some constant specified value. The fatigue damage may be enhanced by strain accumulation under a pressure-ratchet (bulging) mechanism or a moment-ratchet (bending) mechanism. It is assumed that there is no prior fatigue damage to the piping system and that there exists no fabrication defects (i.e., all flaws are smaller than the workmanship flaw sizes in ASME Code Section XI Article IWB-3510), As a practical matter FM_{FL} is the ratio of peak acceleration of the failure level input to the peak acceleration of the level of input at the Code allowable stress or strain. i.e.

$$FM_{FL} = \frac{a_f}{a_c}$$

where

a_f = peak acceleration of failure level input

a_c = peak acceleration of input at Code allowable

- FM_{FD} = margin on duration of seismic loading to cause fatigue failure for a given level of seismic loading, pressure and temperature.

This is the expected number of applications of the given seismic input at the maximum level permitted under a given set of ASME Code design rules that will produce a through-wall crack in the piping system. The pressure and temperature in the piping system are at some constant specified value. The fatigue damage may be enhanced by strain accumulation under a pressure-ratchet (bulging) mechanism or a moment-ratchet (bending) mechanism. It is assumed that there is no prior fatigue damage to the piping system and that there exists no fabrication defects (i.e., all flaws are smaller than the workmanship flaw sizes in ASME Code Section XI Article IWB-3510).

- FM_{DL} = margin on level of seismic loading to cause deformation failure for a given duration of seismic loading, pressure and temperature.

Under large dynamic loading, piping may experience excessive accumulated strains or progressive deformations, leading to insufficient moment-carrying capacity to resist applied external weight or inertia moments (moment collapse occurs). Loss of moment-carrying capacity can be a result of wall thinning (tensile instability), local wall buckling (wrinkling), reduction of section modulus (cross-section shape change), plastic flow (hinging) or an interactive combination of these mechanisms.

There is no widely used margin definition for this potential failure mode. Therefore, it is given the following definition. It is the minimum level of the given input that will produce excessive strain or deformation in the piping system during one application of this level of the input divided by the maximum level of input permitted under a given set of ASME Code piping design rules. The pressure and temperature in the piping system are at some constant specified value. The point at which excessive strain or deformation occurs is defined here as the lesser of the following:

(1) Five percent ratcheted strain averaged through the wall thickness.

(2) Ten degrees of ratcheted plastic rotation at a piping component.

(3) Piping deflection limits specified in the piping Design Specification.

The rotation limit was imposed in the initial versions of the new rules, but subsequently removed. It is maintained in the above margin definition.

4.2.2 TCG Margin Assessment

The TCG and STGIPC have reported that minimum margins on load greater than 4.0 were experimentally demonstrated during the PFDRP component testing. This was based on the use of ±15% peak broadened spectra in the margin evaluations. In addition, adjustments to the results of the test with the minimum load margin (Test 36) to account for the use of broadened spectra vs. unbroadened spectra and worst case loading conditions not actually tested resulted in a reduced load margin near 2.0, which the TCG considered to be adequate for Service Level D loadings. The TCG derivation of the test based load margins and adjustments to these load margins are summarized in the following.

4.2.2.1 Test Based Broadened Spectrum Load Margins

Table 3 provides details of the derivation by the TCG and STGIPC of margins demonstrated during PFDRP testing. Fatigue failure margins on levels of seismic load, FM_{FL}, based on the previous rules and on the new rules are provided in Columns B and D, respectively. Table 3 is extracted from Table 2-1 of the STGIPC report. As reported earlier, several runs of the highest levels of inputs were usually required to induce failures during the component tests. Accordingly, extrapolations of the test results were required to determine the level of the input necessary to induce failure during one application of the input as required in the definition of FM_{FL}. These extrapolations were based on a cyclic damage model that adopts the -0.5 log-log slope of the ASME Code fatigue failure curve in the low cycle regime.

The calculated load margins are based on results of GE linearly elastic response spectrum analyses utilizing the measured sled accelerations with ±15% peak broadening and a damping value of 2% of critical.

Margin extrapolations from analyses with 2% of critical damping to the new rules requiring analyses with 5% of critical damping were conducted using a constant response reduction factor of 1.67 which is the ratio of the peak values of the unbroadened 2% damped and 5% damped acceleration response spectra for the targeted sled input time-history.

Based on these extrapolations, minimum load margins of 10.6 and 4.2 were obtained in Test 36 based on the previous rules and new rules respectively. Details of the load margin derivations are provided in the following in which (X) represents the entries in Column X of Table 3 where X = A, B, C, D, E.

Column A: Measured Load Margin 3 Sm Criterion

$$(A) = \left(B_2 \frac{M}{Z}\right) \Big/ (3Sm)$$

where

B_2 = ASME Code B_2 stress index for the maximum B_2 stress location in the test configuration

M = Calculated moment at the maximum B_2 stress location in the test configuration during the highest level testing based on linear elastic response spectrum analysis of the test configuration using measured sled accelerations and ±15% peak broadening with a damping value of 2% of critical

Z = Section modulus based on nominal dimensions of pipe of same size and schedule as the maximum B_2 stress location in the test configuration

S_m = Applicable ASME Code material allowable stress

Column B: Cycle Corrected Load Margin 3 Sm Criterion

$$(B) = \sqrt{N} \times (A)$$

where

N = Number of high-level test runs to induce failure reported in Appendix A of Reference 4-4

The use of $\sqrt{N}$ factor to adjust the Column A stress magnitude is a direct consequence of the assumed relationship between B_2 based stress amplitude and cycles to failure, specifically, a log-log plot of B_2 based stress amplitude versus cycles to failure would be linear with a slope of -0.5, i.e., $B_2M/Z = \alpha N^{-0.5}$, where α is a constant.

Except for Test 37, for partial runs, N is based on the time fraction of the full test run. For Test 37, N is based on assuming a full test run is of 20 seconds duration. This was in light of Test 37 being almost 2 minutes in duration, while the majority of the other tests were of durations of approximately 20 seconds. Some of the Test 30 test runs were also two minutes in duration, however, no special treatment was given to Test 30.

Column C: Earthquakes to Fail 3 Sm Criterion

$$(C) = (B)^2$$

This is also a direct consequence of the -0.5 log-log slope of the assumed B_2 stress versus cycle damage model.

Column D: Cycle Corrected Load Margin 4.5 Sm Criterion

$$(D) = (C)/(1.5 \times 1.67) = (C)/2.5$$

The 1.5 factor is a uniform reduction in load margin for increasing the allowable from $(3S_m, 2S_y)_{min}$ to $4.5S_m$, and 1.67 is a uniform reduction in load margin to account for reductions in predicted moments when replacing the previous use of 2% of critical damping for SSE loading with 5% of critical damping.

Column E: Earthquakes to Fail 4.5 Sm Criterion

$$(E) = (D)^2$$

This is also a direct consequence of the -0.5 log-log slope of the assumed B_2 stress versus cycle damage model.

4.2.2.2 Load Margin Extrapolations

Two issues were raised by the NRC staff members on the STGIPC related to the influence on PFDRP component test margins of: 1) the use of test inputs with peak acceleration response spectrum frequencies near the fundamental frequency of the test configurations, and 2) the conduct of all component testing at room temperature.

Lacking additional tests to resolve these issues, the TCG performed analytical extrapolations of the test demonstrated load margins. The lowest margin test, Test 36, was selected by the TCG to investigate the impact of the two issues. NRC staff members on the STGIPC disagreed with the decision to only evaluate the impact using Test 36.

4.2.2.2.1 Load Margin Extrapolations for Off-Resonance Tests

During STGIPC meetings, the NRC staff members had raised concerns regarding the exclusive use of near resonant testing in the PFDRP. The concerns were that: 1) margins demonstrated during PFDRP testing would not apply to other cases where the input frequency is not near the fundamental frequency of the component, and 2) lower margins would be obtained for low frequency components.

A study performed for the NRC by Brookhaven National Laboratory (BNL) (Enclosure to Reference 4-5) verified the first of these two staff concerns. The BNL study was not based on fatigue failure, but on ductility ratios, μ, i.e., the ratios of the maximum displacement during the loading inputs to the displacement at yield. However, since displacements and strain ranges are strongly correlated, the same trends are expected to be valid for fatigue-based failures.

A related concern had been raised earlier by PFDRP researchers in Reference 4-6 regarding the softening of piping system higher response modes into the peak of the input acceleration response spectrum. Figure 20 is from a GE spring-mass-damper harmonic motion study using idealized nonlinear force-displacement relationships. This figure suggests two things relative to load margins defined by elastic based stress levels. First, in the region where most of the component tests had been conducted, $0.88 < R_{\omega} < 0.93$, the elastic analysis can be very conservative. R_{ω} is the ratio of the frequency of the peak of the input response spectrum to the natural frequency of the test configuration.

Second, in the region $R_{\omega} < 0.7$, even conservative low damped (2%) elastic analyses can result in unconservative predictions in comparison to inelastic response. The use of peak broadening would reduce the analytical unconservatism, but will not eliminate it. If component tests had been conducted with a R_{ω} ratio less than 0.7, and as expected, they required the same displacement (strain) ranges to cause failure in a similar number of cycles as the existing tests, the effect of less conservatism in the elastic analyses, even possibly an unconservatism in the analyses, would result in lower computed load margins. The load margins are directly related to the amount of conservatism elastic analyses contain when predicting inelastic response. Part III of this report contains further discussion of this aspect of the load margins and the relationship of load margins to other elements of the design process.

In response to the previously described NRC staff members' concerns the TCG developed margin adjustments based on the PFDRP test with the lowest margin, i.e. Test 36. These arguments were developed by the TCG using a number of computations. The cantilever configuration was converted to an equivalent idealized rotational spring mass model. Moment arm corrections were required since the Test 36 failure was not at the base of the test configuration. Best fits to the ASME Section III Code background document fatigue data were developed and simplified ductility dependent bilinearized plastic flow models were developed.

These structural elements were input into a pair of EPRI-developed time-history codes. One was a time-history elasto-plastic dynamic analysis single-degree-of-freedom (SDOF) response code that used implicit direct integration. This code, REMS3, was reported to have been benchmarked against classical solutions and inelastic finite element codes. The other was an auxiliary code, REMSFATI, that used the rotational cyclic strain ranges from REMS3 to compute the accumulated fatigue damage. A fatigue correlation factor is used based on the testing to "calibrate" REMSFATI such that failure would be predicted at the end of the failure level test run. (However, as discussed in 3.1.1, the actual failure of Test 36 occurred midway in the first high-level test run.) It was then assumed this fatigue correlation factor would be appropriate for other frequency ratios.

A series of REMS3/REMSFATI ("REMS") analyses were performed. First, one representing the actual Test 36 test conditions was performed which gave a load margin of 9.9 against the previous rules. This value closely matched the cycle corrected load margin of 10.6 (Table 3 Column B) discussed earlier.

The NRC staff members of the STGIPC pointed out that these results should not match because the REMS time-history solution is analogous to unbroadened response spectrum analysis results and ± 15% peak broadening was used in the GE moment predictions. Eventually, it was agreed unbroadened response spectrum results should be used in the margin derivations. The 15% broadening was intended to cover uncertainties in input loading for which there were none in the laboratory tests.

The REMS margins were then reduced by a factor of 2.5 to account for the use of 5% damping instead of 2% damping (factor of 1.67) and 4.5 S_M instead of 3.0 S_M (factor of 1.5). This was a standard TCG conversion. The 1.67 damping adjustment is based on the peaks of the targeted response spectra.. However, the Test 36 natural frequency was outside the peak-broadened range. Table 2 indicates, based on the GE Test 36 predicted moments from 2% and 5% damped solutions, that the correct damping adjustment factor for Test 36 is 1.48.

Other REMS analyses were then performed for different frequency ratios, R_ω, from 0.1 to 3.2.

Computed margins were sensitive to the details of the methodologies used to vary R_ω and develop the bilinear load-deflection curves. Studies were conducted using correlations to Test 36 measured responses as guidelines for the selection of the best methodologies.

The "best" REMS methodologies resulted in the load margin plots shown in Figure 21 as a function of R_ω. By normalizing the results to the Test 36 test condition ($R_\omega = 0.77$), "margin reduction factors" (MRF's) for other frequency ratios could be inferred. The lowest margin over the range $0.5 \le R_\omega \le 3.2$ was 3.1 corresponding to a test with $R_\omega = 3.2$. (The new rules limit applicability of the revised criteria to systems with $R_\omega \ge 0.5$.) The margin at the test condition was 4.0. Therefore, the most severe MRF was 3.1/4.0 = 0.78.

However, several aspects of the development of the Figure 21 plot were questioned by the NRC staff members and after a series of written exchanges (Referenced 4-7 through 4-9), the TCG agreed, except as noted, that the REMS developed Test 36 load margins for the new rules should have been (see Reference 4-9):

(1) Adjusted so that the REMS solution at the test point of $R_\omega = 0.77$ matched the unbroadened response spectrum results.

(2) Adjusted downward by the factor $\sqrt{0.5} \approx 1/1.4 = 0.71$ to correct the REMS "test calibration" that did not properly account for failure occurring in Test 36 Run 8 about midway through the full test duration.

(3) Adjusted downward by the factor $(4.5S_M - S_p)/4.5S_M = 79{,}945/90{,}000 = 0.89$ to remove pressure stress adjustment from the load margins to provide consistency with the Table 3 load margin derivations. The TCG did not necessarily agree to the need for this adjustment, but accepted it.

The resulting Reference 4-10 REMS based Test 36 load margins with the cycle count and pressure adjustments is provided in Figure 22. For example, at $R_\omega = 0.77$ (the test condition), the load margin reduces from 4.0 to (0.71)(0.89)(4.0) = 2.5. The minimum margin of 1.95 occurs on the "soft side" close to the TCG (minimum) "acceptable margin" of 2.0 shown on Figure 21.

The NRC staff members of the STGIPC believed the actual failure location was incorrectly considered in the calculation of allowable Code moment in the REMS model. The TCG disagreed and considered the adjustment of moment stresses for location to be included in the "test calibration" and adequate.

The NRC staff members of the STGIPC maintained that consistency between the REMS solutions and acceleration response spectrum ~~solutions~~ should be achieved using unbroadened spectrum, and would be if the above moment location adjustment was made.

It was eventually confirmed for the R_ω test condition that the REMS solution matched the unbroadened acceleration response spectrum solution, despite, or possibly as a result of (in combination with the simplified 2% to 5% damping conversion), the lack of a moment location correction. The GE reported B_2 moment stress using 5% damping and an unbroadened spectrum was 314 ksi. Making the cycle correction and ignoring pressure stresses, the load margin agrees with the REMS based solution:

$$(314/4.5S_m)/1.4 = (314/90)/1.4 = 2.5$$

Again, over the range of R_ω studied, the minimum load margin for Test 36 in Figure 22 is 1.95 for values of $R_\omega > 0.5$. The TCG argued that the frequency adjustments on the "soft side" of resonance ($R_\omega > 1.0$) were not rational and prepared "normalizations" such as depicted in Figure 23 (see Reference 4-9) to defend this position. The details of the normalization have not been documented, however, according to Reference 4-11, the background information was presented and debated in a full day joint meeting in September 1993 of the WGPD and SGD.

An errata to a TCG study background paper presented in June 1994 (Reference 4-12) contains discussion of an alternate margin definition that has a margin plot similar in trend to Figure 23. However, ETEC reviewers and members of the PRG have yet to understand the plot nor why the alternate margin definition is any different than the original margin definition. Nevertheless, if a case can be made that no "soft side" adjustments to load margins are needed, then the minimum load margins will be at $R_\omega = 0.5$. Based on Figure 22, the Test 36 load margin for $R_\omega = 0.5$ is 2.1. Note that Figure 23 contains a lower load margin at $R_\omega = 0.5$ of about 1.7.

4.2.2.2.2 Load Margin Adjustments for Temperature Effects

A TCG study was conducted on the potential for lower demonstrated margins had the tests been run at higher temperature. The results of this study were presented in Appendix F to the STGIPC report for an assumed test temperature of 650°F. The TCG reasoned that the increased temperature would have reduced the Code allowable, reduced the yield strength and reduced the fatigue strength. The reduced allowable would increase the margin had the same test levels been achieved. The decreased yield strength would increase the strain range and in combination with the reduced fatigue strength, REMS3/REMSFATI solutions inferred a decrease in margin for Test 36 on the order of 0.83. Notably, there was no discussion of a possible nonlinear increase of pressure ratcheting effects on fatigue with increased temperature. Reference 4-13 results indicate a nonlinear relationship between hoop stress and ratcheting which is complicated by the nonlinear relationship with temperature between the S_M-based allowable pressure hoop stress and the material yield strength.

The TCG stated that even with the temperature correction, based on the then current Figure 21 minimum ambient margin of 3.1, the resulting temperature corrected margin near 2.5 would be acceptable. However, after the later Figure 22 minimum ambient margin of 2.1 was evolved, the 0.83 temperature adjustment drops the margin below the 2.0 level the TCG considered to be acceptable.

On the other hand, it is argued in the STGIPC report that ignoring the mid-level test run and high-level sinesweep test runs in the single event cycle adjustment introduced offsetting conservatism and the STGIPC did not support further adjustments to the ambient margins to account for temperature effects.

The NRC staff members on the STGIPC took exception to the TCG temperature arguments. First, the argument that ignoring lower level runs would offset the unconservatism of testing at ambient temperature had not been demonstrated, second, this argument may not be applicable to other tests, and third, the adjustment based on temperature trends in fatigue strength does not address temperature effects on the Test 37, 39 and 40 type of failures due to excessive deformation.

Note that the TCG margins for Test 36 are based on the use of a tee B_{2R} value of 2.52. The issue of the appropriate B_2 value for the attachment weld failure location will be discussed later in this report.

4.3 References

4-1 EPRI TR-102792-V5, "Piping and Fitting Dynamic Reliability Program, Volume 5 - Piping Design Rules Revisions," EPRI, 1994

4-2 Preliminary Report for ASME SCIII, SGD from Special Task Group on Integrated Piping Criteria (STGIPC), April 16, 1993

4-3 "Technical Core Group Report on FOAKE Task E1: ASME Piping," Advanced Reactor Corporation report, April 1993

4-4 EPRI TR-102792-V2, "Piping and Fitting Dynamic Reliability Program, Volume 2 - Component Tests," EPRI, 1994

4-5 NRC Memorandum, Fair, J.R. to Norberg, J.A., "Review of EPRI Pipe Component Test Margins," October 29, 1992.

4-6 English, W. F., "Piping and Fitting Dynamic Reliability Program Fourth Semi-Annual Progress Report, November 1986 - April 1987," General Electric Company, NEC-31542, January 1988

4-7 ASME Committee Correspondence, Subgroup on Design, SC-III, Tagart, S.W. to Fair, J., "Response to Negative Letter Ballots by Keith Wichman for LB 93-08, LB93-09A, LB 93-09B, and LB 93-10," August 14, 1993

4-8 ASME Committee Correspondence, Special Task Group on Piping, Subgroup on Design, SC-III, Fair, J. to Tagart, S.W., "Minority Response," August 24, 1993

4-9 ASME Committee Correspondence, Subgroup on Design, SC-III, Tagart, S.W. to Fair, J., "Response to your 8/24/96 letter," September 4, 1993

4-10 Branch, E.B., "Minority Report Comments" (Revised REMS Based Frequency Adjustment), Presentation to ASME Subgroup on Design, September 14, 1993.

4-11 ASME Committee Correspondence, Main Committee, Tagart, S.W. to Members Main Committee, "Background Information Agenda #N-12, Revise NB-3200 & NB/NC/ND-3600," November 30, 1993

4-12 Adams, T.M. and Branch, E.B., "Analytical Study for Frequency Effects on the EPRI/USNRC Piping Component Tests: Part II - Numerical Results and Conclusions, ERRATA", Proceedings of 1994 ASME Pressure Vessel and Piping Conference, PVP-Vol. 275-1, July 1994

4-13 EPRI TR-102792-V4, "Piping and Fitting Dynamic Reliability Program, Volume 4 - Fatigue-Ratchet Tests", EPRI, 1994

5 Results of ETEC Review

The results of the ETEC review of the technical bases for the new ASME Code piping design criteria for reversing dynamic loads are provided in the following. This review was based on the GE semi-annual and EPRI PFDRP reports (References 5-1 to 5-9), ANCO "Quick Look" test reports, ANCO test videos, and the STGIPC and TCG reports (References 5-10 and 5-11), supplemented by a collection of ASME rule committee correspondence and presentation packages.

The ETEC review of the technical bases for the new rules identified 12 general issues and 3 specific rule issues as follows.

5.1 Identified General Issues

5.1.1 Collapse Failure Mode

The evaluations supporting the new rules provided in the GE, STGIPC and the TCG reports concluded that the failure mode in piping systems due to reversing dynamic loads is ratchet-fatigue and not collapse and, consequently, the elimination of reversing dynamic loads from the ASME Code collapse design criteria is justified. However, this conclusion is not supported by the results of PFDRP component testing. Test 37 and Test 40 demonstrated incipient instability due to incremental collapse. A review of the test video records confirmed visually and by the recorded comments of the test engineer, that a collapse of the cross-sections had occurred. The moment-rotation plot for the last test run of Test 37 in Appendix I-C of this report clearly shows a degradation of moment capability as the test progressed.

The PFDRP component margin studies at CIT presented in Part II of this report indicate the existence of a regime of flexible piping behavior where large P-delta effects can lead to instability (e.g., see Figure 3.21 in Appendix II-A of this report, the cliff-like rise in fatigue damage is due to unstable behavior). The CIT studies show displacement margins for the high R_ω (higher piping period) regime can be as low as the fatigue margins for the low R_ω regime, yet it is the adequacy of the fatigue margins in the low R_ω regime that has been the focus of attention. Since the general trend is lower required input acceleration levels to reach failure levels at the higher R_ω values, there are worst case studies in the CIT work that indicate low displacement margin at low input levels to failure. For instance, for reducer Test 40, using B_2 = 1.0, Figure 4.41 in Appendix II-A of this report indicates extrapolated displacement margins at 650°F under Regulatory Guide 1.60 loading that are less than 2.0 for failure level input accelerations less than 1g.

The P-delta study conducted in Appendix G of the STGIPC report does not address the more important sustained eccentric weight effect. The 14,000 pounds offset at 0.08 radians on an 83 inch vertical riser introduces approximately 10,000 psi nominal bending stress in 6-inch NPS pipe at the base. However, when combined with the dynamic stresses, this "unaccounted for" weight stress is not expected to initiate ratcheting since there is no sustained weight eccentricity in the perfectly vertical setup. However, if a maximum allowed 0.5 S_m (10,000 psi) sustained eccentric weight stress existed at the start, then the biased loading might progressively have increased the 0.08 radian offset on one side of the cycle and the resulting progressively increasing sustained eccentric weight effect would accelerate the collapse process.

Test 39 was also stopped early due to excessive rotations. It is believed that the progressively increasing sustained eccentric weight effect during rotational ratcheting contributed to the collapse and deformation failure modes observed in the unpressurized Tests 37, 39, and 40. But low pressure alone is not strongly correlated to collapse. Unpressurized Test 8 did not rotationally ratchet in 8 high level test runs despite substantial ovalization and had pressurized Tests 12, 15, 35, and 36 not cracked, "collapse" might have been observed in these tests since rotations at cracking exceeded 10 degrees.

The reducer Test 40, although Schedule 40 test components and not considered "thin-walled" surprisingly experienced a compressive wall instability failure in the straight pipe spool described by the GE researchers in Reference 5-6 as "*inelastic buckling under high stress/strains experienced during ratcheting*" GE termed this behavior "ratchet buckling". The ANCO test engineer clarified this behavior in the QL report: "*The nature of the failure appears to be a sudden compression induced plastic instability failure rather than an incremental collapse of the section*". A review of the test video indicated a large inward wall crimp had formed in the straight pipe between the two reducers.

It was also not demonstrated that the use of test inputs having large displacements at low frequencies would not have resulted in sudden collapse. The displacement capability of the test sleds was limited. Only the low frequency elbow Test 37 in the later stages of the last test run leading to section collapse addressed this behavior. The same large offset weight loading, considered a key contributor to the collapse, would have occurred had the sled been able to move substantially out from under the inertial arm added weights.

It is also noted that the Test 37 measured ultimate moment, M_U, divided by the Code allowable moment (F_S value in Table 2) is the lowest for all the elbows and is roughly half the magnitude of all the other elbow tests except Test 30. Test 30 also had a low F_S value and is the only other low frequency test. An understanding of this Test 37 outlier behavior is still being sought.

The underlying mechanistic concerns are (1) weight moments calculated based on initial geometry and small displacement theory could be significantly under-predicted under large displacement loading of flexible systems and (2) low frequency response could result in adequate time for sustained weight loadings to grossly deform the system if moment capacities are exceeded. This issue is paramount when siting designs on the West Coast where there has been observations of a limited number of severe magnitude ground displacements in the near-field records of recent earthquakes. Exploratory CIT margin studies of PFDRP Test 14 using Northridge near-field records have indicated very low values for the deformation based failure margin discussed in Part II of this report, despite the fatigue damage margin being very high. Although the large displacement portion of the near field loading would be non-oscillatory, the potential for a "whip effect" (e.g., piping still going East under initial ground motion while the building heads West under the subsequent reversing ground motion) leads to collapse concerns. On the other hand, as discussed in Shipley's PRG member commentary in Appendix III-D of this report, it is highly unlikely future nuclear plants will be sited in close proximity to (known) major earthquake faults.

Limiting the piping displacement is one approach to reducing concerns with the weight eccentricity and P-Δ effects. Most piping systems will have an array of weight and seismic supports that, provided they don't fail, will limit system displacements and thus component rotations. However, review of the evolution of the new rules indicates there may be some industry resistance in this area. The early drafts of the new rules required large deflection analysis be used to meet Design Specification displacement limits, with reference to Code Appendix N methods, but this was deleted in later versions.

Also, the incremental collapse of Test 37 may have been enhanced by a rotational ratchet mechanism in elbows due to the non-symmetry of opening and closing plastic behavior of elbows. This potential mechanism is expected to be sensitive to the elbow ovalization characteristic (Code h value). When combined with the pressurization effect observed in Test 3 that ratcheted the elbow in the opening direction, and weight eccentricity effects, the rotational ratchet behavior of elbows is clearly complex.

Extrapolation of elbow collapse margins away from the test points will require a better understanding of the basic interactions of these mechanisms. It is recognized that ETEC's use of geometrically symmetric component test studies like the REMS studies for Test 36 (or Test 11, 14, 36 and 40 CIT studies discussed in Part II of this report) to extrapolate elbow behavior in the Section 6.0 (and Appendix II-B of this report) margin studies is questionable. A study at CIT on non-symmetric elbow hysteresis modeling has been initiated.

Finally, the interaction of section collapse and fatigue failure modes needs to be further studied. There was no Schedule 10 straight pipe tested in the PFDR program. The D_o/t applicability limit of 50 for the new rules is near the D_o/t value observed in static monotonic limit tests of straight pipe above which local wall wrinkling reduced the moment capacity below the theoretical limit moments (Reference 5-26). The D_o/t limit of 50 may prevent local wall wrinkling at $4.5S_M$ levels of stress given the observed increase in moment capacity under reversing dynamic loads seen in Table 2 and discussed in Rodabaugh's PRG member commentary in Appendix III-C of this report, however, this needs to be confirmed. The concern is local wall crimping will create strain concentrations that initiate cracks under reversing loads.

The TCG report claims that collapse is not a realistic failure mode at the new code limits. Resolution of this issue will require more adequate technical support for the elimination from consideration of the collapse failure mode including acceptable explanations for Tests 37 and 40, and satisfactory demonstration of the preceding claim over the full range of potential loading and geometrical conditions.

5.1.2 Inelastic Analysis Criterion

The new rules introduced the previously described fatigue and ratcheting strain limits for dynamic inelastic piping analyses in the Code design-by-analysis Subsection NB-3200. This is termed a "strain control approach" in the PFDRP summary report (Reference 5-5, Appendix B). It is stated the simplified design criteria for linearly elastic analysis based designs in the Subsection NB/NC/ND-3600 new rules are "designed to meet the intent of the general dynamic strain criteria," a reference to the new Subsection NB-3200 criteria.

First, although the results of the PFDRP materials testing provide some insight into the ratchet-fatigue interaction, the PFDRP Volume 4 report conclusions regarding adequacy of the new NB-3200 criteria is not systematically and quantitatively tied to the test data. The test results as summarized provide qualitative, but not quantitative support for the specified limits.

Second, the PFDRP Volume 1 Appendix B discussion of the basis for the new NB-3200 rules argues that the Code shakedown criteria used to validate the fatigue analysis is not necessarily required, and limiting the wall-averaged ratchet strain to 5% assures the Code fatigue procedure will be reasonably accurate. This discussion does not refer directly to the PFDRP materials testing as the basis for this assertion, but suspecting it is, then resolution of this issue will require a clearer and more defensible representation of the EPRI Volume 4 materials testing data and findings.

Third, the demonstration that compliance with the simplified criteria assures compliance with the NB-3200 criteria is lacking. The presentation and discussions of results for five benchmark piping analyses performed by the TCG illustrated the methodology proposed by the TGIPC for evaluating failure margins in new criteria but did not provide a clear proof the NB-3200 strain criteria would be met with the stress criteria (and applicability limits) eventually adopted in the new NB/NC/ND-3600 rules. The simplified criteria in NB/NC/ND-3600 had been developed on a semi-empirical "indirect" basis using correlations to the PFDRP component tests. This is a separate issue which is addressed below. However, it will make it difficult to clearly demonstrate that meeting the new NB/NC/ND-3600 criteria assures meeting the new NB-3200 criteria.

Implementation of the NB-3200 criteria will require that dynamic inelastic piping analyses be performed and the high sensitivity of the solutions to the nonlinear material modeling (constitutive relationships) will also require significant validation efforts to justify the selection of material models. The likelihood that regulatory acceptable nonlinear design analyses will be performed in the near term is negligible. It is therefore recommended that the new NB-3200 "strain control" criteria be deleted at this time to allow review and regulatory approval efforts to focus on the justifications offered for acceptance of the simplified linearly elastic analysis based NB/NC/ND-3600 criteria.

5.1.3 Margin Basis

The GE, STGIPC and TCG margin evaluations are based on linearly elastically calculated stress ratios, which is understandable given that the new rules provide limits on linearly elastically calculated pseudo-stresses. As discussed earlier, this essentially reduces the margin definition to an acceleration ratio. However, acceleration is an inconclusive measure of adequacy in flexible piping systems where displacement response can be equally, if not more, important. Seismic displacements are important when considering the significance of P-delta effects on collapse, the potential for piping system interactions, the operability of in-line equipment and the predictability of support loads. A margin based on strain, displacement and/or rotation limits, as introduced earlier in this report, should be used to augment the pseudo-stress margins.

Further, the use of acceleration ratios loses accountability of the reality of the acceleration levels being studied and these can be affected by the details of the margin studies. For example, when the margin effect of frequency ratio R_ω is studied by changing the time step of the input sled record, effectively shrinking or stretching the input time histories, as done in the REMS studies, the levels of required input accelerations to reach the Code limits increase as R_ω increases. If the input loading remains unchanged and the physical test configuration is altered to change the natural frequencies, as done in the later CIT studies, the levels of required input accelerations <u>decrease</u> as R_ω increases. However, the acceleration ratio based margins are identical for the two cases.

CIT studies have also shown margins are highly dependent on the time-history loadings used and that there is a strong correlation between margin and acceleration levels. These findings indicate the simplistic acceleration ratio based margins are not adequately integrating all the seismic performance issues in the actual design environment.

Resolution of this issue will require a more acceptable definition of margin that includes consideration of deformations, addresses the influences on and reality of the input levels needed for failures and either avoids sensitivity to the input time-history or accounts for the sensitivity appropriately.

5.1.4 Acceptable Margin Level

No technical framework to establish an acceptable seismic margin was provided. The STGIPC report (Reference 5-10) recommended that minimum acceptable margins on ASME service levels C or D reversing dynamic loading be in the range of 2.0 to 2.5. The basis offered was limited to comparison to precedents in other Code margins on other failure modes and loadings.

A defensible technical approach was needed to establish acceptable levels of seismic margins. Towards that end, ETEC retained R. Kennedy to develop such an approach based on piping not impacting plant seismic PRA evaluations. This development is presented in References 5-12 and 5-13. When correctly used to establish acceptable levels of minimum demonstrated seismic margins for the new rules, it is expected to resolve this issue.

5.1.5 Predicted Loads for Design

As the piping pressure boundary rules are relaxed for seismic events, it is expected fewer seismic supports will be used. The reduction in the number of supports will make the proper functioning of the remaining supports more critical. With increased allowables and gross section plastic response, loads may redistribute and some supports, vessel nozzles or equipment anchorages can be loaded higher than predicted by linear analysis.

Concerns with the ability of linear analysis methods to predict support loads have led to many experimental test programs including support load measurements as part of the collected data. A review of some of the most significant testing was conducted by the TCG in Appendix A to Reference 5-10. Notably missing was the Reference 5-14 Argonne National Laboratory evaluations of the Reference 5-15 SHAM tests which indicated, on-average, 40% underpredicted support loads using PVRC recommended (Code Case N-411) damping. The final TCG recommendation was that the linear analysis predicted support loads using 5% damping and ±15% peak broadening should be increased by a factor of 1.2.

The initial versions of the new rules contained this requirement, however, as it passed through the higher committee approval process, the rule was deleted, purportedly due to arguments there were adequate margins in the support design process to cover unconservatism in the predicted loads. Shipley provides a perspective in his PRG member commentary in Appendix III-D of this report that a Code factor on linear analysis predicted loads provides the designer with a false sense of security and the primary issue is whether sufficient support ductility is provided to accommodate possible overloads due to nonlinear piping behavior.

Support load adjustments also do not address the underprediction of nozzle loads and equipment anchorage loads.

Resolution of this issue will require the development of an acceptable methodology for the determination of reaction loads and/or a presentation of the justifications the new rules maintain acceptable seismic margins in supports, nozzles and equipment anchorages.

5.1.6 Limited Test Data

As previously described, the seismic tests in the PFDRP testing were conducted almost exclusively at near resonance conditions. The effects of off-resonance loading have only been studied analytically and use extrapolations of the existing data base that have yet to be verified by test. Off-resonance tests are desirable to benchmark the analytical extrapolations.

As discussed in 5.1.1, tests have not been conducted with large displacements at low frequency and there were no Schedule 10 straight pipe tests.

Only one time-history was used in the PFDRP tests. Analytical studies at CIT have shown that for the same R_ω considerable differences in margins can result using different time histories. In particular, at the higher R_ω values, broad-band time-histories typical of ground level floor response can lead to lower margins than the narrow-band PFDRP test time-history. The International Piping Integrity Research Group (IPIRG) program test results (Reference 5-16) also showed different time-histories with the same acceleration response spectrum could affect the failure behavior.

Only room temperature component tests were conducted. Simplistic analytical temperature adjustments to room-temperature test ratchet-fatigue margins based on the temperature trends of elastic moduli and yield strengths in static monotonic tension tests and the reduced fatigue strength in low-cycle uniaxial fatigue data have been conducted. However, these adjustments do not address temperature dependent cyclic hardening and softening behavior and temperature dependent strain rate effects.

Extrapolation of room temperature failure data or moment capacities to high temperatures for carbon steel piping components is particularly problematic due to a phenomenon known as dynamic strain aging (Reference 5-17). At higher strain rates, near 1 sec^{-1}, there is a temperature-dependent switch in dynamic post-yield strength trends. At room temperature, the dynamic ultimate strength may increase 15 percent above static values, however, at 550°F, the dynamic ultimate strength may decrease by 15 to 30% versus static data (References 5-18 and 5-19). However, this is monotonic test data. Little data exists on the cyclic stress-strain curves of carbon steels at different strain rates and temperatures. The large differences in room temperature ultimate state moments measured in the PFDRP dynamic cyclic component tests versus the static monotonic piping component test data is considered due in large part to cyclic hardening and to a lessor extent due to strain rate effects. Due to dynamic strain aging, it is not clear that this large increase in cyclic dynamic moments over monotonic static moments at room temperature will exist at high temperature, and in fact, it is possible the dynamic data will lie below the static data.

A final testing limitation is that none of the PFDRP component tests included test articles with intentional workmanship defects. A review in Reference 5-20 of piping fatigue test data with workmanship flaw sizes satisfying Section XI IWB-3610 showed that the fatigue life was reduced enough so that the safety margin of 2 on stress or 20 on life was completely eroded. Additional work by Battelle (Reference 5-21) showed that such small flaws could also reduce the low cycle fatigue-ratchet life. Consideration of the effect of such pre-service or in-service allowable workmanship flaw sizes should be given in the assessment of the actual margins

Resolution of these issues appears to require additional selective validation testing.

5.1.7 Semi-Empirical Basis for New Rules

The new NB/NC/ND-3600 criteria utilize static limit load indices for the control of the cyclic ratchet-fatigue failure mode. This approach was purportedly chosen in part for consistency with current design practice and to lessen industry confusion and misunderstanding. Although observations of failure locations and failure characteristics of the ratchet-fatigue failures suggest gross-section plasticity is playing a significant part in the ratchet-fatigue failure mode, the use of static limit load indices is not fully accounting for differences in ratchet-fatigue resistance between different piping components. Further, there is no accounting for the number of major cycles which can vary for a given earthquake depending on the predominant mode frequencies of the piping system and the building's seismic response characteristics at pipe support locations. Therefore, the criteria is at best semi-empirical and it's adequacy must be argued based on overall failure level correlations to the test data.

A number of limitations on concurrent pressure and weight stresses and applicability restrictions were introduced to assure that adequate protection against the ratchet-fatigue failure mode was achieved and more importantly, the failure mode would be limited to ratchet-fatigue.

The limitations introduced appear to have relevance and the reasons for them are generally understood, but they have been correlated to the PFDRP component tests only and may not be appropriate to general piping systems. An argument has not been provided that piping system behavior can not introduce mechanisms that require additional limitations

Also, the semi-empirical approach was based on a particular set of Code B_2 indices selected for the piping components under evaluation. As discussions in the ETEC margin assessment will illustrate, the appropriate selection of B_2 indices for many of the PFDRP tests is controversial. Those issues deal with observed failure locations outside the pipe fittings and/or failure characteristics not indicative of fitting behavior. A different B_2 selection issue addresses the observation fitting B_2 values used in design evaluations may be lower than those used in the empirical correlations as permitted by the Code procedures. This would reduce the seismic margins. For example, lower B_2 indices for out-of-plane elbow moments are currently available but were not used in the data correlations. And there is a continual effort to improve the existing stress indices. Future changes to Code B_2 indices will now need to address their semi-empirical use in the NB/NC/ND-3600 reversing dynamic load criteria.

5.1.8 Component versus System Behavior

The new rules were based essentially on the PFDRP SDOF component testing. The multiple degrees of freedom (MDOF) system tests were dismissed as merely confirmatory and no margins were presented.

The an important system issue that needs to be addressed is higher mode response illustrated by the PFDRP System Test 2 fatigue failure induced by a predominant second mode response. It was recognized that the first mode would not be excited by the single direction sled loading perpendicular to the plane of the first mode shape and the test was "tuned" to excite the second mode. Similarly, in a real piping system, there are locations that will not respond predominantly in the first mode. Although the first mode frequency will meet the R_ω greater than 0.5 applicability limit, the predominant modes may not and margins can be less than the PFDRP component data base extrapolated to $R_\omega = 0.5$.

Two other system issues that need to be addressed are raised by the GE damping study observations quoted earlier. First, the component cantilever test configuration damping will be greater than had the component been subjected to the same level of loading within a redundant piping system (and was the only highly stressed component). Second, the system response frequency will not "detune" from the driving frequency as in the component tests.

Another system issue that needs addressing is the beneficial effect of redundancy that through load redistribution, allows loadings on components to exceed their ultimate capacity without loss of system integrity.

A final system concern not able to be addressed by the PFDRP component testing is that concurrent sustained thermal expansion (TE) and thermal anchor motion (TAM) moments will drive a ratchet mechanism in high seismically stressed areas. The new NB-3200 rules recognize that the thermal loadings need to be considered in conjunction with the mechanical loadings to adequately address potential ratchet mechanisms. Dynamic shaker tests (Reference 5-22) at University of California, Berkeley on a piping system with TE loading simulated by cold spring demonstrated the piping system will "walk" in the direction of the thermal loading.

The main concern with the TE ratchet mechanism is the distortions could have detrimental effects on support performance. A specific concern is weight hanger travel. A piping system that thermally "walked" during the seismic event might lead to the weight hanger bottoming out and then failing under the seismic inertial loads. The weight stress increase resulting from the hanger failure might then induce a collapse failure.

A demonstration that criteria based on SDOF tests are adequate for effects in MDOF piping systems is required. This demonstration should include higher mode failures as observed in the PFDRP System Test 2 and address the issues raised by the GE damping study and UC Berkeley concurrent thermal load study.

5.1.9 Concurrent SAM Loadings

The new rules provide separate limits on the SSE inertia and SAM loadings. An evaluation conducted by Stevenson and Associates (S&A) concluded (Reference 5-23) the effect of the maximum new rule allowed concurrent SAM moments on the Test 36 seismic margins would be at most a 15% reduction.

Two issues were raised during ETEC's review of the S&A study. First, the use of Test 36 only to study the potential effect of concurrent SAMs was too limited. Second, the combination of seismic inertia and SAM moments used by S&A was by Square Root of the Sum of the Squares (SRSS), which is accepted design practice, but may not be appropriate for flexible piping systems. It is expected past studies of SAM and inertia loading interaction have generally been confined to stiffer designs under the old rules.

The study focus on Test 36 ignores other piping components having different relationships between B_2 and C_2 indices. For example, at a girth butt weld,

$$B_1 = 0.5$$

$$B_2 = 1.0$$

$$C_2 = 1.0$$

If the wall thickness is sized at the minimum allowed by NB-3640 for the Design Pressure, then the pressure term in the new rules at the Design Pressure would be near

$$B_1P_DD_o/2t = 0.5\ S_m$$

This leads to an allowed inertia moment stress of

$$D_oM_E/2I = 4\ S_m$$

and in terms of moment range,

$$D_o\Delta M_E/2I \leq 8\ S_m$$

The SAM moment (range) stress limit becomes:

$$D_oM_{AM}/2I \leq 6\ S_m$$

Although rarely the case for current designs, the inertia and SAM loadings could in flexible design situations be directly additive. Combined by algebraic sum, the inertia plus SAM moment range stress limit becomes:

$$D_o(M_E + M_{AM})/2I \leq 14\ S_m$$

The percent increase of moment due to SAM contribution is

$$(14 - 8) / 8 \times 100\% = 75\%$$

The decrease in seismic margin is 43% which is not of little consequence.

Resolution of this issue will require identification of the appropriate combination of SAM and inertia loading for flexible systems and including the potential SAM effects in the seismic margin assessments.

5.1.10 Evaluation of Flaws Greater Than Code Workmanship Flaws

Although the ASME Code Section III rules are applicable to new designs, the implications of the higher allowable stresses in the new rules with respect to the reliability of piping systems constructed to the new rules was evaluated. The concern was that the flaw tolerance of such systems may be significantly degraded and impact the plant operability adversely.

ETEC contracted a study at Battelle (Reference 5-24) that concluded that when flaws in piping at the new stress limits are larger than the Code acceptable workmanship standard flaws, the existing Code Section XI pipe flaw evaluation rules for justification of continued operation can not be used. Hence the piping would need to be repaired or replaced.

Resolution of this issue may require development of a new evaluation methodology based on nonlinear corrections to the elastically calculated stresses.

The implications of the higher allowables in the new rules on margins in degraded piping were not considered in the ETEC reviews, but is clearly a serious issue.

5.1.11 Applicability Limits and Exclusions

The reasons for most of the applicability conditions that must be met to use the new rules were generally understood, although the justifications for some of the specific limits chosen were lacking. The need for the SAM axial stress limit was questioned by a member of the ETEC Peer Review Group since moment stress limits indirectly provide control of axial stresses.

The PFDRP component test data base did not include threaded joints. The seismic experience data base indicates failed threaded joints in earthquakes when connection details akin to the butt welded PFDRP component test articles survived. This issue needs to be resolved before the new rules are applied to design of these fatigue prone connections.

Bimetallic welds were also not tested. These welds can have localized soft zones and/or metallurgical notch effects that could result in accelerated ratchet-fatigue failures. Many of the PFDRP component tests failed at welds. Adequate margins at bimetallic welds need to be demonstrated before the new rules can be applied to these designs.

There also has been recent incentives to use nonlinear pipe supports such as limit stops and energy absorbers. The new rules do not address whether piping systems with these devices are permitted to use the higher allowables. Justification for their allowance have not been forthcoming and until such time, piping systems using nonlinear pipe supports should be excluded from use of the new rules.

5.1.12 Variation in Seismic Margins Predicted for PFDRP Component Testing

Extrapolated seismic fatigue margins of less than 1.0 for PFDRP component tests have been repeatedly calculated by ETEC using the same definition of margin and REMS frequency effect extrapolation as used by the TCG for Test 36. The ETEC margins are based on a different, but defensible, set of B_2 stress indices than used by the TCG and includes nominal versus minimum strength adjustments and pressure, weight and temperature adjustments not included in the TCG margin evaluations. A systematic accounting for the number of events to cause failure based on test measured rotations is also used. This evaluation refines the original 1993 ETEC minimum margin evaluation reported in Reference 5-25. Another set of nominal margins was calculated based on CIT studies and will be presented in Part II of this report.

The historic variability in ETEC predicted seismic margins by themselves clearly illustrates that calculated seismic margins are very sensitive to the basic assumptions and details of the margin data reductions. For example, the ETEC predicted seismic margin in this report (prior to the SAM adjustment) for Test 36 is 0.84 in comparison to the 1.7 and 2.1 TCG values while other documented ETEC margin predictions for Test 36 have ranged between 0.7 and 2.9. Resolution of this issue requires concurrence on the correct assumptions and details to use ~~in the~~ the margin evaluations.

5.2 Identified Specific Rule Issues

5.2.1. Deletion of S_y-based Allowable Stress.

An S_y-based allowable stress on limit load design equations was introduced in the 1983 ASME Section III Code following studies of limit load capabilities by Rodabaugh and Moore (Reference 5-26). This change was made to bring the Code limits into better agreement with the theoretical and experimental work on limit loads. Still, at the Service Level D $3S_M$, $2S_y$ limit, the primary loads could exceed the limit-loads by over 50% and the rule couldn't be defended on the basis of single-hinge limit moment capacity arguments. In their Reference 5-27 discussion of the implication of this for dynamic loads, the authors believed the loads would be applied and removed so quickly that gross plastic deformation does not have time to occur. However, observation of the Test 37 video footage indicates this may not be true for low frequency piping systems.

The location of ratchet-fatigue failures in some of the PFDRP component tests occur not at the highest peak stress locations in the bodies of the fittings but rather in the lower stressed adjacent straight pipe. Also, static limit moment tests of similar fittings have shown the limit moment capacity of the fitting is as great or greater than attached adjacent straight pipe of the same schedule. Indeed, limit moment tests of these fittings often involve use of rigid inserts or solid rounds instead of adjacent straight pipe to force the failure in the fitting. These two observations suggest that the high-level margin tests are inducing cyclic cracking failures in regions of gross section plasticity instead of peak stress regions where more conventional lower-level fatigue tests create failures.

For this reason, the concept of failure mode tied to the B_2 indices gains merit, but more consistently for different materials if it is also tied to S_y. It is clear that material yield strength is an important failure parameter and the S_y-based allowable stress should be reinstated.

5.2.2 6 S_m Allowable Stress for Seismic Anchor Motion

Introduction of a limit on seismic anchor motions (SAMs) is certainly warranted. However, the 6 S_m limit needs to be justified. The earthquake experience data base for piping systems indicates SAM failures are more prevalent than inertia failures (some would argue exclusively so), yet the PFDRP testing and TCG criteria developments (and NRC reviews) have focused almost entirely on the inertia failure mode.

It is not clear that the ratchet-fatigue failure mode cares if the moment loads are inertial or SAM induced. Margin evaluations may need to combine damage effects of the two loadings as done in the Section 6 margin assessment. The technical basis for the SAM criteria needs to address this issue.

5.2.3. S_m-based Allowable Stress for Code Safety Class 2 and 3 Systems

The early versions of the new rules contained S_h-based limits for Code Safety Class 2 and 3 piping systems. These were replaced by Code Safety Class 1 S_m-based limits. This presents a problem for materials in Class 2 and 3 that are not permitted in Class 1. Resolution of this issue will require the development of S_h-based criteria and should include consideration of the differences between Class 1, 2 and 3 construction.

5.3 References

5-1 English, W.F, "Piping and Fitting Dynamic Reliability Program First Semi-Annual Progress Report, May 1985 - October 1985," General Electric Company, NEC-31272, November 1985.

5-2 English, W.F, "Piping and Fitting Dynamic Reliability Program Second Semi-Annual Progress Report, November 1985 - April 1986," General Electric Company, NEC-31364, November 1986.

5-3 English, W.F, "Piping and Fitting Dynamic Reliability Program Third Semi-Annual Progress Report, May - October 1986," General Electric Company, NEC-31450, June 1987.

5-4 English, W.F, "Piping and Fitting Dynamic Reliability Program Fourth Semi-Annual Progress Report, November 1986 - April 1987," General Electric Company, NEC-31542, January 1988.

5-5 EPRI TR-102792-V1, "Piping and Fitting Dynamic Reliability Program, Volume 1 - Project Summary," EPRI, 1994

5-6 EPRI TR-102792-V2, "Piping and Fitting Dynamic Reliability Program, Volume 2 - Component Tests," EPRI, 1994

5-7 EPRI TR-102792-V3, "Piping and Fitting Dynamic Reliability Program, Volume 3 - System Tests," EPRI, 1994

5-8 EPRI TR-102792-V4, "Piping and Fitting Dynamic Reliability Program, Volume 4 - Fatigue-Ratchet Tests," EPRI, 1994

5-9 EPRI TR-102792-V5, "Piping and Fitting Dynamic Reliability Program, Volume 5 - Piping Design Rules Revisions," EPRI, 1994

5-10 Preliminary Report, ASME SCIII, SGD, Special Task Group on Integrated Piping Criteria (STGIPC), April 16, 1993

5-11 "Technical Core Group Report on FOAKE Task E-1: ASME Piping," Advanced Reactor Corporation report, April 1993

5-12 Kennedy, R.P., et. al., "Towards Appropriate Seismic Margins in Nuclear Plant Piping", Proceedings of 1996 ASME Pressure Vessel and Piping Conference, PVP-Vol. 340, July 1996

5-13 Kennedy, R.P., "Establishing Seismic Design Criteria to Achieve an Acceptable Seismic Margin", Proceedings of 24th Water Reactor Safety Information Meeting, USNRC, October 1996

5-14 Srinivasan, M.G., et.al., "Verification of Piping Response Calculations of SMACS Code with Data from Seismic Testing of an In-Plant Piping System," ANL Report NUREG/CR-5757, September 1991.

5-15 Kot, C.A., et.al., "SHAM: High-Level Seismic Tests of Piping at the HDR", Nuclear Engineering and Design, Vol. 118, pp. 305-318, 1990.

5-16 Hopper, A., et.al., "The Second International Piping Integrity Research Group (IPIRG-2) Program - Final Report," NUREG/CR-6452, BMI-2195, March 1997

5-17 Marschall, C.W., et.al., "Effect of Dynamic Strain Aging on the Strength and Toughness of Nuclear Ferritic Piping at LWR Temperatures," NUREG-CR-6226, October 1994

5-18 Miyazaki, K., et.al., "Fracture Behavior Under Monotonic and Low Cycle Loading in Carbon Steel Pipes and Welded Pipe Joints with a Defect", ASME PVP-Vol. 323, July 1996

5-19 Rudland, D., Brust, F., and Wilkowski, G.M., "The Effects of Cyclic and Dynamic Loading on the Fracture Resistance of Nuclear Piping Steels," NUREG/CR-6440, BMI-2190, December 1996

5-20 Wilkowski, G., Rahman, S., and Mohan, R., "Low-Cycle Fatigue Crack Growth Considerations in Pipe Fracture Analyses," ASME PVP-Vol. 280, June 1994

5-21 Scott, P.M. and Wilkowski, G.M., "A Comparison of Recent Full-Scale Component Fatigue Data with ASME Section III Fatigue Design Curves," ASME PVP Vol. 306, pp. 129-138, July 1995

5-22 Schneider, S. et.al., "Response of a Piping System Under Seismic and Thermal Loading," Paper K12/8, Proceedings of the 7th SMiRT Conference, Chicago, 1983.

5-23 Adams, T. "Effect of SAM on the ARC EPRI Criteria", Stevenson and Associates FAX to TCG members, July 26, 1993, attached to November 1993 Agenda of ASME WGPD meeting, Attachment 4, J. Minichiello; "Proposed [TCG] Responses to WGPD Concerns"

5-24 Zhao, Y. and Wilkowski, G.M., "A Case Study for Assessment of Consistency Between ASME Section III and Section XI Rules", Proceedings of 1996 ASME Pressure Vessel and Piping Conference, PVP Vol. 340, pp. 331-344, 1996

5-25 Chokshi, N.C., et.al., "The US NRC Seismic Analysis of Piping Research Program" Proceedings of the 14th SMiRT Conference, Paper K13/2, Vol. 8, pp. 1 - 8, Lyon 1997

5-26 Rodabaugh, E.C. and Moore, S.E., "Evaluation of the Plastic Characteristics of Piping Products in Relation to ASME Code Criteria", NUREG/CR-0261, July 1978

5-27 Moore, S.E. and Rodabaugh, E.C., "Background for the ASME Nuclear Code Simplified Method for Bounding Primary Loads in Piping Systems", Proceedings of the 1981 Pressure Vessel and Piping Conference, PVP-Vol. 50, pp. 143 - 164, 1981

6 ETEC Minimum Fatigue Margin Evaluation

6.1 Overview

Results of the TCG and STGIPC assessments of component test margins demonstrated during PFDRP testing, based on broadened spectrum and FM_{FL} margins, are provided in Section 4.2.2.1 and Table 3 of this report. Test 36 adjustments by the TCG for unbroadened spectrum, weight stress and pressure stresses, and, analytical extrapolations for frequency conditions not tested are provided in Section 4.2.2.2 of this report. It was predicted that the Test 36 configuration would have exhibited a margin of 2.1 (Figure 22) or 1.7 (Figure 23) if it had been tested at $R_{\omega} = 0.5$. This is based on a B_2 value of 2.52.

An ETEC comparative FM_{FL} margin assessment was conducted along similar lines, but extended the coverage to other PFDRP tests and also included adjustments for; 1) actual test article thickness vs. nominal thickness, 2) actual test article strength versus ASME Code minimum strength, and 3) reduced fatigue resistance at elevated temperature.

In addition, ASME Code B_2 stress indices based on actual failure locations were used and refinements to the TCG/STGIPC data reductions were made to 1) eliminate the assumed fixed ratio between the 5% damping response spectrum solution and the 2% damping solution for all of the tests and 2) extrapolate to single event failure levels based on more quantitative response measures.

In the adjustments for frequency conditions not tested, the same REMS based extrapolations used by the TCG for Test 36 were applied to all tests. This provides consistent comparisons with earlier ETEC margin studies that did not have the benefit of the CIT studies. Other ETEC margin assessments directly using the results of the CIT studies are reported separately in Appendix II-B of this report. The Appendix II-B margin studies are based on nominal geometry and material properties and revised B_2 stress indices consistent with Kennedy's recommendations in his PRG member commentary in Appendix III-B of this report.

The FM_{FL} margins reported in this section of the report use the same margin definition and damage model as in the TCG Test 36 study. However, the adjustments for actual geometry and property values and temperature effects is intended to provide "minimum" margins. In actuality, these are not true minimums since the CIT studies indicate that the frequency effects on margins can be more severe than concluded in the REMS studies, time-history selection is important, and a deformation based margin is required to supplement the fatigue margin in order to account for the interaction of strain accumulation on the fatigue damage extrapolations off of the test point. Additionally, recent high temperature fatigue studies indicate less temperature effect for stainless steel and more temperature effect for carbon steel than used in the ETEC minimum margin study.

It must be emphasized that the TCG and both ETEC margin studies are for FM_{FL} margins. The ETEC margins in this section of the report are based on a fatigue damage model, while the temperature adjustment is based on ratchet-fatigue data. The Appendix II-B margins includes a more direct consideration of the ratchet strain interaction with fatigue damage. However, none of these margin studies address the collapse failure mode. Only the CIT Test 40 study in Part II of this report addresses the FM_{DL} margin.

The point being made by the ETEC minimum fatigue margin assessment in this section of the report is that within the same framework of margin definition and damage models used by the TCG, the details of the data extrapolations to "minimum margins" significantly affect the resulting values. The ETEC margin assessment was conducted strictly as an independent comparative evaluation, and does not signify acceptance of the TCG margin definitions and damage models.

Most importantly, the only direct comparison to the TCG results is for Test 36. The extrapolations beyond the test demonstrated margins (Column M of Table 4) are an ETEC initiative, and the TCG only provided margin extrapolations for Test 36, the test with minimum TCG calculated margin at the test point.

Table 4 provides the different adjustments used in the comparative margin assessment and each of the column entries are discussed in the notes to the Table.

For the non-elbow tests, the most significant effect on margin prediction is the choice of stress indices. For this reason, two of the tests, Test 11 and Test 36 had two values of stress indices evaluated. The second most significant effect was the frequency adjustment. The other adjustments individually had an effect of less than 30% on margin, generally decreasing it, but not always.

6.2 Assumptions and Details

6.2.1 B_2 Indices Selection

The B_2 indices were selected based on the location of failures in the PFDRP component tests. Table 1 provides information on the failures contained in the QL reports. The choice of B_2 indices for the ETEC margin assessment will be discussed here.

To assist in the indices selection, the failures under the seismic inertia loading were compared to failures which occurred during cantilever fatigue testing conducted by Markl (References 6-1 and 6-2). The Markl tests were mechanically motion-controlled tests driven using an eccentric slot/key design to provide a harmonic motion-controlled loading to the end of the cantilevers.

6.2.1.1 Elbow Indices

In the PFDRP elbow tests, failure occurred by through-wall cracks in the pressure boundary, except for Tests 8, 19 and 37 which will be discussed separately. All of the elbow test pressure boundary failure locations occurred in the elbows except for Test 31. Based on failure location, the standard Code elbow B_2 indices were considered appropriate for the PFDRP elbow tests except for Test 31. Test 31 cracked circumferentially in the adjacent straight pipe at the weld. Test 30 also cracked circumferentially at the attachment weld, but on the elbow side of the weld.

Tests 30 and 31 are pressurized Schedule 10 in-plane loaded elbows. Their failure locations do not agree with the Markl elbow data in Reference 6-1. All of Markl's in-plane loaded elbows, both pressurized and unpressurized, failed with longitudinal cracks at the sidewall. These were Schedule 40 elbows. Failures at the end welds did occur in Markl's elbow tests, however, these were pressurized out-of-plane tests. These Markl weld line failures are not unexpected because the strains in the center of the elbow are lower (for the same moment) for out-of-plane loading versus in-plane loading. The "carryover effect" of the elbow ovalization at the ends combined with the weld strain concentration could lead to higher strains at the welds than in the center of the body.

The elbow "carryover effect" is greater in thinner walled piping and there is greater potential for strain concentration in the as-welded welds of thinner piping (greater sensitivity to diameter mismatches and the weld thickness to wall thickness discontinuity is greater). Therefore circumferential cracking at the welds for in-plane tested Schedule 10 elbows is not totally unexpected.

Another explanation surfaced when review of the Test 31 QL report indicated the Schedule 10 elbows in the PFDRP were purchased from a vendor who sometimes cold-worked the elbows after forming to eliminate a small bulge that more often than not appeared at some location on the side of the elbow. *"The standard procedure for eliminating this bulge. . . . . is to impact the bulge area with an aluminum ball pien hammer. This is done until the area is sufficiently flattened."* If not followed by an annealing cycle, this might introduce sufficient cold work into the elbow to result in the non-typical Test 31 failure location. Examination of Table 2 in this report indicates the MM/ML and Mu/ML ratios for Tests 3, 30 and 31 are out of line with the remainder of the data base.

The appropriate B_2 index for Test 31 became a moot point when it was discovered the test matrix was too mixed to permit margin data reductions.

Failure of the pressure boundary did not occur in elbow Tests 8, 19 and 37. Test 8 had no cracks, Test 19 had surface cracks in the sidewall but the test was stopped early to provide information on crack propagation, and Test 37 was stopped to avoid an incremental ratchet collapse failure due to large distortions centered in the elbow. Standard Code elbow B_2 indices were considered appropriate for these tests, although Test 37 was not considered in the margin assessment since the study was limited to the ratchet-fatigue failure mode and not collapse.

6.2.1.2 Reducer Indices

Two of the three reducer tests experienced pressure boundary failures in the straight pipe between the two reducers. Reducer Test 40 did not fail the pressure boundary, but was stopped due to excessive distortions, confined entirely to the straight pipe. The pressure boundary failures were circumferential cracks at the middle (Test 15) and edge (Test 16) of diametrical bulges remote from welds. These were pressurized Schedule 40 reducer tests. This does not match reducer test failure locations reported by Markl in Reference 6-2.

In Markl's tests, the highest loaded reducer failed in the straight pipe at the edge of the attachment weld, and the lower loaded reducers failed in the attachment weld. There was no mention of bulging. However, these failure location differences are only an issue associated with appropriate i, C_2 and K_2 values because the B_2 indices are all 1.0 for butt weld, straight pipe and reducers.

6.2.1.3 Straight Pipe Indices

In pressurized straight pipe Test 34, the failure was a circumferential crack at a bulge in the straight pipe. The straight pipe B_2 index of 1.0 is therefore appropriate.

6.2.1.4 Tee Indices

To this point, the choice of B_2 indices has been consistent with those chosen by the TCG. This is not the case for the tee tests. A review of the Markl tee test data in Reference 6-2 observed the following. Markl tested tees in three configurations. Position 1 anchored one run leg and loaded through the branch, Position 2 anchored the branch leg and loaded through the run and Position 3 anchored one run leg and loaded through the other run. Twenty in-plane and twenty-one out-of-plane tests were conducted. Only two of the test setup and load directions matched the PFDRP component test configurations considering the PFDRP inertia arm equivalent to the Markl load arm:

Position 1, Out-of-Plane: PFDRP Tests 38 and 39. Position 3, In-Plane: PFDRP Test 36. There were no Markl tests equivalent to PFDRP tee Tests 9, 10, 11, 12 and 14. These will be discussed separately.

All of the Markl Position 1 failures were on the side of the tee remote from the welds. The observed crack patterns are identical to those observed in the Markl elbow tests when the unloaded run leg is ignored and the load path through the remaining run and branch is viewed as that through an elbow.

The Test 38 failure was a crack in the body of the tee that matched those in the Markl tests. It is therefore appropriate that the standard Code tee B_2 index be used for Test 38. The tee B_{2b} branch index was selected for the ETEC margin assessment based on the inertia load path through the branch and is in agreement with the Reference 6-3 NUREG-1367 use of the B_{2b} value.

Test 39 was stopped early due to excessive distortion of the tee and for that reason was not included in the ETEC (ratchet-fatigue) margin assessment.

Markl conducted three "through run" Position 3 in-plane tests identical to Test 36. All failed adjacent to, in, or across the branch welds. Two of the three in-plane data points lay near an $i = 1.13$ trend line. The third was the highest test point (lowest i value) of the 41 tee tests, even laying above the baseline butt weld line of $i = 1.0$. Markl ignored the Position 3 tests in the i value correlations for simplicity because they did not line up with the other tee data.

The Test 36 failure was a circumferential crack in the tee adjacent to the lower run attachment weld. The tee was a Schedule 40 tee while the lower attached straight pipe was Schedule 80. There was a 4:1 slope transition on the Schedule 80 side of the connection. However, the geometry restrictions of NB-3683.5(a) and (b) for Class 1 welded transitions can not be met because the wall thickness variation on the tee side within $\sqrt{D_o}$ of the weld exceeds the 0.875t to 1.1t limits. Strictly speaking, the weld connection is not permitted for Class 1 unless special indices are developed. However, the details affect the appropriate choice of C_1, C_2 and C_3 indices, and not the B_2 indices. It is clearly a test configuration that introduces a significant amount of plastic strain concentration at the connection weld between the tee and the tapered transition joint. It might even be argued that the reduced thickness section introduces sufficient local overstrain that the Code guidance in NC-3672.6(b)(2) is applicable and the use of linear analyses to infer margins is inappropriate for Test 36.

Nevertheless, continuing the line of thought that the Test 36 setup contains standard design details used in service, the B_{2r} index for a tee could be argued as appropriate due to the tee body containing the failure. However, the observation that the initial failure location (the crack propagated to 285° of the circumference) was adjacent to the weld on the opposite side of the run from the branch undermines this argument. This is an area where gross bending behavior is not significantly affected by the presence of the branch.

To illustrate the subtlety and controversy of the issue, it is noted a B_2 selection for a tee was used in NUREG-1367, however, Rodabaugh, after publication of the NUREG and further consideration of the details of the failure, concurred during follow-up NRC staff inquiries that a more conservative B_2 value of 1.0 is the better choice (for functionality issues). Since then, Rodabaugh in an ETEC requested review of the appropriate indice for Test 36 supported use of an indice close to 2.5 in the context of protecting against a ratchet-fatigue failure by the new rules in acknowledgment of the severe "notch effect" introduced by the change in schedule and weld details. Since the test margin can be deemed applicable to either a transition weld or a tee (or both), results for B_2 indices of 1.0 for the transition weld and 2.52 for the tee were both included in the ETEC margin assessment.

The PFDRP tee Tests 9, 10, 11, 12 and 14 have no Markl test equivalents because they were tested with both run ends supported. The pipe nipples attaching each end to the sled fixture were the same length leading to each run leg reacting approximately the same moment load. This minimized the ratio of run moment to branch moment and may explain the failure locations not being in the tee bodies for most of these double run supported tests.

Only Test 11 of the five double run supported tests failed in the tee. The other four failed in the attached straight pipe. All failed with circumferential cracks. Tests 9, 10 and 14 cracked in the straight pipe adjacent to the attachment weld to the tee. Test 12 cracked in the straight pipe at a diametrical bulge. Test 11 failed in the tee adjacent to the branch weld.

GE in Reference 6-4 offers the explanation for the straight pipe failures versus tee body failures as the higher yield strength of the weld material. At high strain ranges, "the weld acts like a clamp or band on the pipe, similar to a taper transition connection." GE goes on to recommend the code butt-weld indices be increased for dynamic load reversals. Based on it's margin assessment results, ETEC strongly supports this recommendation.

The B_2 indices were selected as 1.0 for the ETEC margin assessment of all the double run supported tests except Test 11. ETEC supports a Test 11 B_2 value selection based on the tee branch B_{2b} value. Tests 9, 10 and 14 are considered by ETEC to be butt weld failures, and Test 12 is considered by ETEC to be a straight pipe failure.

The ETEC support of B_{2b} for Test 11 bears discussion. According to NUREG-1367 the deformations were limited to a local cylindrical zone at the weld and a B_2 value of 1.0 was considered conservative for the functionality study. However, based on ETEC staff experience with the detailed stress analyses of thin-walled elbows for the liquid metal breeder reactor designs, ETEC believes that the body effects of Schedule 10 tees extends into the connection welds and that since the failure was on the tee side of the weld, the use of B_{2b} is appropriate. However, similar to Test 36, the test may be argued to apply also to the weld for the attached branch pipe, and accordingly, results for a B_2 index value of 1.0 are also included in the margin assessment.

6.2.2 Calculated Moments

TCG test margin values for the new rules were uniformly scaled from the test margins for the previous rules using a constant scale factor of 2.5. The STGIPC report establishes the factor of 2.5 based on 1.5 for the increase in Eq. (9) allowables and 1.67 for decreased response due to an increase in damping from 2% to 5% ($1.5 \times 1.67 = 2.5$). Table 3 divides the "cycle corrected load margin" for the "3.0 S_m criterion" by this fixed 2.5 factor to obtain the "cycle corrected load margin" for the "4.5 S_m criterion".

The constant factor of 1.67 for increasing damping from 2% to 5% is the ratio of the peaks of the 2% and 5% damped targeted input spectra. However, Table 2 of this report includes a column labeled "M2/M5" which lists the ratios of the Reference 6-5 Appendix B computed moments based on the measured sled spectra with 2% and 5% damping. The ratios vary from 1.48 to 1.96.

To avoid the error introduced by use of a constant scaling factor, the ETEC assessment used the ~~5%~~ damped, 15% peak broadened response spectrum based moments directly from Reference 6-5 in Column C of Table 4.

Unbroadened response spectrum moments are needed in the margin calculations, but were only available for Test 36. To convert Column C peak-broadened response spectrum moments to Column E unbroadened response spectrum moments, the 5% damped response spectrum from the measured sled acceleration time-history was used. For situations where the fundamental frequency was within 15% of the peak frequency ($0.87 < R_\omega < 1.15$), R, the ratio of the acceleration at the test system natural frequency to the acceleration at the top of the peak-broadened response spectrum was used to scale downward the peak-broadened spectrum predicted moments. This assumes single degree of freedom behavior, a reasonable assumption for the major damage contributing test runs of the tests evaluated in the ETEC margin assessment. The only test significantly outside the R_ω range of applicability of this data reduction was Test 36, however, GE fortunately had run unbroadened spectrum solutions for this test.

6.2.3 Actual Geometry

There was no repeated testing in the test matrix to address component geometry variability and no effort to select test articles with nominal dimensions. In fact, the differences between nominal and actual thickness were significant in some cases. If a nominal thickness component had been tested instead, the test margins would have been different. The Table 1 listed (section-averaged) thickness at the failure location was used in the ETEC margin assessment to correct for off-nominal dimensions. For all tests except Test 36, these were averages of four measured values at 90 degree circumferentially separated locations.

The Test 36 failure location was not dimensionally measured prior to the testing. However, an adjacent location in the attached straight pipe close to the failure location provided wall thinning information that was used to scale up the final measured thickness at the failure location as an estimate of the starting thickness.

The initial diameters were very close to nominal and off-nominal effects of diameter were ignored. Column F is the Section Modulus calculated using failure location pre-test thickness. Nominal dimensions were used in all stress indices calculations.

6.2.4 Event Count

The event count used by GE and adopted by the TCG appears to be an ad hoc screening of test runs into significant high-level runs and those contributing negligible damage. Each full duration high-level run was considered "one event". Partially completed high-level runs seemed to generally be recorded as "1/2 event", based on the total counts being rounded to the closest 0.5 value. However, Test 38 which was reported as a 3.6 event test series, indicates a more sophisticated partial event count may have been used.

In an attempt to be more representative of a desired, but not achievable, event count based on failure location peak strain range, the ETEC margin assessment used "measured" rotation as the indicator of relative levels of strain range in each test run. Rotations were not directly measured but inferred from measured relative displacements between the inertia arm and bottom of the test configuration. The ANCO/GE researchers established a "rotation" data reduction reported in the QL reports. This plotted data was used by ETEC to establish the maximum range of rotation in any test run cycle, and is reported in Appendix I-B of this report .

The equivalent event count is based on the assumption that the cyclic failure can be correlated by the slope of a fatigue curve. Specifically, a fatigue curve with a slope of -0.5 in log-log space, as used in the TCG margin study. The ETEC margin assessment assumes rotation is linearly related to strain range or pseudo-stress range and ignores the nonlinear strain concentrations unaccounted for in such an approach. It is considered a reasonable approach for determining the relative magnitude of damage induced between different test runs and offers a quantitative way of accounting for different test run levels consistent with the assumed failure model.

The results of the ETEC margin assessment event count is tabulated in Appendix I-B of this report, and listed in Column I of Table 4. For comparison, the event count from Reference 6-6 Appendix A used by GE and the TCG is given in Column H. The lowest ratio of the ETEC event count to the GE/TCG event count is 0.61 for Test 3 which will reduce the calculated margin by a factor of 0.78. The highest ratio is 2.74 for Test 36 which will increase the calculated margin by a factor of 1.66.

6.2.5 Concurrent Loads

The PFDRP component tests were conducted with pressure loadings in some cases and weight loading in all cases. The new rules require that pressure stresses and weight stresses be combined with the seismic inertia stresses when meeting the 4.5 S_m limits. These stresses are relatively small compared to the seismic inertia stresses, but are nevertheless included in the ETEC "Equation (9)" derivations. Column K ~~in~~ Table 4 are the Eq. (9) pressure and weight stresses, based on actual thickness, as discussed earlier.

6.2.6 Test Margin Calculation

Table 4 Column J contains the ETEC single event corrected Eq. (9) stress level. Dividing entries in this column by 90,000 psi (4.5 S_m) minus the Column K pressure plus weight stress adjustment, leads to Column M "test margins." This is not the only manner in which concurrent pressure and weight stress adjustments can be computed with regard to the seismic margin.

An alternative data reduction is to add the Column K pressure and weight stresses to the Column J seismic stresses and divide the sum by 90,000. This leads to lower computed margins. It can be argued that the presence of high pressure and weight stresses generally does not increase the ability to accommodate seismic loadings, but rather decreases it. Pressurized components can withstand more moment loading before collapse than unpressurized components, particularly in thin-walled piping, but one of the ratchet-fatigue failure modes being addressed in the margin assessment (pressure bulging ratchet) is clearly worsened by higher pressures. Concurrent weight moments are also difficult to perceive as adding seismic capability.

Nevertheless, the manner of adjusting the allowable downward for concurrent pressure and weight stresses is consistent with plant PRA margin assessments and simplifies the subsequent temperature and frequency (fatigue-based) adjustments by keeping the margin linear in the cyclic (seismic) contribution.

6.2.7 Actual Material

A review of the failure location room temperature mill test data listed in Table 1 indicates a clear trend of higher than minimum material strength in the test articles. This is not surprising since no efforts were taken to select test articles with minimum permitted strength. Logically, to infer the margins apply conservatively to any design, adjustments should be made to account for possible minimum strength material in designs.

Following Beaney's lead (Reference 6-7), the margins are normalized on the basis of material yield strength. Beaney discovered that the scatter in his failure data could be significantly reduced by this normalization (see Figures 24 and 25). In the ETEC margin assessment, the ratio of the Code minimum yield strength to the mill test yield strength for each failure location was used to adjust the test demonstrated margins. Column N of Table 4 is this ratio.

On the other hand, for carbon steels, material fatigue strength is inversely correlated to ultimate strength as pointed out by the TCG researchers in Reference 6-8 and supported by the Code carbon steel fatigue design curves being dependent on ultimate strength. To address this effect, the ETEC margin assessments included an upward margin adjustment for higher than minimum mill test ultimate strengths for the failure locations in the carbon steel component tests. This adjustment is based on the (minimum) 60 ksi ultimate strength extrapolation of the two Code carbon steel fatigue curve values at 200 cycles assuming they are tied to materials with ultimate strengths of 115 ksi and 80 ksi, respectively. The resulting adjustment is presented in the Column P Note to Table 4.

Table 4 Column Q is the end of the series of margin adjustments on the actual tests conducted. The remaining adjustments are for test conditions not conducted.

6.2.8 Elevated Temperature Adjustments

Column R of Table 4 contains adjustments for reduced margin had the tests been conducted at elevated temperature. It was agreed among program researchers and NRC staff that use of 650°F for the elevated temperature adjustment would be representative of "hot" service conditions.

The effect of temperature on margin raises several issues. Two basic failure modes were observed in the PFDRP data, ratchet-fatigue cracking and excessive deformation. The following addresses ratchet-fatigue cracking margins, FM_{FL}, only and is not appropriate for FM_{DL} margin adjustments when the failure mode is excessive deformation.

6.2.8.1 Carbon Steel

Appendix F of Reference 6-9 addresses margin reduction due to the effect of temperature. For Test 36 this margin reduction was estimated to be approximately 17%. However, since the lower level test runs had been ignored in the single event correction step for the Test 36 margin derivation, it was considered justifiable to ignore the reduced margin at higher temperature. Since the ETEC margin assessment now includes all the test runs, the temperature effects will be evaluated explicitly.

Elevated temperatures will result in a reduction in ratchet-fatigue margin at the minimum margin frequency ratio point ($R_{\omega} = 0.5$) due to reduced Elastic Modulus and reduced yield strength (effectively reducing the room temperature R_{ω} value), and lower fatigue strengths. The Reference 6-9 Appendix F study focused on the carbon steel Test 36 behavior using the REMS/FATI model. The combined effect of reduced yield at 650°F and fatigue curve reductions were studied and a relationship between fatigue strength reduction and margin reduction at 650°F was established. Upward margin adjustments for the reduced allowables at higher temperature were included. It was determined by the TCG that the margin reduction at 650°F for carbon steel Test 36 was 0.83.

On the basis of a TCG observation that fatigue strength dominated over yield effects, a simplified derivation of the 650°F correction was investigated. The ratio of room temperature S_m to 650°F S_m value was 20/17 = 1.18. Based on a TCG stated fatigue strength (S-N curve) reduction at 650°F of 0.7, a simplistic correction of (1.18)(0.7) = 0.82 was derived. This compared well with the REMS/FATI based number of 0.83, and the simplified method was used to derive a correction for stainless steel tests.

6.2.8.2 Stainless Steel

Repeating the carbon steel "simplified" temperature adjustment for stainless steel leads to the following. The ratio of room temperature S_m to 650°F S_m is 20/16.7 = 1.2. Figure 26 shows the Type 304 stainless steel fatigue-ratchet data plots in Reference 6-10 Appendix B at room temperature and 550°F. Values on the 10 ksi mean stress curves were used to address pressure and weight mean stress effects at higher temperatures. The lowest cycle 10 ksi mean stress data points were log-linearly extrapolated back to 100 cycles to failure and the resulting values for the room temperature and 550°F data sets were near 2.2 and 1.4 respectively. The resulting fatigue-ratchet strength reduction for temperature effects at 550°F becomes 1.4/2.2 = 0.64. No extrapolation to 650°F was attempted, and the final overall temperature effect adjustment factor of (1.2)(0.64) = 0.76 was used for the stainless steel tests

6.2.9 Frequency Adjustments

Adjustments for frequency effects were based on the latest frequency effect results reported by the TCG in Reference 6-11 for Test 36, as shown in Figure 22, and, the assumption that the "shape" of this curve is applicable to all tests. This shape assumption is questionable based on the studies at CIT presented in Part II of this report. However, it provides consistency with the TCG Test 36 studies.

The frequency adjustment is intended to correct for reduced margins had the testing been done at a frequency ratio with lower margin. The extrapolated "hard side" margins at R_ω equal to 0.5 were investigated.

Margin adjustments for tested R_ω values were obtained by dividing the Figure 22 margin at $R_\omega = 0.5$ (i.e., near 2.1) by the Figure 22 margin for the particular R_ω value tested. As discussed earlier, the "shape" of Figures 21 and 22 are identical, but Figure 22 has been lowered slightly. The same margin reduction for frequency effect would be obtained using either curve. Tables of values for Figure 21 are available from several published sources and these values were used to derive the margin reduction factor expression in Note U to Table 4 over the range of $0.74 < R_\omega < 1.0$.

6.3 Margin Study Results

Table 4 of this report provides the ETEC minimum fatigue margin study results in Column V. The value for Test 36 using a B_2 of 2.52 is 2.16 which compares well with the comparable TCG value of 2.1. This is purely coincidental. Most importantly, Test 36 is not the lowest test value, several other tests had lower margins. The lowest margin is for Test 11 using a B_2 index of 1.0, but as stated earlier, ETEC believes the more appropriate B_2 value for Test 11 is 3.35 which raises the margin above 1.0 (it still remains one of the four lowest margin tests however). The lowest margin test for which there is no B_2 issue from ETEC's perspective is Test 14 where the margin is slightly below 1.0. This result implies that if Test 14 was performed at the new rule allowable stress levels on a minimum strength butt weld connection at 650°F using a test loading with frequency ratio of 0.5, it would fatigue fail before the completion of the seismic event.

Part II of this report contains more recent and more refined margin evaluations by CIT of Test 14, and other tests, that is considered the only defensible margin results on the PFDRP component test data to date.

The key result of the margin study in this section of the report is that it demonstrates significant variation in margin values can be obtained by changing the details of the data reduction. The most important detail is the appropriate choice of B_2 indices. This is the issue raised in Section 5.1.12 of this report.

6.4 References

6-1 Markl, A.R.C., "Fatigue Tests of Welding Elbows and Comparable Double-Mitre Bends", Pressure Vessel and Piping Design, Collected Papers 1927-1959, ASME, 1960, pp. 371-381, reprinted from ASME Transactions, 1947

6-2 Markl, A.R.C., "Fatigue Tests of Piping Components", Pressure Vessel and Piping Design, Collected Papers 1927-1959, ASME, 1960, pp. 402-418, reprinted from ASME Transactions, 1952.

6-3 Terao, D. and Rodabaugh, E.C., Functional Capability of Piping Systems, NUREG-1367, November 1992.

6-4 English, W.F, "Piping and Fitting Dynamic Reliability Program Fourth Semi-Annual Progress Report, November 1986 - April 1987," General Electric Company, NEC-31542, January 1988.

6-5 EPRI TR-102792-V2, "Piping and Fitting Dynamic Reliability Program, Volume 2 - Component Tests," EPRI, 1994

6-6 EPRI TR-102792-V1, "Piping and Fitting Dynamic Reliability Program, Volume 1 - Project Summary," EPRI, 1994

6-7 Beaney, E.M., "Response of Pipes to Seismic Excitation - Effect of Pipe Diameter/Wall Thickness Ratio and Material Properties," CEGB Report TPRD/B/0637/N85, Berkeley Nuclear Laboratories, July 1985.

6-8 Branch, E.B., "ETEC Margin Calculations", ASME Committee Correspondence, ASME SCIII, SGD ember, to Ed Wais, February 1995

6-9 Preliminary Report, ASME SCIII, SGD, Special Task Group on Integrated Piping Criteria (STGIPC), April 16, 1993

6-10 EPRI TR-102792-V4, "Piping and Fitting Dynamic Reliability Program, Volume 4 - Fatigue-Ratchet Tests," EPRI, 1994

6-11 Branch, E.B., "Minority Report Comments" (Revised REMS Based Frequency Adjustment), Presentation to ASME Subgroup on Design, September 14, 1993

Table 1: PFDRP Component Test Basic Data and Failure Information

BASIC DATA								FAILURE LOCATION GEOMETRY & STRENGTH DATA										FAILURE DATA				
TEST ID	MTL	P	LOAD	Fn	Fl	Rw		NOM T	TEST T	TST/NOM	III-Sy	III-Su	III-Sm	T-Sy	T-Su	T/III Sy	T/III Su	PB	ROT	OVAL	CIRC	FAILURE LOCATION / NOTES
ELBOW TESTS:																						
1 EL,80,LR	CS	2600	IP	8.40	7.60	0.905		0.432	0.455	1.05	35	60	20	40	69	1.14	1.15	YES	NA	1.00	1.02	SIDEWALL
2 EL,80,LR	CS	2600	OP	6.40	5.50	0.859		0.432	0.459	1.06	35	60	20	40	69	1.14	1.15	YES	NA	1.00	1.04	IN BODY AT WELD
3 EL,10,LR	SS	400	IP	4.00	3.90	0.975		0.134	0.156	1.16	30	75	20	34	82	1.13	1.09	YES	NA	1.00	1.01	IN BODY AT WELD
4 EL,40,LR	CS	1000	IP	7.00	6.80	0.971		0.280	0.307	1.10	35	60	20	48	71	1.37	1.18	YES	NA	1.00	1.04	SIDEWALL
5 EL,40,LR	CS	1700	IP	7.40	6.50	0.878		0.280	0.300	1.07	35	60	20	48	71	1.37	1.18	YES	7.5	1.00	1.11	SIDEWALL
6 EL,40,LR	SS	1700	IP	7.20	6.30	0.875		0.280	0.311	1.11	30	75	20	54	84	1.80	1.12	YES	17.5	1.00	1.06	SIDEWALL
7 EL,40,LR	SS	1000	IP	7.00	6.50	0.929		0.280	0.314	1.12	30	75	[illegible]	[illegible]	[illegible]	1.80	1.12	YES	5	1.00	1.01	SIDEWALL
8 EL,40,LR	SS	0	IP	7.20	6.60	0.917		0.280	0.313	1.12	30	75	20	54	[illegible]	1.80	1.12	NO	2	1.10	1.00	8 RUNS, NO CRACKS
13 EL,40,SR	CS	1000	IP	7.00	6.70	0.957		0.280	0.421	1.50	35	60	20	47	79	1.34	1.32	YES	2	1.00	1.00	SIDEWALL
19 EL,40,LR	SS	2500	IP	6.80	6.70	0.985		0.280	0.323	1.15	30	75	20	54	84	1.80	1.12	NO	7	1.00	1.01	PARTIAL CRACKS @ MID SIDE
30 EL,10,LR	SS	400	IP	1.44	1.45	1.007		0.134	0.145	1.08	30	75	20	34	82	1.13	1.09	YES	2	1.10	1.01	CIRC CRACK @ WELD
31 EL,10,LR	SS	400	IP	4.00	3.50	0.875		0.134	0.131	0.98	30	75	20	39	86	1.30	1.15	YES	6	1.02	1.01	CIRC CRACK IN ST @ WELD
35 EL,40,LR	CS	1700	IP	4.40	4.10	0.932		0.280	0.304	1.09	35	60	20	42	79	1.20	1.32	YES	16	1.10	1.04	AXIAL CRACK @ MID SIDE
37 EL,10,LR	SS	0	IP	1.44	1.40	0.972		0.134	0.156	1.16	30	75	20	34	82	1.13	1.09	NO	21	1.80	1.00	INCIPIENT COLLAPSE
41 EL,40,LR	CS	1700	IP	7.00	6.50	0.929		0.280	0.304	1.09	35	60	20	44	67	1.26	1.12	YES	5	1.02	1.02	CIRC CRACK @ DIE STAMP
OTHERS:																						
9 TEE,40	SS	1700	OP,2	7.00	6.60	0.943		0.280	0.269	0.96	30	75	20	51	84	1.69	1.12	YES	2	1.00	1.00	CIRC CRACK IN ST @ BR WELD
10 TEE,40	SS	1000	OP,2	7.20	6.70	0.931		0.280	0.282	1.01	30	75	20	51	84	1.69	1.12	YES	4	1.00	1.00	CIRC CRACK IN ST @ BR WELD
11 TEE,10	SS	400	OP,2	5.80	5.00	0.862		0.134	0.139	1.04	30	75	20	40	64	1.32	1.12	YES	0	1.00	1.00	CIRC CRACK @ BR WELD
12 TEE,40	SS	1700	IP,2	8.40	7.60	0.905		0.280	0.282	1.01	30	75	20	51	84	1.69	1.12	YES	15	1.00	1.07	CIRC CRACK IN ST @ BULGE
14 TEE,40	CS	1700	OP,2	7.20	6.60	0.917		0.280	0.286	1.02	35	60	20	54	73	1.54	1.21	YES	3	1.00	1.00	CIRC CRACK IN ST @ BR WELD
15 RED,40	SS	1700	BEND	7.20	6.50	0.903		0.237	0.228	0.96	30	75	20	37	79	1.23	1.05	YES	13	1.00	1.01	CIRC CRACK IN ST @ BULGE
16 RED,40	CS	1700	BEND	7.40	6.70	0.905		0.237	0.234	0.99	35	60	20	50	72	1.41	1.20	YES	8	1.10	1.05	CIRC CRACK IN ST @ BULGE
34 PIPE,40	CS	1000	BEND	5.80	5.30	0.914		0.280	0.278	0.99	35	60	20	45	78	1.29	1.30	YES	3	1.10	1.08	CIRC CRACK @ BULGE
36 TEE,40	CS	1700	IP,1	6.80	5.30	0.779		0.280	0.293	1.05	35	60	20	46	72	1.30	1.20	YES	21	1.00	1.01	CIRC CRACK @ RUN WELD
38 TEE,40	SS	1700	OP,1	7.00	6.50	0.929		0.280	0.371	1.33	30	75	20	40	80	1.34	1.07	YES	7	NA	1.12	45 DEG CRACK IN BODY
39 TEE,40	SS	0	OP,1	6.80	6.50	0.956		0.280	0.283	1.01	30	75	20	40	80	1.33	1.07	NO	22	1.50	0.96	EXCESSIVE DEFORMATION
40 RED,40	SS	0	BEND	7.00	6.50	0.929		0.237	0.216	0.91	30	75	20	37	79	1.23	1.05	NO	22	1.30	1.01	INSTABILITY IN STRAIGHT

Notes to Table 1

BASIC DATA

TEST	PFDRP test identification number assigned by GE and ANCO to the test.
D	Piping Product description: XX/YY/ZZ
	XX = EL, Butt-welded 6 inch nominal diameter 90-degree elbow
	XX = TEE, Butt-welded 6 inch nominal diameter equal-leg tee
	XX = RED, Butt-welded 6 to 4 inch nominal diameter reducer
	YY = 10, 40, 80: Pipe Schedule
	ZZ = LR, Long radius (1-1/2 times nominal diameter bend radius)
	ZZ = SR, Short radius (1 times nominal diameter bend radius)
MTL	CS = carbon steel, SA-106 Grade B Pipe, SA-234 WPB Fittings
	SS = stainless steel, Type 316, SA-312 Pipe, SA-403 Fittings
P	Internal pressure, psig (see Footnote 1)
LOAD	IP = Sled motion in the plane of the pipe fitting
	OP = Sled motion out of the plane of the pipe fitting
	BEND = Straight cantilever beam bending test setup
	XX,1 = Only one run leg of tee attached to sled
	XX,2 = Both run legs of tee attached to sled
Fn	Measured natural frequency of test configuration, Hz. (see Footnote 1)
Fl	Frequency at peak of measured sled acceleration LERS, Hz (see Footnote 1)
Rw	Rw, Ratio of Fl/Fn (see Footnote 1)

FAILURE LOCATION GEOMETRY & STRENGTH DATA

NOM T	Nominal wall thickness, inch
TEST T	Pre-test measured wall thickness in proximity failure location, inch (see Footnote 2)
TST/NOM	Ratio (TEST T)/(NOM T)
III-Sy	ASME Code listed yield strength for component, ksi
III-Su	ASME Code strength for component, ksi
III-Sm	ASME Code allowable stress intensity for component, ksi
T-Sy	Mill test yield strength for failed pipe component, ksi
T-Su	Mill test ultimate strength for failed test component, ksi
T/III Sy	Ratio (T-SY)/(III-SY)
T/III Su	Ratio (T-SU)/(III-SU)

FAILURE DATA

PB	YES, Through-wall leak
	NO, No through-wall leak
ROT	Inertia arm off-vertical rotation at end of test, deg., NA if not available
OVAL	Failure location proximity (max diameter)/(min diameter), NA if not available
CIRC	Failure location proximity average diameter pre-test/post-test
FAILURE LOCATION / NOTES	Information on failure

Footnote 1: Values in Table 1 are nominal values that can vary in test runs. Appendix I - B contains individual test run details.

Footnote 2: Test 36 failure location thickness not measured pre-test. Value was estimated from final thickness and assumption percent thinning was the same as measured in adjacent straight.

Table 2: Moment Data from PFDRP Component Testing

BASIC DATA								ANALYTICAL MOMENTS								TEST MOMENTS						RPK FACTORS	
A	B	C	D	E	F	G	H	I	J	K	L	M	N	O	P	Q	R	S	T	U	V	W	X
								S_P	M_{CODE}	M_{LIMIT}		M2,M5						RATIO			RATIO	F_S	F_{S2}
TEST	MTL	B_1 USED	B_2 USED	NOM T	D	NOM Z	P	B_1PD / 2000T	$(90 - S_P)$ * Z / B_2	4 / PI * ZSy	GE M_{WT}	TEST RUN	M2	M5	RATIO M2/M5	GE MM	QL MM	QL/GE MM	M_{UD}	M_{UD} NOTE	M_{UD} / MM	M_{UD} / M_{CODE}	M_{UD} / M_{LIMIT}
ELBOW TESTS:																							
1	CS	0.062	2.373	0.432	6.625	12.2	2600	1.2	457	545	2.81	8	4560	2803	1.63	569	567	1.00	na	na	na	na	na
2	CS	0.062	2.373	0.432	6.625	12.2	2600	1.2	457	545	1.94	8	4597	2570	1.79	574	na	na	na	na	na	na	na
3	SS	0.000	5.513	0.134	6.625	4.35	400	0.0	71	166	1.07	10	1006	593	1.70	153	158	1.03	162	1	1.03	2.28	na
4	CS	0.000	3.270	0.280	6.625	8.50	1000	0.0	234	379	1.07	8	2732	1675	1.63	na	403	na	429	1	1.06	1.83	na
5	CS	0.000	3.270	0.280	6.625	8.50	1700	0.0	234	379	1.07	8	3199	1741	1.84	478	470	0.98	534	1	1.14	2.28	na
6	SS	0.000	3.270	0.280	6.625	8.50	1700	0.0	234	325	1.07	8	2992	1638	1.83	na	470	na	520	1	1.11	2.22	na
7	SS	0.000	3.270	0.280	6.625	8.50	1000	0.0	234	325	1.07	8	3548	1953	1.82	na	406	na	523	1	1.29	2.23	na
8	SS	0.000	3.270	0.280	6.625	8.50	0	0.0	234	325	1.07	8	3726	2004	1.86	na	396	na	508	1	1.28	2.17	na
13	CS	0.000	4.290	0.280	6.625	8.50	1000	0.0	178	379	1.54	10	2487	1345	1.85	400	418	1.05	379	1	0.91	2.13	na
19	SS	0.000	3.270	0.280	6.625	8.50	2500	0.0	234	325	1.07	8	3439	1826	1.88	450	498	1.11	633	1	1.27	2.71	na
30	SS	0.000	5.510	0.134	6.625	4.35	400	0.0	71	166	8.46	4	486	279	1.74	133	133	1.00	115	1	0.87	1.62	na
31	SS	0.000	5.513	0.134	6.625	4.35	400	0.0	71	166	1.07	11	1098	583	1.88	150	na	na	192	3	1.28	2.71	na
35	CS	0.000	3.270	0.280	6.625	8.50	1700	0.0	234	379	20.11	9	na	1677	na	na	410	na	470	2	1.15	2.01	na
37	SS	0.000	5.513	0.134	6.625	4.35	0	0.0	71	166	8.46	5	510	294	1.73	57	64	1.12	72	1	1.13	1.01	na
41	CS	0.000	3.270	0.280	6.625	8.50	1700	0.0	234	379	1.07	12	3972	2023	1.96	398	na	na	510	3	1.28	2.18	na
OTHERS:																							
9	SS	0.500	1.000	0.280	6.625	8.50	1700	10.1	679	325	7.42	6	5011	2808	1.78	na	584	na	629	1	1.08	0.93	1.94
10	SS	0.500	1.000	0.280	6.625	8.50	1000	5.9	714	325	7.42	7	5097	2851	1.79	na	560	na	641	2	1.15	0.90	1.98
11(P)	SS	0.500	1.000	0.134	6.625	4.35	400	4.9	370	166	7.42	6	1171	777	1.51	na	138	na	369	1	2.67	1.00	2.22
12	SS	0.500	1.000	0.280	6.625	8.50	1700	10.1	679	325	7.42	6	6262	3412	1.84	na	634	na	726	2	1.15	1.07	2.24
14	CS	0.500	1.000	0.280	6.625	8.50	1700	10.1	679	379	7.42	6	4223	2373	1.78	na	600	na	617	1	1.03	0.91	1.63
15	SS	0.500	1.000	0.237	4.500	3.21	1700	8.1	263	123	6.55	9	2528	1376	1.84	178	220	1.24	333	1	1.51	1.26	2.71
16	CS	0.500	1.000	0.237	4.500	3.21	1700	8.1	263	143	6.55	6	6352	3244	1.96	260	278	1.07	385	1	1.38	1.46	2.69
34	CS	0.500	1.000	0.280	6.625	8.50	1000	5.9	714	379	2.21	12	6210	3562	1.74	605	na	na	775	3	1.28	1.08	2.05
36(P)	CS	0.500	1.000	0.280	6.625	8.50	1700	10.1	679	379	7.42	8	3043	2053	1.48	512	634	1.24	700	1	1.10	1.03	1.85
38	SS	0.500	2.020	0.280	6.625	8.50	1700	10.1	336	325	7.42	6	4989	2756	1.81	na	567	na	649	2	1.15	1.93	2.00
39	SS	0.500	2.020	0.280	6.625	8.50	0	0.0	379	325	7.42	4	5255	2837	1.85	463	549	1.19	629	2	1.15	1.66	1.94
40	SS	0.500	1.000	0.237	4.500	3.21	0	0.0	289	123	6.55	5	4320	2524	1.71	202	na	na	314	1	1.56	1.09	2.56

M_{UD} Notes (See Appendix I - C for CIT moment plots and spreadsheet of M_{UD} calculations)

Note 1 M_{UD} = CIT PM_{CIT} times QL MM_{MAX} / MM_{CIT}

Note 2 M_{UD} = C2 times QL MM_{MAX}, based on trend average of the 15 available comparative test runs (Test 11 excluded). C2 = 1.15

Note 3 M_{UD} = C3 times GE MM_{MAX}, based on trend average of the 12 available comparative test runs (Test 11 excluded) C3 = 1.28

Notes to Table 2

	COLUMN	
TEST	A	PFDRP test identification number. Special cases: (E) stress indices for elbow used. (W) stress indices for weld used.
MTL	B	Carbon steel (CS) or stainless steel (SS) test article.
B_1 USED	C	Except as noted, used ASME Code NB-3650 based B_1 value for pipe product that failed, calculated using nominal dimensions. Elbow B_1 index was used for Test 31 even though it failed on the straight pipe side of the weld.
B_2 USED	D	Except as noted, ASME Code NB-3650 based B_2 value for pipe product that failed, calculated using nominal dimensions. Elbow B_2 index used for Test 31. B2 = 1.0 used for Tests 11 and 36 even though failed on tee side of weld.
NOM T	E	Nominal wall thickness, inch.
D	F	Nominal outside diameter, inch.
NOM Z	G	Section Modulus, Z, based on nominal dimensions, in^3.
P	H	Internal pressure, psig (see Table 1 Footnote 1).
S_P	I	Code pressure stress computed as indicated, ksi.
M_{CODE}	J	Code allowable moment computed as indicated, in-kip.
M_{LIMIT}	K	Straight pipe theoretical limit moment computed as indicated, in-kip.
GE M_{WT}	L	Reference 3-7 Table 7-2 listed weight moment, in-kip.
TEST RUN	M	Test run with highest reported M2 and M5 values in Reference 3-7 Appendix B.
M2	N	Reference 3-7 Appendix B highest level test run's sled accelerometer based 15% peak broadened, 2% damped, linearly elastic response spectrum (LERS) moment at failure location, in-kips. Test 14 M2 at failure location was extrapolated from tee moment.
M5	O	Reference 3-7 Appendix B highest level test run's sled accelerometer based 15% peak broadened, 5% damped, linearly elastic response spectrum (LERS) moment at failure location, in-kips. Test 14 M5 at failure location was extrapolated from tee moment.
RATIO M2/M5	P	Column N divided by Column O.
GE MM	Q	Reference 3-7 Appendix B reported measured moment for Column M test run, in-kips.
QL MM	R	ANCO QL test report measured moment maximum single cycle moment range divided by 2 for Column M test run, in-kips.
QL/GE MM	S	Column R divided by Column Q.

M_{UD}	T	Appendix I-C based ultimate dynamic moment amplitude demonstrated for all test runs. Based on Appendix I-C CIT test moments and scaled to maximum level test run. Scaling used trend averages per spreadsheet in Appendix I-C, in-kips.
M_{UD} NOTE	U	Basis for M_{UD} calculation in Appendix I-C.
M_{UD}/MM	V	Column T divided by Column R (1st choice) or Column Q (2nd choice).
M_{UD}/M_{CODE}	W	Kennedy Appendix III-B "strength factor", F_S, Column T divided by Column J.
M_{UD}/M_{LIMIT}	X	Kennedy Appendix III-B alternate "strength factor", F_{S2}, Column T divided by Column K.

Table 3: ARC-TCG Seismic Margin Evaluations for PFDRP Component Tests

PFDR COMPONENT TEST NUMBER	3 S_m CRITERION			4.5 S_m CRITERION	
	A	B	C	D	E
	MEASURED LOAD MARGIN	CYCLE CORRECTED LOAD MARGIN	EARTH-QUAKES TO FAIL	CYCLE CORRECTED LOAD MARGIN	EARTH-QUAKES TO FAIL
1	15	35.0	1225	14.0	197
2	15	46.1	2129	18.5	341
3	21	39.2	1537	15.7	246
4	18	28.4	807	11.4	129
5	21	39.2	1537	15.7	246
6	19	35.5	1258	14.2	201
7	23	48.7	2371	19.5	379
8	24	53.6	2869	21.4	459
9	21	25.7	659	10.3	105
10	21	33.1	1098	13.3	176
11	16	11.3	127	4.5	20
12	27	42.6	1815	17.0	290
13	22	34.7	1205	13.9	193
14	18	22.0	484	8.8	77
15	13	29.0	842	11.6	135
16	30	21.2	448	8.5	72
17	20	34.6	1195	13.8	191
18	20	10.9	120	4.4	19
19	22	38.0	1446	15.2	231
20	16	22.0	484	8.8	78
21	19	12.0	144	4.8	23
22	19	13.4	180	5.4	29
30	10	17.3	299	6.9	48
31	23	42.9	1844	17.2	295
34	12	24.0	574	9.6	92
35	18	40.2	1614	16.1	258
36	15	10.6	112	4.2	18
37	10	14.1	199	5.6	32
38	20	37.9	1434	15.1	229
39	21	41.9	1757	16.8	281
40	22	31.1	964	12.4	154
41	25	35.3	1245	14.1	199

Table 4: Minimum Strength, 650F, Hard Side REMS Test 36 MRF, Upper-Bound (Fatigue Only) Ratchet-Fatigue Margins

HIGH LEVEL TEST RUN INERTIA STRESS W/ THK ADJ							EVENT CORRECTION			TEST MARGIN			MIN SY,SU ADJ				TEMP ADJ		FREQ ADJ		
A	B	C	D	E	F	G	H	I	J	K	L	M	N	O	P	Q	R	S	T	U	V
TEST	B_2 USED	GE BR M5	R = TEST S(Fn)/Sa	TEST BASED $M5_U$	Z ACT T	B_2M5_U /Z ACT T	GE # OF EVNT	ROT # OF EVNT	EVNT CORR BM/Z	EQ 9 P,WT ACT T	P + WT ADJ 4.5 Sm	ACT T TEST MRGN	III/T Sy	CS T-60 Su	Sy Su ADJ	MIN III TEST MRGN	ADJ 650F /70F	650F TEST MRGN	MEAS Rw	REMS MRF@ 0.5	DYN MRGN
ELBOW TESTS:																					
1	INSUFFICIENT DATA																				
2	INSUFFICIENT DATA																				
3	5.51	593	0.85	505	5.01	556	3.5	2.13	811	1.18	88.8	9.13	0.88		0.88	8.06	0.76	6.12	0.975	0.40	2.44
4	3.27	1675	0.80	1340	9.20	476	2.5	2.70	783	0.38	89.6	8.73	0.73	11	0.76	6.62	0.82	5.43	0.971	0.40	2.18
5	3.27	1741	0.62	1071	9.02	388	3.5	2.40	602	0.39	89.6	6.71	0.73	11	0.76	5.09	0.82	4.17	0.919	0.46	1.91
6	3.27	1638	0.54	885	9.30	311	3.5	3.40	573	0.38	89.6	6.40	0.56		0.70	4.48	0.76	3.40	0.875	0.52	1.76
7	3.27	1953	0.82	1601	9.38	558	4.5	4.80	1223	0.37	89.6	13.65	0.56		0.70	9.55	0.76	7.26	0.929	0.45	3.23
8	3.27	2004	0.67	1343	9.35	469	5.0	5.10	1060	0.37	89.6	11.83	0.56		0.70	8.28	0.76	6.29	0.917	0.46	2.89
13	4.29	1345	0.77	1033	11.97	370	2.5	3.69	711	0.55	89.4	7.95	0.74	19	0.80	6.33	0.82	5.19	0.957	0.42	2.16
19	3.27	1826	0.99	1800	9.61	613	3.0	2.34	937	0.36	89.6	10.45	0.56		0.70	9.22	0.76	7.01	0.985	0.39	2.73
30	5.51	279	1.00	279	4.68	328	3.0	3.59	622	9.96	80.0	7.78	0.88		0.88	6.86	0.76	5.21	1.007	0.38	1.98
31	COMPLEX MIX SINESWEEPS AND MUTI-FREQUENCY HIGH LEVEL RUNS																				
35	3.27	1677	0.71	1198	9.12	429	5.0	4.81	942	7.21	82.8	11.37	0.83	19	0.89	10.14	0.82	8.32	0.932	0.44	3.67
37	LARGE ROTATION STOPPED TESTING BEFORE R-F FAILURE																				
41	INSUFFICIENT DATA																				
OTHERS:																					
9	1.00	2808	0.88	2462	6.20	300	1.5	1.84	407	11.37	78.6	5.18	0.59		0.70	3.63	0.76	2.76	0.943	0.43	1.18
10	1.00	2851	0.79	2246	8.55	263	2.5	1.74	347	6.74	83.3	4.16	0.59		0.70	2.91	0.76	2.21	0.931	0.44	0.98
11(T)	3.35	766	0.49	378	4.50	282	0.5	0.93	272	10.29	79.7	3.41	0.76		0.76	2.58	0.76	1.96	0.862	0.54	1.05
11(W)	1.00	777	0.49	384	4.50	85	0.5	0.93	82	6.42	83.6	0.98	0.76		0.76	0.74	0.76	0.57	0.862	0.54	0.30
12	1.00	3412	0.72	2444	8.55	286	2.5	2.49	451	10.85	79.1	5.70	0.59		0.70	3.99	0.76	3.03	0.905	0.47	1.44
14	1.00	2373	0.77	1837	8.65	212	1.5	1.69	276	10.70	79.3	3.48	0.65	13	0.73	2.55	0.82	2.09	0.917	0.46	0.96
15	1.00	1376	0.66	904	3.11	291	5.0	5.69	693	10.49	79.5	8.72	0.81		0.81	7.07	0.76	5.37	0.903	0.48	2.56
16	1.00	3244	0.65	2097	3.18	659	0.5	0.75	571	10.23	79.8	7.16	0.71	12	0.74	5.28	0.82	4.33	0.905	0.47	2.05
34	COMPLEX MIX SINESWEEPS AND MUTI-FREQUENCY HIGH LEVEL RUNS																				
36(T)	2.52	GE UNBR M5:		1058	8.84	302	0.5	1.37	353	11.73	78.3	4.51	0.77	12	0.80	3.62	0.82	2.97	0.779	0.73	$\boxed{2.16}$
36(W)	1.00	GE UNBR M5:		1058	8.84	120	0.5	1.37	140	10.45	79.6	1.76	0.77	12	0.80	1.41	0.82	1.16	0.779	0.73	0.84
38	2.02	2756	0.82	2270	10.80	425	3.6	3.17	756	8.98	81.0	9.33	0.75		0.75	6.98	0.76	5.31	0.929	0.45	2.36
39	LARGE ROTATION STOPPED TESTING BEFORE R-F FAILURE																				
40	LARGE ROTATION STOPPED TESTING BEFORE R-F FAILURE																				

Notes to Table 4

	COLUMN	
TEST	A	PFDRP test identification number. Special cases: (T) B_2 for tee (failed pipe product) used; (W) B_2 = 1.0 used.
B_2 USED	B	Except as noted, ASME Code NB-3650 based B_2 value for pipe product that failed, calculated using nominal dimensions. Elbow B_2 indices were also used for Tests 8 and 19 which did not fail.
GE BR M5	C	Reference 6-5 reported highest level test run's sled accelerometer based 15% peak broadened, 5% damped, linearly elastic response spectrum (LERS) moment at failure location, M5, in-kips. Test 14 M5 at failure location was extrapolated from tee moment.
R = TEST S(Fn)/Sa	D	Ratio of acceleration values from M5 test run's ANCO QL test report plot of sled accelerometer based unbroadened 5% damped LERS: $$R = S(F_N) / S_a$$ S_a is the acceleration at the peak of the LERS plot. $S(F_N)$ is the acceleration off the LERS plot at the ANCO QL report natural frequency of the test configuration. R values for Tests 7 and 8 had to be based on a high level test run different than the test run used for M5 values, as noted in Appendix I-B. R values for Test 6 were based on R_W versus R data trends plotted for all tests in Appendix I-B.
TEST BASED $M5_U$	E	Estimation of M5 test run unbroadened 5% damped LERS analysis moment at failure location, $M5_U$, in-kips: $$M5_U = (\text{Column C})(\text{Column D})$$ Test 36 $M5_U$ values provided in Reference 6-5 were used directly.
Z ACT T	F	Section Modulus, Z, at failure location based on pre-test section-averaged ANCO QL report proximity thickness measurements, listed in Table 1 as TEST T, in^3.
B_2M5_U/Z ACT T	G	M5 test run 5% damped unbroadened LERS inertia moment stress, ksi; $$B_2M5_U / Z = (\text{Column B})(\text{Column E}) / (\text{Column F})$$
GE # OF EVNT	H	Reference 6-6 reported number of high level test runs used in TCG margin evaluations. Provided for comparison only.

ROT # OF EVNT I

Number of fatigue damage equivalent M5 level test runs for all significant test runs based on measured maximum cycle rotation range for each test run. Appendix I-B contains individual test run maximum cycle rotation range data. The number of equivalent M5 level test runs for a fully completed test run "X" is calculated as:

$$\frac{(\text{maximum cycle rotation range Test Run X})^2}{(\text{maximum cycle rotation range Test Run M5})^2}$$

This effectively assumes that the rotation-cycle damage curve is linear in log-log space with a -0.5 slope. Adjustments for partially completed test runs based on CIT test history rotation-fatigue calibrations are provided in Appendix I-B. Tests 3, 13 and 30 required special data reductions for missing rotation data. Test 36 included two high level sinesweep test runs that were simplistically assumed equivalent in damage to seismic runs with the same maximum cycle rotation ranges.

EVNT CORR BM/Z J

TCG margin study based extrapolation of the 5% damped unbroadened LERS maximum inertia moment stress amplitude causing failure at the end of one test run computed as:

$$(\text{Column } \overset{O}{\cancel{D}})\,(\text{Column } \overset{I}{\cancel{F}})^{1/2}$$

This effectively assumes that the B_2M/Z-cycle damage curve is linear in log-log space with a slope of -0.5.

EQ 9 P,WT ACT T K

ASME Code B indices based pressure plus weight stresses at failure location using ANCO measured pre-test thicknesses, ksi. Weight moments are listed in Table 2.

P + WT ADJ 4.5 Sm L

Pressure and weight stress adjusted Code seismic inertia moment stress allowable, ksi:

$$90 - (\text{Column K})$$

ACT T TEST MARGIN M

Single PFDRP test time history TCG seismic inertia stress ratchet-fatigue margin for tested component and PFDRP test conditions:

$$(\text{Column J}) / (\text{Column L})$$

III/T Sy N

Ratio ASME Code listed yield strength / mill test yield strength for the material at the failure location. Values are listed in Table 1 as III-Sy and T-Sy, respectively.

CS T-60 Su O

Computed difference between the failure location mill test ultimate strength and 60 ksi Code minimum ultimate strength, ksi. Mill test ultimate strength values are listed in Table 1 as T-Su. Only carbon steel components use this term.

y Su ADJ	P	Adjustment factor for Code minimum material strength effects on TCG seismic inertia moment stress ratchet-fatigue margin using Column N and Column O entries. For stainless steel components, it is the ratio of minimum Code yield to mill test yield: Column N A maximum reduction of 30% is imposed. For carbon steel components, the above adjustment is modified to reflect increased fatigue resistance with reduced ultimate strength as follows: (Column N) (166 / (166 - 0.561 O) The basis for this adjustment is discussed in Section 6.2.7.
MIN III TEST MRGN	Q	Single PFDRP test time history TCG seismic inertia stress ratchet-fatigue margin for tested conditions, adjusted for ASME Code minimum strength effects: (Column M) (Column P)
ADJ 650F / 70F	R	Adjustment in ratchet-fatigue margin at $R_W = 0.5$ for 650F temperature effects on hysteretic response and fatigue strength. The bases are ratios of ASME Code stress allowables at room and elevated temperatures, and TCG temperature effect studies in Reference 6-9, discussed in Section 6.2.8. The reduction factors are: 0.76 margin reduction for stainless steel components 0.82 margin reduction for carbon steel components
650F TEST MRGN	S	Single PFDRP test time history TCG seismic inertia stress ratchet-fatigue margin, adjusted for ASME Code minimum strength effects and 650F temperature effects: (Column Q) (Column R)
MEAS Rw	T	ANCO QL test report based frequency ratio, R_W, of input loading predominant frequency divided by the test configuration natural frequency: $R_W = FI / F_N$ F_N, the test configuration natural frequency is the ANCO reported peak frequencies from spectral analyses conducted on preliminary (fphz) or elastic (fehz) level test runs. The input loading predominant frequency, FI, is the frequency at the peak of the measured sled acceleration linearly elastic response spectrum for the high level test run from which M5 was calculated. Values of FI and F_N for all test runs are provided in Appendix I-B and for the M5 test run in Table 1. Test 4 was missing F_N data and Tests 6, 7 and 8 were missing FI data. The GE Reference 6-5 reported value of F_N for Test 4 was used and the relationship: FI = (143 / test duration in seconds), based on response spectra of the targeted sled time history, was used for Test 6. FI values for other high level test runs identical to the M5 test run were used for Tests 7 and 8.

REMS MRF @ 0.5	U	The TCG REMS study results of frequency effect on Test 36 ratchet-fatigue margin in Figure 22 from Reference 4-10 were used over the range $0.5 < R_W < 1.0$ to infer margins at $R_W = 0.5$ from the margins at the tested R_W's. These "hard side" margin reduction factors (MRF's) were computed from Column T entries using: $$MRF = 0.869 / [1 + 5.04 (T - 0.74)]$$
DYN MRGN	V	Single PFDRP test time history TCG seismic inertia stress ratchet-fatigue margin, adjusted for ASME Code minimum strength effects, 650F temperature effects and frequency effects: (Column S) (Column U)

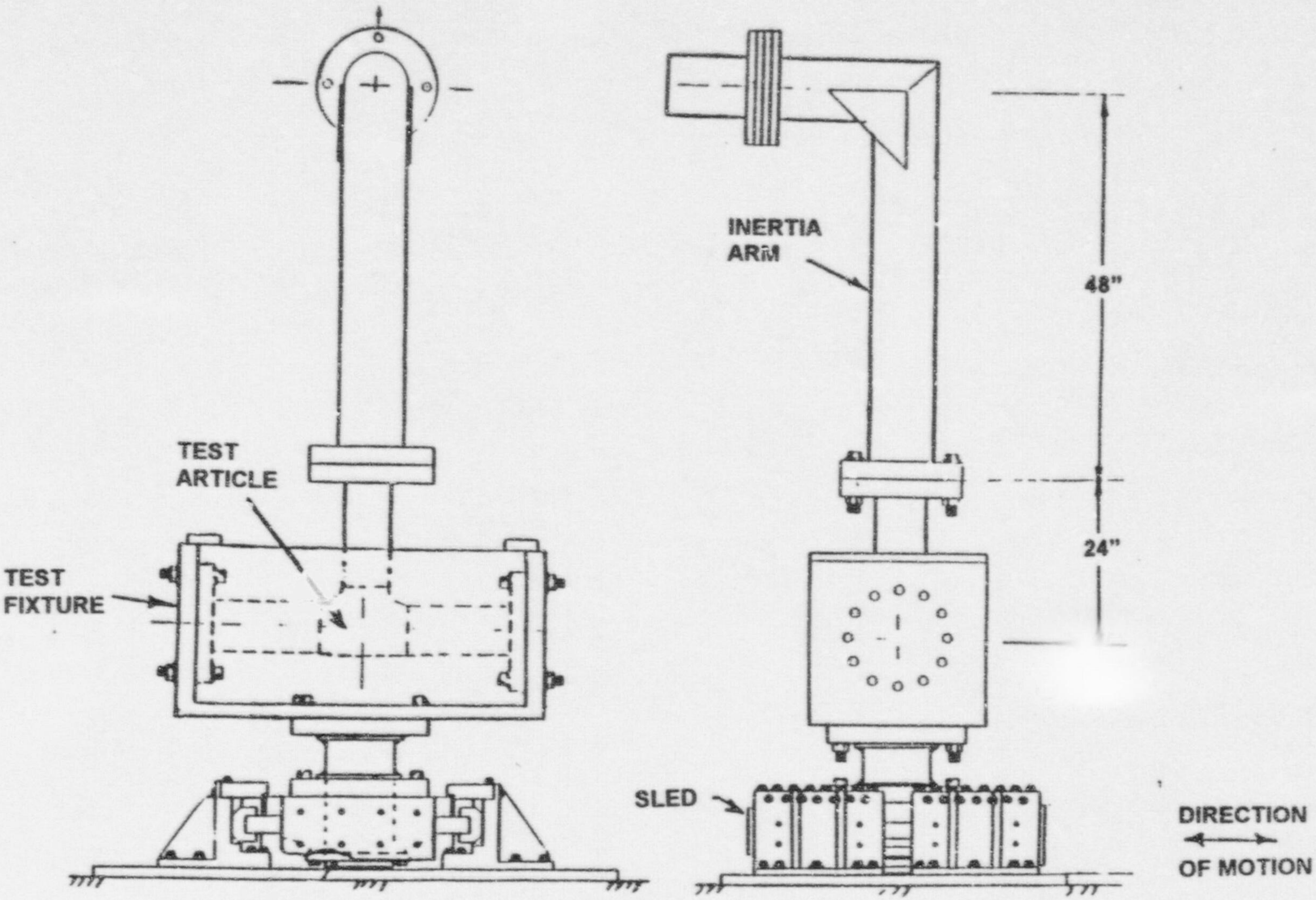

Figure 1: PFDRP Test 11 Configuration

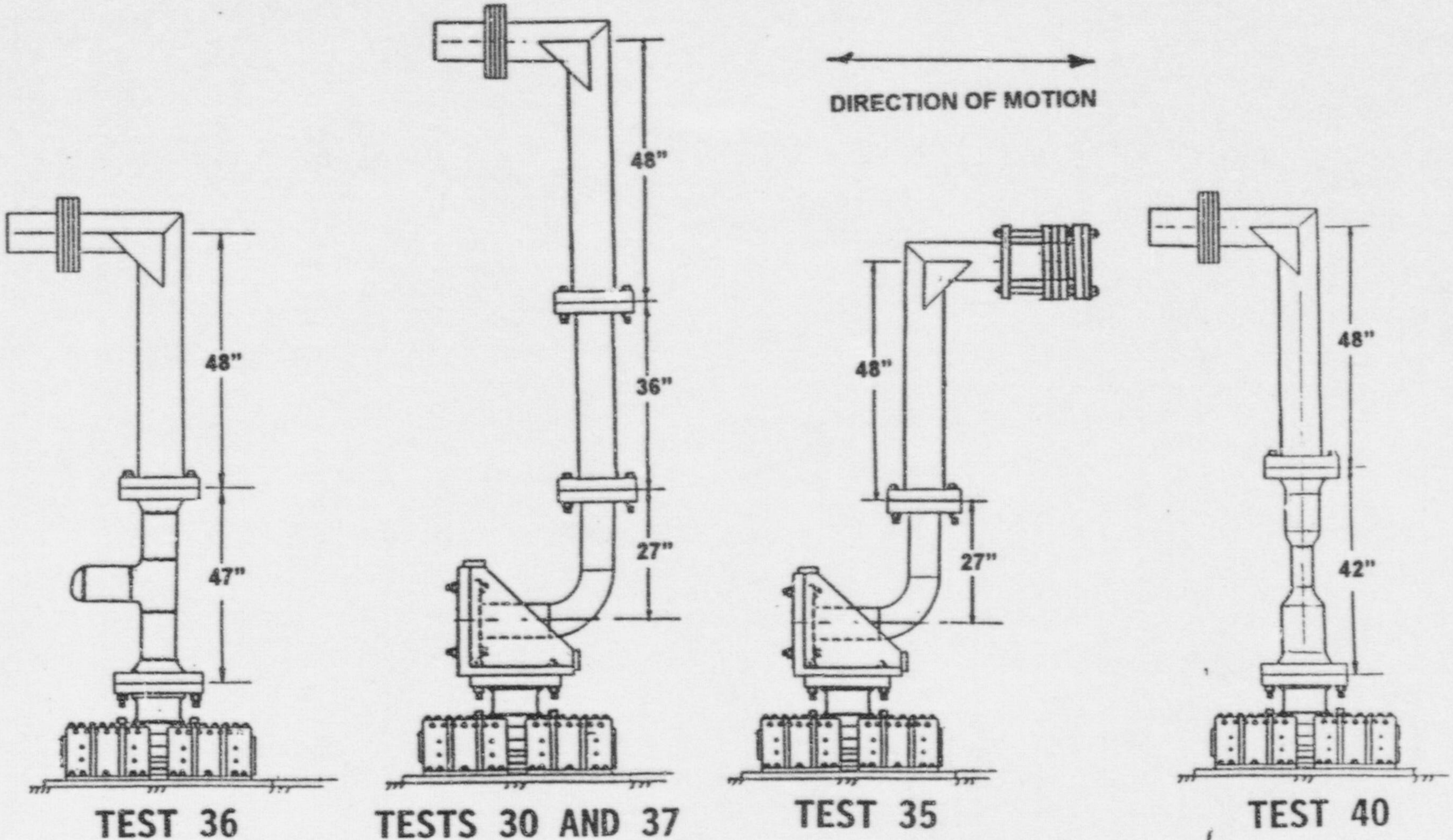

Figure 2: Other Key PFDRP Test Configurations

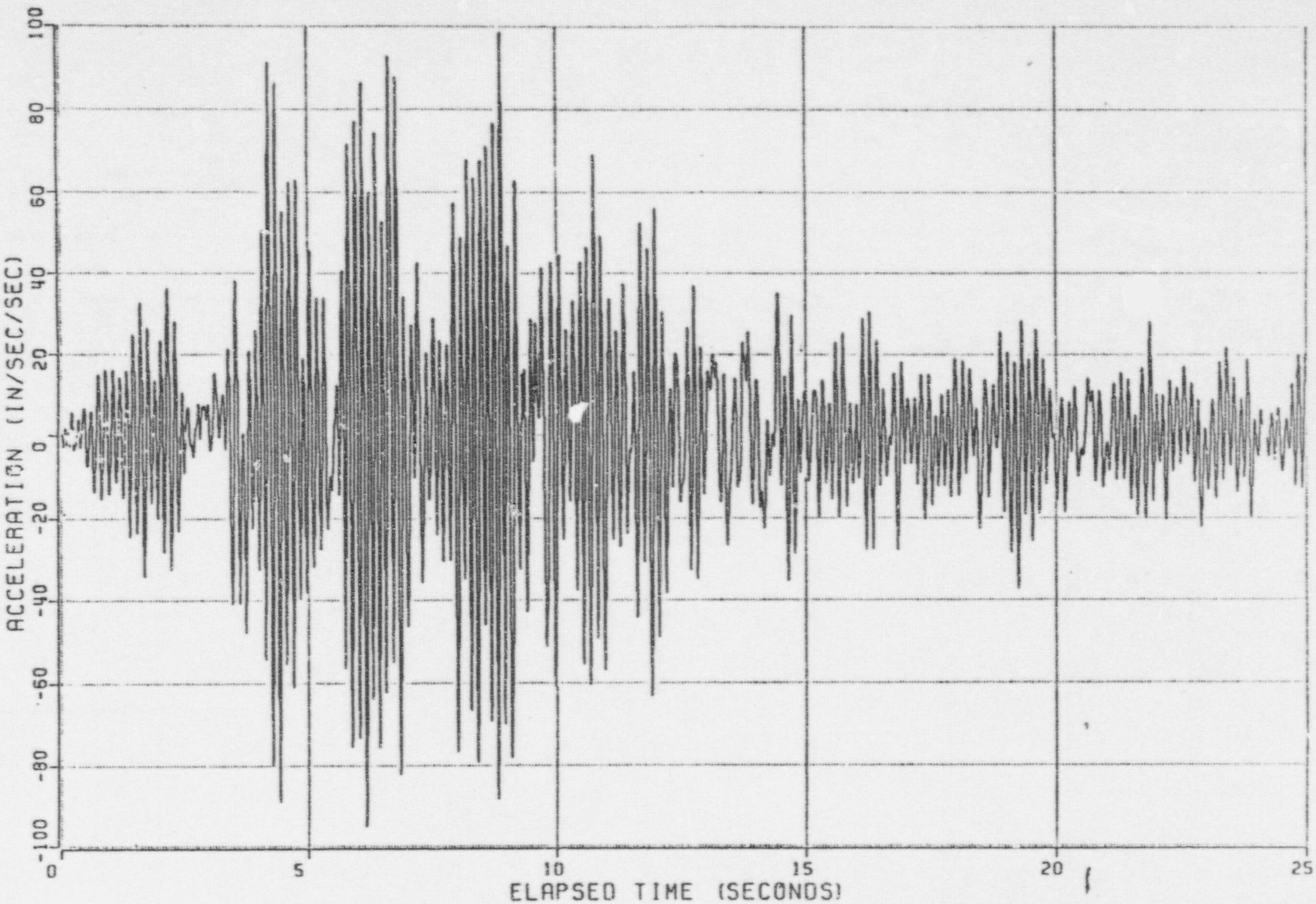

Figure 3: Typical Targeted PFDRP Sled Acceleration Time History

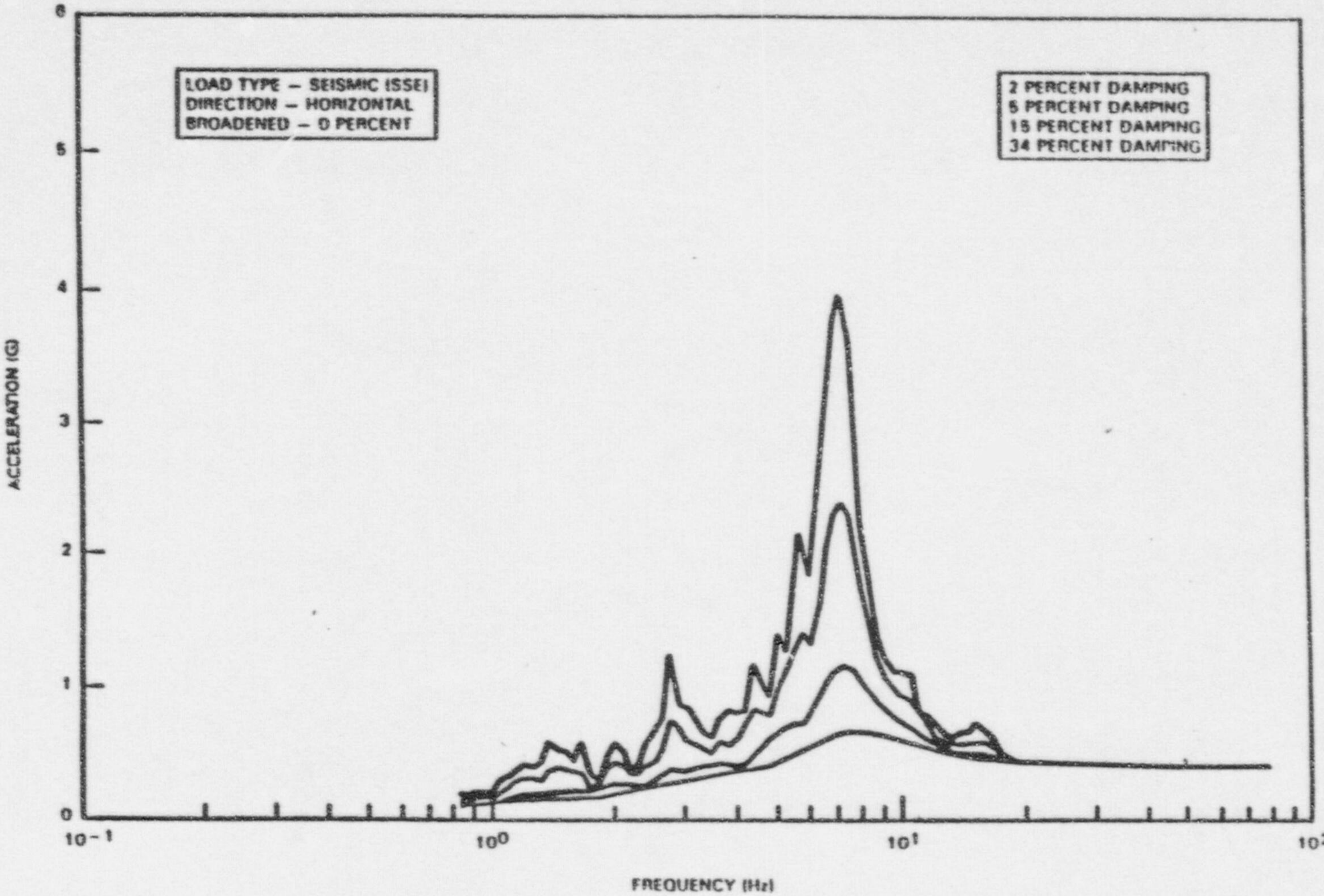

Figure 4: Response Spectra of PFDRP Targeted Sled Acceleration Time History

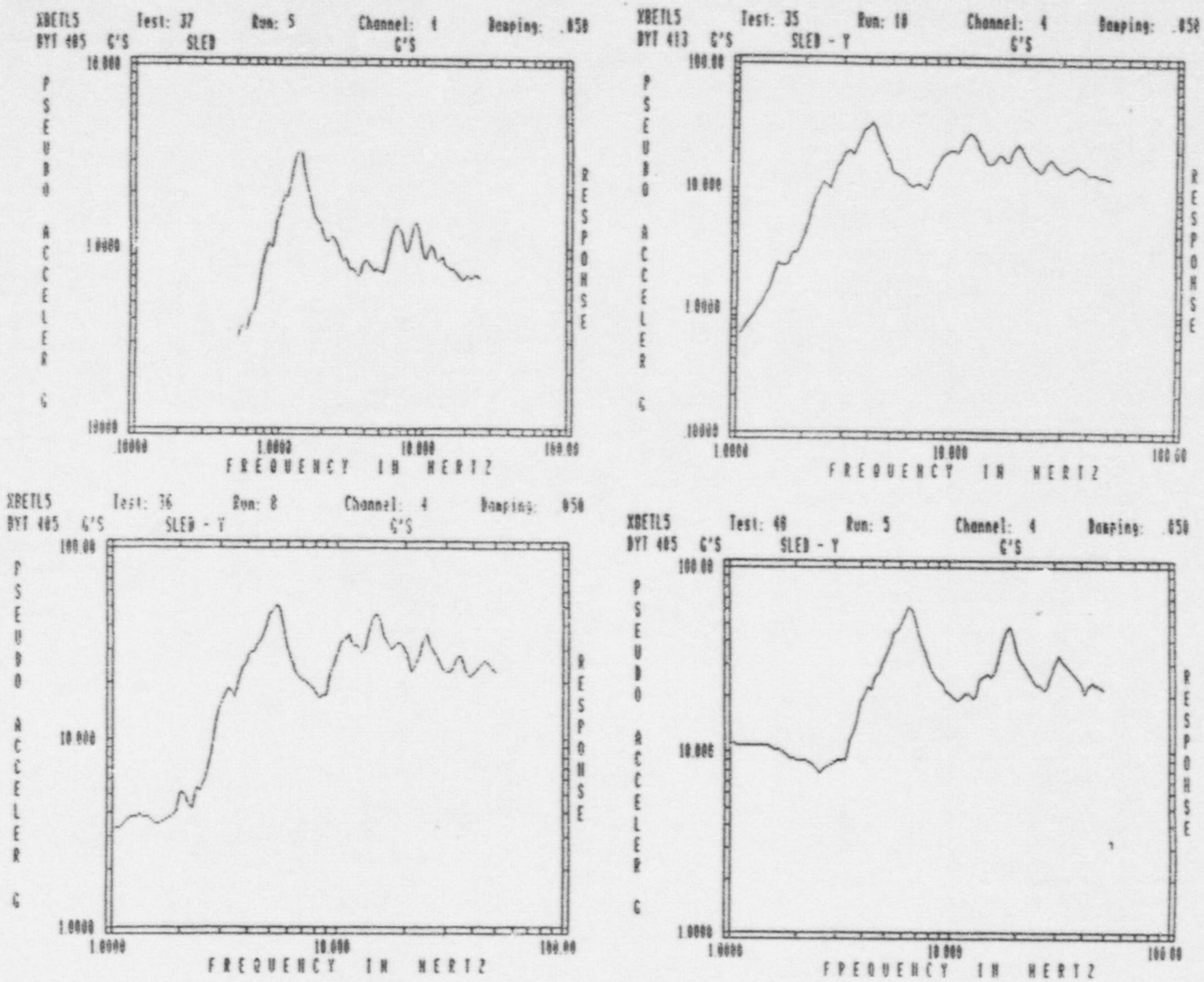

Figure 5: Response Spectra of Measured PFDRP Sled Acceleration Time History

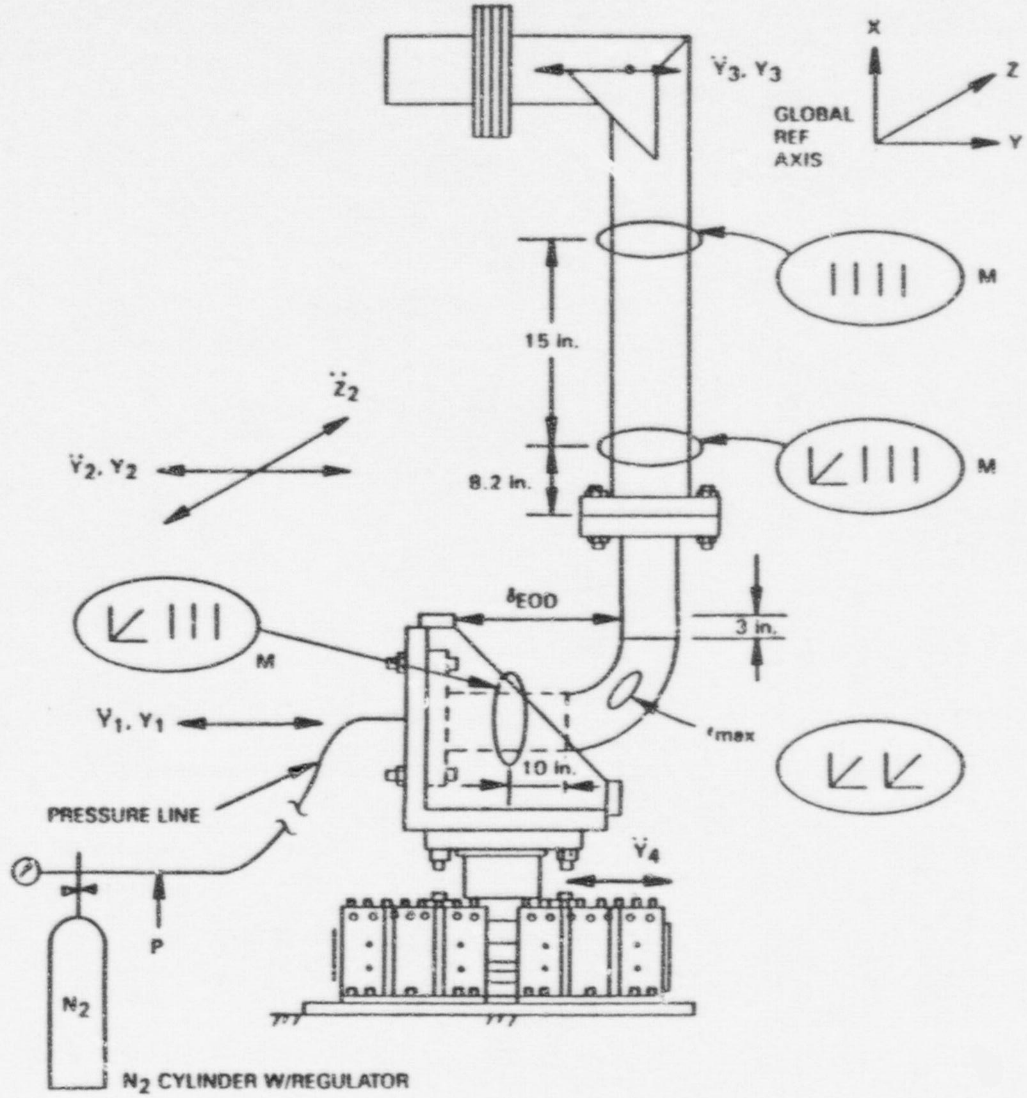

SYMBOL	STRAIN GAGE ORIENTATION
	ROSETTE ORIENTATION
	AXIAL ORIENTATION

SYMBOL	DESCRIPTION	DATA CHANNELS
$\ddot{Y}_1$	ACCELERATION	1
$\ddot{Y}_2, \ddot{Z}_2$	ACCELERATION	2
$\ddot{Y}_3$	ACCELERATION	1
$\ddot{Y}_4$	ACCELERATION	1
Y_1	HORIZONTAL DISPLACEMENT	1
Y_2	HORIZONTAL DISPLACEMENT	1
Y_3	HORIZONTAL DISPLACEMENT	1
δ_{EOD}	ELBOW OPENING/ CLOSING DISPL	1
P	PRESSURE	1
M	MOMENT FORCE RESULTANT	16
ϵ_{max}	PEAK STR	6
	TOTAL	32

Figure 6: Instrumentation Layout for PFDRP Elbow Tests

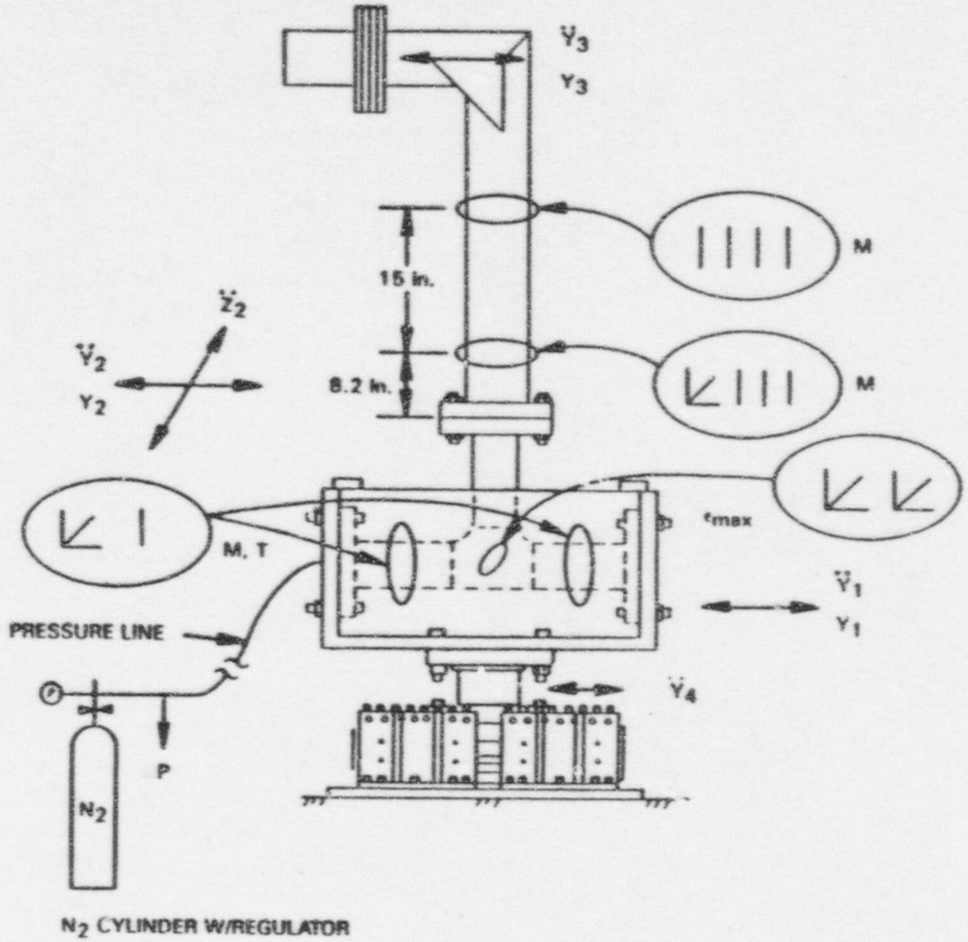

SYMBOL	STRAIN GAGE ORIENTATION
	ROSETTE ORIENTATION
|	AXIAL ORIENTATION

SYMBOL	DESCRIPTION	DATA CHANNELS
$\ddot{Y}_1$	ACCELERATION	1
$\ddot{Y}_2$, $\ddot{Z}_2$	ACCELERATION	2
$\ddot{Y}_3$	ACCELERATION	1
$\ddot{Y}_4$	ACCELERATION	1
Y_1	HORIZONTAL DISPLACEMENT	1
Y_2	HORIZONTAL DISPLACEMENT	1
Y_3	HORIZONTAL DISPLACEMENT	1
δ_{EOD}	END OPENING/ CLOSING DISPL	1
P	PRESSURE	1
M	MOMENT FORCE RESULTANT	18
ϵ_{max}	PEAK STR	6
	TOTAL	34

Figure 7: Instrumentation Layout for PFDRP Tee Tests

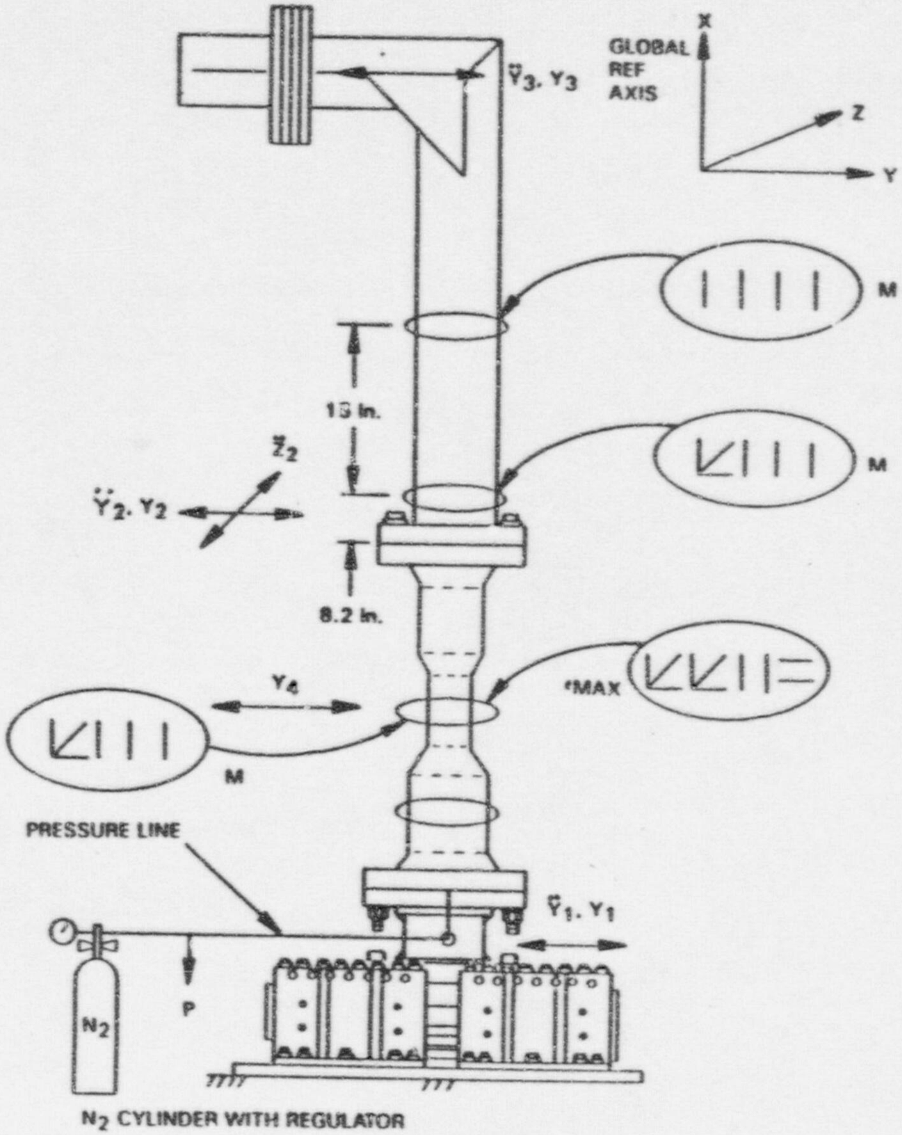

SYMBOL	STRAIN GAGE ORIENTATION
∠	ROSETTE ORIENTATION
|	AXIAL ORIENTATION

SYMBOL	DESCRIPTION	DATA CHANNELS
$\ddot{Y}_1$	ACCELERATION	1
$\ddot{Y}_2$	ACCELERATION	1
$\ddot{Y}_3$	ACCELERATION	1
$\ddot{Z}_2$	ACCELERATION	1
Y_1	HORIZONTAL DISPLACEMENT	1
Y_2	HORIZONTAL DISPLACEMENT	1
Y_3	HORIZONTAL DISPLACEMENT	1
Y_4	HORIZONTAL DISPLACEMENT	1
P	PRESSURE	1
M	MOMENT FORCE RESULTANT	16
εMAX	PEAK STR	10
	TOTAL	35

Figure 8: Instrumentation Layout for PFDRP Reducer Tests

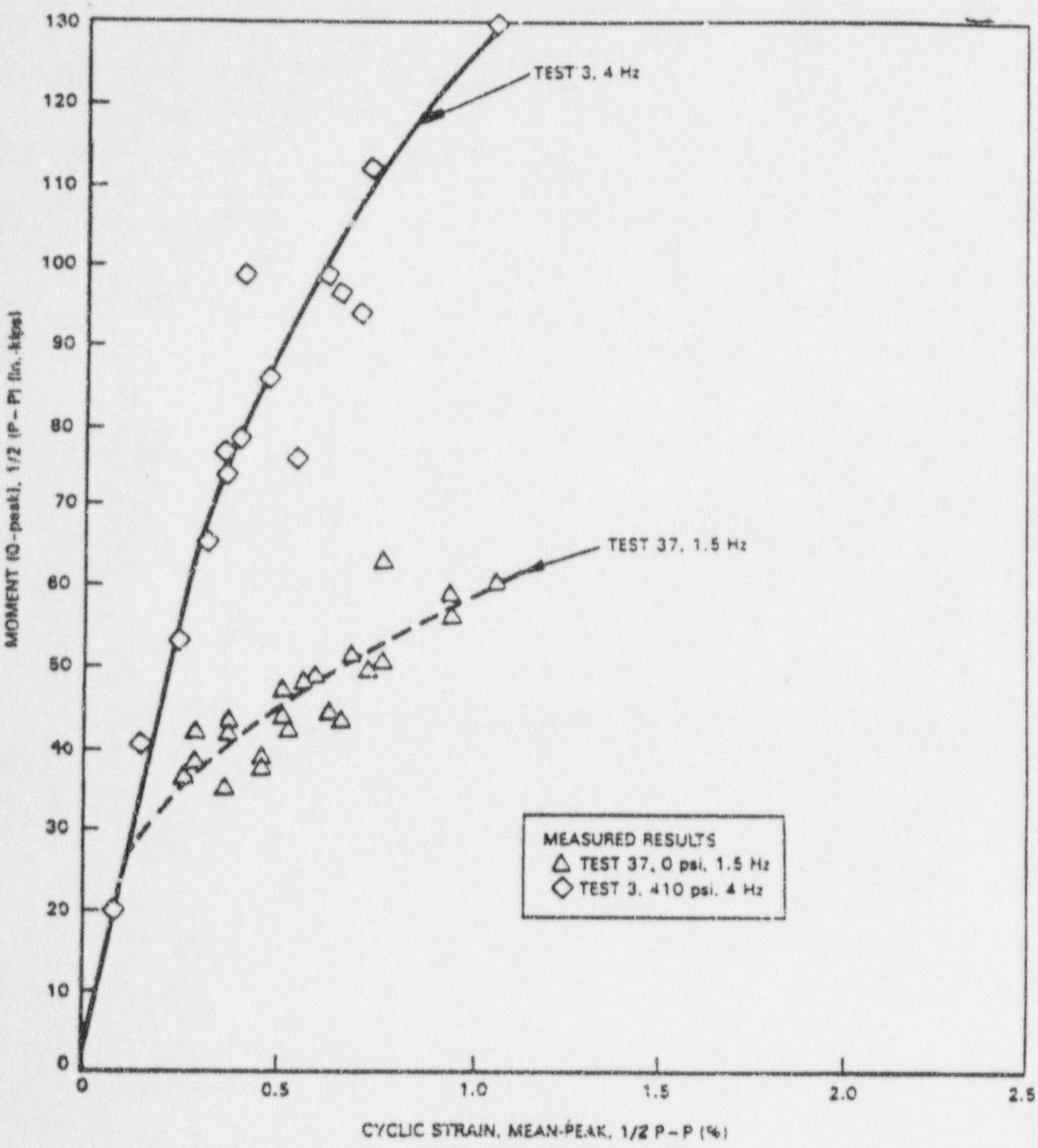

Figure 9: Comparison of Moments Versus Strain, PFDRP Elbow Tests 3 and 37

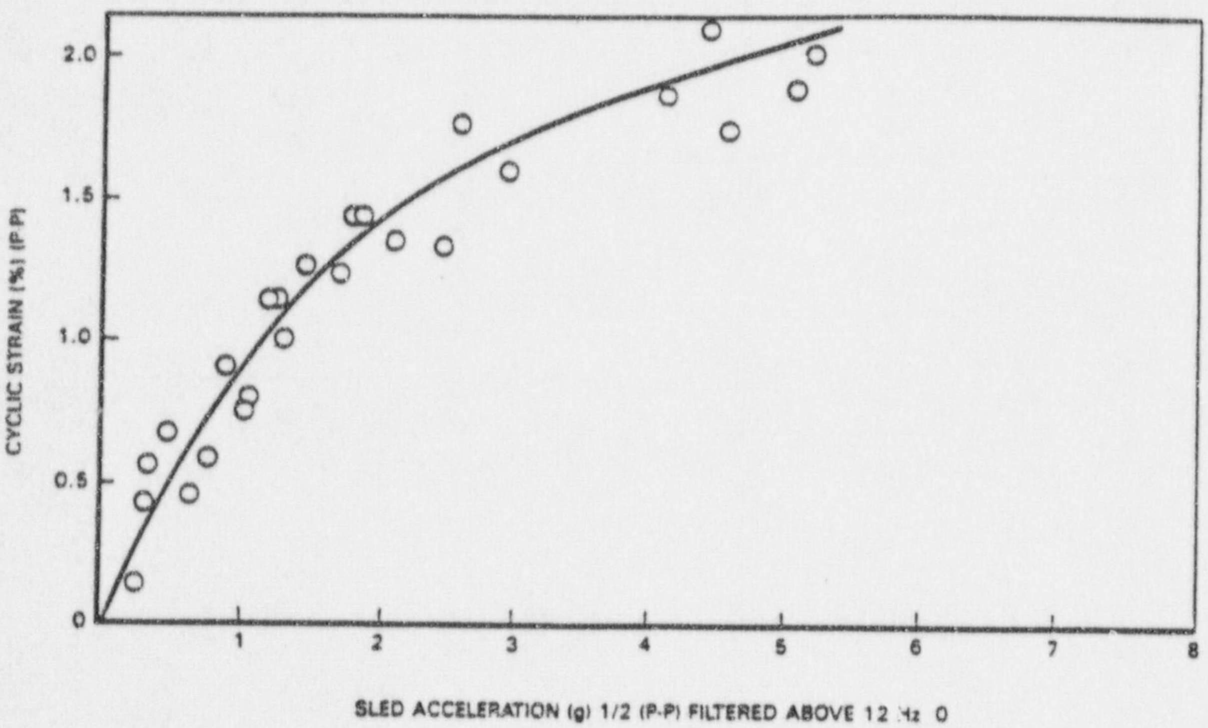

Figure 10: Strain Versus Sled Acceleration, PFDRP Elbow Test 3

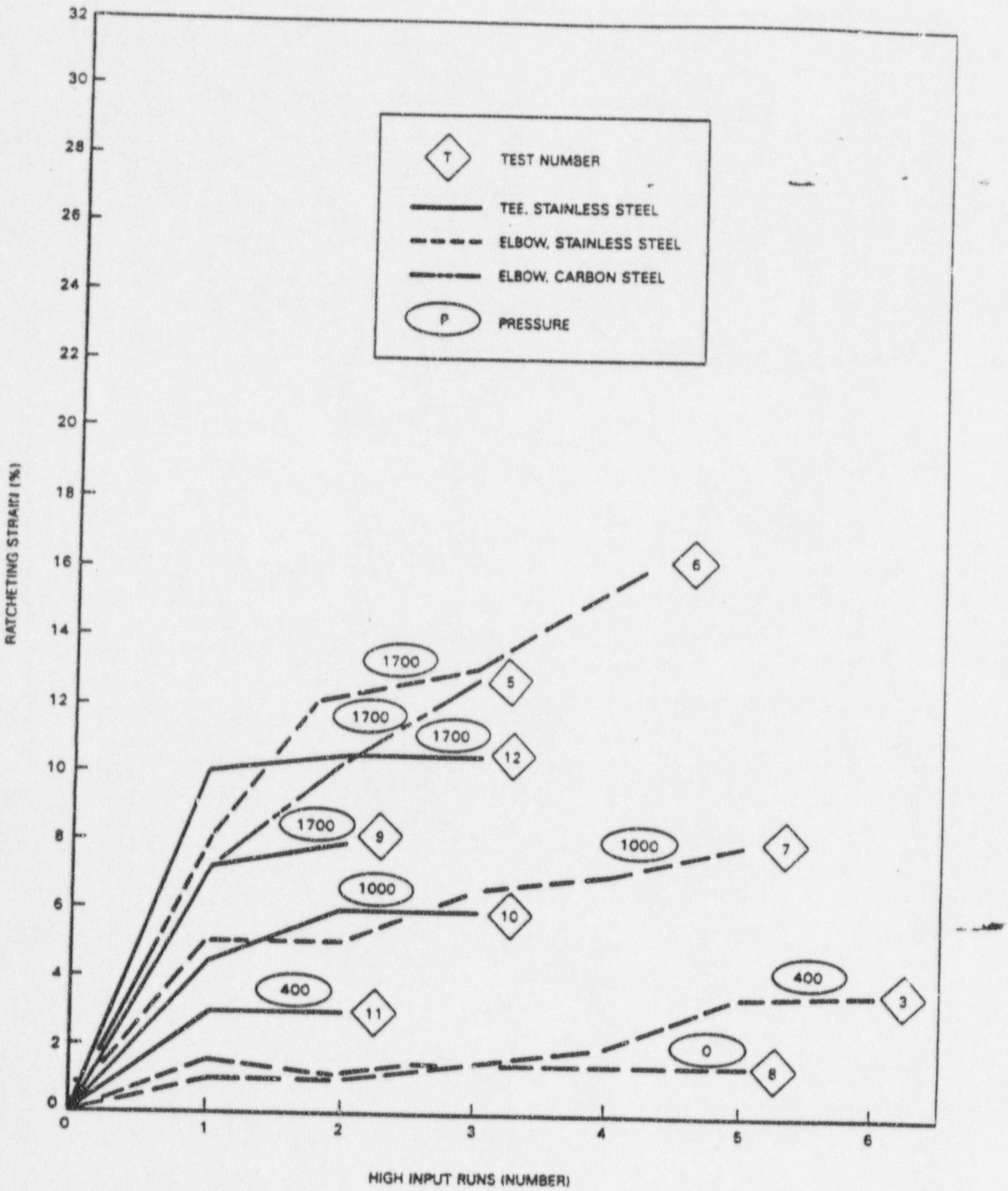

Figure 11: PFDRP Scratch Mark Based Strain Accumulation

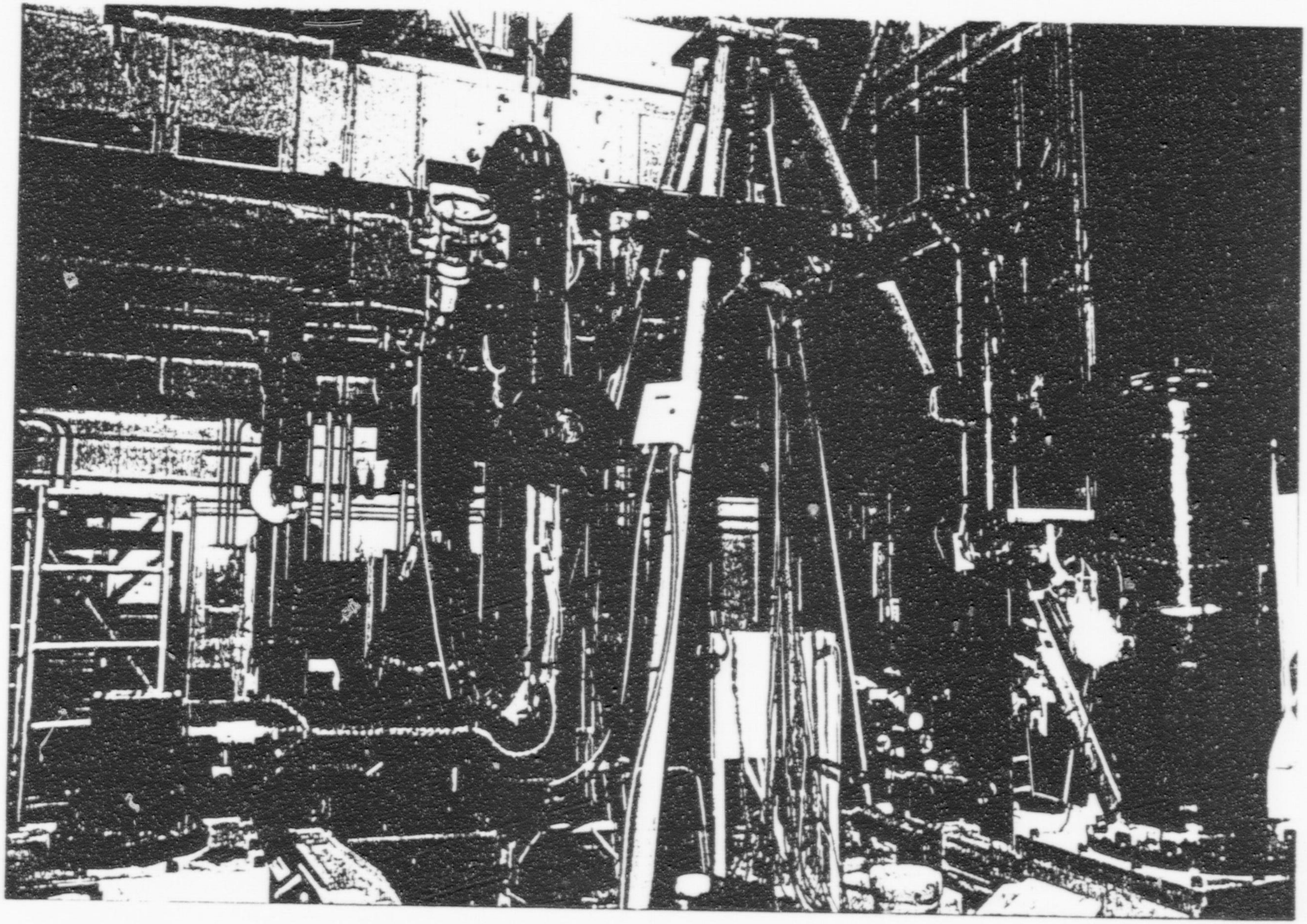

Figure 12: PFDRP Piping System 1, Photo

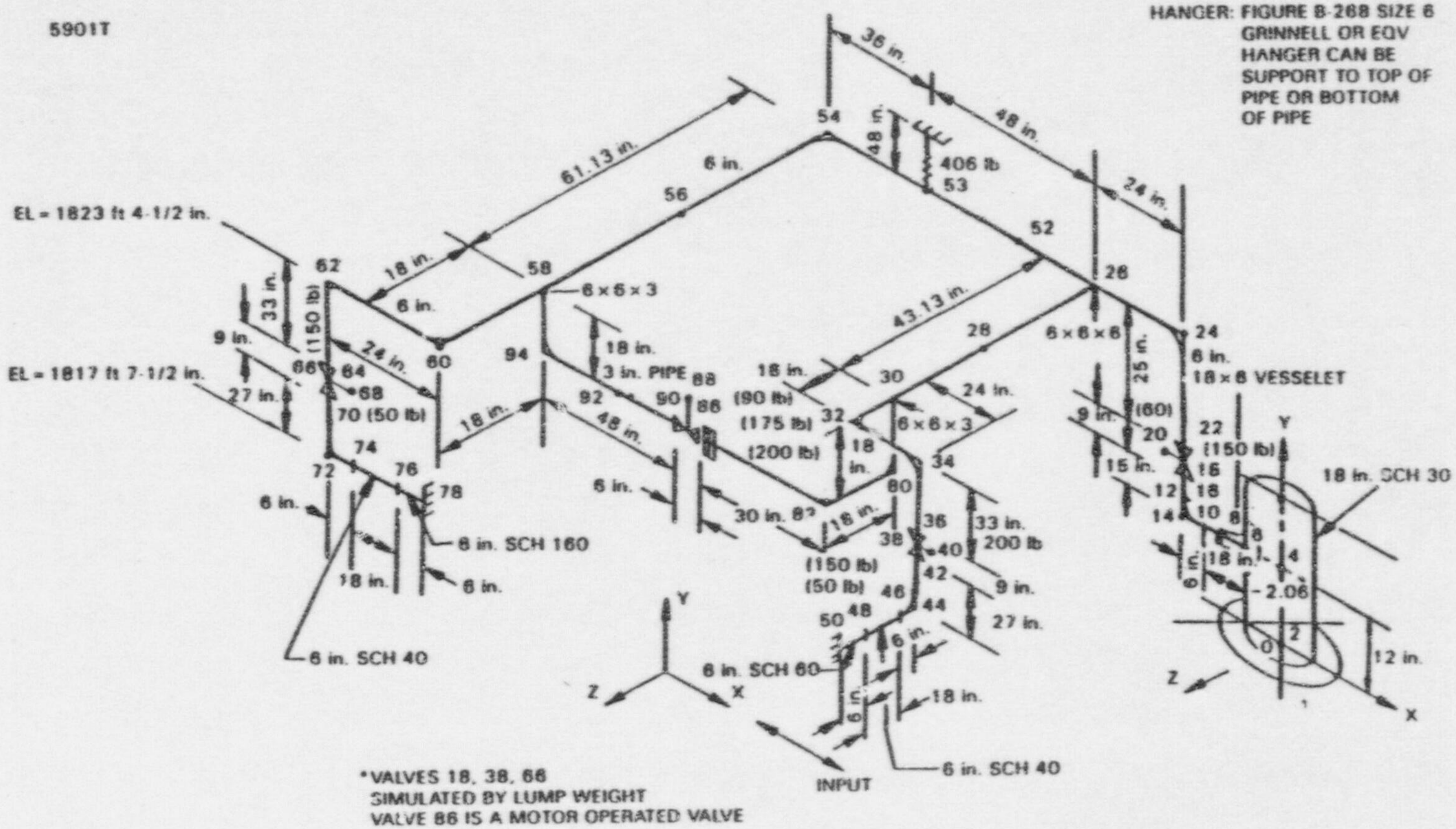

Figure 13: PFDRP Piping System 1, Isometric

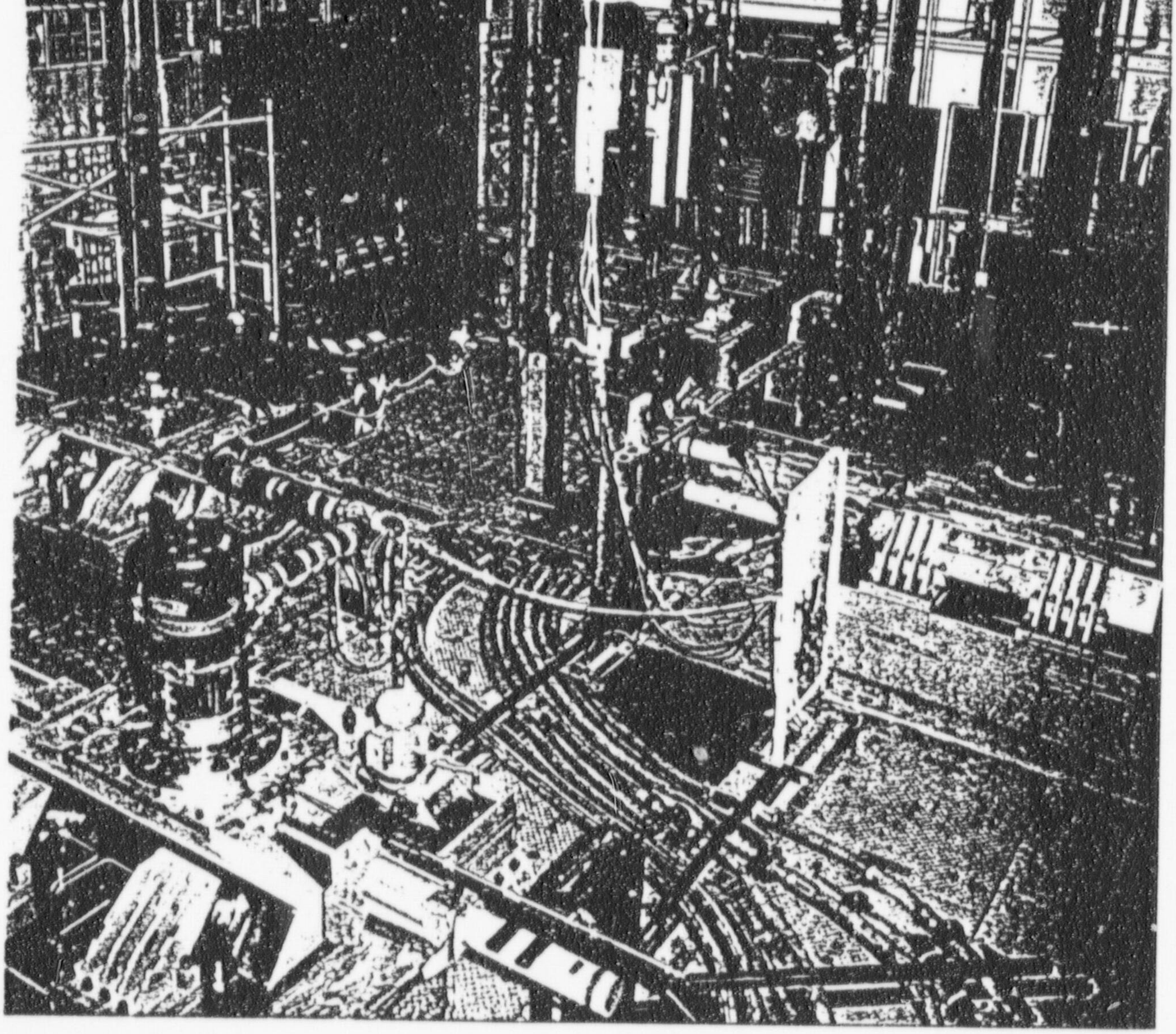

Figure 14: PFDRP Piping System 2. Photo

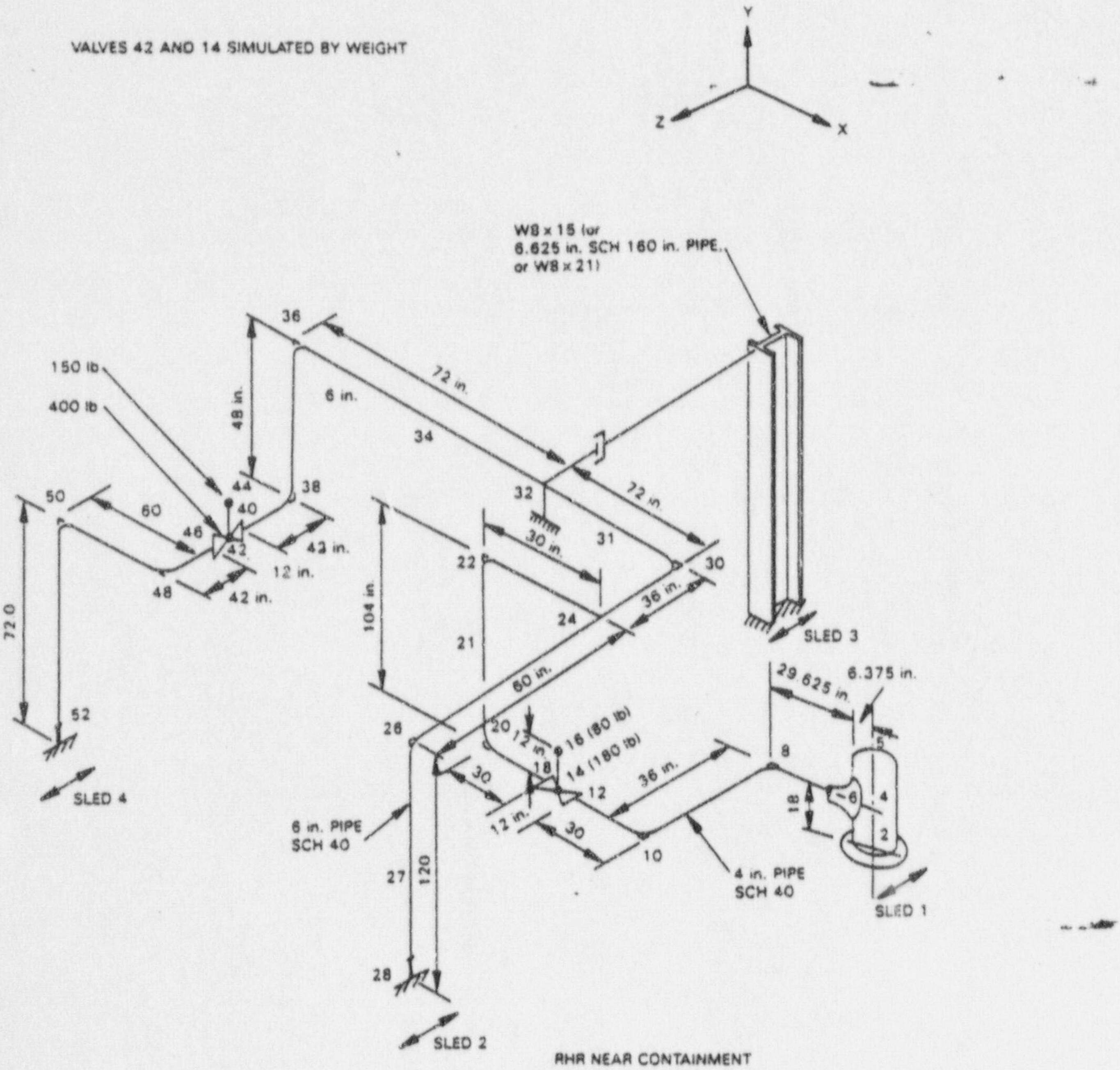

Figure 15: PFDRP Piping System 2, Isometric

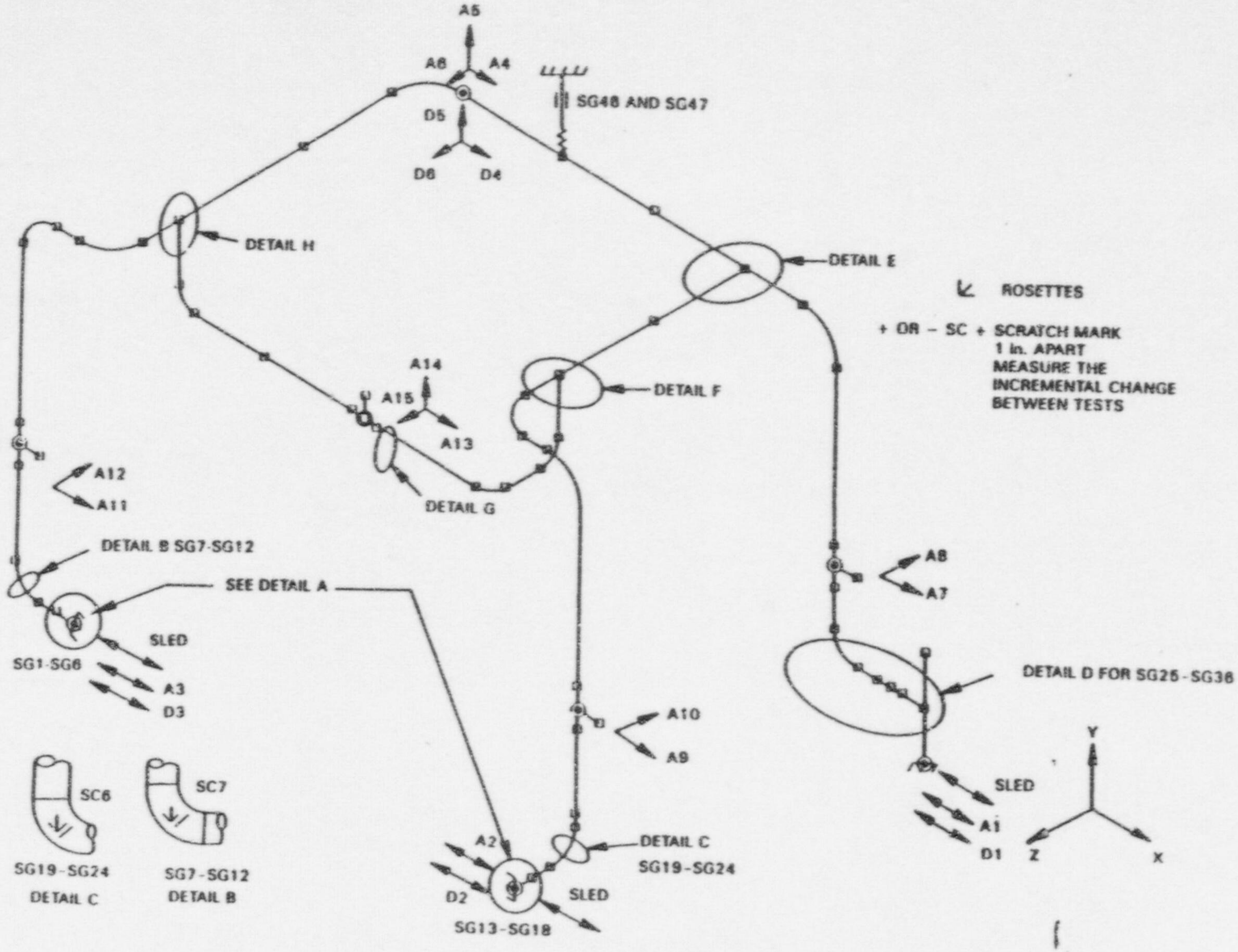

Figure 16: PFDRP System 1 Instrumentation Layout

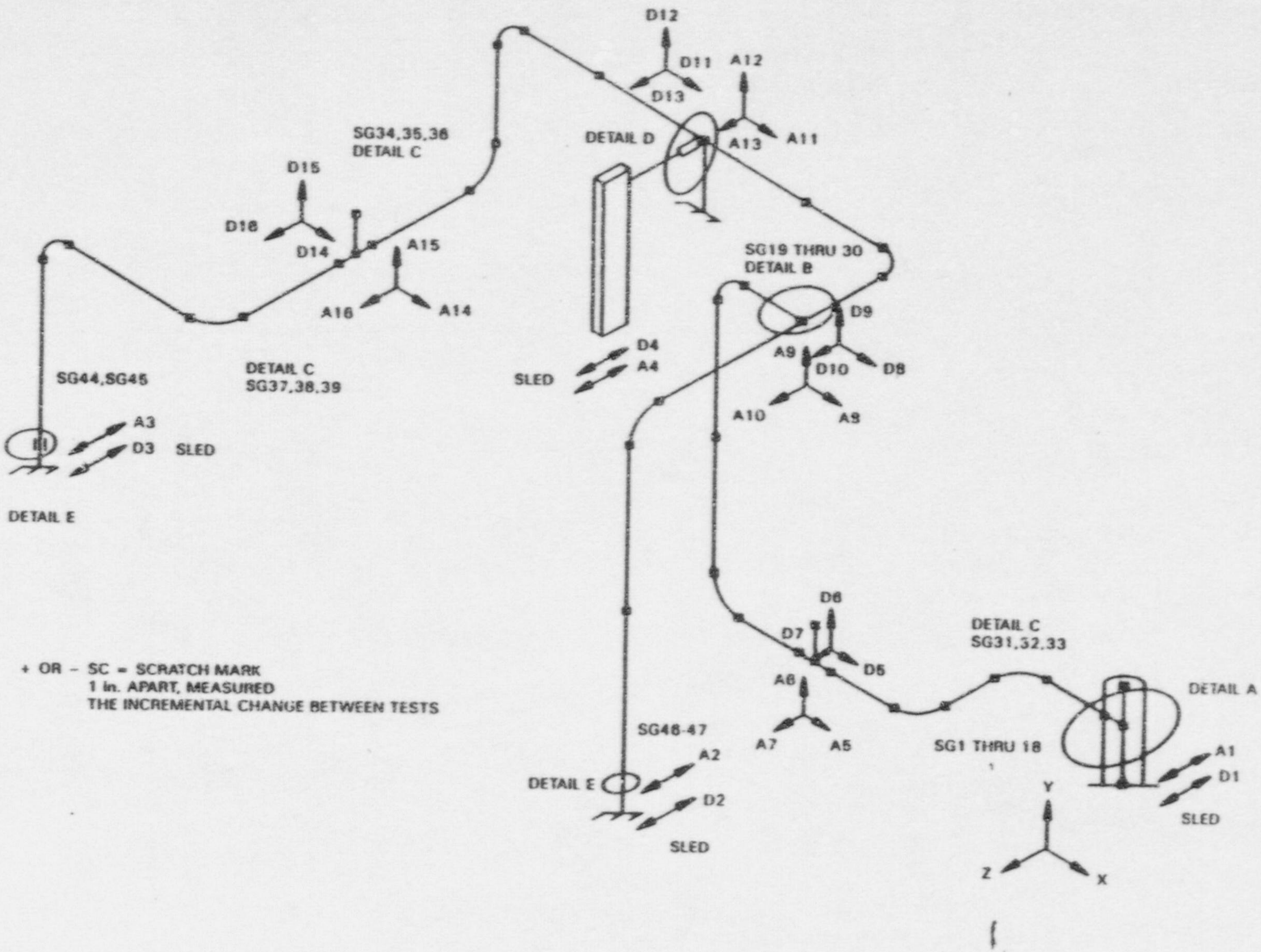

Figure 17: PFDRP System 2 Instrumentation Layout

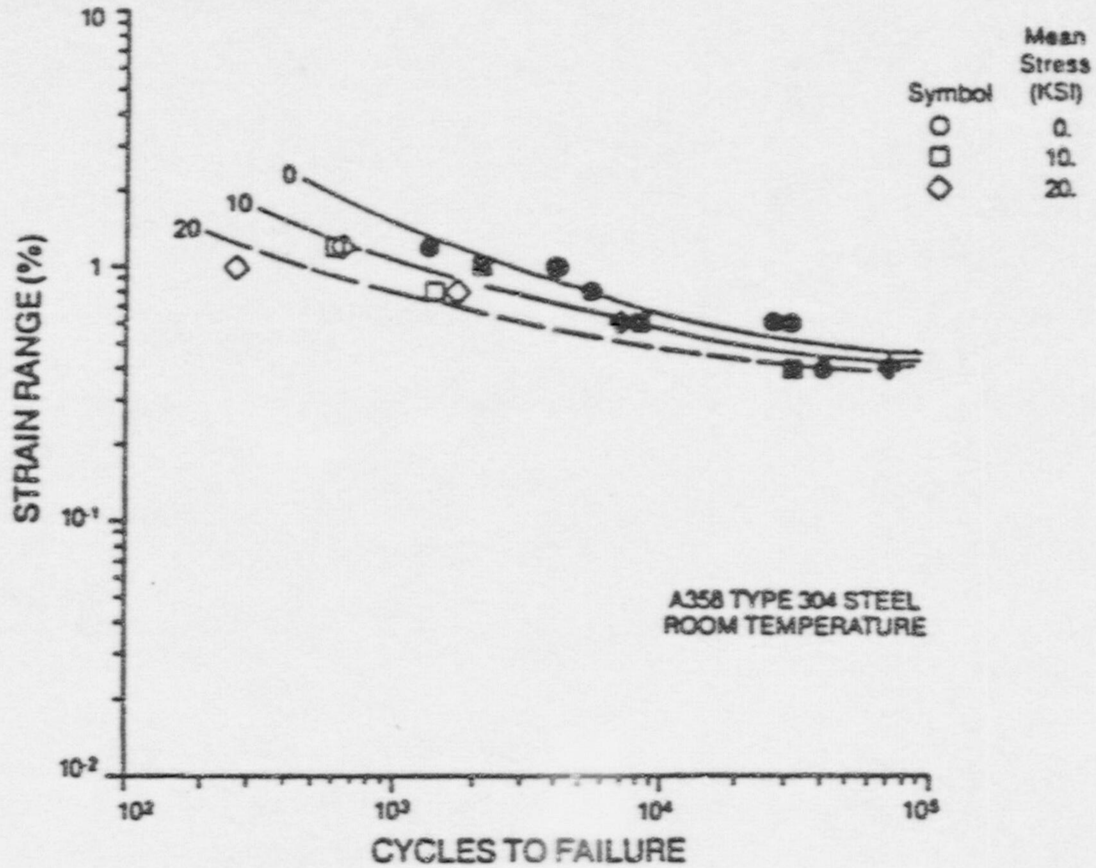

Figure 18: Typical PFDRP 2-Bar Failure Map, Room Temperature

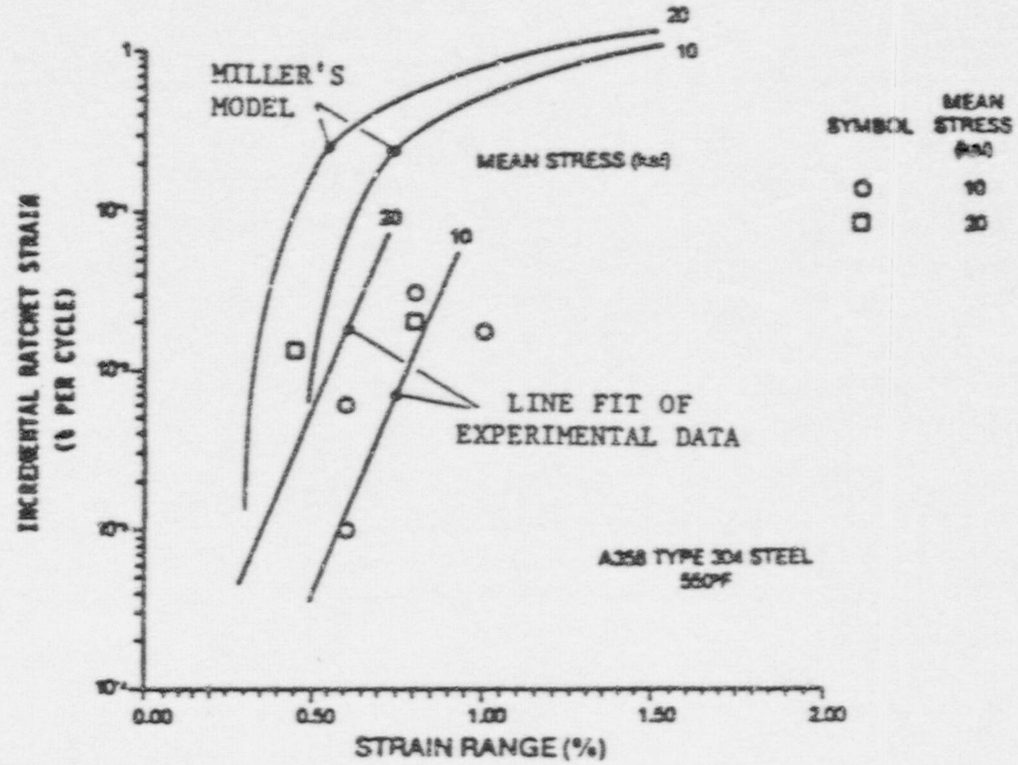

Figure 19: Typical PFDRP 2-Bar Failure Map, 550°F

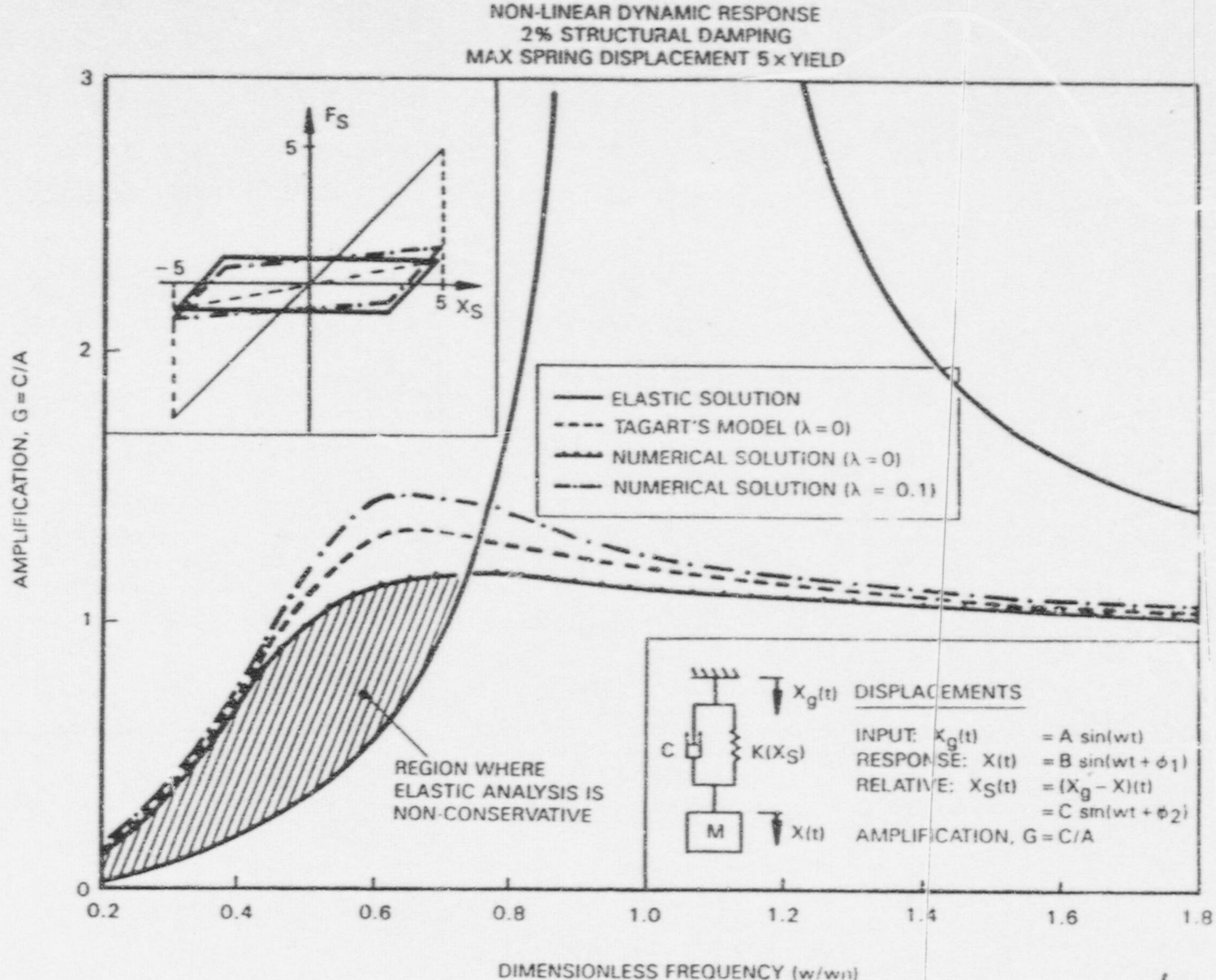

Figure 20: Dynamic Amplification for Elastic and Elastic-Plastic Systems

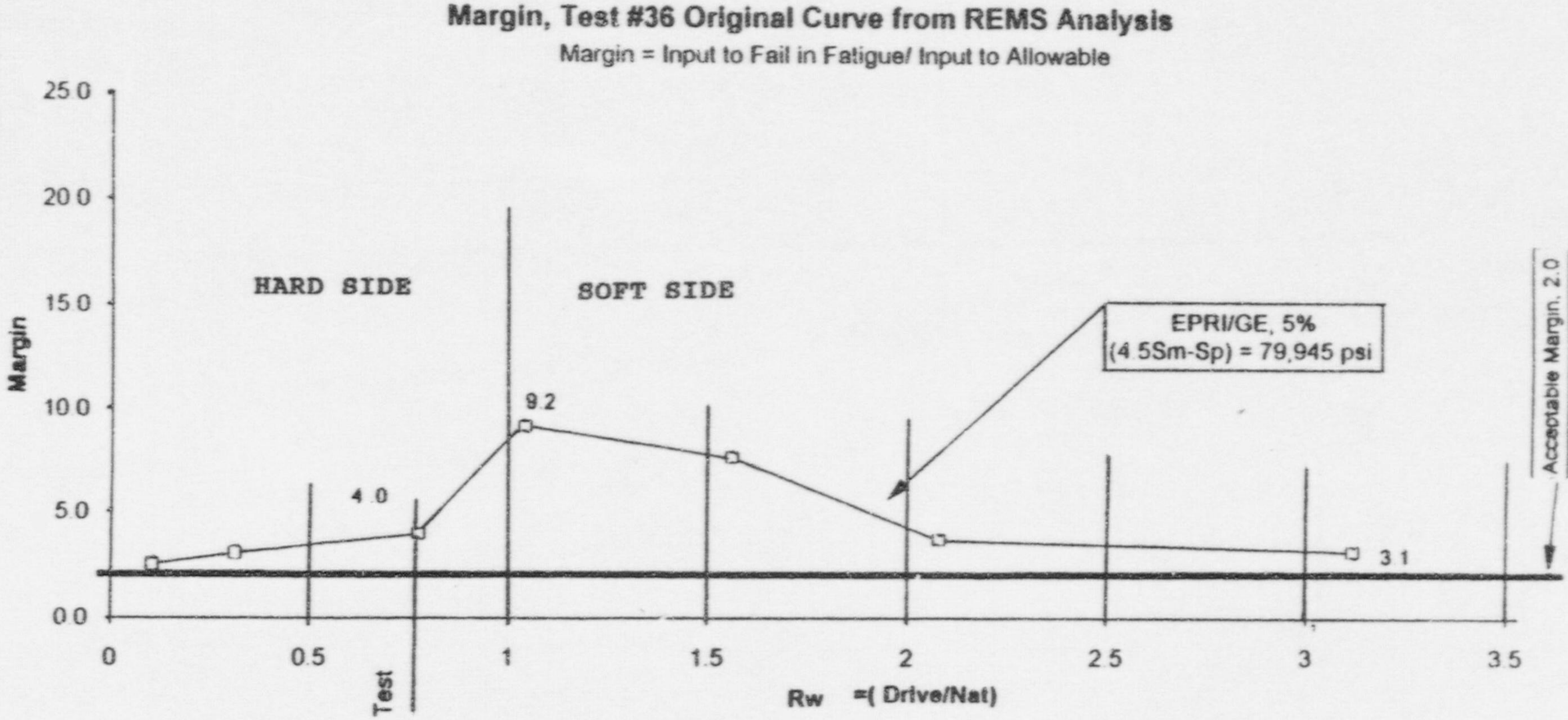

Figure 21: Initial REMS Based Test 36 Frequency Dependent Margins

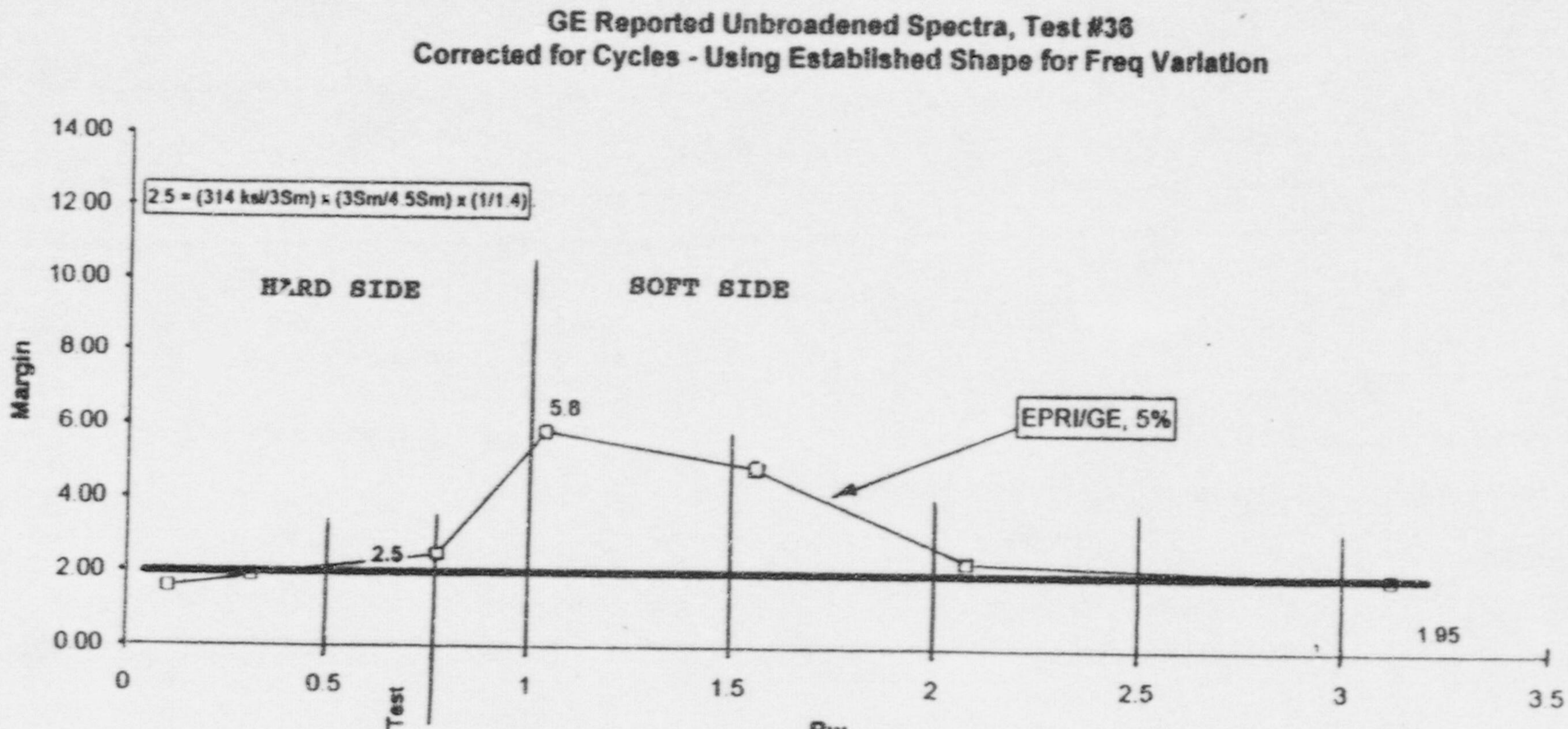

Figure 22: 9/93 Revised REMS Based Test 36 frequency Dependent Margins

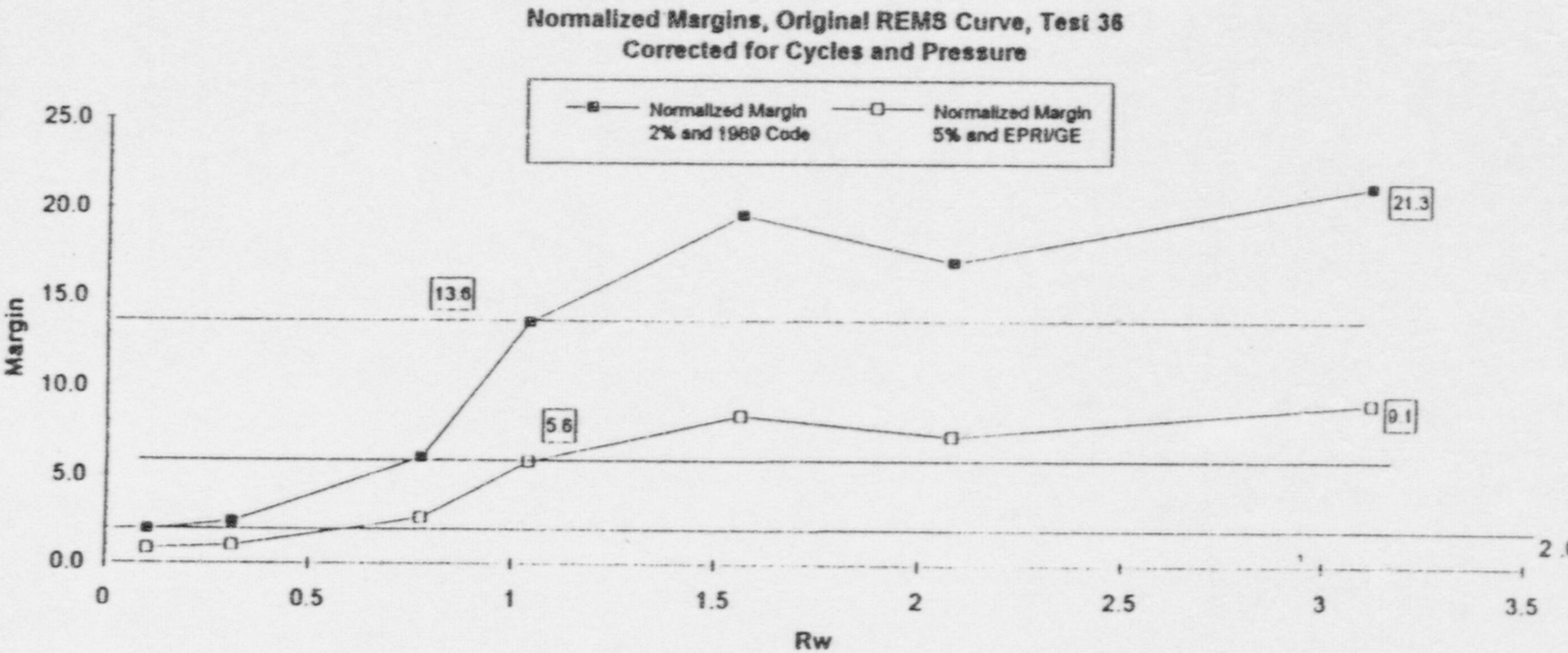

Figure 23: 9/93 Revised REMS Based Test 36 Normalized Frequency Dependent Margins

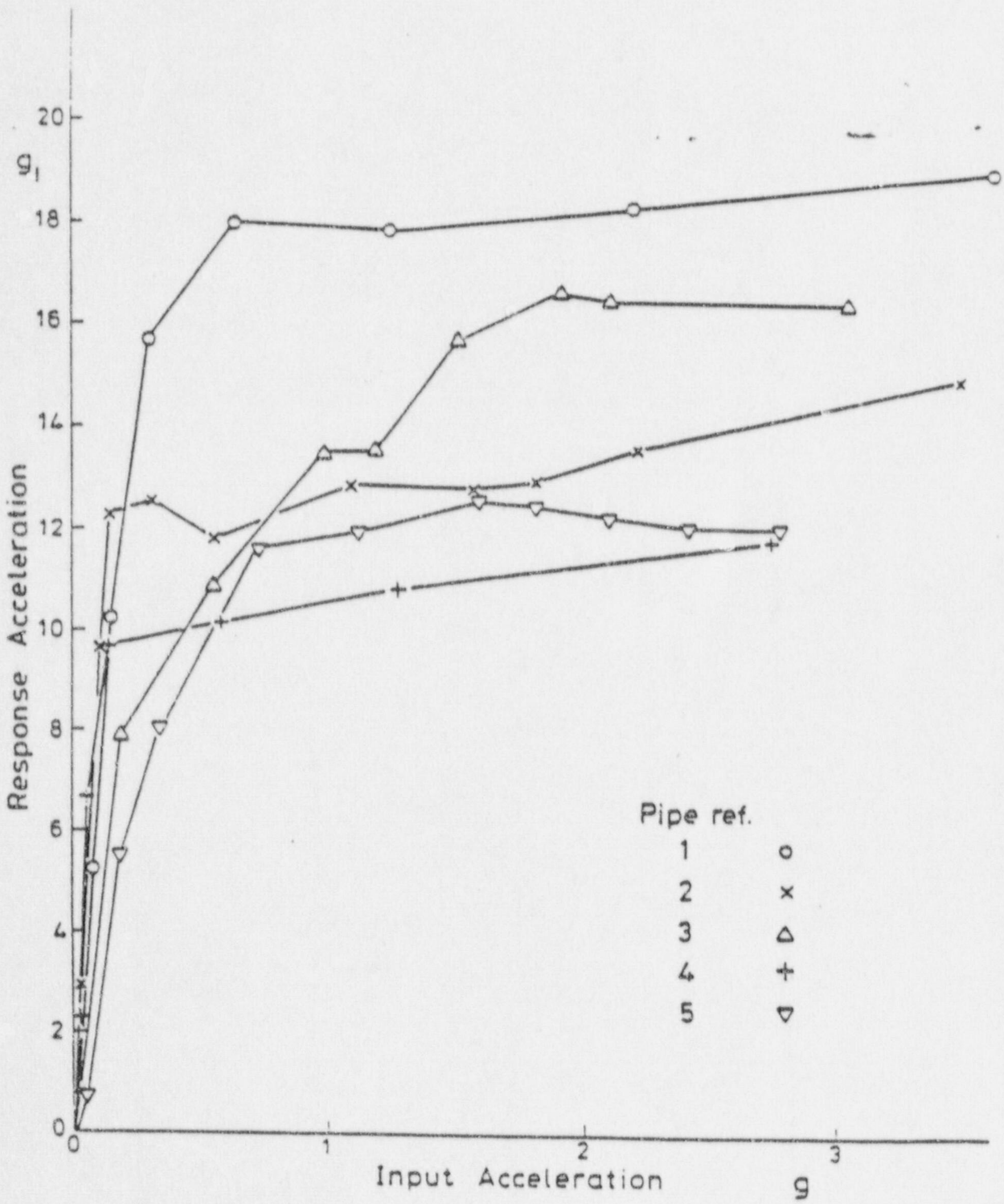

Figure 24: Beaney 1-inch Diameter Pipe Test Data

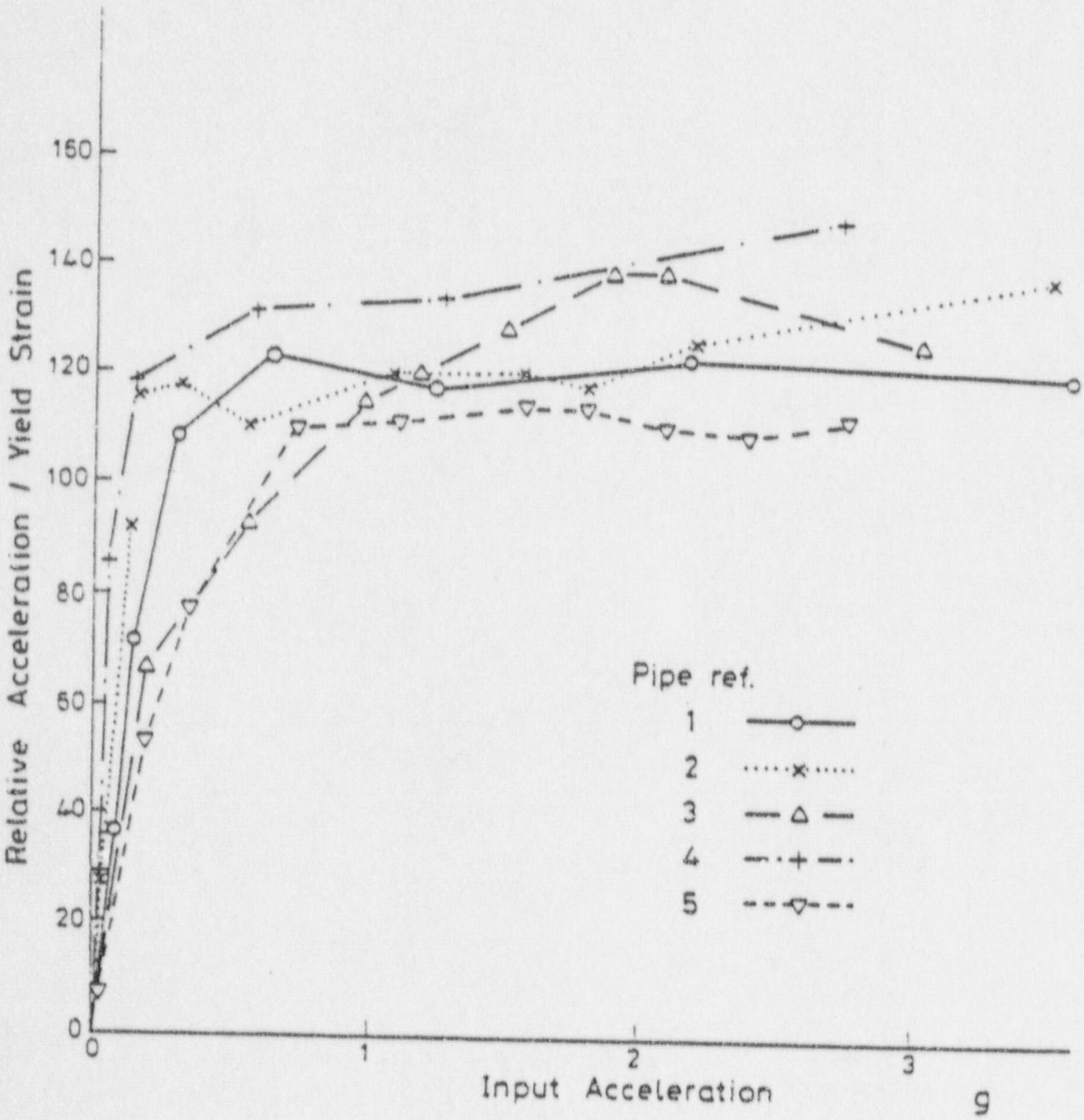

Figure 25: Beaney Yield Correction of Figure 24 Data

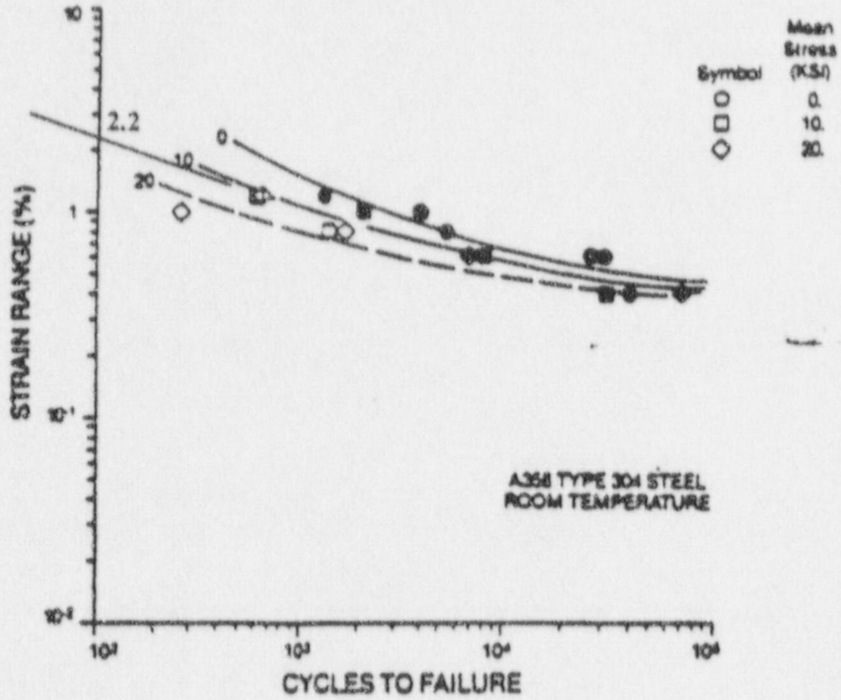

Figure B-6. Strain Range Versus Cyclic Life – A358 Type-304 Stainless Steel RT (Includes Both Fatigue and Ratchet Failure)

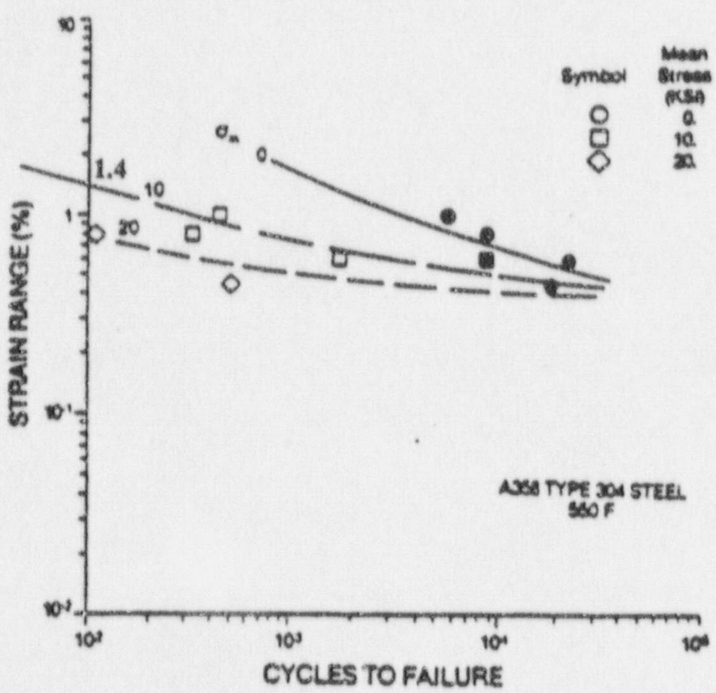

Figure B-8. Strain Range Versus Cyclic Life – A358 Type-304 Stainless Steel 550°F (Includes Both Fatigue and Ratchet Failure)

Figure 26: Derivation of Stainless Steel Fatigue Strength Reduction

Appendix I-A: New Rules

ASME Main Committee #93-374 Agenda Item (passed 2/2/94)

PART II SEISMIC MARGIN ASSESSMENTS

1 Introduction

Part II of this report includes a comprehensive assessment by researchers affiliated with the California Institute of Technology (CIT) of frequency, P-delta, temperature, load eccentricity and worst case combined effects on seismic margins undertaken in response to issues identified in Part I of this report. Margin results for Tests 11, 14, 36 and 40 are presented. These results were then used by ETEC to develop nominal seismic fatigue margins consistent with recent definitions of acceptable margin level, including consideration of revised stress indices. R. Kennedy then performed a data confidence study of the ETEC margins and presented a briefing on his study July 15, 1997 to the US NRC staff. At that time, Kennedy was developing the ultimate moment capacity based design rule approach presented in Part III, Appendix II-B of this report, and the ETEC margin study was referred to in his briefing as "the alternate approach".

The format of Part II is self-contained Appendices. Appendix II-A presents the CIT effort and Appendix II-B is the ETEC margin study followed by the Kennedy data confidence study briefing charts.

The Sub-Section discussions and final conclusions in Appendix II-A provide an excellent description of the CIT study findings regarding specific margin trends under the chosen variables. Only four brief oversight observations by ETEC will be offered. First, the margins are extremely variable. It will be difficult to know the actual margin in any piping system without performing nonlinear analyses. Fortunately, the minimum margins tend to be isolated in the very "stiff" and very "flexible" frequency ratio regions. Unfortunately, providing design criteria to cover these minimums will result in excess conservatism for most frequency ratio regions. On the other hand, multi-mode piping system behavior complexes the issue and it is not clear how many piping systems will have all significant modes lying outside one of these minimum regions. Second, the minimum margin values in the CIT studies are much lower than the test point margins and substantiate the need in the PFDRP test program for very high "superseismic" loadings. Third, although there tended to be a low input level associated with the high margin regions and a high input level associated with the low margin regions, this is not without exception. Figure 4.39 in Appendix II-A illustrates one of these exceptions at the high R_{ω} end. Another unpublished CIT study of low-filtered broad banded input also indicated the possibility of lower input levels at failure in the low R_{ω} region. Finally, the CIT studies to date have been limited to non-elbow tests since elbow non-symmetric plastic behavior requires a special hysteretic modeling development (planned to be conducted at CIT in the Fall of 1997). Clearly, elbow response is a primary consideration for any piping system and until the analytical test margin extrapolations for elbows are completed, the CIT study must be considered incomplete. Nevertheless, the information gained to date has expanded the knowledge of piping dynamic plastic behavior tenfold beyond that learned in the PFDRP testing. The Appendix II-A results will be very valuable in assessing Kennedy's "F_N" term should rule developments proceed along that path, and in general, provides researchers with a much better understanding of piping component margin trends.

The Appendix II-B data tables and briefing charts are offered without discussion due to time constraints at the publishing date of this draft. The final draft is planned to include some discussion. Essentially, the same spreadsheet exercise as conducted for Table 4 in Part I was conducted except nominal properties and geometries were used and the CIT margin reduction factors for Test 14 were used. These reduction factors were for a CIT study that included temperature effects and the lower-bound displacement-based margin was used. The margin result for Test 14 was then compared to the CIT Test 14 value (within about 10%) and all the margins were then scaled by this 10% "correlation factor". The correlated table was also modified to provide margins using the minimum $B_2 = 2$ index recommendation of Kennedy.

NB-3213.33 Ratcheting. Ratcheting is a progressive incremental inelastic deformation or strain which can occur in a component that is subjected to variations of mechanical stress, thermal stress, or both.

NB-3213.34 Shakedown. Shakedown of a structure occurs if, after a few cycles of load application, ratcheting ceases. The subsequent structural response is elastic, or elastic–plastic, and progressive incremental inelastic deformation is absent. Elastic shakedown is the case in which the subsequent response is elastic.

NB-3213.35 Reversing Dynamic Loads. Reversing dynamic loads (Figure NB-3213-1) are those loads which cycle about a mean ~~[illegible]~~ value and include building filtered loads, earthquake and the reflected waves in a piping system due to flow transients resulting from sudden opening or closure of valves.

NB-3213.36 Nonreversing Dynamic Loads. Nonreversing dynamic loads (Figure NB-3213-1) are those loads which do not cycle about a mean value and include the initial thrust force due to sudden opening or closure of valves and waterhammer resulting from entrapped water in two-phase flow systems.

NB-3214 Stress Analysis

A detailed stress analysis of all major structural components shall be prepared in sufficient detail to show that each of the stress limitations of NB-3220 and NB-3230 is satisfied when the component is subjected to the loadings of NB-3110. As an aid to the evaluation of these stresses, formulas and methods for the solution of certain recurring problems have been placed in Appendix A.

NB-3215 Derivation of Stress Intensities

One requirement for the acceptability of a design (NB-3210) is that the calculated stress intensities shall not exceed specified allowable limits. These limits differ depending on the stress category (primary, secondary, etc.) from which the stress intensity is derived. This paragraph describes the procedure for the calculation of the stress intensities which are subject to the specified limits. The steps in the procedure are stipulated in (a) through (e) below.

(a) At the point on the component which is being investigated, choose an orthogonal set of coordinates, such as tangential, longitudinal, and radial, and designate them by the subscripts t, l, and r. The stress components in these directions are then designated σ_t, σ_l, and σ_r for direct stresses and τ_{tl}, τ_{lr}, and τ_{rt} for shear stresses.

(b) Calculate the stress components for each type of loading to which the part will be subjected, and assign each set of stress values to one or a group of the following categories:[4]

(1) general primary membrane stress P_m (NB-3213.8);

(2) local primary membrane stress P_L (NB-3213.10);

(3) primary bending stress P_b (NB-3213.7 and NB-3213.8);

---

[4]See Tables NB-3217-1 and NB-3217-2 and Note (2) of Fig. NB-3221-1.

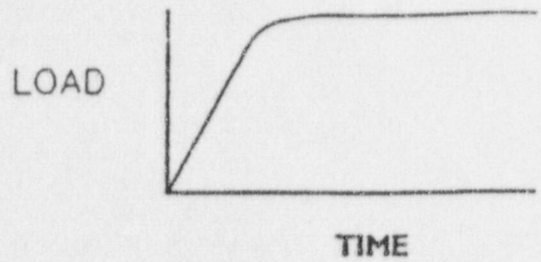

NONREVERSING DYNAMIC LOAD
(RELIEF/SAFETY VALVE OPEN END DISCHARGE)
1(a)

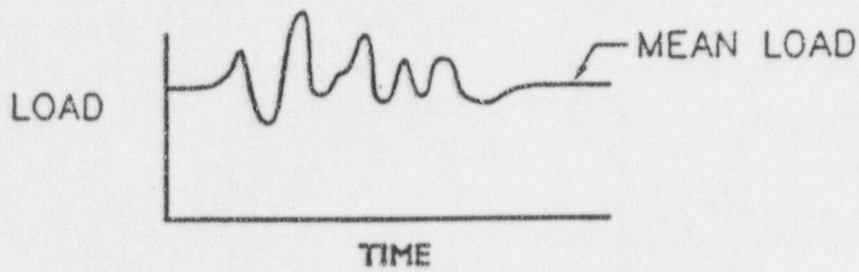

REVERSING DYNAMIC LOAD
(EARTHQUAKE LOAD CYCLING ABOUT NORMAL OPERATING CONDITION)
1(b)

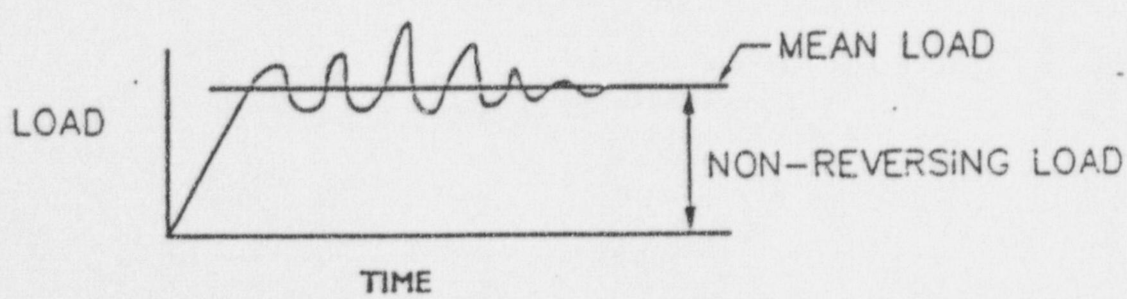

NONREVERSING FOLLOWED BY REVERSING
(INITIAL WATER SLUG FOLLOWED BY REFLECTED PRESSURE PULSES)
1(c)

FIG. NB-3213-1
EXAMPLES OF REVERSING AND NONREVERSING DYNAMIC LOADS

TABLE NB-3217-2
CLASSIFICATION OF STRESS INTENSITY IN PIPING, TYPICAL CASES

Piping Component	Locations	Origin of Stress	Classification	Discontinuities Considered: Gross	Discontinuities Considered: Local
Pipe or tube, elbows, and reducers. Intersections and branch connections, except in crotch regions	Any, except crotch regions of intersections	Internal pressure	P_m P_L and Q F	No Yes Yes	No No Yes
		Sustained mechanical loads, including weight Nonreversing Dynamic Loads	P_b P_L and Q F	No Yes Yes	No No Yes
		Expansion Axial thermal gradient Reversing Dynamic Loads	P_e F Q F Note 2	Yes Yes Yes Yes	No Yes No Yes
Intersections, including tees and branch connections	In crotch region	Internal pressure, sustained mechanical loads, expansion and nonreversing dynamic loads	P_L and Q [Note (1)] F	Yes Yes	No Yes
		Axial thermal gradient Reversing Dynamic Loads	Q F Note 2	Yes Yes	No Yes
Bolts and flanges	Any	Internal pressure, gasket compression, and bolt load	P_m Q F	No Yes Yes	No No Yes
		Thermal gradient	Q F	Yes Yes	No Yes
		Expansion	P_e F	Yes Yes	No Yes
Any	Any	Nonlinear radial thermal gradient	F	Yes	Yes
		Linear radial thermal gradient	F	Yes	No
		Anchor point motions, including those resulting from earthquake	Q	Yes	No

NOTE:
(1) Analysis is not required when reinforced in accordance with NB-3643.
(2) The stress intensity resulting from this loading has special requirements which must be satisfied. For Level B Service Limits these are provided in NB-3223(b)(2) and for Level D Service Limits in NB-3228.6

Stress Category	Primary			Secondary		Peak
	General Membrane	Local Membrane	Bending	Expansion	Membrane plus Bending	
Description (for examples see Table NB-3217-1)	Average primary stress across solid section. Excludes effects of discontinuities and concentrations. Produced by pressure and mechanical loads.	Average stress across any solid section. Considers effects of discontinuities but not concentrations. Produced by pressure and mechanical loads, including inertia earthquake effects.	Component of primary stress proportional to distance from centroid of solid section. Excludes effects of discontinuities and concentrations. Produced by pressure and mechanical loads, including inertia earthquake effects. [Note (1)]	Stresses which result from the constraint of free end displacement. Considers effects of discontinuities but not local stress concentration (not applicable to vessels).	Self-equilibrating stress necessary to satisfy continuity of structure. Occurs at structural discontinuities. Can be caused by pressure, mechanical loads, or differential thermal expansion. Excludes local stress concentrations.	(1) Increment added to primary or secondary stress by a concentration (notch). (2) Certain thermal stresses which may cause fatigue but not distortion.
Symbol [Note (2)]	P_m	P_L	P_b	P_e	Q	F
Combination of stress components and allowable limits of stress intensities						

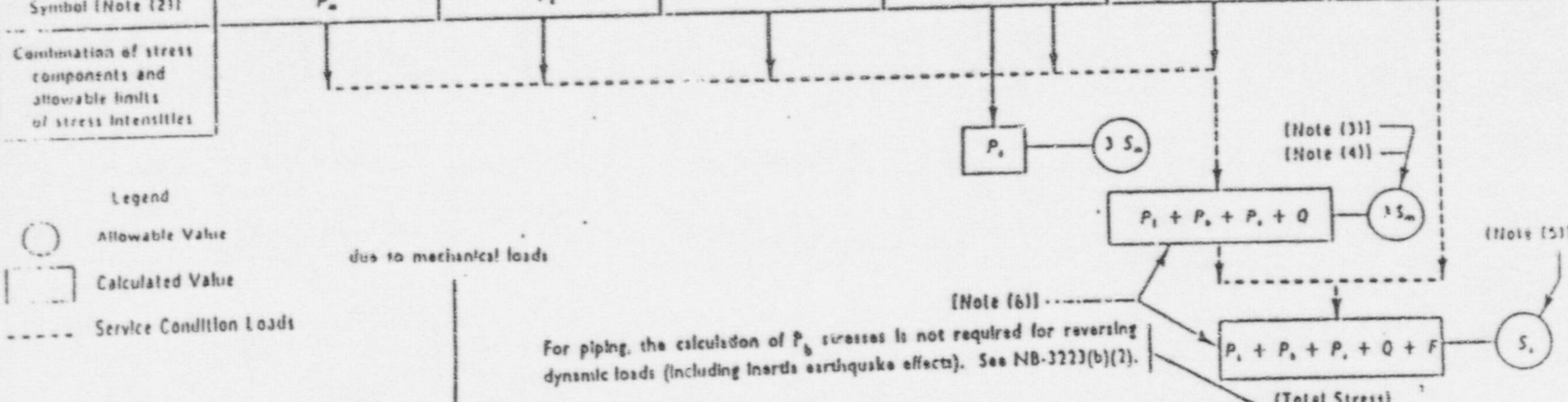

NOTES:

(1) Bending component of primary stress for piping shall be the stress proportional to the distance from centroid of pipe cross section.

(2) The symbols P_m, P_L, P_b, P_e, Q, and F do not represent single quantities, but sets of six quantities representing the six stress components σ_t, σ_l, σ_r, τ_{tl}, τ_{lr}, and τ_{rt}.

(3) When the secondary stress is due to a temperature transient at the point at which the stresses are being analyzed or to restraint of free end deflection, the value of S_m shall be taken as the average of the tabulated S_m values for the highest and the lowest temperatures of the metal during the transient. When part or all of the secondary stress is due to mechanical load, the value of S_m shall not exceed the value for the highest temperature during the transient.

(4) Special rules for exceeding $3S_m$ are provided in NB-3228.5. The allowable stress intensity for the full range of fluctuation is $2S_a$.

(5) S_a is obtained from the fatigue curves, Figs. I-9.0.

(6) The stresses in category Q are those parts of the total stress that are produced by thermal gradients, structural discontinuities, etc., and they do not include primary stresses that may also exist at the same point. However, it should be noted that a detailed stress analysis frequently gives the combination of primary and secondary stresses directly and, when appropriate, the calculated value represents the total of $P_m + P_b + Q$, and not Q alone. Similarly, if the stress in category F is produced by a stress concentration, the quantity F is the additional stress produced by the notch over and above the nominal stress. For example, if a point has a nominal stress intensity P_m and has a notch with a stress concentration factor K, then $P_m \leq S_m$, $P_b = 0$, $Q = 0$, $F = P_m(K - 1)$, and the peak stress intensity equals $P_m + P_m(K - 1) = KP_m$. However, P_L is the total membrane stress that results from mechanical loads, including discontinuity effects, rather than a stress increment. Therefore, the P_L value always includes the P_m contribution.

FIG. NB-3222-1 STRESS CATEGORIES AND LIMITS OF STRESS INTENSITY FOR LEVEL A AND LEVEL B SERVICE LIMITS

B-3223 Level B Service Limits

~~For components operating within the temperature nits of this Subsection the requirements of (a), (b), id (c) below apply.~~

(a) For components other than piping operating within the temperature limits of this subsection the requirements of (1), (2) and (3) below shall apply.

(1)

~~(a)~~ The values of Level A Service Limits shall apply r Level B Service Limits. In addition, if a pressure r which Level B Limits are designated exceeds the esign pressure, the stress limits of Fig. NB-3221-1 iall apply using allowable stress intensity values of 10% of those given on Fig. NB-3221-1 and the loadgs for which Level B Limits are designated.

(2)

~~(b)~~ In evaluating possible exemption from fatigue ialysis by the methods of NB-3222.4(d), Service oadings for which Level B Limits are designated shall : considered as though Level A Limits were desigated.

(3)

~~(c)~~ Any deformation limits prescribed by the Design pecifications shall be satisfied.

(b) For piping components operating within the temperature limits of this subsection the requirements of (1) or (2) below shall apply.

(1) For Level B Service Limits which do not include reversing dynamic loads (NB-3213.35) or have reversing dynamic loads combined with nonreversing dynamic loads (NB-3213.36) the requirements of (a)(1), (2) and (3) above shall be satisfied.

(2) For Level B Service Limits which include reversing dynamic loads that are not required to be combined with nonreversing dynamic loads the requirements of NB-3222.2 and NB-3222.4(e) shall be satisfied in lieu of (b)(1) above. In addition any deflection limits prescribed by the Design Specification must be satisfied.

NB-3224 Level C Service Limits

If the Design Specifications specify any Service Loadings for which Level C Service Limits are designated [NCA-2142.2(b)(3)], and NB-3113(b)] for components other than piping. The rules used in evaluating these loadings shall be those used for other loadings, except as modified by the following subparagraphs and as summarized in Fig. NB-3224-1. For piping special requirements are provided in NB-3224.7.

NB-3224.1 Primary Stress Limits. The primary stress limits of NB-3221 shall be satisfied using an S_m value equal to the greater of 120% of the tabulated S_m value or 100% of the tabulated yield strength, with both values taken at the appropriate temperature. In addition, for ferritic material, the P_m elastic analysis limits for pressure loadings alone shall be equal to the greater of $1.1S_y$ or $0.9S_m$.

NB-3224.2 External Pressure. The permissible external pressure shall be taken as 120% of that given by the rules of NB-3133.

NB-3224.3 Special Stress Limits. The permissible values for special stress limit shall be taken as 120% of the values given in NB-3227.4 and NB-3228.

NB-3224.4 Secondary and Peak Stresses. The requirements of NB-3222.2, NB-3222.4, NB-3222.5, and NB-3227.3 need not be satisfied.

NB-3224.5 Fatigue Requirements. Service Loadings for which Level C Service Limits are designated need not be considered when applying the procedures of NB-3222.4(a) to determine whether or not a fatigue analysis is required.

NB-3224.6 Deformation Limits. Any deformation limits prescribed by the Design Specifications shall be considered.

NB-3224.7 Piping Requirements.

(a) For Level C Service Limits which do not include reversing dynamic loads or have reversing dynamic load combined with nonreversing dynamic loads the requirements of NB-3224.1 thru NB-3224.6 above shall be satisfied.

(b) As an alternative to (a) above, for Level C Service Limits which include reversing dynamic loads that are not required to be combined with nonreversing dynamic loads the requirements of NB-3228.6 may be satisfied using 70% of the specified allowable strain values.

Stress Category	Primary [Notes (1) and ~~(2)]~~ and (6)]			Secondary [Note (1)] and (6)]	Peak [Note (1)] and (6)]
	General Membrane	Local Membrane	Bending	Membrane plus Bending	
Description (for examples see Table NB-3217-1)	Average primary stress across solid section. Excludes discontinuities and concentrations. Produced only by mechanical loads.	Average stress across any solid section. Considers discontinuities but not concentrations. Produced only by mechanical loads.	Component of primary stress proportional to distance from centroid of solid section. Excludes discontinuities and concentrations. Produced only by mechanical loads.	Self-equilibrating stress necessary to satisfy continuity of structure. Occurs at structural discontinuities. Can be caused by mechanical load or by differential thermal expansion. Excludes local stress concentration.	(1) Increment added to primary or secondary stress by a concentration (notch). (2) Certain thermal stresses which may cause fatigue but not distortion of vessel shape.
Symbol [Note (1)]	P_m NB-3213.6 and NB-3213.8 [Note (3)]	P_L NB-3213.10	P_b NB-3213.7 and NB-3213.8	Q NB-3213.9	F NB-3213.11
Combination of stress components and allowable limits of stress intensities					

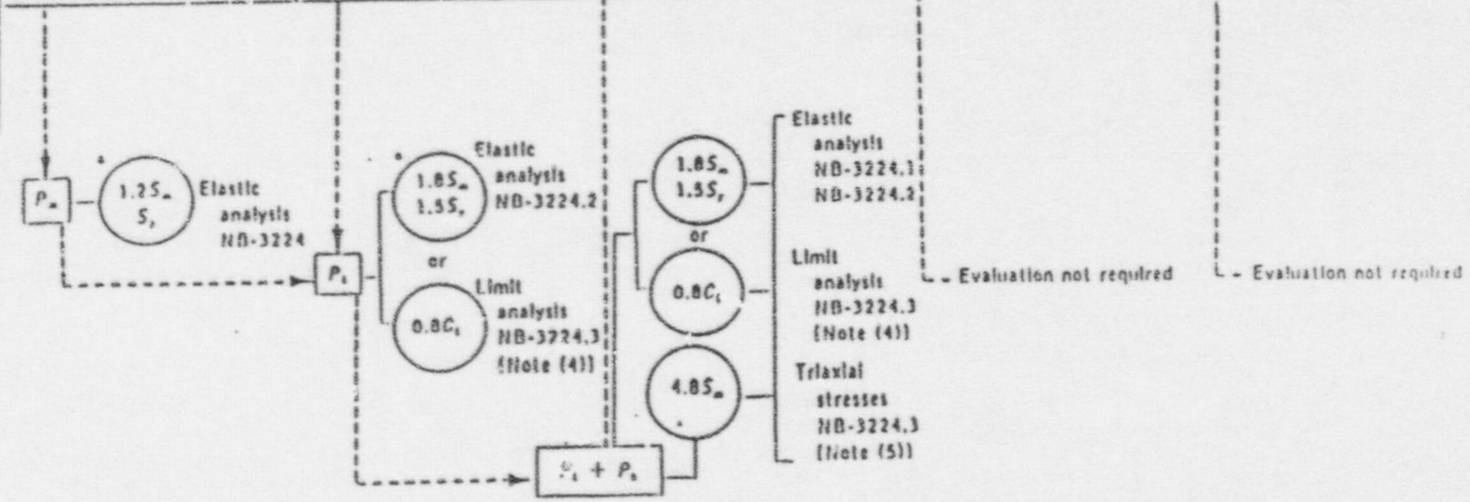

NOTES:

(1) The symbols P_m, P_L, P_b, Q, and F do not represent single quantities, but rather sets of six quantities representing the six stress components σ_t, σ_l, σ_r, τ_{tl}, τ_{lr}, and τ_{rt}.

(2) For configurations where compressive stresses occur, the stress limits shall be revised to take into account critical buckling stresses [NB-3211(c)].

(3) The limits shown are for stresses resulting from pressure in combination with other mechanical loads. For ferritic materials, the P_m elastic analysis limits for pressure loadings alone shall be equal to the greater of $1.1S_m$ or $0.9S_y$.

(4) C_L the collapse load calculated on the basis of the lower bound theorem of limit analysis and yield strength values specified in Section II, Part D, Subpart 2, Table Y-1

(5) The triaxial stresses represent the algebraic sum of the three primary principal stresses ($\sigma_1 + \sigma_2 + \sigma_3$) for the combination of stress components.

* Use the greater of the values specified.

FIG. NB-3224-1 STRESS CATEGORIES AND LIMITS OF STRESS INTENSITY FOR LEVEL C SERVICE LIMITS

(6) For piping, alternative requirements are provided in NB-3224.7.

-3225 Level D Service Limits

-f the Design Specifications specify any Service adings for which Level D Limits are designated CA-2142.2(b)(4)], the rules contained in Appendix may be used in evaluating these loadings, independ-ntly of all other Design and Service Loadings.

B-3226 Testing Limits

The evaluation of pressure test loadings (NCA-42.3) shall be in accordance with (a) through (e) low, except that these rules do not apply to the items NB-3500.

(a) The general primary membrane stress intensity shall not exceed 90% of the tabulated yield strength at test temperature.

(a) For components other than piping, if

STET

(b) For piping fabricated from material designated P Nos. 1 thru 9 in Table 2A, Section II, Part D, if the Design Specifications specify any Service Loading for which Level D limits are designated [NCA-2142.2(b)(4)], the rules contained in NB-3228.6 may be used as an alternative to those contained in Appendix F. ~~For other piping materials the rules of Appendix F~~ may be used in evaluating these loadings, independently of all other Design and Service Loadings.

~~MOVE TO NB 3228.6~~

~~NEED INTRODUCTION TO BE DRAFTED.~~

INSERT FROM NB-3225(b)

NB-3228.6 Reversing Dynamic Loading in Piping. As an alternative to ~~In lieu of~~ meeting the ~~simplified design~~ requirements of Appendix F ~~NB-3650, the following may be satisfied.~~ for ~~P~~piping components subjected to reversing type dynamic loading as defined in NB-3213.365 ~~must be protected against fatigue or fatigue ratchet failure~~the requirements of (a)(1) and (2) below shall be satisfied. However, ~~W~~when the specified Level D Load combination includes nonreversing dynamic loads (NB-3213.36) alone or coincident with earthquake and other reversing dynamic loads for which the Design Specification requires satisfaction of Level D Service Limits the requirements of ~~NB-3225(a)~~ Appendix F must be satisfied for Level D.

(a) ~~The following requirements shall be satisfied. when the specified Level D Load combination includes earthquake and other reversing dynamic loads not occurring coincident with nonreversing dynamic loads for which the Design Specification requires satisfaction of Level D Service Limits.~~ Deflections, deformations, and strains, including those caused by incremental ratcheting must be evaluated on an inelastic basis to assure compliance with these limits.

(1) The effective ratchet strain averaged through the wall thickness of the piping component due to the application of all simultaneously applied loading including pressure, the effects of gravity, thermal expansion ranges, earthquake inertia ranges, anchor motion ranges, (including thermal, earthquake, etc.) and reversing dynamic loading ranges shall not exceed 5%.

(2) The effective local peak cyclic single-amplitude strain ϵ_{an}, in the wall of the piping component due to the application of all simultaneously applied loading ranges considered in (1) above shall not exceed the following.

$$\epsilon_{an} \le \frac{S_{a10}}{(E\sqrt{N})}$$

where:

S_{a10} = The S_a value at 10 cycles from the applicable Design Fatigue Curve in Appendix I

E = Young's Modulus

N = 10 for earthquake event. For other reversing dynamic loads N is the number of cycles defined in the Design Specification. However N can never be taken as less than 10.

INSERT DEFINITIONS OF EQUIVALENT STRAINS FROM INSERT PAGE,

INSERT PAGE

ADD TO
NB-3228.6
9/14/93

Sam W. Tagart, Jr.
September 10, 1993

~~A Definition of Equivalent Strains~~

The equivalent strain range is defined as follows.

Step 1. Identify all strain components for each point, i, in time (εxi, εyi, εzi, Γxyi, Γyzi, Γzxi) for a complete cycle of interest.

Step 2. Select a time point when conditions are at an extreme for the cycle, either maximum or minimum. Refer to this time point as o.

Step 3. Calculate the history of the change in strain components by subtracting the values at the time, o, from the corresponding components at each point in time, i, during the cycle.

$$\delta\varepsilon xi = \varepsilon xi - \varepsilon xo$$

$$\delta\varepsilon yi = \varepsilon yi - \varepsilon yo$$

etc;

Step 4. Calculate the equivalent strain ranges for each point in time as:

$$\delta\varepsilon equiv,i = \frac{\sqrt{2}}{3}\left[(\delta\varepsilon xi - \delta\varepsilon yi)^2 + (\delta\varepsilon yi - \delta\varepsilon xi)^2 + (\delta\varepsilon zi - \delta\varepsilon xi)^2 + \frac{3}{2}(\delta\Gamma xyi^2 + \delta\Gamma yzi^2 + \delta\Gamma zxi^2)\right]^{1/2}$$

Step 5. The equivalent strain range is the maximum value of the above calculated equivalent strain ranges, $\delta\varepsilon equiv,i$.

The effective cyclic single-amplitude strain is half the equivalent strain range for one typical cycle of loading.

The equivalent ratchet strain is the value of the above calculated equivalent strain range over all the cycles of loading.

33A

NB-3622 Dynamic Effects

NB-3622.1 Impact. Impact forces caused by either external or internal loads shall be considered in the piping design.

~~**NB-3622.2 Earthquake.** The effects of earthquake shall be considered in the design of piping, piping supports, and restraints. The loadings, movements (earthquake anchor movements), and number of cycles to be used in the analysis shall be part of the Design Specifications. The stresses resulting from these earthquake effects must be included with weight, pressure, or other applied loads when making the required analysis.~~

NB-3622.2 Reversing Dynamic Loads. Reversing dynamic loads (Figure NB-3622-1) are those loads which cycle about a mean valve and include building filtered loads, earthquake and the reflected waves in a piping system due to flow transients resulting from sudden opening or closure of valves. A reversing dynamic load shall be treated as a nonreversing dynamic load in applying the rules of NB-3600 when either of the following conditions exist:

(a) The frequency ratio of the dynamic DOMINANT load driving frequency to the lowest piping system natural frequency is less than 0.5

(b) The number of reversing dynamic load cycles, exclusive of earthquake, exceed 20.

NB-3622.3 Vibration. Piping shall be arranged and supported so that vibration will be minimized. The designer shall be responsible, by design and by observation under startup or initial service conditions, for ensuring that vibration of piping systems is within acceptable levels.

~~**NB-3622.4 Relief and Safety Valve Thrust.** The effects of thrusts from relief and safety valve loads from pressure and flow transients shall be considered in the design of piping, pipe supports, and restraints. See Appendix O.~~

NB-3622.4 Nonreversing Dynamic Loads. Nonreversing dynamic loads (Figure NB-3622-1) are those loads which do not cycle about a mean value and include the initial thrust force due to sudden opening or closure of valves and waterhammer resulting from entrapped water in two-phase flow systems.

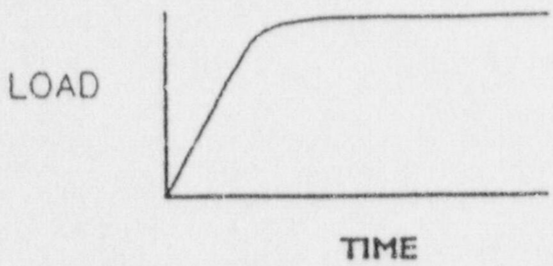

NONREVERSING DYNAMIC LOAD
(RELIEF/SAFETY VALVE OPEN END DISCHARGE)
1(a)

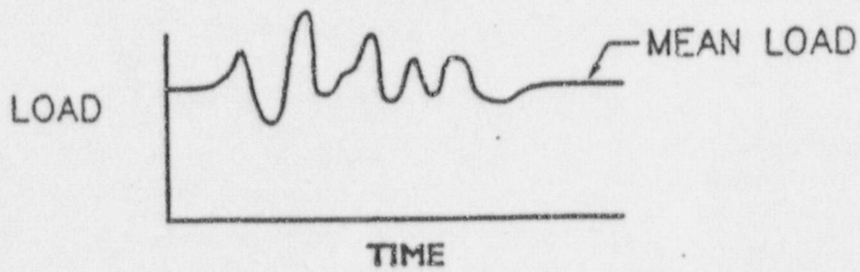

REVERSING DYNAMIC LOAD
(EARTHQUAKE LOAD CYCLING ABOUT NORMAL OPERATING CONDITION)
1(b)

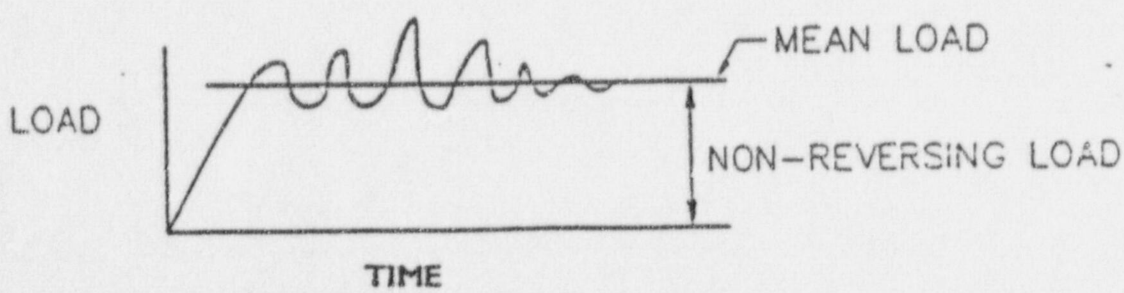

NONREVERSING FOLLOWED BY REVERSING
(INITIAL WATER SLUG FOLLOWED BY REFLECTED PRESSURE PULSES)
1(c)

FIG. NB-3622-1
EXAMPLES OF REVERSING AND NONREVERSING DYNAMIC LOADS

NB-3653.1

(i.e., resultant moments from different load sets shall not be used in calculating the moment range M_i). Weight effects need not be considered in determining the loading range since they are noncyclic in character. If the method of analysis is such that only magnitudes without relative algebraic signs are obtained, the most conservative combination shall be assumed. If a combination includes ~~earthquake effects~~ reversing dynamic loads, M_i shall be either: (1) the resultant range of moment due to the combination of all loads considering one-half the range of the ~~earthquake~~ reversing dynamic loads; or (2) the resultant range of moment due to the full range of the ~~earthquake~~ reversing dynamic loads alone, whichever is greater.

$T_a(T_b)$ = range of average temperature on side $a(b)$ of gross structural discontinuity or material discontinuity, °F. For generally cylindrical shapes, the averaging of T (NB-3653.2) shall be over a distance of $\sqrt{d_a t_a}$ for T_a and over a distance of $\sqrt{d_b t_b}$ for T_b.

$d_a(d_b)$ = inside diameter on side $a(b)$ of a gross structural discontinuity or material discontinuity, in.

$t_a(t_b)$ = average wall thickness through the length $\sqrt{d_a t_a}$ ($\sqrt{d_b t_b}$), in. A trial and error solution for t_a and t_b may be necessary.

$\alpha_a(\alpha_b)$ = coefficient of thermal expansion on side $a(b)$ of a gross structural discontinuity or material discontinuity, at room temperature, 1/°F (Section II, Part D, Subpart 2, Table TE)

E_{ab} = average modulus of elasticity of the two sides of a gross structural discontinuity or material discontinuity at room temperature, psi (Section II, Part D, Subpart 2, Table TM)

P_o = range of service pressure, psi

NB-3654 Consideration of Level B Service Limits

NB-3654.1 Permissible Pressure. For Level B Service Limits [NCA-2142.4(b)(2)], the permissible pressure shall not exceed the pressure P_a, calculated in accordance with Eq. (3) of NB-3641.1, by more than 10%.

NB-3654.2 Analysis of Piping Components. ~~For Service Loadings for which Level B Service Limits are designated,~~ the conditions of Eq. (9) shall be met using Service Level B coincident pressure P and moments M_i which result in the maximum calculated stress. The allowable stress to be used for this condition is $1.8S_m$, but not greater than $1.5S_y$. In addition, the procedures for analyzing Service Loadings for which Level B Service Limits are designated are the same as those given in NB-3653 for Level A Service Limits.

S_y = yield strength value, psi, taken at average fluid temperature of the transient under consideration

For Service Loadings for which Level B Service Limits are designated the requirements of (a) or (b) below shall apply.

(a) For Service Loadings for which Level B Service Limits are designated which do not include reversing dynamic loads (NB-3622.2) or have reversing dynamic loads combined with nonreversing dynamic loads (NB-3622.4).

(b) For Service Loadings for which Level B Service Limits are designated which include reversing dynamic loads that are not required to be combined with nonreversing dynamic loads the requirements of NB-3653 for Level A Service Limits shall be met. In addition any deflection limits prescribed by the Design Specification must be satisfied.

NB-3655 Consideration of Level C Service Limits

NB-3655.1 Permissible Pressure. When Level C Service Limits [NCA-2142.4(b)(3)] are specified, the permissible pressure shall not exceed the pressure P_a, calculated in accordance with Eq. (3) of NB-3641.1, by more than 50%.

NB-3655.2 Analysis of Piping Components. ~~Under any Service Loadings for which Level C Service Limits are designated [NCA-2142.4(b)(3)],~~ the conditions of Eq. (9) of NB-3652 shall be met using Service Level C coincident pressure P and moments M_i which result in the maximum calculated stress. The allowable stress to be used for this condition is $2.25S_m$ but not greater than $1.8S_y$.

NB-3655.3 Deformation Limits. Any deformation limits prescribed by the Design Specifications shall be considered with respect to Level C Service Limits.

and NB-3113(b)

For Service Loadings for which Level C Service Limits [NCA-2142.4(b)(3) and NB-3113(b)] are designated the requirements of (a) or (b) below shall apply.

(a) For Service Loadings for which Level C Service Limits are designated which do not include reversing dynamic loads or have reversing dynamic loads combined with nonreversing dynamic loads.

(b) For Service Loadings for which Level C Service Limits are designated which include reversing dynamic loads that are not required to be combined with nonreversing dynamic loads the requirements of NB-3656(b) shall be satisfied using the allowable stress in NB-3656(b)(2), 70% of the allowable stress in NB-3656(b)(3) and 70% of the allowable loads in NB-3656(b)(4).

or deflection

NB-3656 Consideration of Level D Service Limits

~~*(a)* If the Design Specifications specify any Service Loadings for which Level D Service Limits are designated [NCA-2142.4(b)(4)], the rules contained in Appendix F may be used in evaluating these Service Loadings independently of all other Design and Service Loadings.~~

~~*(b)* As an alternative, the conditions of Eq. (9) shall be met. The allowable stress to be used for this condition is 3.0 S_m, but not greater than 2.0 S_y. The permissible pressure shall not exceed 2.0 times the pressure P_a calculated in accordance with Eq. (3) of NB-3641.1.~~

For piping ~~fabrication~~ fabricated from material designated P No. 1 thru 9 in Table 2A, Section II, Part D, If the Design Specifications specify any Service Loading for which Level D Limits are designated [NCA-2142.2(b)(4)] the requirements of (a), (b) or (c) below shall apply.

(a) For Service Loadings for which Level D Service Limits are designated which do not include reversing dynamic loads or have reversing dynamic loads combined with nonreversing dynamic loads the requirements of (1) and (2) shall apply.

(1) The permissible pressure shall not exceed 2.0 times the pressure P_a calculated in accordance with Eq. (3) of NB-3641.1

(2) The conditions of Eq. (9) of NB-3652 shall be met. The allowable stress to be used for this condition is 3.0 S_m but not greater than 2.0 S_y.

(b) ~~for~~ Service Loadings for which Level D Service Limits are designated which include reversing dynamic loads that are not required to be combined with nonreversing dynamic loads the requirements of (1) thru (5) shall apply.

(1) The pressure occurring coincident with the earthquake or other reversing type loading shall not exceed the Design Pressure.

(2) The sustained stress due to weight loading shall not exceed the following:

$$B_2 \frac{D_o}{2I} M_O \le 0.5\ S_m$$

W

where

W

M_O = resultant moment due to weight effects (NB-3623)

(3) The stress due to weight and inertial loading due to reversing dynamic loads in combination with the Level D coincident pressure shall not exceed the following:

$$B_1 \frac{P_D D_o}{2t} + B_2 \frac{D_o}{2I} M_E \le 4.5\ S_m$$

where

P_D = the pressure occurring coincident with the reversing dynamic load

M_E = the amplitude of the resultant moment due to the inertial loading from the earthquake, other reversing type dynamic events and weight. Earthquake and other reversing dynamic loads shall be computed from a linear elastic response spectrum analysis as defined in Appendix N-1226 except the spectrum peak broadening value Δ_{1g} in N-1226.3 shall not be less than 15 percent and, in place of the damping values for both large and small diameter piping systems in Table N-1230-1 for Operating Basis Earthquake and Safe Shutdown Earthquake, a value of 5 shall be used. The ground motion design input for generating the floor response spectrum to be used in the linear elastic analysis shall meet the requirements of Appendix N-1211(a) and N-1211(b). Moments and forces may be computed using a methodology other than prescribed above if the alternate methodology is demonstrated to produce results which envelope the prescribed methodology results. In the combination of loads, all directional moment components in the same direction shall be combined before determining the resultant moment. If the method of analysis is such that only magnitude without algebraic signs are obtained, the most conservative combination shall be assumed.

(4) The range of the resultant moment M_{AM} and the amplitude of the longitudinal force F_{AM} resulting from the anchor motions due to earthquake and other reversing type dynamic loading shall not exceed the following:

$$C_2 \frac{M_{AM} D_o}{2I} < S_1$$

$$\frac{F_{AM}}{A_M} < S_2$$

where: $S_1 = 6S_m$
$S_2 = 1.0S_m$
A_M = cross-sectional area of metal in the piping component wall

(5) Piping displacements shall satisfy Design Specification limitations.

(c) As an alternative to NB-3656(a) and (b), the rules contained in Appendix F may be used in evaluating these service loadings independently of all other Design and Service Loadings.

NB-3658.3 Level D Service Limits

(a) The pressure shall not exceed 2.0 times the Rated Pressure.

(b) The limitation given by Eq. (17) of NB-3658.2(b) shall be met, where P_{fd} and M_{fd} are pressures, psi, and moments, in.-lb, occurring concurrently.

The allowable M_{fd} calculated from Eq. (17) shall be increased by 40%.

NB-3658.4 Test Loadings. Analysis for Test Loadings is not required.

for NB-3656(b) & NC-3655(b) add
"and applicable to D/t ≤ 50"

NC-3600 PIPING DESIGN

NC-3610 GENERAL REQUIREMENTS

NC-3611 Acceptability

The requirements for acceptability of a piping system are given in the following subparagraphs.

NC-3611.1 Allowable Stress Values. Allowable stress values to be used for the design of piping systems are given in Tables I-7.0.

NC-3611.2 Stress Limits

(a) Design and Service. Loadings shall be specified in the Design Specification.

(b) Design Loadings. The sum of stresses due to design internal pressure, weight, and other sustained loads shall meet the requirements of Eq. (8), NC-3652.

(c) Service Loadings. The following service limits shall apply to Service Loadings as designated in the Design Specifications.

(1) Level A and B Service Limits. For Service Loadings for which Level A and B Service Limits are designated in the Design Specification, the requirements of NC-3653 shall be met. ~~The stress range due to thermal expansion shall not exceed S_A, or the sum of stresses due to internal pressure, weight, and other sustained loads, and the stress range due to thermal expansion shall not exceed the sum of S_A and S_h. This requirement is satisfied by meeting Eq. (10) or (11), NC-3653.2. In addition, for Service Loadings for which Level B Service Limits are designated in the Design Specification, the sum of stresses due to internal pressure, live and dead load, and those due to occasional loads such as wind or earthquake shall meet the requirements of NC-3653.1.~~ When Level B Limits apply, the peak pressure P_{max} alone shall not exceed 1.1 times the pressure P_a calculated in accordance with Eq. (5), NC-3641.1.

(2) Level C Service Limits. For Service Loadings for which Level C Service Limits are designated in the Design Specification, the sum of stresses ~~due to internal pressure, live and dead load, and those due to occasional loads~~ shall meet the requirements of NC-3654. ~~When Level C Limits apply, the peak pressure P_{max} alone shall not exceed 1.5 times the pressure P_a calculated in accordance with Eq. (5), NC-3641.1.~~

(3) Level D Service Limits. For Service Loadings for which Level D Service Limits are designated in the Design Specification, the sum of stresses shall meet the requirements of NC-3655. ~~When Level D Limits apply, the peak pressure P_{max} alone shall not exceed 2.0 times the pressure P_a calculated in accordance with Eq. (5), NC-3641.1.~~

(4) Test Conditions. Testing shall be in accordance with NC-6000. Occasional loads shall not be considered as acting at time of test.

NC-3622 Dynamic Effects

NC-3622.1 Impact. Impact forces caused by either external or internal loads shall be considered in the piping design.

~~**NC-3622.2 Earthquake.** The effects of earthquake shall be considered in the design of piping, piping supports, and restraints. The loadings, movements, including earthquake anchor movements, and number of cycles to be used in the analysis shall be part of the Design Specifications. The stresses resulting from these earthquake effects must be included with weight, pressure, or other applied loads when making the required analysis.~~

NC-3622.3 Vibration. Piping shall be arranged and supported so that vibration will be minimized. The designer shall be responsible, by design and by observation under startup or initial service conditions, for ensuring that vibration of piping systems is within acceptable levels.

NC-3622.4 Exposed Piping. Exposed piping shall be designed to withstand wind loadings, using meteorological data to determine wind forces. When State, Province, or Municipal ordinances covering the design of building structures are in effect and specify wind loadings, these values shall be considered the minimum design values. However, it is not necessary to consider earthquake and wind loadings to be acting concurrently.

~~**NC-3622.5 Relief and Safety Valve Thrust.** The effects of thrusts from relief and safety valve loads from pressure and flow transients shall be considered in the design of piping, pipe supports, and restraints. See Appendix O.~~

NC-3622.2 Reversing Dynamic Loads. Reversing dynamic loads (Figure NC-3622-1) are those loads which cycle about a mean valve and include building filtered loads, earthquake and the reflected waves in a piping system due to flow transients resulting from sudden opening or closure of valves. A reversing dynamic load shall be treated as a nonreversing dynamic load in applying the rules of NC-3600 when either of the following conditions exist:

(*a*) The frequency ratio of the dynamic DOMINANT load driving frequency to the lowest piping system natural frequency is less than 0.5

(*b*) The number of reversing dynamic load cycles, exclusive of earthquake, exceed 20.

NC-3622.5 Nonreversing Dynamic Loads. Nonreversing dynamic loads (Figure NC-3622-1) are those loads which do not cycle about a mean value and include the initial thrust force due to sudden opening or closure of valves and waterhammer resulting from entrapped water in two-phase flow systems.

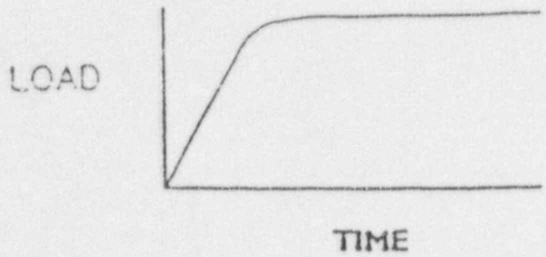

NONREVERSING DYNAMIC LOAD
(RELIEF/SAFETY VALVE OPEN END DISCHARGE)
1(a)

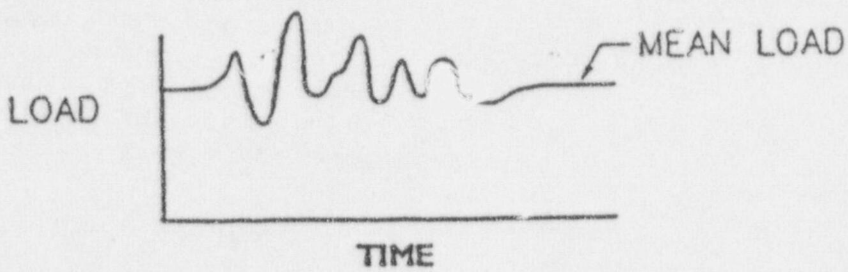

REVERSING DYNAMIC LOAD
(EARTHQUAKE LOAD CYCLING ABOUT NORMAL OPERATING CONDITION)
1(b)

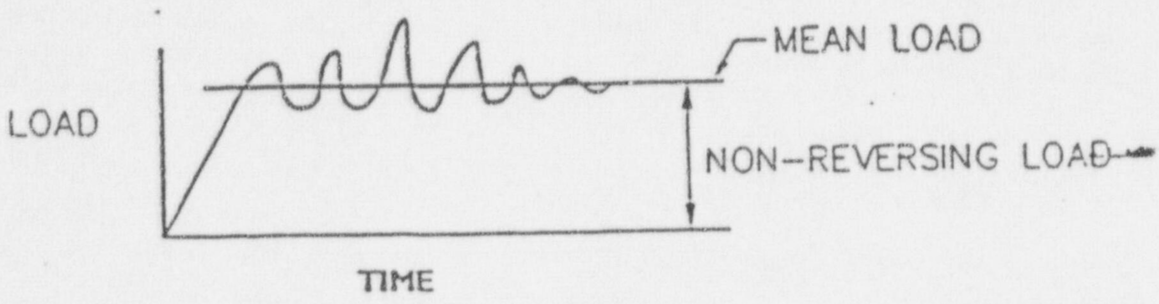

NONREVERSING FOLLOWED BY REVERSING
(INITIAL WATER SLUG FOLLOWED BY REFLECTED PRESSURE PULSES)
1(c)

FIG. NC-3622-1
EXAMPLES OF REVERSING AND NONREVERSING DYNAMIC LOADS

(*f*) The Certificate Holder's Data Report shall state which of the above procedures was utilized to verify the design.

(*g*) If there are two or more types of stress cycles which produce significant stresses, their cumulative effect shall be evaluated as stipulated in Steps 1 through 5 below.

Step 1: Designate the specified number of times each stress cycle of types 1, 2, . . ., n, will be repeated during the life of the component as n_1, n_2, . . ., n_n, respectively.

NOTE: In determining n_1, n_2, . . ., n_n, consideration shall be given to the superposition of cycles of various origins which produce a total stress difference S_1, S_2, . . ., S_n greater than the stress difference of the individual cycles. For example, if one type of stress cycle produces 1,000 cycles of stress difference variation from zero to +60,000 psi and another type of stress cycle produces 10,000 cycles of a stress difference variation from zero to − 50,000 psi, the two types of cycles to be considered are defined by the following parameters:

Type 1 cycle n_1 = 1000,
S_1 = (60,000 + 50,000) = 110,000 psi
Type 2 cycle n_2 = 9000,
S_2 = (50,000 + 0) = 50,000 psi

Step 2: For each value S_1, S_2, . . ., S_n, use the applicable design fatigue curve and corresponding method of analysis to determine the maximum number of stress cycles which would be allowable if this type of cycle were the only one acting. Call these values N_1, N_2, . . ., N_n. The fatigue curve used may be either the S_f plot defined in NC-3649.4(d) or the curve consistent with NC-3649.4(e)(2) or (3). If the fatigue curve has been developed based on a total stress difference, then the full value of S_1, S_2, . . ., S_n, of Step 1 must be used to determine N; however, if the curve is based on an alternating stress, then the values S_1, S_2, . . ., S_n become the alternating stresses.

Step 3: For each type of stress cycle, calculate the usage factors, U_1, U_2, . . ., U_n, from $U_1 = n_1/N_1$, $U_2 = n_2/N_2$, . . ., $U_n = N_n/N_n$.

Step 4: Calculate the cumulative usage factor U from $U = U_1 + U_2 + \ldots + U_n$.

Step 5: The cumulative usage factor U shall not exceed 1.0.

(*h*) The Certificate Holder shall submit a report which demonstrates compliance with NC-3649.

(*i*) Where necessary to carry the pressure, the cylindrical ends of the bellows may be reinforced by suitable collars. The design method used to assure that the stresses generated will not cause premature failure of the bellows material or weldment shall include the attachment weld between the bellows and end connections.

(*j*) The spring rates of the expansion joint assembly shall be provided by the Certificate Holder. The spring rates of a bellows can be defined by several methods due to the hysteresis loop which can occur during deflection; a restoring force may be required to return the bellows to the original neutral position after deflection. When applicable, the Design Specifications shall state the maximum allowable force that can be imposed on the connecting parts or shall require the Certificate Holder to determine the maximum force necessary to deflect the bellows a given distance, such as the maximum movement to be absorbed.

NC-3650 ANALYSIS OF PIPING SYSTEMS

NC-3651 General Requirements[26]

(*a*) The design of the complete piping system shall be analyzed between anchors for the effects of thermal expansion, weight, and other sustained and occasional loads. The system design shall meet the limits of NC-3650. The pressure portion of Eqs. (8) and (9) may be replaced with the expression

$$S_{LP} = B_1 \frac{2Pd^2}{D_o^2 - d^2}$$

The pressure portion of Eq. (11) may be replaced by the expression

$$S_{LP} = \frac{Pd^2}{D_o^2 - d^2}$$

where the terms are the same as in NC-3652, except

$P = P$ or P_{max}, psi
d = nominal inside diameter of pipe, in.

(*b*) When evaluating stresses in the vicinity of expansion joints, consideration must be given to actual cross-sectional areas that exist at the expansion joint.

(*c*) For analysis of flanged joints, see NC-3658.

NC-3652 Consideration of Design Conditions

The effects of pressure, weight, and other sustained mechanical loads must meet the requirements of Eq. (8):

$$S_{SL} = B_1 \frac{PD_o}{2t_n} + B_2 \frac{M_A}{Z} \leq 1.5S_h \qquad (8)$$

B_1, B_2 = primary stress indices for the specific product under investigation (NB-3680)
P = internal Design Pressure, psi
D_o = outside diameter of pipe, in.

[26] The pressure term in Eqs. (8), (9), and (11) may not apply for bellows and expansion joints.

NC-3653 Consideration of Level A and B Service Limits

NC-3653.1 Occasional Loads.[27] The effects of pressure, weight, other sustained loads, and occasional loads, ~~including earthquake~~, for which Level B Service Limits are designated, must meet the requirements of Eq. (9): including nonreversing dynamic loads

$$S_{OL} = B_1 \frac{P_{max} D_o}{2t_n} + B_2 \left(\frac{M_A + M_B}{Z} \right) \leq 1.8 S_h \qquad (9)$$

but not greater than $1.5 S_y$. Terms are the same as in NC-3652, except:

P_{max} = peak pressure, psi

M_B = resultant moment loading on cross section due to ~~occasional loads, such as thrusts from relief and safety valve loads from pressure and flow transients, and earthquake, if the Design Specifications require calculation of moments due to earthquake, in. lb. For earthquake, use only one half the range. Effects of anchor displacement due to earthquake may be excluded from Eq. (9) if they are included in Eqs. (10) and (11) (NC-3653.2).~~ nonreversing dynamic loads

S_y = material yield strength at temperature consistent with the loading under consideration, psi

S_h = material allowable stress at temperature consistent with the loading under consideration, psi

NC-3653.2 Therma' Expansion. For Service Loadings for which Level A and B Service Limits are designated, the requirements of either Eq. (10) or Eq. (11), and Eq. (~~12~~) 11a must be met.

(a) The effects of thermal expansion must meet the requirements of Eq. (10):

$$S_E = \frac{iM_C}{Z} \le S_A \qquad (10)$$

Terms same as above except:

M_C = range of resultant moments due to thermal expansion, in.-lb.; also include moment effects of anchor displacements due to ~~earthquake~~ nonreversing dynamic loads if anchor displacement effects were omitted from Eq. (9) (NC-3653.1)

S_A = allowable stress range for expansion stresses (NC-3611.2), psi

i = stress intensification factor (NC-3673.2)

(b) The effects of any single nonrepeated anchor movement shall meet the requirements of Eq. (10a):

$$\frac{iM_D}{Z} \le 3.0S_c \qquad (10a)$$

Terms same as in NC-3653.2, except:

M_D = resultant moment due to any single nonrepeated anchor movement (e.g., predicted building settlement), in.-lb.

(c) The effects of pressure, weight, other sustained loads, and thermal expansion shall meet the requirements of Eq. (11):

$$S_{TE} = \frac{PD_o}{4t_n} + 0.75i\left(\frac{M_A}{Z}\right) + i\left(\frac{M_C}{Z}\right) \le (S_h + S_A) \qquad (11)$$

$0.75i$ shall not be less than 1.0.

(d) The effects of reversing dynamic loads must meet the requirements of Eq. (~~12~~) 11a

$$S_R = \frac{iM_R}{Z} \le \cancel{S_A}\ 2.0S_A \qquad (11a)$$

Terms same as above except:

MR = range of resultant moments due to inertia and anchor motion effects of reversing dynamic loads

~~3654 Consideration of Level C Service Limits~~

~~r Service Loadings for which Level C Service ts are designated, the conditions of Eq. (9) shall net. In calculating the resultant moment loading the effects of anchor displacement due to earth-e or other secondary effects need not be included. allowable stress to be used for this condition is S_h but not greater than $1.8S_y$~~

~~S_y = material yield strength at temperature consistent with the loading under consideration, psi~~

~~S_h = material allowable stress at temperature consistent with the loading under consideration, psi~~

NC-3654.1 Permissible Pressure. When Level C Service Limits [NCA-2142.4(b)(3) and NB-3113(b) are specified, the permissible pressure shall not exceed the pressure P_a, calculated in accordance with Eq. (5) of NC-3641.1, by more than 50%.

NC-3654.2 Analysis of Piping Components. For Service Loadings for which Level C Service Limits [NCA-2142.4(b)(3) and NB-3113(b)] are designated the requirements of (a) or (b) below shall apply.

(a) For Service Loadings for which Level C Service Limits are designated which do not include reversing dynamic loads or have reversing dynamic loads combined with nonreversing dynamic loads, the conditions of Eq. (9) of NC-3653.1 shall be met using Service Level C coincident pressure P and moments M_i which result in the maximum calcualted stress. The allowable stress to be used for this condition is $2.25S_m$ but not greater than $1.8S_y$.

(b) For Service Loadings for which Level C Service Limits are designated which include reversing dynamic loads that are not required to be combined with nonreversing dynamic loads the requirements of NC-3655(b) shall be satisfied using the allowable stress in NC-3656(b)(2), 70% of the allowable stress in NC-3655(b)(3) and 70% of the allowable loads in NC-3656(b)(4).

NC-3654.3 Deformation Limits. Any deformation or deflection limits prescribed by the Design Specifications shall be considered with respect to Level C Service Limits.

NC-3655 Consideration of Level D Service Limits

~~For Service Loadings for which Level D Service Limits are designated, the conditions of Eq. (9) shall be met. In calculating the resultant moment loading M_B, the effects of anchor displacement due to earthquake or other secondary effects need not be included. The allowable stress to be used for this condition is $3.0S_h$ but not greater than $2.0S_y$.~~

~~S_y = material yield strength temperature consistent with the loading under consideration, psi~~

~~S_h = material allowable stress at temperature consistent with the loading under consideration, psi~~

~~NEW INTRODUCTION TO BE DRAFTED~~

For piping fabricated from material designated P No. 1 thru 9 in Table 2A Section II, Part D, if the Design Specifications specify any Service Loading for which Level D Limits are designated [NCA-2142.2(b)(4)] the requirements of (a), (b) or (c) below shall apply.

(a) For Service Loadings for which Level D Service Limits are designated which do not include reversing dynamic loads or have reversing dynamic loads combined with nonreversing dynamic loads the requirements of (1) and (2) shall apply.

(1) The permissble pressure shall not exceed 2.0 times the pressure P_a calculated in accordance with Eq. (3) of NC-3641.1

(2) The conditions of Eq. (9) of NC-3653.1 shall be met. The allowable stress to be used for this condition is $3.0\ S_m$ but not greater than $2.0\ S_y$.

(b) For Service Loadings for which Level D Service Limits are designated which include reversing dynamic loads that are not required to be combined with nonreversing dynamic loads the requirements of (1) thru (5) shall apply.

(1) The pressure occurring coincident with the earthquake or other reversing type loading shall not exceed the Design Pressure.

(2) The sustained stress due to weight loading shall not exceed the following:

M_W M_W

$$B_2 \frac{D_o}{2I} M_D \leq 0.5\ S_m$$

where

M_D = resultant moment due to weight effects

(3) The stress due to weight and inertial loading due to reversing dynamic loads in combination with the Level D coincident pressure shall not exceed the following:

$$B_1 \frac{P_D D_o}{2t} + B_2 \frac{D_o}{2I} M_E \leq 4.5\ S_m$$

where

P_D = the pressure occurring coincident with the reversing dynamic load

M_E = the amplitude of the resultant moment due to the inertial loading from the earthquake, other reversing type dynamic events and weight. Earthquake and other reversing dynamic loads shall be computed from a linear elastic response spectrum analysis as defined in Appendix N-1226 except the spectrum peak broadening value Δ_{f_g} in N-1226.3 shall not be less than 15 percent and, in place of the damping values for both large and small diameter piping systems in Table N-1230-1 for Operating Basis Earthquake and Safe Shutdown Earthquake, a value of 5 shall be used. The ground motion design input for generating the floor response spectrum to be used in the linear elastic analysis shall meet the requirements of Appendix N-1211(a) and N-1211(b). Moments and forces may be computed using a methodology other than prescribed above if the alternate methodology is demonstrated to produce results which envelope the prescribed methodology results. In the combination of loads, all directional moment components in the same direction shall be combined before determining the resultant moment. If the method of analysis is such that only magnitude without algebraic signs are obtained, the most conservative combination shall be assumed.

(4) The range of the resultant moment M_{AM} and the amplitude of the longitudinal force F_{AM} resulting from the anchor motions due to earthquake and other reversing type dynamic loading shall not exceed the following:

$$C_2 \frac{M_{AM} D_o}{2I} < S_1$$

$$\frac{F_{AM}}{A_M} < S_2$$

where: $S_1 = 6S_m$
$S_2 = 1.0S_m$
A_M = cross-sectional area of metal in the piping component wall

(5) Piping displacements shall satisfy Design Specification limitations.

(c) As an alternative to NC-3655(a) and (b), the rules contained in Appendix F may be used in evaluating these service loadings independently of all other Design and Service Loadings.

NC-3658.3 ANSI B16.5 Flanged Joints With High Strength Bolting. Flanged joints using flanges, bolting, and gaskets as specified in ANSI B16.5 and using bolting material having an S value at 100°F not less than 20,000 psi may be analyzed in accordance with the following rules.

(a) Design Limits and Levels A and B Service Limits

(1) The pressure shall not exceed the rated pressure for Level A Service Limits or 1.1 times the rated pressure for Level B Service Limits.

(2) The limitations given by Eqs. (12) and (13) shall be met:

$$M_{fs} \leq 3125(S_y/36{,}000)CA_b \qquad (12)$$

$$M_{fd} \leq 6250(S_y/36{,}000)CA_b \qquad (13)$$

where the value of Sy/36,000 shall not be taken as greater than unity.

(b) Level C Service Limits

(1) The pressure shall not exceed 1.5 times the rated pressure.

(2) The limitation given by Eq. (17) shall be met:

$$M_{fd} \leq [11{,}250A_b - (\pi/16)D_f^2 P_{fd}]C(S_y/36{,}000) \qquad (17)$$

where the value of Sy/36,000 shall not be taken as greater than unity.

(c) Level D Service Limits

(1) The pressure shall not exceed 2.0 times the rated pressure.

(2) The limitation given by Eq. (17) shall be met, where P_{fd} and M_{fd} are pressures, psi, and moments, in.-lb, occurring concurrently.

The allowable M_{fd} calculated from Eq. (13) shall be increased by 40%.

(d) Test Loadings. Analysis for test loadings is not required.

Appendix II-A: Analytical Study of Frequency Effects on Margins

Prepared by

Dr. C. T. Huang

California Institute of Technology

Supervised by

Dr. W. D. Iwan

California Institute of Technology

Appendix II-B: PFDRP Component Tests Seismic Ratchet-Fatigue Margins

margins developed by

K. R. Jaquay

Energy Technology Engineering Center

data confidence study by

R. P. Kennedy

Structural Mechanics Consulting, Inc.

CIT TEST 14 MARGINS

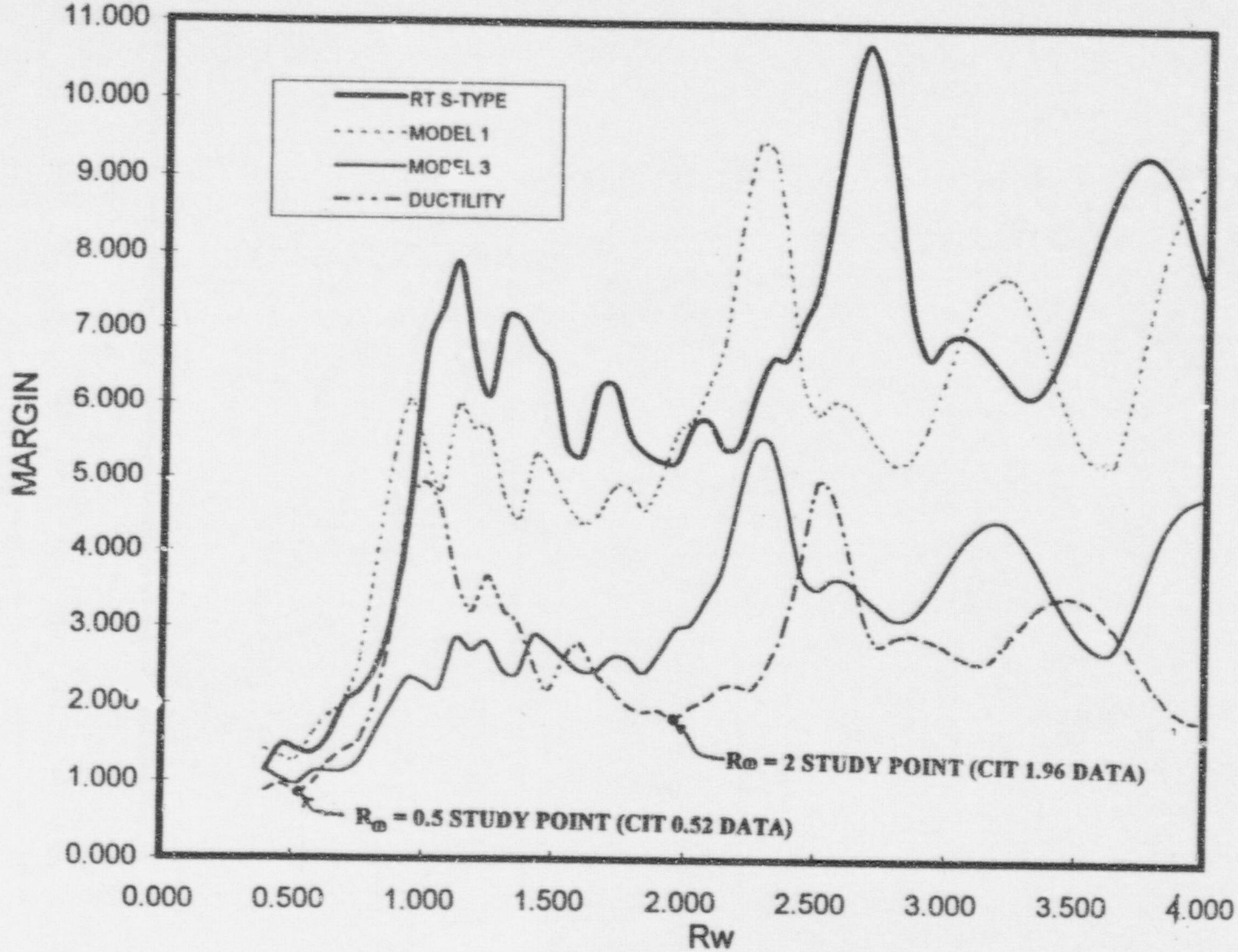

Nominal Properties, 650F CIT MRF Rw = 0.5 and 2.0 Lower Bound Ratchet-Fatigue Margins, **Uncorrelated**

HI LEVEL TEST RUN INERTIA STRESS W/ NOMINALTHK							EVENT CORRECTION			TEST MARGIN			CIT TEMP + FREQ ADJ				
A	B	C	D	E	F_{MOD}	G	H	I	J	K	L	M	T	U_{MOD}	U_{NEW}	V_{MOD}	V_{NEW}
																DYN MRGN	
TEST	B_2 USED	GE BR M5	R = TEST S(Fn)/Sa	TEST BASED $M5_U$	Zn NOM T	B_2M5_U /Z NOM T	GE # OF EVNT	ROT # OF EVNT	EVNT CORR BM/Z	EQ 9 P,WT NOM T	P+WT ADJ 4.5Sm	NOM T TEST MRGN	MEAS Rw	CIT MRF@ 0.5	CIT MRF@ 2.0	Rw 0.5	Rw 2.0
ELBOW TESTS:																	
3	5.51	593	0.85	505	4.35	641	3.5	2.13	935	1.36	88.6	10.6	0.975	0.153	0.325	1.62	3.43
4	3.27	1675	0.80	1340	8.50	516	2.5	2.70	847	0.41	89.6	9.5	0.971	0.158	0.335	1.50	3.17
5	3.27	1741	0.62	1071	8.50	412	3.5	2.40	639	0.41	89.6	7.1	0.919	0.222	0.470	1.58	3.35
6	3.27	1638	0.54	885	8.50	340	3.5	3.40	628	0.41	89.6	7.0	0.875	0.276	0.585	1.94	4.10
7	3.27	1953	0.82	1601	8.50	616	4.5	4.80	1350	0.41	89.6	15.1	0.928	0.208	0.440	3.13	6.63
8	3.27	2004	0.67	1343	8.50	517	5.0	5.10	1167	0.41	89.6	13.0	0.917	0.222	0.470	2.89	6.12
13	4.29	1345	0.77	1033	8.50	521	2.5	3.69	1002	0.78	89.2	11.2	0.957	0.175	0.370	1.96	4.15
19	3.27	1826	0.99	1800	8.50	693	3.0	2.34	1060	0.41	89.6	11.8	0.985	0.144	0.305	1.70	3.61
30	5.51	279	1.00	279	4.35	354	3.0	3.59	670	10.73	79.3	8.5	0.993	0.135	0.285	1.14	2.41
35	3.27	1677	0.71	1198	8.50	461	5.0	4.81	1011	7.74	82.3	12.3	0.932	0.201	0.425	2.47	5.22
OTHERS:																	
9	1.00	2808	0.88	2462	8.50	290	1.5	1.64	393	10.93	79.1	5.0	0.943	0.187	0.395	0.93	1.96
10	1.00	2851	0.79	2246	8.50	264	2.5	1.74	349	6.79	83.2	4.2	0.930	0.203	0.430	0.85	1.80
11	3.35	766	0.49	378	4.35	292	0.5	0.93	281	10.66	79.3	3.5	0.862	0.295	0.625	1.05	2.22
12	1.00	3412	0.72	2444	8.50	288	2.5	2.49	454	10.93	79.1	5.7	0.905	0.241	0.510	1.38	2.93
14	1.00	2373	0.77	1837	8.50	216	1.5	1.69	281	10.93	79.1	3.6	0.917	0.222	0.470	0.789	1.671
15	1.00	1376	0.66	904	3.21	281	5.0	5.69	671	10.11	79.9	8.4	0.903	0.246	0.520	2.06	4.37
16	1.00	3244	0.65	2097	3.21	652	0.5	0.75	565	10.11	79.9	7.1	0.905	0.241	0.510	1.70	3.61
36	1.00	GE UNBR :		1058	8.50	125	0.5	1.37	146	10.93	79.1	1.8	0.779	0.383	0.810	0.71	1.49
38	2.02	2756	0.82	2270	8.50	540	3.6	3.17	961	11.82	78.2	12.3	0.928	0.208	0.440	2.55	5.41

TEST 14 CIT MARGIN:	0.866	1.832
CORRELATION:	1.096	1.096

Nominal Properties, 650F CIT MRF Rw = 0.5 and 2.0 Lower Bound Ratchet-Fatigue Margins, Minimum B_2 = 2, Correlated

HI LEVEL TEST RUN INERTIA STRESS W/ NOMINALTHK							EVENT CORRECTION			TEST MARGIN			CIT TEMP + FREQ ADJ					
A	B	C	D	E	F_{MOD}	G	H	I	J	K	L	M	T	U_{MOD}	U_{NEW}	V_{MOD}	V_{NEW}
																DYN MRGN	
TEST	B_2 USED	GE BR M5	R = TEST S(Fn)/Sa	TEST BASED $M5_U$	Zn NOM T	B_2M5_U /Z NOM T	GE # OF EVNT	ROT # OF EVNT	EVNT CORR BM/Z	EQ 9 P,WT NOM T	P+WT ADJ 4.5Sm	NOM T TEST MRGN	MEAS Rw	CIT MRF@ 0.5	CIT MRF@ 2.0	Rw 0.5	Rw 2.0
ELBOW TESTS:																	
3	5.51	593	0.85	505	4.35	641	3.5	2.13	935	1.36	88.6	10.6	0.975	**0.168**	**0.356**	1.77	3.76
4	3.27	1675	0.80	1340	8.50	516	2.5	2.70	847	0.41	89.6	9.5	0.971	**0.173**	**0.367**	1.64	3.47
5	3.27	1741	0.62	1071	8.50	412	3.5	2.40	639	0.41	89.6	7.1	0.919	**0.243**	**0.515**	1.73	3.67
6	3.27	1638	0.54	885	8.50	340	3.5	3.40	628	0.41	89.6	7.0	0.875	**0.303**	**0.641**	2.12	4.49
7	3.27	1953	0.82	1601	8.50	616	4.5	4.80	1350	0.41	89.6	15.1	0.928	**0.228**	**0.482**	3.43	7.27
8	3.27	2004	0.67	1343	8.50	517	5.0	5.10	1167	0.41	89.6	13.0	0.917	**0.243**	**0.515**	3.17	6.71
13	4.29	1345	0.77	1033	8.50	521	2.5	3.69	1002	0.78	89.2	11.2	0.957	**0.192**	**0.406**	2.15	4.55
19	3.27	1826	0.99	1800	8.50	693	3.0	2.34	1060	0.41	89.6	11.8	0.985	**0.158**	**0.334**	1.87	3.95
30	5.51	279	1.00	279	4.35	354	3.0	3.59	670	10.73	79.3	8.5	0.993	**0.148**	**0.312**	1.25	2.64
35	3.27	1677	0.71	1198	8.50	461	5.0	4.81	1011	7.74	82.3	12.3	0.932	**0.220**	**0.466**	2.70	5.73
OTHERS:																	
9	2.00	2808	0.88	2462	8.50	580	1.5	1.84	786	11.80	78.2	10.1	0.943	**0.204**	**0.433**	2.05	4.35
10	2.00	2851	0.79	2246	8.50	529	2.5	1.74	698	7.66	82.3	8.5	0.930	**0.223**	**0.471**	1.89	3.99
11	3.35	766	0.49	378	4.35	292	0.5	0.93	281	10.66	79.3	3.5	0.862	**0.324**	**0.686**	1.15	2.43
12	2.00	3412	0.72	2444	8.50	575	2.5	2.49	908	11.80	78.2	11.6	0.905	**0.264**	**0.559**	3.07	6.49
14	2.00	2373	0.77	1837	8.50	432	1.5	1.89	562	11.80	78.2	7.2	0.917	**0.243**	**0.515**	1.75	3.70
15	2.00	1376	0.66	904	3.21	563	5.0	5.69	1342	12.15	77.9	17.2	0.903	**0.269**	**0.570**	4.64	9.63
16	2.00	3244	0.65	2097	3.21	1305	0.5	0.75	1130	12.15	77.9	14.5	0.905	**0.264**	**0.559**	3.83	8.11
36	2.00	GE UNBR :		1058	8.50	249	0.5	1.37	292	11.80	78.2	3.7	0.779	**0.419**	**0.888**	1.57	3.32
38	2.02	2756	0.82	2270	8.50	540	3.6	3.17	961	11.82	78.2	12.3	0.928	**0.228**	**0.482**	2.80	5.93
											RPK:	16.8				4.52	9.57

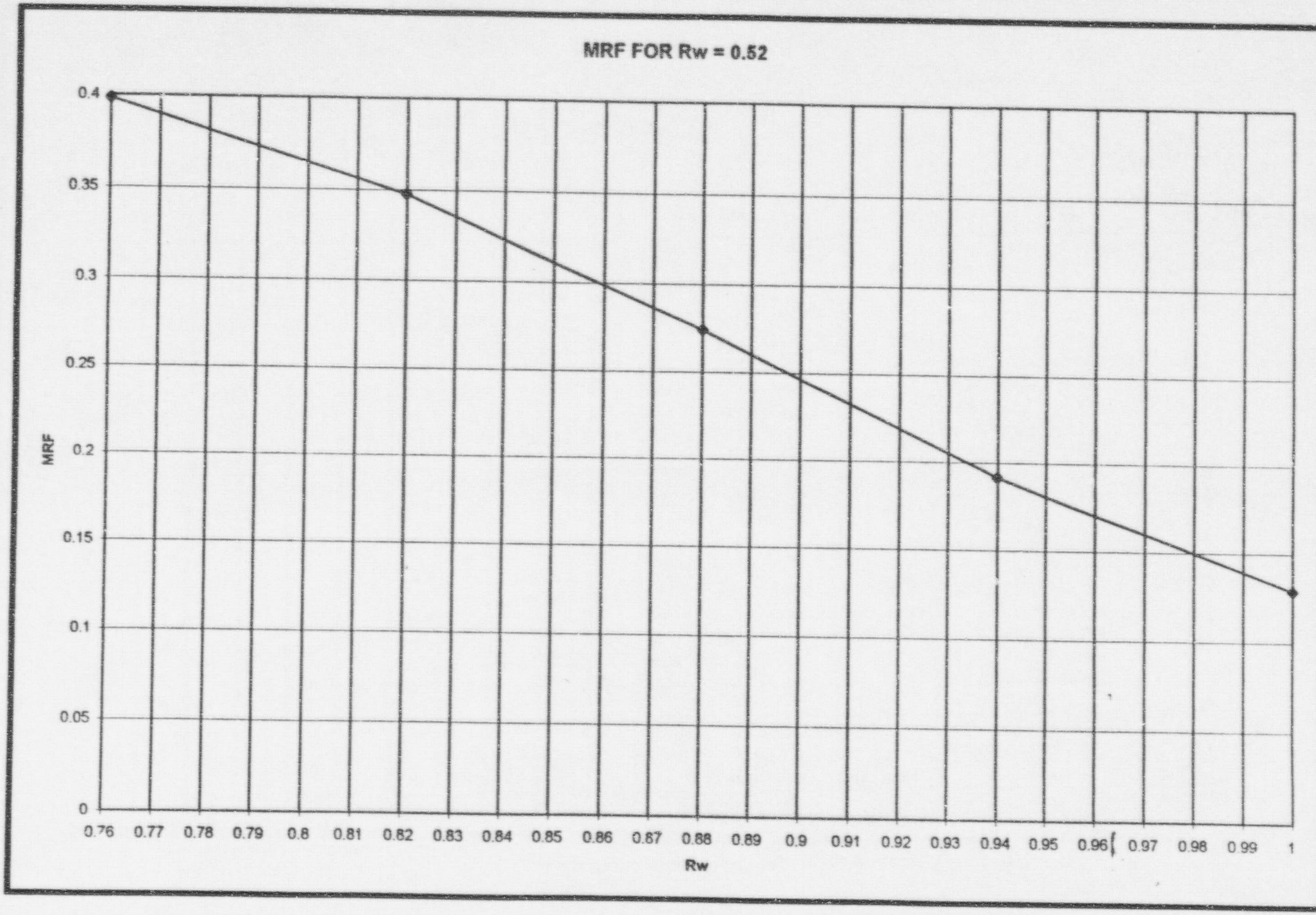
MRF FOR Rw = 0.52
MRF
0.4
0.35
0.3
0.25
0.2
0.15
0.1
0.05
0
0.76 0.77 0.78 0.79 0.8 0.81 0.82 0.83 0.84 0.85 0.86 0.87 0.88 0.89 0.9 0.91 0.92 0.93 0.94 0.95 0.96 0.97 0.98 0.99 1
Rw

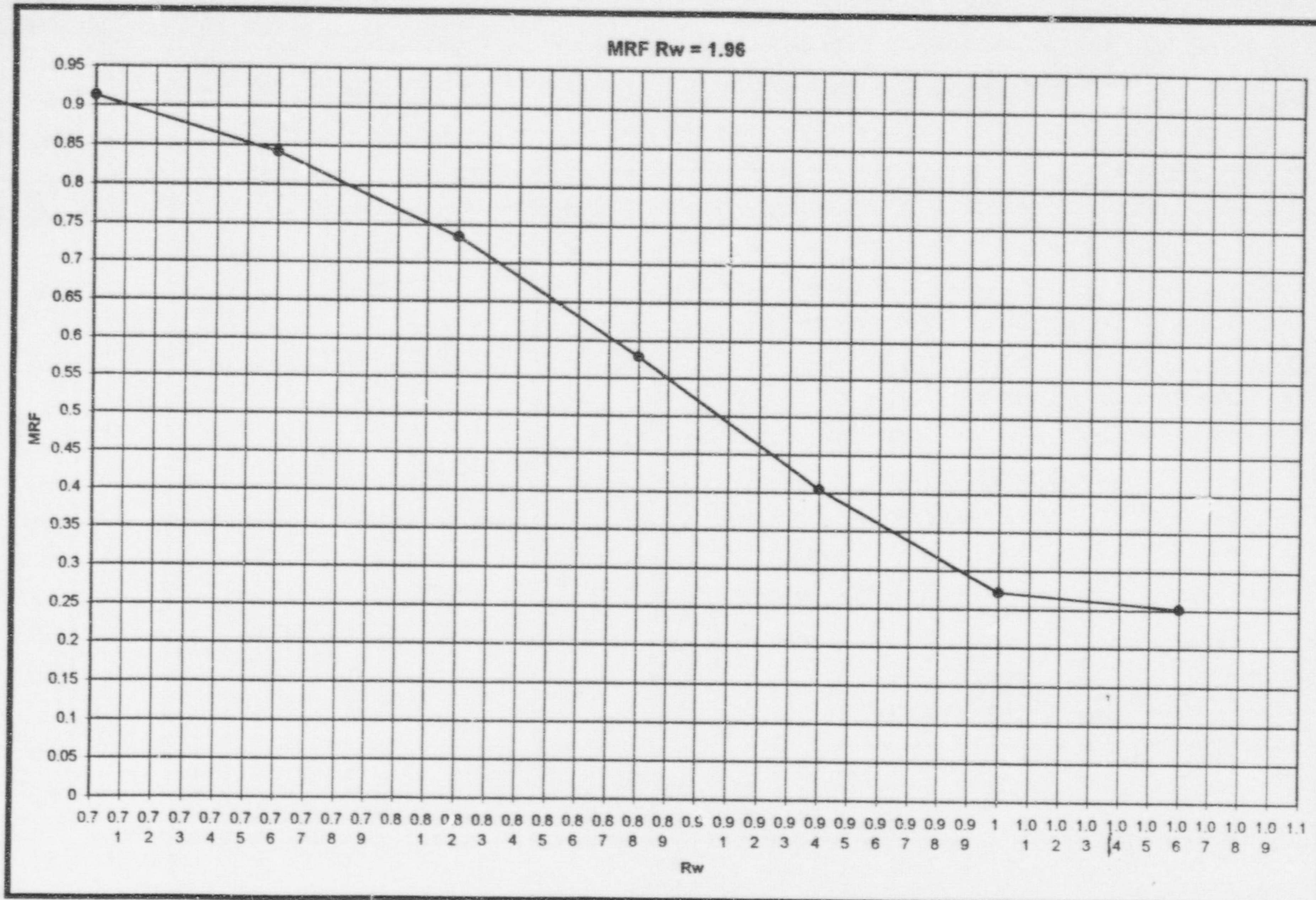
MRF Rw = 1.96
MRF
0.95
0.9
0.85
0.8
0.75
0.7
0.65
0.6
0.55
0.5
0.45
0.4
0.35
0.3
0.25
0.2
0.15
0.1
0.05
0
0.7 0.71 0.72 0.73 0.74 0.75 0.76 0.77 0.78 0.79 0.8 0.81 0.82 0.83 0.84 0.85 0.86 0.87 0.88 0.89 0.9 0.91 0.92 0.93 0.94 0.95 0.96 0.97 0.98 0.99 1 1.01 1.02 1.03 1.04 1.05 1.06 1.07 1.08 1.09 1.1
Rw

Alternate Approach

- Use frequency corrected component test margins to study case of $4.5S_M$ allow, with Min $B_2 = 2.0$

Component	B_2	Event Corrected Test Margin R_{CPT}	Lower Bound Freq. Corr.		Lower Bound Component Margin R_{CP}	
			R_W=0.5	R_W=2.0	R_W=0.5	R_W=2.0
Elbow						
3	5.51	10.6	.168	.356	1.77	3.76
4	3.27	9.5	.173	.367	1.64	3.47
5	3.27	7.1	.243	.515	1.73	3.67
6	3.27	7.0	.303	.641	2.12	4.49
7	3.27	15.1	.228	.482	3.43	7.27
8	3.27	13.0	.243	.515	3.17	6.71
13	4.29	11.2	.192	.406	2.15	4.55
19	3.27	11.8	.158	.334	1.87	3.95
30	5.51	8.5	.148	.312	1.25	2.64
35	3.27	12.3	.220	.466	2.70	5.73
Non Elbow						
9	2.0	10.1	.204	.433	2.05	4.35
10	2.0	8.5	.223	.471	1.89	3.99
11	3.35	3.5	.324	.686	1.15	2.43
12	2.0	11.6	.264	.559	3.07	6.49
14	2.0	7.2	.243	.515	1.75	3.70
15	2.0	16.8	.269	.570	4.52	9.57
16	2.0	14.5	.264	.559	3.83	8.11
36	2.0	3.7	.419	.888	1.57	3.32
38	2.02	12.3	.228	.482	2.80	5.93
$R_{CP50\%}$	=	9.5			2.19	4.63
β_{RCP}	=	0.42			0.37	0.37
$R_{CP1\%}$	=	3.5			0.92	1.94

Problems With Alternate Approach

- Uncorrected test margins are for a very narrow frequency input motion, and are unrealistically high for a broad frequency input motion

- Frequency corrections are extreme lower bound corrections appropriate only for a very narrow frequency input motion

- Scatter of results are very large and are not significantly reduced by applying frequency correction factors

- Because of these issues, all of these results are very controversial and argumentative

- Despite these problems, the $R_W = 2.0$ frequency corrected results might represent a reasonable compromise at least for situations where $R_W > 0.7$.

- Does not include any redundancy margin which exists in actual piping systems but not in component tests

Study Homogeneity of Data

$R_W = 2.0$ Frequency Corrected

	Elbow			Non-Elbow			Combined
	CS	SS	Combined	CS	SS	Combined	
$R_{CP_{50\%}}$ =	4.27	4.53	4.42	4.64	5.00	4.87	4.63
β_{RCP} =	0.23	0.38	0.31	0.49	0.47	0.45	0.37
$R_{CP_{1\%}}$ =							1.94

- Reasonable to combine data into a single data set so long as Min B_2 = 2.0 is used for Non-Elbow data

$R_{CP_{1\%}} \approx 2.0$ for

4.5 S_M Allow

$B_2 \geq 2.0$ Min

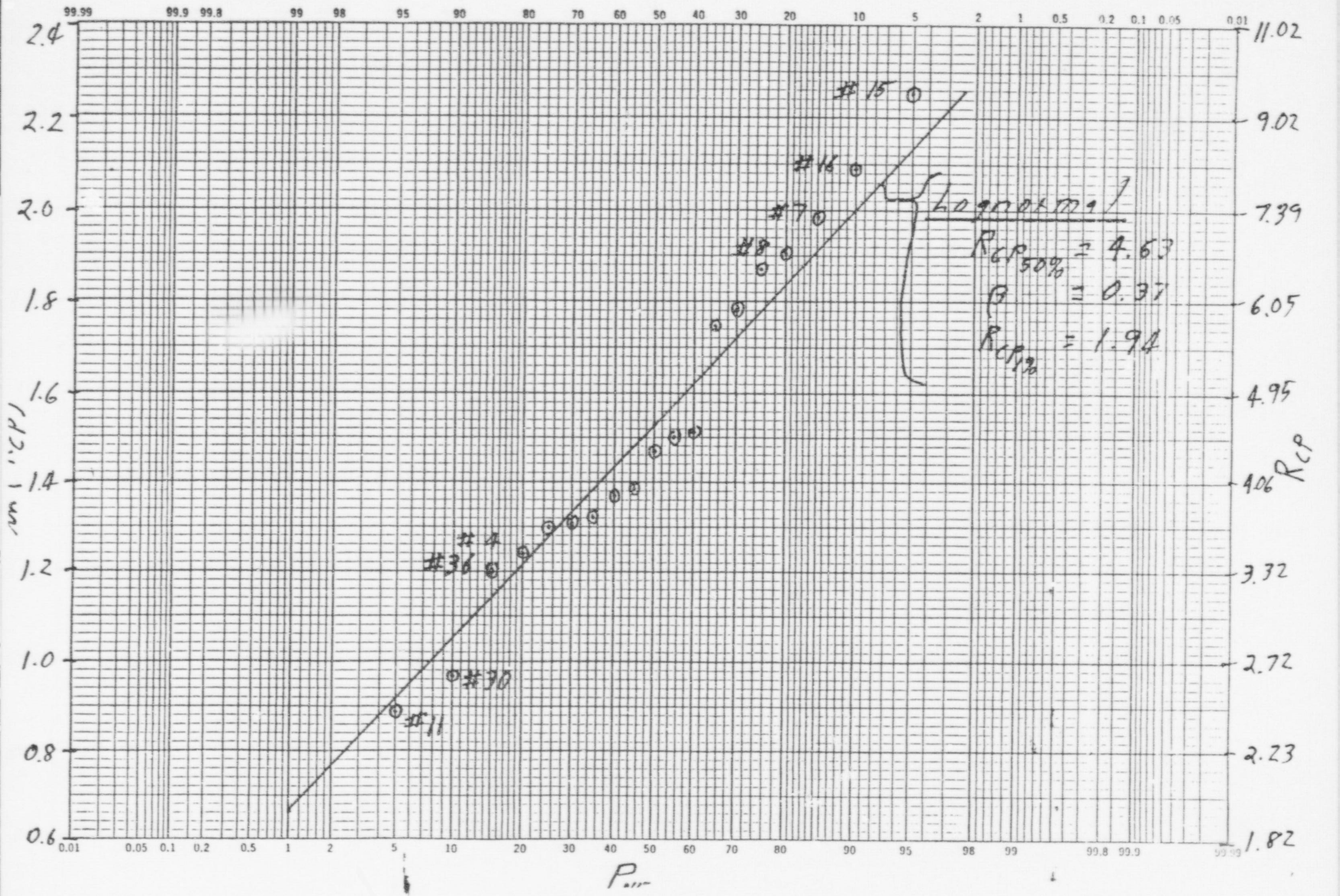
Lognormal
$R_{cp_{50\%}} = 4.63$
$\beta = 0.37$
$R_{cp_{1\%}} = 1.94$
#15
#16
#7
#8
#4
#36
#30
#11
R_{cp}
11.02
9.02
7.39
6.05
4.95
4.06
3.32
2.72
2.23
1.82
2.4
2.2
2.0
1.8
1.6
1.4
1.2
1.0
0.8
0.6
$P_{\ldots}$

Tentative Conclusions

- Data reasonably fits lognormal distribution

- In my judgment, this alternate Margin Approach is suspect, because it contains several adjustment factors on the data, and the resulting Log. Std. Dev. (β) is large

- However, results reasonably support judgment that HCLPF seismic margin is about 2.0 when:

Allowable	: $4.5\ S_M$
So Long As Min	$B_2 = 2.0$

PART III PEER REVIEW GROUP MEMBER INPUTS

1 Introduction

The members of the Seismic Analysis of Piping program's Peer Review Group (PRG) were invited to provide commentaries following their reviews of Part I of this report. They were also asked to review and comment on R. Kennedy's write-up "Using Component Test Data in Establishing Code Criteria to Achieve the Desired Seismic Capacity Margin for Piping" contained in Attachment 2 to Appendix III-B of this report. Part III of this report contains these PRG member commentaries as separate appendices, in alphabetical order of last names.

Appendix III-A is the inputs from Professor Bill Iwan at the California Institute of Technology (CIT). The opinions expressed are those of Dr. Iwan as an individual, and should not be construed as representing in any way the position of CIT. Dr. Iwan concludes there is insufficient basis for the current ASME seismic code provisions for nuclear piping systems and the new rules can lead to inadequate margin of safety in both stiff and flexible piping. He discusses the basis for his conclusion. Although he supports system displacement-based criterion as the best approach, he concurs with the Kennedy component moment control design approach as the best alternative. He raises some issues with Kennedy's approach and the adequacy of the current data base to resolve them. He concludes with a list of studies that are needed to confirm the validity of Kennedy's moment control design approach.

Appendix III-B is the inputs from Dr. Robert Kennedy at Structural Mechanics Consulting, Inc.. Dr. Kennedy is of the opinion a number of open issues exist with the new rules and the previously published technical basis for the new rules is inadequate. He considers the issues resolvable under a proper focus of involved parties provided a candidate path forward can be identified and agreed upon. Towards that end, in his Attachments 1 and 2 he suggests a seismic capacity margin approach using ultimate dynamic moments achieved in component tests that will resolve most of the issues and achieve sufficient conservatism in piping design so that piping does not control the High-Confidence-Low-Probability-of-Failure (HCLPF) seismic margin of the nuclear power plant. His only significant reservation is that nonlinear or pseudo-linear methods are needed to realize the full nonlinear dynamic benefit existing in the majority of piping systems. Lacking such, excess conservatism will be typically introduced by his approach to address the odd case.

Appendix III-C is the inputs from Everett Rodabaugh at E.C. Rodabaugh and Associates. Rodabaugh provides a series of letters that study the test demonstrated dynamic moment capacity issue central to the seismic capacity margin approach suggested by Kennedy. Special attention is given to the Test 37 results which do not follow the higher than static data trend observed in other PFDRP component tests. He provides an approximation for the pressure effects on elbow behavior that may be a contributor to this outlier behavior.

Appendix III-D is the inputs from Larry Shipley at ARES Corporation. Shipley is concerned the ETEC evaluation has become an increasingly academic exercise and may be diverging from the objective of providing realistic criteria. He recommends the approval of the current criteria for a subset of piping systems in order to obtain actual use of the criteria needed to assess the risk/benefit the new criteria brings. He is critical of the extrapolation of the collapse failure mode observed in the component tests to piping systems that are within the bounds of good engineering practice and disputes the importance of near-field events. He also supports a ductility control approach rather than a factored load approach to assuring adequate pipe support design.

Appendix III-E is the inputs from Dr. Edward Wais at Wais and Associates, Inc.. Dr. Wais is of the opinion that the basis for the new rules was incomplete and that while one can argue with the details of the data reductions, it still has not been demonstrated that sufficient margin exists with the new rules. He points out the ASME has established a Special Working Group - Seismic Rules that has identified over 40 specific issues identified with the new rules, including all of those identified in the ETEC effort. He believes there is now an improved understanding of piping behavior that provides a basis for establishing rules with a complete justification. He supports consideration of Kennedy's "ultimate moment" approach.

Appendix III-F is the inputs from Dr. Gery Wilkowski at Battelle-Columbus. The input was co-authored by his co-worker R. J. Olsen. They believe that the new rules are in need of further validation before they are deemed acceptable. The basis for this position are weaknesses in six technical areas; (1) incomplete material selections and use of room temperature tests only in the PFDRP component test program, (2) testing lacked components with Code allowable workmanship flaws, (3) testing lacked concurrent restrained thermal expansion and seismic anchor loading, (4) margin data reductions did not account for actual loading, use of greater than Code minimum strength test components nor actual failure location, (5) the test time history was not adequately characterized as to damage propensity and (6) specific issues exist with the margin definition, lack of published details of the REMS analytical extrapolations and the choice of stress indices.

Appendix III-A: W. Iwan Inputs

Seismic Analysis of Piping Peer Review Group Report

Submitted by W. D. Iwan
California Institute of Technology

Conclusions

Based upon information presented up to the time of the meeting of the Seismic Analysis of Piping Peer Review Group held on July 15-16 at the NRC office in Rockville, MD and the ensuing discussions, it is concluded that there is insufficient basis for the current ASME seismic code provisions for nuclear piping systems. Furthermore, it is concluded that the current code provisions provide an inadequate margin of safety for some piping system components in both the stiff and flexible system frequency ranges. However, it appears that an adequate seismic margin may be assured if a relatively simple change is made to the current code provisions.

Basis for Conclusions

The recently completed studies of frequency and temperature effects on seismic margin indicate the following:

1. The results of the new study of frequency effects differ significantly from the previous REMS results which were used by ASME in the development of the new code provisions both as regards the nature of the margin versus frequency relationship and the level of input acceleration required to cause failure.
2. Collapse failure of piping systems cannot be ruled out, especially for soft (long period or high R_w) piping systems.
3. The level of ASME seismic code margin obtained in the new study is strongly dependent on the earthquake input employed. There is a high degree of variability in the margin results for different piping frequencies and input accelerograms. This variability must be taken into account when interpreting the margin results.
4. For narrow-banded PFDR and broad-banded RG 1.60 type inputs, ASME code margins of the order of one are routinely observed for stiff (short period or low R_w) systems.
5. For narrow-banded PFDR-type inputs, displacement-based margins for soft (long period or high R_w) systems may be as low as two.
6. For narrow-banded PFDR-type inputs, the level of acceleration required to cause failure generally decreases with increasing piping system flexibility (increasing period or R_w), rather than increasing as indicated by previous REMS studies.
7. Displacement-based margins are generally significantly lower than fatigue-based margins for flexible piping system.
8. There is a strong correlation between margin and level of acceleration required to cause failure.
9. The degree of fatigue damage can be very sensitive to the level of input acceleration, particularly for systems with a large P-Δ moment.

10. Both the fatigue-based and collapse-based failures observed in the new study are associated with large deformations of the piping components corresponding to highly ductile nonlinear material behavior. Therefore, excessive deformation appears to be the primary factor leading to both fatigue and collapse failure.

Recommendations

It is the writer's opinion that the best approach to insuring the safety of piping systems would be to place deformation limits on the dynamic response of the piping components. These limits would be selected to allow a significant degree of ductile behavior while limiting the possibility of low cycle fatigue or collapse failure. Based on the test results, it would appear that limiting the response deformations to the equivalent of a ductility of four would be acceptable. It would be acceptable for design purposes to demonstrate satisfaction of the deformation limits using a linear analysis with prescribed viscous damping.

Although deformation limits are generally preferred by the writer, in design practice it may be easier to place limits on the moment that can be safely applied to each piping component. This is basically the approach suggested by Dr. Kennedy. The writer concurs with this approach as the best alternative to a displacement-based criterion.

Kennedy has shown that a 1% probability of failure code capacity factor, R_{CP}, of at least 2.0 is adequate to assure that piping does not become a significant contribution to the seismic risk of a nuclear power plant. This corresponds to a HCLPF seismic margin of 1.4-1.5 which is somewhat higher than that projected for existing plants (about 1.25). Kennedy argues that the 1% $R_{CP}\geq 2$ condition can be achieved if the corresponding 1% exceedance ratio, F_S, of the ultimate moment capacity of the piping components to the code-based moment is greater than or equal to 1.5. This condition being independent of any earthquake duration or cycle count considerations.

From the test data, the above condition on F_S is satisfied for the collection of elbow components tested near resonance using the current ASME code evaluation procedure with 4.5 S_M. It is not satisfied for the collection of non-elbow components including those for which $B_2=1$. However, the condition will be satisfied if the value of B_2 is not allowed to be less than 2.0. Test 37 appears to represent a special case that needs further consideration. Based on these observations, Kennedy suggests using the current ASME criterion of 4.5 S_M but requiring the B_2 index to be greater than or equal to 2.0 for all components. Since the B_2 index is not really applicable for this type of analysis, the introduction of a new index (β_2?) is recommended in its place. The Kennedy approach is believed by the writer to be sound and should insure adequate seismic margins for seismic inputs of the types considered.

For the PFDR and RG 1.60 input motions considered in the present study, failure appears to be largely dependent on the peak amplitude of the response while the time history of the response, including fatigue cycles and duration effects, plays only a secondary role. This might not be the case for some other types of input motions, particularly those of long duration. For such cases, the fatigue margin may be lower than the displacement margin for low R_w systems.

Another concern about the proposed approach is that it seems to be on the conservative side for the near-resonance condition and would leave some significant excess margin for the number of piping components that were observed to have F_S values considerably in excess of

1.5. It would be appropriate to allow this margin to be recovered by the designer if it could be demonstrated that the maximum moment based on linear analysis did not exceed 1.5 times the ultimate moment of the component as determined from static tests of a validated finite element analysis.

Issues Requiring Further Study

It is believed that the following issues warrant further study in order to confirm the validity of the proposed moment control design approach that has been endorsed by the author. These studies may also reveal whether the proposed approach is overly conservative.

1. The effect of prior fatigue damage due to normal aging and transient pressure events should be investigated. This would be a straight forward study using the models developed for the current margin versus frequency study. All that would be required is to begin the margin calculation with some non-zero level of fatigue cumulative usage factor.

2. A long duration input motion should be examined in order to extend the present off-resonance margin results and verify the assumptions of the Kennedy approach or any other response amplitude based approach for this case.

3. Test 37 requires further study to resolve apparent inconsistencies with other test data as regards the ratio of ultimate to code moment.

4. The effects of unsymmetric elbow hysteresis loops on the seismic margin would be investigated to confirm that the proposed moment controlled design approach is valid for these cases.

Appendix III-B: R. Kennedy Inputs

Peer Review Comments Concerning
ETEC Studies of New ASME
Code Criteria for Seismic Design of Piping

by

Robert P. Kennedy
July 1997

The new ASME code criteria for the moment capacity M_{CODE} of piping components subject to seismic loads is:

$$M_{CODE} = \left[4.5S_M - \frac{B_1PD_0}{2t}\right]\frac{Z_N}{B_2} \qquad (1)$$

ETEC has been reviewing the technical basis for this revised criteria. In particular ETEC has extensively reviewed the EPRI dynamic piping component test data and its usage in justifying Eqn. (1).

The ETEC report *"Seismic Analysis of Piping-Vol. 1: Issue Identification"* does an excellent job of identifying issues and concerns associated with the prior technical basis for Eqn. (1). Clearly a number of open issues exist and the previously published basis is inadequate. However, I believe it would be inappropriate to stop with just identifying issues and concerns. A practical way forward to resolve most of these issues can and should also be presented. In this regard, hopefully the remainder of my comments will be helpful.

Previously (see Attachment 1) I recommended that a desirable goal for piping seismic design criteria would be to design piping systems sufficiently conservatively that piping did not control the High-Confidence-Low-Probability-of-Failure (HCLPF) seismic margin of the nuclear power plant. In this way piping would not become an important contributor to the overall seismic risk of the plant. Furthermore, I suggest in Attachment 1 that this goal is reasonably achieved so long as the 1% non-exceedance probability (NEP) Seismic Capacity (Code) Margin $R_{CP_{1\%}}$ is about 2.0.

In Attachment 2, I suggest an approach to use the data presented in the ETEC Volume 1 together with the many nonlinear piping studies conducted by Cal Tech for ETEC to reasonably conservatively establish a Code Moment Capacity M_{CODE} so as to achieve $R_{CP_{1\%}}$ of at least about 2.0 for a wide variety of piping systems, differing seismic inputs, and both low cycle fatigue and excessive displacement (collapse) failure modes. My recommendations are summarized below.

The ultimate moment M_{UD} achieved under dynamic cyclic loading appears to be a stable and predictable parameter which is reliably reached prior to failure irrespective of whether the ultimate failure mode is low cycle fatigue or excessive deformation. Therefore, it is recommended that the Code Moment Capacity M_{CODE} be established based upon:

$$M_{CODE} = \frac{M_{UD_{1\%}}}{F_S} \qquad (2)$$

where $M_{UD_{1\%}}$ is the 1% non exceedance probability (NEP) ultimate dynamic moment capacity demonstrated in the dynamic component tests and F_S is an appropriate strength factor of safety. Based upon my interpretation of the Cal Tech nonlinear studies, I suggest that F_S should lie in the 1.1 to 1.5 range in order to reliably achieve an overall 1% NEP seismic capacity (code) margin $R_{CP_{1\%}}$ of about 2.0. The remainder of this capacity margin is accommodated by nonlinear-dynamic behavior and redundancy benefits.

With the exception of Elbow Component #37, I show that the 1994 Addenda ASME Code Moment Capacity Eqn. (1) with an allowable stress of $4.5S_M$ reliably achieves a strength factor of safety F_S of at least 1.5 for Elbows. However, Eqn. (1) does not reliably achieve an adequate F_S for Non-Elbow Components when $B_2 < 2.0$. Two alternates are proposed to overcome this deficiency.

I prepared Attachment 2 not because I believe it is necessarily the final answer. However, I present it as a possible way forward to resolve many, but not all, of the important open issues. Two major open issues which need more work are:

1. Why did Elbow Component #37 excessively deform at a M_{UD} so low that M_{CODE} from Eqn. 1 provides a strength factor F_S of only about 1.0 for this component, whereas Elbow Component #30 which is essentially identical and was tested with essentially identical input has a M_{UD}/M_{CODE} ratio of 1.6? The only apparent difference was that the hoop pressure stress $\left(\frac{PD}{2t}\right)$ was approximately 10 ksi for Component #30 and zero for Component #37.

2. All the tested components were at room temperature. What adjustments if any need to be made to Eqn. (1) for application at elevated temperature?

My major concern is that a path forward is needed. Otherwise I fear that people will look at all of the identified open issues and concerns and just give up. Volunteer committees are likely to disband without a clear path to resolution. Then all of the extremely valuable Industry and NRC sponsored research together with the many hundreds of volunteer committee hours will have been wasted. I reject the notion that most of the open issues and concerns are nct resolvable so long as all parties are focused on seeking reasonable and technically justifiable compromises, and a candidate path forward has been identified and agreed upon. The ongoing ETEC and Cal Tech studies provide the necessary data base expansion to enable such forward progress so long as all parties involved wish to progress.

My only significant reservation with my proposed "strawman" path forward summarized in Attachment 2 is that the resulting Seismic Capacity Margin R_{CP} is likely to be exceedingly and unnecessarily high for the majority of piping systems. However, this likely excessive margin is generically unreliable because generically large nonlinear dynamic benefits are unreliable as is shown in the Cal Tech studies. The only way I know of to avoid this problem that the average Seismic Capacity Margins are likely to be exceedingly and unnecessarily high would be to perform either nonlinear or pseudo-linear piping evaluations against a strain or inelastic rotation failure criteria in order to reasonably account for the nonlinear dynamic and redundancy benefits that exist for the specific situation being analyzed. Short of performing such analyses, I recommend living with the excessive conservatism which will be typically introduced by establishing the Code Moment Capacity M_{CODE} from Eqn. (2) with an appropriately low F_S so as to avoid unconservatism for the odd case where the nonlinear dynamic benefit is low.

Establishing the Required Seismic Margin for Piping Systems in Nuclear Power Plants

Robert P. Kennedy
May 1995

1. Introduction & Background

Dr. Nilesh Chokshi of the U.S. Nuclear Regulatory Commission (NRC) and Dr. W. Paul Chen of ETEC have requested that I document my thoughts concerning how one might establish the required seismic margin for piping systems in nuclear power plants. This brief report attempts to summarize my initial thoughts on this matter.

First, the required seismic margin for a piping system will depend upon the required seismic margin for the plant as a whole for some damage state such as seismic induced core damage. Currently, the NRC has requested that all existing plants define their plant seismic margin in terms of the High-Confidence-Low-Probability-of-Failure (HCLPF) seismic capacity. The seismic margin for the design basis Safe Shutdown Earthquake (SSE) is then defined by the ratio R_H between the HCLPF and SSE ground motion levels, ie.,

$$R_H = \left(\frac{HCLPF}{SSE} \right) \quad (1)$$

Initially, the HCLPF seismic capacity was defined as the level at which one had approximately 95% confidence of less than about 5% probability of failure. However, in Ref. 1 the NRC has suggested that this HCLPF seismic capacity can be approximated as the 1% composite (mean) probability of failure. With this approximation, one does not have to separate their estimates of variability into "uncertainty," and "randomness," but can work with a single composite (mean) fragility curve which defines mean probability of failure versus ground motion level. For simplicity, this composite (mean) approximation of the HCLPF capacity will be used herein.

After anchorage, seismic-interaction, or other significant deficiencies caught as a result of a careful seismic walkdown of a plant have been corrected, seismic probabilistic risk assessments (PRA) and seismic margin studies conducted on existing nuclear power plants have reported (Ref. 2) that:

$$R_H \geq 1.25 \quad (\textit{Existing Plants}) \quad (2)$$

RPK Structural Mechanics Consulting, Inc.
18971 Villa Terrace, Yorba Linda, CA 92686 • (714) 777-2163

In addition, as a target goal for the standardized Advance Light Water Reactor (ALWR), the NRC has suggested:

$$R_H \geq 1.67 \quad (ALWR) \tag{3}$$

These levels for R_H will be used herein to establish the required seismic margin for piping systems.

In addition, based upon current seismic design criteria, seismic PRA and seismic margin studies have concluded that piping is not a significant contributor to the seismic risk of a nuclear power plant and does not control the High-Confidence-Low-Probability-of-Failure (HCLPF) seismic capacity of the plant. A desirable goal is to not liberalize piping seismic design criteria so much that piping begins to control the HCLPF seismic capacity of the plant.

However, because of the large number of at-least partially independent piping segments, piping will control the plant HCLPF capacity unless piping has substantially less than a 1% Prob. Of Failure at the Plant HCLPF capacity. In order to provide reasonable assurance that piping will not control the plant HCLPF capacity, I suggest that the probability of failure P_{Pf} of a piping segment be limited to about 0.1% at the plant HCLPF seismic capacity level, ie.:

$$P_{P_f} \leq 0.1\% \quad at \quad Plant \quad HCLPF \quad Level \tag{4}$$

2. <u>Derivation of Required Seismic Margin for Structures and Other Components</u>

The ratio of the median (50% probability of failure) seismic capacity of any component to the design basis SSE can be defined by a median factor of safety $F_{50\%}$ given by:

$$F_{50\%} = \left(\frac{Median}{SSE}\right) \tag{5}$$

This median factor of safety can be defined by the product of the median capacity factor $F_{C50\%}$, and the median response factor of conservatism, $F_{R50\%}$, ie.:

$$F_{50\%} = \left(F_{C_{50\%}}\right)\left(F_{R_{50\%}}\right) \tag{6}$$

The variability (logarithmic standard deviation or approximate coefficient of variation), β, on the factor of safety can be obtained by adding capacity and response variances (β_C^2 and β_R^2, respectively) or:

$$\beta^2 = \beta_C^2 + \beta_R^2 \tag{7}$$

Since the plant HCLPF is defined at the 1% probability of failure, then:

$$R_H = F_{50\%} e^{-2.326\beta} \tag{8}$$

where (-2.326) is the standardized normal coefficient corresponding to the 1% probability of failure.

The code minimum ultimate, code limit-state, or code Service Level D capacities that I have investigated all lead to a capacity margin $R_{C1\%}$ greater than unity on the 1% non-exceedance probability (NEP) capacity. Thus:

$$F_{C_{50\%}} = R_{C_{1\%}} e^{2.326\beta_c} \tag{9}$$

Similarly, in my judgment, response analyses conducted in accordance with the Standard Review Plan (SRP) are aimed at defining the seismic response at the 84% NEP. However, because of either excess conservatism in some aspects of the SRP response requirements, or because of excess conservatism introduced by the analyst, most response analyses achieve a response margin $R_{R84\%}$ greater than unity when compared to a probabilistic computed 84% NEP response. Thus:

$$F_{R_{50\%}} = R_{R_{84\%}} e^{\beta_R} \tag{10}$$

By combining Equations (6) through (10):

$$R_H = (R_{C_{1\%}})(R_{R_{84\%}})(f_\beta) \tag{11}$$

where:

$$f_\beta = e^{\beta_R - 2.326(\beta - \beta_C)} \tag{12}$$

However, for structures and most other components, the factor f_β will be very close to unity over the likely range of β_C from 0.2 to 0.4 and β_R from 0.2 to 0.3 as is shown in Table 1. Therefore, R_H may be closely approximated by:

$$R_H \approx (R_{C_{1\%}})(R_{R_{84\%}}) \qquad (13)$$

Thus, to approximately achieve a seismic margin ratio R_H defined as the ratio of the HCLPF/SSE capacity, it is sufficient to establish the capacity margin $R_{C1\%}$ above the 1% NEP capacity and to establish the response margin $R_{R84\%}$ on the 84% NEP response. Equation (13) can then be used to estimate R_H without having to explicitly estimate the variabilities β_C and β_R. Equation (13) defines the essence of the Conservative-Deterministic-Failure-Margin (CDFM) method for finding the HCLPF seismic capacity.

For structures, and other non-distribution system components, I have estimated that:

$$R_{C_{1\%}} = 1.25 \text{ to } 1.9 \qquad (14)$$

My lower estimate of 1.25 corresponds to brittle failure modes where there is negligible inelastic energy absorption such as a welded connection, or out-of-plane shear failure of a concrete member without shear reinforcement. My high estimate is for ductile failure modes with significant inelastic energy absorption capability defined as the ratio by which linear elastically computed responses can exceed the ultimate capacity for oscillatory, limited duration dynamic events.

Based upon my review of design basis response analyses, for structures and other non-distribution system components I estimate that:

$$R_{R_{84\%}} = 1.0 \text{ to } 2.0 \qquad (15)$$

At low elevations for structures founded on rock, $R_{R84\%} = 1.0$ for response analyses which satisfy the SRP. Higher values often occur at higher elevations and for structures embedded in soil. However, there is no consistency in these higher values so that they cannot be counted upon to reduce the required capacity margin $R_{C1\%}$. In my judgment, all that can be counted upon is:

$$\begin{aligned} R_{R_{84\%}} &\geq 1.0 \quad \text{(Existing Plants)} \\ R_{R_{84\%}} &\geq 1.25 \quad \text{(ALWR)} \end{aligned} \qquad (16)$$

The estimate that $R_{R84\%} \geq 1.25$ for standardized ALWR plants is based on the design seismic responses for these plants being an envelope of the responses computed for many sites and thus being conservative for any particular site.

Thus, combining Equations (13) and (16) with the plant seismic margin R_H goals defined by Equations (2) and (3):

	R_H	$R_{R_{84\%}}$	$R_{C_{1\%}} = \left(R_H / R_{R_{84\%}}\right)$
(Existing Plants)	1.25	1.0	1.25
(ALWR)	1.67	1.25	1.33

In conclusion, for structures and other non-distribution system components, I believe an adequate capacity margin $R_{C1\%}$ on the 1% probability of failure capacity is in the range of 1.25 to 1.33. However, I do not believe that this is an adequate capacity margin for distribution systems such as piping which have a large number of at-least partially independent failure locations (segments).

3. Derivation of Required Seismic Margin for Piping and Other Distribution Systems With Large Numbers of Segments

As summarized in Equation (4), I recommend that the probability of failure P_{Pf} for piping and other multiple segment distribution systems be limited to about 0.1% at the plant HCLPF level. To achieve this lesser probability of failure, Equations (11) and (12) must be modified for piping as follows:

$$R_{CP_{1\%}} = \left(R_H / R_{RP_{84\%}}\right)\left(f_{\beta P}\right)^{-1} \tag{17}$$

where:

$$f_{\beta P} = e^{\beta_{RP} + X_{CP}\beta_{CP} - X_{fP}\beta_P}$$
$$X_{CP} = 2.326 \quad (1\%\text{NEP}) \tag{18}$$
$$X_{fP} = 3.090 \quad (0.1\%\text{NEP})$$

and the subscript P refers to piping specific estimates.

For distributed piping systems, the capacity variability β_{CP} and possibly the response variability β_{RP} are typically larger than those tabulated in Table 1 for structures and other non-distribution system components. In addition, the coefficient X_{fP} of 3.090 in Equation (18) for $f_{\beta P}$ associated with 0.1% NEP is larger than the corresponding coefficient of 2.326 in Equation (12) for f_β associated with 1% NEP. Table 2 presents the resulting estimates for $(f_{RP})^{-1}$ for piping systems. Note that $(f_{\beta P})^{-1}$ is nearly constant over the estimated typical ranges of β_{CP} and β_{RP}. The mean value $(\bar{f}_{\beta P})^{-1}$ is 1.42 with a small coefficient of variation (COV) of 0.07. I recommend that $(f_{RP})^{-1}$ be taken at about the 84% NEP level given by:

$$(f_{\beta P})^{-1} = (\bar{f}_{\beta P})^{-1}(1+COV) \approx 1.50 \tag{19}$$

For piping the response margin $R_{RP84\%}$ is highly variable and is often excessively conservative particularly at high elevations in structures at frequencies near resonance with the structure frequencies. In my judgment:

$$R_{RP_{84\%}} = 1.0 \quad \text{to} \quad 4.0 \tag{20}$$

Here again, at low elevations for structures founded on rock, $R_{RP84\%} = 1.0$ for response analyses which satisfy the SRP. Therefore, I don't see how one can take credit for the potentially excess but highly uncertain conservatism in $R_{RP84\%}$. I recommend setting $R_{RP84\%}$ equal to $R_{RP84\%}$ from Equation (16).

Thus, from Equations (17) and (18):

	$\left(R_H/R_{RP_{84\%}}\right)$	$R_{CP_{1\%}}$
(Existing Plants)	1.25	1.875
(ALWR)	1.33	2.0

In conclusion, I recommend that an adequate capacity margin $R_{CP1\%}$ on the 1% probability of failure piping capacity is in the range of 1.875 to 2.0.

However, it may not be possible to define the 1% probability of failure piping capacity from a limited number of component seismic tests. Therefore, it may be necessary to define the required capacity margin $R_{CPY\%}$ in terms of some higher Y% probability of failure. At a Y% other than 1%, the desired stability of $(f_{\beta P})^{-1}$ shown in Table 2 for Y = 1% will not be so well achieved. For example at Y = 5% the Coefficient of variation (COV) increases to 0.12 versus 0.07 at Y = 1%. Even so, this COV is still reasonably small. For Y > 1% the largest $(f_{\beta P})^{-1}$ will always occur at the largest typical β_{CP} of 0.6. Therefore, at some other Y% probability of failure, the required capacity margin $R_{CPY\%}$ can be slightly conservatively estimated from:

$$R_{CP_{Y\%}} = \left(R_{CP_{1\%}}\right)e^{\alpha\beta_{CP\,max}} \tag{21}$$

where:

$$\beta_{CP_{max}} = 0.6$$
$$\alpha = 2.326 - X_{CP_{Y\%}}$$

Y	$X_{CP_{Y\%}}$	α	$\left(R_{CP_{Y\%}}/R_{CP_{1\%}}\right)$
1%	2.326	0	1.0
2%	2.054	0.272	1.175
3%	1.881	0.445	1.30
5%	1.645	0.681	1.50

Thus, if $R_{CP_{1\%}} = 2.0$ is deemed sufficient for piping as per my recommendation, then:

Y	$R_{CP_{Y\%}}$
1%	2.0
2%	2.35
3%	2.6
5%	3.0

The required capacity margin for piping on the Y% probability of failure seismic capacity can be specified by any of these $R_{CP_{Y\%}}$ values. Thus, for the 1% to 5% probability of failure capacities, the required seismic capacity margin should range from about 2.0 at 1% NEP capacity to 3.0 at the 5% NEP capacity.

Table 1

Typical Values for Factor f_β for Structures
and Other Non-Distribution System Components

β_C	f_β	
	$\beta_R = 0.2$	$\beta_R = 0.3$
0.2	1.01	0.93
0.3	1.06	1.01
0.4	1.09	1.07

Table 2
Typical Values for Factor
$f_{\beta P}$ for Piping Systems

β_{CP}	$(f_{\beta P})^{-1}$		
	$\beta_{RP} = 0.2$	$\beta_{RP} = 0.3$	$\beta_{RP} = 0.4$
0.3	1.24	1.37	1.56
0.4	1.29	1.37	1.52
0.5	1.35	1.40	1.52
0.6	1.43	1.46	1.54

References

1. "Procedural and Submittal Guidance for the Individual Plant Examination of External Events for Severe Accident Vulnerabilities," NUREG-1407, U.S. NRC, June 1991

2. "An Approach to Seismic Scope Re-Assessment for Individual Plant Examination of External Events," ERI/NRC 94-502, Energy Research, Inc. Sept. 1994

Attachment 2

Using Component Test Data to Assist in Establishing Code Criteria to Achieve the Desired Seismic Capacity Margin for Piping

Robert P. Kennedy
July 1997

1. Introduction

Revised and more relaxed dynamic load design criteria for piping were published in the 1994 Addenda of the ASME Boiler and Pressure Vessel Code, Section III (ASME Code). By this new criteria, for dynamic loads similar to seismic the code moment capacity M_{CODE} resulting from weight stress, SSE inertia effects, and other mechanical loads is limited to:

$$M_{CODE} = \left[S_A - \frac{B_1 P D_0}{2t}\right]\frac{Z_N}{B_2}$$
$$S_A = 4.5 S_M \quad (1)$$

where: S_A is the allowable stress

S_M = ASME Code material allowable stress

P = Pressure coincident with SSE loading

D_0 = Outside pipe diameter

t = Pipe wall thickness

Z_N = Nominal Section Modulus

B_1, B_2 = ASME Code Stress Indices

This new code criterion (Eqn. (1)) has been primarily based on a series of dynamic component tests extensively discussed in Ref. 1 and analyzed in Ref 2. The open question is whether this new code criterion (Eqn.(1)) provides an adequate seismic capacity (code) margin. Previously (Ref. 3), I recommended that the seismic capacity margin $R_{CP_{1\%}}$ corresponding to a 1% probability of failure should be about 2.0. The purpose of this brief report is to first determine whether the new code criterion achieves this recommended goal based on the component test data summarized in Ref. 1. Secondly, some changes are recommended to enable the desired seismic capacity margin goal to be reliably achieved over a wide variety of seismic inputs and piping natural frequencies.

It is most convenient to consider the Seismic Capacity Margin R_{CP} to be composed of the product of three parts, i.e.:

$$R_{CP} = F_S F_{NL} F_{Red} \tag{2}$$

where F_S is a strength factor and F_{NL} is the additional factor due to non linear dynamic behavior and F_{Red} is a redundancy factor associated with the load redistribution that will occur when a region is overstressed in an actual piping system.

The strength factor F_S is given by:

$$F_S = \frac{M_{UD}}{M_{CODE}} \tag{3}$$

where M_{UD} is the ultimate moment achieved in any component under dynamic cyclic loading prior to failure. This strength margin can be estimated with minimum controversy from the available component test data since M_{UD} can be estimated with little uncertainty for each tested component. In all of the component tests described in Ref. 1 and for all of the additional analyses presented in Ref. 2, the nonlinear hysteretic behavior of the component prior to failure was similar to that shown in Figure 1. A moment capacity close to the ultimate moment capacity M_{UD} was reached at a relatively small rotation (typically in the range of 0.02 to 0.04 radians). However, failure did not occur until a substantially greater rotation (typically 0.06 to 0.1 radians) was exceeded. This behavior occurred irrespective of whether the ultimate failure was a low cycle ratchet-fatigue failure or was excessive deformation (collapse or deflection based failure). The seismic margins shown by the analyses presented in Ref. 2 are highly variable and are sensitive to the ratio R_W between the component and input frequency, the breadth of the input motion frequency content, and the postulated failure mode (fatigue versus displacement). For example, see Figures 2 and 3. However, in each analysis case the maximum moment reached prior to failure was approximately M_{UD}. Therefore, M_{UD} remains a stable description of the component strength irrespective of the input time history, the component frequency, and the failure mode (low cycle fatigue or deformation). As such, F_S is a stable strength factor for each tested component.

The nonlinear factor F_{NL} is highly sensitive to both the ratio R_W of the component natural frequency to the central frequency of the input motion, and the breadth of the frequency content of the input motion as well as the assumed failure mode (low cycle fatigue versus deformation): Therefore, it will be very difficult and probably impossible to reliably estimate F_{NL} for an actual piping system without performing a nonlinear dynamic analyses coupled with a nonlinear acceptable strain or inelastic rotation criterion. However, the nonlinear component analyses presented in Ref. 2 do enable some reasonably conservative estimates of F_{NL} to be made as will be discussed in Section 3.

The redundancy factor F_{Red} is unity in the component tests because no redundancy benefit exists in these tests. For actual piping systems F_{Red} will vary somewhat from system to system. However, some reasonably conservative generic estimates of F_{Red} can be made as will be discussed in Section 4.

From Eqn. (2), the 1% probability of failure capacity margin $R_{CP_{1\%}}$ can be estimated from:

$$R_{CP_{1\%}} = F_{S_{1\%}} \left(F_{NL} F_{Red}\right)_{CONS.} \tag{4}$$

where $F_{S_{1\%}}$ is the 1% non-exceedance probability (NEP) strength factor which can be directly estimated from the component test data, and $(F_{NL}F_{Red})_{CONS.}$ represents a reasonably conservative generic estimate of the product of F_{NL} and F_{Red}. Based on the considerations presented in Ref. 4, the product $(F_{NL}F_{Red})_{CONS.}$ should be established sufficiently conservatively that there is less than about a 16% probability that the actual product would be less for any specific piping system and seismic input. It is recommended that a conservative generic estimate be made by consensus of a committee using the Ref. 2 results as guidance. Some further guidance is given in Section 4.

Once a consensus estimate of $(F_{NL}F_{Red})_{CONS.}$ is established, then the required strength factor $F_{S_{1\%}}$ needed to achieve the goal of $R_{CP_{1\%}} = 2.0$ is given by:

$$F_{S_{1\%}} \frac{2.0}{\left(F_{NL} F_{Red}\right)_{CONS.}} \tag{5}$$

$(F_{NL}F_{Red})_{CONS.}$	$F_{S_{1\%}}$
1.0	2.0
1.33	1.5
1.5	1.33
2.0	1.0

i.e., the required strength factor $F_{S_{1\%}}$ should lie in the range of 1.0 to 2.0 depending upon how much consensus credit is given for $(F_{NL}F_{Red})_{CONS}$.

2. Component Test Data Strength Factor F_S

In order to estimate the strength factor F_S for each of the component tests, the appropriate values of B_2, M_{UD}, and S_M must be established for each of these tests. Some controversy exists over the appropriate B_2 value to use for each test. Also M_{UD} is not directly measured in the test at the failure location and must be extrapolated to this location based on an analytical model of the test. The values used herein are those recommended in Table 2 of Ref. 1. For all tested components:

$$S_M = 20 \text{ ksi}$$
$$4.5\, S_M = 90 \text{ ksi}$$

Table 1 summarizes the parameter used herein for each component test and the resulting test strength factor F_S.

In this discussion, it will be assumed that the seismic strength factor can be approximated as being lognormally distributed. Such a distribution has been shown to reasonably approximate many seismic capacity situations. It will subsequently be shown that the piping component seismic strength factor data also reasonably fits a lognormal distribution.

With the assumed lognormal distribution, the seismic strength factor $F_{S_{1\%}}$ corresponding to a 1% probability of failure can be estimated by:

$$F_{S_{1\%}} = F_{S_{50\%}} e^{-2.326\beta_S} \tag{6}$$

where $F_{S_{50\%}}$ is the median seismic strength factor from the test data, and β_S is the logarithmic standard deviation of the test data. The value $F_{S_{50\%}}$ is obtained from the mean value of the logarithm of the test data, and β_S is the standard deviation of the natural logarithm of the test data, and is approximately the coefficient of variation of the test data.

Table 2 presents statistical distribution information on the strength factor F_S for the Elbow Components for which $B_2 > 3.0$ versus the Non-Elbow Components with $B_2 = 1.0$. Elbow Component #37 has been left out of the Elbow Component distribution in Table 2 because its F_S is clearly not of the same distribution as the other Elbow Components. The median F_S for the other 12 Elbow components is

2.18 with $\beta_S = 0.14$. Thus the F_S of Elbow Component #37 lies 5.5 standard deviations below the median of the other 12 Elbow components. If all of the Elbow component F_S were part of the same distribution, the likelihood that one out of 13 tests would lie at least 5.5 standard deviations below the median is infinitesimally small. Elbow Component #37 is clearly an outlier from the other tested Elbow components and must be separately considered.

Table 2 shows that the Code Moment Capacity Eqn. (1) produces similar strength factors F_S for the tested carbon steel (CS) components as for the stainless steel (SS) components. Therefore, the strength factors for the carbon steel and stainless steel components can be combined.

However, Table 2 shows that the 10 Non-Elbow Components with $B_2 = 1.0$ have a strength factor F_S which is only about 50% of that obtained for the Elbow components. Thus, the Code Moment Capacity Eqn. (1) does not provide for a uniform seismic strength factor. Although the strength factor F_S is likely to be acceptable for the Elbow components tested (except Elbow Component #37), it is not acceptable for Non-Elbow components tested. Some modification should be made to the Code Moment Capacity Eqn. (1) in order to increase the F_S for the Non-Elbow components with $B_2 = 1.0$ up to that of the Elbow components. Several candidate modifications exist. Two alternates will be discussed herein.

2.1 Proposed Alternate #1

Replace B_2 in Eqn. (1) by B_2' for oscillatory dynamic loads defined by:

$$B_2' = B_2 \text{ or } 2.0\text{, whichever greater} \tag{7}$$

This change has the advantage of being very simple. However, it has the disadvantage that B_2' does not represent an elastic stress indice.

Alternate #1 produces no change in the code moments and strength factors F_S reported in Table 1 for the Elbow components. Table 3 shows the revised M_{CODE} and F_S for the 12 Non-Elbow components based on Alternate #1.

2.2 Proposed Alternate #2

Limit the Code Moment Capacity to the idealized limit state moment M_{LS} for unpressurized straight pipe, i.e.:

$$M_{CODE} \leq \left(\tfrac{4}{\pi}\right) S_Y Z_N \tag{8}$$

Contents

1 Introduction 1

1.1 Acknowledgments 1

1.2 Overview 1

1.3 Organization 2

2 Modeling, Identification and Fatigue Analysis 3

2.1 Description of the PFDR Component Tests 3

2.2 Generalized Analytical Model 3

2.2.1 Simplified Equation of Motion 3

2.3 Hysteresis Loop Identification 4

2.4 Modeling and Identification of the Restoring Moment 4

2.4.1 Modeling of Hysteretic Component 4

2.4.2 Parameter Identification 5

2.5 Fatigue Model 6

2.6 Modeling and Calibration Results 6

2.6.1 Test 40 6

2.6.2 Test 36 7

2.6.3 Test 14 7

2.6.4 Test 11 8

3 Analytical Seismic Margins 30

3.1 ASME Code Margins 30

3.1.1 Frequency Ratio 30

3.1.2 Approaches in Varying Frequency Ratio 30

3.2 Varying System Parameter (VSP) Approach 31

3.2.1 Evaluation of a_c 31

3.2.2 Evaluation of a_f 32

3.2.3 Margin Spectra: Parametric Representation 32

3.3 Varying Earthquake Time-scale (VET) Approach 33

3.3.1 Alternative Statement 33

3.3.2 Relation to VSP Approach 34

3.4 Analytical Code Margin Results 35

3.4.1 Input Earthquakes 35

3.4.2 Code Allowable Moment . . . 35
3.4.3 Analytical Margin Results . . . 36
3.5 Response Implications . . . 36
3.6 Displacement Based Margin . . . 37

4 Additional Considerations Affecting Margins 56
4.1 Eccentric Weight Moment Effects . . . 56
4.1.1 Parametric Models . . . 56
4.1.2 Physical Models . . . 57
4.2 Temperature Effects . . . 58
4.2.1 Hysteretic Model . . . 58
4.2.2 Material ϵ-N Curve . . . 59
4.2.3 Code Allowable Moment . . . 59
4.2.4 Simulation Results . . . 59
4.3 Worst-Case Considerations . . . 60

5 Summary and Conclusions 88

References 90

List of Tables

2.1 System identification and fatigue analysis results 10

3.1 Calculation of Code allowable moment 35

4.1 Code moment calculation for Test 14 physical models at room temperature, $S_m = 20.0$ ksi 61

4.2 Code moment calculation for Test 40 physical models at room temperature, $S_m = 20.0$ ksi 61

4.3 Material properties for Test 14 (carbon steel) 61

4.4 Material properties for Test 40 (stainless steel) 61

4.5 Code moment calculation for worst-case physical model at $650°F$, $S_m^* = S_m R_m$, $S_m = 20$ ksi for both stainless steel and carbon steel, $R_m = 0.850$ for carbon steel, $R_m = 0.835$ for stainless steel 61

List of Figures

2.1 Two types of skeleton curve and closed-loop hysteretic moment 5
2.2 Generalized PFDR test configuration 9
2.3 SDOF analytical model, solid lines: undeformed analytical model, dashed lines: deformed analytical mode, dotted line: geometric relation for a lumped mass to the base 9
2.4 Material S-N curves for carbon steel and stainless steel, E: Young's Modulus 10
2.5 Response comparison, solid line: fully nonlinear analysis using Eqn. (2.1), dashed line: simplified analysis using Eqn. (2.10) 11
2.6 Comparison of measured and simulated response given by the optimal model for Test 40, Run 4 . . . 12
2.7 Comparison of measured and simulated hysteresis loops for Test 40, Run 4 13
2.8 Comparison of measured and simulated response given by the optimal model for Test 40, Run 5 . . . 14
2.9 Comparison of measured and simulated hysteresis loops for Test 40, Run 5 15
2.10 Comparison of measured and simulated response given by the optimal model for Test 36, Run 7 . . . 16
2.11 Comparison of measured and simulated hysteresis loops for Test 36, Run 7 17
2.12 Comparison of measured and simulated response given by the optimal model for Test 36, Run 8 . . . 18
2.13 Comparison of measured and simulated hysteresis loops for Test 36, Run 8 19
2.14 Simulated strain response and evolutionary CUF for Test 36, β=0.685 20
2.15 Comparison of measured and simulated response given by the optimal model for Test 14, Run 6 . . . 21
2.16 Comparison of measured and simulated hysteresis loops for Test 14, Run 6 22
2.17 Comparison of measured and simulated response given by the optimal model for Test 14, Run 7 . . . 23
2.18 Comparison of measured and simulated hysteresis loops for Test 14, Run 7 24
2.19 Simulated strain response and evolutionary CUF for Test 14, β=0.49 25
2.20 Comparison of measured and simulated response given by the optimal model for Test 11, (top) Run 6 and (bottom) Run 7 26
2.21 Comparison of measured and simulated hysteresis loops for Test 11, Run 6 27
2.22 Comparison of measured and simulated hysteresis loops for Test 11, Run 7 28
2.23 Simulated strain response and evolutionary CUF for Test 11, β=1.20 29

3.1 Response and restoring force segments of a hysteretic response 34
3.2 PFDR input: peak acceleration = 0.383 g, dominant frequency = 7.5 Hz 39
3.3 RG 1.60 input: acceleration time history, peak acceleration = 1 g, dominant frequency = 7.5 Hz . . . 39
3.4 PFDR input: response spectra 40
3.5 PFDR input: displacement response spectra 40
3.6 RG 1.60 input: pseudo-acceleration response spectra 41

3.7 RG 1.60 input: displacement response spectra . . . 41

3.8 Test 36, PFDR input: margin spectra for various values of α_w, $\zeta_s = 2\%$, Sequential Method . . . 42

3.9 Test 36, PFDR input: margin spectra for various fatigue evaluation methods, $\alpha_w = -5\%$, $\zeta_s = 2\%$. 42

3.10 Test 36, RG 1.60 input: margin spectra for various values of α_w, $\zeta_s = 2\%$, Sequential Method . . . 43

3.11 Test 36, RG 1.60 input: margin spectra for various methods, $\alpha_w = -5\%$, $\zeta_s = 2\%$ . . . 43

3.12 Test 11, PFDR input: margin spectra for various values of α_w, $\zeta_s = 3\%$, Sequential Method . . . 44

3.13 Test 11, PFDR input: margin spectra for various fatigue evaluation methods, $\alpha_w = -5\%$, $\zeta_s = 3\%$. 44

3.14 Test 11, RG 1.60 input: margin spectra for various values of α_w, $\zeta_s = 3\%$, Sequential Method . . . 45

3.15 Test 11, RG 1.60 input: margin spectra for various methods, $\alpha_w = -5\%$, $\zeta_s = 3\%$ . . . 45

3.16 Test 14, PFDR input: margin spectra for various values of α_w, $\zeta_s = 2.5\%$, Sequential Method . . . 46

3.17 Test 14, PFDR input: margin spectra for various fatigue evaluation methods, $\alpha_w = -2\%$, $\zeta_s = 2.5\%$ 46

3.18 Test 14, RG 1.60 input: margin spectra for various values of α_w, $\zeta_s = 2.5\%$, Sequential Method . . . 47

3.19 Test 14, RG 1.60 input: margin spectra for various methods, $\alpha_w = -2\%$, $\zeta_s = 2.5\%$ . . . 47

3.20 Test 36, CUF as a function of R_w and peak acceleration of linearly amplified PFDR input, $\alpha_w = 0\%$, $c_p = 0.01$, $\zeta_s = 2\%$, sequential method . . . 48

3.21 Test 36, CUF as a function of R_w and peak acceleration of linearly amplified PFDR input, $\alpha_w = -5\%$, $c_p = 0.01$, $\zeta_s = 2\%$, sequential method . . . 48

3.22 Test 36, response time history for systems with R_w=0.5, 1.5 and 3.0 subjected to PFDR input, CUF=1, $\alpha_w = -3\%$, $c_p = 0.01$, $\zeta_s = 2\%$, sequential method . . . 49

3.23 Test 14, CUF as a function of R_w and peak acceleration of linearly amplified PFDR input, $\alpha_w = 0\%$, $c_p = 0.01$, $\zeta_s = 2.5\%$, sequential method . . . 50

3.24 Test 14, CUF as a function of R_w and peak acceleration of linearly amplified PFDR input, $\alpha_w = -2\%$, $c_p = 0.01$, $\zeta_s = 2.5\%$, sequential method . . . 50

3.25 Test 14, response time history for systems with R_w=0.5, 1.5 and 3.0 subjected to PFDR input, CUF=1, $\alpha_w = -1\%$, $c_p = 0.01$, $\zeta_s = 2.5\%$, sequential method . . . 51

3.26 Test 36, PFDR input: displacement margin spectra for various values of α_w . . . 52

3.27 Test 36, RG 1.60 input: displacement margin spectra for various values of α_w . . . 52

3.28 Test 14, PFDR input: displacement margin spectra for various values of α_w . . . 53

3.29 Test 14, RG 1.60 input: displacement margin spectra for various values of α_w . . . 53

3.30 Test 11, PFDR input: displacement margin spectra for various values of α_w . . . 54

3.31 Test 11, RG 1.60 input: displacement margin spectra for various values of α_w . . . 54

3.32 Test 40, PFDR input: displacement margin spectra for various values of α_w . . . 55

3.33 Test 40, RG 1.60 input: displacement margin spectra for various values of α_w . . . 55

4.1 Modification of hysteretic model . . . 58

4.2 Three postulated models for ϵ-N relationship at $650°F$ . . . 59

4.3 Test 14, Parametric models, PFDR input: fatigue margin spectra for various values of α_l, $\alpha_w = 0\%$, Sequential Method . . . 62

4.4 Test 14, Parametric models, PFDR input: displacement margin spectra for various values of α_l, $\alpha_w = 0\%$ 62

4.5 Test 14, Parametric models, PFDR input: fatigue margin spectra for various values of α_l and α_w, Sequential Method . . . 63

4.6 Test 14, Parametric models, PFDR input: displacement margin spectra for various values of α_l and α_w 63

4.7 Test 14, Parametric models, RG 1.60 input: fatigue margin spectra for various values of α_l, $\alpha_w = 0\%$, Sequential Method . . . 64

4.8 Test 14, Parametric models, RG 1.60 input: displacement margin spectra for various values of α_l, $\alpha_w = 0\%$ . . . 64

4.9 Test 14, Parametric models, RG 1.60 input: fatigue margin spectra for various values of α_l and α_w, Sequential Method . . . 65

4.10 Test 14, Parametric models, RG 1.60 input: displacement margin spectra for various values of α_l and α_w . . . 65

4.11 Test 40, Parametric models, PFDR input: displacement margin spectra for various values of α_l, $\alpha_w = 0\%$ 66

4.12 Test 40, Parametric models, PFDR input: displacement margin spectra for various values of α_l and α_w 66

4.13 Test 40, Parametric models, RG 1.60 input: displacement margin spectra for various values of α_l, $\alpha_w = 0\%$ . . . 67

4.14 Test 40, Parametric models, RG 1.60 input: displacement margin spectra for various values of α_l and α_w . . . 67

4.15 Test 14: physical models without eccentricity, $l_1 = l_2 = 0$ in. . . . 68

4.16 Test 14: physical models with eccentricity, $l_1 = l_2 = 56$ in. . . . 68

4.17 Test 14: physical models with eccentricity, $l_1 = l_2 = 85$ in. . . . 69

4.18 Test 40: physical models without eccentricity, $l_1 = l_2 = 0$ in. . . . 69

4.19 Test 40: physical models with eccentricity, $l_1 = l_2 = 30$ in. . . . 70

4.20 Test 40: physical models with eccentricity, $l_1 = l_2 = 49$ in. . . . 70

4.21 Test 14, Physical models, RG 1.60 input: frequency effects on fatigue margin spectrum and displacement margin spectrum and required acceleration levels , $l_1, l_2 = 0$ in., Sequential Method . . . 71

4.22 Test 14, Physical models, RG 1.60 input: fatigue margin spectra and required acceleration levels for various degrees of eccentricity, Sequential Method . . . 72

4.23 Test 14, Physical models, RG 1.60 input: displacement margin spectra and required acceleration levels for various degrees of eccentricity . . . 73

4.24 Test 40, Physical models, RG 1.60 input: displacement margin spectra and required acceleration levels 74

4.25 Test 14, Parametric models, PFDR input: temperature effects (S-type) on fatigue based margin spectra, $\alpha_w = 0\%$, $R_y = 0.726$, Sequential Method . . . 75

4.26 Test 14, Parametric models, PFDR input: temperature effects (S-type) on displacement margin spectra, $\alpha_w = 0\%$, $R_y = 0.726$ . . . 75

4.27 Test 14, Parametric models, PFDR input: temperature effects (H-type) on fatigue based margin spectra, $R_h = 1.5$, $\alpha_w = 0\%$, Sequential Method . . . 76

4.28 Test 14, Parametric models, PFDR input: temperature effects (H-type) on displacement margin spectra, $R_h = 1.5$, $\alpha_w = 0\%$ . . . 76

4.29 Test 14, Physical models, RG 1.60 input: temperature effects (S-type) on fatigue margin spectra and required acceleration levels, $l_1 = l_2 = 0$, $R_y = 0.726$, Sequential Method 77

4.30 Test 14, Physical models, R. G 1.60 input: temperature effects (H-type) on fatigue margin spectra and required acceleration levels, $l_1 = l_2 = 0$, $R_h = 1.5$, Sequential Method 78

4.31 Test 14, Physical models, R. G 1.60 input: temperature effects (S-type and H-Type) on displacement margin spectra and required acceleration levels, $l_1 = l_2 = 0$, $R_h = 1.5$, $R_y = 0.726$ 79

4.32 Test 40, Parametric models, PFDR input: temperature effects on displacement margin spectra, $\alpha_w =$ 0%, $R_y = 0.584$ 80

4.33 Test 40, Parametric models, RG 1.60 input: temperature effects on displacement margin spectra, $\alpha_w = 0\%$, $Ry = 0.584$ 80

4.34 Test 14: worst-case physical models with eccentricity, $l_1 = l_2 = 78$ in. 81

4.35 Test 40: worst-case physical models with eccentricity, $l_1 = l_2 = 44$ in. 81

4.36 Test 14, Physical models, PFDR input: worst-case consideration ($l_1 = l_2 = 0$ in, Period = [0: 0.25] second), fatigue and displacement margin spectra and required acceleration levels, $R_y = 0.726$ 82

4.37 Test 14, Physical models, PFDR input: worst-case consideration ($l_1 = l_2 = 78$ in, Period = [0.25, 1.75] second), fatigue and displacement margin spectra and required acceleration levels, $R_y = 0.726$ 83

4.38 Test 14, Physical models, RG 1.60 input: worst-case consideration ($l_1 = l_2 = 0$ in, Period = [0: 0.25] second), fatigue and displacement margin spectra and required acceleration levels, $R_y = 0.726$ 84

4.39 Test 14, Physical models, RG 1.60 input: worst-case consideration ($l_1 = l_2 = 78$ in, Period = [0.25, 1.75] second), fatigue and displacement margin spectra and required acceleration levels, $R_y = 0.726$ 85

4.40 Test 40, Physical models, PFDR input: worst-case displacement margins and required acceleration levels, $R_y = 0.584$ 86

4.41 Test 40, Physical models, RG 1.60 input: worst-case margins, $R_y = 0.584$ 87

1 Introduction

1.1 Acknowledgments

This research project is part of the US Nuclear Regulatory Commission (NRC) Seismic Analysis of Piping (SAOP) research program conducted at the Energy Technology Engineering Center (ETEC). Any opinions, findings, and conclusions or recommendations expressed in this report are those of the authors and do not necessarily reflect the views of NRC or ETEC.

The authors would like to thank N. C. Chokshi and J. Fair of the US NRC for valuable comments and continuous support during the course of this study. Thanks are also given to K. Jaquay of ETEC for his important technical assistance and guidance on this research project. The authors would also like to thank R. P. Kennedy for his encouragement and insightful discussion of this project.

This research is dedicated to the memory of Dr. W. P. Chen, the former program manager of the SAOP research program at ETEC.

1.2 Overview

This report documents an analytical study of frequency effects on seismic margins. This study is based on selected piping component tests conducted as part of the previous joint Electric Power Research Institute (EPRI) and NRC Piping and Fitting Dynamic Reliability (PFDR) program. The seismic margin was taken to be the ratio of the peak acceleration required to cause failure of the component in one application of a given earthquake excitation to the peak acceleration corresponding to the ASME Code allowable stress obtained from a linear response spectrum analysis.

The majority of the PFDR component tests were performed using a narrow-banded earthquake excitation input that was tuned to have a peak frequency slightly lower than the fundamental frequency of the test component. Due to these frequency limitations, the PFDR test margins are considered applicable only for near-resonance conditions. However, the natural frequency of a piping system in an actual plant may vary over a rather wide range, and the corresponding seismic margins at the off-resonance condition can also be of great importance. It is the primary objective of this study to analytically extrapolate the PFDR test margins such that the variation of seismic margins due to input-to-system frequency effects can be investigated.

To achieve this goal, a series of nonlinear dynamic models and fatigue damage models are developed for the piping components. The PFDR test data and failure information are used to calibrate the model parameters. With these established models, margin evaluations can then be performed analytically according to the margin definition. Although originally targeted at the PFDR off-resonance test margins, this study represents a framework of margin assessment in which many influential factors on margins are systematically evaluated and the interaction of possible failure modes are identified and characterized.

A summary of some of the significant issues addressed in this report is given below.

- **approaches to alter the frequency ratio**

Two possible approaches to alter the input-to-system frequency ratio are investigated. They are respectively the approach of altering the system's fundamental frequency and the approach of altering the predominate frequency of the input earthquake.

- **seismic loadings**

  This study employs two input excitations, the target PFDR input, representing a narrow-banded spectrum excitation and the Regulatory Guide (RG) 1.60 input, representing a broad-banded spectrum excitation.

- **failure modes**

  Two possible failure modes, fatigue failure and large-displacement induced failure, are considered.

- **effects of structural configurations**

  This study explicitly addresses the effects of dynamically destabilizing factors that include the P-Δ effect and the sustained bias moment effect.

- **effects of elevated operating temperature**

  The effect on seismic margin due to an elevated operating temperature of 650°F is investigated.

1.3 Organization

The results of this study are presented in four major sections as follows.

- Section 2 describes the techniques developed for nonlinear modeling, identification and fatigue analysis for the PFDR component test system. Results of these analyses are presented for PFDR Tests 11, 14, 36 and 40.

- Section 3 presents analytical margin results. Both fatigue-based margins and displacement-based margins are evaluated for PFDR Tests 11, 14 and 36 using both the target PFDR input and RG 1.60 input time histories. Only the displacement-based margin is given for Test 40.

- Section 4 presents additional considerations on seismic margins, including eccentric moment effects and temperature effects, for PFDR Test 14 and Test 40.

- Section 5 gives a summary and conclusions of this study.

2 Modeling, Identification and Fatigue Analysis

2.1 Description of the 1 . DR Component Tests

A typical test configuration used in the PFDR piping component tests is shown in Fig. 2.2. The test component is connected to an over-hanging inertia arm with an attached weight. The input excitation is supplied through a base sled motion. The input acceleration time history as well as the strain, displacement and acceleration response time histories at selected locations are recorded for later analysis.

2.2 Generalized Analytical Model

For the purpose of analysis, the deformation leading to failure is assumed to concentrate at one location in the test component, and the portion of the system above the failure region is assumed to act as a rigid body. This leads to a single-degree-of-freedom (SDOF) model for the piping test system which appears to be supported by the data. The restoring moment given by the piping component at the failure location is modeled by a non-linear rotational spring. The idealized analytical model that is employed in this study is shown in Fig. 2.3.

The idealized analytical model consists of a set of lumped and distributed mass elements. For each mass element in the undeformed configuration, ϕ_i and d_i are the rotational angle and distance from the mass center to the center of the base. The equation of motion governing the rotation response $\theta(t)$ is derived using the Lagrange formulation as

$$I\ddot{\theta} - g\sum S_i \sin(\theta - \phi_i) + m_r(\theta, \dot{\theta}) = -a(t)\sum S_i \cos(\theta - \phi_i) \tag{2.1}$$

where $\dot{\theta}$ and $\ddot{\theta}$ are respectively the rotation velocity and acceleration, I is the total mass moment of inertia, g is the acceleration of gravity, $a(t)$ is the base acceleration, $m_r(\theta, \dot{\theta})$ is the restoring moment of the spring and S_i are a set of system parameters associated with each mass element.

The total mass moment of inertia I is given by

$$I = \sum I_i \tag{2.2}$$

where I_i represents the mass moment of inertia of each mass element that can be expressed as

$$I_i = \begin{cases} m_i d_i^2 & \text{for lumped mass} \\ \rho_i l_i d_i^2 + \frac{\rho_i l_i^3}{12} & \text{for distributed mass} \end{cases} \tag{2.3}$$

The expressions for S_i are given by

$$S_i = \begin{cases} m_i d_i & \text{for lumped mass} \\ \rho_i l_i d_i & \text{for distributed mass} \end{cases} \tag{2.4}$$

In the above equations, m_i is the mass of a lumped mass element, and ρ_i and l_i are the mass density per unit length and the length of a distributed mass element.

2.2.1 Simplified Equation of Motion

A simplified equation of motion can be derived when the rotational angle is assumed to be "small". Using the small angle approximations, $\sin\theta \approx \theta$ and $\cos\theta \approx 1$, Eqn. (2.1) becomes

$$I\ddot{\theta} + m_r(\theta, \dot{\theta}) + k_{p\delta}\theta = -c_f a(t) - f_e - a(t)\theta f_p \quad (2.5)$$

where $k_{p\delta}$ is the $P - \Delta$ stiffness, c_f is the participation constant, f_e is a static eccentric moment and f_p is a parametric excitation constant. The expressions for these terms are given by

$$\begin{aligned} k_{p\delta} &= -g\sum S_i \cos\phi_i \\ c_f &= \sum S_i \cos\phi_i \\ f_e &= g\sum S_i \sin\phi_i \\ f_p &= \sum S_i \sin\phi_i \end{aligned} \quad (2.6)$$

The last term in the right-hand side (RHS) of Eqn. (2.5) represents a parametric excitation term which appears only when a bias loading is present. This parametric excitation term is relatively small in general as compared to the first term on the RHS of Eqn. (2.5). By neglecting the parametric excitation term, Eqn. (2.5) is further simplified as

$$I\ddot{\theta} + m_r(\theta, \dot{\theta}) + k_{p\delta}\theta = -c_f a(t) - f_e \quad (2.7)$$

2.3 Hysteresis Loop Identification

Eqn. (2.7) stipulates the dynamic balance associated with the restoring moment. Rearranging the order of this equation yields

$$m_r(\theta, \dot{\theta}) = -I\ddot{\theta} - k_{p\delta}\theta - c_f a(t) - f_e \quad (2.8)$$

Given the rotational displacement and acceleration time histories, the RHS of Eqn. (2.8) is an explicit function of the physical parameters of the test system only. The left-hand side (LHS) represents the restoring moment developed in the piping component. Hence, Eqn. (2.8) can be used to deduce the restoring moment-rotation characteristics using the physical parameters and measured response data.

Note that Eqn. (2.7) is a simplified equation of motion where the geometric nonlinearity and the parametric excitation terms are neglected. The same technique can be applied to Eqn. (2.1) to obtain moment-rotation characteristics with geometric nonlinearity fully considered.

2.4 Modeling and Identification of the Restoring Moment

The restoring moment $m_r(\theta, \dot{\theta})$ is assumed to consist of both linear and nonlinear components, and is modeled as

$$m_r(\theta, \dot{\theta}) = c\dot{\theta} + k_l\theta + h(\theta, \dot{\theta}) \quad (2.9)$$

where c is a linear damping constant governing the amount of linear viscous damping, k_l is a linear stiffness constant governing the post-yielding moment, and $h(\theta, \dot{\theta})$ represents the hysteretic component having a zero ultimate stiffness.

Substituting Eqn. (2.9) into Eqn. (2.7) yields

$$I\ddot{\theta} + c\dot{\theta} + k_l\theta + k_{p\delta}\theta + h(\theta, \dot{\theta}) = -c_f a(t) - f_e \quad (2.10)$$

Eqn. (2.10) can be solved numerically given the availability of an appropriate hysteretic model for $h(\theta, \dot{\theta})$.

2.4.1 Modeling of Hysteretic Component

The hysteretic model employed for $h(\theta, \dot{\theta})$ is a class of hysteretic models capable of representing a broad range of curved non-deteriorating hysteretic behavior. These models are of the continuous parallel-distributed-element type [1] and permit both steady-state and transient dynamic analysis. For both analyses, the hysteretic behavior is fully determined by the initial loading (skeleton) curve.

Two different types of continuous, monotonically increasing skeleton curves are considered. The expressions for the skeleton curve, v, as a function of the rotational angle θ are given by

- Type 1:

$$v(\theta) = f_y(1 - \exp(\frac{k_{ini}}{f_y})|\theta|)\mathrm{sgn}(\theta) \qquad (2.11)$$

- Type 2:

$$v(\theta) = f_y \tanh(\frac{k_{ini}\theta}{f_y}) \qquad (2.12)$$

where f_y and k_{ini} are the parameters governing the ultimate yielding moment and the initial hysteretic stiffness respectively. A comparison of the closed-loop moment characteristics resulting from these skeleton curves is shown in Fig. 2.1. These two moment characteristics represe different degrees of rounding of the hysteretic loops.

2.4.2 Parameter Identification

A parameter identification procedure associated with this class of models is also developed. The purpose of the parameter identification is to obtain a set of model parameters based on a certain minimization criterion. The minimization is set in such a way that the model generated response is as "close" to the measured data as possible. This process is formulated as an optimization problem defined in a space spanned by the model parameters.

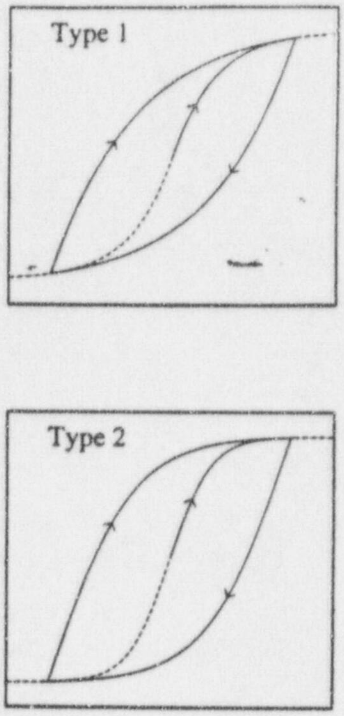

Figure 2.1: Two types of skeleton curve and closed-loop hysteretic moment

The model parameters of interest are the parameters of the restoring moment $m_r(\theta, \dot{\theta})$. As formulated in Eqn. (2.9), the restoring moment is separated into linear and nonlinear hysteretic components. The nonlinear hysteresis is fully determined by only two parameters k_{ini} and f_y once the type of skeleton curve is selected. Therefore, this poses a four-dimensional optimization problem formulated as

$$\text{Min} \qquad J = J(k_{ini}, k_l, f_y, c) \qquad (2.13)$$

where J symbolizes the objective function to be minimized. The objective function defines a measure of the error between the measured and simulated response data. In the present study, this is taken as the sum square error between the model simulated and measured rotational responses.

The solution to the optimization problem is performed numerically using a computer code developed specifically for this study. The code is called PIPES (Parameter Identification using Parallel-distributed-Element Systems). PIPES involves an integration of successive function evaluations and an optimization search scheme. The function evaluation is performed by a subroutine, using the extended Masing's Hypothesis [2, 3] to generate transient hysteretic loops. The response variables are integrated in time using an explicit fourth-order Runge-Kutta scheme. The optimization search is based on a first-order gradient method [4]. The moment characteristics evaluated from Eqn. (2.8) are used to guide the optimal search within a plausible parameter range.

2.5 Fatigue Model

The fatigue analysis is based on the assumption that the local strain, ϵ, is linearly proportional to the rotational angle, θ, according to the relationship

$$\epsilon = \beta\theta \tag{2.14}$$

where β is a constant proportionality factor. The factor β is determined from test data such that the cumulative usage factor (CUF) reaches unity at the instant that the fatigue failure was observed in the test. The calibration procedure is based on the Sequential Method of range-pair selection and the Miner's Linear Hypothesis [5]. The material S-N curves are then used to evaluate the fatigue usage. The expression for the material S-N curves for carbon steel and stainless steel are given in Eqn. (2.15) and Eqn. (2.16) respectively [7].

$$S = 21,645 + 8,660,000N^{-\frac{1}{2}} \tag{2.15}$$

$$S = 43,500 + 8,420,000N^{-\frac{1}{2}} \tag{2.16}$$

In these equations, S (psi) is the strain amplitude multiplied by the Young's Modulus (psi) and N is the number of cycles to failure. The characteristics for these curves are illustrated in Fig. 2.4.

2.6 Modeling and Calibration Results

The modeling and identification processes are implemented for four piping component tests, Tests 40, 36, 14 and 11. The last three tests failed in fatigue and are subjected to fatigue analysis. Table 2.1 summaries the modeling, identification and calibration results. Detailed descriptions are given in subsections that follow.

2.6.1 Test 40

Test 40 was conducted for an unpressurized Schedule 40 reducer. Run 4 and Run 5 were subjected to high level earthquake input. The adjacent pipe spool failed in buckling during Run 5 and the test sequence was terminated. The Run 4 data is used to obtain an optimal analytical model.

The response of Test 40 exhibits significant response ratcheting with excessive accumulated deformation. However, the accumulated deformation is not directly described in the measured data because the test measurement transducers were re-zeroed before each new run. To simulate the actual test sequences and to recover the deformation time history, the optimal model is subjected to a sequential base excitation of Run 4 and Run 5. Test 40 is also used as a benchmark test for the validity of the small angle assumptions. Both the fully nonlinear equation of motion, Eqn. (2.1), and the simplified equation of motion, Eqn. (2.10), are examined and compared.

The simulation results are given in Fig. 2.5. The final offset in θ is estimated as 0.06 radians for Run 4. After Run 5 starts, the rate of ratcheting accelerates and the rotational angle exceeds 0.20 radians at the end of the excitation. The linear and nonlinear analyses show almost identical solutions for $\theta \leq 0.1$ radians. Only a slightly difference is observed for $0.10 \leq \theta \leq 0.20$, and the linear assumption gives a more conservative response amplitude. This result demonstrates that the small angle assumption offers accurate response approximations and is well suitable as an alternative solution approach.

Comparisons of the rotation time histories and hysteresis loops are given in Figs. 2.6 - 2.9. In Run 4, excellent performance of the optimal model is demonstrated for both the ratcheting rate and the response amplitude. In the Run 5 rotation plot, the measured rotation is adjusted by an initial offset of 0.06 radians to recover a lost initial condition due to the re-zeroing process. The optimal model still accurately predicts the response for a duration of about 10 seconds but response discrepancies become apparent after that.

2.6.2 Test 36

Test 36 was a through-run test of a Schedule 40 pressurized tee. Run 7 and Run 8 were the only runs subjected to high level earthquake input. The test was terminated in Run 8 due to a through-wall crack. The identification procedure is based on the Run 8 data.

The optimal model obtained from Run 8 data is then continuously subjected to the input of Run 7 and Run 8 in a manner similar to that performed for Test 40. The comparison of the simulated and measured response of Run 7 is given in Fig. 2.10, and the hysteresis loops are compared in Fig. 2.11. These results clearly indicate that the response level of Run 7 is close to being within the linear range.

The response time history and hysteresis loops of Run 8 are compared in Figs. 2.12 and 2.13 respectively. The component failure causes an abrupt change in both the response time history and the restoring moment characteristics at a time around 17 seconds. The response given by the optimal model agrees well with the measured data prior to failure.

A subsequent fatigue analysis is performed using the simulated Run 7 and Run 8 data. The results of the fatigue calibration is illustrated in Fig. 2.14. The proportionality factor β is determined to be β=0.685. This fatigue model predicts $CUF = 1$ at 17 seconds into the simulated Run 8. It is observed that the simulated Run 8 consumes over 95 % of the fatigue usage and the contribution of Run 7 is insignificant. This implies that the fatigue consumption prior to Run 7 is also negligible due to a much smaller input intensity.

2.6.3 Test 14

Test 14 was a pressurized out-of-plane Schedule 40 tee test. The tee was subjected to increasingly higher levels of excitation in Runs 5, 6 and 7. A through-wall crack due to fatigue occurred during Run 7 which terminated the test sequence. This crack was in the upper branch nipple adjacent to the tee-nipple weld.

Run 6 test data are used in PIPES to obtain an optimal model. The measured restoring moment characteristics and the model simulated hysteretic loops are compared in Fig. 2.16. The measured restoring moment exhibits a smooth yielding hysteretic behavior. The optimal model provides good agreement in the overall hysteretic loop shape.

The measured and simulated rotational angle response is compared in Fig. 2.15. Slight ratcheting response is observed for this run which results in a final offset angle of approximately 0.02 radians. The optimal model demonstrates excellent performance in both the response amplitude and phase, as well as the rate of ratcheting.

The optimal model is further subjected to Run 7 excitation for a response prediction. Good agreement between the predicted and measured response is again achieved as demonstrated in Figs. 2.17 and 2.18. The component failed at around 11 seconds into this run at an accumulated final offset rotation of approximately 0.04 radians.

The fatigue calibration procedure is illustrated in Fig. 2.19. The value of β that causes the model to reach $CUF = 1$ at the time of the actual occurrence of fatigue failure is $\beta = 0.49$. It is observed that Run 6 and Run 7 together consume over 95 % of the fatigue usage while the contribution from Run 5 is insignificant.

2.6.4 Test 11

Test 11 was an out-of-plane Schedule 10 tee test. The component was internally pressurized at 400 psi. Run 5 was a low level earthquake test for a full time history. Run 6 and Run 7 were subjected to higher level earthquake input with only one third of the full time history. A through-wall crack occurred during Run 7 which terminated the test sequence.

The parameter identification is performed on the Run 6 data. The optimal model is then used to simulate the test sequences consisting of Runs 5, 6 and 7. The simulated responses of Run 6 and Run 7 are compared to the measured data in Fig. 2.20. The comparison of hysteresis loops of Run 6 and Run 7 is given in Fig. 2.21 and Fig. 2.22 respectively.

Good response fitting is again achieved for the Run 6 data. Since only one third of the earthquake input is used, the total duration of the base excitation is estimated as 10 seconds. After the 10-second excitation period, the system undergoes free vibration response where a slight response discrepancy is observed.

This optimal model also provides an excellent response prediction for Run 7 during the duration of main excitation. The sudden change in the measured response corresponds to the component failure that occurred at roughly 7 seconds into this run.

The simulated test sequences of Runs 5, 6 and 7 and the fatigue calibration results are illustrated in Fig. 2.23. The proportionality factor is determined to be $\beta = 1.20$. The fatigue usage contributed from the lower level run (Run 5) is again seen to be insignificant to the total CUF. Most of the fatigue usage is accumulated in only a 17-second time interval, i.e., 10 seconds in Run 6 and 7 seconds in Run 7.

The 17-second interval of fatigue usage in Test 11 is found to be almost identical to that of Test 36 Run 8. In addition, similar levels of rotational angle response are observed for both tests. However, the calibrated β value for Test 11 differs significantly from that for Test 36. One reason is that Test 36 exhibits a larger number of rotation range-pairs. A more significant factor is the difference in component materials and corresponding S-N curves (stainless steel for Test 11 in contrast to carbon steel for Test 36).

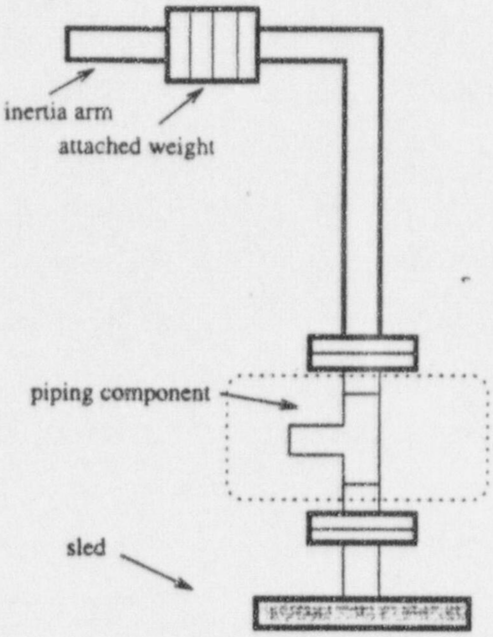

Figure 2.2: Generalized PFDR test configuration

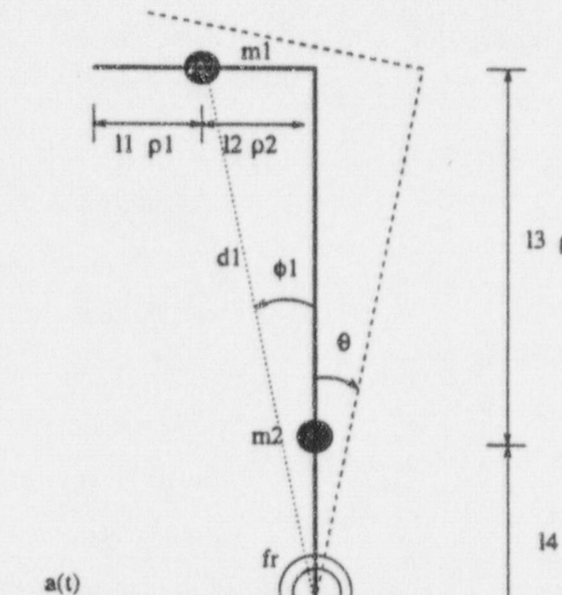

Figure 2.3: SDOF analytical model, solid lines: undeformed analytical model, dashed lines: deformed analytical mode, dotted line: geometric relation for a lumped mass to the base

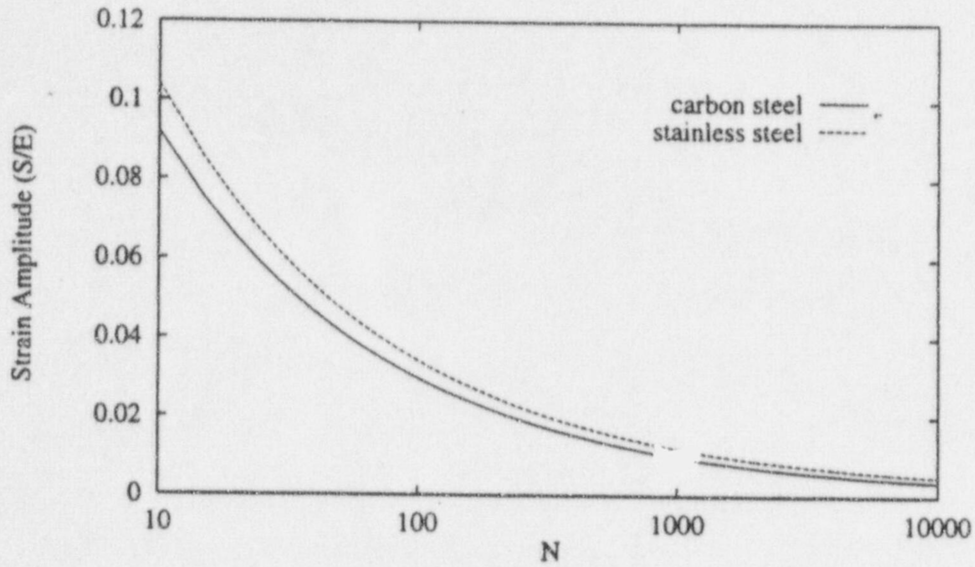

Figure 2.4: Material S-N curves for carbon steel and stainless steel, E: Young's Modulus

Test No.	damping ratio (%)	natural frequency (Hz)	skeleton curve	k_{ini} (kips-in)	f_y (kips-in)	k_l (kips-in)	c (kips-in-sec)	β
40	4.5	7.5	Type 2	16108	221	54.9	30.9	N/A
36	3.1	6.8	Type 1	18350	708	345.5	26.8	0.685
14	2.5	7.8	Type 2	14302	558	116.3	14.7	0.490
11	3.0	5.9	Type 1	8189	600	50.9	13.2	1.200

Table 2.1: System identification and fatigue analysis results

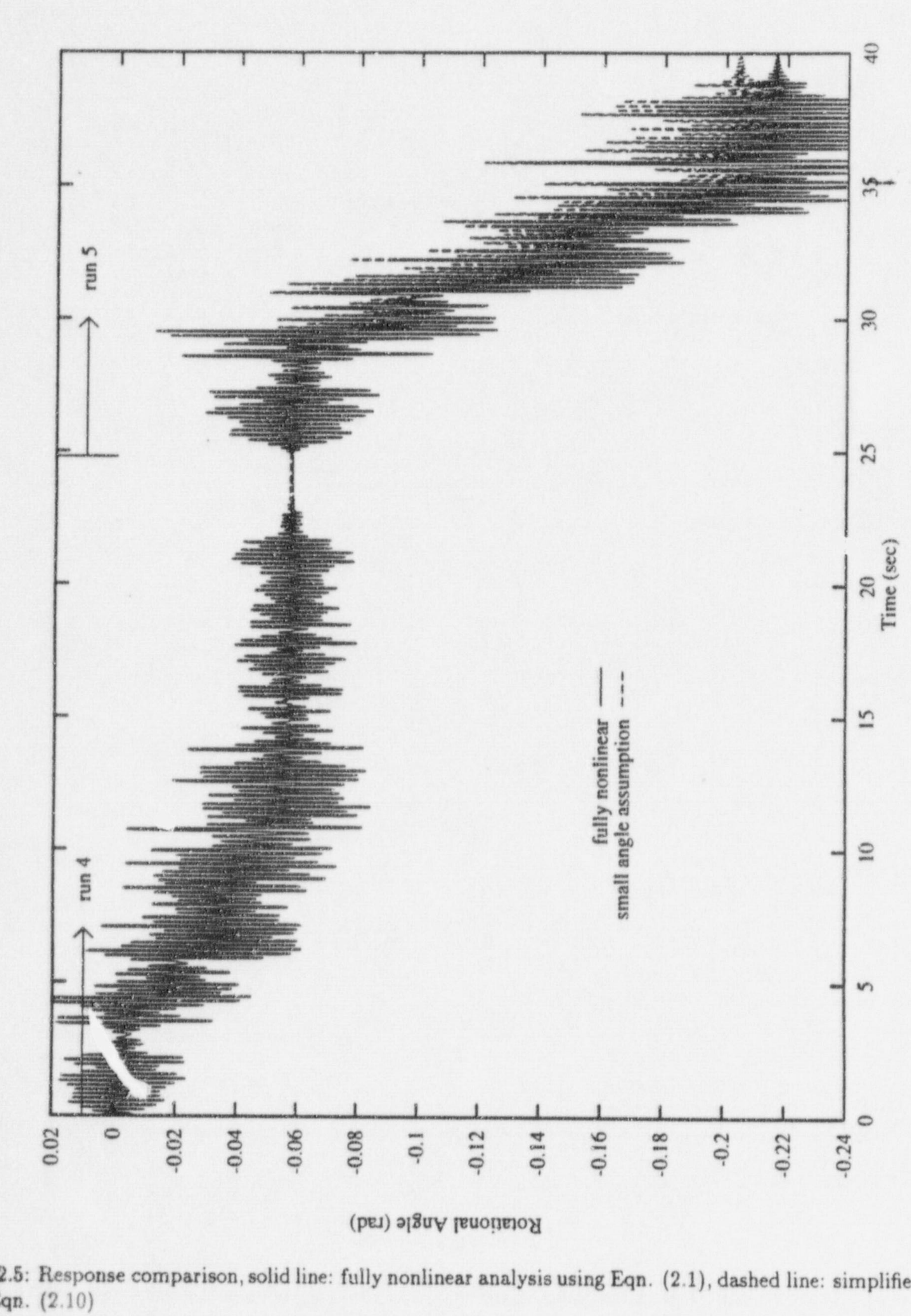

Figure 2.5: Response comparison, solid line: fully nonlinear analysis using Eqn. (2.1), dashed line: simplified analysis using Eqn. (2.10)

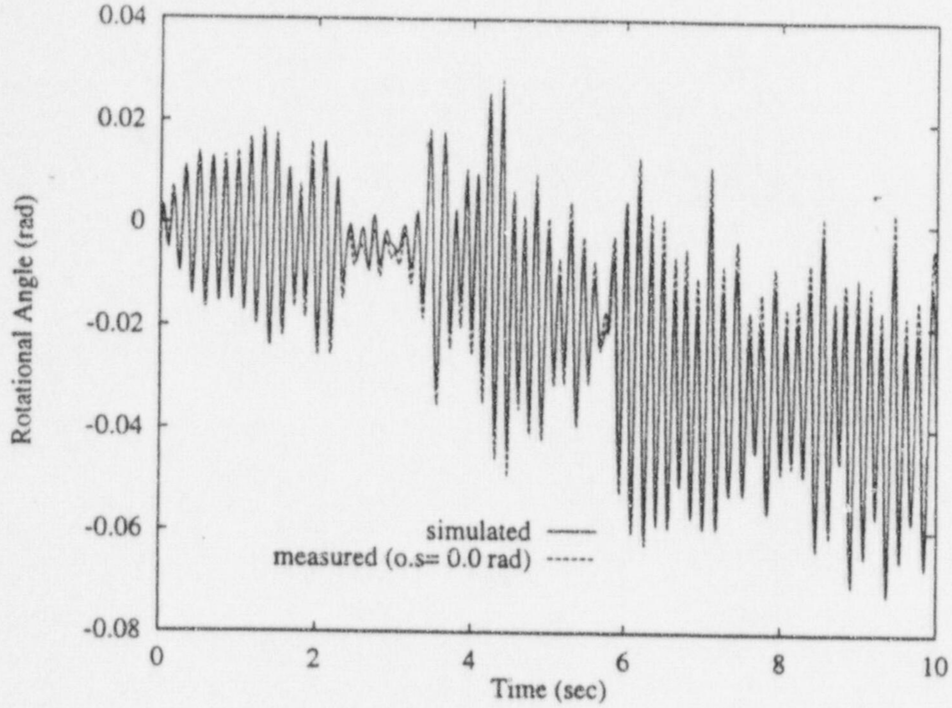

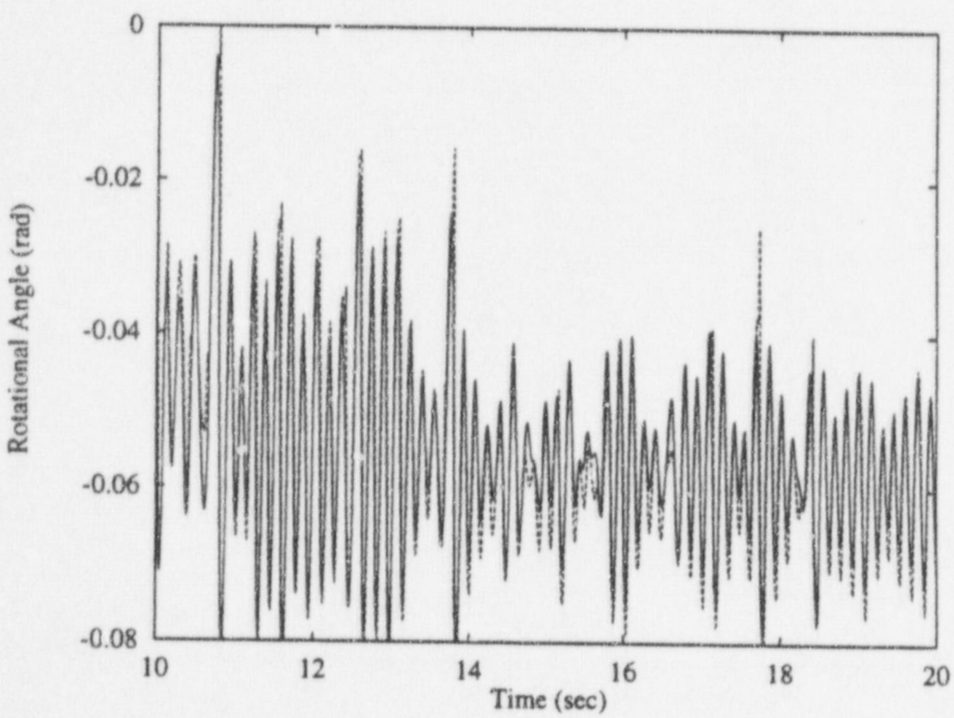

Figure 2.6: Comparison of measured and simulated response given by the optimal model for Test 40, Run 4

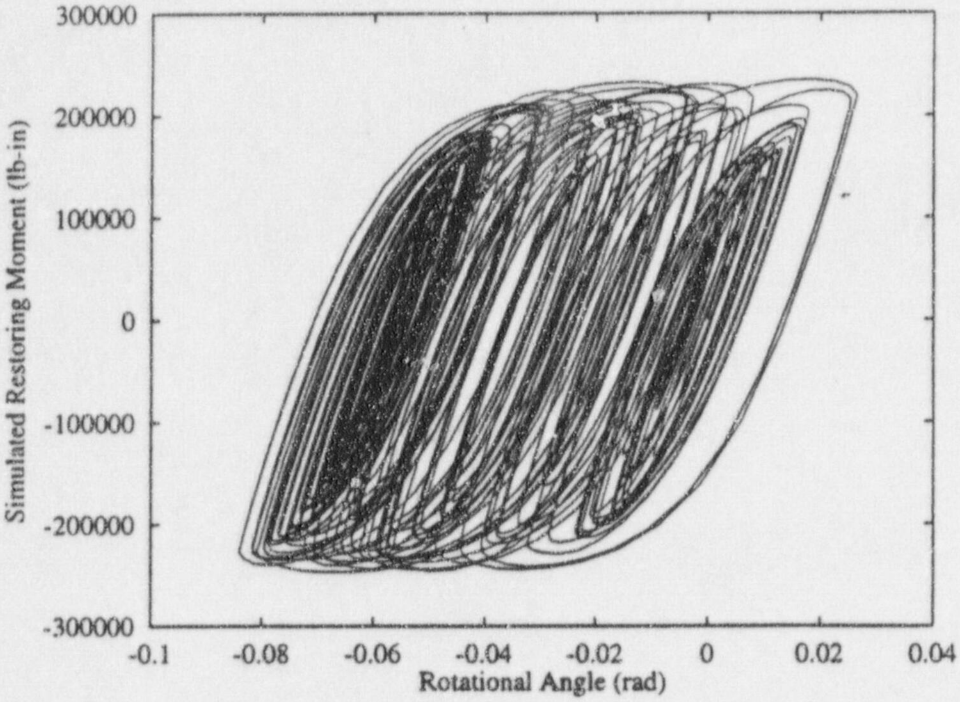

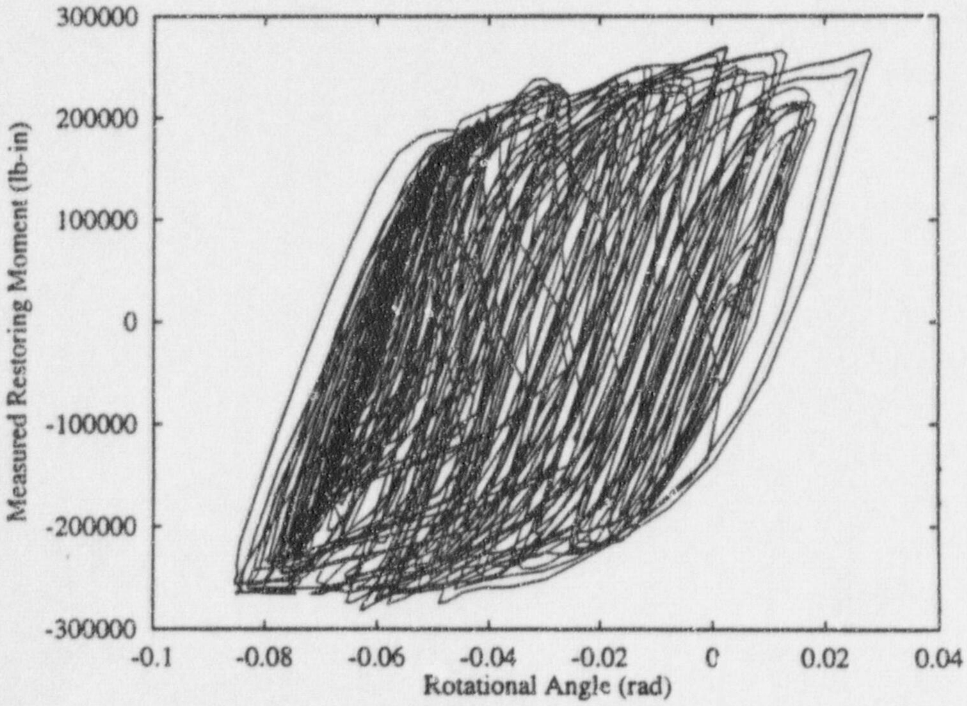

Figure 2.7: Comparison of measured and simulated hysteresis loops for Test 40, Run 4

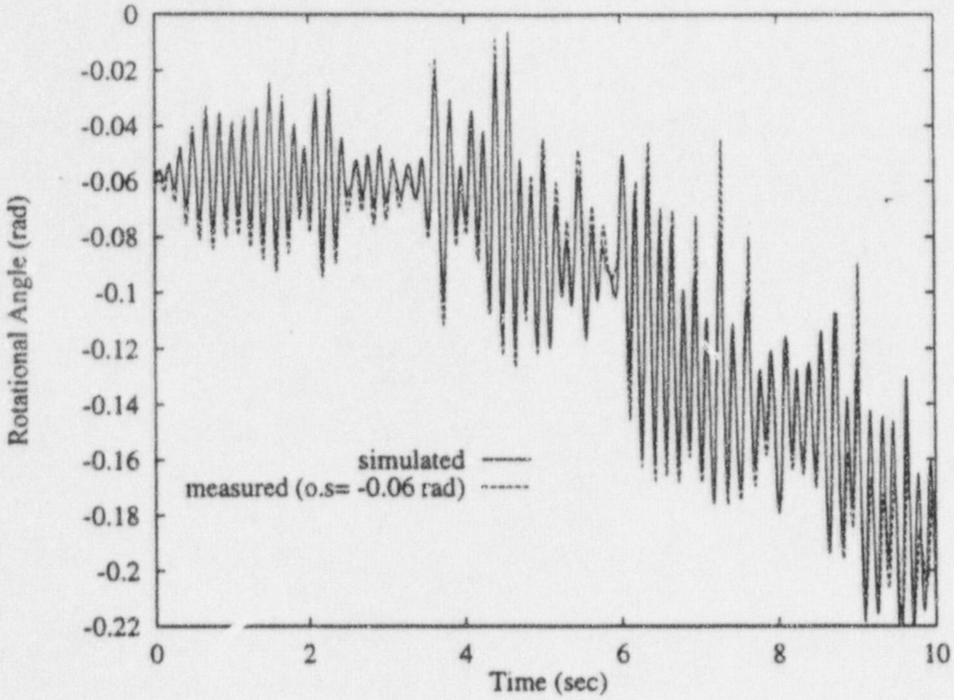

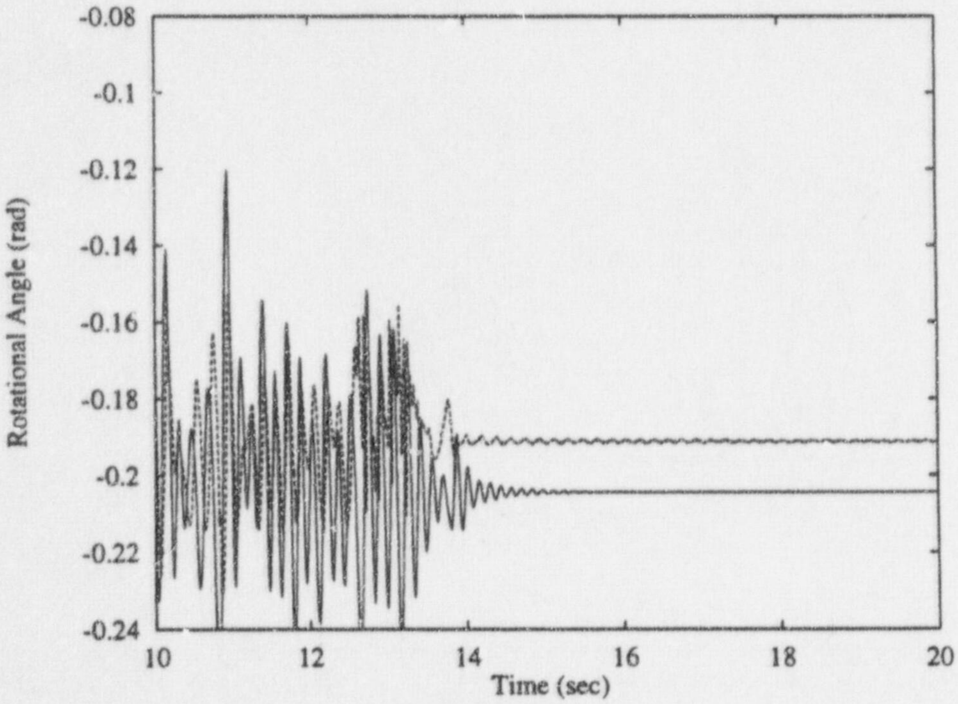

Figure 2.8: Comparison of measured and simulated response given by the optimal model for Test 40, Run 5

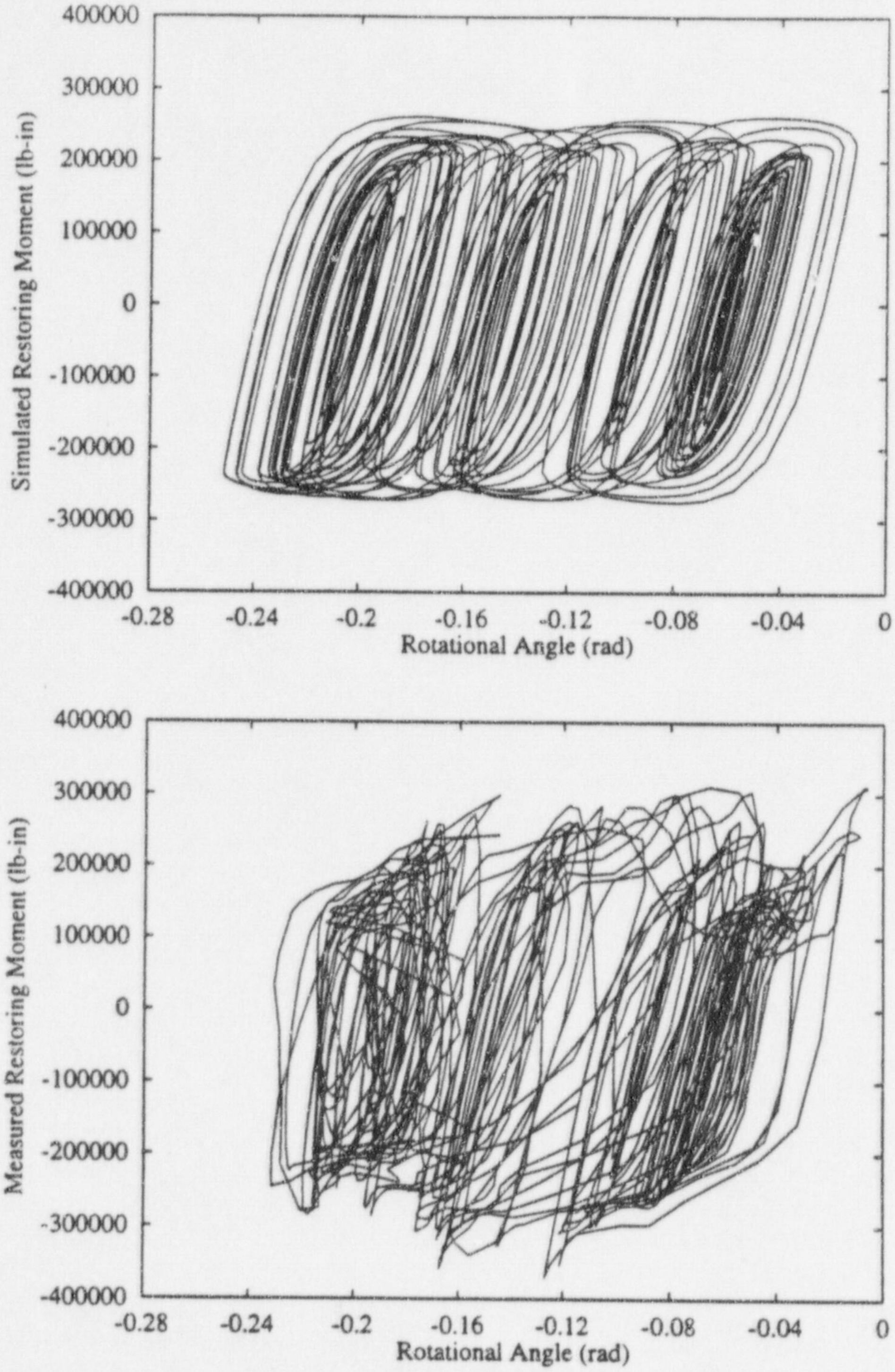

Figure 2.9: Comparison of measured and simulated hysteresis loops for Test 40, Run 5

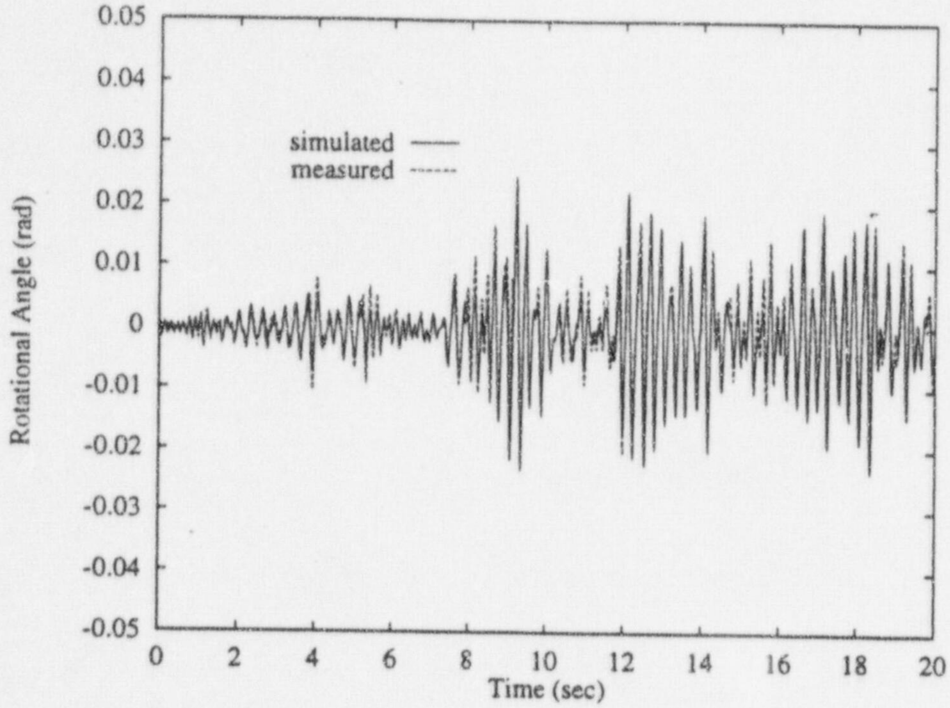

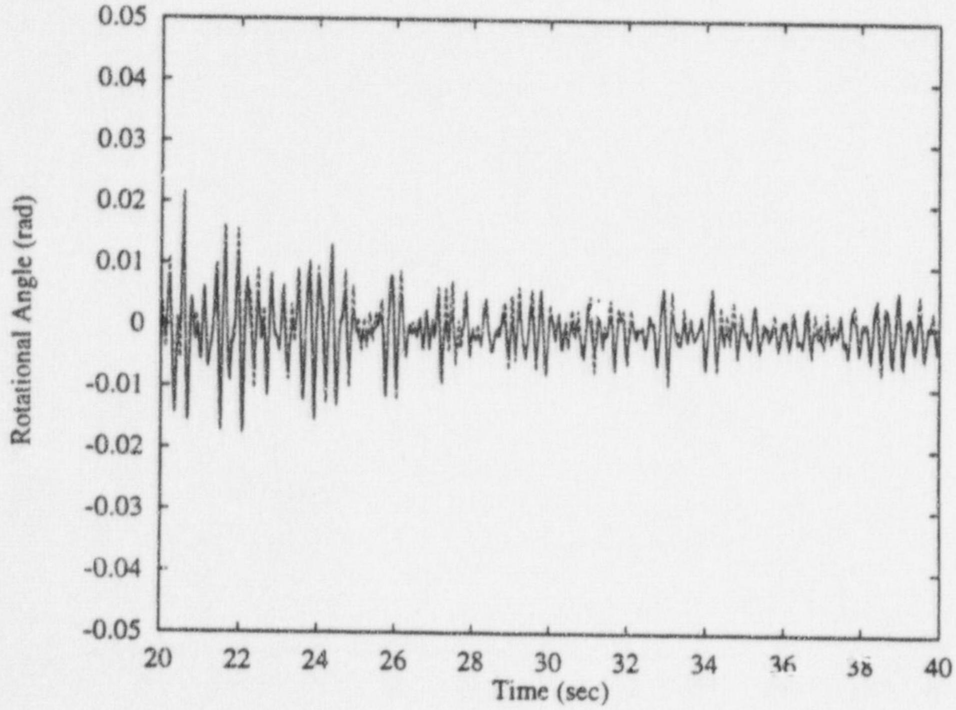

Figure 2.10: Comparison of measured and simulated response given by the optimal model for Test 36, Run 7

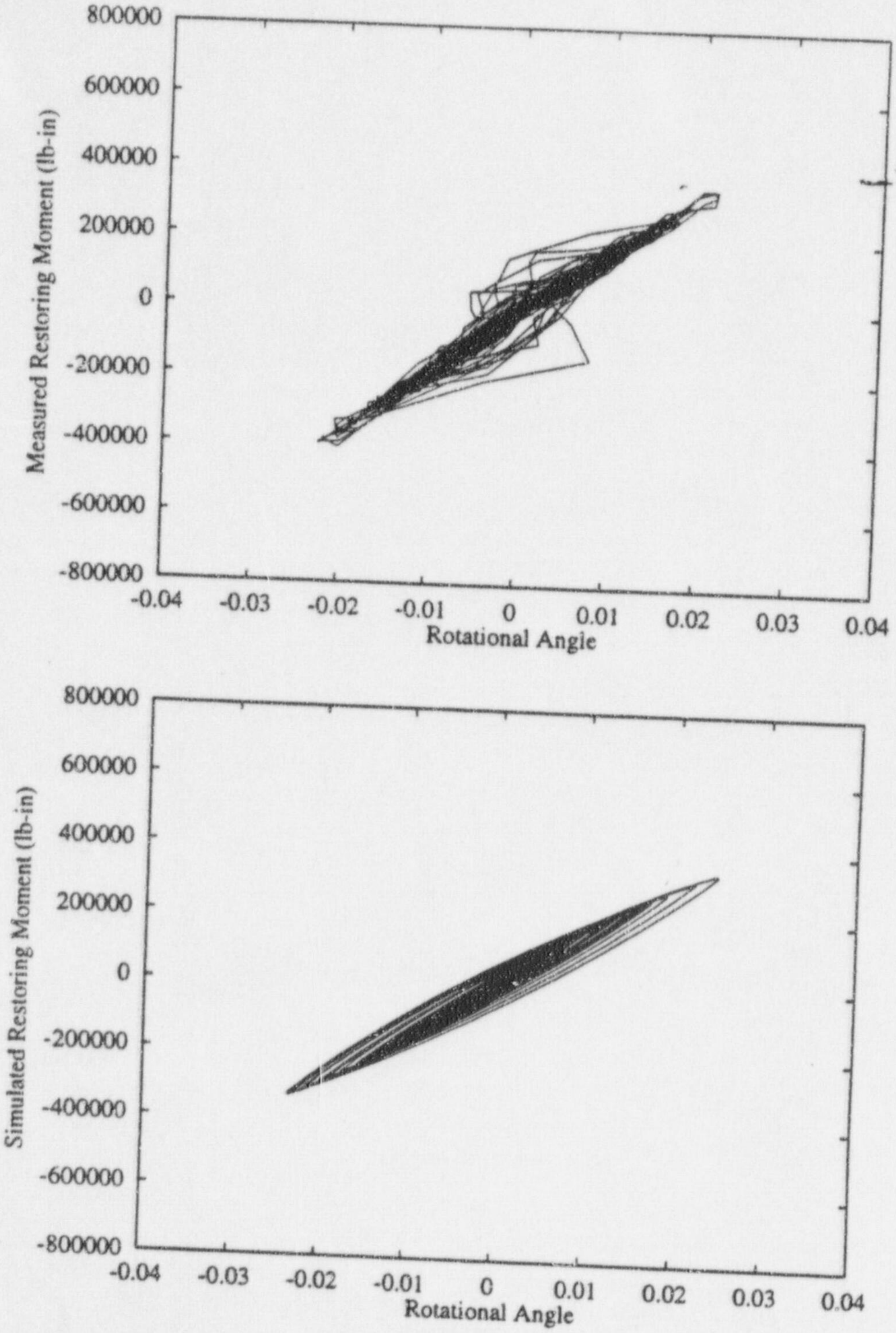

Figure 2.11: Comparison of measured and simulated hysteresis loops for Test 36, Run 7

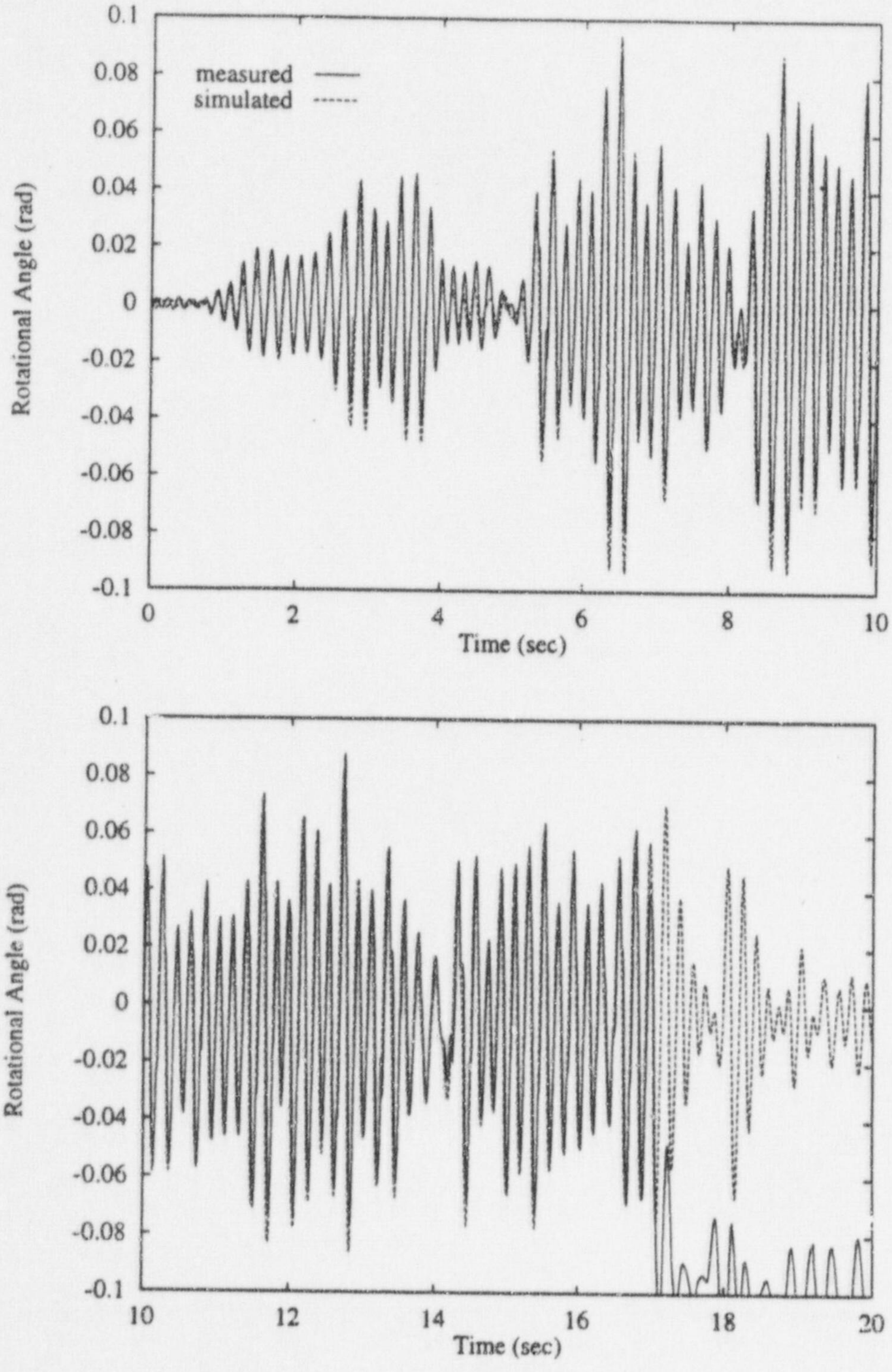

Figure 2.12: Comparison of measured and simulated response given by the optimal model for Test 36, Run 8

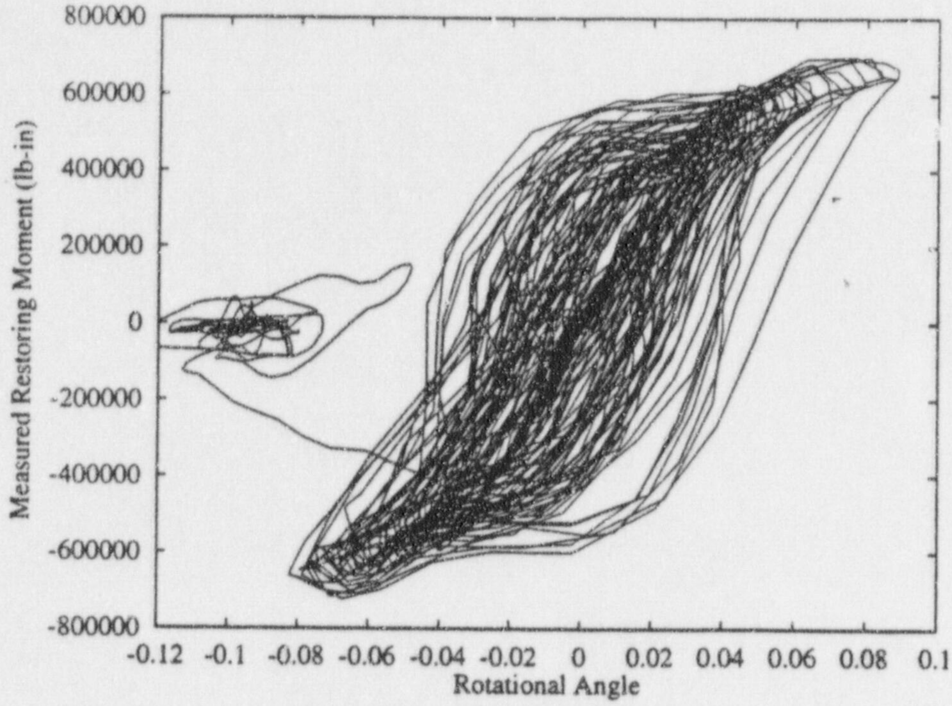

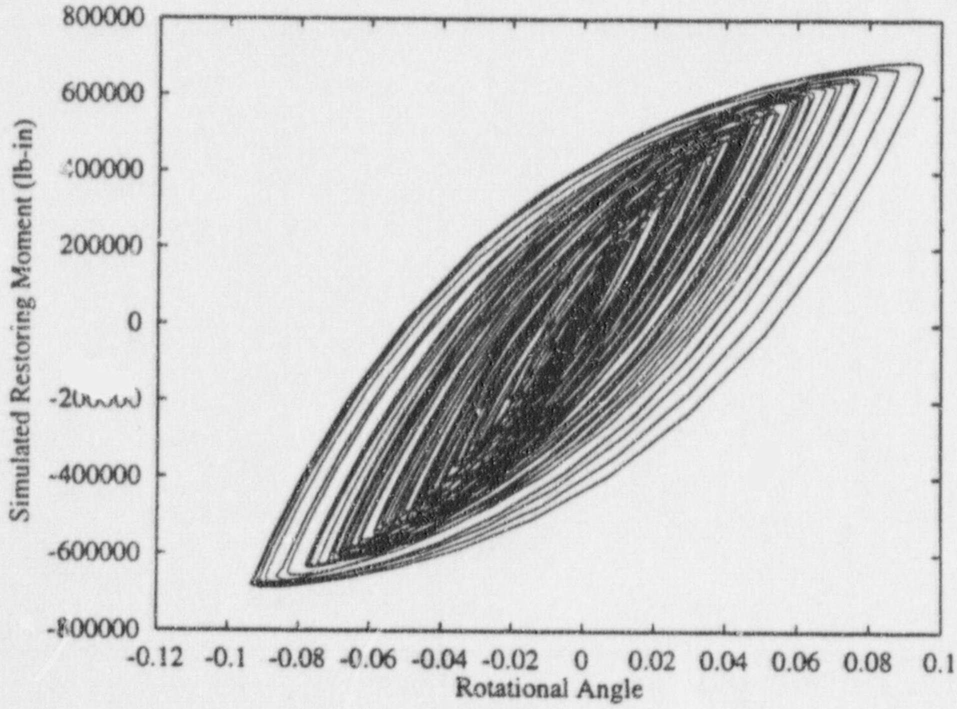

Figure 2.13: Comparison of measured and simulated hysteresis loops for Test 36, Run 8

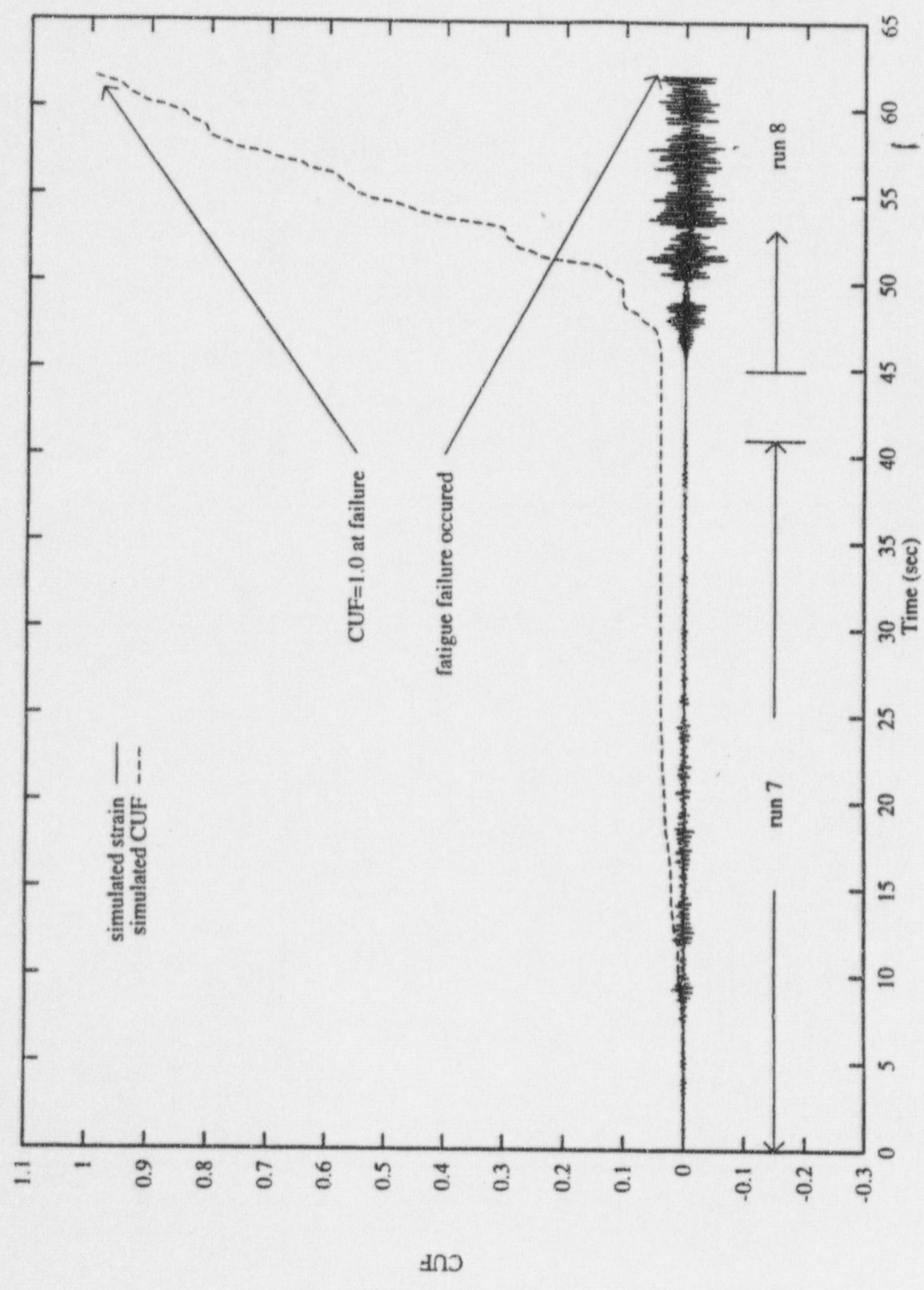

Figure 2.14: Simulated strain response and evolutionary CUF for Test 36, β=0.685

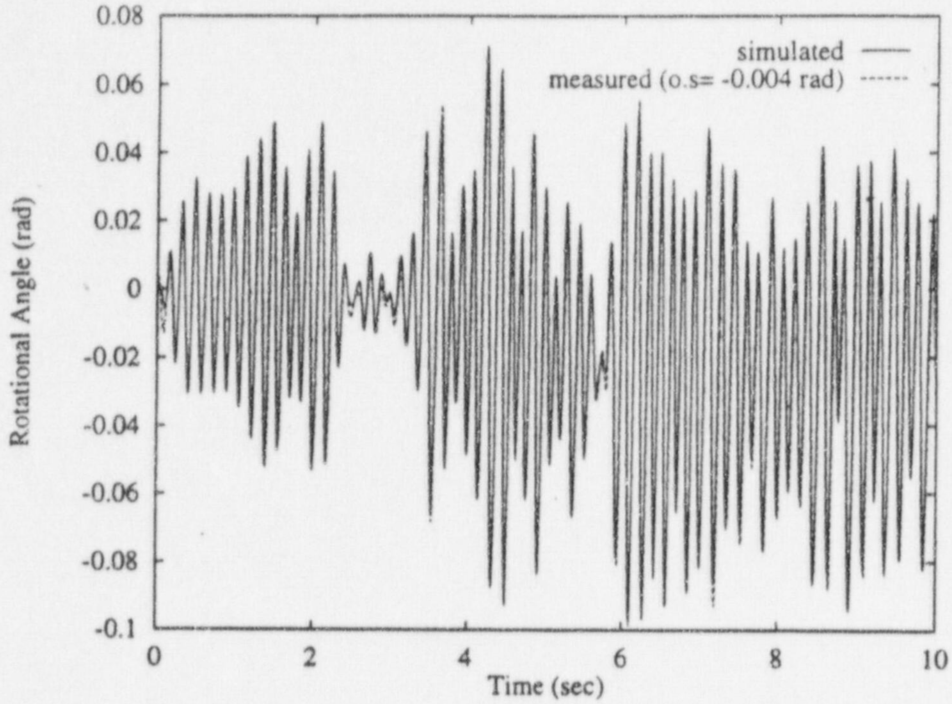

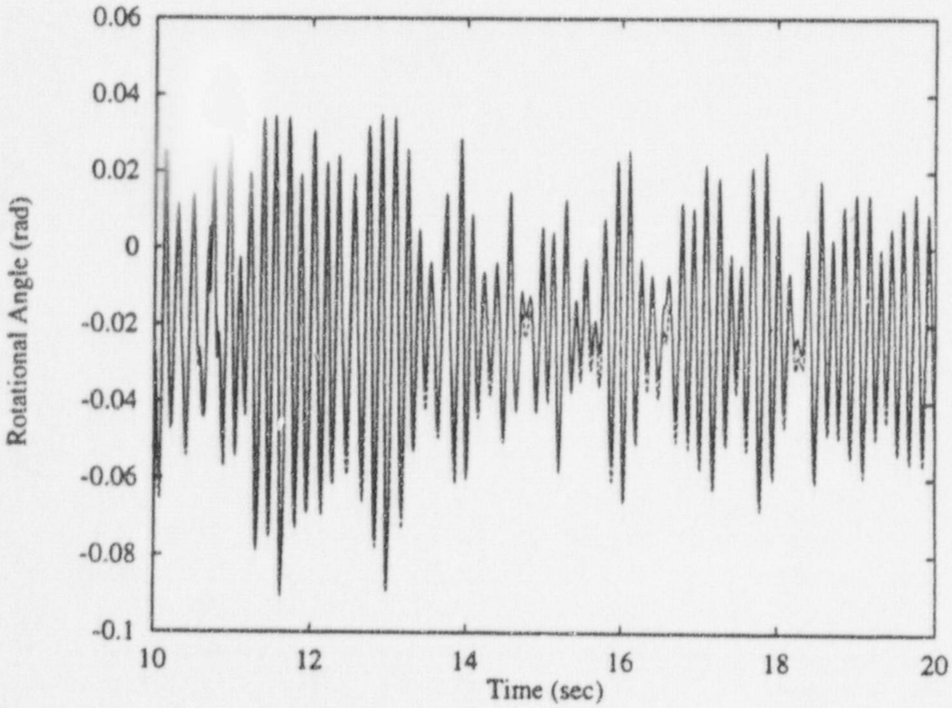

Figure 2.15: Comparison of measured and simulated response given by the optimal model for Test 14, Run 6

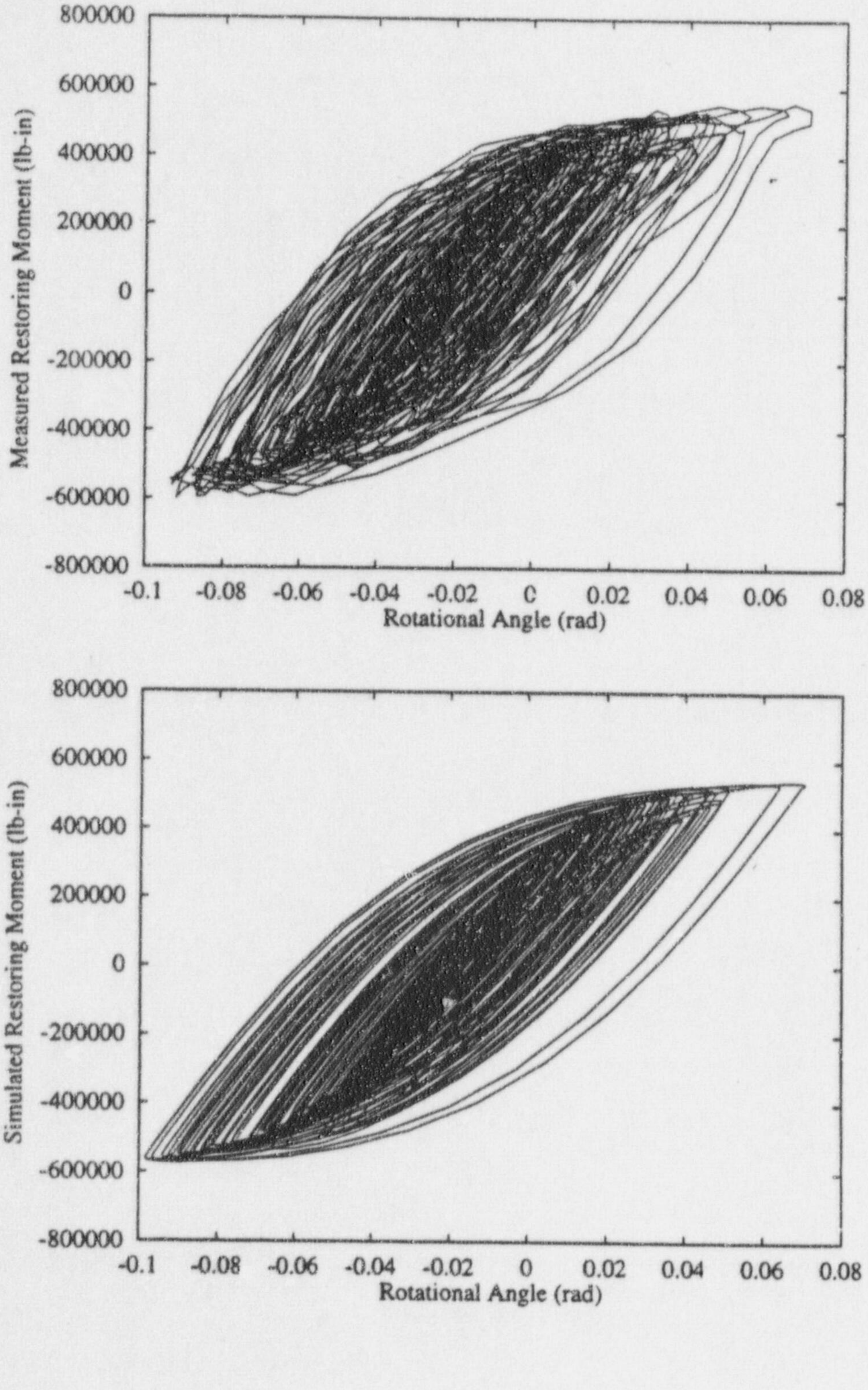

Figure 2.16: Comparison of measured and simulated hysteresis loops for Test 14, Run 6

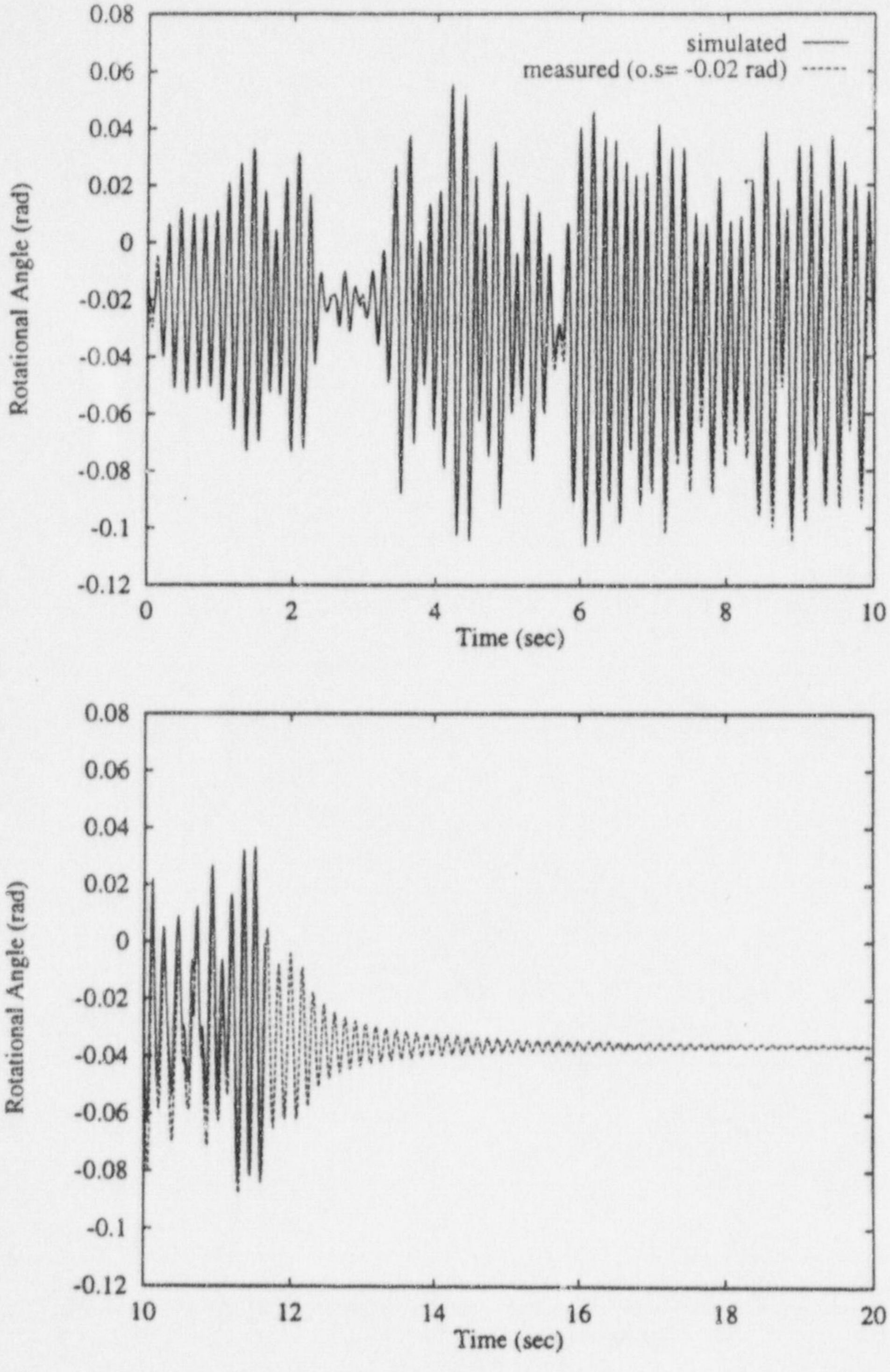

Figure 2.17: Comparison of measured and simulated response given by the optimal model for Test 14, Run 7

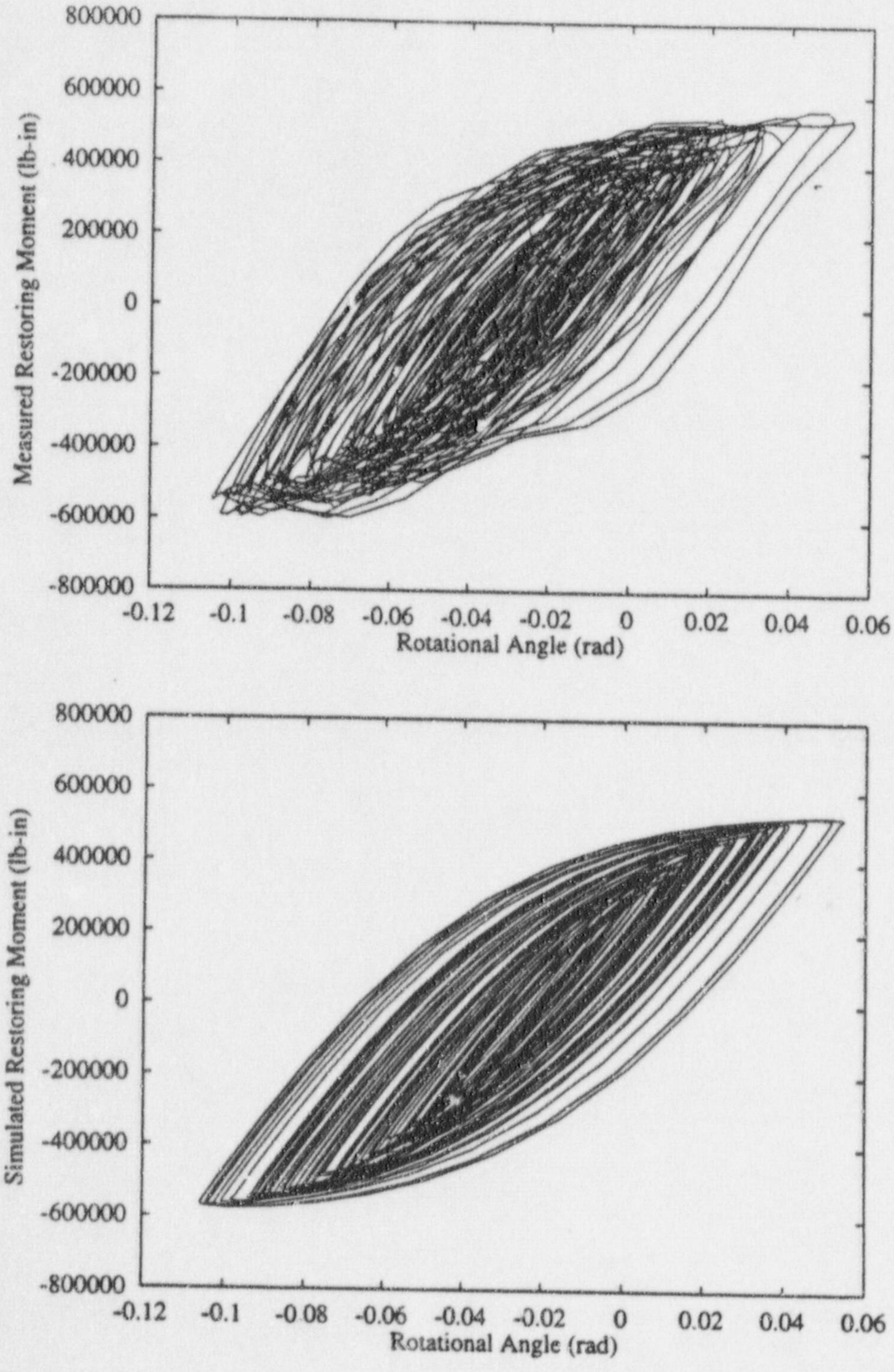

Figure 2.18: Comparison of measured and simulated hysteresis loops for Test 14, Run 7

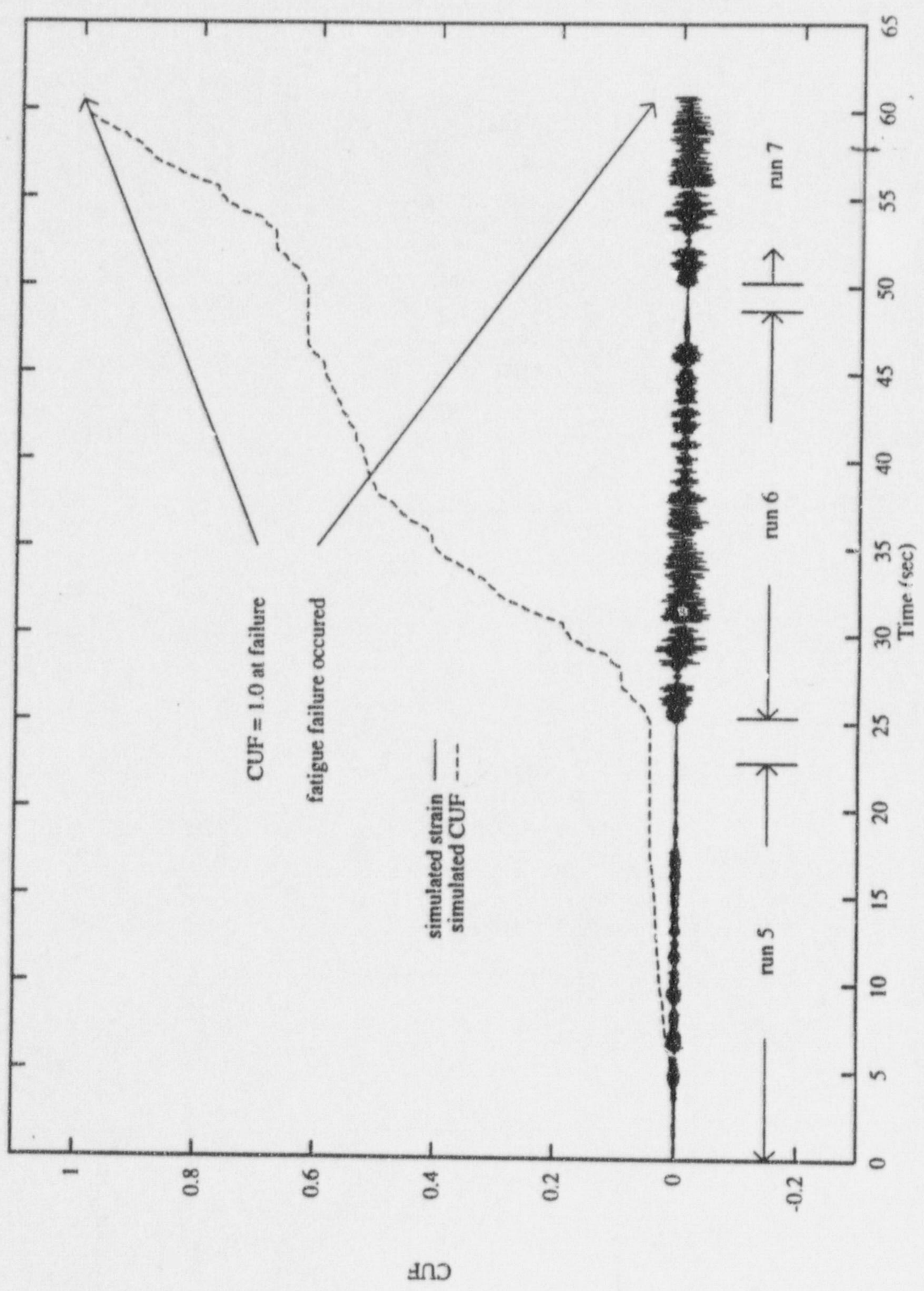

Figure 2.19: Simulated strain response and evolutionary CUF for Test 14, β=0.49

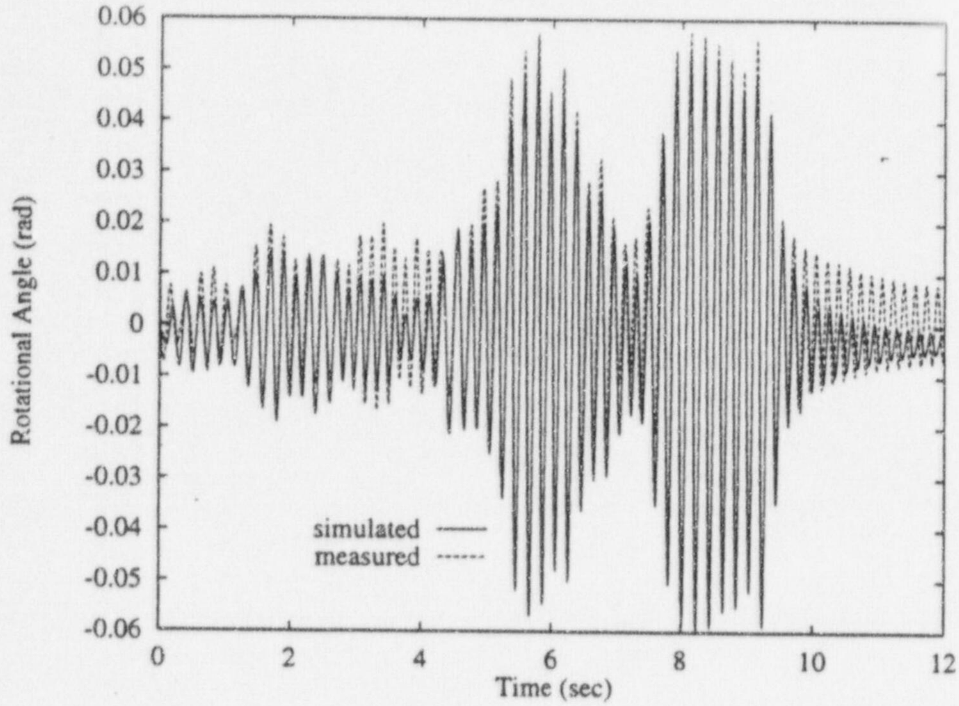

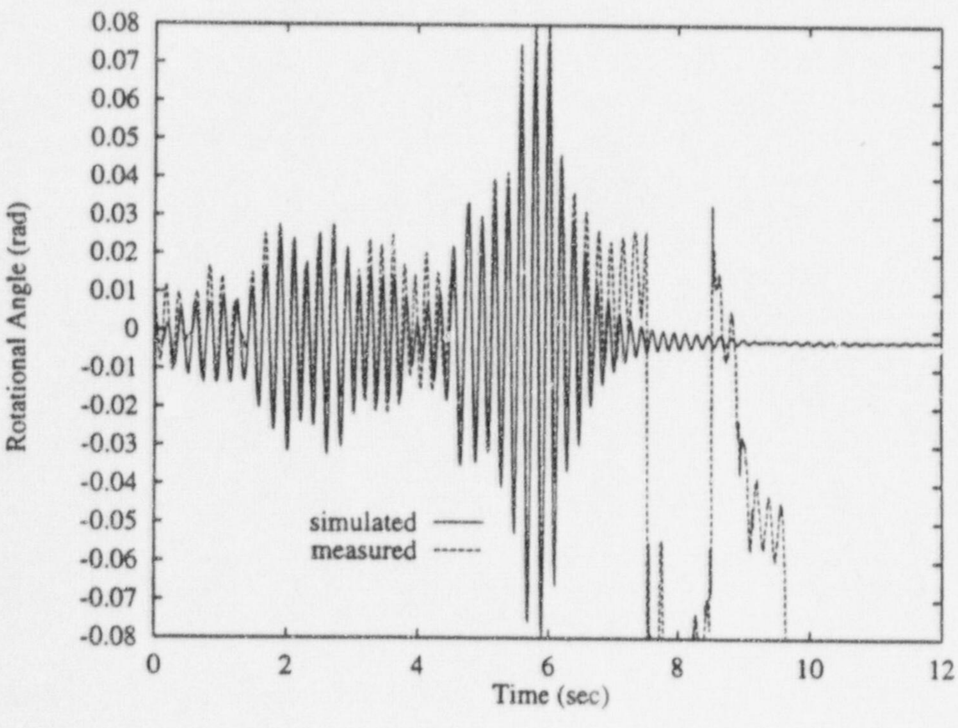

Figure 2.20: Comparison of measured and simulated response given by the optimal model for Test 11, (top) Run 6 and (bottom) Run 7

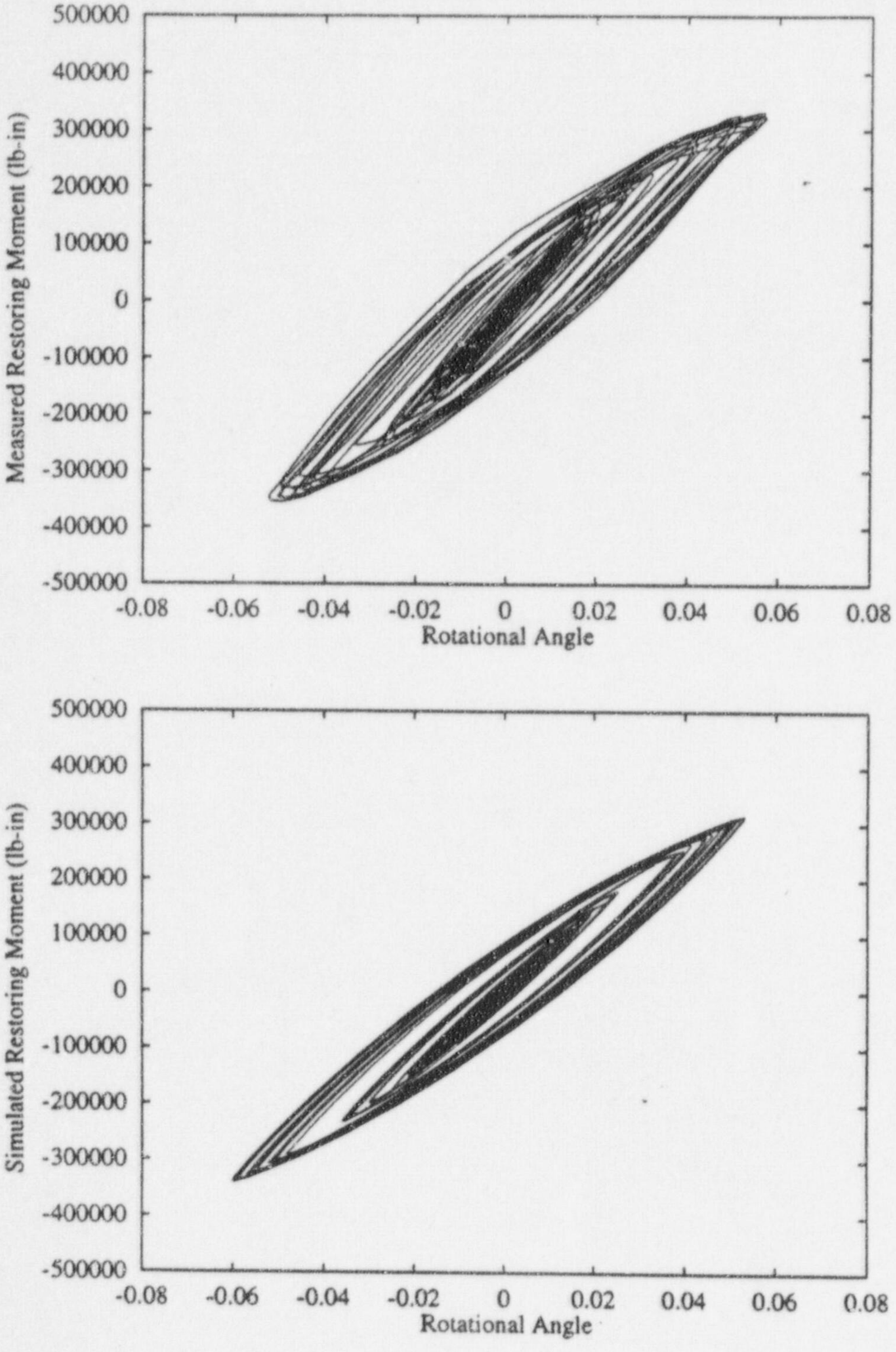

Figure 2.21: Comparison of measured and simulated hysteresis loops for Test 11, Run 6

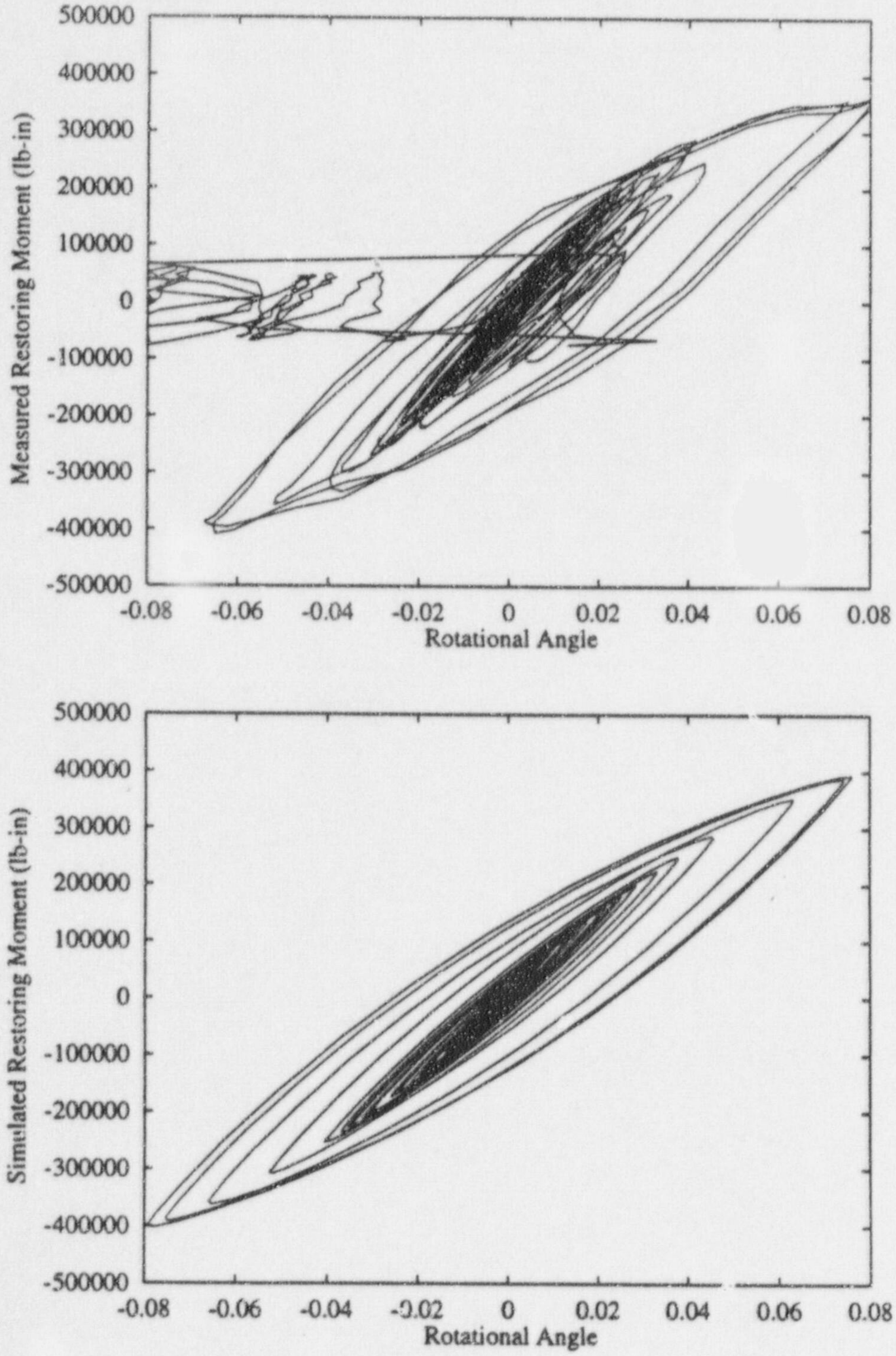

Figure 2.22: Comparison of measured and simulated hysteresis loops for Test 11, Run 7

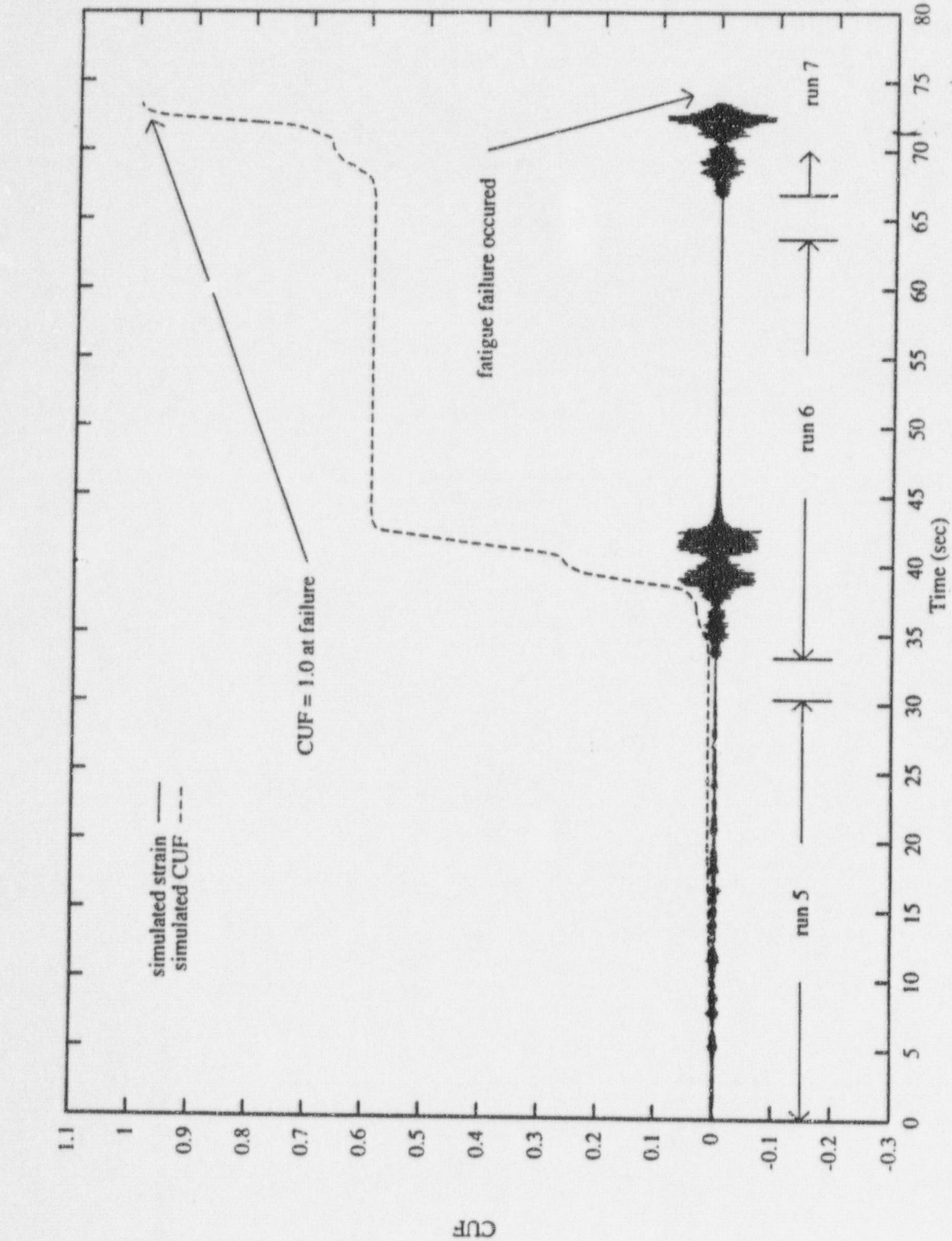

Figure 2.23: Simulated strain response and evolutionary CUF for Test 11, β=1.20

3 Analytical Seismic Margins

The objective of the analytical seismic margin study is to extend the limited frequency range of the PFDR test results to other frequencies and other dynamic loadings not tested. This study is based on the previously obtained dynamic models and fatigue damage models.

3.1 ASME Code Margins

The ASME Code (fatigue) margin M_r for a given earthquake excitation is defined as

$$M_r \equiv \frac{a_f}{a_c} \tag{3.1}$$

where a_f is the peak acceleration of the linearly amplified earthquake required to result in fatigue failure at the conclusion of the earthquake excitation. The factor a_c is the peak acceleration of the linearly amplified earthquake excitation resulting from application of the Code design procedure for calculating the maximum allowable stresses.

The Code design procedure was modified to use an *unbroadened* 5 % damped response spectra. This Code design procedure modification reflects the latest ASME consensus on margin definition. The ASME Code margin will be referred to as the fatigue margin in what follows.

3.1.1 Frequency Ratio

In the current margin study, the margin is presented in terms of a frequency ratio R_w defined as

$$R_w \equiv \frac{\omega_e}{\omega_n} \tag{3.2}$$

where ω_e is the predominant frequency of an earthquake input and ω_n is the natural frequency of the component test system.

3.1.2 Approaches in Varying Frequency Ratio

There are two possible approaches to achieving a different frequency ratio from that was tested. The first approach is to adjust the natural frequency of the test systems by physical means such as lengthening or shortening the inertial arm and adding or removing attached weight while leaving the input excitation unchanged. This approach is referred to as the Varying System Parameter (VSP) approach since it results in a variation of the system parameters in the governing equation of motion.

The second approach is referred to as the Varying Earthquake Time-scale (VET) approach. In this approach, the test system configuration is unaltered and the predominant frequency of the input excitation is adjusted by compression or stretching of the excitation time scale.

For both approaches, the model's nonlinear restoring moment characteristics must be left unchanged to preserve the test calibration. The sustained eccentric moment is excluded in the following consideration for simplicity. The VSP approach is described in Section 3.2 and the VET approach is described in Section 3.3.

3.2 Varying System Parameter (VSP) Approach

The VSP approach is considered as a parametric generalization of all possible physical means in altering the fundamental frequency of the test system. By pursuing the VSP approach, one considers an equation of motion given by

$$I\ddot{\theta}(t) + k_{p\delta}\theta(t) + m_r(\theta, \dot{\theta}) = c_f a(t) \tag{3.3}$$

where

$$m_r(\theta, \dot{\theta}) = c\dot{\theta}(t) + k_l\theta(t) + h(\theta, \dot{\theta}) \tag{3.4}$$

Eqn. (3.3) is identical to Eqn. (2.10) except that the bias moment term is removed and the excitation sense is reversed. All the symbols are as previously defined.

Substituting Eqn. (3.4) into Eqn. (3.3), and dividing the resulting equation by I, the equation of motion is rewritten as

$$\ddot{\theta}(t) + 2\zeta\omega_n\dot{\theta}(t) + \alpha_w\omega_n^2\theta(t) + (1-\alpha_w)\omega_n^2 z(\theta, \dot{\theta}) = c_p a(t) \tag{3.5}$$

where α_w is the ratio of $k_{p\delta}$ to the total linearized stiffness defined as

$$\alpha_w \equiv \frac{k_{p\delta}}{k_{p\delta} + k_{ini} + k_l} \tag{3.6}$$

c_p is a force participation factor given by

$$c_p = \frac{c_f}{I} \tag{3.7}$$

ω_n is the linearized natural frequency given by

$$\omega_n = \sqrt{\frac{k_{p\delta} + k_{ini} + k_l}{I}} \tag{3.8}$$

ζ is the damping ratio of the system given by

$$\zeta = \frac{c}{2\sqrt{I(k_{ini} + k_l + k_{p\delta})}} \tag{3.9}$$

$z(\theta, \dot{\theta})$ is a normalized hysteresis given by

$$z(\theta, \dot{\theta}) = \frac{k_l\theta + h(\theta, \dot{\theta})}{k_l + k_{ini}} \tag{3.10}$$

Clearly, the normalized hysteresis $z(\theta, \dot{\theta})$ has an initial slope of unity.

3.2.1 Evaluation of a_c

Evaluation of a_c is based on a linear version of Eqn. (3.5). Since the normalized hysteretic restoring moment $z(\theta, \dot{\theta})$ has an initial slope of unity, this results in a linearized equation of motion

$$\ddot{\theta}(t) + 2\zeta\omega_n\dot{\theta}(t) + \omega_n^2\theta(t) = c_p a(t) \tag{3.11}$$

The restoring moment in Eqn. (3.4) for this case is therefore given by

$$m_r(\theta, \dot{\theta}) = c\dot{\theta}(t) + (k_{ini} + k_l)\theta(t) \tag{3.12}$$

The factor a_c is evaluated under the condition that the restoring moment reaches maximum Code allowable moment. The peak restoring moment usually occurs at a zero velocity, and is therefore approximated by

$$\text{Max} \ \left|m_r(\theta, \dot{\theta})\right| \approx \text{Max} \ \left|(k_{ini} + k_l)\,\theta(t)\right| \tag{3.13}$$

The maximum Code allowable moment is denoted as M_c, and ζ_c is the 5% damping ratio specified in the Code design procedure. The factor a_c is evaluated based on

ζ_c such that

$$\text{Max} \quad |(k_{ini} + k_l)\,\theta(t)| = M_c$$

For a given ζ_c and M_c and given piping parameters k_{ini} and k_l, the factor a_c is governed by ω_n and c_p only. Replacing the dependent parameter ω_n by the frequency ratio R_w, the functional dependency for a_c can be expressed as

$$a_c = a_c(R_w, c_p) \tag{3.14}$$

3.2.2 Evaluation of a_f

A similar procedure is used to evaluate a_f except that the nonlinear response is considered and fatigue failure is used as the condition. The fatigue failure condition is reached when the cumulative fatigue usage factor CUF reaches unity at the end of one earthquake excitation. For illustration purposes, Eqn. (3.5) is rewritten here.

$$\ddot{\theta}(t) + 2\zeta\omega_n\dot{\theta}(t) + \alpha_w\omega_n^2\theta(t) + (1-\alpha_w)\omega_n^2 z(\theta,\dot{\theta}) = c_p a(t) \tag{3.15}$$

As shown by Eqn. (3.9), the analytical damping ratio ζ in Eqn. (3.15) becomes frequency-dependent when a fixed-value damping constant c is used. However,

1. The linear damping mechanism in the actual system is generally poorly known.

2. The damping constant c generally exhibits a certain degree of uncertainty as a result of the system identification procedure.

3. The total system damping is strongly dominated by the hysteretic damping in the nonlinear failure analysis.

It is thus preferred to provide a constant damping ratio ζ_s such that a frequency-independent damping ratio is uniformly assigned for all altered test systems. The value of ζ_s can be selected according to engineering considerations or be selected based on the system damping ratio identified from the test data.

Examining Eqn. (3.15), the free parameters controlling a_f involve not only ω_n and c_p but also the stiffness fraction α_w. More specifically, to achieved the failure condition $CUF = 1$, the system may undergo a highly yielding response where the post-yielding stiffness k_l and the geometrical stiffness $k_{p\delta}$ may play significant roles. Therefore, the parameter dependency for a_f becomes

$$a_f = a_f(R_w, \alpha_w, c_p) \quad . \tag{3.16}$$

3.2.3 Margin Spectra: Parametric Representation

Substituting Eqns. (3.16) and (3.14) into the ASME Code margin definition yields

$$M_r(R_w, \alpha_w, c_p) = \frac{a_f(R_w, \alpha_w, c_p)}{a_c(R_w, c_p)} \tag{3.17}$$

The above functional dependency can be further simplified by considering the role of c_p. Let λ be some arbitrary constant. Then, the factor a_c follows an amplification rule given as

$$a_c(R_w, \lambda c_p) = \frac{1}{\lambda} a_c(R_w, c_p) \tag{3.18}$$

Although nonlinear analysis is used, a similar amplification rule is also valid for a_f. That is,

$$a_f(R_w, \alpha_w, \lambda c_p) = \frac{1}{\lambda} a_f(R_w, \alpha_w, c_p) \tag{3.19}$$

Then, using Eqn. (3.17) and the amplification rules, Eqn. (3.18) and Eqn. (3.19), the ASME Code margin of a system with a participation factor λc_p is derived as

$$\begin{aligned} M_r(R_w, \alpha_w, \lambda c_p) &= \frac{a_f(R_w, \alpha_w, \lambda c_p)}{a_c(R_w, \lambda c_p)} \\ &= \frac{a_f(R_w, \alpha_w, c_p)}{a_c(R_w, c_p)} \\ &= M_r(R_w, \alpha_w, c_p) \quad (3.20) \end{aligned}$$

Eqn. (3.20) shows the margin is *independent* of the value of c_p for any system expressible in the form of Eqn. (3.5), and leads to the following parametric representation for the ASME Code margin

$$M_r = M_r(R_w, \alpha_w) \quad (3.21)$$

Motivated by the simplicity of this parametric representation, a *margin spectrum* is herein proposed where the margin curve is plotted as a function over a desired R_w range using a fixed value of α_w. In addition, multiple margin curves with different values of α_w can be simultaneously presented to account for the $P-\Delta$ effects.

3.3 Varying Earthquake Time-scale (VET) Approach

The VET approach maintains the physical test system unaltered, but changes the predominant earthquake frequency by compressing or stretching the earthquake data in time. By this process, the total excitation duration will also be changed due to the change in the time step of the earthquake data.

Let the earthquake time history $a(t)$ be altered as $a(\lambda t)$, where λ is an arbitrary constant. The equation of motion for the VET approach can then be described by

$$\begin{aligned} &\ddot{\theta}(t) + 2\zeta\omega_n\dot{\theta}(t) + \alpha_w\omega_n^2\theta(t) + (1-\alpha_w)\omega_n^2 z(\theta, \dot{\theta}) \\ &= c_p a(\lambda t), \quad 0 \le t \le \frac{t_f}{\lambda} \quad (3.22) \end{aligned}$$

where t_f represents the end of the excitation duration.

3.3.1 Alternative Statement

Consider the process of subdividing the response given by Eqn. (3.22) into peak to peak response segments as illustrated in Fig. 3.1. Each response segment starts with zero initial velocity and also ends with zero velocity.

The restoring force associated with each response segment represents a segment of the hysteresis curve between consecutive turning points. In general, this restoring force is a nonlinear function of the displacement variable only. This statement holds for hysteretic models ranging from elasto-plastic type, bilinear type, to the class of curved-hysteresis models as currently employed.

Denote each segment of restoring force as $\phi_i(\theta)$, which is a nonlinear function of θ only. The equation of motion governing this response segment can be written as

$$\begin{aligned} &\ddot{\theta}(t) + 2\zeta\omega_n\dot{\theta}(t) + \alpha_w\omega_n^2\theta(t) + (1-\alpha_w)\omega_n^2\phi_i(\theta) \\ &= c_p a(\lambda t), \quad t_i \le t \le t_{i+1} \quad (3.23) \end{aligned}$$

Introducing a new time variable $\tau = \lambda t$, it follows

$$\ddot{\theta}(t) = \lambda^2\theta''(\tau), \qquad \dot{\theta}(t) = \lambda\theta'(\tau) \quad (3.24)$$

Substituting Eqn. (3.24) into Eqn. (3.23) and dividing

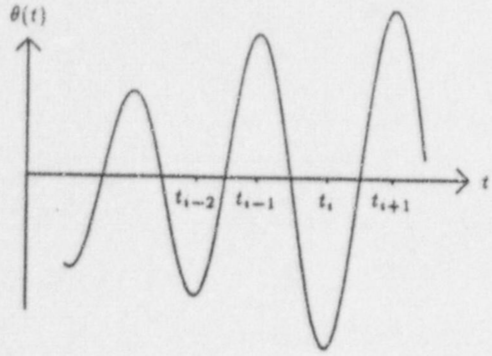

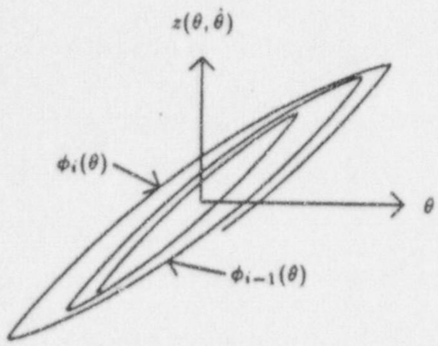

Figure 3.1: Response and restoring force segments of a hysteretic response

the resulting equation by λ^2 yields

$$\theta''(\tau) + 2\zeta\tfrac{\omega_a}{\lambda}\theta'(\tau) + \alpha_w(\tfrac{\omega_a}{\lambda})^2\theta(\tau) +$$
$$(1-\alpha_w)(\tfrac{\omega_a}{\lambda})^2\phi_i(\theta) = \tfrac{c_p}{\lambda^2}a(\tau),\ \lambda t_i \le \tau \le \lambda t_{i+1} \quad (3.25)$$

One can start this transformation from the first response segment and continue until the end of the response process. By concatenating each equation segment represented by Eqn. (3.25), an alternative statement to Eqn. (3.22) can thus be formed as

$$\theta''(\tau) + 2\zeta\tfrac{\omega_a}{\lambda}\theta'(\tau) + \alpha_w(\tfrac{\omega_a}{\lambda})^2\theta(\tau) +$$
$$(1-\alpha_w)(\tfrac{\omega_a}{\lambda})^2 z(\theta,\theta') = \tfrac{c_p}{\lambda^2}a(\tau),\ 0 \le \tau \le t_f \quad (3.26)$$

The validity of the above representation is substantiated by the observation that the hysteretic force depends on the sign but not the magnitude of velocity response. Therefore, the restoring force $z(\theta,\theta')$ offers exactly the same sequence of restoring functions $\{\phi_0, \phi_1, \cdots, \phi_i, \cdots\}$ as that given by $z(\theta,\dot{\theta})$.

Further considering the time variable τ in Eqn. (3.26) as a dummy time variable and replacing the τ variable by the conventional time variable t, a new system is constructed as

$$\ddot{\theta}(t) + 2\zeta\tfrac{\omega_a}{\lambda}\dot{\theta}(t) + \alpha_w(\tfrac{\omega_a}{\lambda})^2\theta(t) +$$
$$(1-\alpha_w)(\tfrac{\omega_a}{\lambda})^2 z(\theta,\dot{\theta}) = \tfrac{c_p}{\lambda^2}a(t),\ 0 \le t \le t_f \quad (3.27)$$

Given any solution function $\theta^*(t)$ that satisfies Eqn. (3.27), then $\theta^*(\lambda t)$ will satisfy Eqn. (3.22) automatically. Therefore, the displacement responses of Eqn. (3.27) and Eqn. (3.22) have identical response shape and response magnitude except for a different time scale in the time histories. Consequently, the peak response amplitude and fatigue damage of the two systems would also be identical. It is also noticed that a linear consideration of Eqn. (3.22) is only a sub-case of the nonlinear hysteretic case presented. Therefore, the margin and the failure acceleration levels for Eqn. (3.22) can identically be obtained by analyzing Eqn. (3.27).

3.3.2 Relation to VSP Approach

By pursuing the VSP approach to achieve the same frequency ratio, one alters the equation of motion as

$$\ddot{\theta}(t) + 2\zeta\tfrac{\omega_a}{\lambda}\dot{\theta}(t) + \alpha_w(\tfrac{\omega_a}{\lambda})^2\theta(t) +$$
$$(1-\alpha_w)(\tfrac{\omega_a}{\lambda})^2 z(\theta,\dot{\theta}) = c_p a(t),\ 0 \le t \le t_f \quad (3.28)$$

Eqn. (3.28) and Eqn. (3.27) differ only by a constant divider λ^2 in the force participation factor. Applying the argument that margin is independent of the force participation factor as shown previously, it is concluded that the margin will be identically obtained by either the VET approach or the VSP approach.

However, the VET approach and VSP approach will give different acceleration levels required for failure. Denote the over-hat symbols $\hat{a}_c$ and $\hat{a}_f$ as the required acceleration levels for the VET approach to reach Code allowable moment and fatigue failure respectively. By the amplification rules stated in Eqn. (3.18) and Eqn. (3.19), $\hat{a}_c$ and $\hat{a}_f$ satisfy the following relationship.

$$\begin{aligned} \hat{a}_c &= \lambda^2 a_c \\ \hat{a}_f &= \lambda^2 a_f \end{aligned} \qquad (3.29)$$

where a_c and a_f are the acceleration levels for the VSP approach as previously defined.

This λ^2 relationship yields a very different curve shape for $\hat{a}_c$ and $\hat{a}_f$ when plotted as functions of R_w. Since the R_w of the altered system is directly proportional to λ, the $\hat{a}_c$ and $\hat{a}_f$ curves are proportional to a_c and a_f by a factor of R_w^2.

3.4 Analytical Code Margin Results

3.4.1 Input Earthquakes

Two earthquake loadings are considered: the PFDR time history B (abbreviated as PFDR) input and the Regulatory Guide (RG) 1.60 earthquake. The PFDR input is a 25-second excitation that represents a narrow-banded input motion and its response spectrum is sharply peaked at a frequency of 7.5 Hz. The PFDR time history is shown in Fig. 3.2, and the pseudo-acceleration and displacement response spectra are given in Fig. 3.4 and Fig. 3.5 respectively. The RG 1.60 input represents a typical broad-banded earthquake motion. The reference frequency of RG 1.60 input for purpose of calculation of R_w is arbitrarily taken at 7.5 Hz to facilitate the comparison. The acceleration time history is shown in Fig. 3.3, and the corresponding response spectra are given in Figs. 3.6 and 3.7. It is observed from the acceleration time histories that the duration of strong shaking for the PFDR input is about 10 seconds and for the RG 1.60 input is about 20 seconds.

3.4.2 Code Allowable Moment

For the Service Level D SSE loading, the new ASME rule for calculating the Code allowable moment is

$$\frac{B_1\, P\, D_0}{2\,t} + \frac{B_2\, M}{Z} \leq 4.5 S_m \qquad (3.30)$$

where S_m is the Code material allowable stress, B_1 and B_2 are stress indices, P is the pressure, D_0, Z and t are component geometric properties, and M is the resultant moment amplitude due to weight, SSE inertia effects and other mechanical loads.

Rearranging Eqn. (3.30), the maximum allowable Code moment, M_c, satisfies

$$B_2 M_c = Z\,(4.5 S_m) - \frac{P\, Z\, D_0\, B_1}{2t} \qquad (3.31)$$

Using $S_m = 20,000$ psi at $100°F$, the component data and the calculated Code allowable moment for PFDR Tests 11, 36, 14 and 40 are tabulated in Table 3.1.

Test No.	P (psi)	Z (in^3)	t (in)	D_0 (in)	B_1	$B_2 M_c$ (in-lb)
36	1700	8.5	0.28	6.625	0.5	679,526
11	400	4.35	0.134	6.625	0.5	369,994
14	1700	8.5	0.28	6.625	0.5	679,526
40	0	3.21	0.237	4.5	0.5	288,900

Table 3.1: Calculation of Code allowable moment

3.4.3 Analytical Margin Results

The analytical procedures of ASME Code margins for PFDR Tests 11, 14 and 36 are presented using the proposed parametric representation following the VSP approach. The margins are normalized by the ASME primary stress index B_2, and are plotted over a range of $0.5 \leq R_w \leq 4.0$. The primary stress index has been factored out of the margin as there is debate over just what value this index should have for several of the component tests considered. Three levels of P-Δ effect, α_w = 5%, 0% and -5 %, are evaluated using the Sequential Method of cycle counting in the fatigue analysis. The $\alpha_w = -5\%$ case is also analyzed using the Rainflow Method of cycle counting for comparison. These margin results are shown in Fig. 3.8 - Fig. 3.19.

General observations concerning the results are summarized below.

1. For the R_w range considered, both the PFDR and RG 1.60 fatigue margins follow a general increasing trend as R_w increases. For $R_w \leq 1$, low margin factors on the order of unity are frequently observed for both the PFDR and RG 1.60 inputs.

2. The degree of irregularity of the margin spectra seems to correspond to the degree of irregularity in the shape of the input spectra. The PFDR fatigue margins exhibit a more irregular curve shape as compared to the smoother RG 1.60 fatigue margins.

3. For the PFDR input, a rapid increase in margin is observed as R_w increases from 0.5 towards 1.

4. The effect of P-Δ stiffness is observed to be a relatively insignificant contribution to both the magnitude and shape of the margin curves for most tests considered except for the $\alpha_w = -5\%$ case in Test 14. It is believed that this exception is because Test 14 has a small k_l to k_{ini} ratio.

5. Fatigue analyses based on either the Sequential or the Rainflow cycle count method give similar margin results

3.5 Response Implications

Although the P-Δ effect is generally observed to be inconsequential to the fatigue margins, important additional insight is gained by plotting CUF as a function of R_w and the peak acceleration of the linearly amplified PFDR input. This indicates a cliff-like profile due to the influence of the negative (destabilizing) P-Δ stiffness (See Figs. 3.20 and 3.21 for Test 36, and Figs. 3.23 and 3.24 for Test 14). The sudden increase in the CUF profile at the "cliff" is caused by excessive rotational ratcheting. This shows a region where the CUF can be highly responsive to small increases in input excitation level.

The possible occurrence of unstable displacement response is also indicated in Figs. 3.22 and 3.25. These figures show three rotational response time histories corresponding to R_w = 0.5, 1.5 and 3.0 under relatively mild P-Δ effects. Each of these rotation time histories results from a different level of PFDR input intensity, but they all correspond to the same fatigue failure condition that CUF = 1. Both the response for R_w = 1.5 and 3.0 exhibit ratcheting behavior with very large peak rotations. To explain this, one notices that for a SDOF system undergoing a fixed duration of excitation, the total number of response cycles decreases as the natural period increases. Hence, a higher R_w system generally requires larger average response-ranges to achieve

CUF = 1, particularly in the low cycle failure region where the fatigue damage is relatively less sensitive to increases in strain amplitude. Such response behavior introduces deformation response issues not adequately addressed by the consideration of fatigue damage alone.

3.6 Displacement Based Margin

The potential occurrence of excessive rotational response raises concern about possible deformation-induced failure modes, such as bucking or collapse. Moreover, quantitative assessments of fatigue damage for such large displacements are highly uncertain since

- the analysis for large displacements may extend beyond the range of applicability of the analytical model, and
- the fatigue damage correlation does not include known detrimental effects of coincident accumulated mean strain.

To address these issues, a displacement-based margin (displacement margin) is developed to complement the use of the fatigue margin. By analogy to the fatigue margin, the proposed displacement $M_r^{(\theta)}$ is defined as

$$M_r^{(\theta)} = \frac{a_\theta}{a_c} \tag{3.32}$$

where a_θ is the loading intensity required to reach a prescribed rotation limit θ_m and a_c is as previously defined. The value of of θ_m can be prescribed according to engineering considerations or set equal to the rotational capability demonstrated in the tests. The introduction of this displacement-based failure condition also provides a basis for margin analysis for those tests that did not fail in fatigue, such as Test 40.

The frequency ratio effects on displacement margins can be represented using the same parametric approach adopted for fatigue margins. It can also be concluded that $M_r^{(\theta)}$ is a two-parameter function that can be represented as

$$M_r^{(\theta)} = M_r^{(\theta)}(R_w, \alpha_w) \tag{3.38}$$

The discussions regarding parametric representation for the fatigue margin are also applicable to the displacement margin.

The numerical results of displacement margins are presented in Figs. 3.26 - 3.33. The θ_m prescribed for Tests 14, 36 and 11 are respectively 0.12, 0.09 and 0.08 radians. These selected values are the maximum test rotations. This conservatively assumes rotations in excess of those demonstrated in the tests will lead to immediate failure. For Test 40, θ_m is set equal to 10 degrees in rotation, an early Code rule limit addressing collapse - later dropped, which is approximately equal to 0.17 in radians.

The displacement-based margins are observed to be generally lower than the fatigue margins, particularly for higher R_w systems. This indicates the greater tendency for ratcheting associated with higher R_w systems undergoing yielding response. The effect of P-Δ stiffness is seen to be inconsequential to the displacement margins for Tests 36, 14 and 11. For Test 40, the P-Δ effect results in greater variations in displacement margins due to its larger θ_m.

During the numerical iteration process to determine the displacement margins, it was observed that the rotational responses are relatively insensitive to variations in the input intensity around the prescribed θ_m even at the $\alpha_w = -5\%$ level. This is because that the displacement-based failure region, as a function of R_w and peak input acceleration, is located in a region of stable response and is sufficiently far away from the "cliff" observed in the fatigue margin analysis. This property indicates that the proposed displacement-based margin is a more stable margin than the highly input sensitive fatigue margin.

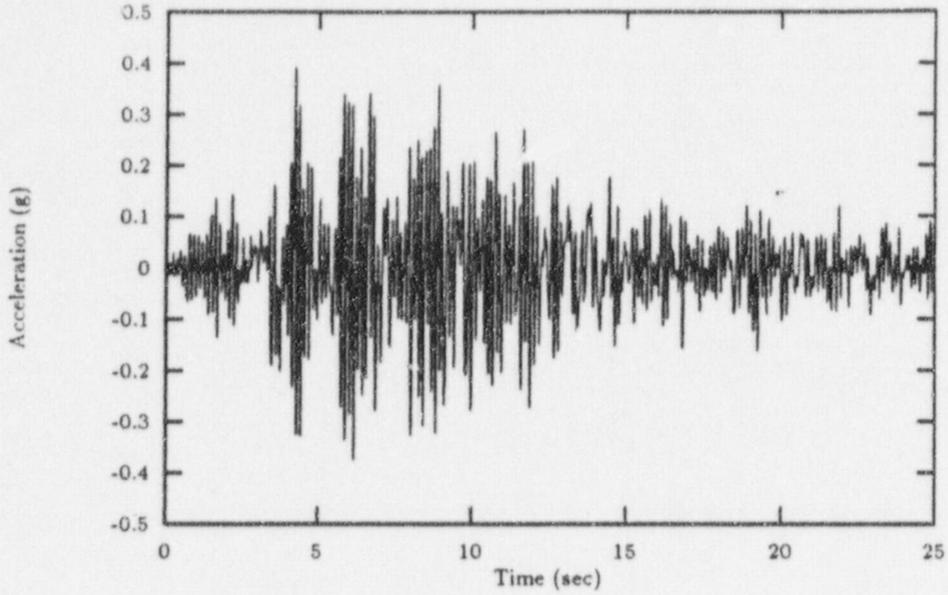

Figure 3.2: PFDR input: peak acceleration = 0.383 g, dominant frequency = 7.5 Hz

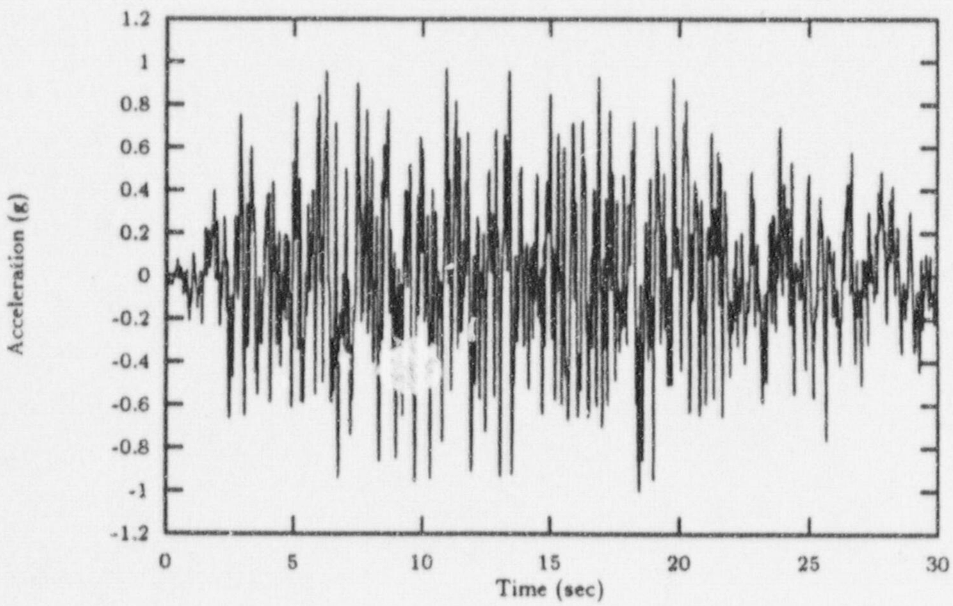

Figure 3.3: RG 1.60 input: acceleration time history, peak acceleration = 1 g, dominant frequency = 7.5 Hz

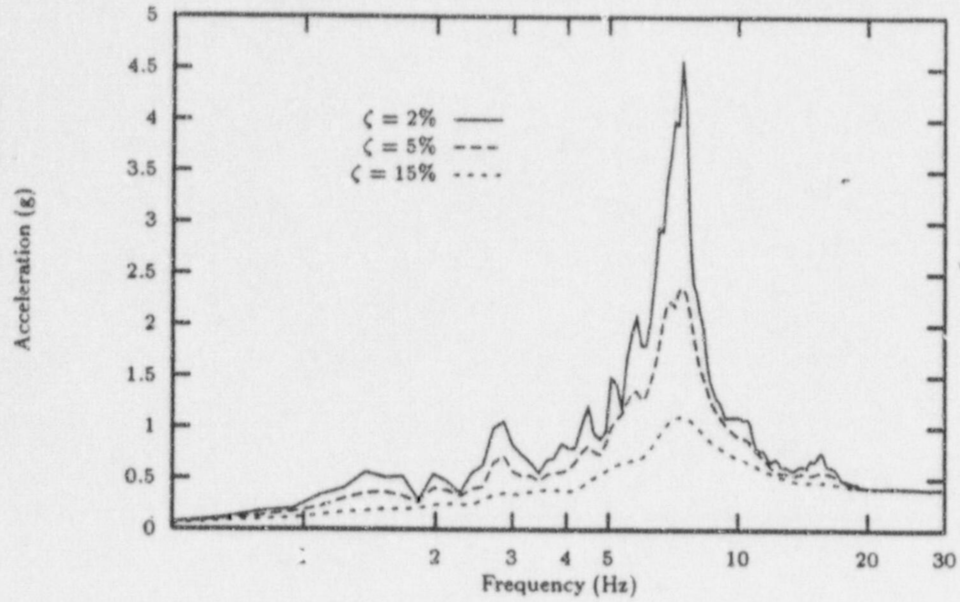

Figure 3.4: PFDR input: response spectra

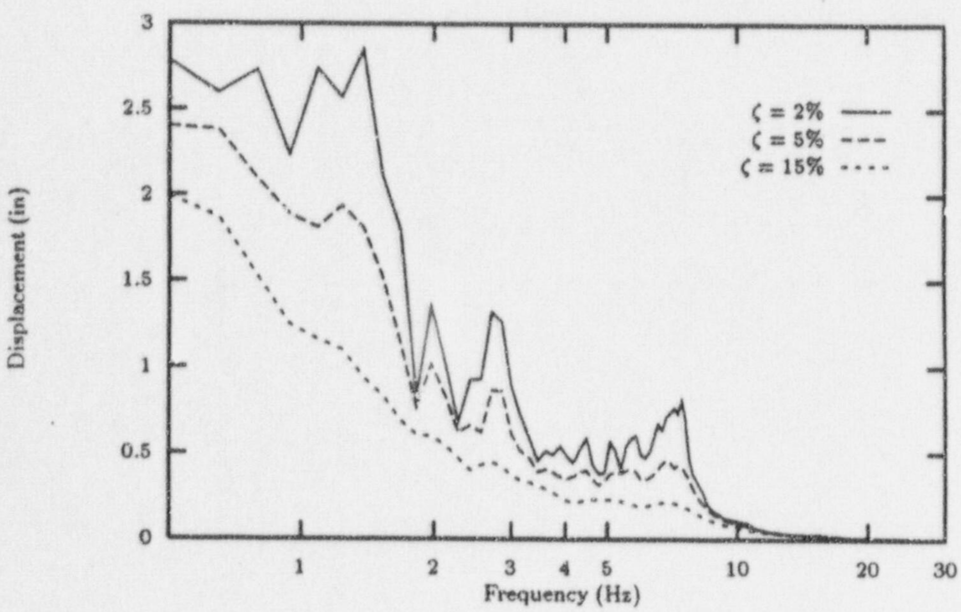

Figure 3.5: PFDR input: displacement response spectra

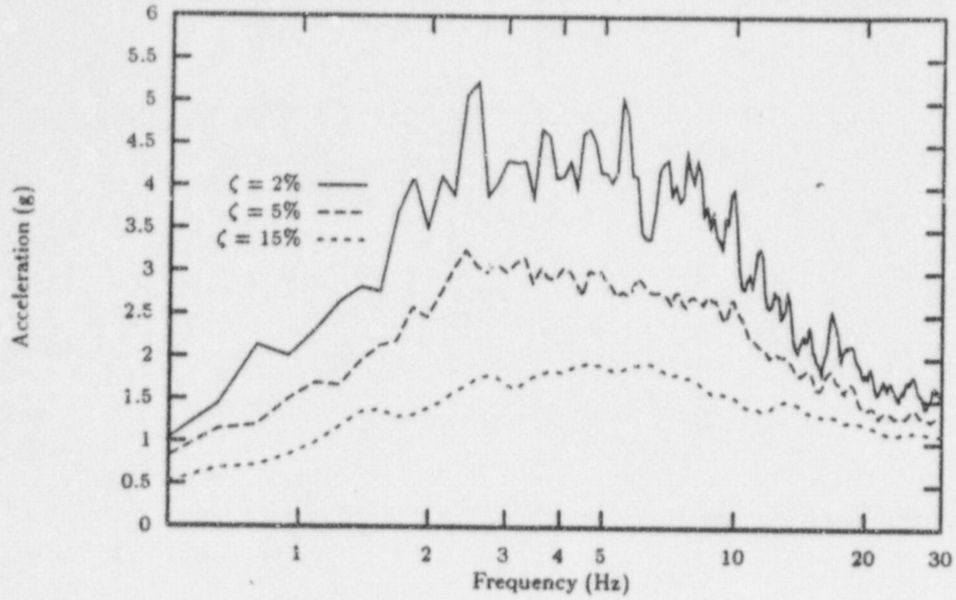

Figure 3.6: RG 1.60 input: pseudo-acceleration response spectra

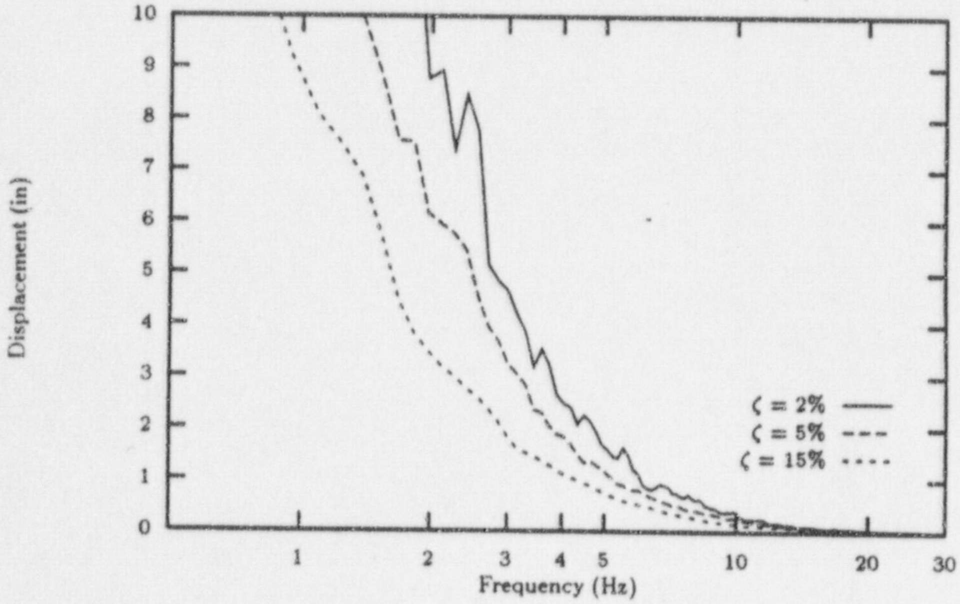

Figure 3.7: RG 1.60 input: displacement response spectra

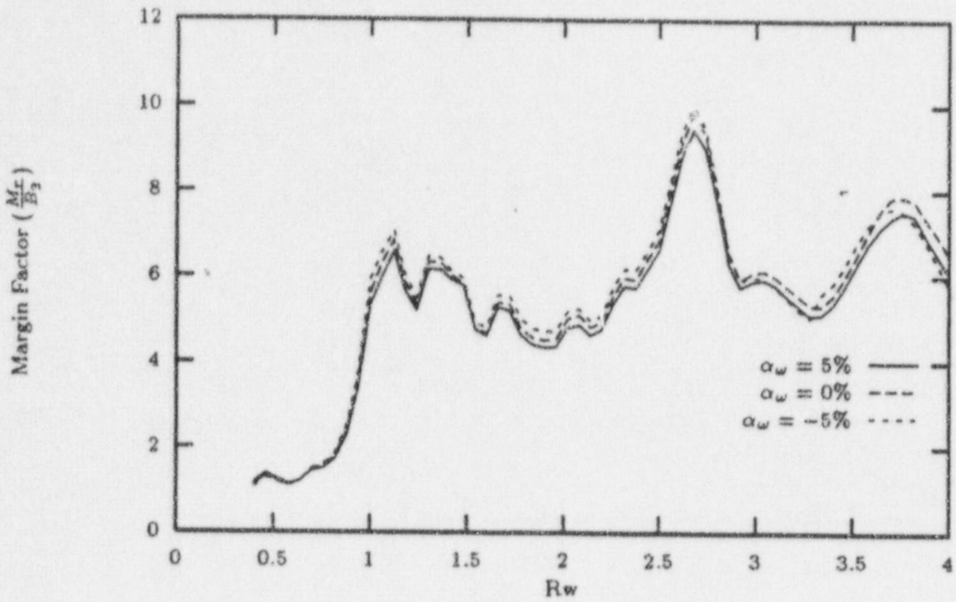

Figure 3.8: Test 36, PFDR input: margin spectra for various values of α_w, $\zeta_s = 2\%$, Sequential Method

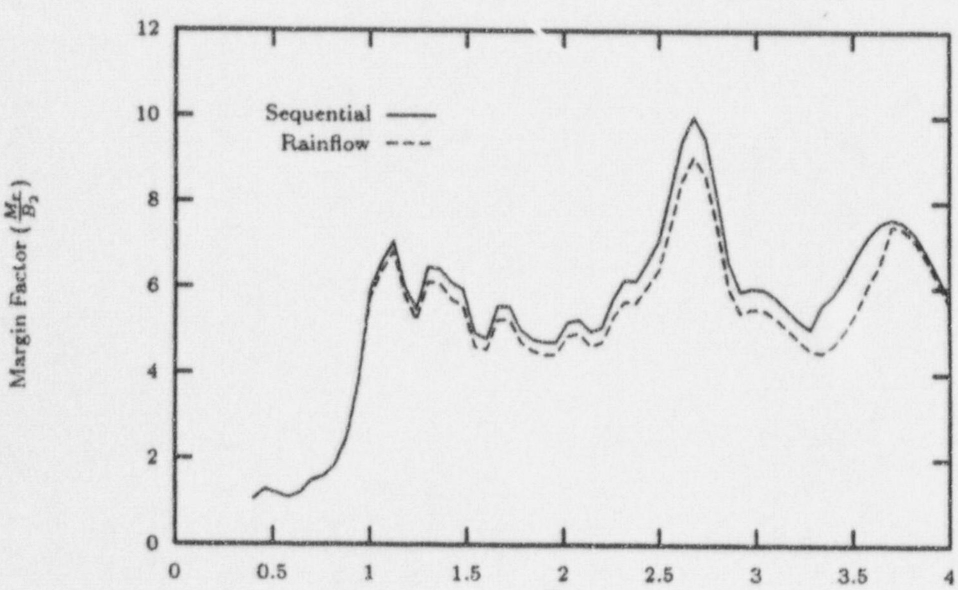

Figure 3.9: Test 36, PFDR input: margin spectra for various fatigue evaluation methods, $\alpha_w = -5\%$, $\zeta_s = 2\%$

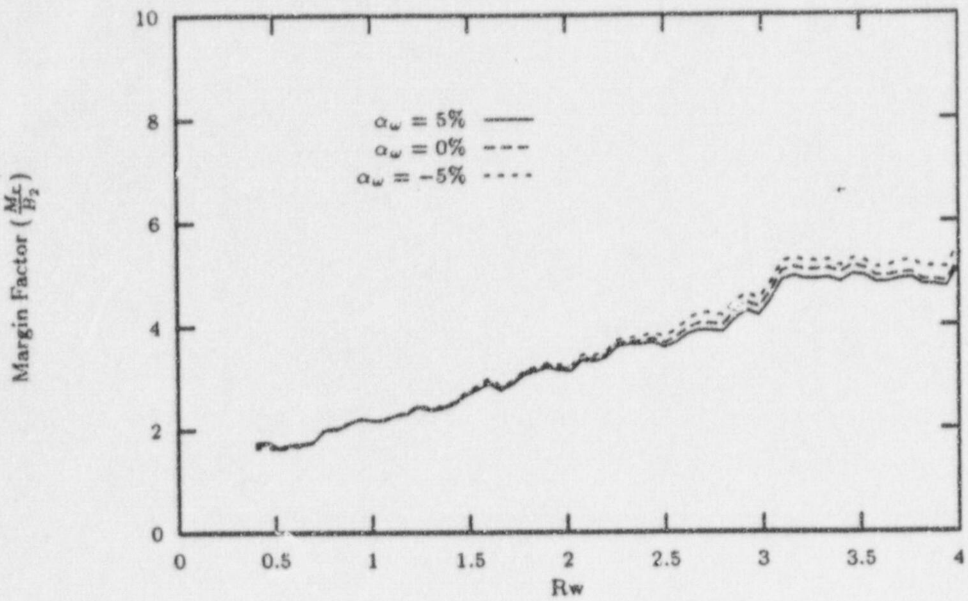

Figure 3.10: Test 36, RG 1.60 input: margin spectra for various values of α_w, $\zeta_s = 2\%$, Sequential Method

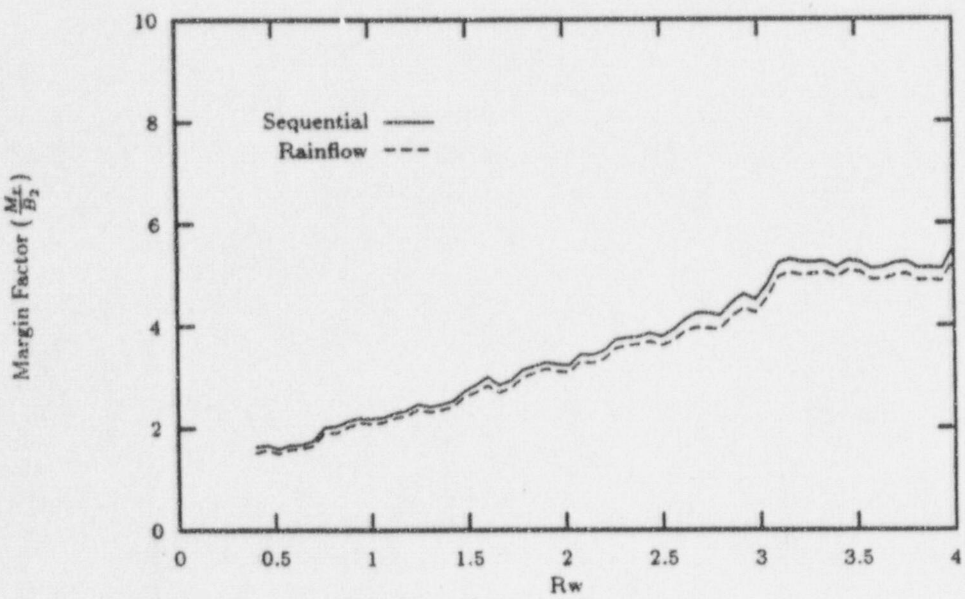

Figure 3.11: Test 36, RG 1.60 input: margin spectra for various methods, $\alpha_w = -5\%$, $\zeta_s = 2\%$

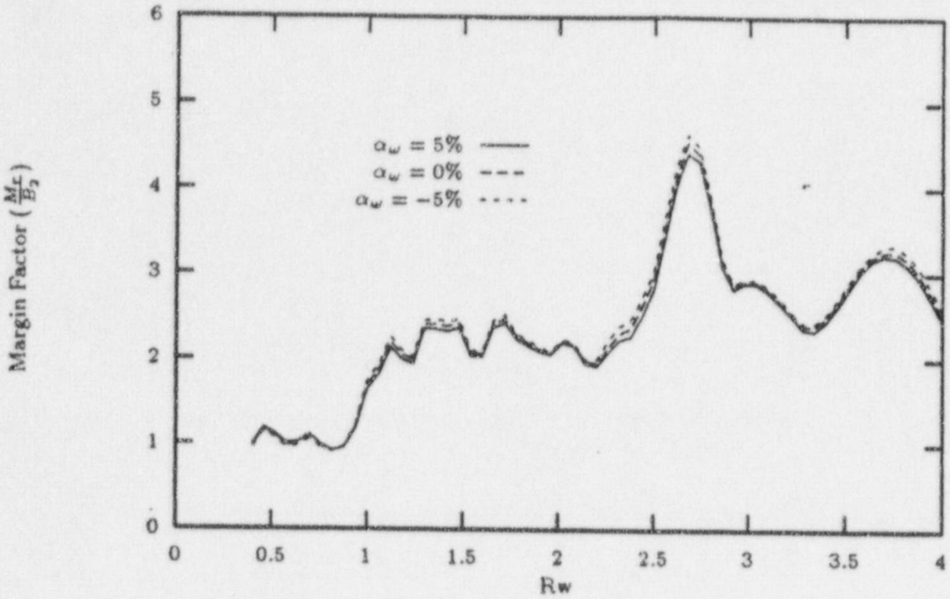

Figure 3.12: Test 11, PFDR input: margin spectra for various values of α_w, $\zeta_s = 3\%$, Sequential Method

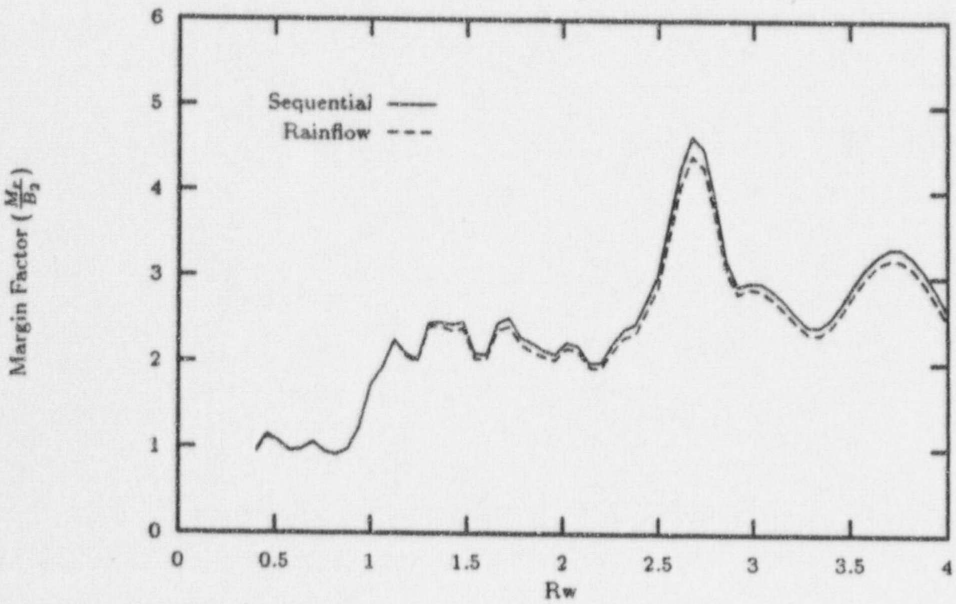

Figure 3.13: Test 11, PFDR input: margin spectra for various fatigue evaluation methods, $\alpha_w = -5\%$, $\zeta_s = 3\%$

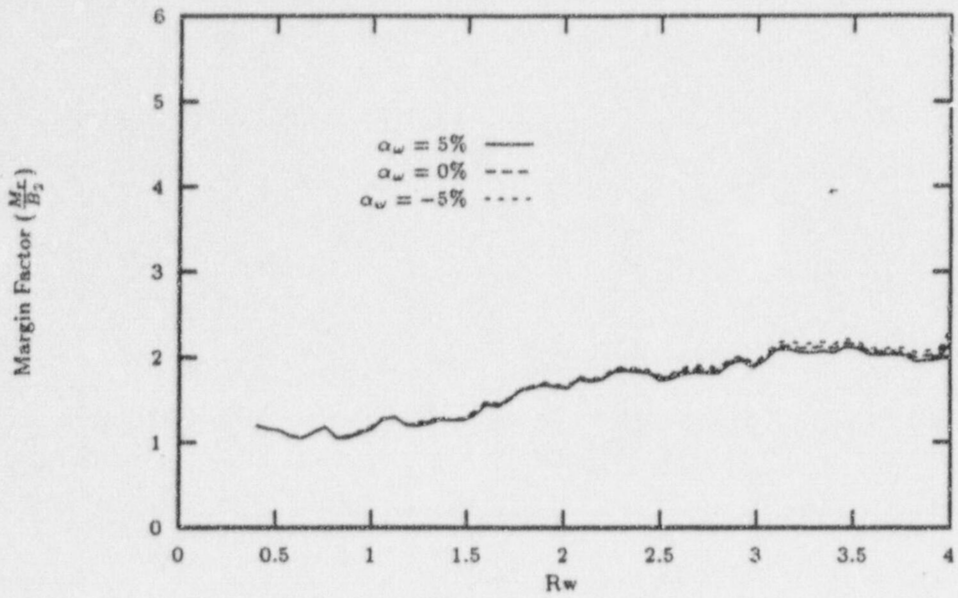

Figure 3.14: Test 11, RG 1.60 input: margin spectra for various values of α_w, $\zeta_s = 3\%$, Sequential Method

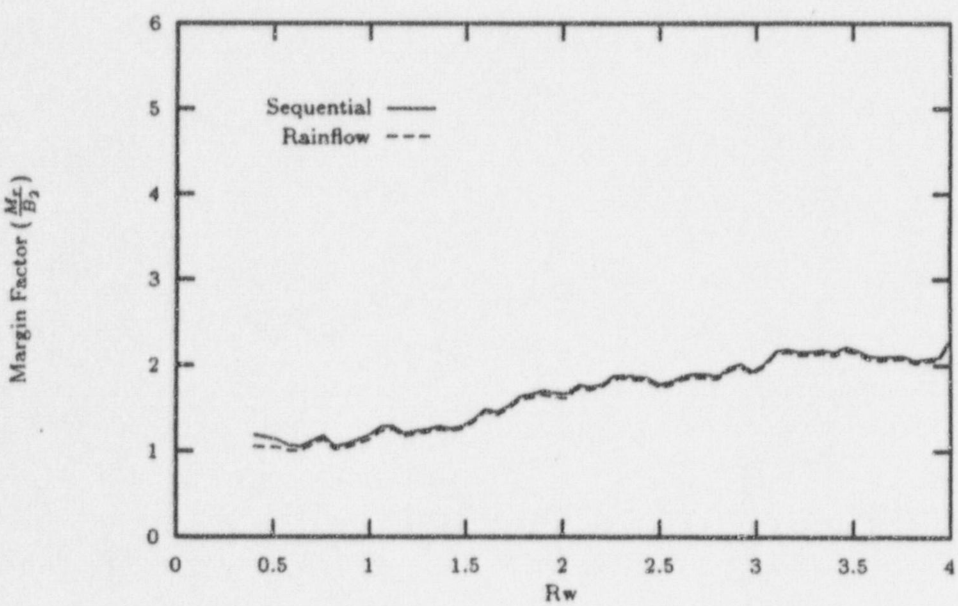

Figure 3.15: Test 11, RG 1.60 input: margin spectra for various methods, $\alpha_w = -5\%$, $\zeta_s = 3\%$

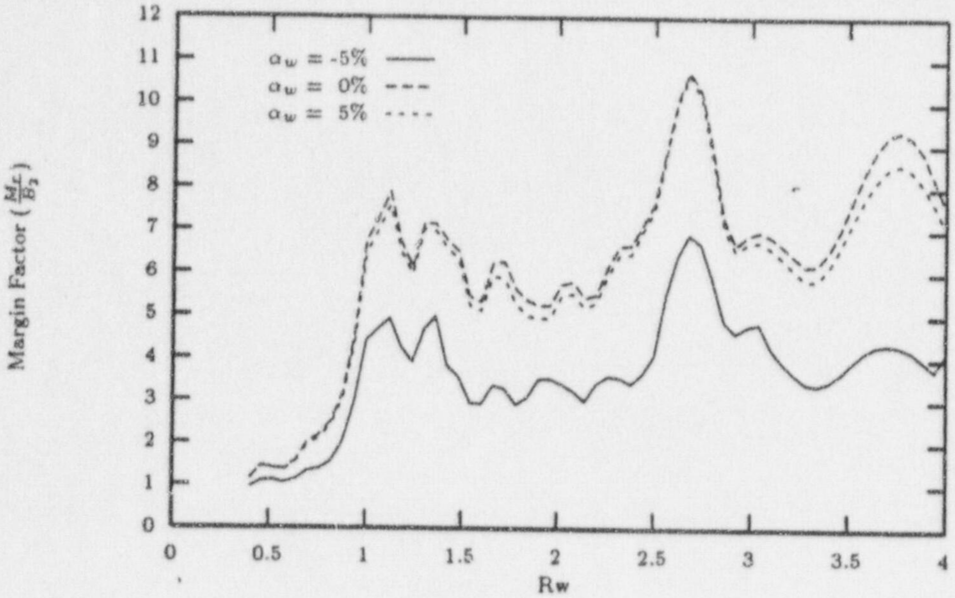

Figure 3.16: Test 14, PFDR input: margin spectra for various values of α_w, $\zeta_s = 2.5\%$, Sequential Method

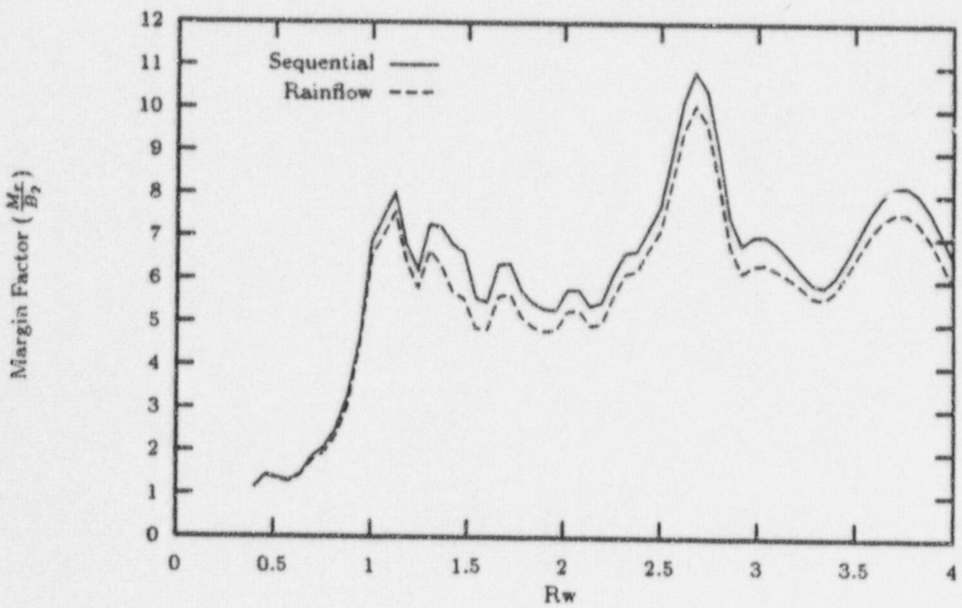

Figure 3.17: Test 14, PFDR input: margin spectra for various fatigue evaluation methods, $\alpha_w = -2\%$, $\zeta_s = 2.5\%$

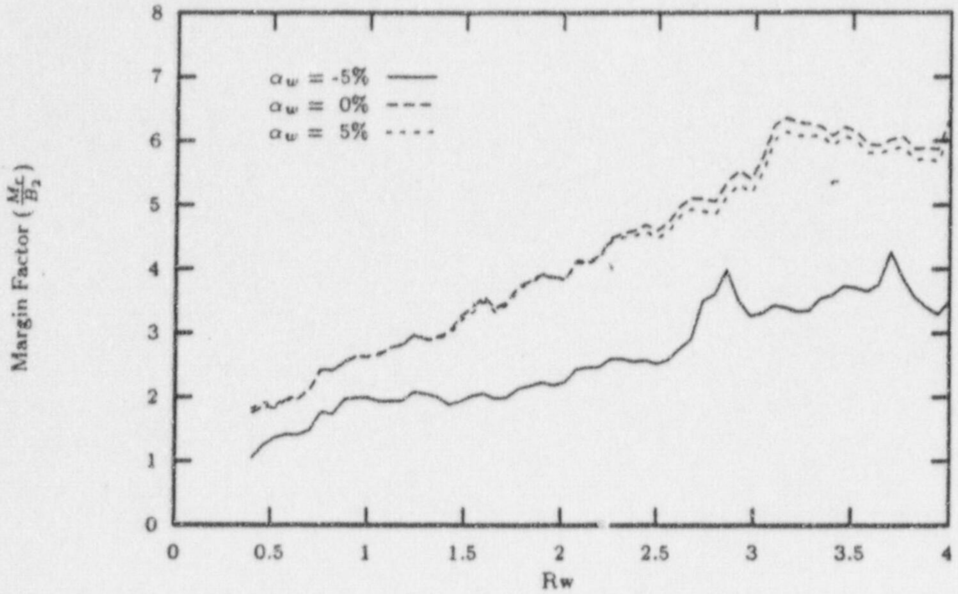

Figure 3.18: Test 14, RG 1.60 input: margin spectra for various values of α_w, $\zeta_s = 2.5\%$, Sequential Method

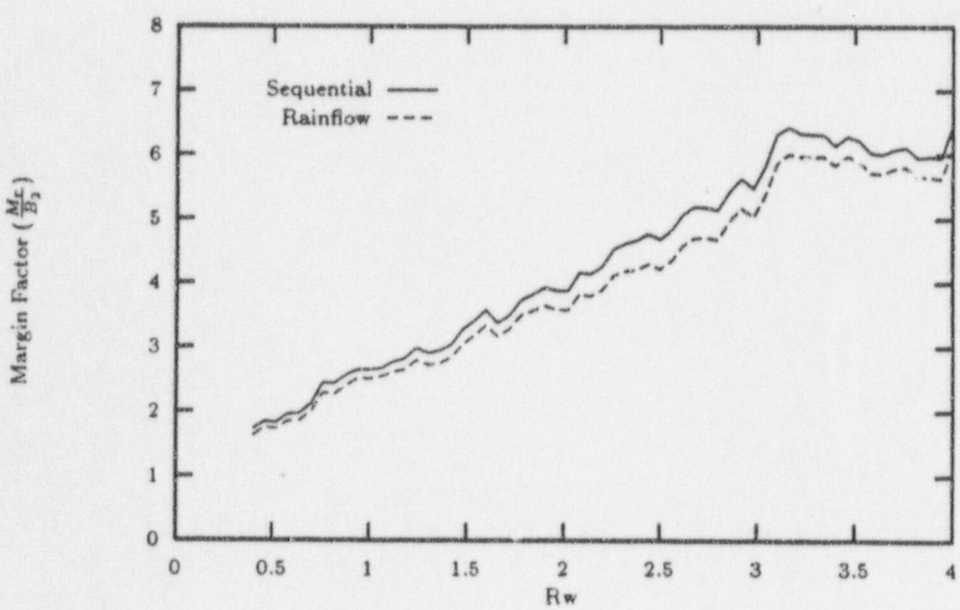

Figure 3.19: Test 14, RG 1.60 input: margin spectra for various methods, $\alpha_w = -2\%$, $\zeta_s = 2.5\%$

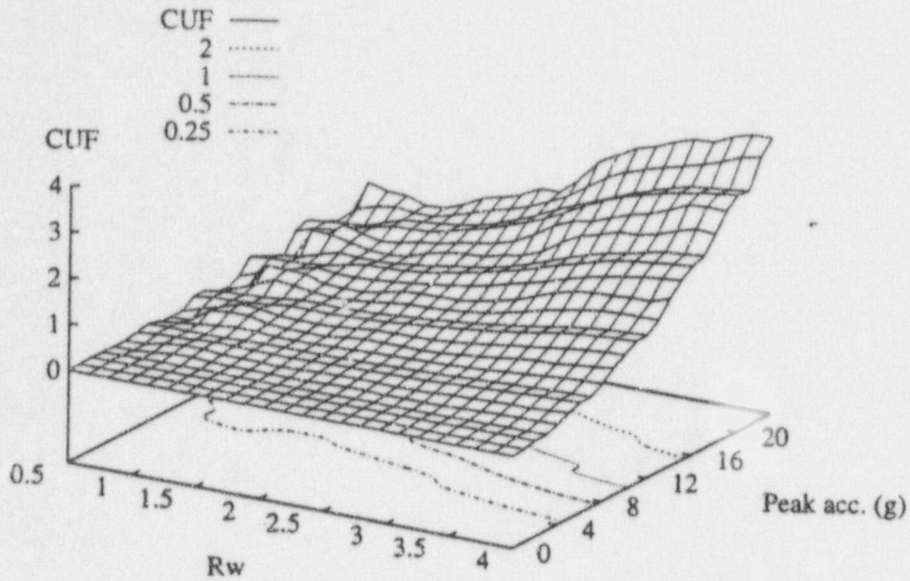

Figure 3.20: Test 36, CUF as a function of R_w and peak acceleration of linearly amplified PFDR input, $\alpha_w = 0\%$, $c_p = 0.01$, $\zeta_s = 2\%$, sequential method

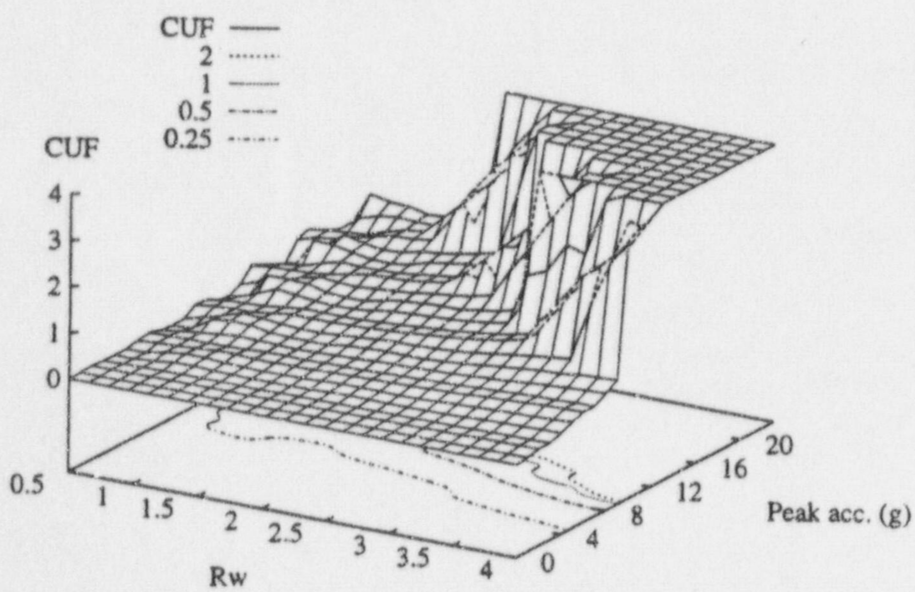

Figure 3.21: Test 36, CUF as a function of R_w and peak acceleration of linearly amplified PFDR input, $\alpha_w = -5\%$, $c_p = 0.01$, $\zeta_s = 2\%$, sequential method

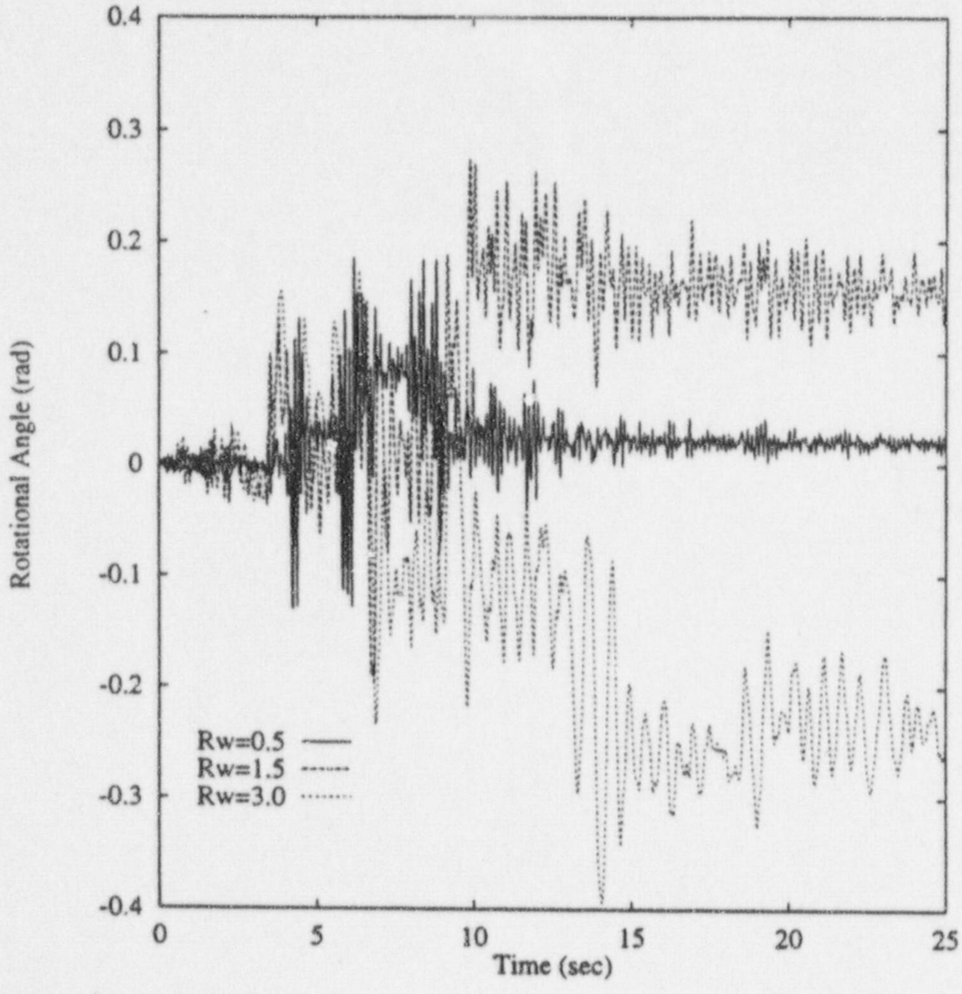

Figure 3.22: Test 36, response time history for systems with R_w=0.5, 1.5 and 3.0 subjected to PFDR input, CUF=1, $\alpha_w = -3\%$, $c_p = 0.01$, $\zeta_s = 2\%$, sequential method

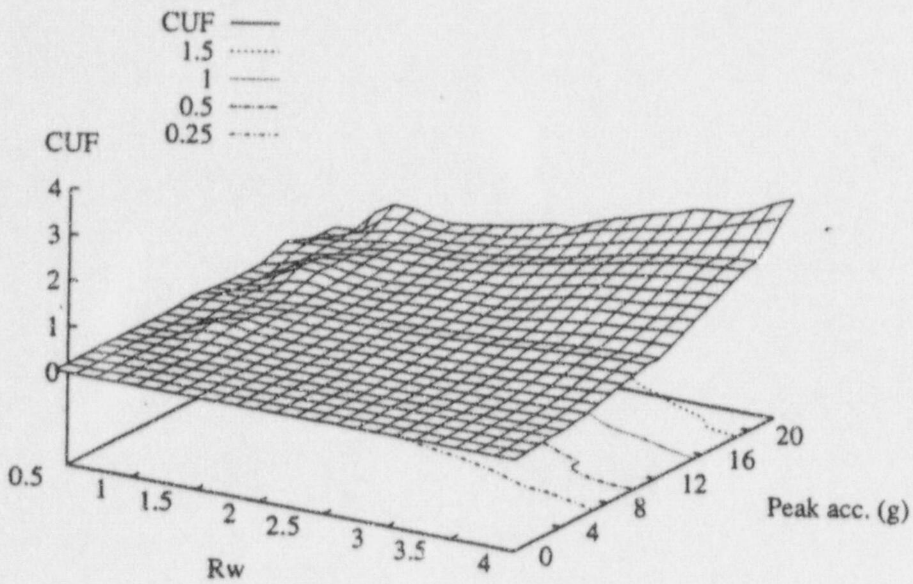

Figure 3.23: Test 14, CUF as a function of R_w and peak acceleration of linearly amplified PFDR input, $\alpha_\omega = 0\%$, $c_p = 0.01$, $\zeta_s = 2.5\%$, sequential method

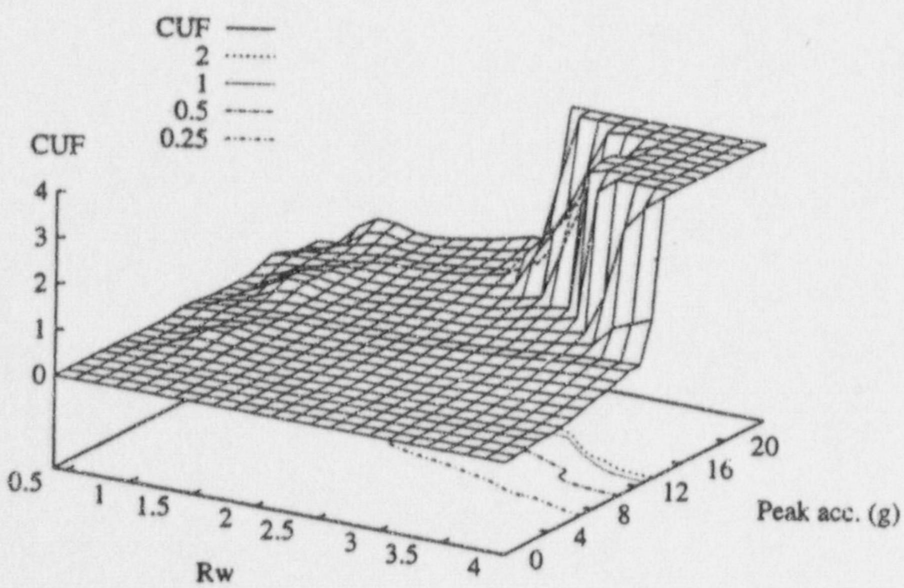

Figure 3.24: Test 14, CUF as a function of R_w and peak acceleration of linearly amplified PFDR input, $\alpha_\omega = -2\%$, $c_p = 0.01$, $\zeta_s = 2.5\%$, sequential method

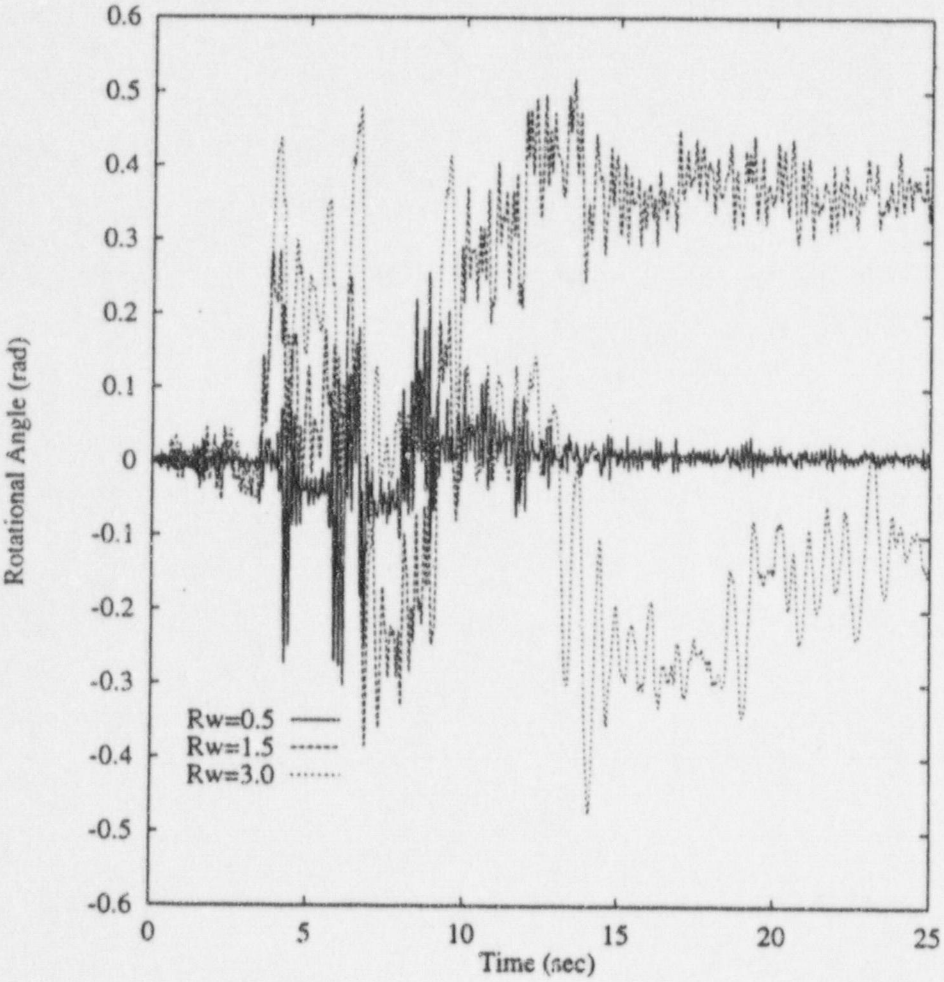

Figure 3.25: Test 14, response time history for systems with R_w=0.5, 1.5 and 3.0 subjected to PFDR input, CUF=1, $\alpha_w = -1\%$, $c_p = 0.01$, $\zeta_s = 2.5\%$, sequential method

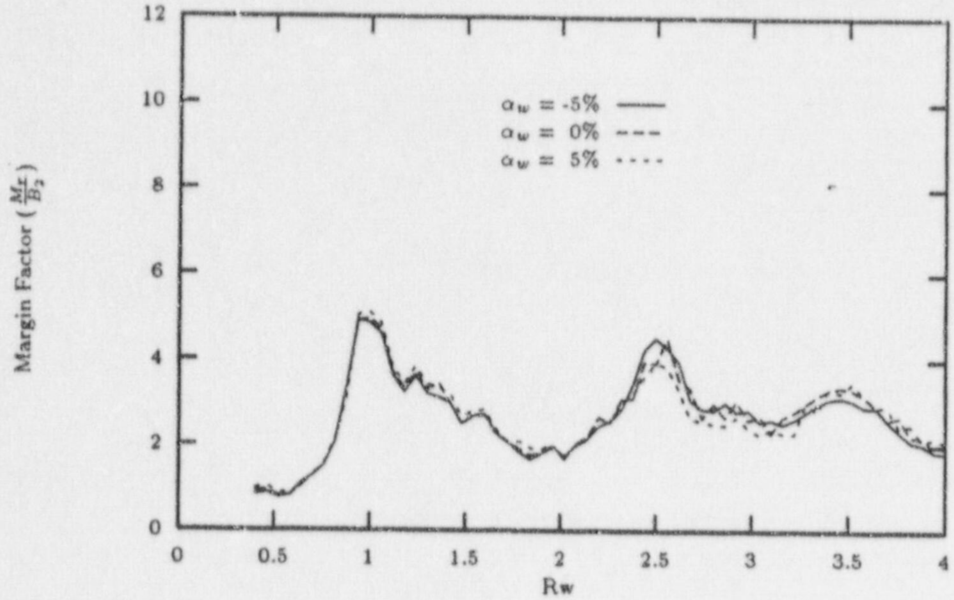

Figure 3.26: Test 36, PFDR input: displacement margin spectra for various values of α_w

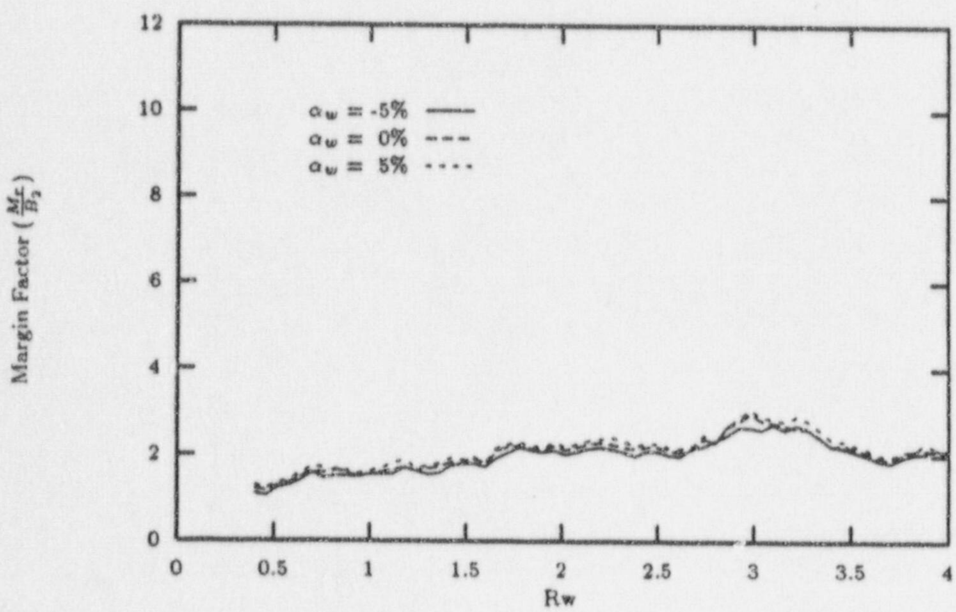

Figure 3.27: Test 36, RG 1.60 input: displacement margin spectra for various values of α_w

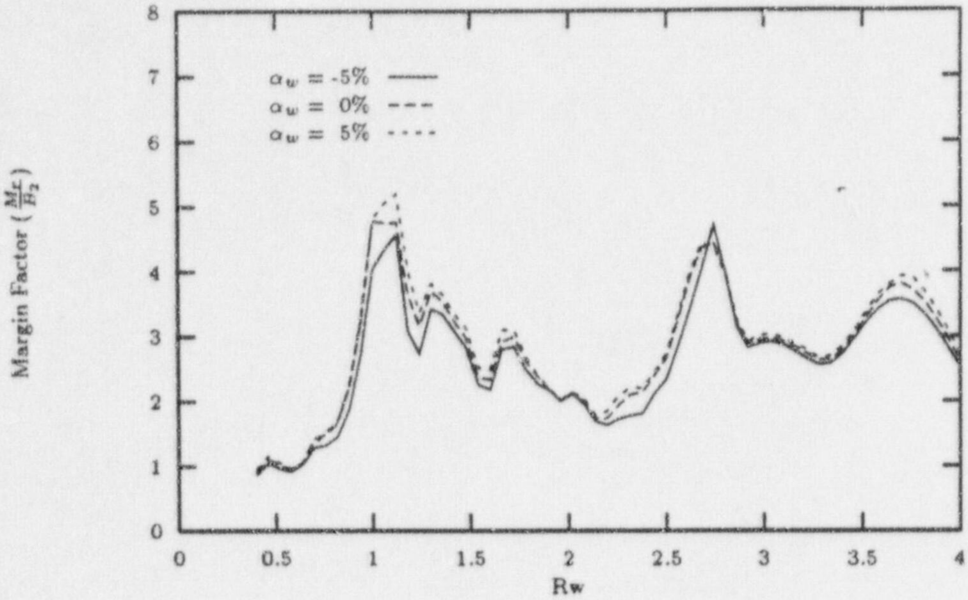

Figure 3.28: Test 14, PFDR input: displacement margin spectra for various values of α_w

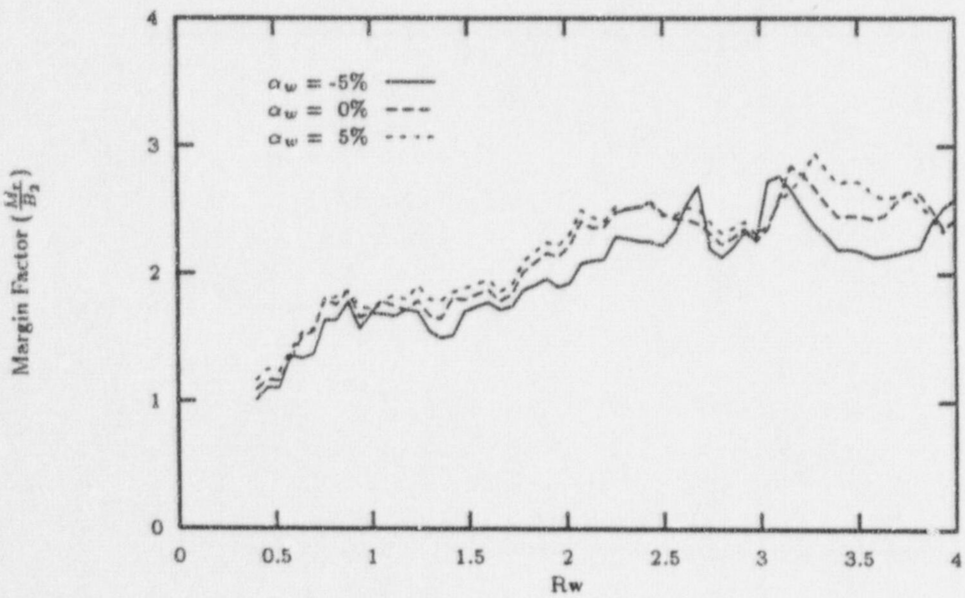

Figure 3.29: Test 14, RG 1.60 input: displacement margin spectra for various values of α_w

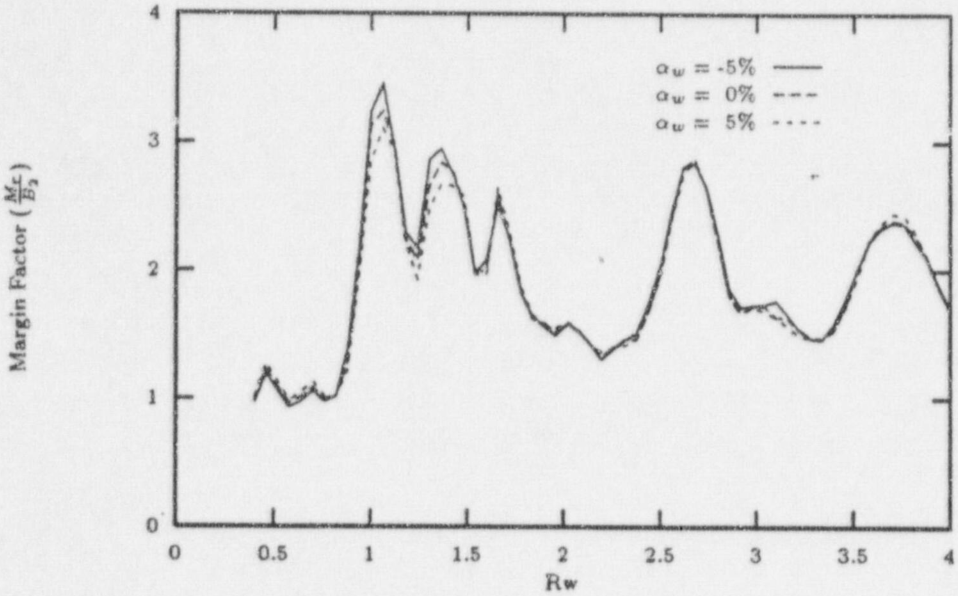

Figure 3.30: Test 11, PFDR input: displacement margin spectra for various values of α_w

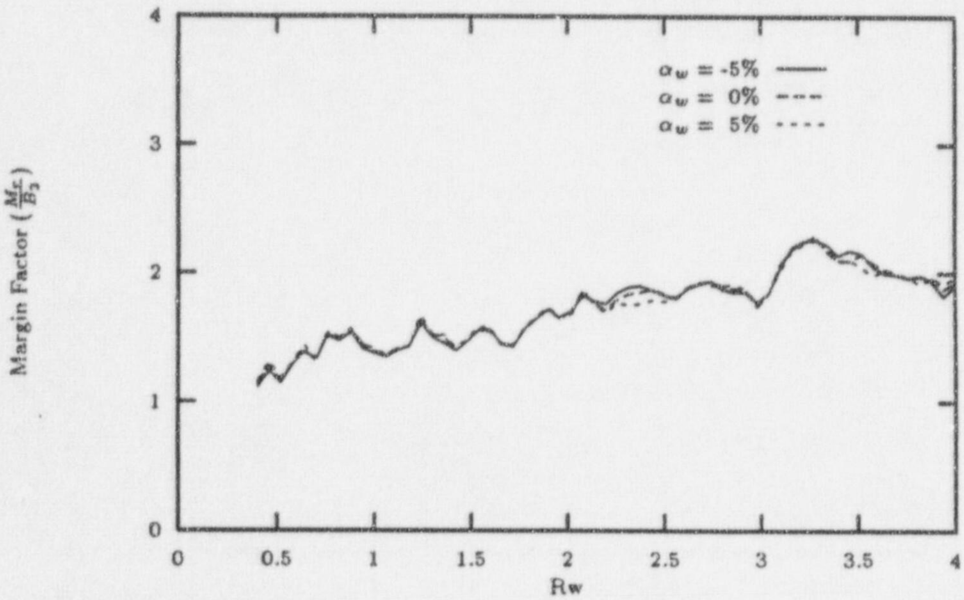

Figure 3.31: Test 11, RG 1.60 input: displacement margin spectra for various values of α_w

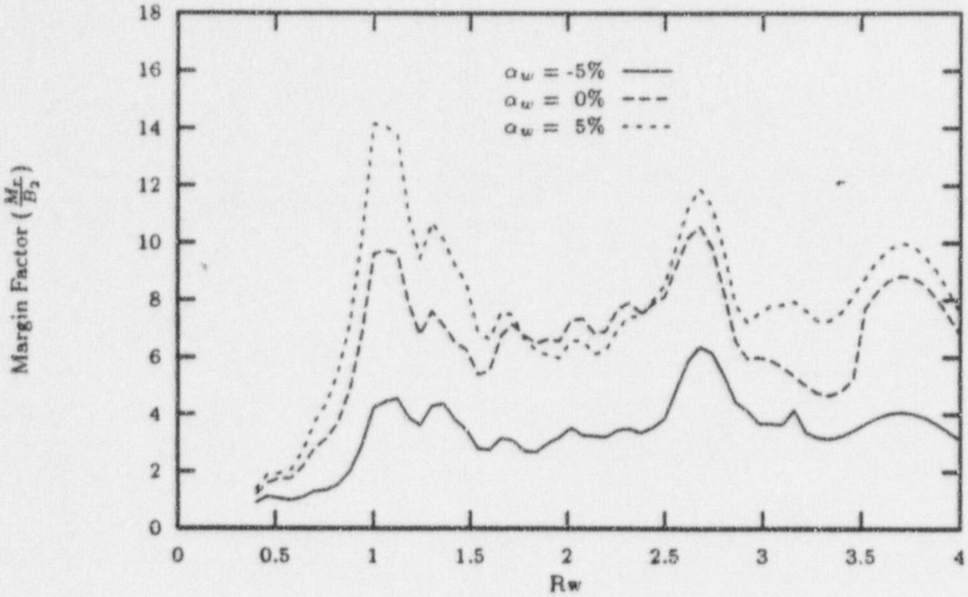

Figure 3.32: Test 40, PFDR input: displacement margin spectra for various values of α_w

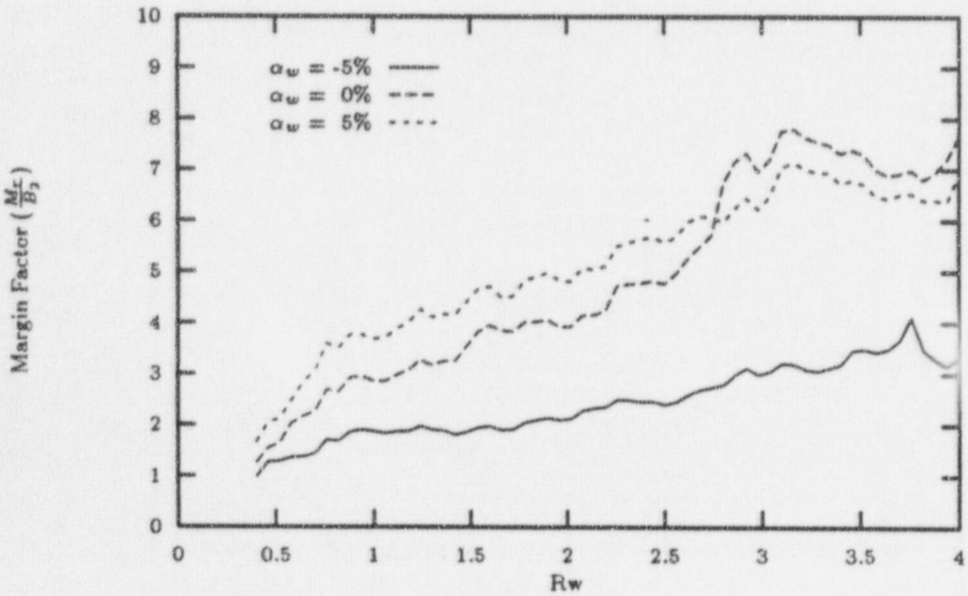

Figure 3.33: Test 40, RG 1.60 input: displacement margin spectra for various values of α_w

4 Additional Considerations Affecting Margins

The following sections address additional considerations affecting seismic margins that allow issues including eccentric moment effects, temperature effects and worst-case margin to be examined. Analytical results for these considerations are presented for Tests 14 and 40.

4.1 Eccentric Weight Moment Effects

In the previous margin studies, the eccentric weight moment effects were excluded from consideration for the sake of simplicity. However, several PFDR test data suggest that the eccentric moment caused by the bias static weight significantly influences the test system's response characteristics, particularly for flexible systems under low-frequency base motion. The typical response characteristic is the rotation ratcheting in the preferred weight direction that substantially increases the final displacement offset. It is the objective of this section to examine the implications of eccentric weight moment effects on seismic margins.

To incorporate the eccentric weight moment in margin analysis, Eqn. (2.7) is rearranged in a form similar to Eqn. (3.5) as

$$\ddot{\theta}(t) + 2\zeta\omega_n\dot{\theta}(t) + \alpha_w\omega_n^2\theta(t) + (1-\alpha_w)\omega_n^2 z(\theta,\dot{\theta}) = c_p a(t) + \alpha_l c_p g \quad (4.1)$$

where all the symbols are defined previously except for a newly introduced symbol α_l whose expression is related to the physical configuration parameters as

$$\alpha_l = \frac{\sum S_i \sin\phi_i}{\sum S_i \cos\phi_i} \quad (4.2)$$

This indicates that α_l represents a dimensionless length ratio that is approximately the ratio of the offset distance of the eccentric weight to the height of the test system. Thus, the higher the value of α_l, the higher the degree of weight eccentricity.

This additionally introduced system parameter results in a three-parameter representation,

$$M_r = M_r(R_w, \alpha_w, \alpha_l) \quad (4.3)$$

for both fatigue margin and displacement margin. This higher-dimensional margin function implies a more complicated correspondence between physical systems and its parametric space. Consequently, using a parametric approach to study margins may not necessarily provide a plausible parametric combination for physical systems. As a remedy to this inherent difficulty, this study also employs a physical-model approach in addition to the parametric-model approach. The two approaches are described separately in the subsections that follow.

4.1.1 Parametric Models

The parametric-model approach is based on Eqn. (4.3). Three degrees of α_l, 0%, 15% and 30%, with $\alpha_w = 0\%$, are first examined. An additional study considers two cases of parametric combination, $\alpha_l = 15\%$ with $\alpha_w = -2\%$, and $\alpha_l = 30\%$ with $\alpha_w = -5\%$. For simplicity, the weight stress due to the eccentric weight moment is neglected in the allowable Code moment evaluation. Cases with negative α_l are not performed. That is, the directional effect is not investigated in this parametric-model approach, but will be addressed in the physical-model approach later.

The margin results for Test 14 are given in Figs. 4.3 - 4.10 and those for Test 40 are given in Figs. 4.11 - 4.14. It is observed that the effect of eccentric weight moment is relatively insignificant for low R_w systems (stiff systems), and generally causes much larger margin reduction for high R_w systems (flexible systems).

4.1.2 Physical Models

The physical-model approach is based on three groups of physical models categorized by different levels of resulting eccentric weight stress. The three levels of weight stress are respectively 0 S_m, 0.25 S_m and 0.5 S_m. The last level, 0.5 S_m, is the maximum Code weight stress allowed. The physical configurations and corresponding systems parameters for these models are illustrated in Figs. 4.15- 4.17 for Test 14, and Figs. 4.18- 4.20 for Test 40.

The margins study using physical models differs from that using parametric models in the following aspects:

- The selected physical models encompass a much broader frequency range; one that covers from 0.05 second to 1.5 second in natural period. In the physical-model approach, both fatigue-based and displacement-based seismic margins are presented as functions of natural period, T, instead of frequency ratio R_w.
- In the physical-model approach, the acceleration levels required to reach failure conditions are presented together with the seismic margins.
- The weight stress is now considered in the allowable Code moment evaluation due to the significant weight stress in some of the selected physical models. The calculation of the allowable Code moment is illustrated in Table 4.1 and Table 4.2 for Tests 14 and 40 respectively.
- The directional effect in the input base excitation is taken into account. Specifically, two applications of base excitation in opposite sign sled directions are performed. The margin results are presented as the minimum margin from these two analyses.

The physical models are subjected to the previously defined RG 1.60 input and the margin results are given in Fig. 4.22 - Fig. 4.23 for Test 14. and are given in Fig. 4.24 for Test 40. For short-period systems, the results indicate that fatigue margins may possibly increase when the eccentric weight effect is considered. The reason is mainly due to the reduction in the Code allowable seismic moment. However, both the fatigue and displacement margins show a decreasing trend as the eccentricity level increases for most flexible systems ($T \geq 0.5$ second for Test 14 and $T \geq 0.3$ second for Test 40). For some period ranges, both margins are significantly reduced by as much as half at the case when maximum weight stress is assumed.

For the RG 1.60 input, the acceleration levels for failure are observed to follow a generally decreasing trend as the system natural period increases. The acceleration levels associated with displacement margin are observed to be within the 1 - 2 g range for the more flexible physical models.

4.2 Temperature Effects

The material dynamic constitutive relationship and material fatigue life are highly dependent on operating temperature. Consequently, temperature variations may lead to significant variations in the dynamic response process, failure conditions and seismic margins. The PFDR component tests were conducted at room temperature, and the subsequent margin analysis is considered meaningful only for this temperature. The objective of this study is to investigate seismic margins at an elevated temperature of $650°F$.

This study employs a set of reduction factors for carbon steel and stainless steel that are calculated in Table 4.3 and Table 4.4 respectively. In these tables, S_m is the ASME Code allowable stress, S_y is the ASME yield stress and E is Young's Modulus. The set of reduction factors, R_m, R_y and R_e, is defined as

$$R_m = \frac{S_m \text{ @ } 650°F}{S_m \text{ @ } 100°F} \quad (4.4)$$

$$R_y = \frac{S_y \text{ @ } 650°F}{S_y \text{ @ } 100°F} \quad (4.5)$$

$$R_e = \frac{E \text{ @ } 650°F}{E \text{ @ } 100°F} \quad (4.6)$$

The analytical models established at room temperature are modified according to these reduction factors to obtain corresponding models for $650°F$. Modifications of the analytical models as well as the margin analysis procedure are detailed below.

4.2.1 Hysteretic Model

Modifications of the analytical hysteresis models are based on the following assumptions.

- The stiffness properties of the restoring moment decrease by a factor of R_e as the temperature increases from room temperature to $650°F$. That is,

$$k^*_{ini} = k_{ini}R_e$$
$$k^*_l = k_l R_e$$

where a superscript $*$ is used to denote the corresponding material property at the elevated temperature level.

- The ultimate yielding moment, f_y, is varied by a factor of R_y when strain softening material behavior is assumed (S-type), and by a factor of R_h when strain hardening (H-Type) material behavior is assumed for $650°F$. That is,

$$f^*_y = f_y R_y \text{ for S-Type}$$
$$f^*_y = f_y R_h \text{ for H-Type}$$

where R_h is a hardening factor that will be used to consider material dynamic strain aging behavior for carbon steel.

- The frequency-independent damping ratio, ζ_s, used in room temperature studies remains unaltered at $650°F$, despite the fact that k^*_{ini} and k^*_l are varied.

These modifications are illustrated in Fig. 4.1.

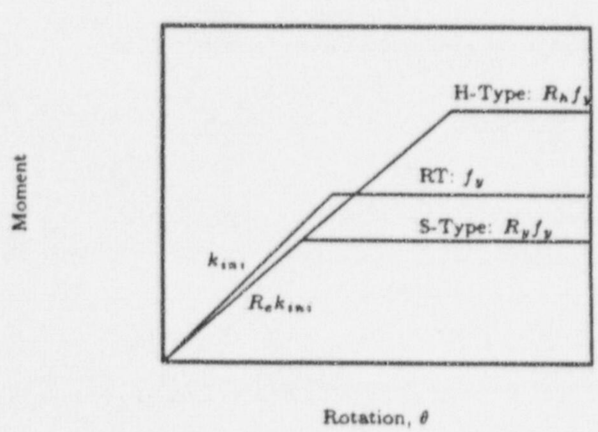

Figure 4.1: Modification of hysteretic model

4.2.2 Material ϵ-N Curve

Material fatigue data show that an increase in temperature generally causes a decrease in strain amplitude for failure in a given number of fatigue cycles. In this study, the fatigue analysis is performed on three postulated temperature ϵ-N models at $650^\circ F$. These models are based on variations of the ASME material ϵ-N curve by different levels of reduction in strain amplitude (See Fig. 4.2). They are respectively:

- Model 1: unaltered S-N curve
- Model 2: 20 % reduction in strain amplitude
- Model 3: 40 % reduction in strain amplitude

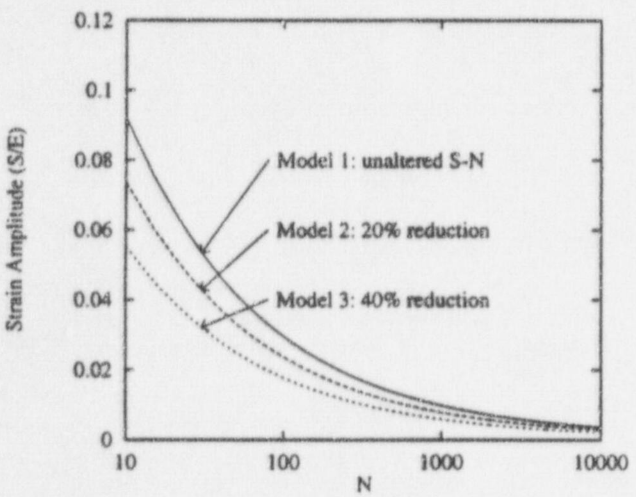

Figure 4.2: Three postulated models for ϵ-N relationship at $650^\circ F$

4.2.3 Code Allowable Moment

The Code allowable moment is reduced by a factor of R_m when the pressure stress is neglected, since the S_m value is reduced to $R_m S_m$ at $650^\circ F$.

4.2.4 Simulation Results

The temperature effect is investigated using both parametric models ($\alpha_w = 0\%$, $\alpha_l = 0\%$) and physical models without eccentric moment. In plotting the margin results, the R_w or period at room temperature is still used as the reference R_w or period at $650^\circ F$ to facilitate comparison. Both H-type and S-type of yielding response are considered for Test 14 (Figs. 4.25 - 4.31). However, only the S-type yielding response is considered for Test 40 (Figs. 4.32 - 4.33).

It is observed that the temperature effect causes either a left-shifted or a right-shifted trend for the margin curves. To explain this, one must consider two factors, namely the *linear effect* and the *nonlinear effect*. The linear effect is due to the linear stiffness reduction at $650^\circ F$ in the analytical model. With the linear effect, the system's behavior at $650^\circ F$ will resemble a more flexible system at room temperature, and consequently the margin curve exhibits a left-shifted trend. For the H-type (S-type) materials, the nonlinear effect is due to an increase (decrease) in the yielding level. Alternatively, this can be viewed as an increase (decrease) in the effective stiffness, and hence results in a right-shifted (left-shifted) trend.

Using the above arguments, the margin results can be summarized as follows.

- For the S-type yielding model, the fatigue margin curves exhibit a left-shift trend with a decrease in magnitude. In this case, the linear and nonlinear effects are added together.
- By contrast, H-type yielding models on the order of $R_h = 1.5$ have fatigue margin curves that generally exhibit a right-shift trend with an increase in

magnitude. This indicates that these systems may need to undergo highly nonlinear response to reach fatigue failure. Thus, the nonlinear effect can far exceed the linear effect.

- Obviously, the higher the reduction in the material S-N curves, the higher will be the reduction in the fatigue margins.
- Most displacement margins show a left-shifted trend without significant variations in magnitude. This observation suggests that the response is strongly dominated by the linear effect when a rotation limit is imposed.

4.3 Worst-Case Considerations

The worst-case considerations on margins are based on simultaneous consideration of the eccentric weight moment effects and temperature effects. For each test, the worst-case (WC) margins are evaluated separately for stiff systems and flexible systems following the physical-model approach. The representative groups of physical models are:

1. **WC stiff systems:**
   Short-period physical models, $T \leq 0.25$ second, without eccentric moment at $650°F$ (See Fig. 4.15 for Test 14 and Fig. 4.18 for Test 40).
2. **WC flexible systems:**
   Long-period physical models, $0.25 \leq T \leq 1.75$ second, with maximum allowable weight stress at $650°F$ (See Fig. 4.34 for Test 14 and Fig. 4.35 for Test 40). Due to the reduction of S_m at $650°F$, the selected WC flexible systems have smaller eccentric weight stress than that allowed at room temperature.

These models are further subjected to the following conditions in the margin analysis.

- S-Type of yielding moment characteristics is assumed. The R_y used for Test 14 is 0.726, and for Test 40 is 0.584.
- Model 3 of the S-N curve (40% reduction in strain) is assumed in calculating the fatigue margin.
- Code allowable moment at $650°F$ is used.
- Weight stress is included in the Code moment evaluation when an eccentric weight moment is present.

A summary of the Code moment calculation for the WC physical models is given in Table 4.5. Both PFDR and RG 1.60 inputs are used in this study. The worst-case margins as well as the failure acceleration levels are shown in Figs. 4.36 - 4.39 for Test 14, and are shown in Figs. 4.40 and 4.41 for Test 40.

	M_{wt} (lb-in)	$\frac{M_{wt}}{Z}$ (psi)	weight stress	pressure stress	$\frac{B_2 M_{eq}}{Z}$
$l_1 = l_2 = 0$ in.	0	0	0.000 S_m	0.503 S_m	3.997 S_m
$l_1 = l_2 = 56$ in.	42,279	4,974	0.248 S_m	0.503 S_m	3.749 S_m
$l_1 = l_2 = 85$ in.	82,025	9,650	0.482 S_m	0.503 S_m	3.515 S_m

Table 4.1: Code moment calculation for Test 14 physical models at room temperature, $S_m = 20.0$ ksi

	M_{wt} (lb-in)	$\frac{M_{wt}}{Z}$ (psi)	weight stress	$\frac{B_2 M_{eq}}{Z}$
$l_1 = l_2 = 0$ in.	0	0	0.000 S_m	4.500 S_m
$l_1 = l_2 = 30$ in.	15,510	4,832	0.242 S_m	4.258 S_m
$l_1 = l_2 = 49$ in.	32,068	9,990	0.500 S_m	4.000 S_m

Table 4.2: Code moment calculation for Test 40 physical models at room temperature, $S_m = 20.0$ ksi

Test 14	Room Temp. (100° F)	$650° F$	Reduction Factor
S_m(ksi)	20.0	17.0	$R_m = 0.850$
S_y(ksi)	35.0	25.4	$R_y = 0.726$
$E/10^3$ (ksi)	29.5	26.7	$R_e = 0.885$

Table 4.3: Material properties for Test 14 (carbon steel)

Test 40	Room Temp. (100° F)	650° F	Reduction Factor
S_m (ksi)	20.0	16.7	$R_m = 0.835$
S_y (ksi)	30.0	17.5	$R_y = 0.584$
$E/10^3$ (ksi)	28.3	25.3	$R_e = 0.885$

Table 4.4: Material properties for Test 40 (stainless steel)

	M_{wt} (lb-in)	$\frac{M_{wt}}{Z}$ (psi)	weight stress	pressure stress	$\frac{B_2 M_{eq}}{Z}$
Test 14: $l_1 = l_2 = 0$ in.	0	0	0.000 S_m^*	0.5 S_m^*	4.000 S_m^*
Test 14: $l_1 = l_2 = 78$ in.	71,309	8,389	0.493 S_m^*	0.5 S_m^*	3.507 S_m^*
Test 40: $l_1 = l_2 = 0$ in.	0	0	0.000 S_m^*	0.0 S_m^*	4.500 S_m^*
Test 40: $l_1 = l_2 = 44$ in.	27,204	8,474	0.498 S_m^*	0.0 S_m^*	4.002 S_m^*

Table 4.5: Code moment calculation for worst-case physical model at $650°F$, $S_m^* = S_m R_m$, $S_m = 20$ ksi for both stainless steel and carbon steel, $R_m = 0.850$ for carbon steel, $R_m = 0.835$ for stainless steel

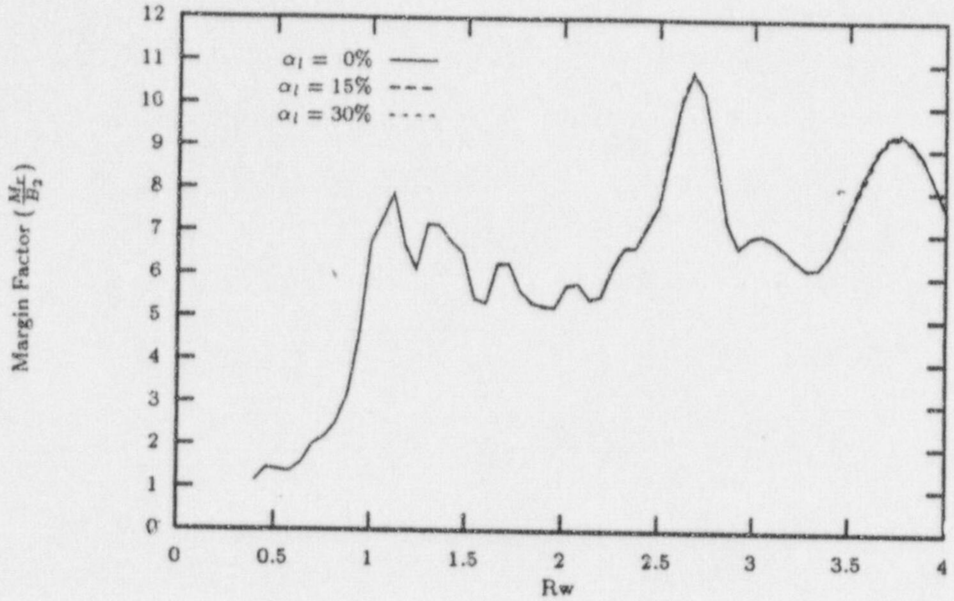

Figure 4.3: Test 14, Parametric models, PFDR input: fatigue margin spectra for various values of α_l, α_w = 0%, Sequential Method

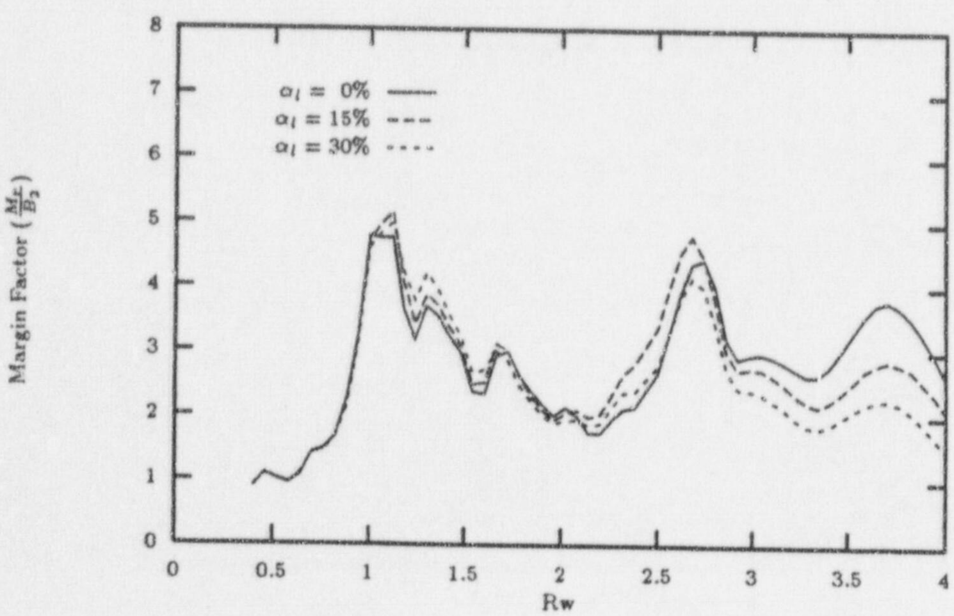

Figure 4.4: Test 14, Parametric models, PFDR input: displacement margin spectra for various values of α_l, α_w = 0%

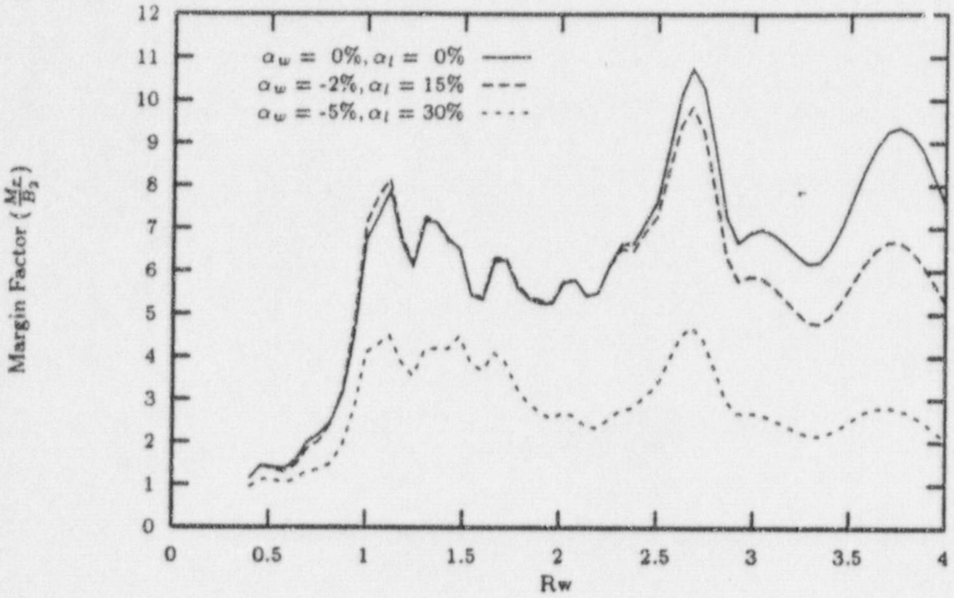

Figure 4.5: Test 14, Parametric models, PFDR input: fatigue margin spectra for various values of α_l and α_w, Sequential Method

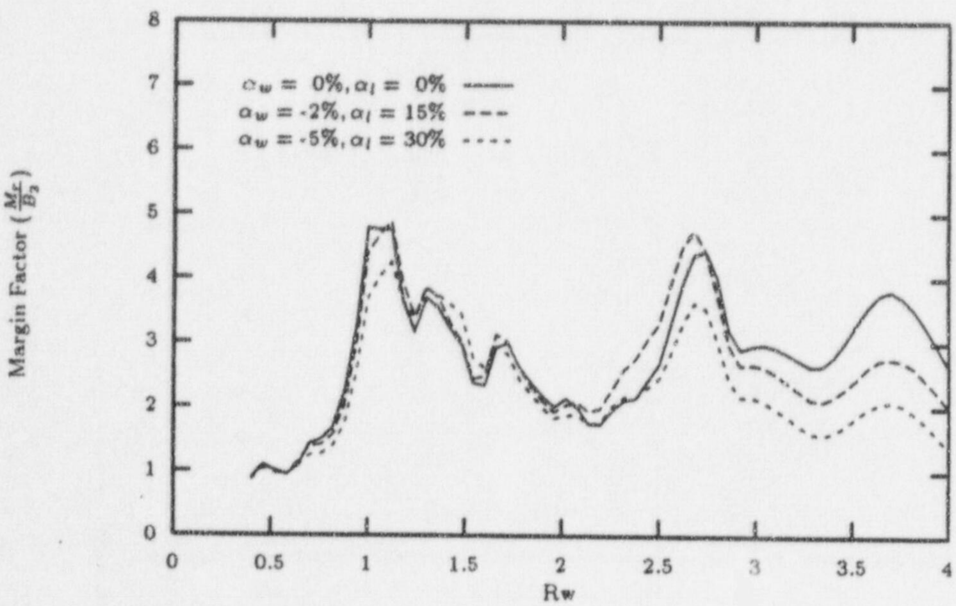

Figure 4.6: Test 14, Parametric models, PFDR input: displacement margin spectra for various values of α_l and α_w

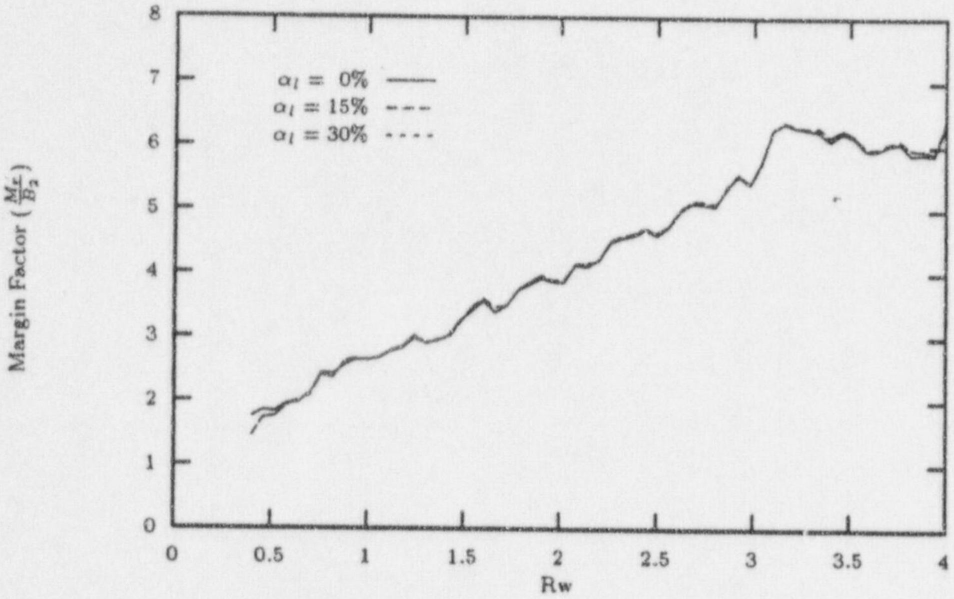

Figure 4.7: Test 14, Parametric models, RG 1.60 input: fatigue margin spectra for various values of α_l, $\alpha_w = 0\%$, Sequential Method

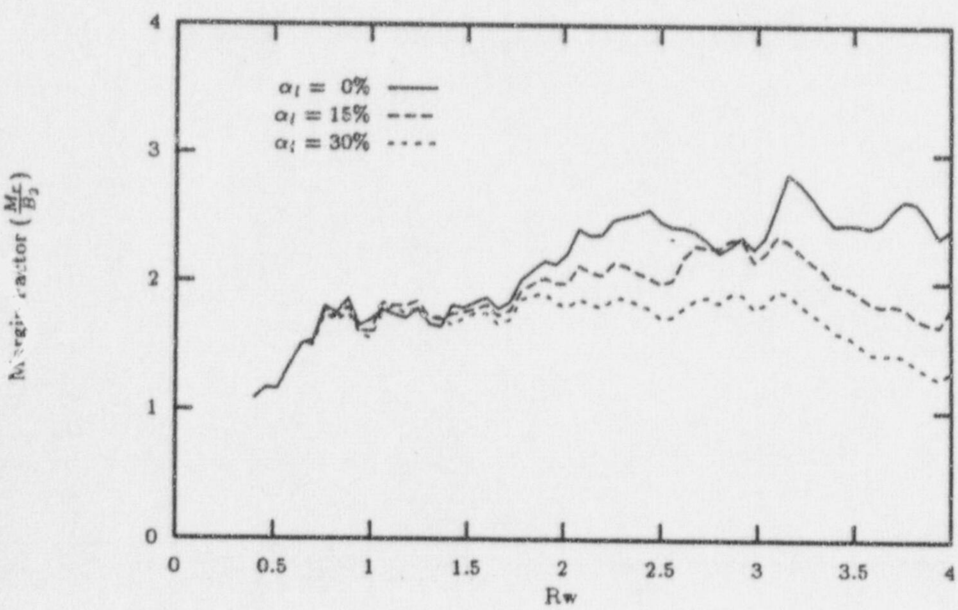

Figure 4.8: Test 14, Parametric models, RG 1.60 input: displacement margin spectra for various values of α_l, $\alpha_w = 0\%$

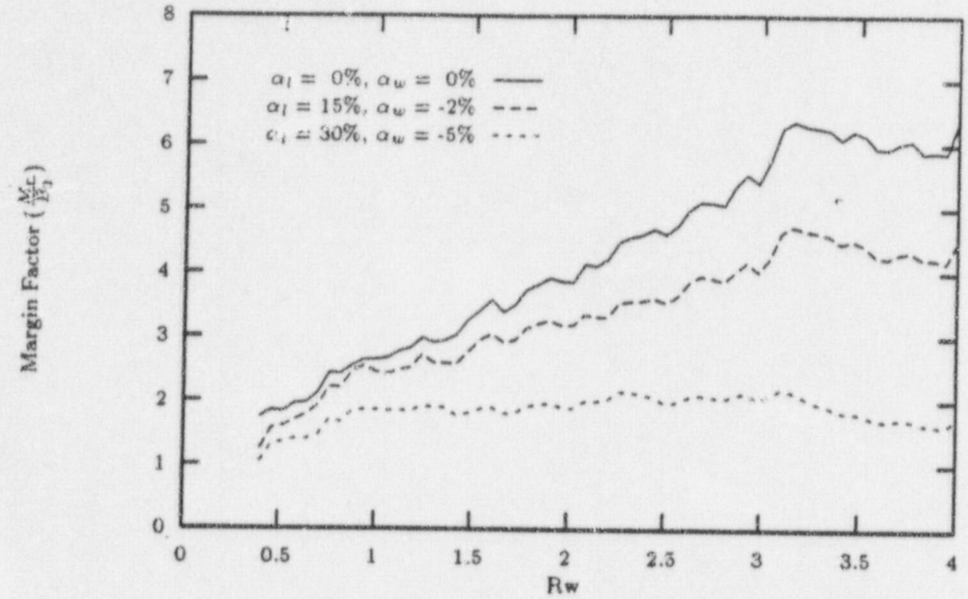

Figure 4.9: Test 14, Parametric models, RG 1.60 input: fatigue margin spectra for various values of α_l and α_w, Sequential Method

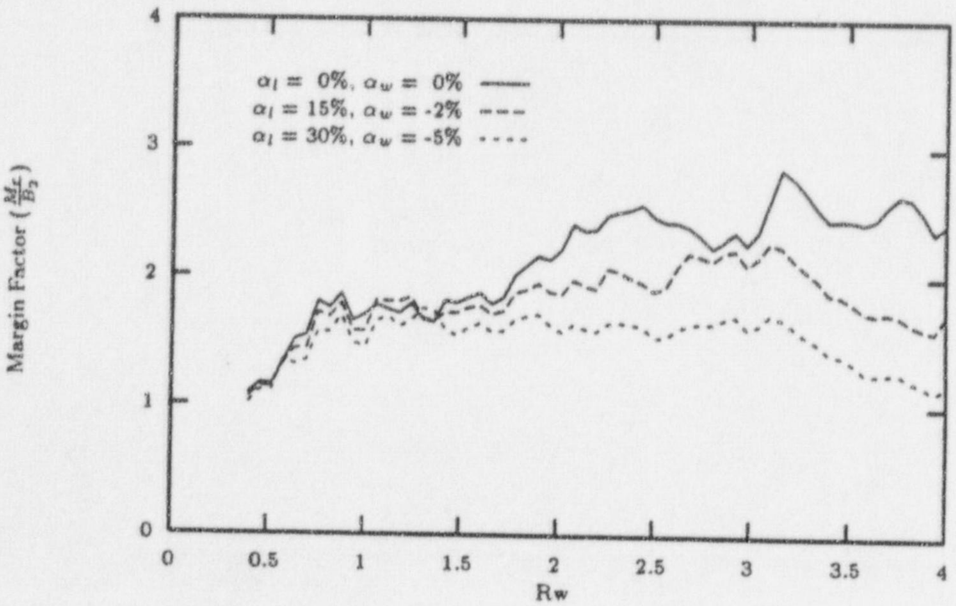

Figure 4.10: Test 14, Parametric models, RG 1.60 input: displacement margin spectra for various values of α_l and α_w

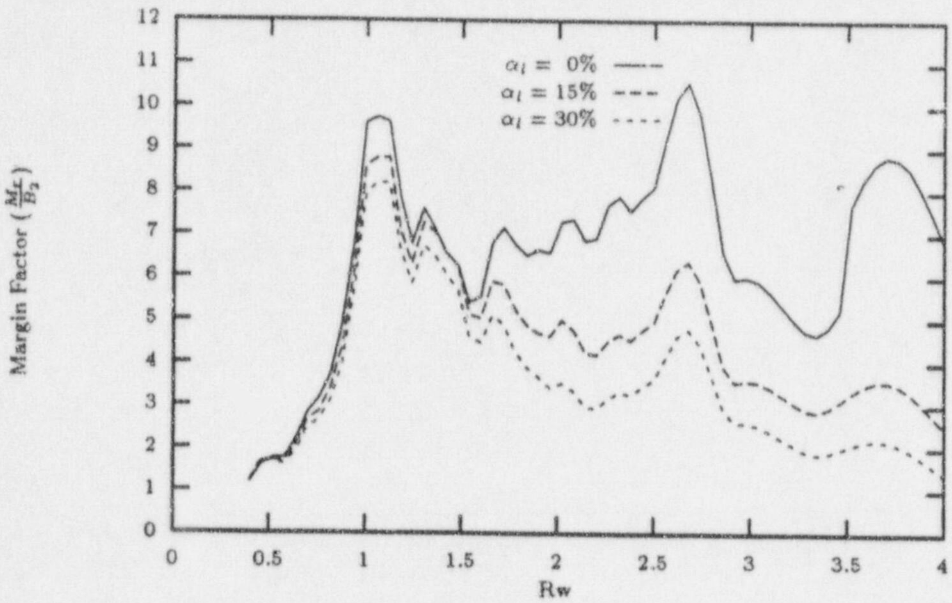

Figure 4.11: Test 40, Parametric models, PFDR input: displacement margin spectra for various values of α_l, $\alpha_w = 0\%$

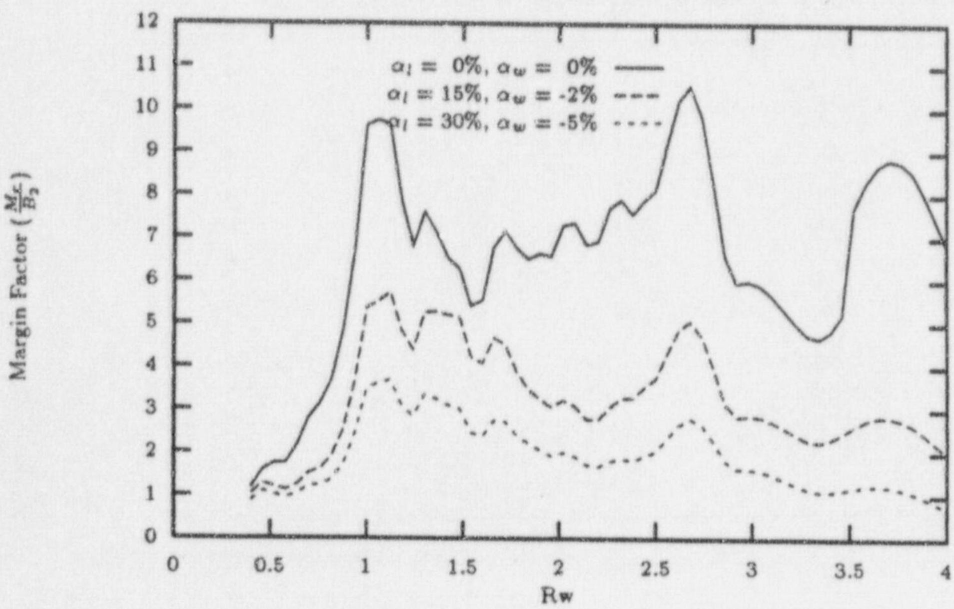

Figure 4.12: Test 40, Parametric models, PFDR input: displacement margin spectra for various values of α_l and α_w

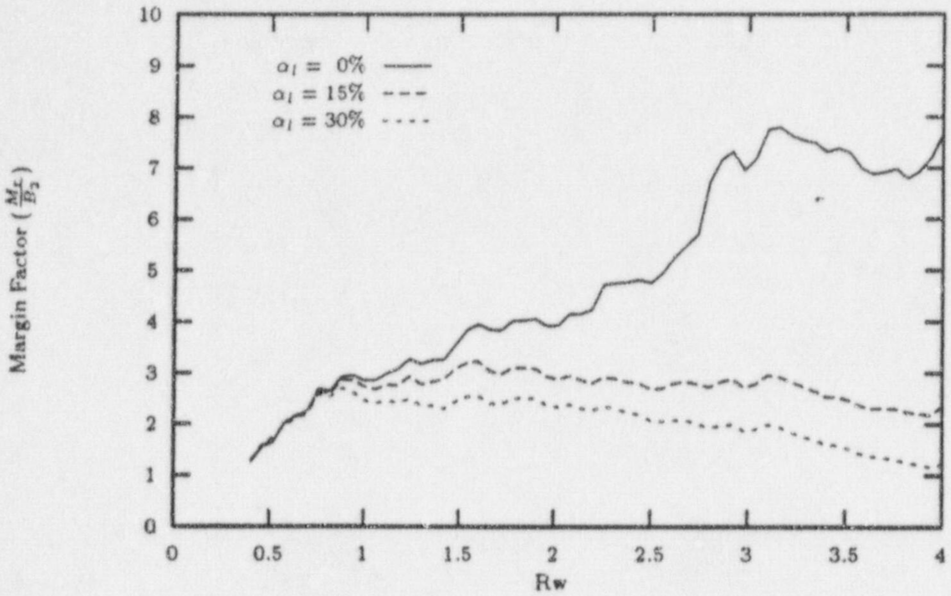

Figure 4.13: Test 40, Parametric models, RG 1.60 input: displacement margin spectra for various values of α_l, $\alpha_w = 0\%$

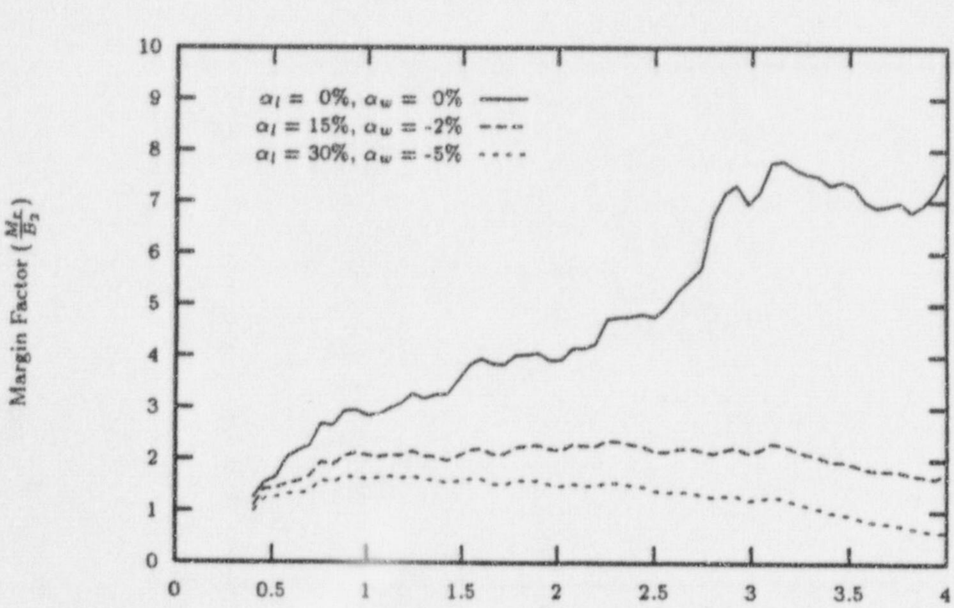

Figure 4.14: Test 40, Parametric models, RG 1.60 input: displacement margin spectra for various values of α_l and α_w

l_3(in)	T(sec)	c_p	α_l(%)	α_w(%)
5	.032	.0659	.0	-0.1
10	.039	.0528	.0	-0.1
20	.056	.0369	.0	-0.1
30	.073	.0281	.0	-0.1
40	.090	.0226	.0	-0.2
50	.109	.0189	.0	-0.2
60	.128	.0163	.0	-0.3
70	.147	.0143	.0	-0.3
80	.167	.0128	.0	-0.4
90	.188	.0116	.0	-0.4
100	.209	.0106	.0	-0.5
150	.320	.0075	.0	-0.7
200	.442	.0058	.0	-1.1
250	.574	.0048	.0	-1.5
300	.715	.0041	.0	-2.0
350	.866	.0036	.0	-2.6
400	1.026	.0032	.0	-3.3
450	1.195	.0028	.0	-4.0
500	1.373	.0026	.0	-4.8

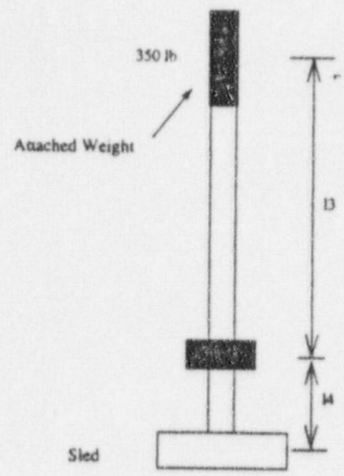

Figure 4.15: Test 14: physical models without eccentricity, $l_1 = l_2 = 0$ in.

l_3(in)	T(sec)	c_p	α_l(%)	α_w(%)
5	.147	.0053	259.1	-0.1
10	.151	.0064	206.8	-0.1
20	.161	.0080	145.9	-0.2
30	.174	.0089	111.7	-0.3
40	.189	.0094	89.7	-0.3
50	.207	.0094	74.5	-0.4
60	.226	.0093	63.4	-0.5
70	.247	.0090	54.9	-0.5
80	.269	.0086	48.2	-0.6
90	.292	.0083	42.8	-0.7
100	.316	.0079	38.4	-0.8
150	.447	.0062	24.5	-1.2
200	.590	.0051	17.3	-1.7
250	.744	.0043	13.0	-2.3
300	.908	.0037	10.2	-3.0
350	1.081	.0032	8.2	-3.7
400	1.263	.0029	6.8	-4.5
450	1.454	.0026	5.7	-5.4
500	1.654	.0024	4.9	-6.4

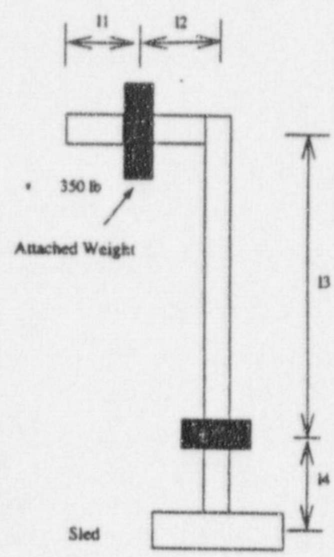

Figure 4.16: Test 14: physical models with eccentricity, $l_1 = l_2 = 56$ in.

l_3(in)	T(sec)	c_p	$\alpha_l(\%)$	$\alpha_w(\%)$
5	.250	.0023	412.4	-0.1
10	.252	.0028	327.2	-0.2
20	.260	.0038	229.8	-0.2
30	.270	.0045	175.7	-0.3
40	.283	.0052	141.3	-0.4
50	.298	.0056	117.6	-0.5
60	.315	.0059	100.3	-0.6
70	.334	.0060	87.0	-0.7
80	.355	.0061	76.6	-0.7
90	.376	.0061	68.2	-0.8
100	.399	.0060	61.3	-0.9
150	.529	.0053	39.7	-1.5
200	.677	.0046	28.4	-2.0
250	.838	.0039	21.6	-2.7
300	1.010	.0035	17.1	-3.4
350	1.192	.0031	13.9	-4.3
400	1.383	.0028	11.6	-5.2
450	1.584	.0025	9.8	-6.1
500	1.794	.0023	8.4	-7.2

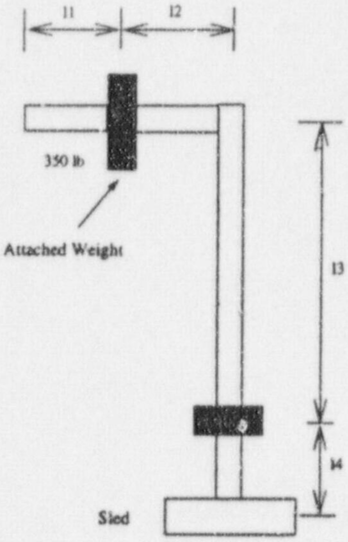

Figure 4.17: Test 14: physical models with eccentricity, $l_1 = l_2 = 85$ in.

l_3(in)	T(sec)	c_p	$\alpha_l(\%)$	$\alpha_w(\%)$
5	.045	.0420	.0	-0.1
10	.052	.0368	.0	-0.1
20	.066	.0290	.0	-0.1
30	.081	.0236	.0	-0.2
40	.097	.0198	.0	-0.2
50	.114	.0171	.0	-0.2
60	.131	.0150	.0	-0.3
70	.149	.0134	.0	-0.3
80	.167	.0121	.0	-0.3
90	.186	.0110	.0	-0.4
100	.205	.0102	.0	-0.4
150	.308	.0073	.0	-0.7
200	.421	.0057	.0	-1.0
250	.544	.0047	.0	-1.4
300	.676	.0041	.0	-1.8
350	.816	.0035	.0	-2.3
400	.966	.0032	.0	-2.9
450	1.123	.0028	.0	-3.5
500	1.289	.0026	.0	-4.2

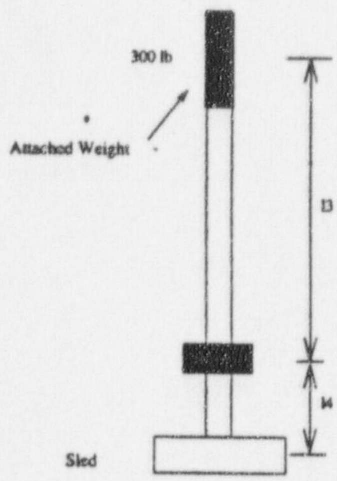

Figure 4.18: Test 40: physical models without eccentricity, $l_1 = l_2 = 0$ in.

l_3(in)	T(sec)	c_p	α_l(%)	α_w(%)
5	.080	.0192	81.0	-0.1
10	.086	.0192	69.7	-0.1
20	.100	.0182	54.0	-0.2
30	.116	.0167	43.6	-0.2
40	.134	.0151	36.3	-0.3
50	.153	.0137	30.8	-0.3
60	.172	.0125	26.6	-0.4
70	.192	.0114	23.3	-0.4
80	.213	.0105	20.6	-0.5
90	.235	.0097	18.4	-0.5
100	.256	.0091	16.6	-0.6
150	.373	.0067	10.6	-0.9
200	.499	.0053	7.5	-1.3
250	.635	.0044	5.6	-1.7
300	.779	.0038	4.3	-2.3
350	.932	.0033	3.5	-2.8
400	1.092	.0030	2.9	-3.5
450	1.261	.0027	2.4	-4.2
500	1.438	.0025	2.0	-5.0

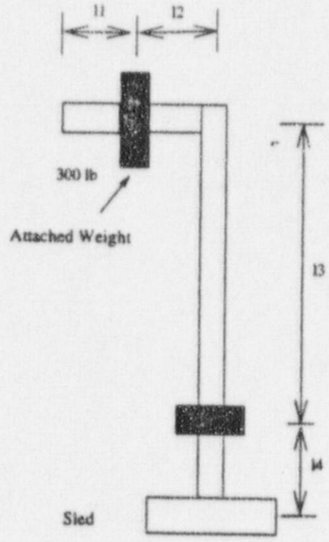

Figure 4.19: Test 40: physical models with eccentricity, $l_1 = l_2 = 30$ in.

l_3(in)	T(sec)	c_p	α_l(%)	α_w(%)
5	.124	.0094	141.1	-0.1
10	.129	.0101	120.9	-0.2
20	.141	.0110	93.3	-0.2
30	.156	.0112	75.3	-0.3
40	.172	.0110	62.7	-0.3
50	.190	.0106	53.4	-0.4
60	.209	.0101	46.2	-0.4
70	.229	.0095	40.6	-0.5
80	.251	.0090	36.0	-0.6
90	.273	.0085	32.3	-0.6
100	.295	.0081	29.1	-0.7
150	.416	.0062	18.9	-1.1
200	.549	.0051	13.5	-1.5
250	.691	.0043	10.2	-2.0
300	.842	.0037	8.0	-2.5
350	1.001	.0032	6.5	-3.2
400	1.169	.0029	5.3	-3.9
450	1.345	.0026	4.5	-4.6
500	1.528	.0024	3.8	-5.5

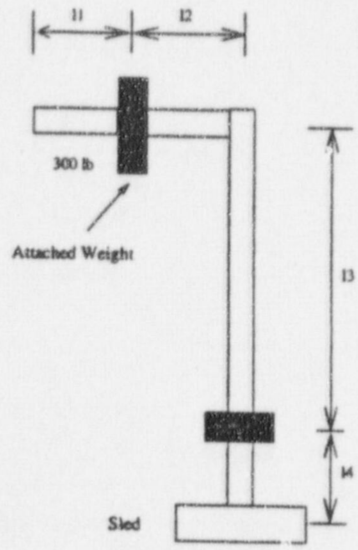

Figure 4.20: Test 40: physical models with eccentricity, $l_1 = l_2 = 49$ in.

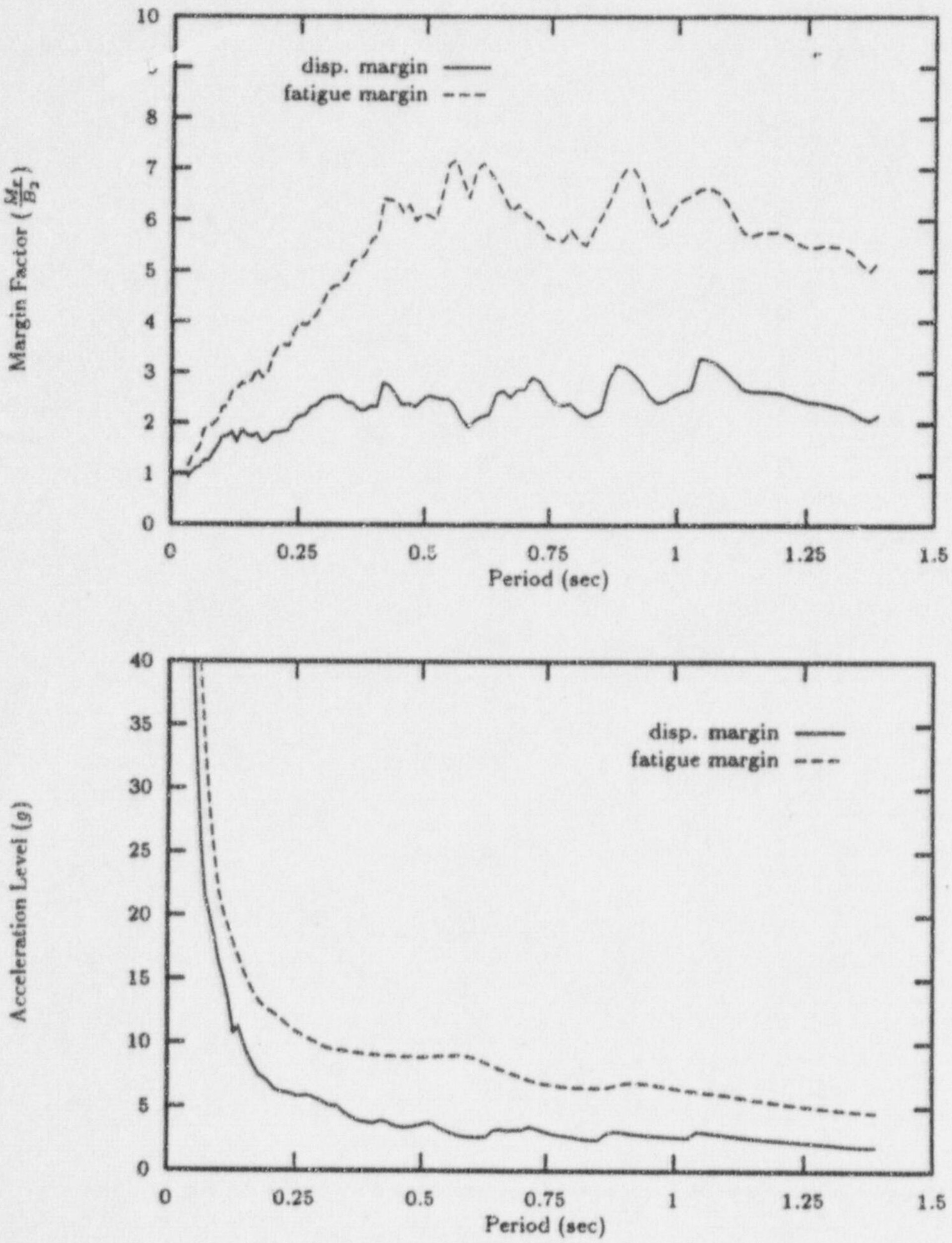

Figure 4.21: Test 14, Physical models, RG 1.60 input: frequency effects on fatigue margin spectrum and displacement margin spectrum and required acceleration levels , $l_1, l_2 = 0$ in., Sequential Method

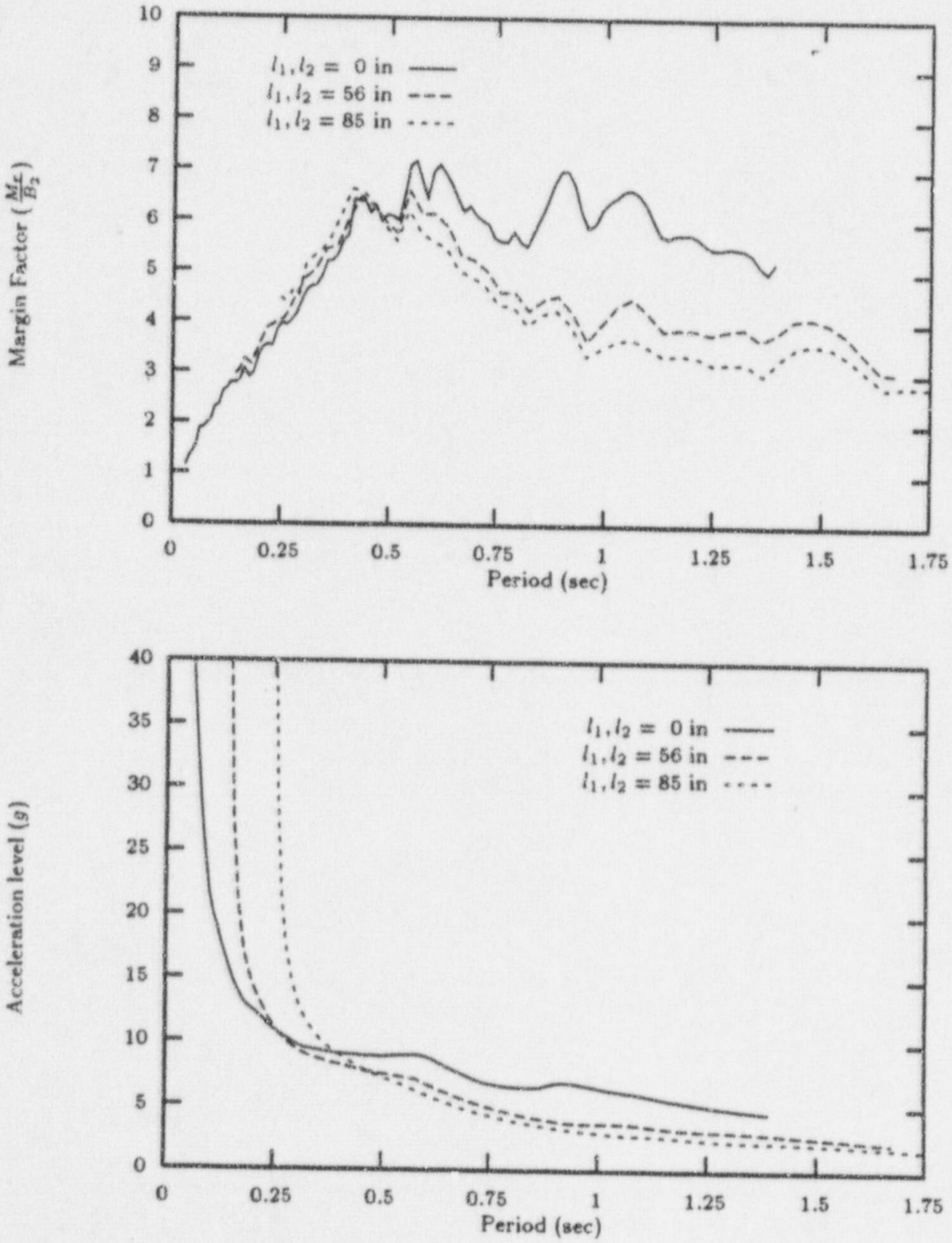

Figure 4.22: Test 14, Physical models, RG 1.60 input: fatigue margin spectra and required acceleration levels for various degrees of eccentricity, Sequential Method

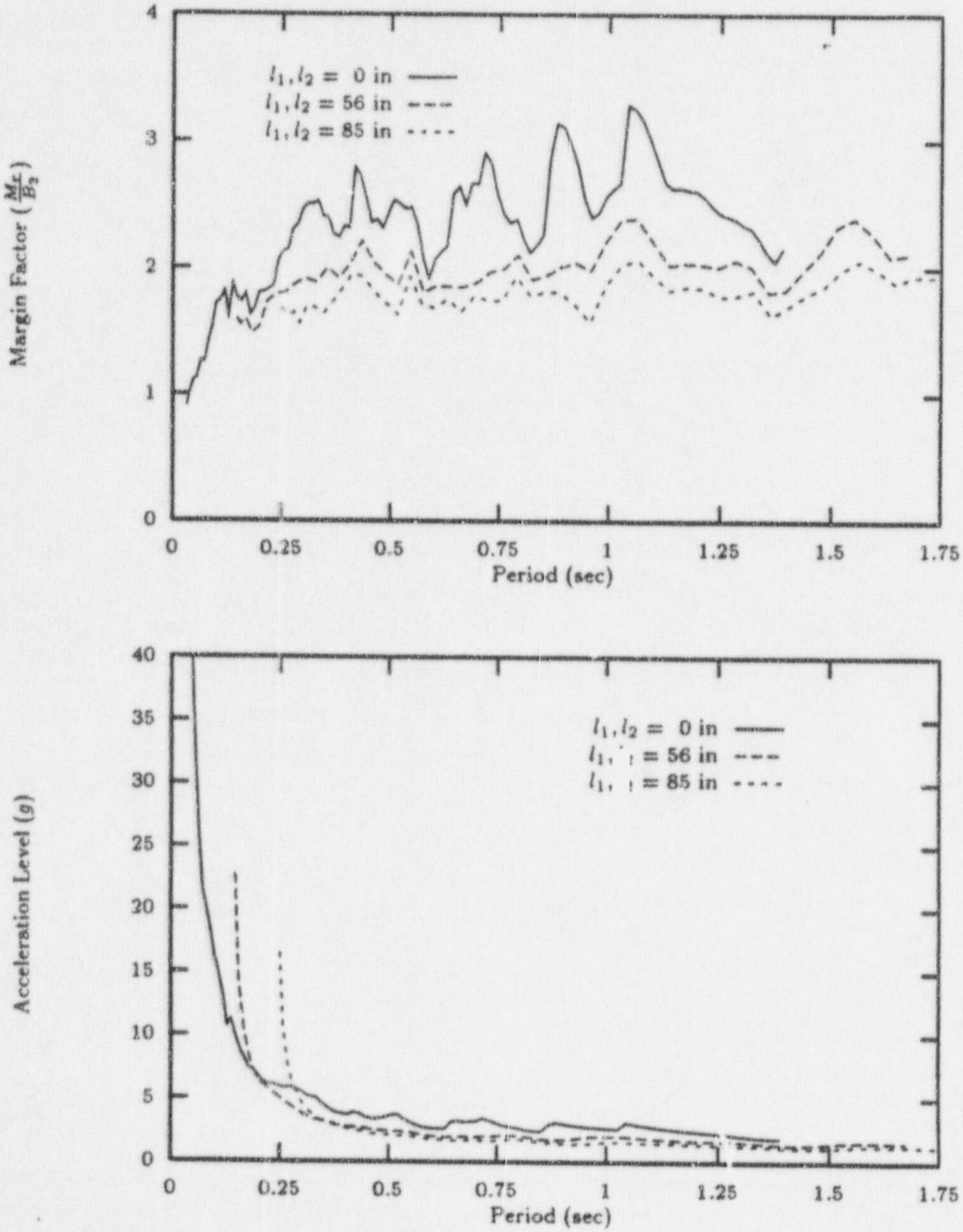

Figure 4.23: Test 14, Physical models, RG 1.60 input: displacement margin spectra and required acceleration levels for various degrees of eccentricity

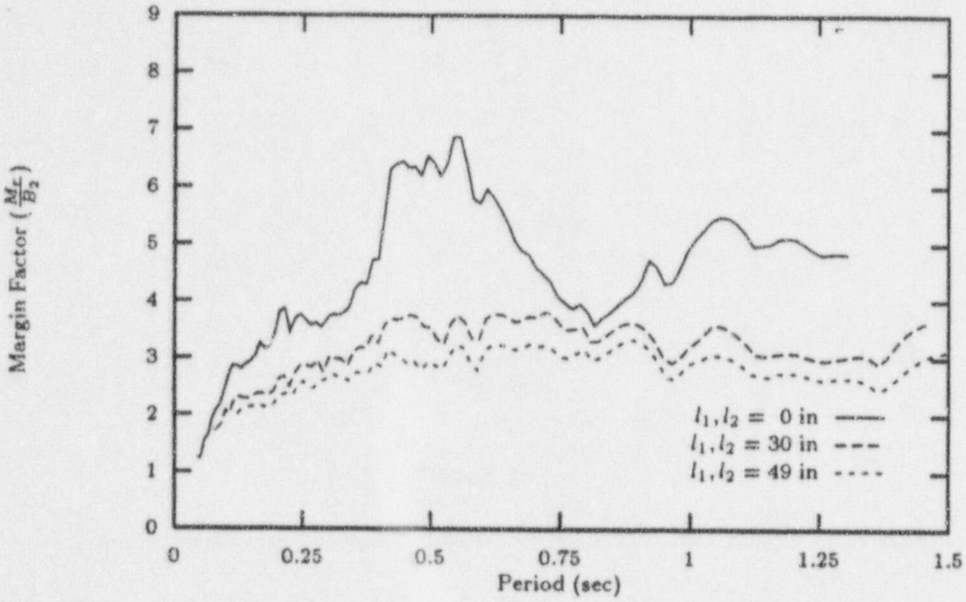

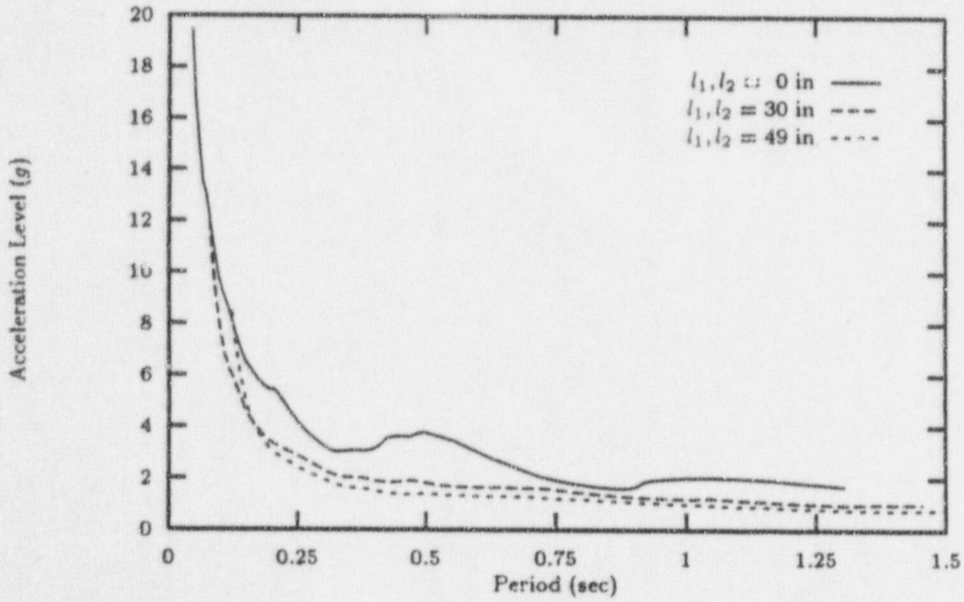

Figure 4.24: Test 40, Physical models, RG 1.60 input: displacement margin spectra and required acceleration levels

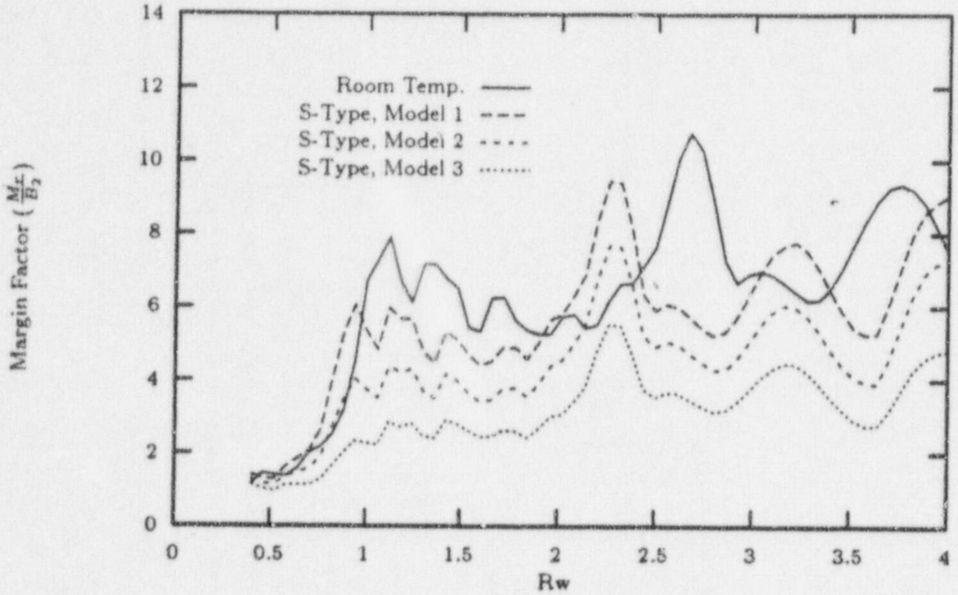

Figure 4.25: Test 14, Parametric models, PFDR input: temperature effects (S-type) on fatigue based margin spectra, $\alpha_w = 0\%$, $R_y = 0.726$, Sequential Method

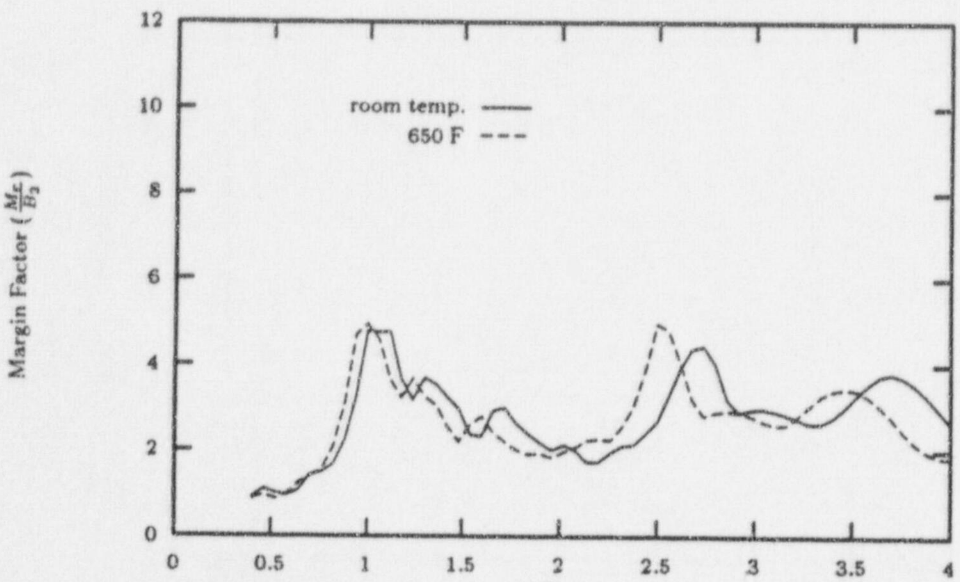

Figure 4.26: Test 14, Parametric models, PFDR input: temperature effects (S-type) on displacement margin spectra, $\alpha_w = 0\%$, $R_y = 0.726$

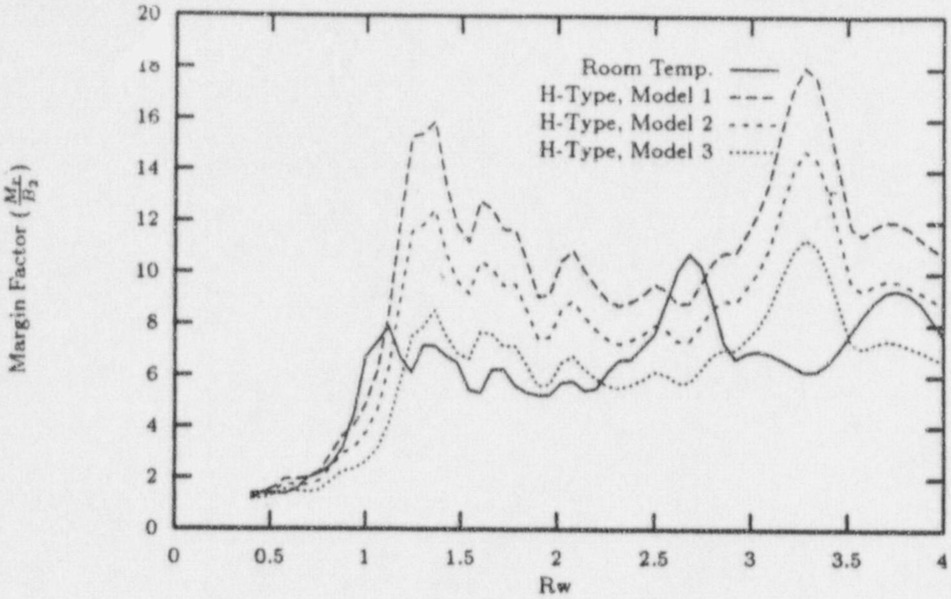

Figure 4.27: Test 14, Parametric models, PFDR input: temperature effects (H-type) on fatigue based margin spectra, $R_h = 1.5$, $\alpha_w = 0\%$, Sequential Method

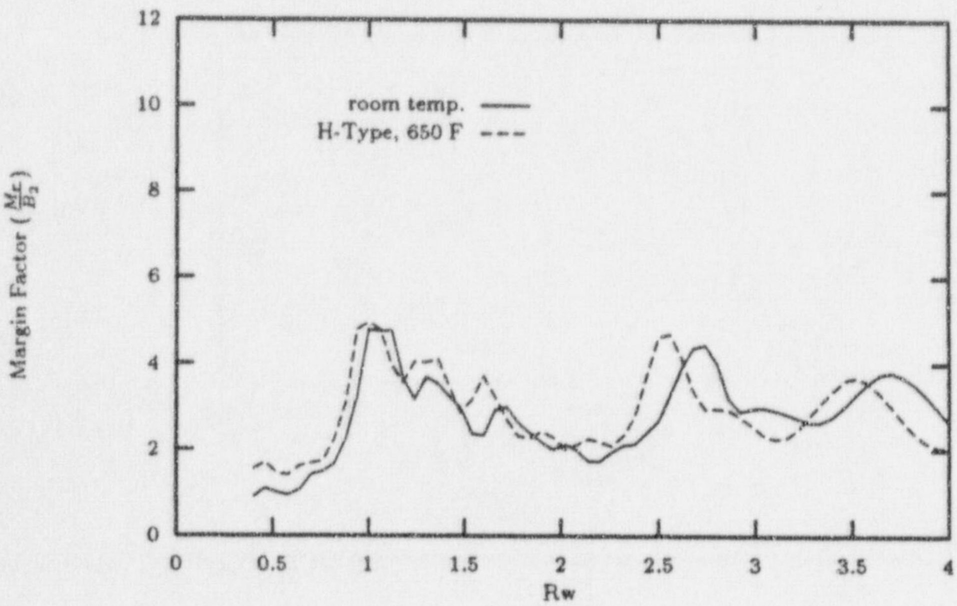

Figure 4.28: Test 14, Parametric models, PFDR input: temperature effects (H-type) on displacement margin spectra, $R_h = 1.5$, $\alpha_w = 0\%$

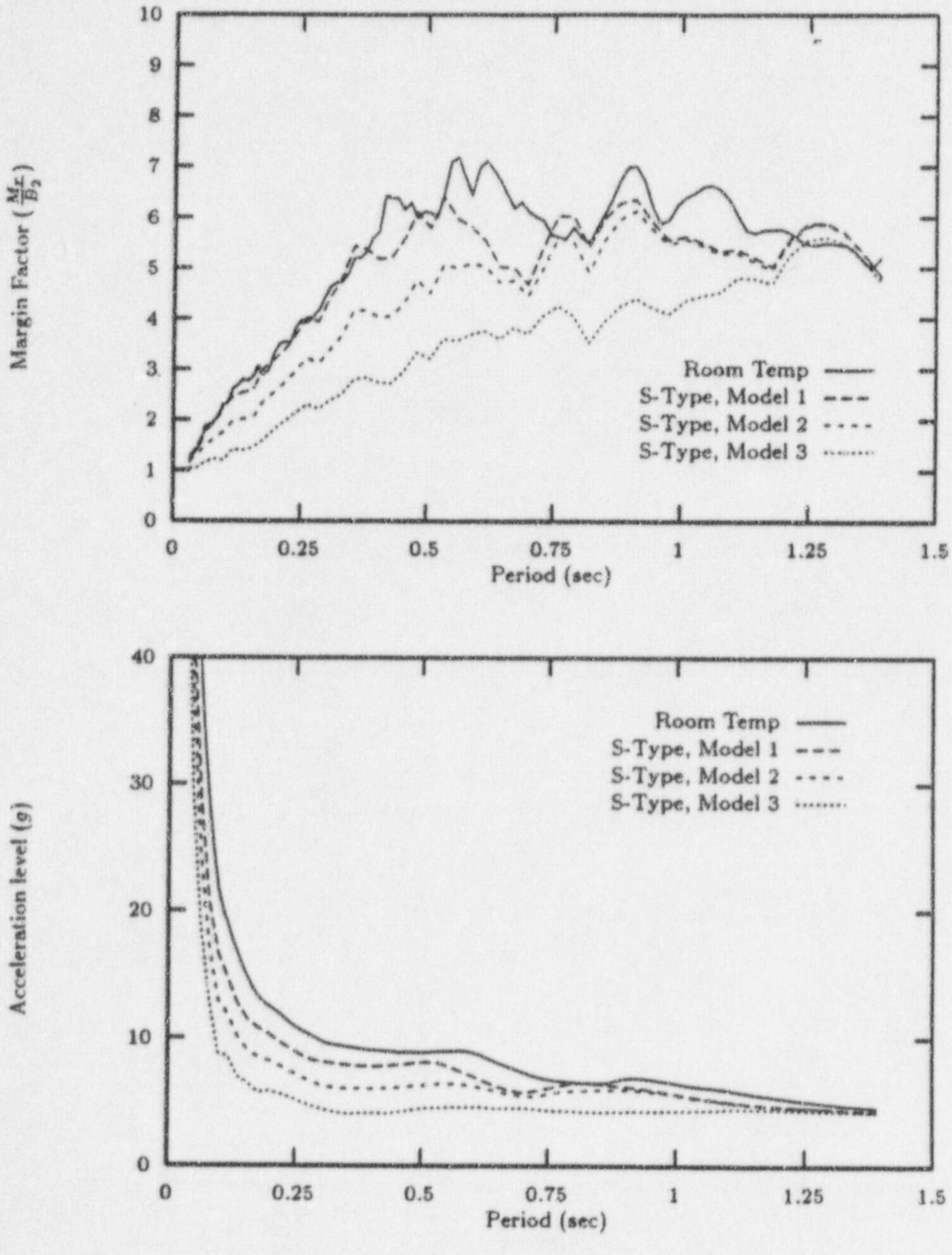

Figure 4.29: Test 14, Physical models, RG 1.60 input: temperature effects (S-type) on fatigue margin spectra and required acceleration levels, $l_1 = l_2 = 0$, $R_y = 0.726$, Sequential Method

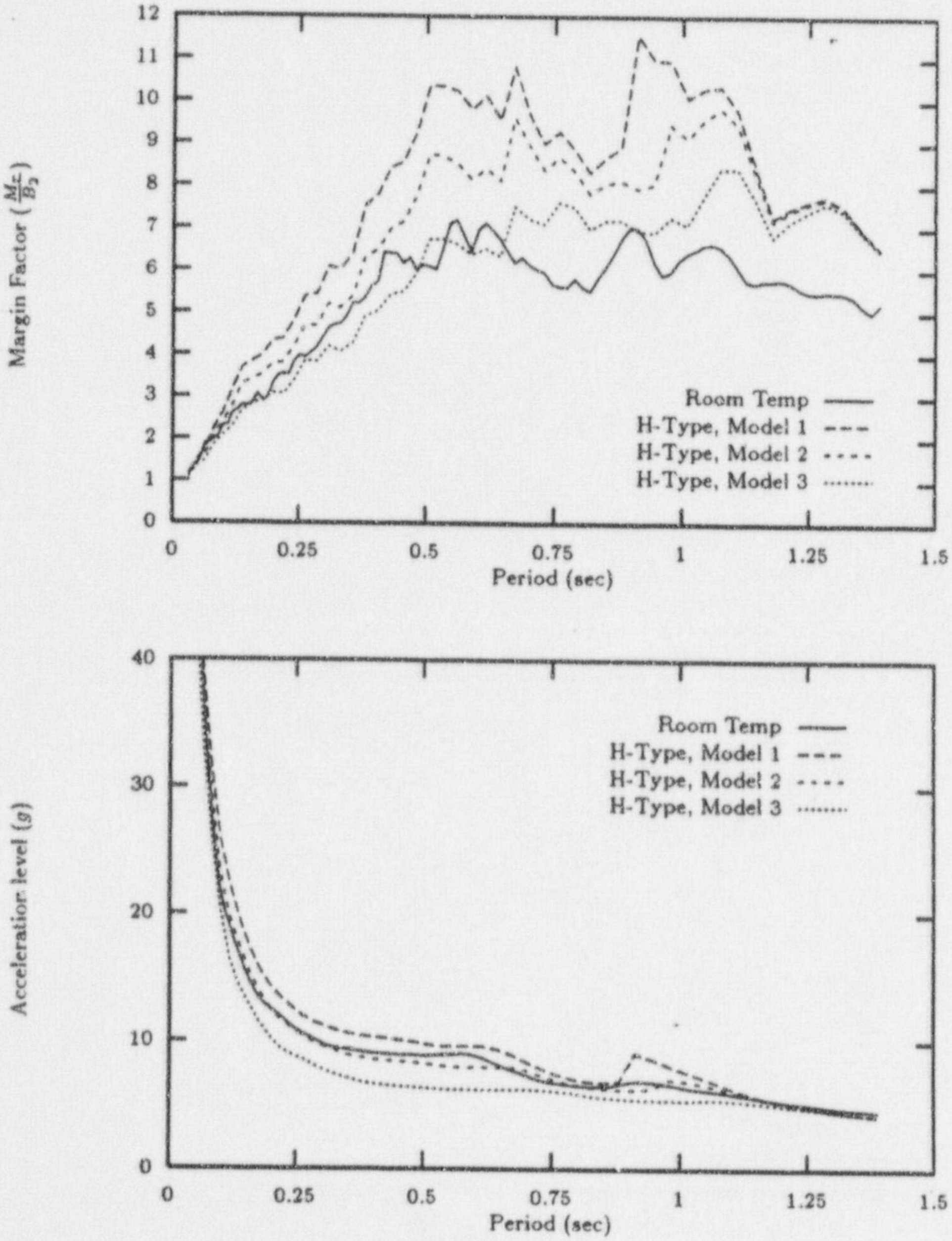

Figure 4.30: Test 14, Physical models, R. G 1.60 input: temperature effects (H-type) on fatigue margin spectra and required acceleration levels, $l_1 = l_2 = 0$, $R_h = 1.5$, Sequential Method

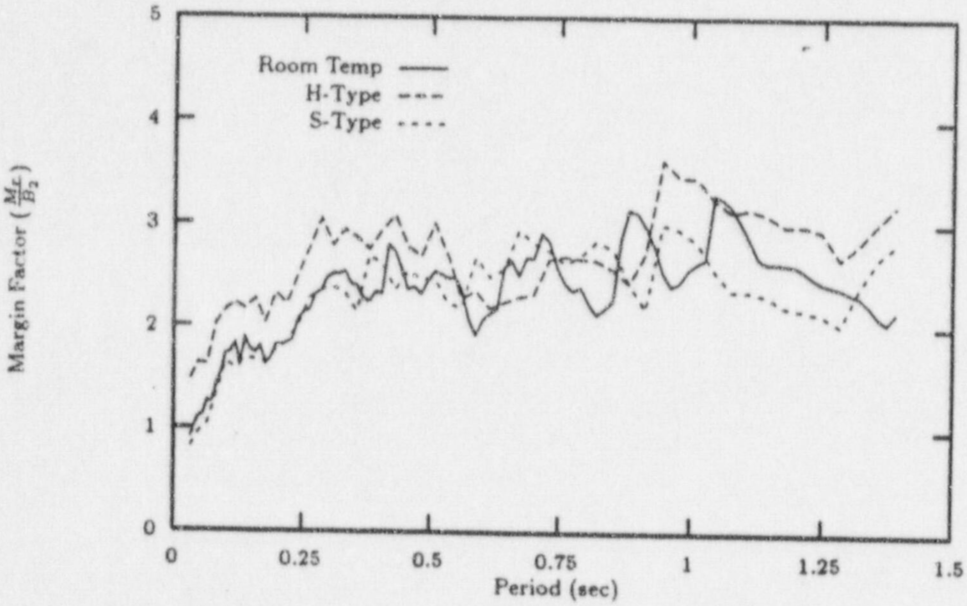

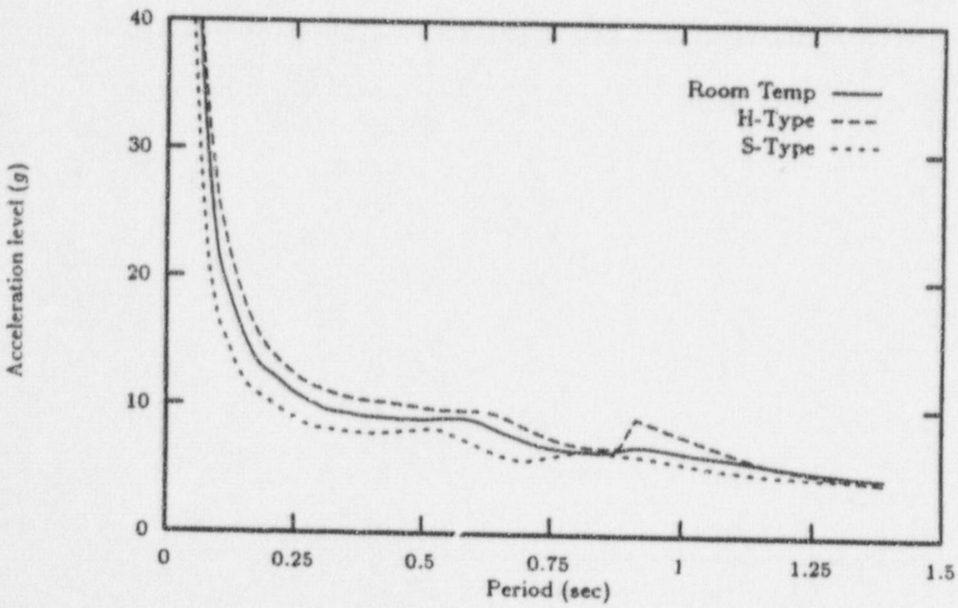

Figure 4.31: Test 14, Physical models, R. G 1.60 input: temperature effects (S-type and H-Type) on displacement margin spectra and required acceleration levels, $l_1 = l_2 = 0$, $R_h = 1.5$, $R_y = 0.726$

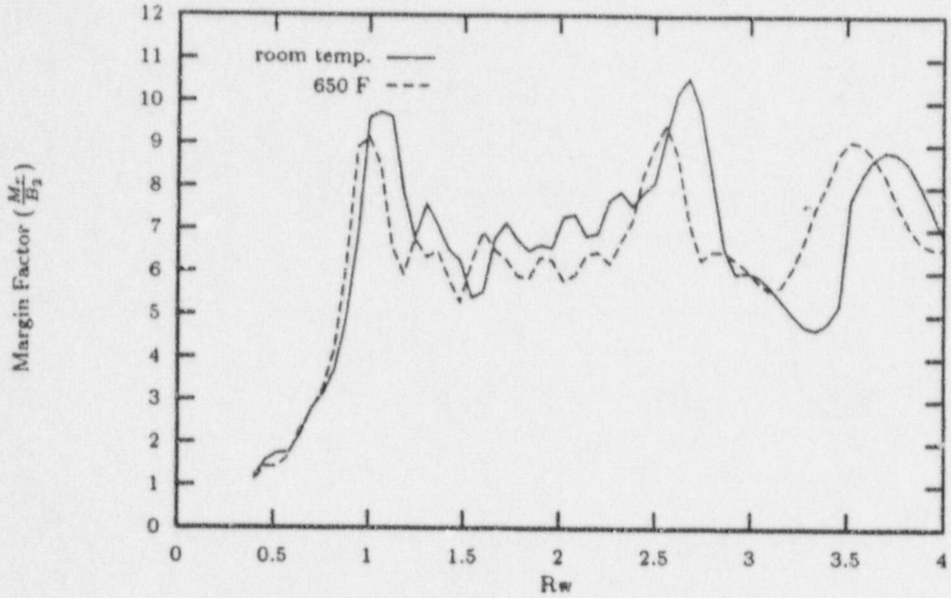

Figure 4.32: Test 40, Parametric models, PFDR input: temperature effects on displacement margin spectra, $\alpha_w = 0\%$, $R_y = 0.584$

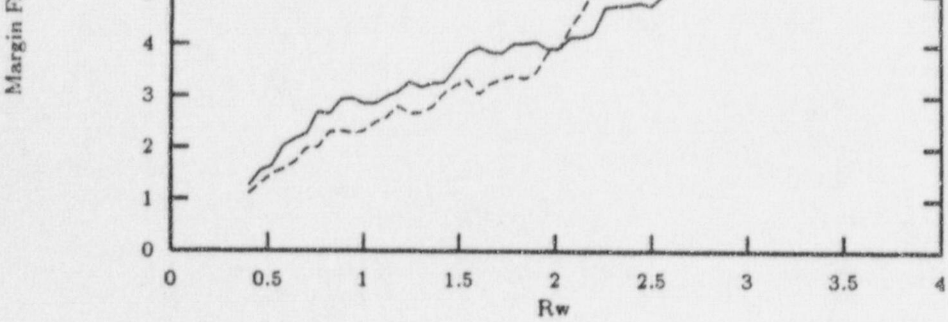

Figure 4.33: Test 40, Parametric models, RG 1.60 input: temperature effects on displacement margin spectra, $\alpha_w = 0\%$, $Ry = 0.584$

l_3(in)	T(sec)	c_p	α_l(%)	α_w(%)
35	.252	.0056	142.8	-0.3
40	.258	.0059	128.7	-0.4
50	.274	.0063	107.1	-0.5
60	.292	.0066	91.2	-0.5
70	.311	.0066	79.2	-0.6
80	.332	.0066	69.7	-0.7
90	.354	.0066	62.0	-0.8
100	.377	.0064	55.7	-0.9
150	.508	.0055	35.9	-1.4
200	.655	.0047	25.6	-2.0
250	.815	.0040	19.5	-2.6
300	.985	.0035	15.4	-3.3
350	1.165	.0031	12.5	-4.1
400	1.354	.0028	10.4	-5.0
450	1.553	.0025	8.8	-6.0
500	1.760	.0023	7.5	-7.0

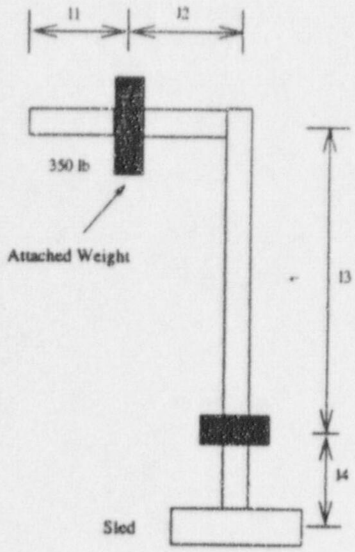

Figure 4.34: Test 14: worst-case physical models with eccentricity, $l_1 = l_2 = 78$ in.

l_3(in)	T(sec)	c_p	α_l(%)	α_w(%)
10	.116	.0119	107.1	-0.2
20	.129	.0125	82.7	-0.2
30	.144	.0125	66.8	-0.3
40	.161	.0120	55.6	-0.3
50	.179	.0114	47.3	-0.4
60	.198	.0107	40.9	-0.4
70	.219	.0101	35.9	-0.5
80	.240	.0094	31.9	-0.5
90	.262	.0089	28.5	-0.6
100	.284	.0083	25.7	-0.7
150	.405	.0064	16.7	-1.0
200	.536	.0051	11.9	-1.4
250	.676	.0043	8.9	-1.9
300	.825	.0037	7.0	-2.5
350	.983	.0033	5.6	-3.1
400	1.149	.0029	4.6	-3.8
450	1.323	.0026	3.9	-4.5
500	1.505	.0024	3.3	-5.3

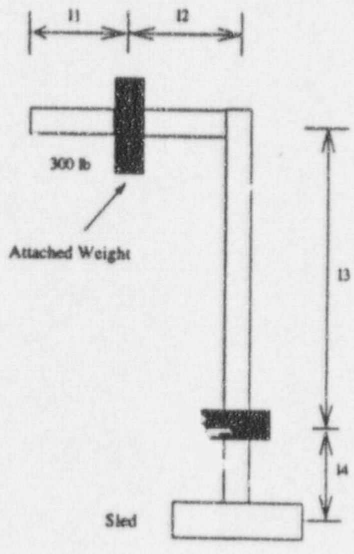

Figure 4.35: Test 40: worst-case physical models with eccentricity, $l_1 = l_2 = 44$ in.

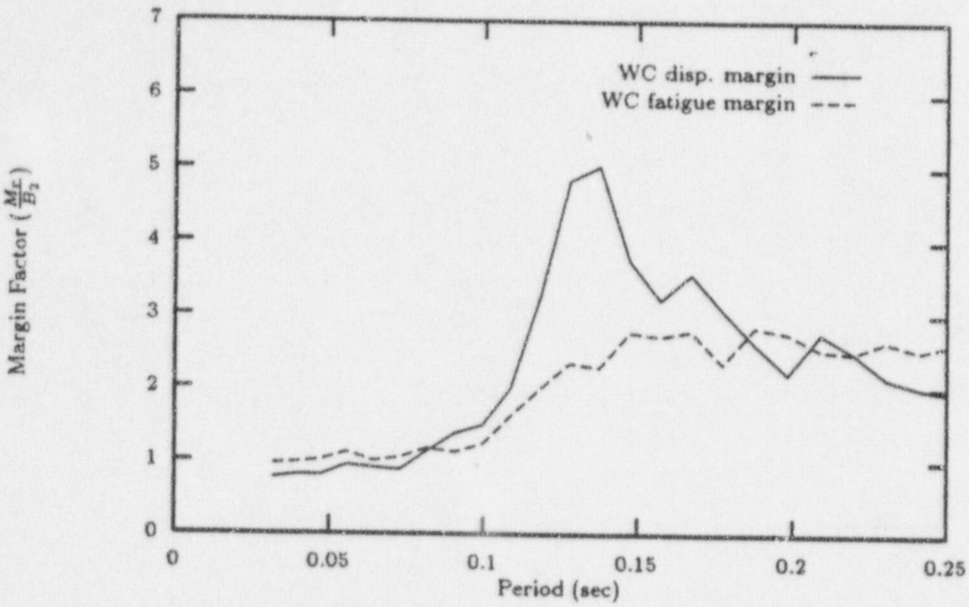

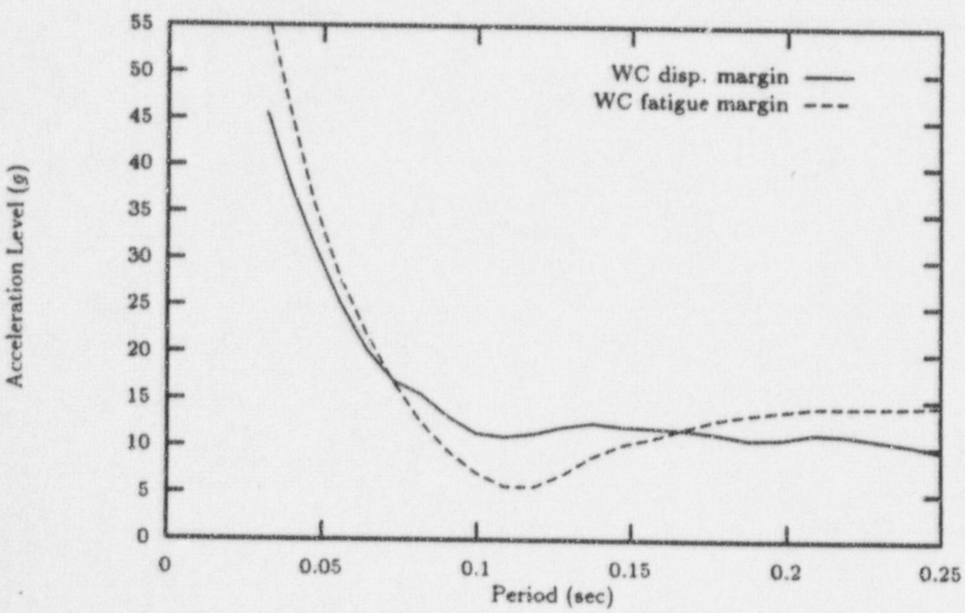

Figure 4.36: Test 14, Physical models, PFDR input: worst-case consideration ($l_1 = l_2 = 0$ in, Period = [0: 0.25] second), fatigue and displacement margin spectra and required acceleration levels, $R_y = 0.726$

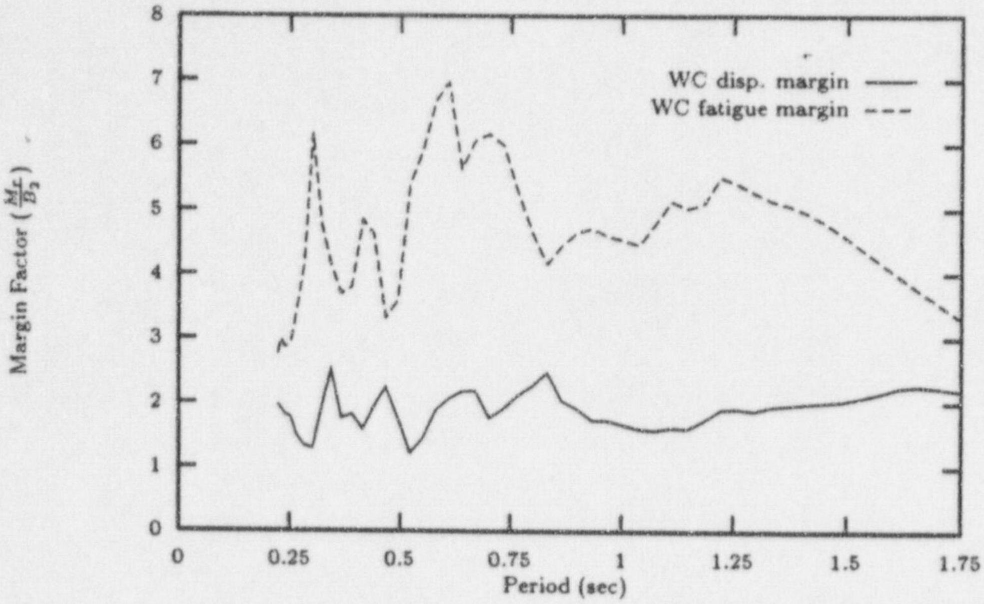

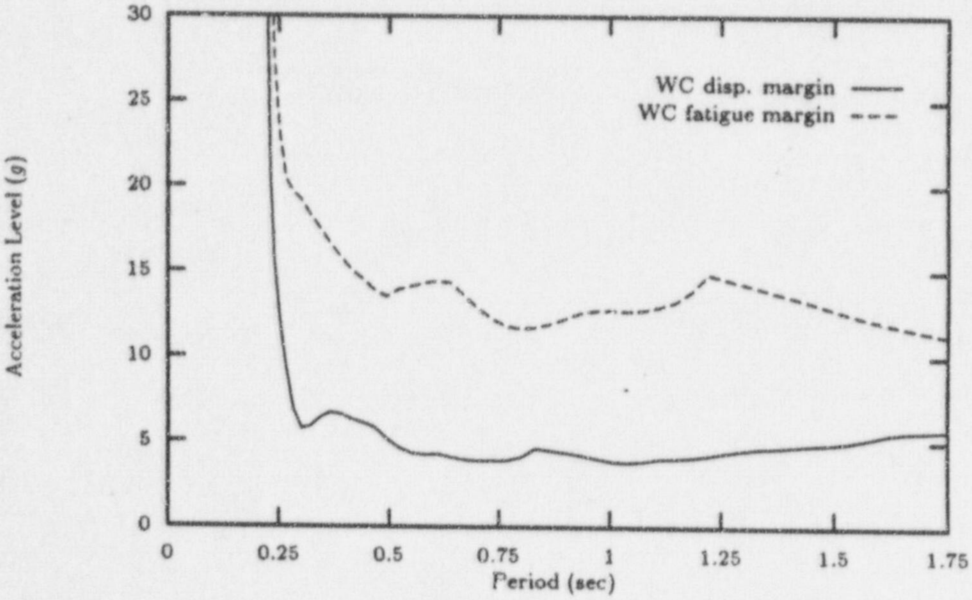

Figure 4.37: Test 14, Physical models, PFDR input: worst-case consideration ($l_1 = l_2 = 78$ in, Period = [0.25, 1.75] second), fatigue and displacement margin spectra and required acceleration levels, $R_y = 0.726$

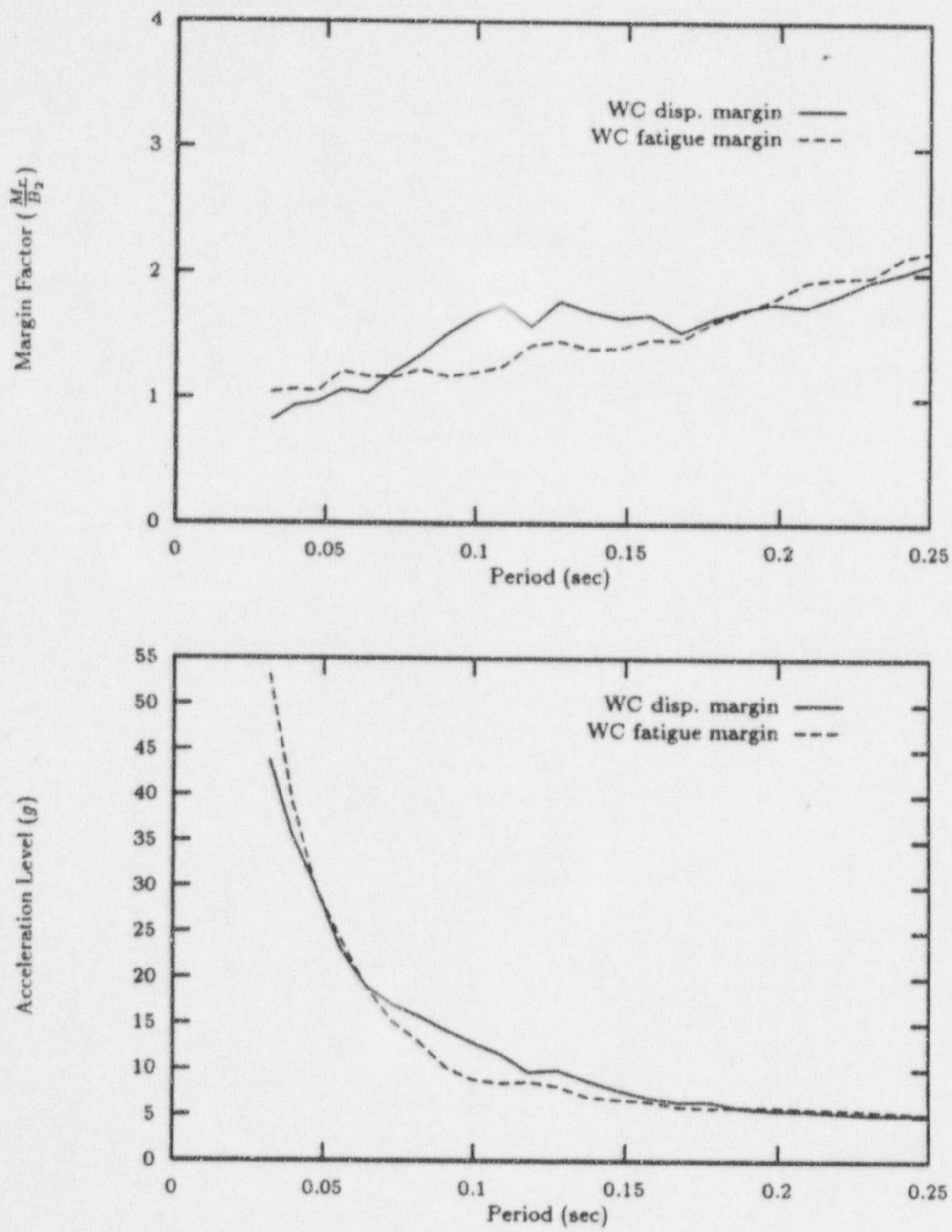

Figure 4.38: Test 14, Physical models, RG 1.60 input: worst-case consideration ($l_1 = l_2 = 0$ in, Period = [0: 0.25] second), fatigue and displacement margin spectra and required acceleration levels, $R_y = 0.726$

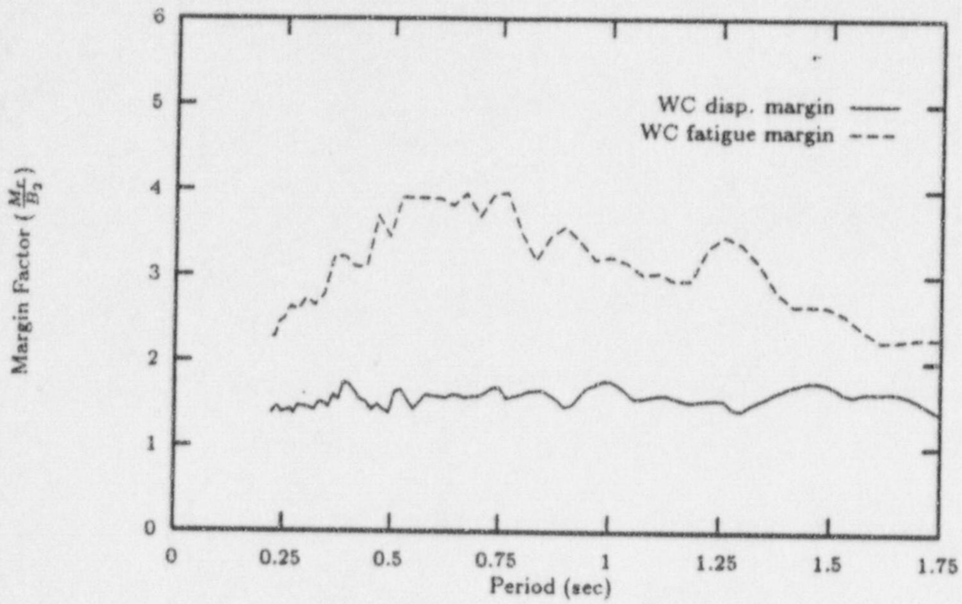

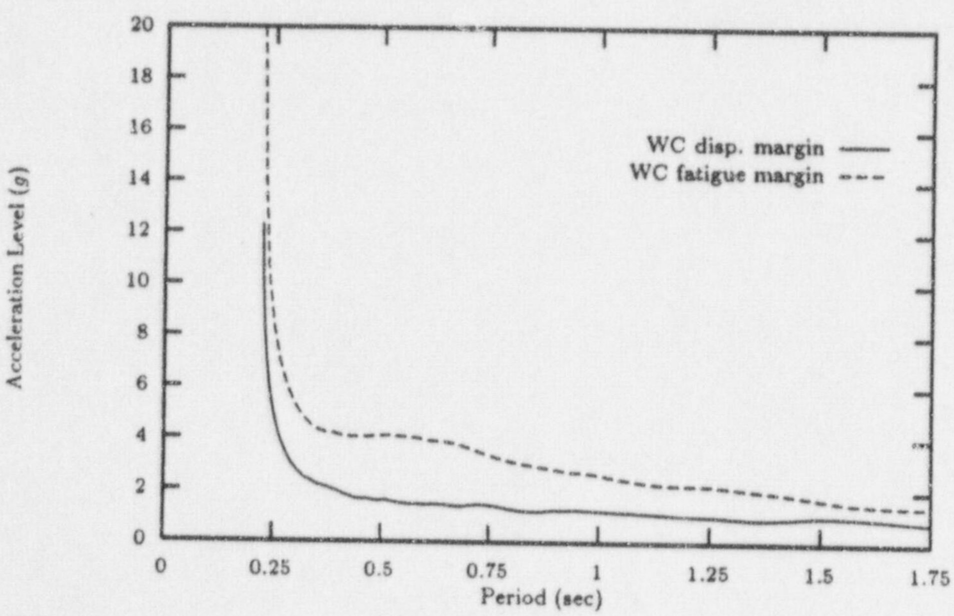

Figure 4.39: Test 14, Physical models, RG 1.60 input: worst-case consideration ($l_1 = l_2 = 78$ in, Period = [0.25, 1.75] second), fatigue and displacement margin spectra and required acceleration levels, $R_y = 0.726$

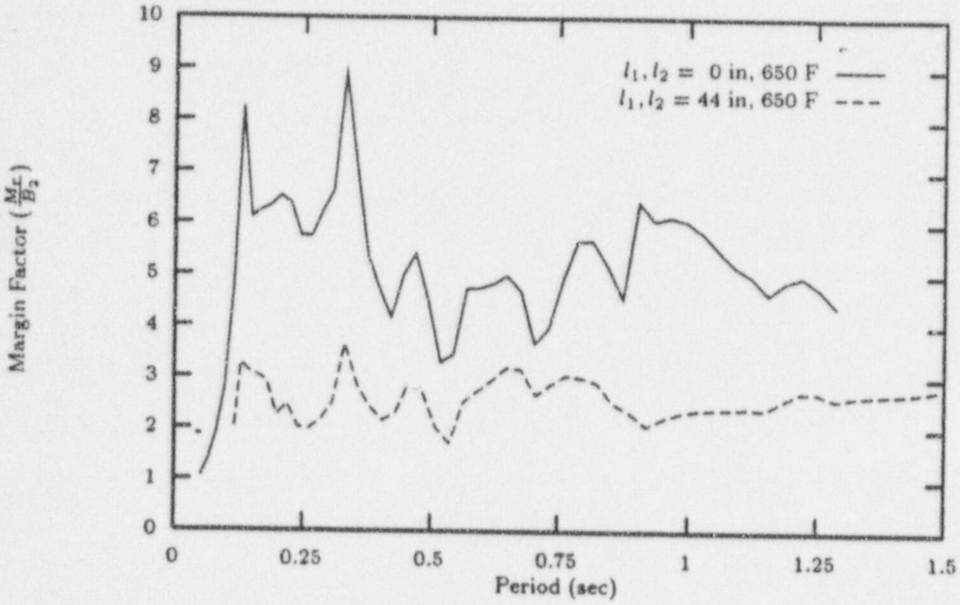

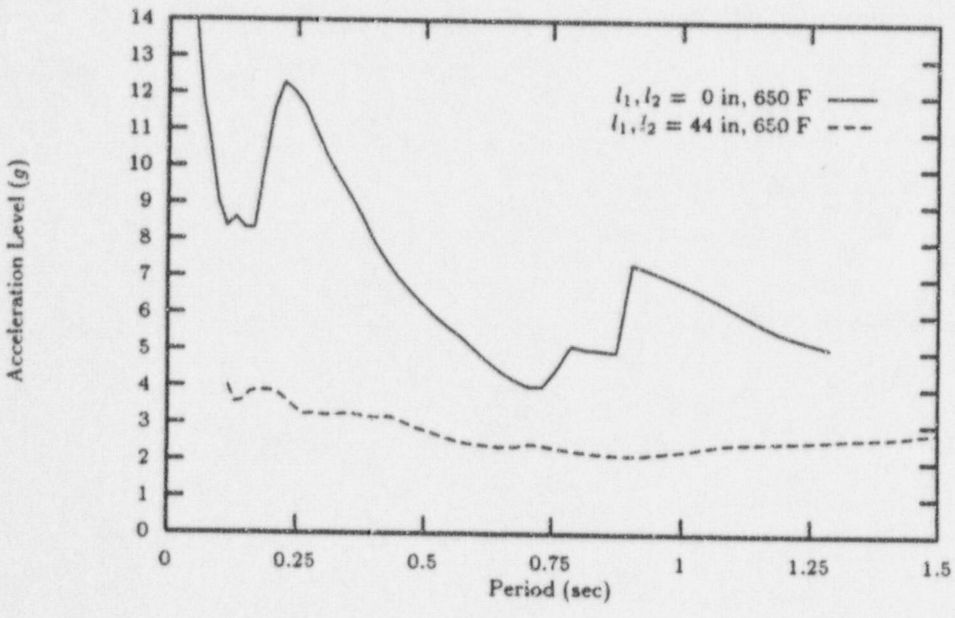

Figure 4.40: Test 40, Physical models, PFDR input: worst-case displacement margins and required acceleration levels, $R_y = 0.584$

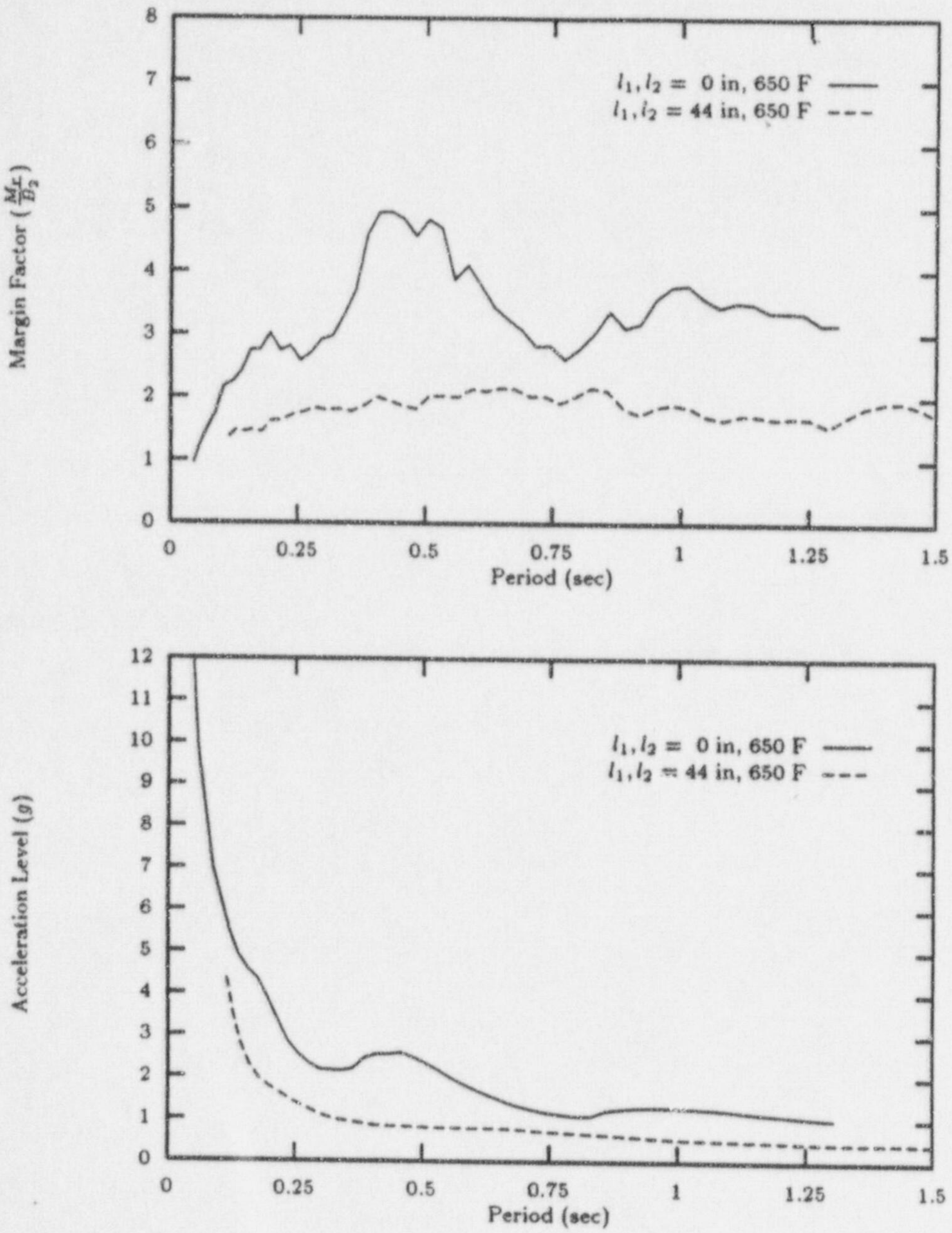

Figure 4.41: Test 40, Physical models, RG 1.60 input: worst-case margins, $R_y = 0.584$

5 Summary and Conclusions

A framework for hysteretic modeling, identification and fatigue analyses for piping component seismic test systems has been developed in this study. The developed models are capable of simulating the nonlinear response of the test system with a high degree of accuracy. A unified treatment of frequency effects on seismic margin is presented. The seismic margin is concluded to be a two-parameter function when the eccentric moment effects are excluded from consideration. Representation of seismic margins can be based on the frequency ratio R_w and the P-Δ stiffness ratio α_w. A proof is provided to show that the effects of R_w on margins can be identically obtained by varying the frequency of the physical model or varying the time scale of the input loading.

The study results suggest the possibility of large-rotation induced damage mechanisms and failure modes that are not being fully addressed by the ASME Code fatigue margin. The concept of displacement-based margin is proposed in this study to complement the use of fatigue-based margin.

Based on the present study of the seismic margins of piping component test systems, the following conclusions are drawn:

1. The fatigue margin versus frequency ratio results from this study differ significantly from those of the previous study that provided the basis for increased allowable primary stress in the 1994 Addendum to the ASME Boiler and Pressure Vessel Code. Generally speaking, the fatigue margin results from the present study are lower than those from the previous study in the stiff system region ($R_w \leq 1$) and greater than those of the previous study in the soft system region ($R_w \geq 1$). The results of the present study are based on more sophisticated modeling and analysis techniques, and are believed to be more accurate than those of previous studies.

2. The fatigue margin for relatively stiff piping systems is observed to be generally lower than for relatively soft piping systems. For a building filtered narrow-banded type of excitation, there is a very rapid increase in fatigue margin as the natural frequency of the piping system decreases in the region of the predominant frequency of the structure. For a broad-band ground type excitation, there is a gradual increase in fatigue margin as the natural frequency of the piping system is decreased.

3. The fatigue margin is directly proportional to the stress index B_2. Therefore, whether or not the fatigue margin results are "acceptable" will depend upon the value of stress index assumed. For example, if B_2 is assumed to be 1.0 for Test 14, the fatigue margin in the stiff region is on the order of unity, which is clearly unacceptable.

4. The fatigue margin for piping systems in the soft region is generally high regardless of the value of B_2 assumed. However, the displacements in this frequency ratio region may become quit large. This can lead to the possibility of failure modes other than fatigue, such as buckling or collapse. Fatigue-based failure margins may not be an appropriate

measure for such cases.

5. A displacement-based failure margin can be useful for piping systems in the soft region. A possible rotation-based failure margin is described in this report. The magnitude of the displacement-based margin in the soft region will depend upon the value of acceptable rotation limit that is assumed. However, the displacement-based failure margin will generally be lower than the fatigue-based failure margin in the soft region.

6. Based on PFDR and RG 1.60 inputs, it is observed that there is a strong correlation between the margins and the acceleration levels required to reach either a fatigue-based or a displacement-based failure condition. For structural systems without bias eccentric weight, the required acceleration level generally follows a decreasing trend with increasing structural natural period, while the margins generally follow an increasing trend with increasing structural natural period.

7. Eccentric moment effects and the temperature effects can significantly reduce both fatigue-based and displacement-based margins for flexible systems. Under the indicated considerations, study results suggest that the minimum "soft-side" displacement margin is only slightly higher than the minimum "hard-side" margin. Thus, concern may be raised about the seismic safety of extremely flexible systems due to the simultaneous occurrence of low seismic margins and low input earthquake intensity levels.

References

[1] W. D. Iwan, A distributed-element model for hysteresis and its steady-state dynamic resonses, *Journal of Applied Mechanics*, 893 (December 1966).

[2] P. Jayakumar, *Modeling and identification in structural dynamics*, Ph. D. Dissertation, California Institute of Technology, Pasadena (1987)

[3] R. S. Thyagarajan, *Modeling and analysis of hysteretic structural behavior*, Ph. D. Dissertation, California Institute of Technology, Pasadena (1989)

[4] S. L. S. Jacoby, J. S. Kowalik and J. T. Pizzo, *Iterative Methods for Nonlinear Optimization Problems*, Prentice-Hall Inc., New Jersey (1972)

[5] J. A. Collins, *Failure of Materials in Mechanical Design*, Wiley-Interscience (1981)

[6] *Piping and Fitting Dynamic Reliability Program Vol. 2: Component Tests*, Electric Power Research Institute (Oct. 1994)

[7] *Criteria of the ASME Boiler and Pressure Vessel Code for Design by Analysis in Section III and VIII* Div. 2, ASME (1969)

Appendix I-B: Data Collection from ANCO Quick Look Test Reports

prepared by

Ken Jaquay

Energy Technology Engineering Center

Spreadsheets for ANCO Quick Look Report Data. Top 10 Lines for ASME SWG-SR

Test	Test ID #	Comments on test (text continued below type identification line)					
type	Note [1]:						
Z	input	Section Modulus, in**3					
B2:	input	Moment stress index at measured moment location					
Mc:	calc	Based on 4.5 Sm = 90 ksi: Mc = 90*Z/B2, ksi, P=WT=0 used.					
QL title:	QL report run titles						
run: test run #	5	6	7	8	9	10	11
Sa [Note 2]:							
LMs range / 2:	Ms range / 2	[Note 4]	calc	calc	calc	calc	calc
TM [Note 3]:	calc	calc	calc	calc	calc	calc	calc
Ms range / 2:	location	Maximum test run measured moment range divided by 2, in-kips					
max rot range:	Extreme range of rotation measured during entire test run, radians						
max rot cycle:	Maximum range of rotation for a single half cycle during test run, radians						
run fraction:	Fraction of full test run when test was stopped or through-wall leak reduced pressure						
sled input freq:	FI, Frequency at peak of 5% damped LERS using sled's measured accel T-H, hz						
S(fn):	Accel at nat freq on 5% damped LERS using sled's measured accel T-H, g's						
R = S(fn) / Sa:	Ratio used to convert broadened LERS moments to unbroadened LERS moments						
GE BR M5:	GE EPRI Vol. 2 reported 15% peak broadened 5% damped LERS moment. in-kips						
R * M5:	"Unbroadened" 5% damped LERS moment for cases .87 < Rw < 1.15, in-kips						
rot/rot(M5)**2:	Run magnitude using "max rot cycle"ratio to value at boxed R*M5 and -0.2 slope S-N						
eff # events:	Run magnitude adjusted for partial run times. Summation inside SUM box.						

[ ] QL test data   SUM [ ] Total # events   *** Problem

[ ] In above table: Spreadsheet calculated values.
In the Test tables: a scaled number or computed using a scaled number. See notes for assumptions used.

na = Not Available

Note [1]: This is a string of text identifiers separated by commas.

Field 1: Type of fitting

LREL	Long radius elbow
SREL	Short radius elbow
TEE	Tee
RED	Reducer

Field 2: Pipe Schedule

Field 3: Material

CS	Carbon steel A106 Grade B pipe and A234WPB fittings
SS	Stainless steel A312 TP316L pipe and A403 WP316L fittings

Field 4: xxxx P Internal pressure, psig

Field 5: xx.x WT Eccentric weight moment, in-kips

Field 6: Direction and/or manner of loading, when applicable

IP	In-plane of fitting
OP	Out-of-plane of fitting
-1 or -2	Number of tee run ends attached to sled

Field 7: xx.x sec — Duration of a full Test Run
(x.x hz) — Targeted sled peak response frequency, hz = 143/duration

Field 8: x.x Fn — EPRI Report Vol. 2 Appendix B stated Natural Freq of test system, hz
( ) — Measured natural frequency of test system, fn, hz

fphz units	based on Fourier analysis of preliminary test run
fehz units	based on Fourier analysis of "elastic level" test run

Field 9: Rw = Ratio of input peak frequency to natural frequency based on;
Test frequency measurements when available
Last full high level run when available

Note [2]: Sa = Acceleration at peak of 5% damped LERS using sled's measured accel T-H, g's

Note [3]: TM = LMs/Mc

Note [4]: LMs = linearly extrapolated measured moment = Sa/Sa(Low EQ) times Ms/2(Low EQ), in-kips

T1: MISSING KEY DATA - INFO ONLY

Test	1	QL has only strain data Runs 6,7,9,10, Rotation is "across elbow"					
type	LREL,80,CS,1500/2600 P,2.8 WT,IP,20.5 sec (7 hz),7.81 Fn (8.4 fehz),Rw = 0.905						
Z	12.23	QL Run titles indicate magnitude relative to Run 6					
B2	2.37	Sa scaled from titles. Eff # events based on Sa estimates.					
Mc (P=WT=0)	464	Based on 4.5 Sm = 90					
QL title	Elastic EQ	High EQ	1.2 X Run 6	1.4 X Run 6	1.4 X Run 6	1.4 X Run 6	
run	5	6	7	8	9	10	RETESTS
Sa	8	60	72	84	84	84	NO DATA
LMs range / 2	201	1508	1809	2111	2111	2111	
TM	0.43	3.25	3.90	4.54	4.54	4.54	
Ms range / 2	mid elbow	na	na	567	na	na	
max rot range	na	na	na	0.039	na	na	
max rot cycle	na	na	na	0.038	na	na	
run fraction	1.00	1.00	1.00	1.00	1.00	1.00	
sled input freq	7.3	na	na	7.6	na	na	
S(fn)	4.8	na	na	60	na	na	
R = S(fn) / Sa	0.60			0.71			
GE BR M5	na	na	na	2803	na	na	
R * M5				2002			
Sa/Sa(M5)**2	0.01	0.51	0.73	1.00	1.00	1.00	SUM
eff # events	0.01	0.51	0.73	1.00	1.00	1.00	4.25

T3: MISSING DATA RECOVERABLE

Test	3	Run 5 Sled Sa na. Sa from M5 ratio to Run 6 M5					
type	LREL,10,SS,400 P,1.1 WT,IP,39.7 sec (3.6 hz),4.0 Fn (4.0 fphz),Rw = 0.975						
Z	4.35	No rotation data. Listed dis values are top of inertia					
B2	2.37	arm total displacements, SDH-3, in., listed range for run.					
Mc (P=WT=0)	165	Based on 4.5 Sm = 90					
QL title	Low Level	Increased Level				High Level	
run	5	6	7	8	9	10	11
Sa	0.715	5	7.6	11	15	27	25
LMs range / 2	25	175	266	385	525	944	874
TM	0.15	1.06	1.61	2.33	3.18	5.72	5.29
Ms range / 2	mid elbow	66	80	96	105	158	156
max dis range	na	6.53	7.68	8.81	12.4	18.96	16.41
max dis cycle	na	6.4	na	na	na	na	na
run fraction	1.00	0.33	0.33	0.33	1.00	1.00	0.42
sled input freq	na	3.9	3.9	3.9	3.9	3.9	3.8
S(fn)	na	4.5	6.8	10.0	13.0	23.0	22.0
R = S(fn) / Sa		0.90	0.89	0.91	0.87	0.85	0.88
GE BR M5	16.3	114	168	252	313	593	561
R * M5		103	150	229	271	505	494
dis/dis(M5)**2	(run range)	0.12	0.16	0.22	0.43	1.00	0.75
eff # events		0.06	0.08	0.10	0.43	1.00	0.46
						SUM	2.13

T4

Test	4	Rotation is inertia arm			
type	LREL,40,CS,1000 P,1.1 WT,IP,22.7 sec (6.3 hz),7.0 Fn ( ),Rw = 0.971				
Z	8.50				
B2	3.27				
Mc (P=WT=0)	234	Based on 4.5 Sm = 90			
QL title	Low level	High level			
run	5	6	7	8	
Sa	7.5	64	68	70	
LMs range / 2	231	1971	2094	2156	
TM	0.99	8.43	8.95	9.22	
Ms range / 2	mid elbow	386	403	400	
max rot range	0.063	0.274	0.278	0.297	
max rot cycle	0.063	0.274	0.261	0.277	
run fraction	1.00	1.00	1.00	0.62	
sled input freq	6.8	6.8	6.8	6.8	
S(fn)	5.8	52	55	56	
R = S(fn) / Sa	0.77	0.81	0.81	0.80	
GE BR M5	na	na	na	1675	
R * M5				1340	
rot/rot(M5)**2	0.05	0.98	0.89	1.00	SUM
eff # events	0.05	0.98	0.89	0.82	2.7

T5: MISSING DATA RECOVERABLE

Test	5	Rotation is inertia arm. Run 6 Sa from Ms ratios and Run 7			
type	LREL,40,CS,1690 P,1.1 WT,IP,22.7 sec (6.3 hz),7.1 Fn (7.4 fphz),Rw = .878				
Z	8.50	Test Run 7 FI used for Rw calc noting Test Run 8 partial run with S(fn) identical Test Runs 7 and 8. LERS Test Run 8 suspect. 75% damage Test Runs 6 and 7.			
B2	3.27				
Mc (P=WT=0)	234	Based on 4.5 Sm = 90			
QL title	Low level	High level			
run	5	6	7	8	
Sa	5.6	64	68	65	
LMs range / 2	163	1863	1979	1892	
TM	0.70	7.96	8.46	8.09	
Ms range / 2	mid elbow	429	458	470	
max rot range	0.043	0.306	0.348	0.341	
max rot cycle	0.043	0.265	0.314	0.308	
run fraction	1.00	1.00	1.00	0.44	
sled input freq	6.8	na	6.8	6.5	
S(fn)	4	na	40	40	
R = S(fn) / Sa	0.71		0.59	0.62	
GE BR M5	na	na	na	1741	
R * M5				1071	
rot/rot(M5)**2	0.02	0.74	1.04	1.00	SUM
eff # events	0.02	0.74	1.04	0.64	2.4

T6: MISSING DATA RECOVERABLE

Test	6	Rotation inertia arm. Run 6 Sa from Ms Run 7. Noisy LVDT Run 6				
type	LREL,40,SS,1700 P,1.1 WT,IP,22.7 sec (6.3 hz),7.1 Fn (7.2 fphz), Rw = 0.875					
Z	8.50	No sled spectra. R value Run 8 from Rw vs R trend plot				
B2	3.27	See sheet 2				
Mc (P=WT=0)	234	Based on 4.5 Sm = 90				
QL title	Low level	High level				
run	5	6	7	8	9	
Sa	5.7	59	64	62	62	
LMs range / 2	156	1615	1752	1697	1697	
TM	0.67	6.90	7.49	7.25	7.25	
Ms range / 2	mid elbow	420	453	460	470	
max rot range	0.042	0.29	0.412	0.370	0.363	
max rot cycle	0.042	0.25	0.374	0.320	0.321	
run fraction	1.00	1.00	1.00	1.00	0.28	
sled input freq	na	na	na	na	na	
S(fn)	na	na	na	na	na	
R = S(fn) / Sa				0.54		
GE BR M5	na	na	na	1638	na	
R * M5				885		
rot/rot(M5)**2	0.02	0.59	1.37	1.00	1.01	SUM
eff # events	0.02	0.59	1.37	1.00	0.38	3.4

T7: MISSING DATA RECOVERABLE

Test	7	Rotation is nipple. Run 10 Sa from Ms Run 9. Run 8 R from Run 6					
type	LREL,40,SS,1000 P,1.1 WT,IP,22.7 sec (6.3 hz),7.0 Fn (7.0 fphz), Rw = 0.929						
Z	8.50						
B2	3.27						
Mc (P=WT=0)	234	Based on 4.5 Sm = 90					
QL title	Low level	High level					
run	5	6	7	8	9	10	
Sa	6	73	75	74	74	74	
LMs range / 2	145	1764	1813	1788	1788	1788	
TM	0.62	7.54	7.75	7.64	7.64	7.64	
Ms range / 2	mid elbow	380	396	404	406	406	
max rot range	0.034	0.319	0.287	0.258	0.288	0.218	
max rot cycle	0.034	0.223	0.218	0.208	0.22	0.218	
run fraction	1.00	1.00	1.00	1.00	1.00	0.28	
sled input freq	6.8	6.5	na	na	na	na	
S(fn)	4.6	60	na	na	na	na	
R = S(fn) / Sa	0.77	0.82		0.82			
GE BR M5	na	na	na	1953	na	na	
R * M5				1601			
rot/rot(M5)**2	0.03	1.15	1.10	1.00	1.12	1.10	SUM
eff # events	0.03	1.15	1.10	1.00	1.12	0.42	4.8

T8 MISSING DATA RECOVERABLE

Test	8	Rotation is inertia arm. Run 8 R unavailable, used Run 4 R					
type	LREL,40,SS,0 P,1.1 WT,IP,22.7 sec (6.3 hz),6.8 Fn (7.2 fehz),Rw = .917						
Z	8.50						
B2	3.27						
Mc (P=WT=0)	234	Based on 4.5 Sm = 90					
QL title	Low level	High level					
run	3	4	5	6	7	8	
Sa	6.2	75	75	76	76	78	
LMs range / 2	150	1815	1815	1839	1839	1887	
TM	0.64	7.76	7.76	7.86	7.86	8.07	
Ms range / 2	mid-elbow	396	328	324	312	300	
max rot range	0.046	0.308	0.304	0.301	0.310	0.285	
max rot cycle	0.046	0.269	0.268	0.257	0.298	0.271	
run fraction	1.00	1.00	1.00	1.00	1.00	1.00	
sled input freq	6.6	6.6	na	na	na	na	
S(fn)	4.2	50	na	na	na	na	
R = S(fn) / Sa	0.68	0.67				0.67	
GE BR M5	na	na	na	na	na	2004	
R * M5						1343	
rot/rot(M5)**2	0.03	0.99	0.98	0.90	1.21	1.00	SUM
eff # events	0.03	0.99	0.98	0.90	1.21	1.00	5.1

T9

Test	9	Rotation is upper nipple		
type	TEE,40,SS,1700 P,7.4 WT,OP-2,22.7 sec (6.3 hz),7.2 Fn (7.0 fphz),Rw = 0.943			
Z	8.50			
B2	1.00			
Mc (P=WT=0)	765	Based on 4.5 Sm = 90		
QL title	Low level	High level		
run	5	6	7	
Sa	9	65	68	
LMs range / 2	246	1777	1859	
TM	0.32	2.32	2.43	
Ms range / 2	upper br	572	584	
max rot range	0.039	0.429	0.486	
max rot cycle	0.039	0.312	0.486	
run fraction	1.00	1.00	0.26	
sled input freq	6.6	6.6	6.5	
S(fn)	7.3	57	58	
R = S(fn) / Sa	0.81	0.88	0.85	
GE BR M5	na	2808	na	
R * M5		2462		
rot/rot(M5)**2	0.02	1.00	2.43	SUM
eff # events	0.02	1.00	0.82	1.84

T10

Test	10	Rotation is nipple			
type	TEE,40,SS,1000 P,7.4 WT,OP-2,22.7 sec (6.3 hz),7.1 Fn (7.2 fphz),Rw = 0.931				
Z	8.50				
B2	1.00				
Mc (P=WT=0)	765	Based on 4.5 Sm = 90			
QL title	Low level	High level			
run	5	6	7	8	
Sa	8.9	62	66	66	
LMs range / 2	256	1783	1898	1898	
TM	0.33	2.33	2.48	2.48	
Ms range / 2	upper br	320	555	560	
max rot range	0.039	0.184	0.188	0.179	
max rot cycle	0.039	0.176	0.183	0.17	
run fraction	1.00	0.29	1.00	0.28	
sled input freq	6.6	6.6	6.7	6.7	
S(fn)	5.8	41	52	52	
R = S(fn) / Sa	0.65	0.66	0.79	0.79	
GE BR M5	na	na	2851	na	
R * M5			2246		
rot/rot(M5)**2	0.05	0.92	1.00	0.86	SUM
eff # events	0.05	0.37	1.00	0.33	1.74

T11 WELD

Test	11	Rotation is nipple		
type	TEE,10,SS,400 P,7.4 WT,OP-2,30.3 sec (4.7 hz),5.8 Fn (5.8 fphz),Rw = 0.862			
Z	4.43			
B2	1.00	Based on weld		
Mc (P=WT=0)	399	Based on 4.5 Sm = 90		
QL title	Low level	Increased level		
run	5	6	7	
Sa	2.7	17	24	
LMs range / 2	46	290	409	
TM	0.12	0.73	1.03	
Ms range / 2	upper br	128	138	
max rot range	0.031	0.112	0.156	
max rot cycle	0.031	0.110	0.156	
run fraction	1.00	0.31	0.19	
sled input freq	5.0	5.0	5.0	
S(fn)	1.4	8.4	14	
R = S(fn) / Sa	0.52	0.49	0.58	
GE BR M5	na	777	na	
R * M5		384		
rot/rot(M5)**2	0.08	1.00	2.01	SUM
eff # events	0.08	0.44	0.42	0.93

T11 TEE: SUSPECT DATA

Test	11	Rotation is nipple		
type	TEE,10,SS,400 P,7.4 WT,OP-2,30.3 sec (4.7 hz),5.8 Fn (5.8 fphz),Rw = 0.862			
Z	4.43			
B2	3.35	Based on tee		
Mc (P=WT=0)	119	Based on 4.5 Sm = 90		
QL title	Low level	Increased level		
run	5	6	7	
Sa	2.7	17	24	
LMs range / 2	24.4	154	217	
TM	0.21	1.29	1.82	
Ms range / 2	lower br	68	74	
max rot range	0.031	0.112	0.156	
max rot cycle	0.031	0.110	0.156	
run fraction	1.00	0.31	0.19	
sled input freq	5.0	5.0	5.0	
S(fn)	1.4	8.4	14	
R = S(fn) / Sa	0.52	0.49	0.58	
GE BR M5	na	766	na	
R * M5		378		
rot/rot(M5)**2	0.08	1.00	2.01	SUM
eff # events	0.08	0.44	0.42	0.93

T12: MISSING DATA RECOVERABLE

Test	12	Rotation is nipple. Run 8 Sa from Ms Run 7			
type	TEE,40,SS,1700 P,7.4 WT,IP-2,20.5 sec (7 hz),8.2 Fn (8.4 fphz),Rw = 0.905				
Z	8.50				
B2	1.00				
Mc (P=WT=0)	765	Based on 4.5 Sm = 90			
QL title	Low level	High level			
run	5	6	7	8	
Sa	12	74	78	77	
LMs range / 2	330	2035	2145	2118	
TM	0.43	2.66	2.80	2.77	
Ms range / 2	upper br	612	634	623	
max rot range	0.079	0.222	0.163	0.137	
max rot cycle	0.079	0.144	0.135	0.126	
run fraction	1.00	1.00	1.00	0.40	
sled input freq	7.30	7.60	7.60	na	
S(fn)	7.7	53	54	na	
R = S(fn) / Sa	0.64	0.72	0.69		
GE BR M5		3412			
R * M5		2444			
rot/rot(M5)**2	0.30	1.00	0.88	0.77	SUM
eff # events	0.30	1.00	0.88	0.31	2.49

T13: MISSING DATA RECOVERABLE

Test	13	Rotation is inertia arm. Run 11 rot from Sa and Run 10					
type	SREL,40,CS,1000 P,1.5 WT,IP,22.7 sec (6.3 hz),7.0 Fn (7.0 fphz), Rw = 0.957						
Z	8.50						
B2	4.29						
Mc (P=WT=0)	178	Based on 4.5 Sm = 90					
QL title	Low level	2x low level	4x low level	6x low level	8x low level	9x low level	10.4x low
run	5	6	7	8	9	10	11
Sa	5.5	12	22	32	44	56	59
LMs range / 2	210	458	840	1222	1680	2138	2253
TM	1.18	2.57	4.71	6.85	9.42	11.99	12.63
Ms range / 2	mid elbow	363	403	410	412	418	410
max rot range	0.047	0.098	0.133	0.154	0.177	0.204	0.215
max rot cycle	0.047	0.095	0.133	0.154	0.168	0.192	0.202
run fraction	1.00	1.00	1.00	1.00	1.00	1.00	0.32
sled input freq	6.5	6.5	6.5	6.5	6.6	6.7	6.7
S(fn)	4	11	18	27	35	43	46
R = S(fn) / Sa	0.73	0.92	0.82	0.84	0.80	0.77	0.78
GE BR M5	134	307	570	839	1095	1345	na
R * M5	97.5	281	466	708	871	1033	
rot/rot(M5)**2	0.06	0.24	0.48	0.64	0.77	1.00	1.11
eff # events	0.06	0.24	0.48	0.64	0.77	1.00	0.50
						SUM	3.69

T14

Test	14	Rotation is inertia arm		
type	TEE,40,CS,1700 P,7.4 WT,OP-2,22.7 sec (6.3 hz),7.2 Fn (7.2 fphz),Rw = 0.917			
Z	8.50	GE M5 at tee center, divided M5 by 1.09 for weld location		
B2	1.00			
Mc (P=WT=0)	765	Based on 4.5 Sm = 90		
QL title	Low level	High level		
run	5	6	7	
Sa	9	62	62	
LMs range / 2	286	1970	1970	
TM	0.37	2.58	2.58	
Ms range / 2	upper br	596	600	
max rot range	0.042	0.171	0.167	
max rot cycle	0.042	0.167	0.164	
run fraction	1.00	1.00	0.45	
sled input freq	6.6	6.6	6.6	
S(fn)	5.5	48	44	
R = S(fn) / Sa	0.61	0.77	0.71	
GE BR M5	na	2373	na	
R * M5		1837		
rot/rot(M5)**2	0.06	1.00	0.96	SUM
eff # events	0.06	1.00	0.63	1.69

T15

Test	15	Rotation is inertia arm					
type	RED,40,SS,1700 P,6.6 WT,22.7 sec (6.3 hz),7.2 Fn (7.2 fphz), Rw = 0.903						
Z	3.22						
B2	1.00						
Mc (P=WT=0)	290	Based on 4.5 Sm = 90					
QL title	Low level	2x low level	3.5x low lvl	5x low level	High level	High level	High level
run	5	6	7	8	9	10	11
Sa	5.2	9.5	18	26	35	34	30
LMs range / 2	99	181	343	495	666	647	571
TM	0.34	0.62	1.18	1.71	2.30	2.23	1.97
Ms range / 2	lower 4nps	138	170	197	220	215	208
max rot range	0.022	0.046	0.078	0.097	0.089	0.111	0.082
max rot cycle	0.022	0.036	0.056	0.066	0.066	0.086	0.082
run fraction	1.00	1.00	1.00	1.00	1.00	1.00	0.38
sled input freq	6.6	6.6	6.6	6.5	6.5	6.5	6.5
S(fn)	3.5	6.9	14	18	23	23	20
R = S(fn) / Sa	0.67	0.73	0.78	0.69	0.66	0.68	0.67
GE BR M5	208	384	740	1044	1376	1332	1204
R * M5	140.0	279	576	723	904	901	803
rot/rot(M5)**2	0.11	0.30	0.72	1.00	1.00	1.70	1.54
eff # events	0.11	0.30	0.72	1.00	1.00	1.70	0.86
						SUM	5.69

T16

Test	16		
type	RED,40,CS,1700 P,6.6 WT,22.7 sec (6.3 hz),7.2 Fn (7.4 fphz),Rw = 0.905		
Z	3.22		
B2	1.00		
Mc (P=WT=0)	290	Based on 4.5 Sm = 90	
QL title	Low level	High level	
run	5	6	
Sa	5.8	82	
LMs range / 2	186	2630	
TM	0.64	9.07	
Ms range / 2	lower 4nps	278	
max rot range	0.025	0.228	
max rot cycle	0.025	0.163	
run fraction	1.00	0.52	
sled input freq	6.7	6.7	
S(fn)	3.9	53	
R = S(fn) / Sa	0.67	0.65	
GE BR M5	230	3244	
R * M5	154.7	2097	
rot/rot(M5)**2	0.02	1.00	SUM
eff # events	0.02	0.73	0.75

T19

Test	19	Rotation is inertia arm.			
type	LREL,40,SS,2500 P,1.1 WT,IP,22.7 sec (6.3 hz),6.8 Fn (6.8 fphz),Rw = .985				
Z	8.50				
B2	3.27				
Mc (P=WT=0)	234	Based on 4.5 Sm = 90			
QL title	Low level	Mid level	3/4 level	High level	
run	5	6	7	8	
Sa	5.5	41	58	70	
LMs range / 2	217	1618	2288	2762	
TM	0.93	6.92	9.79	11.81	
Ms range / 2	mid-elbow	403	462	498	
max rot range	0.068	0.214	0.323	0.315	
max rot cycle	0.069	0.191	0.282	0.300	
run fraction	1.00	1.00	1.00	1.00	
sled input freq	6.7	6.7	6.7	6.7	
S(fn)	5.3	40	57	69	
R = S(fn) / Sa	0.96	0.98	0.98	0.99	
GE BR M5	134	1075	1546	1826	
R * M5	129.1	1049	1519	1800	
comp LMS	217.0	1638	2334	2825	
rot/rot(M5)**2	0.05	0.41	0.88	1.00	SUM
eff # events	0.05	0.41	0.88	1.00	2.34

T30: MISSING DATA RECOVERABLE

Test	30	No low level EQ test, No Run 1-3 Ms , (Run 3 scaled from Run 4 by Sa).					
type	LREL,10,SS, 400 P,8.5 WT,110 sec (1.3 hz),1.4 Fn (1.44 fphz),Rw = 1.007						
Z	4.35	Unpressurized detuned high level Runs 1 and 2, no reduced data					
B2	5.51	GE reported Ms Runs 1 and 2.			Run 1, 22.7 sec (6.3 hz), Rw = 4.6		
Mc (P=WT=0)	71	Based on 4.5 Sm = 90			Run 2, 35.6 sec (4 hz), Rw = 2.9		
QL title	Mid level	High level			Initial detuned high level		Data
run	3	4	5	6	1	2	aliasing
Sa	1.7	3.3	3.3	4.8	77	40	concerns
LMs range / 2	60	116	116	169	2718	1412	cited
TM	0.84	1.64	1.64	2.38	38.25	19.87	Runs 3 - 6
Ms range / 2	mid elbow	116	119	128	133	93	
max rot range	na	0.183	0.185	0.215	na	na	
max rot cycle	na	0.174	0.185	0.215	na	na	
run fraction	1.00	1.00	1.00	0.20	1.00	1.00	
sled input freq	1.45	1.45	1.45	1.45	6.7	4.2	
S(fn)	1.7	3.3	3.3	4.8	2.0	2.3	
R = S(fn) / Sa	1.00	1.00	1.00	1.00	0.03	0.06	Runs 1,2&3
GE BR M5	139	279	271	na	591	536	eff # used
R * M5	139	279	271		not valid	not valid	$S(fn)^2$ ratio
rot/rot(M5)**2	na	1.00	1.13	1.53	na	na	SUM
eff # events	0.27	1.00	1.13	0.34	0.37	0.49	3.59

T35: NON-STANDARD TEST, HIGHLY SUSPECT DATA

Test	35	Highly suspect Ms Run 5. High weight moment. Mixed frequencies					
type	LREL,40,CS,1700 P,20.1 WT,IP,*** sec (*** hz),4.4 Fn (4.4 fphz)						
Z	8.50	*** Runs 5,7,9,10: 37.2 sec (3.85 hz),Rw = 0.932					
B2	3.27				*** Run 6: 32.5 sec (4.4 hz),Rw = 1.07		
Mc (P=WT=0)	234	Based on 4.5 Sm = 90			*** Run 8: 40.7 sec (3.5 hz),Rw = 0.841		
QL title	Low level	High level					on plot est.
run	5	6	7	8	9	10	UNBR R
Sa	3.5	31	34	30	35	34	= 0.68
LMs range / 2	7.3	65	71	63	73	71	
TM	0.03	0.28	0.30	0.27	0.31	0.30	
Ms range / 2	mid elbow	385	404	402	410	408	
max rot range	0.041	0.230	0.235	0.233	0.22	0.212	
max rot cycle	0.041	0.179	0.194	0.210	0.191	0.185	
run fraction	1.00	1.00	1.00	1.00	1.00	0.48	
sled input freq	4.1	4.7	4.1	3.7	4.1	4.1	
S(fn)	2.6	27	26	17	25	24	
R = S(fn) / Sa	0.74	0.87	0.76	on plot	0.71	0.71	
GE BR M5	166	1617	1667	1496	1677	na	
R * M5	123.3	1408	1275	1017	1198		
rot/rot(M5)**2	0.05	0.88	1.03	1.21	1.00	0.94	SUM
eff # events	0.05	0.88	1.03	1.21	1.00	0.64	4.81

T36 WELD: NON-STANDARD TEST

Test	36	No low level EQ., Mixed frequencies. Earlier mid/high level sine sweeps				
type	TEE,40,CS,1700 P,7.4 WT,IP-1,*** sec (*** hz),6.77 Fn (6.8 fphz)					
Z	8.50				*** Test 7: 41 sec (3.5 hz),Rw = 0.551	
B2	1.00	based on weld			*** Test 8: 28.4 sec (5 hz),Rw = 0.779	
Mc (P=WT=0)	765	Based on 4.5 Sm = 90			event count sum includes sine	
QL title	Mid level	High level	Sine sweep	Sine sweep	sweeps as equiv to EQ event	
run	7	8	5	6		
Sa	23	52				
LMs range / 2	345	780				
TM	0.45	1.02				
Ms range / 2	thru run	634	466	520		
max rot range	0.067	0.229	0.08	0.106		
max rot cycle	0.063	0.196	0.08	0.106		
run fraction	1.00	0.60				
sled input freq	3.75	5.3	13.5 to 3.5	13.5 to 3.5		
S(fn)	UNBR avail	UNBR avail				
R = S(fn) / Sa	UNBR avail	UNBR avail			Unbroadened LERS	
GE BR M5	433	2058			Run 7	Run 8
R * M5	UNBR avail	UNBR avail			375	1058
rot/rot(M5)**2	0.10	1.00	0.17	0.29	SUM	
eff # events	0.10	0.81	0.17	0.29	1.37	

T36 TEE: NON-STANDARD TEST

Test	36	No low level EQ., Mixed frequencies. Earlier mid/high level sine sweeps				
type	TEE,40,CS,1700 P,7.4 WT,IP-1,*** sec (*** hz),6.77 Fn (6.8 fphz)					
Z	8.50				*** Test 7: 41 sec (3.5 hz),Rw = 0.551	
B2	2.52	based on tee			*** Test 8: 28.4 sec (5 hz),Rw = 0.779	
Mc (P=WT=0)	304	Based on 4.5 Sm = 90			event count sum includes sine	
QL title	Mid level	High level	Sine sweep	Sine sweep	sweeps as equiv to EQ event	
run	7	8	5	6		
Sa	23	52				
LMs range / 2	345	780				
TM	1.14	2.57				
Ms range / 2	thru run	634	466	520		
max rot range	0.067	0.229	0.08	0.106		
max rot cycle	0.063	0.196	0.08	0.106		
run fraction	1.00	0.60				
sled input freq	3.75	5.3	13.5 to 3.5	13.5 to 3.5		
S(fn)	UNBR avail	UNBR avail				
R = S(fn) / Sa	UNBR avail	UNBR avail			Unbroadened LERS	
GE BR M5	433	2058			Run 7	Run 8
R * M5	UNBR avail	UNBR avail			375	1058
rot/rot(M5)**2	0.10	1.00	0.17	0.29	SUM	
eff # events	0.10	0.81	0.17	0.29	1.37	

T38

Test	38	Rotation out-of-plane, moments SRSS in-plane,out-of-plane				
type	TEE,40,SS,1700 P,7.4 WT,OP-1,22.7 sec (6.3 hz),7 Fn (7.0 fphz),Rw = 0.929					
Z	8.50					
B2	2.02					
Mc (P=WT=0)	379	Based on 4.5 Sm = 90				
QL title	Low level	High level				
run	5	6	7	8	9	
Sa	8.7	68	68	65	66	
LMs range / 2	222	1735	1735	1659	1684	
TM	0.59	4.58	4.58	4.38	4.45	
Ms range / 2	lower br	530	553	560	567	
max rot range	0.054	0.201	0.192	0.178	0.177	
max rot cycle	0.054	0.19	0.192	0.178	0.177	
run fraction	1.00	1.00	1.00	1.00	0.20	
sled input freq	6.6	6.5	6.5	6.5	6.5	
S(fn)	7.2	56	55	54	57	
R = S(fn) / Sa	0.83	0.82	0.81	0.83	0.86	
GE BR M5	na	2756	na	na	na	
R * M5		2270				
rot/rot(M5)**2	0.08	1.00	1.02	0.88	0.87	SUM
eff # events	0.08	1.00	1.02	0.88	0.19	3.17

FROM CIT TEST 14 RUN 6 CUMULATIVE USAGE FRACTION (FATIGUE) STUDY

TF	RF
0	0
0.1	0.084
0.2	0.222
0.3	0.419
0.4	0.597
0.5	0.704
0.6	0.807
0.7	0.856
0.8	0.918
0.9	0.989
1	1

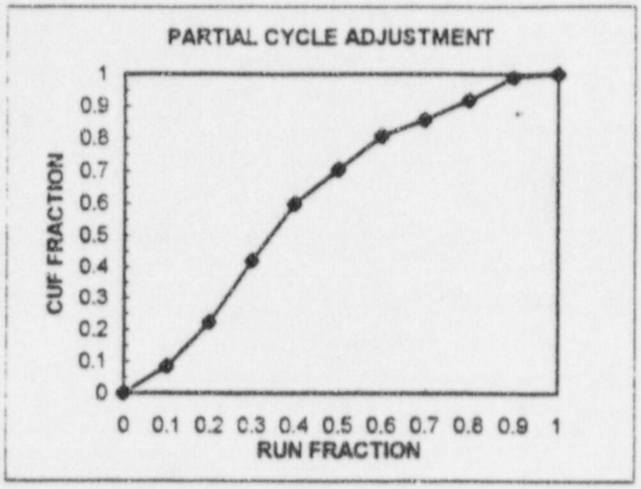

ALL TESTS AT TEST RUN M5 BASED ON (FOR TEST 6 R SELECTION)

Rw	R
0.975	0.85
0.971	0.8
0.919	0.62
0.928	0.82
0.917	0.67
0.943	0.85
0.93	0.79
0.862	0.49
0.905	0.69
0.957	0.77
0.917	0.77
0.903	0.66
0.905	0.65
0.985	0.99
0.932	0.71
0.779	0.51
0.928	0.82

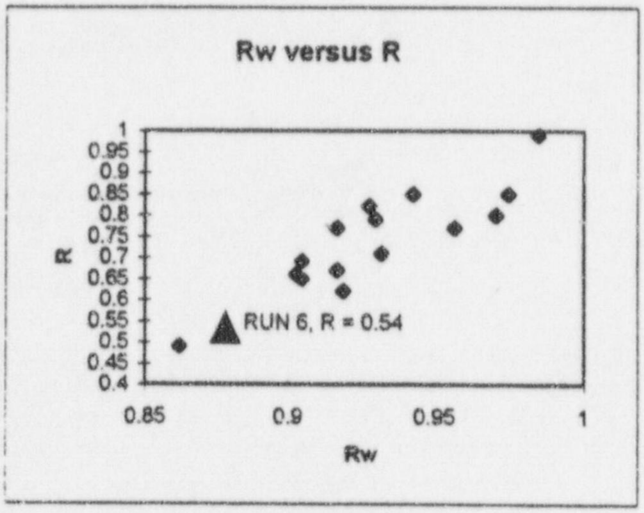

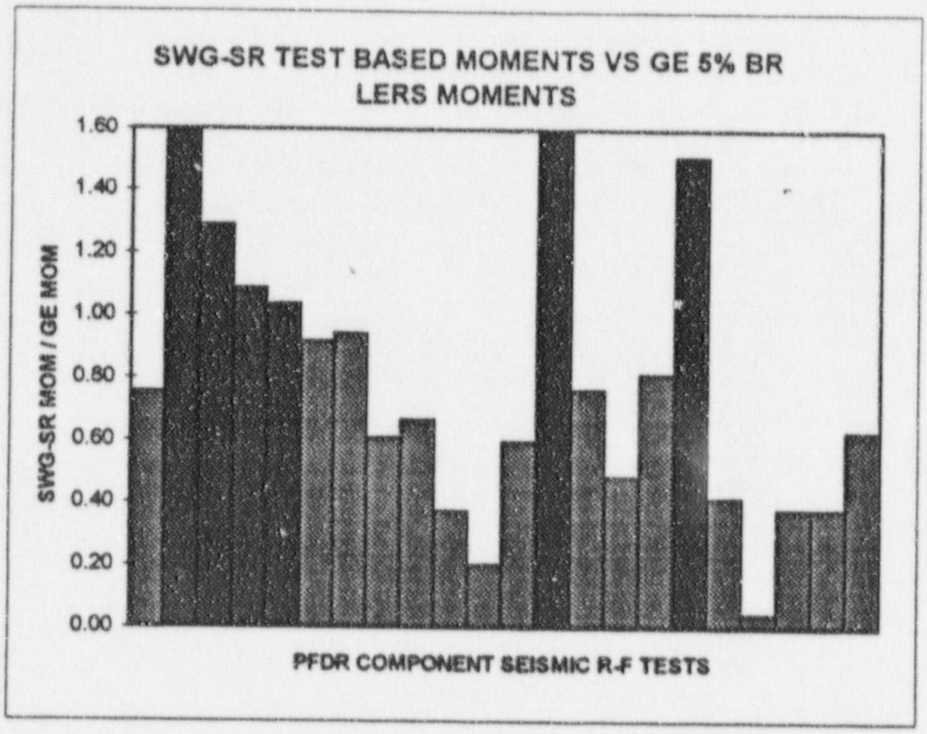
SWG-SR TEST BASED MOMENTS VS GE 5% BR LERS MOMENTS
1.60
1.40
1.20
1.00
0.80
0.60
0.40
0.20
0.00
SWG-SR MOM / GE MOM
PFDR COMPONENT SEISMIC R-F TESTS

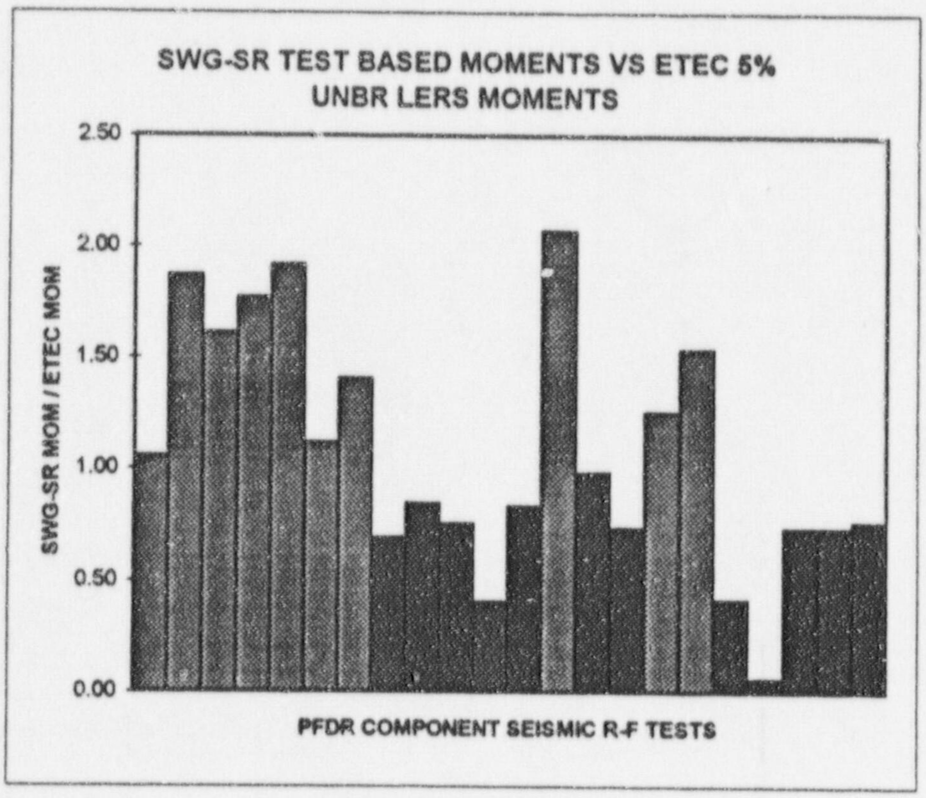
SWG-SR TEST BASED MOMENTS VS ETEC 5% UNBR LERS MOMENTS
2.50
2.00
1.50
1.00
0.50
0.00
SWG-SR MOM / ETEC MOM
PFDR COMPONENT SEISMIC R-F TESTS

COMPARISON SWG-SR Sa-Ms BASED UNBR MOMENTS TO BR M5 AND R VALUE
BASED UNBR MOMENTS FOR TEST RUN WITH MAX LISTED GE BR M5 VALUES

	A	B	C			
	SWG-SR	GE	R TIMES	RATIO	RATIO	
TEST	LMS/2	BR M5	BR M5	A/B	A/C	
1	2111	2803	2002	0.75	1.05	
3	944	593	505	1.59	1.87	
4	2156	1675	1340	1.29	1.61	
5	1892	1741	1071	1.09	1.77	
6	1697	1638	885	1.04	1.92	
7	1788	1953	1601	0.92	1.12	
8	1887	2004	1343	0.94	1.41	
9	1707	2808	2462	0.61	0.69	
10	1898	2851	2246	0.67	0.85	
11P	290	777	384	0.37	0.76	
11T	154	766	378	0.20	0.41	
12	2035	3412	2444	0.60	0.83	
13	2138	1345	1033	1.59	2.07	
14	1970	2587	2003	0.76	0.98	TEE CENTER
15	666	1376	904	0.48	0.74	
16	2630	3244	2097	0.81	1.25	
19	2762	1826	1800	1.51	1.53	
30	116	279	279	0.42	0.42	
35	73	1677	1198	0.04	0.06	
36P	780	2058	1058	0.38	0.74	
36T	780	2058	1058	0.38	0.74	
38	1735	2756	2270	0.63	0.76	

Appendix I-C: Predicted Maximum Moments for Selected PFDR Component Tests

Plots by

C. T. Huang

California Institute of Technology

Maximum Moment Determinations by

Ken Jaquay

Energy Technology Engineering Center

Spreadsheet for Table 2 M_{UD} Values

Scaled to max test run level. Ratioed from QL(1st) or GE(2nd) MM values if no CIT Appendix I-C plotted moment PM_{CIT} values

BASIC DATA			TEST RUN RATIOS			SCALED M_{UD} VALUES				CALC OF AVERAGE RATIOS (MINUS TEST 11)				
	Run #	Attached	GE	GE	QL	Note 1	Note 2	Note 3						
Test	CIT (max)	Plots** PM_{CIT}	or QL MM_{CIT}	or QL MM_{MAX}	MM_{MAX} / MM_{CIT}	CIT M_{UD}	QL M_{UD}	GE M_{UD}	M_{UD}	CIT PM_{CIT}	QL MM_{CIT}	CIT / QL	GE MM_{CIT}	CIT / GE
Elbows														
1		** Circles on attached CIT moment plots indicate values used												
2														
3	10(10)	162	158	158	1.00	162			162	162	158	1.03	153	1.06
4	7(7)	429	403	403	1.00	429			429	429	403	1.06		
5	7(8)	520	458	470	1.03	534			534	520	458	1.14		
6	8(9)	509	460	470	1.02	520			520	509	460	1.11	457	1.11
7	8(9)	520	404	406	1.00	523			523	520	404	1.29	426	1.22
8	7(4)	400	312	396	1.27	508			508	400	312	1.28		
13	10(10)	379	418	418	1.00	379			379	379	418	0.91	400	0.95
19	7(8)	587	462	498	1.08	633			633	587	462	1.27	420	1.40
30	6(1)	111	128	133	1.04	115			115	111	128	0.87		
31	na(7)	na		150				192	192					
35	na(9)	na		410			470		470					
37	5(5)	72	64	64	1.00	72			72	72	64	1.13	57	1.26
41	na(12)	na		398				510	510					
Non-elbows														
9	6(7)	616	572	584	1.02	629			629	616	572	1.08	540	1.14
10	na(8)	na		560			641		641					
11	6(7)	342	128	138	1.08	369			369	342	128		143	
12	na(7)	na		634			726		726					
14	6(7)	613	596	600	1.01	617			617	613	596	1.03	564	1.09
15	8(9)	298	197	220	1.12	333			333	298	197	1.51	172	1.73
16	6(6)	385	278	278	1.00	385			385	385	278	1.38	260	1.48
34	na(12)	na		605				775	775					
36	8(8)	700	634	634	1.00	700			700	700	634	1.10	512	1.37
38	na(9)	na		567			649		649					
39	na(4)	na		549			629		629					
40	4(5)	277	178	202	1.13	314			314	277			178	1.56

SUM2: 17.18 SUM3: 15.37

C2 = SUM2 / 15: $\boxed{1.15}$

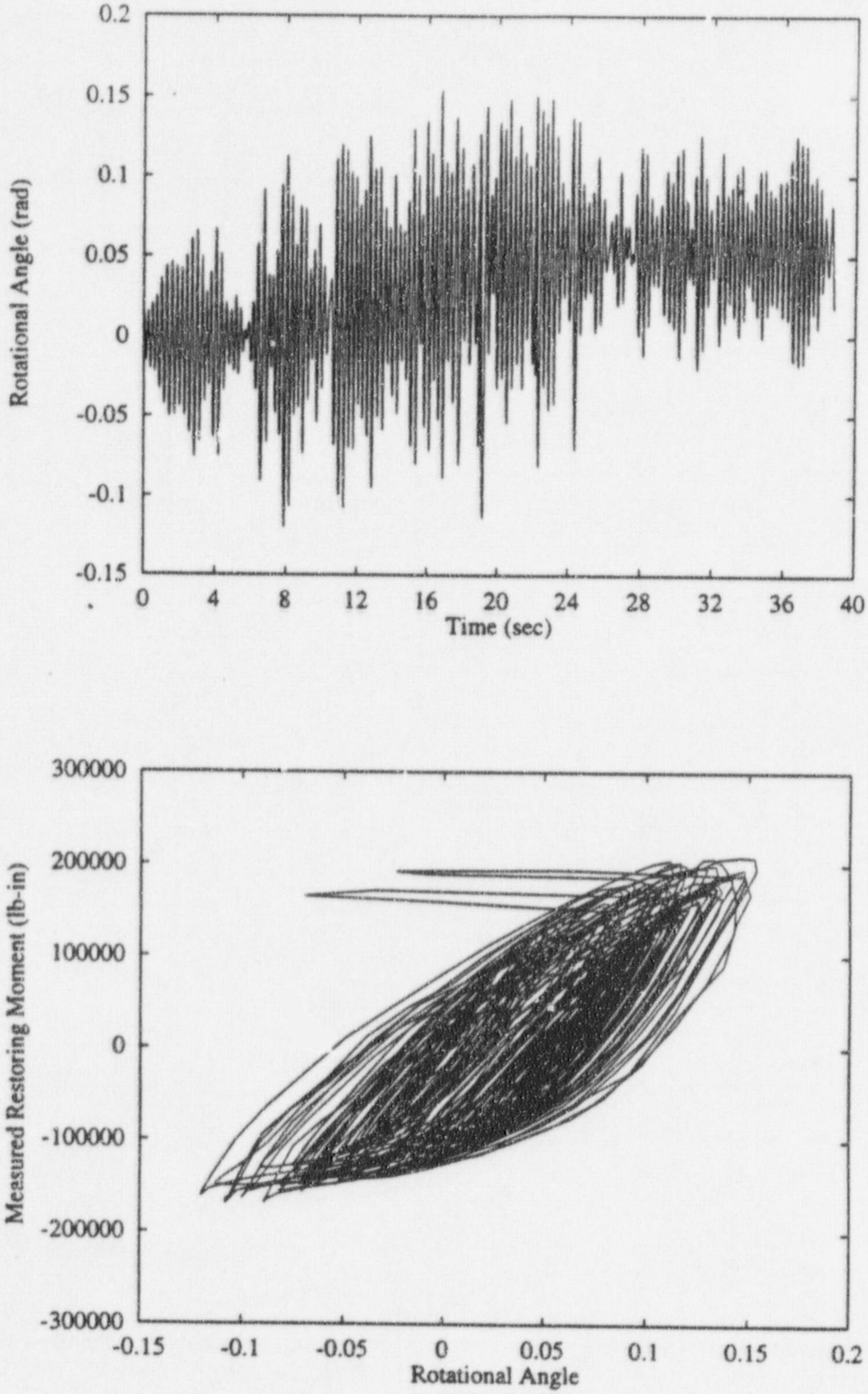

Figure 1: Response time history and hysteretic loops for ANCO Test 3 Run 10

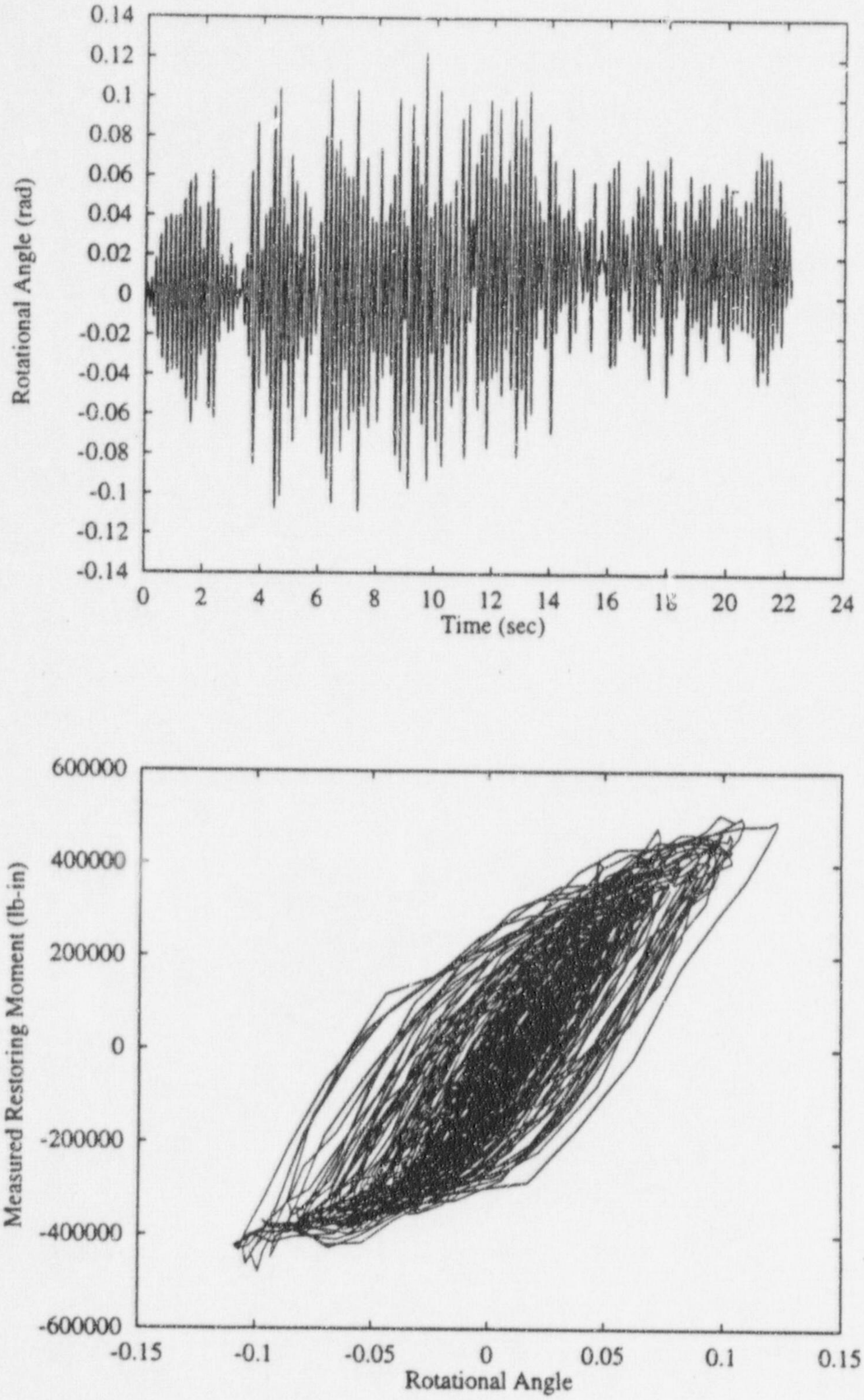

Figure 2: Response time history and hysteretic loops for ANCO Test 4 Run 7

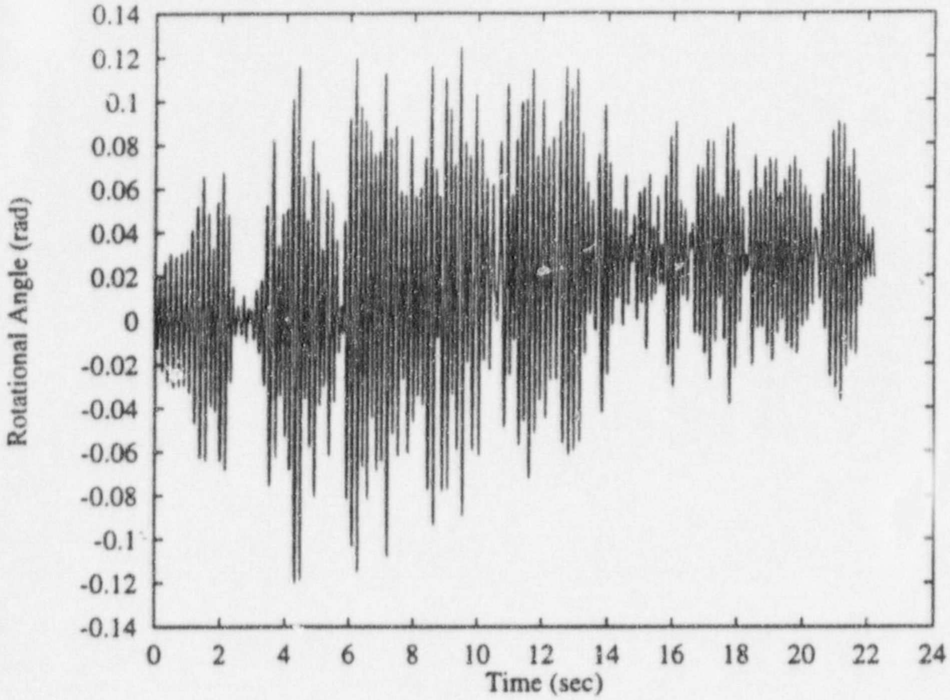

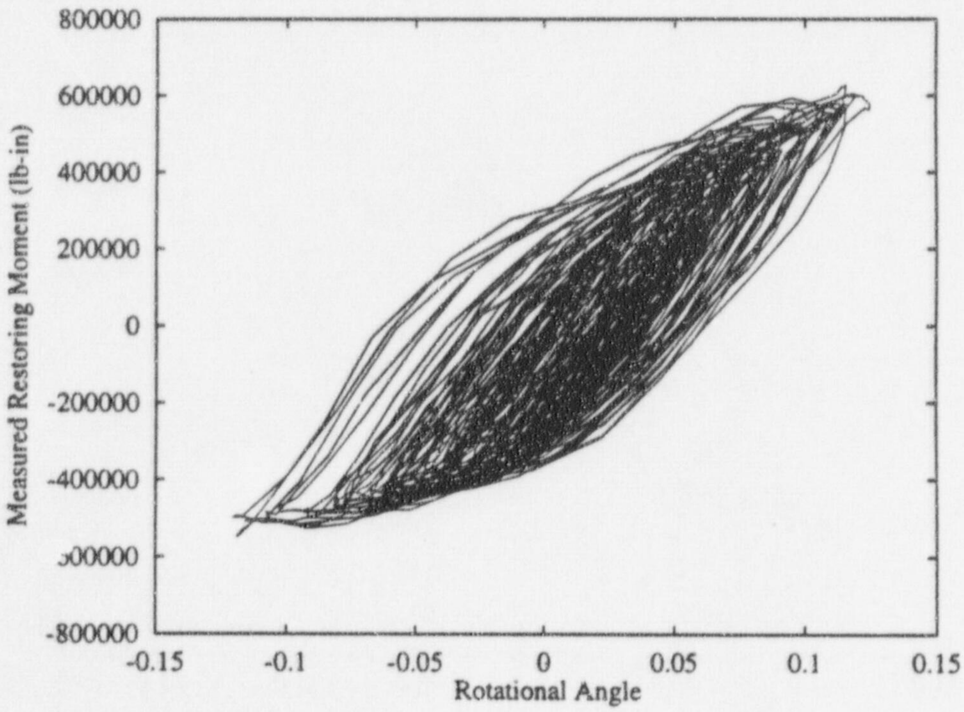

Figure 3: Response time history and hysteretic loops for ANCO Test 5 Run 7

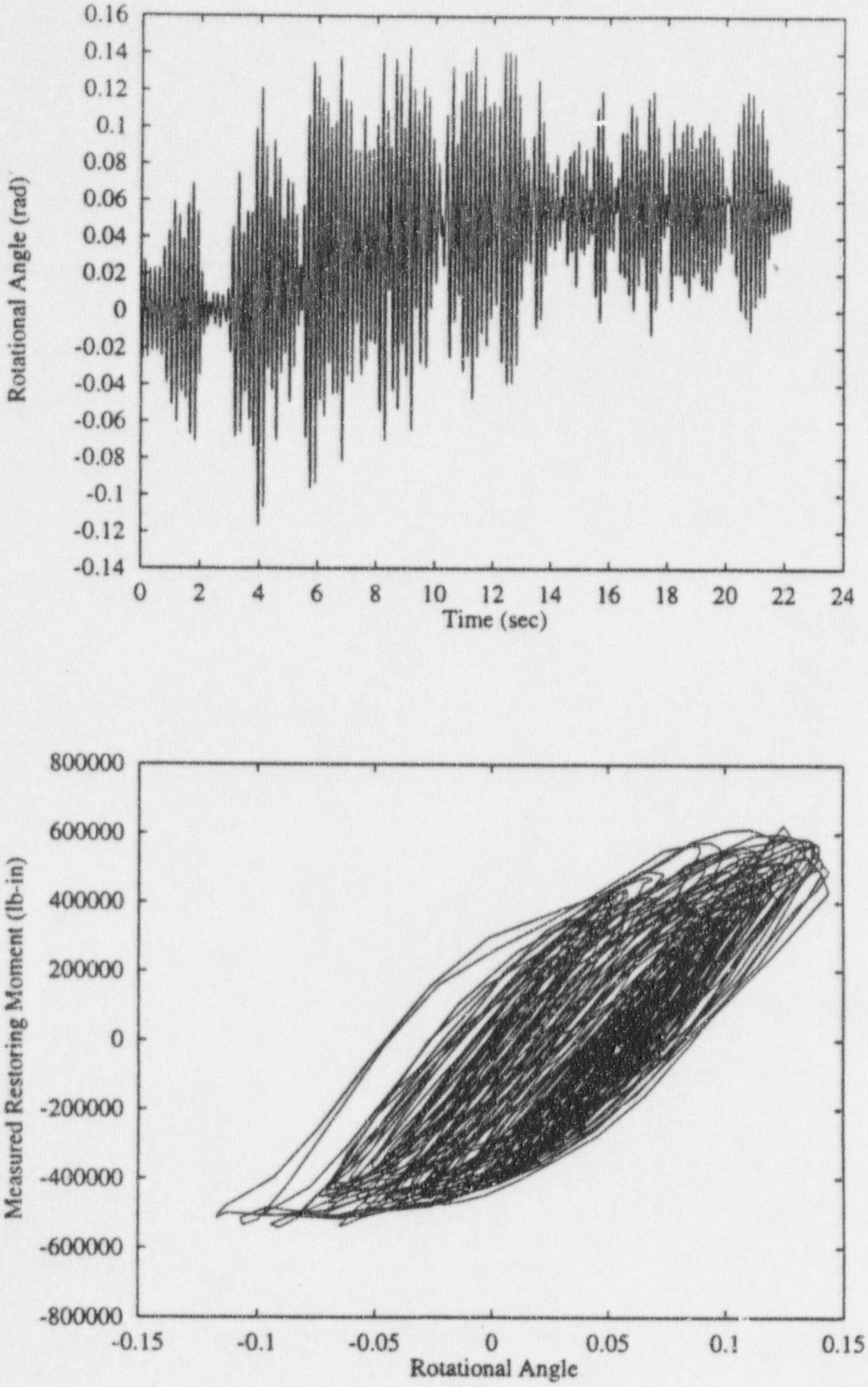

Figure 4: Response time history and hysteretic loops for ANCO Test 6 Run 8

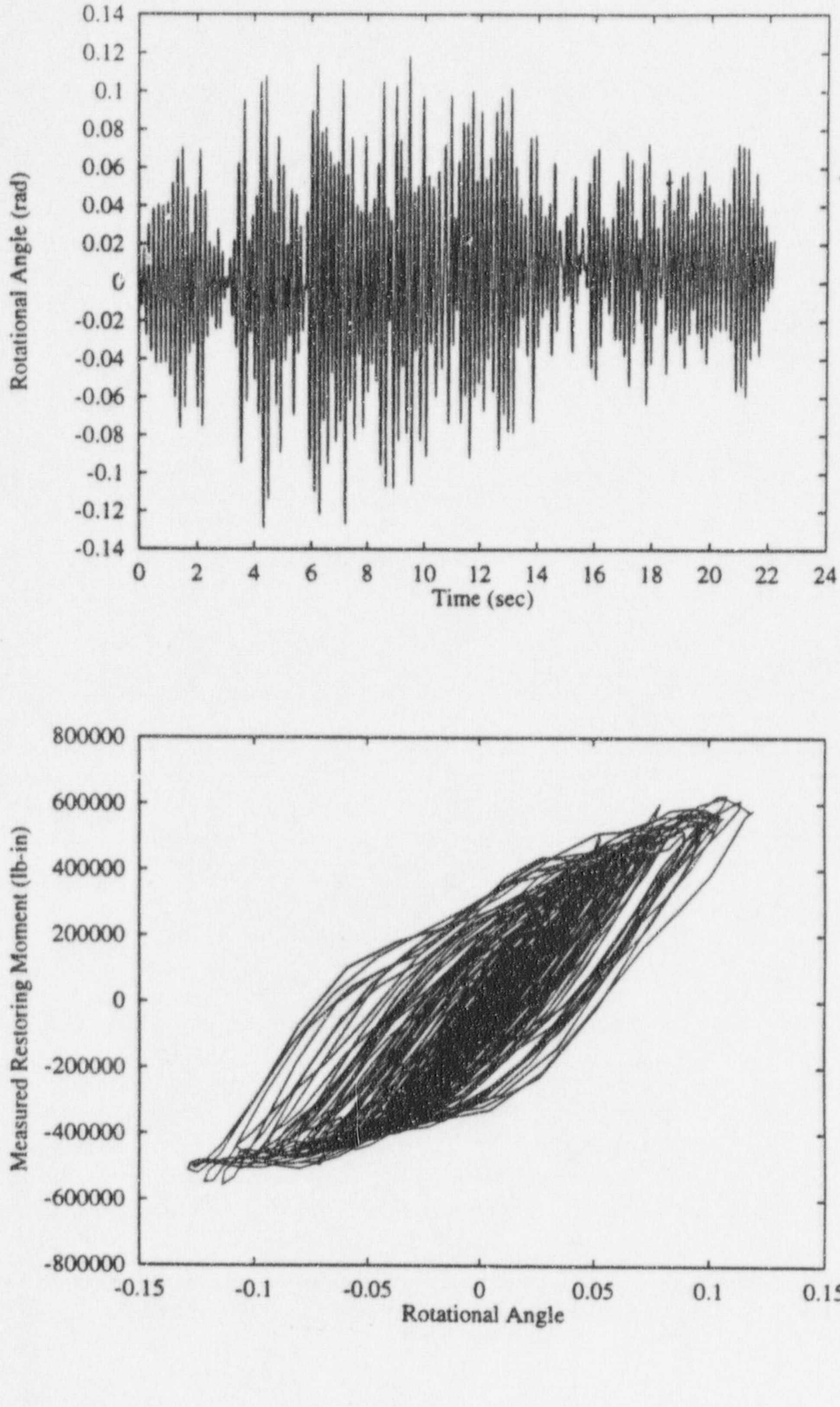

Figure 5: Response time history and hysteretic loops for ANCO Test 7 Run 8

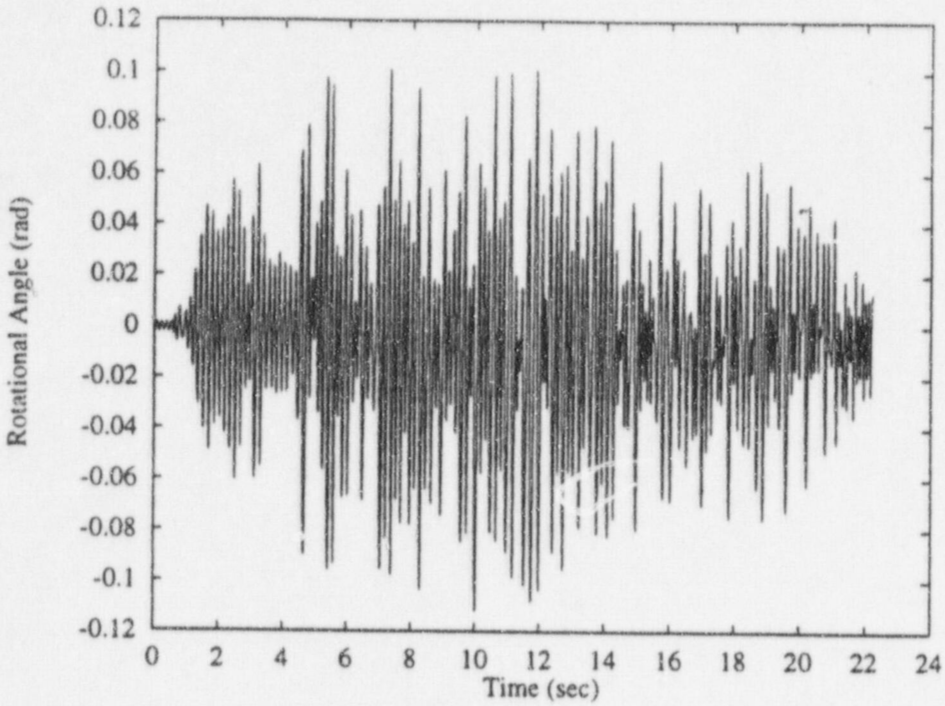

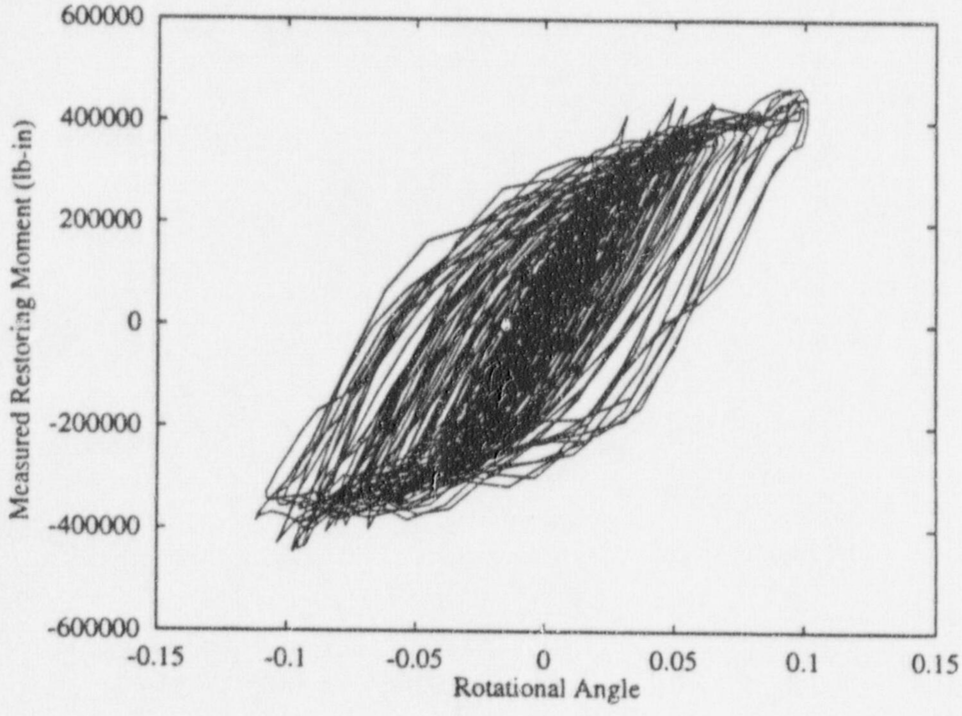

Figure 6: Response time history and hysteretic loops for ANCO Test 8 Run 7

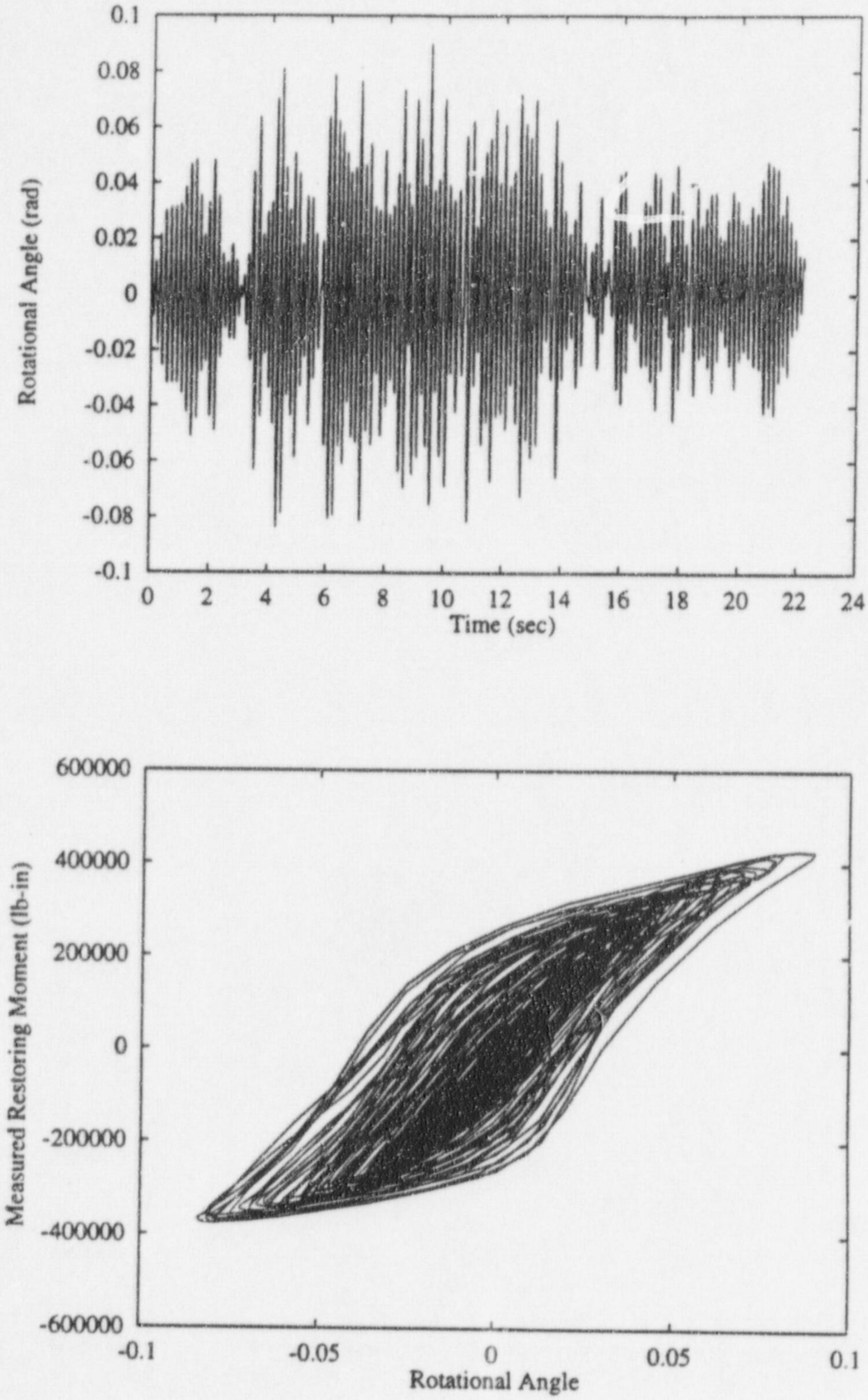

Figure 7: Response time history and hysteretic loops for ANCO Test 13 Run 10

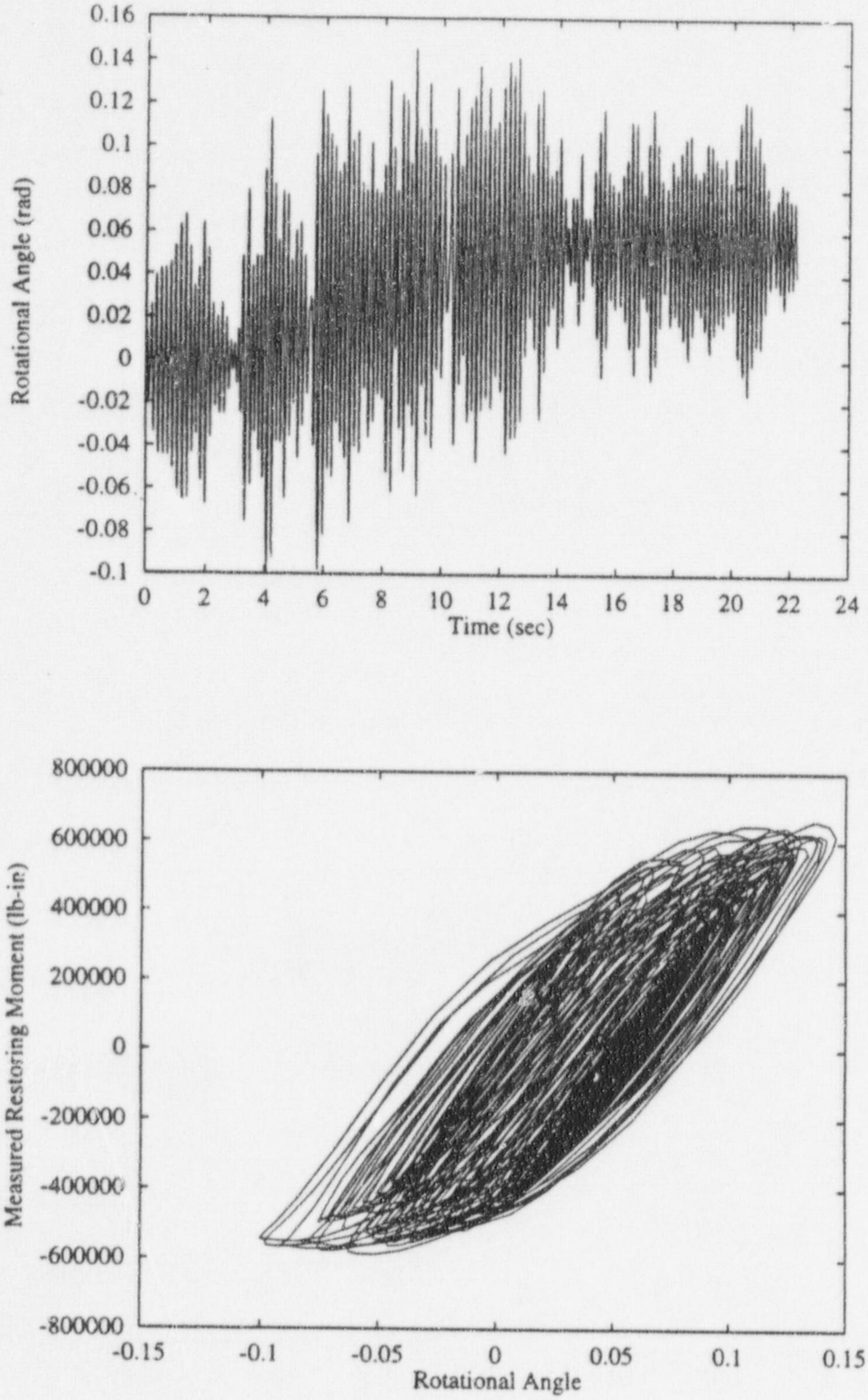

Figure 8: Response time history and hysteretic loops for ANCO Test 19 Run 7

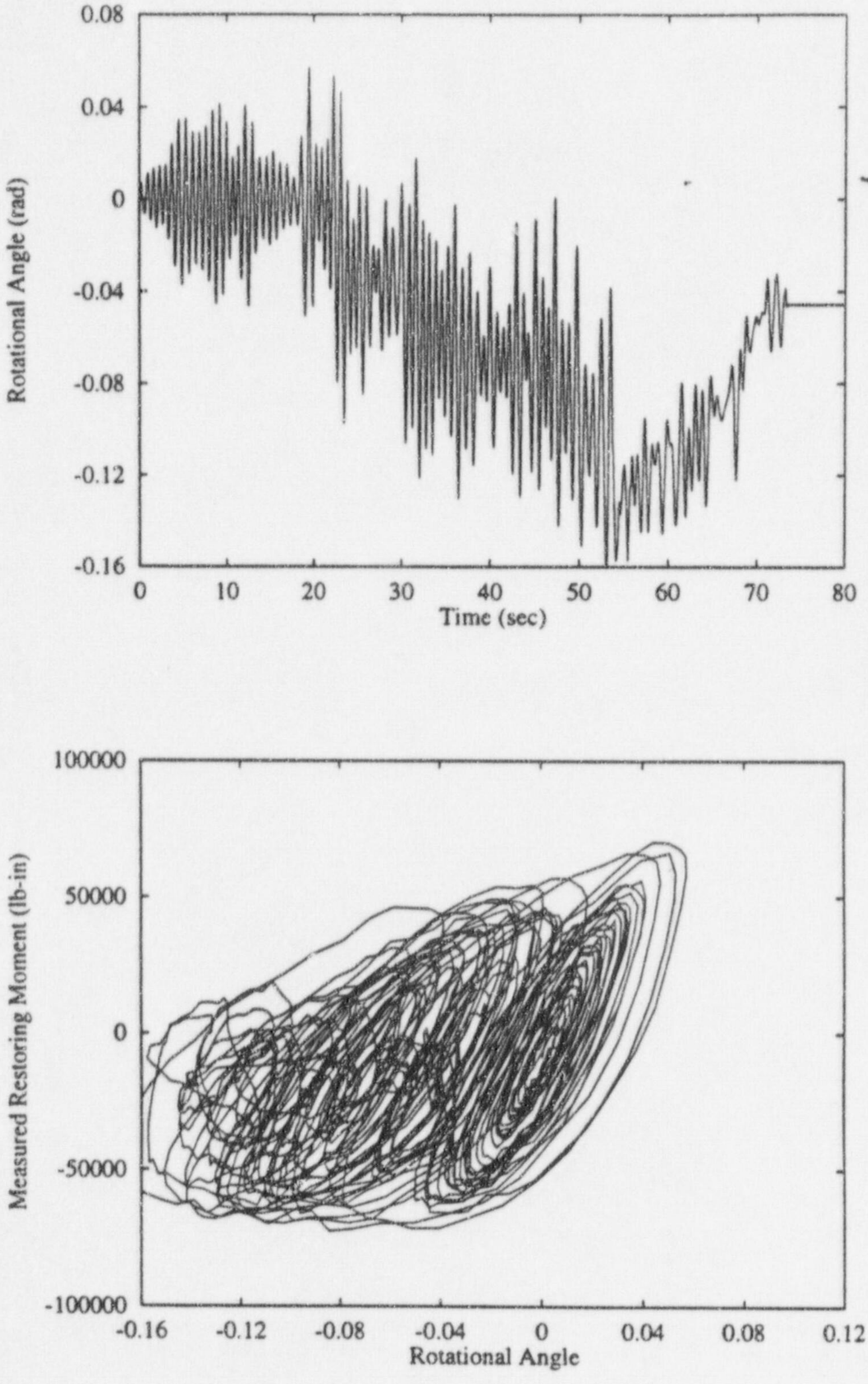

Figure 9: Response time history and hysteretic loops for ANCO Test 37 Run 5

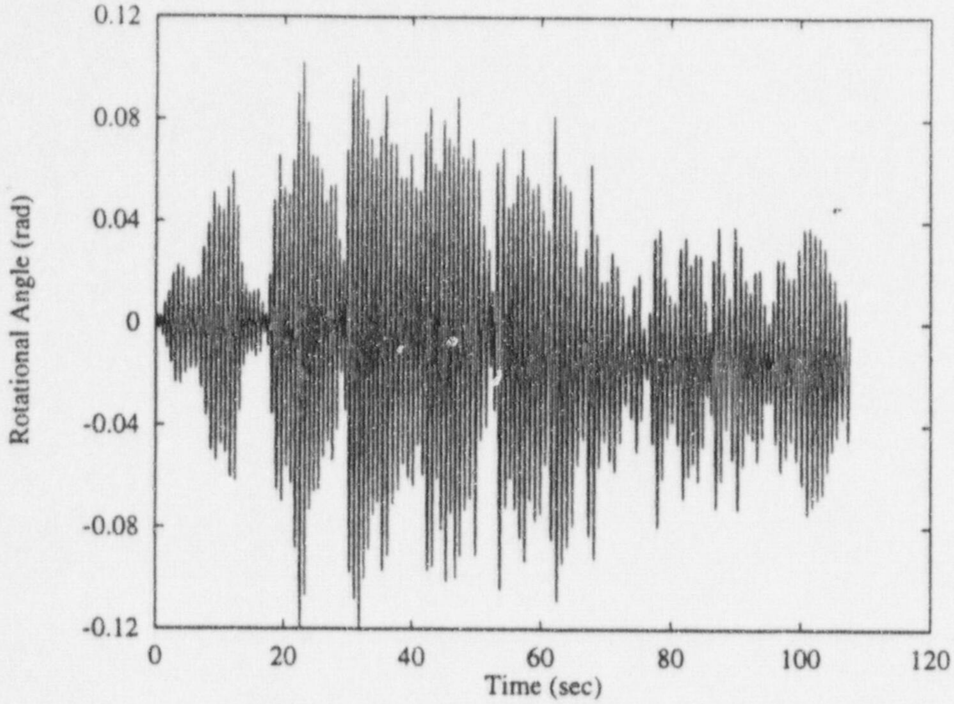

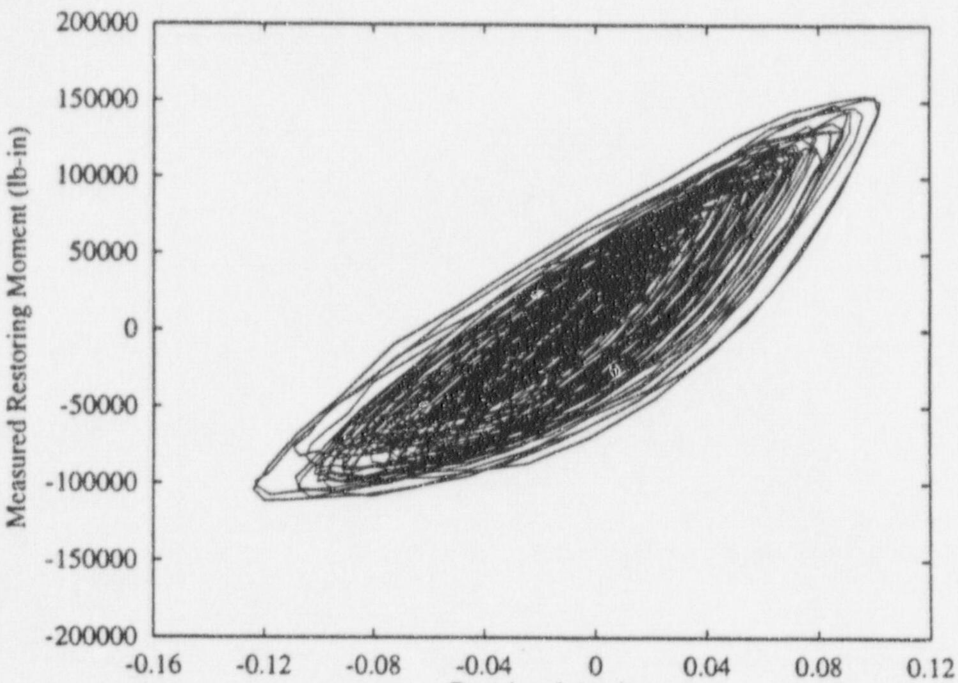

Figure 10: Response time history and hysteretic loops for ANCO Test 30 Run 6

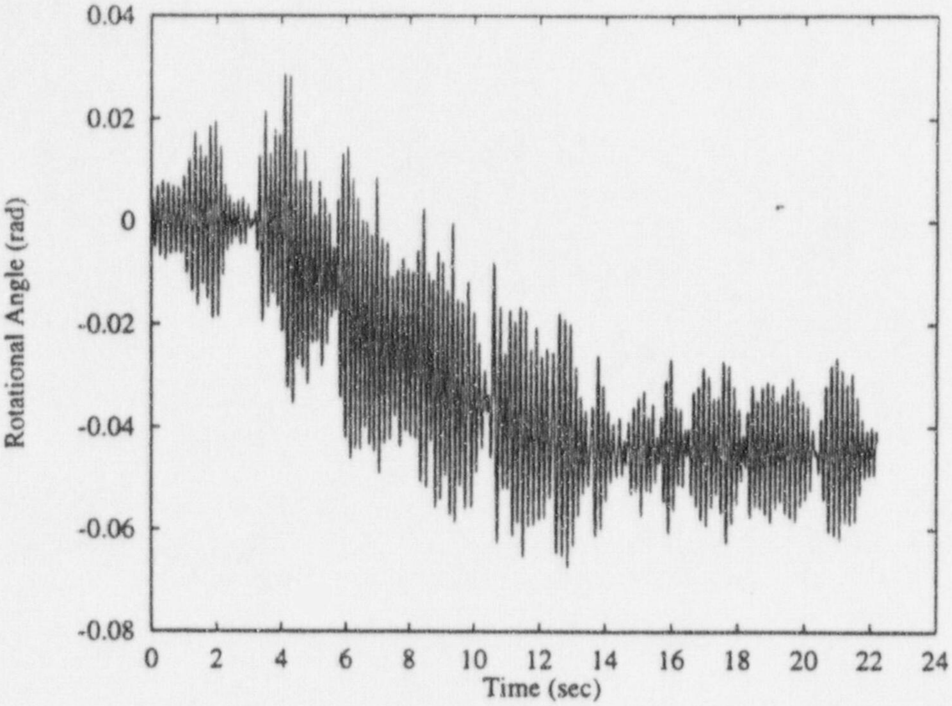

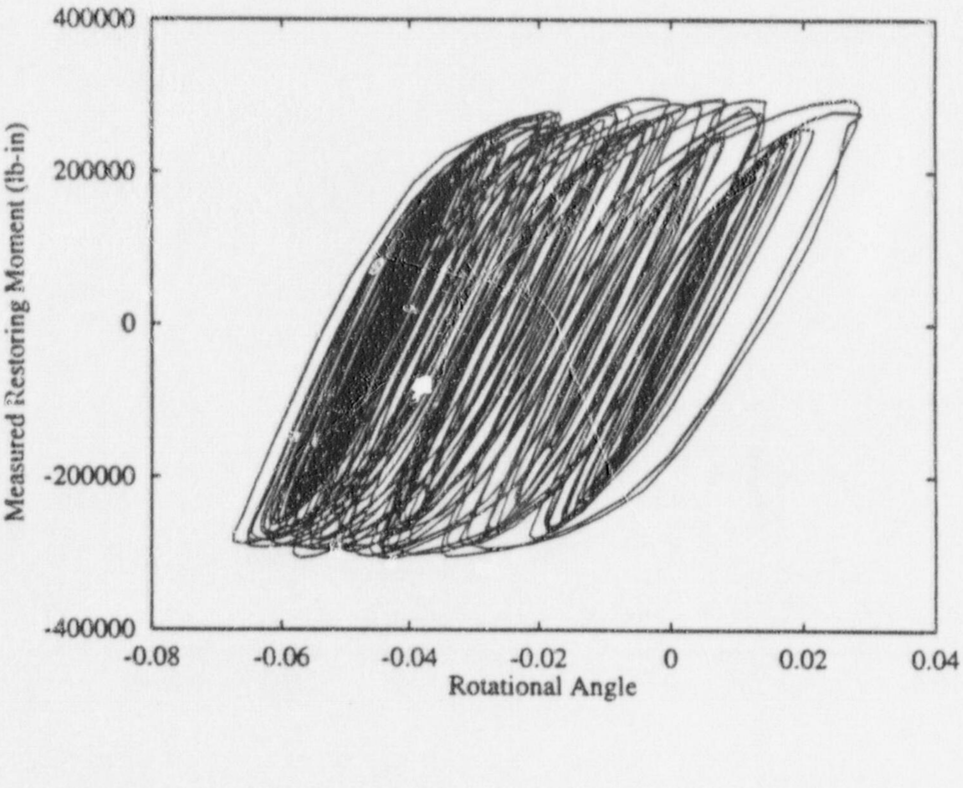

Figure 11: Response time history and hysteretic loops for ANCO Test 15 Run 8

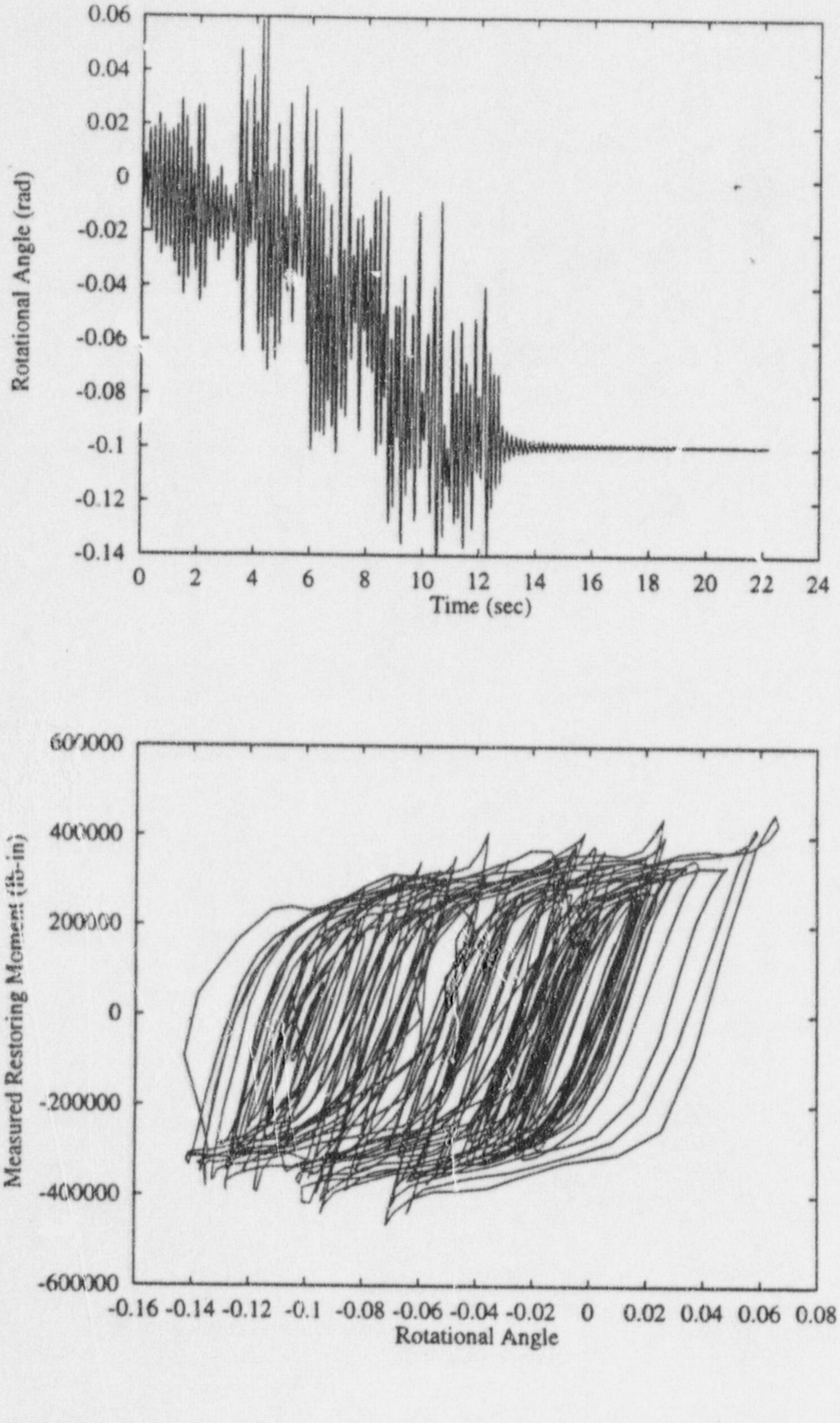

Figure 12: Response time history and hysteretic loops for ANCO Test 16 Run 6

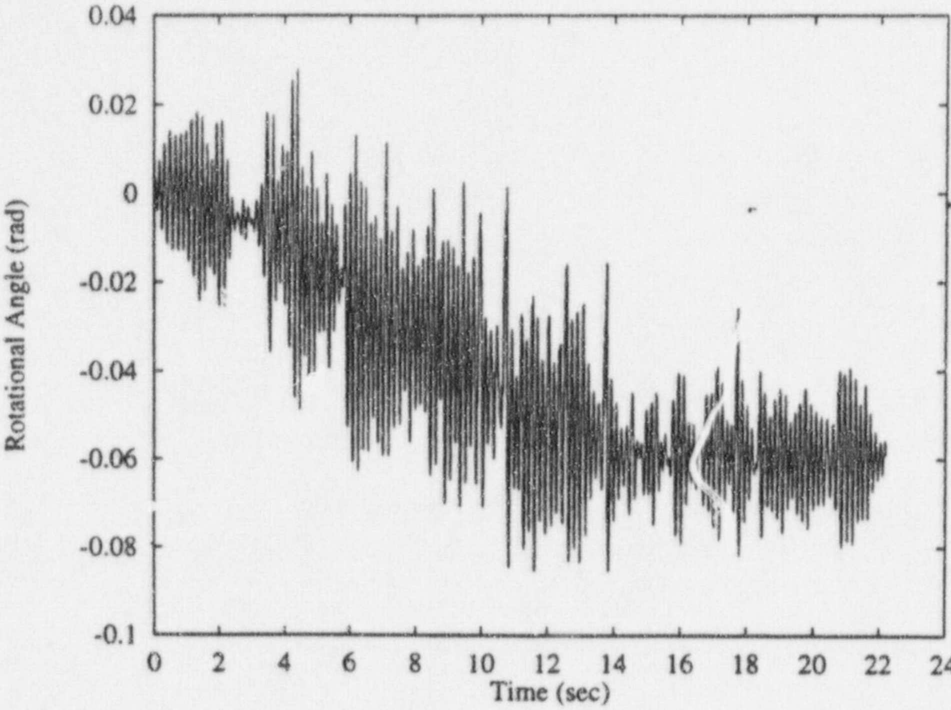

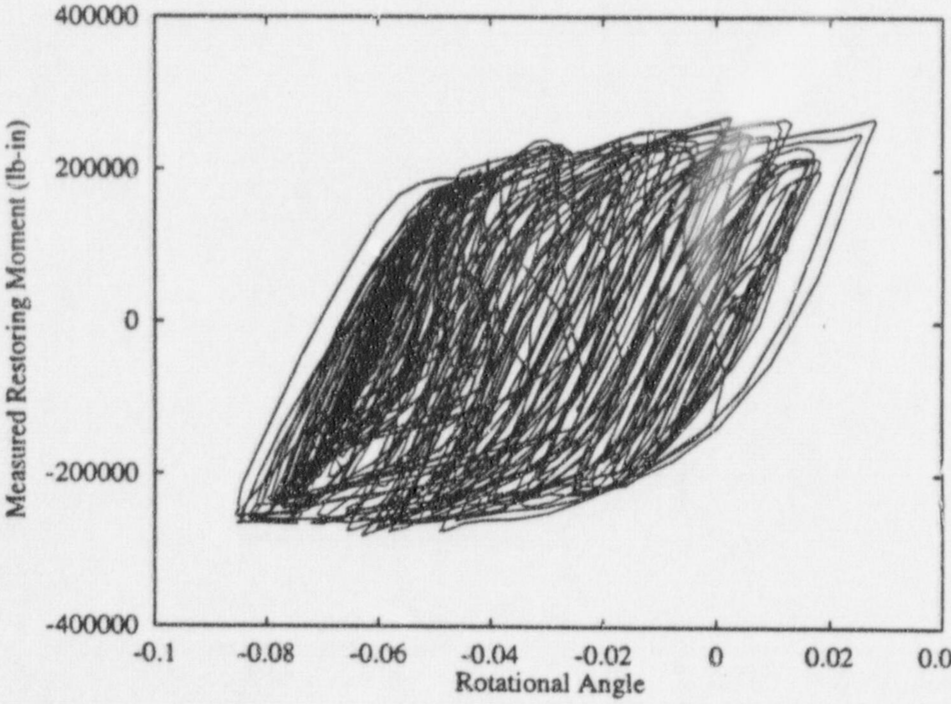

Figure 13: Response time history and hysteretic loops for ANCO Test 40 Run 4

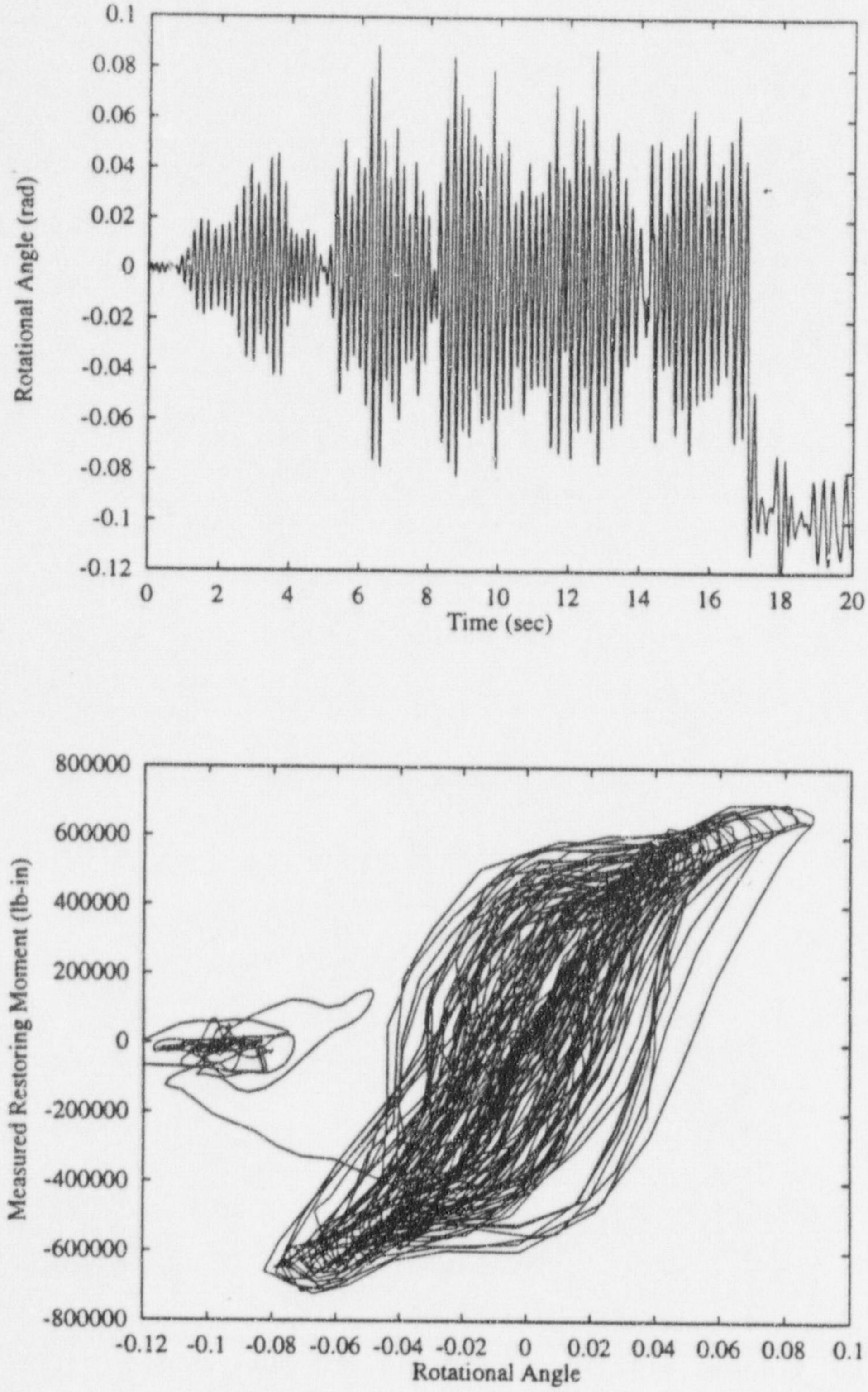

Figure 14: Response time history and hysteretic loops for ANCO Test 36 Run 8

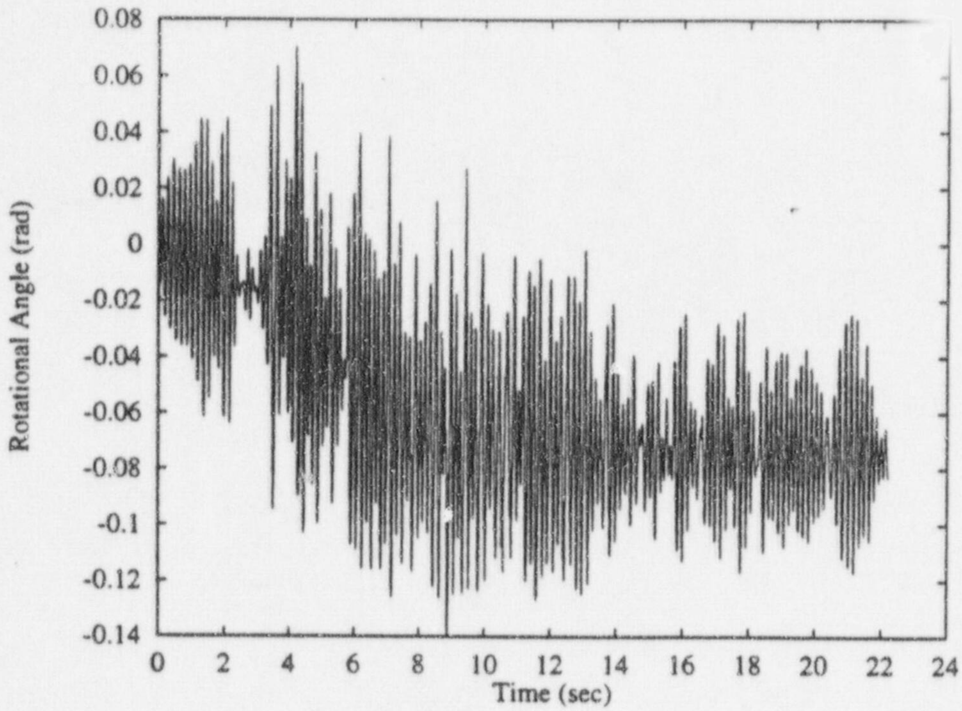

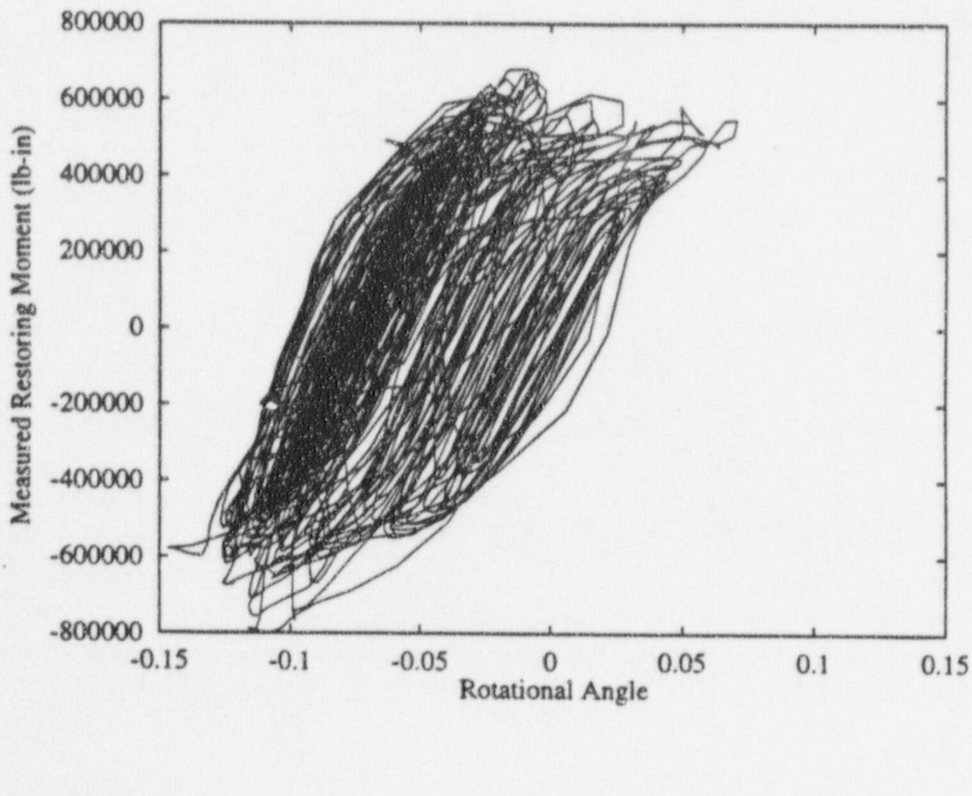

Figure 15: Response time history and hysteretic loops for ANCO Test 9 Run 6

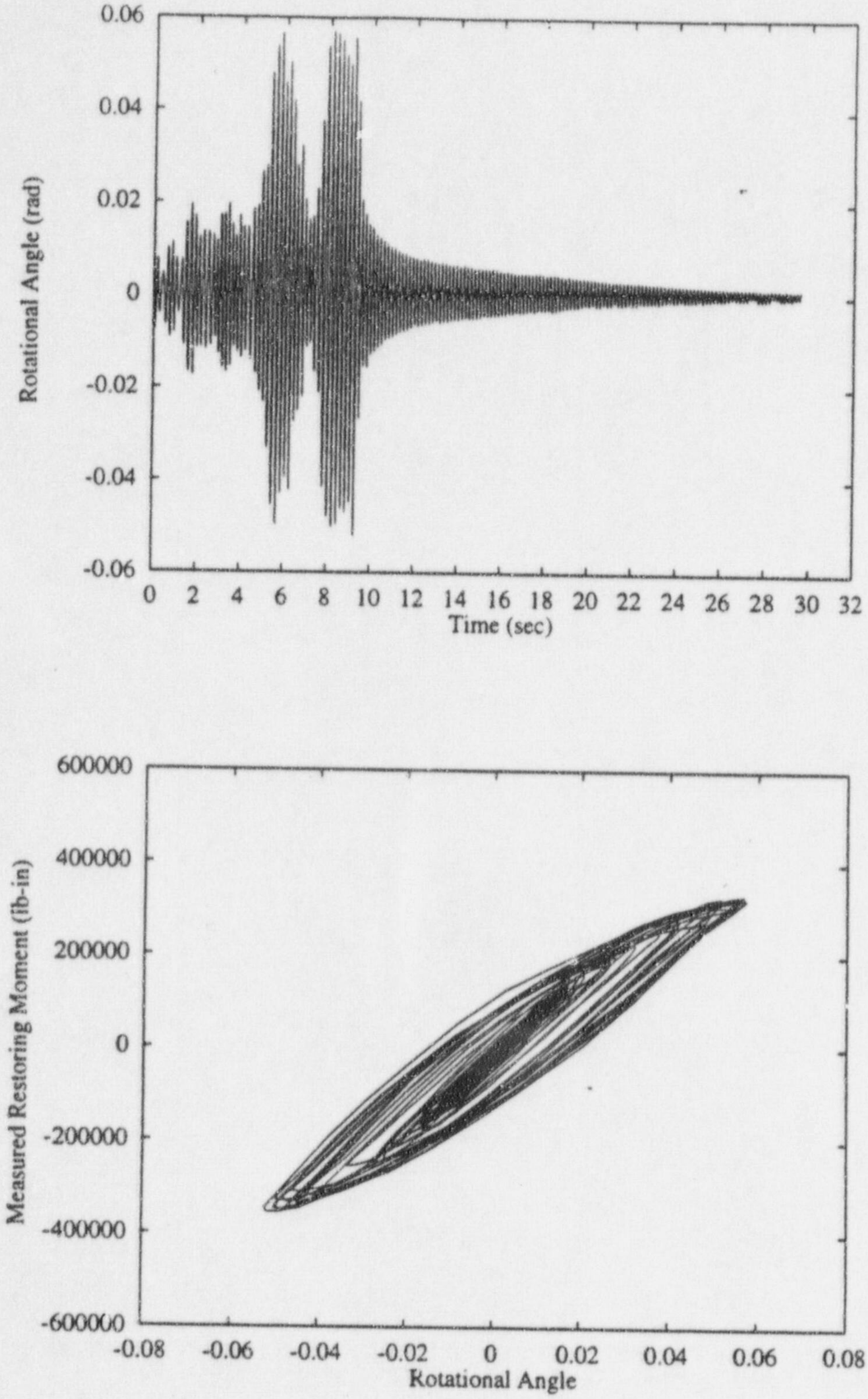

Figure 16: Response time history and hysteretic loops for ANCO Test 11 Run 6

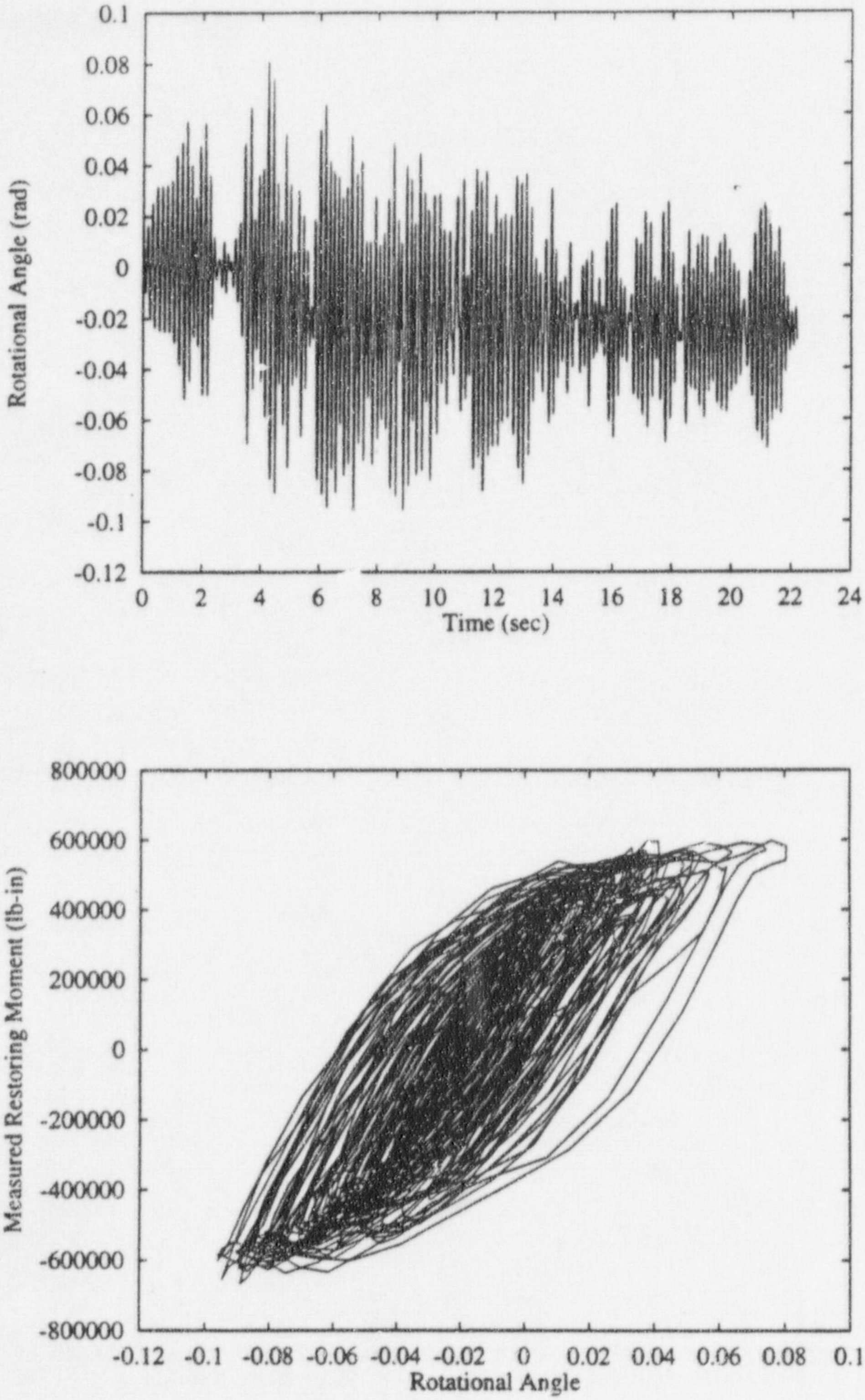

Figure 17: Response time history and hysteretic loops for ANCO Test 14 Run 6

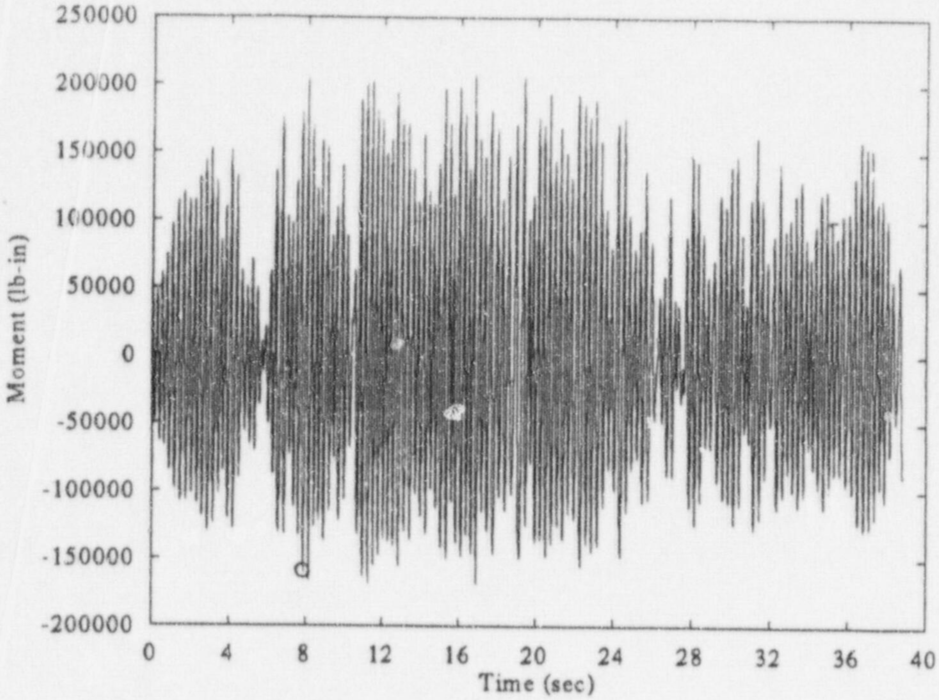

Figure 1: Moment time history for ANCO Test 3 Run 10

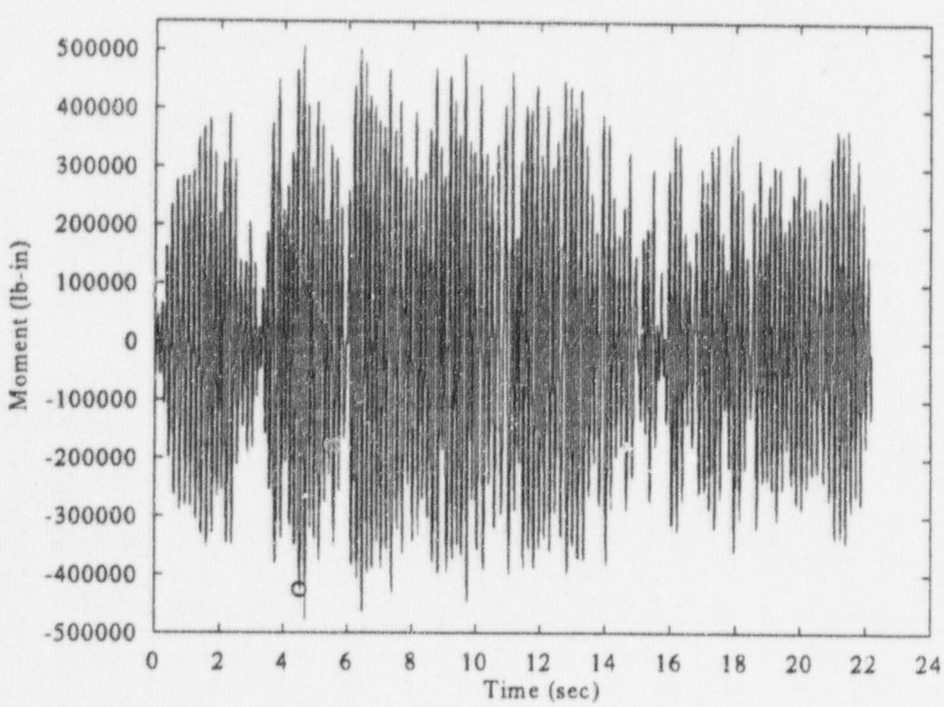

Figure 2: Moment time history for ANCO Test 4 Run 7

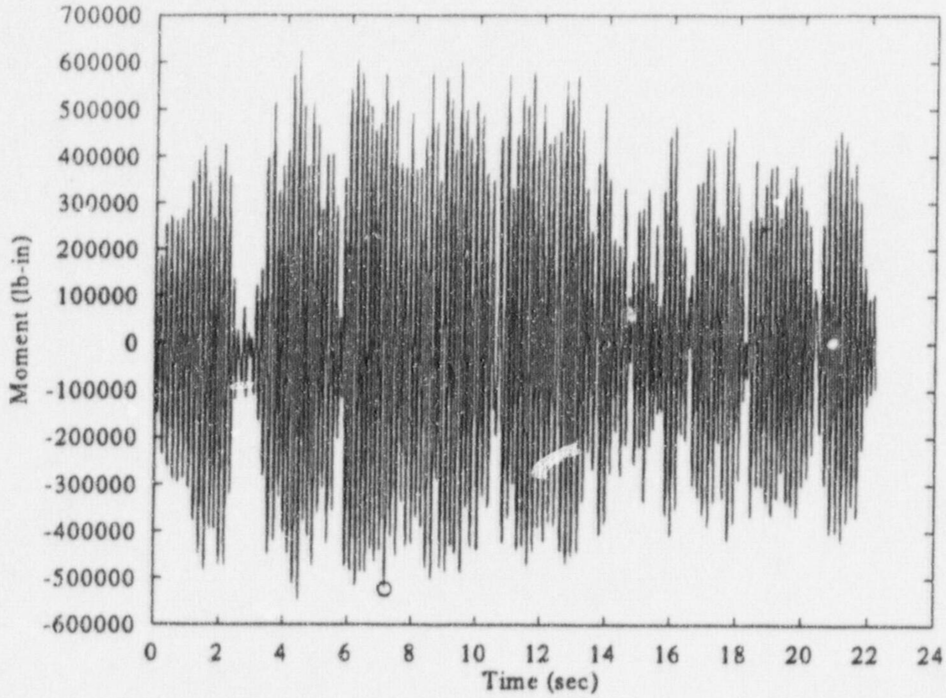

Figure 3: Moment time history for ANCO Test 5 Run 7

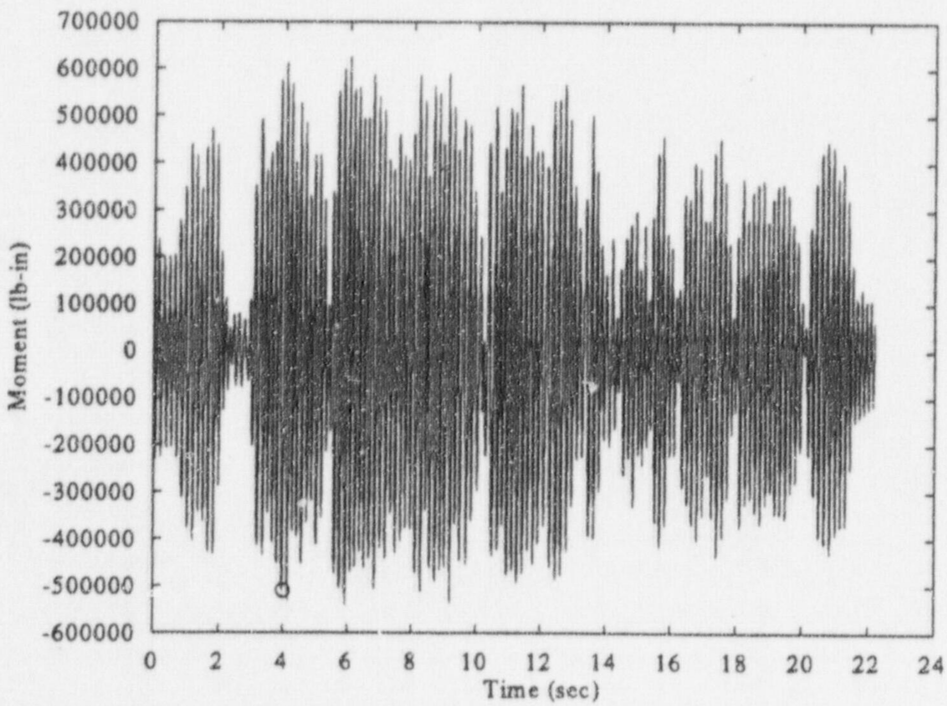

Figure 4: Moment time history for ANCO Test 6 Run 8

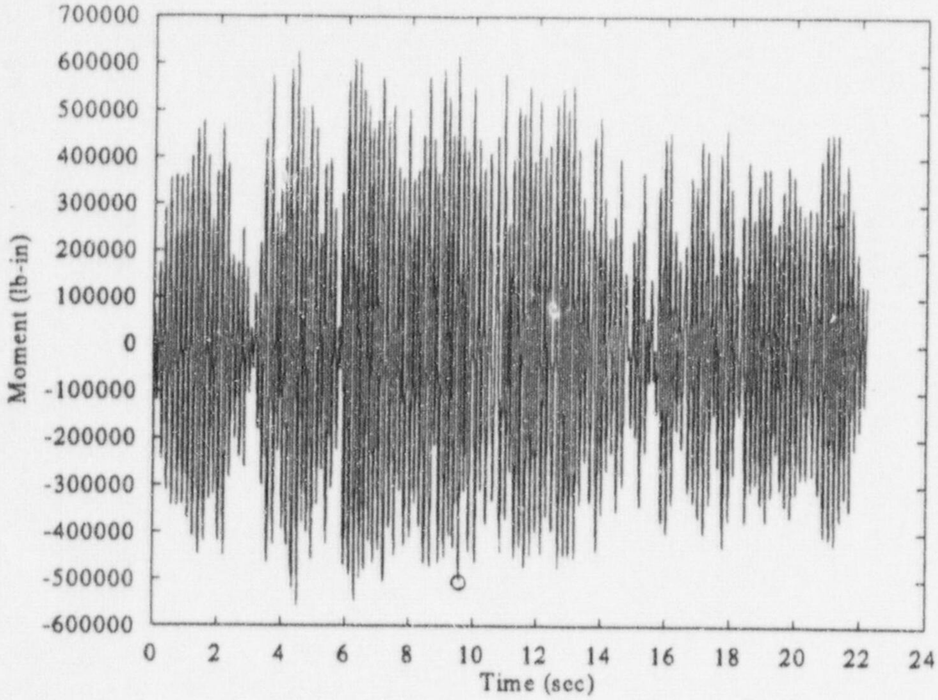

Figure 5: Moment time history for ANCO Test 7 Run 8

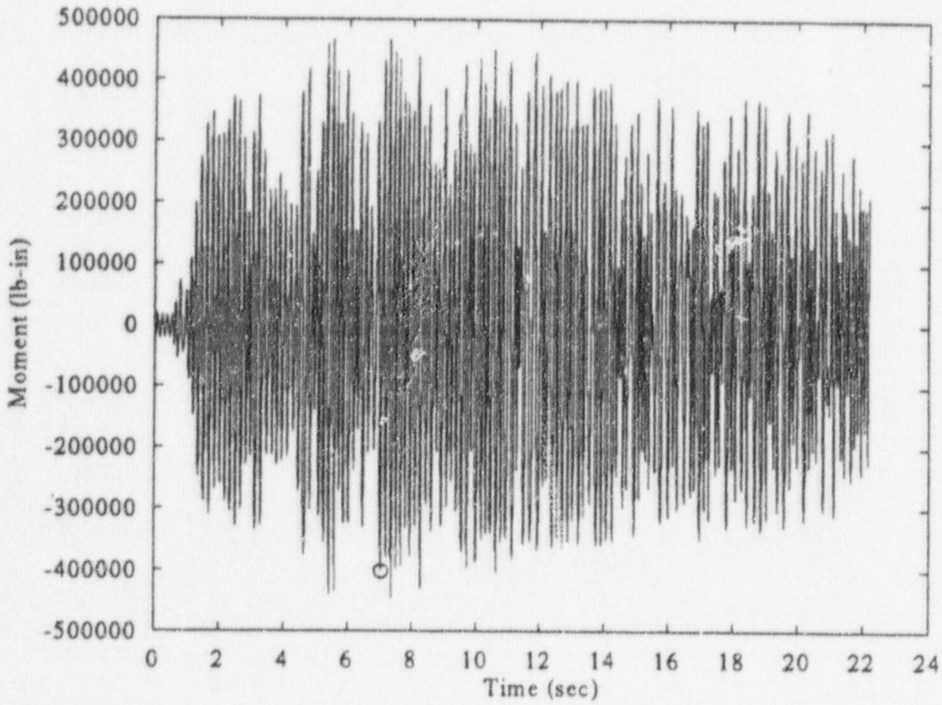

Figure 6: Moment time history for ANCO Test 8 Run 7

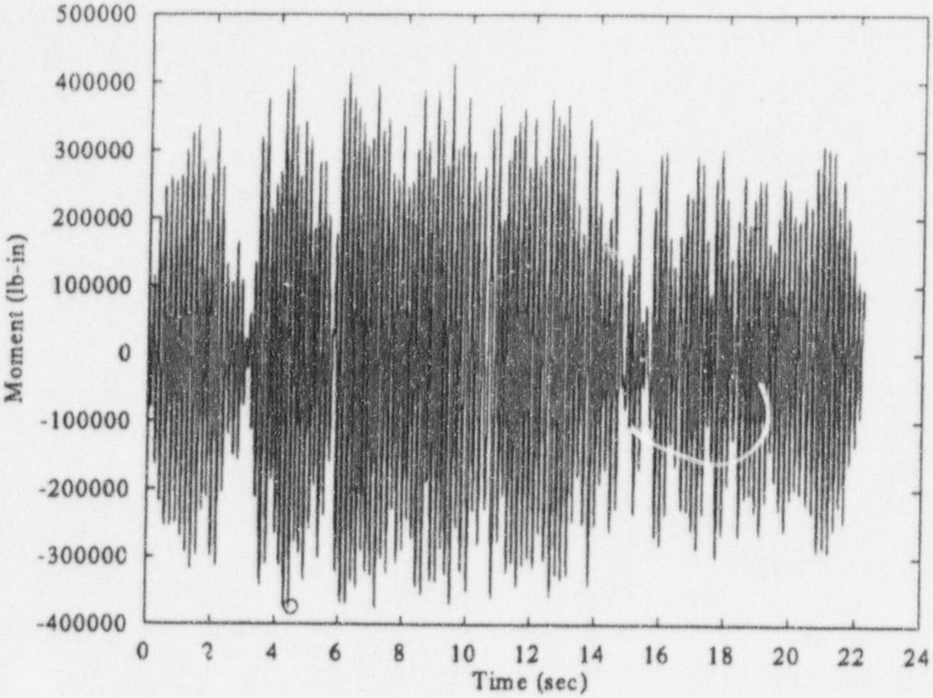

Figure 7: Moment time history for ANCO Test 13 Run 10

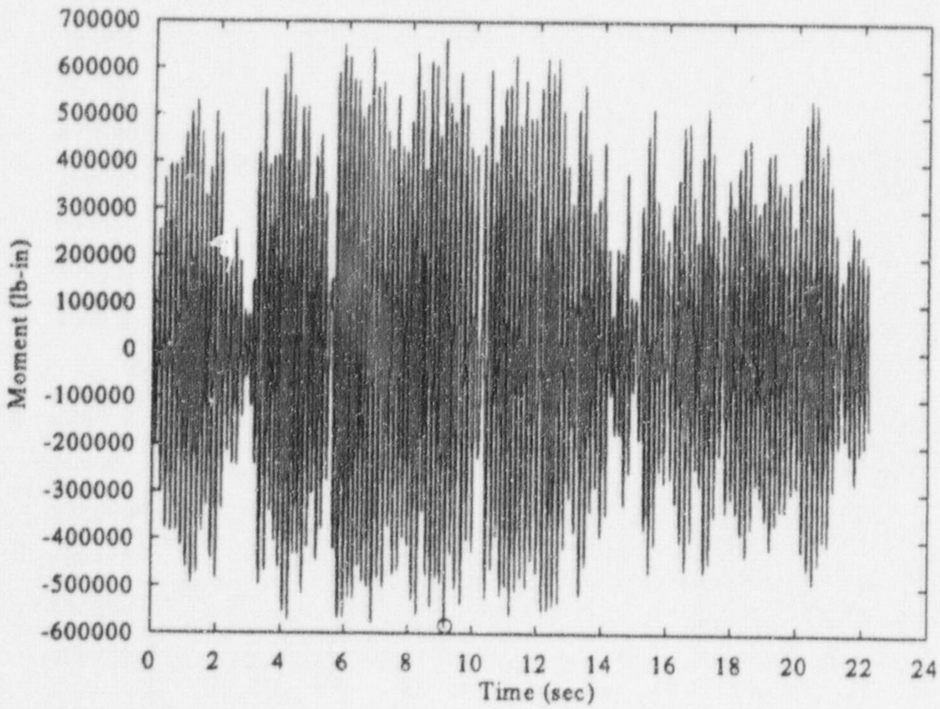

Figure 8: Moment time history for ANCO Test 19 Run 7

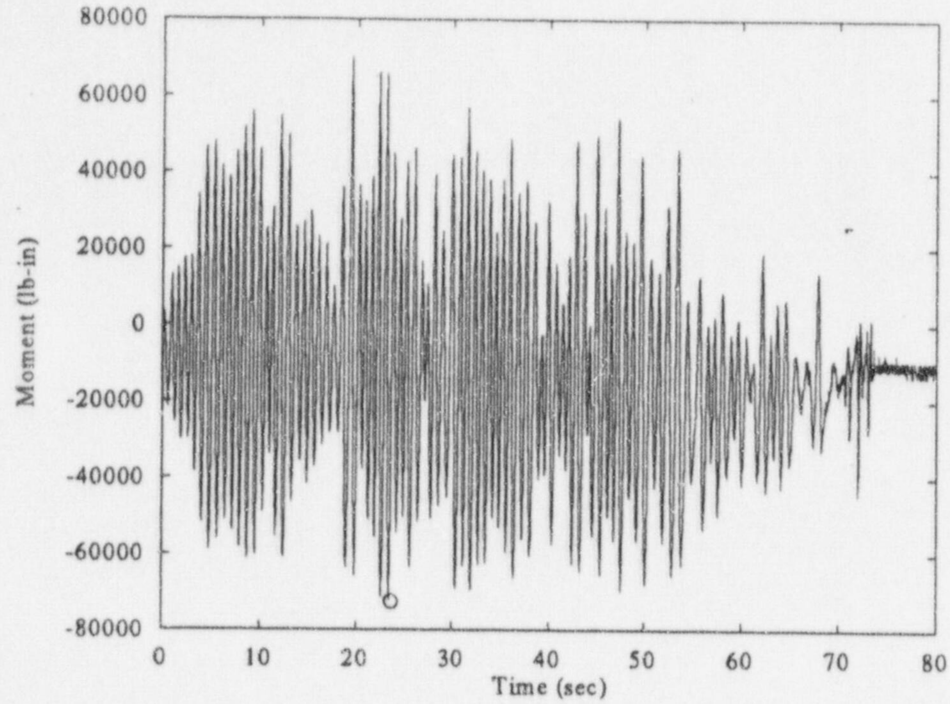

Figure 9: Moment time history for ANCO Test 37 Run 5

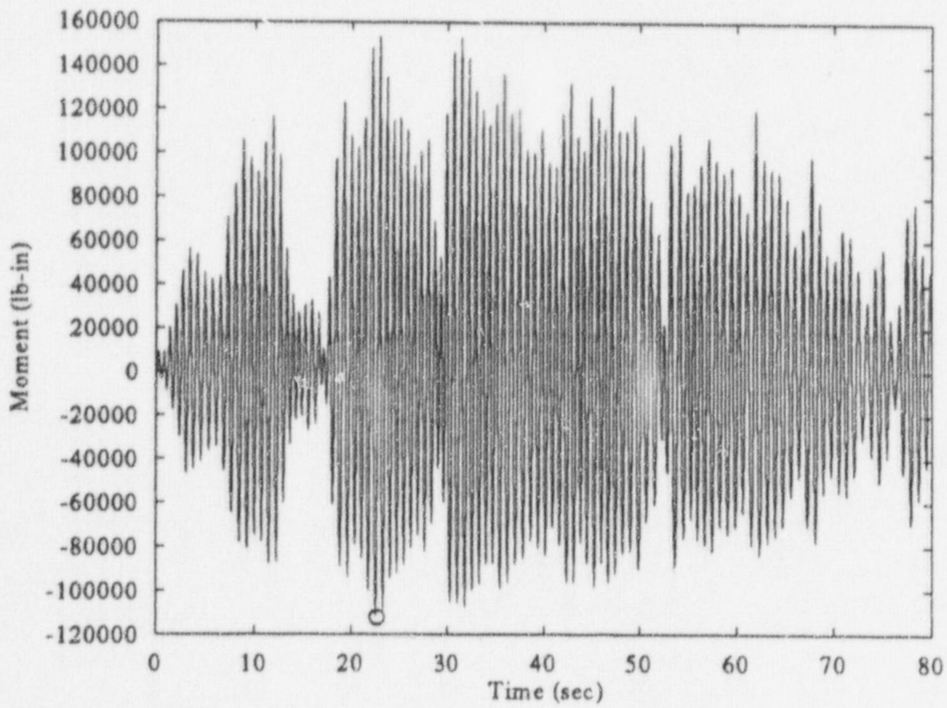

Figure 10: Moment time history for ANCO Test 30 Run 6

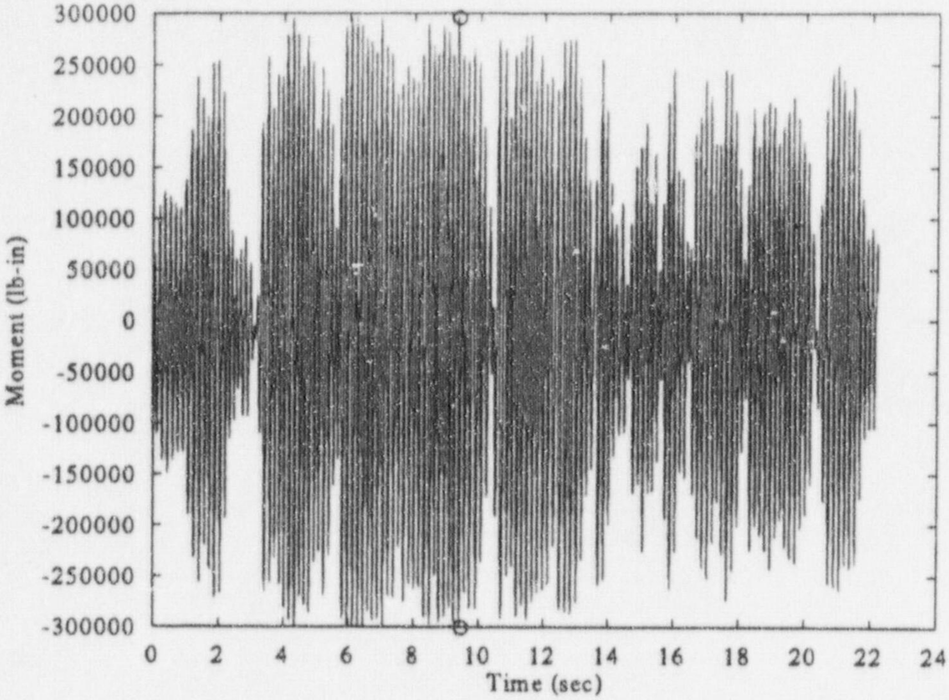

Figure 11: Moment time history for ANCO Test 15 Run 8

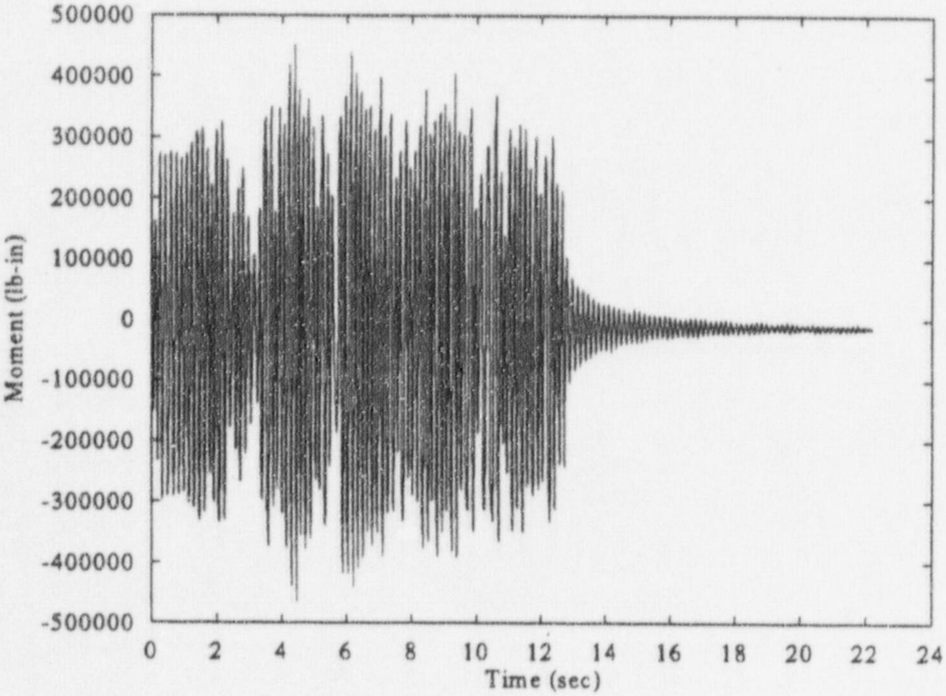

Figure 12: Moment time history for ANCO Test 16 Run 6

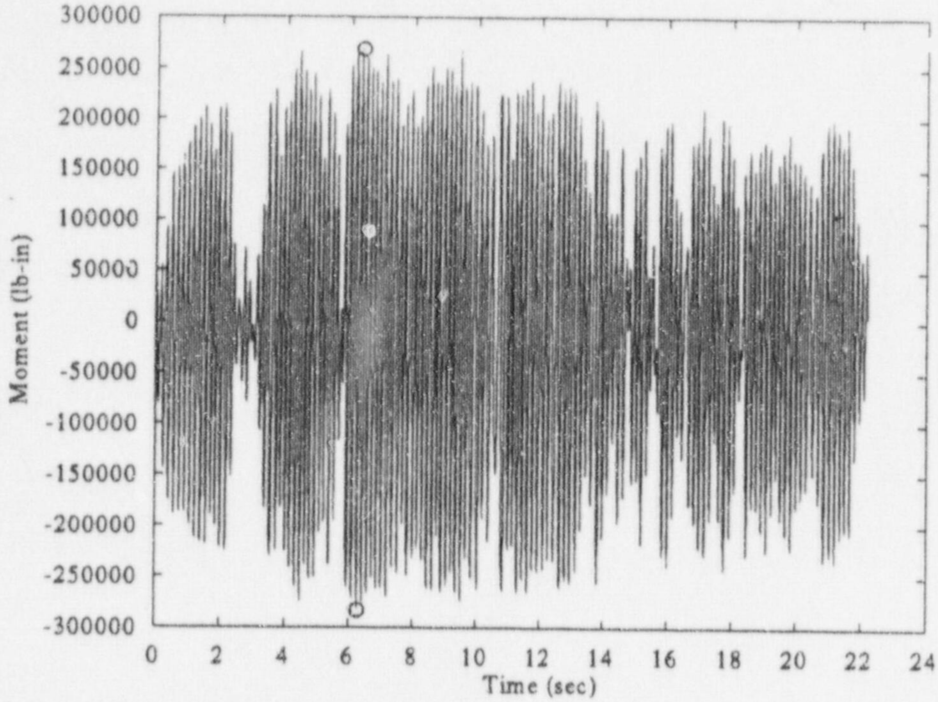

Figure 13: Moment time history for ANCO Test 40 Run 4

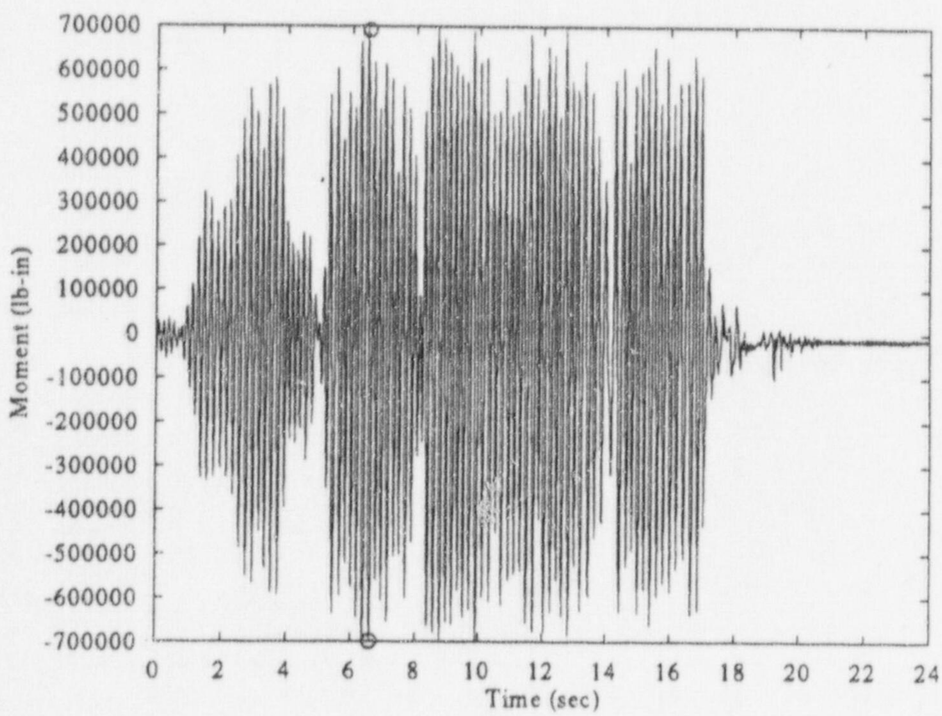

Figure 14: Moment time history for ANCO Test 36 Run 8

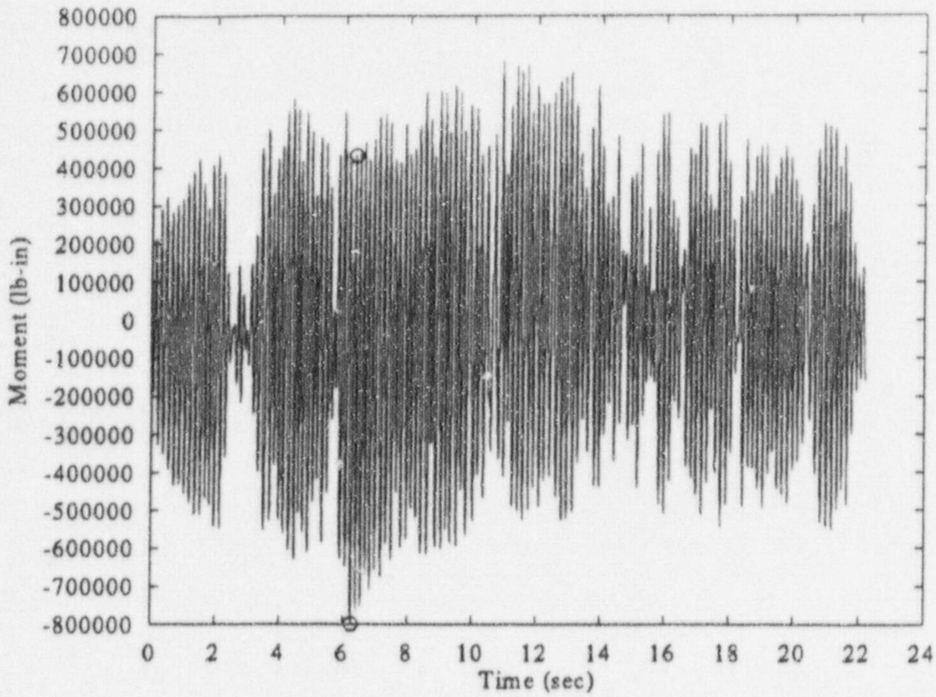

Figure 15: Moment time history for ANCO Test 9 Run 6

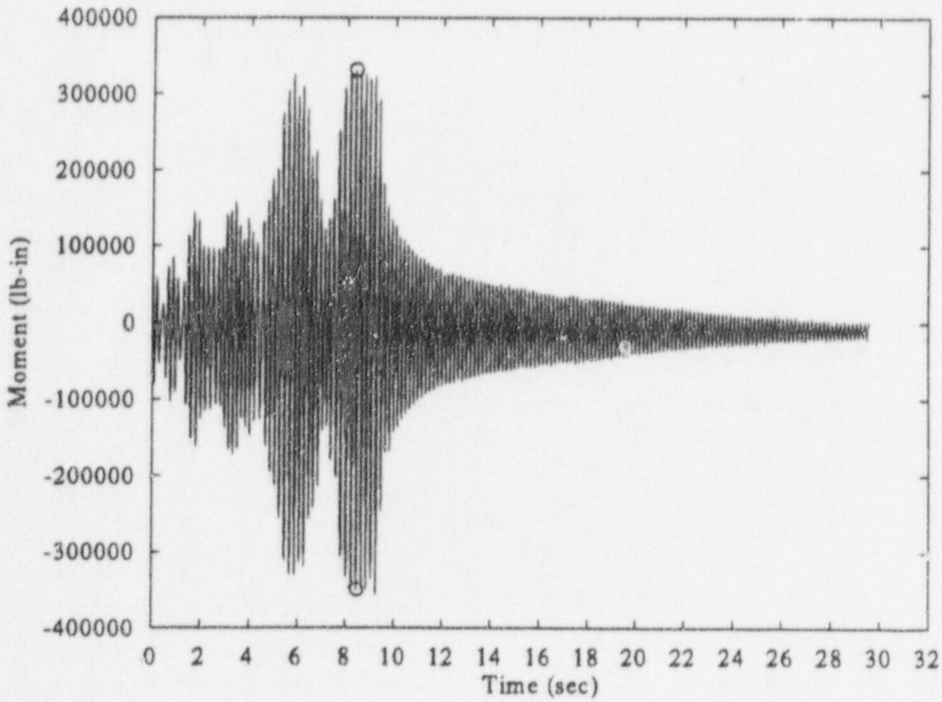

Figure 16: Moment time history for ANCO Test 11 Run 6

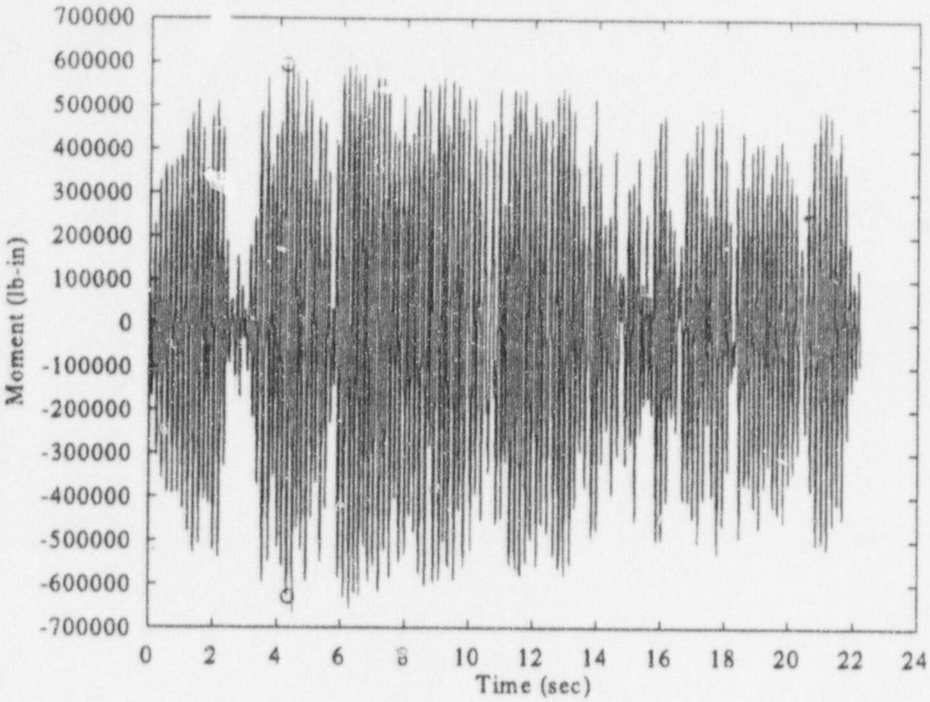

Figure 17: Moment time history for ANCO Test 14 Run 6

Appendix III-C: E. Rodabaugh Inputs

August 13, 1997

E. C. Rodabaugh
7025 Scribner Way
Dublin, Ohio 43017
614-792-9142

Ken Jaquay
Energy Technology Engineering Center
P. O. Box 7930
Canoga Park, CA 91309-7930

Subject: Peer Review Comments Concerning ETEC Studies of New ASME Code Criteria for Seismic Design of Piping

Dear Ken:

My letter to you dated July 28, 1997, the enclosed letter dated August 12, 1997 and this letter constitute my comments.

(1) Letter Dated August 12, 1997

This is a revision of my July 21, 1997 letter. Part (1) of the letter was revised to use the Mud moments per your "Input to Bob Kennedy Mud Study", 7/21/97. It also contains an added paragraph on "time-effects" as possibly significant in explaining the difference between static limit moment tests and Mud moments.

Part (2) of the letter was extensively revised prompted, mainly, by my belated recognition that D-Test #37 was not appropriate for calibration of P-effects. Part (2) may help to explain and/or extrapolate the effect of internal pressure on Mud moments.

(2) Letter Dated July 28, 1997

Equation (a) of my 8/12/97 letter is:

M(Capacity) => M(Demand) (a)

My 8/12/97 letter suggests a simple Code change that, in my view, introduces sufficient conservative on the M(Capacity) side of Eq. (a).

(3) Test # 37

This model failed by "incipient collapse", no pressure boundary failure. In my view, the remaining task relative to Test #37 is to attempt to identify those conditions under which failure such as in Test #37 might occur in piping systems.

NUREG-1367 addressed this potential problem by "the elastic response spectrum analysis must show that the response stress contribution at 2 Hz and less is not more than Sy."

(4) M(Demand)

As a layman in this area, I am not aware of any damage to piping systems in nuclear power plants due to an earthquake. In the USA, this mav represent some 200*10 = 2000 plant years; perhaps another 2000 plant years in nuclear power plants outside the USA.

During these years of operation, there have been numerous piping failures or incipient failures in nuclear power plants due to such causes as water hammer, thermal striping, stress-induced corrosion cracking, corrosion-erosion, fatigue due to vibration in small lines, etc.

As a layman, I do not know what uncertainties or conservatisms are involved in the Code-prescribed elastic analysis used to establish the M(Demand) side of Eq. (a). The operating history suggests to me that M(Demand) has been estimated in a conservative way.

Yours Very Truly,

Everett

E. C. Rodabaugh

Encl: 8/12/97 Letter

File: ken897-2, etec97disc

E. C. Rodabaugh
7025 Scribner Way
Dublin, Ohio 43017
614-792-9142

August 12, 1997

Ken Jaquay
Energy Technology Engineering Center
P. O. Box 7930
Canoga Park, CA 91309-7930

Subject: Use of Static Limit Moment Test Data (S-Tests) and Approximation of Pressure Effect

Dear Ken:

As I see it, the design process consists of satisfaction of the equation:

$$M(\text{Capacity}) \Rightarrow M(\text{Demand}) \quad \text{(a)}$$

In this letter, I will discuss two aspects of the M(Capacity) side of Eq. (a). My only comment concerning the M(Demand) side of Eq. (a) is that the Code has the method pretty well tied down; e.g., linear elastic response spectrum analysis, peak broadened, 5% damping, etc.

(1) Use of Static Limit Moment Test Data (S-Tests)

There was speculation at the July 15,16/1997 meeting that S-Tests would be about the same as D-Tests(Mud) and thus could be used to help establish new Code rules for earthquake evaluations.

In order to examine the premise that S-Tests are about the same as D-Tests (Mud's), I made the enclosed Table X for elbows. My conclusion from Table X is that, except for D-Test #37, M(Capacity) from S-Tests is substantially less than Mud (D-Tests).

Some specific examples from Table X are:

S-Test	M2	Mud	M2/Mud	D-Test
(22)5	334	534	0.63	#5
(22)15	191	508	0.38	#8
(22)16	174	508	0.34	#8
(23)1				
Scaled	55	72	0.76	#37
(13)8	68	72	0.94	#37
GE24	200	508	0.39	#8

The enclosed Fig. X illustrates the significance of M2 and the maximum moment capacity, Mm, from S-tests. In many S-Tests in Table X, the test was not carried to the extent that Mm was reached. However, as indicated in footnote (f) of Table X, some were. For most such tests where both M2 and Mm are available, the difference between M2 and Mm is small. To illustrate this aspect, I have enclosed Fig.

7-28 of the GE/EPRI report. While the tests are a bit on the crude side, roughly M2 = 200 in-kip, Mm = 210 in-kip as compared to Mud = 508 in-kip.

However, there are two exceptions:

S-Test (24)1 M2 = 1500 in-kip: Mm = 3300 in-kip.
Scaled 54.5 in-kip: 120 in-kip
S-Test (13)6: M2 = 184 in-kip; Mm = 313 in-kip.

These two "exceptions" lead to the following comparisons:

S-Test	M2	Mm	Mud	M2/Mud	Mm/Mud	D-Test
(24)1 Scaled	54.5	120	72	0.76	1.67	#37
(13)6	184	313	520	0.35	0.60	#6

S-Test (13)8 also is roughly comparable to D-Test #37; it's Mm is 79 in kips. Thus we have:

S-Test (24)1, Scaled: M2 = 54.5, Mm = 120 Mud = 72
S-Test (13)8, M2 = 68, Mm = 79

Thus, for D-Test #37, the S-Tests are in reasonable agreement with Mud; but not for any other elbow D-Test.

You mentioned, at the July 15,16, 1997 meeting, that in running static limit load tests, there is a "time effect"; an effect that I have also observed. In the plastic response region, if an increment of load is applied in, for example, 5 seconds, then the measured displacement will continue to increase for perhaps another 10 seconds. The enclosed Fig. 7-28, for closing moment, may be showing this effect by the difference between the "initial" and "stabilized" lines. D-Tests involve high rates of loadings and, perhaps, part of the difference between D-Tests and S-Tests may be due to the "time effect".

(2) Approximation of Pressure Effect (P-effect)

There is an existing theory for P-effect in the elastic region:

Sp = So/Fp (b)

where Sp = stress due to moment at P = 0
So = stress due to moment at P > 0
Fp = 1 + 3.25*(pr/t)*(r/t)^(3/2)*(R/r)^(2/3)/E
p = internal pressure
r = elbow mean radius
t = elbow wall thickness
E = modulus of elasticity of elbow material
R = bend radius of elbow

Equation (b) is non-linear; to duplicate the results using finite-element computer programs would require consideration of finite-displacements.

For elastic analysis:

$$So = [1.95/h^{(2/3)}]*M/Z. \qquad (c)$$

where $h = (t/r)*R/r$
M = in-plane moment
Z = section modulus of elbow cross section
$1.95/h^{(2/3)}$ Not to be taken as less then 1.5

This stress, for parameters of main interest, is a bending stresss at the sides of the elbow. To obtain thru-wall plasticity, the stress must be 1.5 Sy, Sy = material yield strength. This concept led to the Code B2-index for elbows; i.e., $B2 = (1.95/1.5)/h^{(2/3)} = 1.3/h^{(2/3)}$. The implicit assumption is the that elbow parameter, h, continues to be valid for plastic response.

I will use Eq. (b) to estimate the P-effect on elbows in the plastic region. The assumption is that the dimensional parameters h, r/t and R/r continue to be valid for plastic response.

Eq. (b) and (c) can be combined to give:

$$Sp = [Co/h^{(2/3)}] * M/Z/ Fp \qquad (d)$$

Where Co and the E in Fp are to be "calibrated" from a dimensional and material identical pair of tests in the plastic regime that differ in internal pressure, p.

The D-tests include four models, with D = 6.625, t = 0.280, R = 9 and P = 0, 1000, 1700 and 2500 psi; D-Tests #8, #7, #6 and #19, respectively. D-Test #8 had no cracks, D-Tests #7 and #8 had through wall cracks in the side wall (the theoretical location); D-Test #19 had partial cracks at the side wall. Ideally, we would like to have a set of tests where through wall cracks occurred; but this set appears to be the most appropriate for "calibration" of Eq. (d).

Using the extremes of pressure, D-Tests #8 and #19, Mud = 508 and 633, respectively, leads to the estimate that the P-effect, for 2500 psi internal pressure, is about a factor of 633/508 = 1.2461.

Thus, a calibrated value of E, E', is obtained by:

$$(pr/t)*3.25*(r/t)^{(3/2)}*(R/r)^{(2/3)}/E' = 1.2461 - 1 \qquad (e)$$

With p = 2500 psi, r = 3.172 inch, R = 9 inch, Eq. (e) gives:

$$E' = (2500*3.172/.280)*3.25*(3.172/.280)^{(3/2)}*(9/3.172)^{(2/3)}/0.2461$$

$$E' = 2.279e7 \text{ psi}$$

To obtain Co, a limiting nominal stress must be assumed. Taking this to be 90000 psi, then:

Co = 90000*h^(2/3)*Z/153000 = 1.958

Some examples of the use of the "calibrated" Eq. (d) are shown in Table Y:

The first and fourth lines of Table Y are simply getting back the calibration input.

It is apparent in Table Y that D-Test #37 is "different"; we think it should be, the failure mode is incipient collapse; not a fatigue failure.

It may be noted in Table X that there are two pair of S-tests in which pressure is the only variable; i.e., (22)2, (22)5 and (13)5, (13(6). The pair (13)5 and (13)6 are stainless steel tests; use of this pair to estimate P-effect, after adjusting for the rather large difference between S-Tests and P-Tests for stainless steel, give results similar to those obtained in the preceding for stainless steel.

To extend the estimates of P-effects to carbon steel, I used the pair (22)2 and (22)5; for which M2(p=0) = 264, M2(p=1500 psi) = 334 in-kip; M2(p=1500)/ M2(p=0) = 334/264 = 1.2652. Using this ratio in Eq. (e), with p = 1500 psi, gives:

E' = 1.592e7: Co = 1.151

To give direct comparison, an adjustment was made by multiplying the results (which are for M2) by a factor such that agreement was obtained with Mud, D-Test #4. This factor is 429/311 = 1.38. This is a much smaller factor than for stainless steel tests and suggests that the difference between S-Tests and D-Tests for carbon steel may be significantly less than for stainless steel.

The results for carbon steel tests are included in Table Y; D-Tests #4, #5, #13, #35 and #41. It may be noted that the P-effect for the "short radius" elbow, D-Test #13, is consistent with the Mud moment.

The last four lines of Table 4 are intended to illustrate that the P-effect results can be extrapolated to most elbows.

The question arises: Can the P-effect be incorporated in Code rules?

Table Y is based on the characteristics of 90 deg.elbows with in-plane closing moments. In piping systems, other than 90 deg. elbows may be used and, in general, the elbows will be subjected to combinations of in-plane, out-of-plane and torsional moments. Further, adjustments must be made for some elbows; related to the 1.75/h^(2/3) not to be taken as less than 1.5.

Thus, my answer to my question is: No.

In brief summary of this letter:

(a) Elbow S-Tests, except for Test #37, are NOT the same as from D-Tests; Mud. The difference is substantial for stainless steel. There is a suggestion, in the P-effect portion of this letter, that the difference may be much less for carbon steel.

(b) P-effects using Eq. (d), after calibration, appears to be a reasonable way to estimate the effect of internal pressure for 90 deg. elbows subjected to in-plane closing moments. However, the scope of Eq. (d), as presently developed, is far too limited to permit its use in Code rules.

Yours Very Truly,

Everett

E. C. Rodabaugh

Encls: Tables X and Y, Fig. X
Fig. 7-28 of GE/EPRI Report, Vol. 2

File: ken897, Disk etec97

Table X: Summary of Static Limit Load Tests on Elbows, all Data for In-plane Closing Moment

S-Test Number (a)	M't'l (b)	D, in (c)	t, in (c)	R, in (c)	Sy, ksi (d)	p, ksi (e)	M2, in-kip (f)	D-Test Number (g)	p, ksi (g)	Mud in-kip (h)
(22)2	C	6.625	0.280	9.00	50.0	0	264			
5	C	6.625	0.280	9.00	50.0	1.5	334	#4	1.0	429
								#5	1.7	534
8	C	6.625	0.432	9.00	37.8	0	428			
11	C	6.625	0.432	6.00	39.6	0	206			
15	S	6.625	0.280	9.00	37.7	0	191	#8	0	508
16	S	6.625	0.280	9.00	37.7	0	174	#8	0	508
17	S	6.625	0.280	6.00	35.6	0	175			
18	S	6.625	0.432	9.00	35.4	0	341			
19	C	6.625	0.280	6.00	46.0	0	202	#13	1.0	379
20	C	6.625	0.432	6.00	34.6	0	369			
(23)1	S	20.00	0.472	30.0	36.3	0	1500			
Scaled		6.625	0.156	9.94	36.3	0	54.5	#37	0	72
(13)1	C	6.504	0.280	9.00	?	1.4	212	#4	1.0	429
								#5	1.7	534
5	S	6.504	0.280	9.00	?	0	153	#8	0	508
6	S	6.504	0.280	9.00	?	1.7	184	#6	1.7	520
								#7	1.0	523
7	S	6.504	0.197	9.00	?	0	114			
8	S	6.504	0.157	9.00	?	0	68	#37	0	72
9	S	3.893	0.226	6.00	?	0	74			
Scaled		6.625	0.385	10.2	?	0	365			
(24)4	S	3.508	0.118	4.50	?	1.2	43.8			
Scaled		6.625	0.223	8.50	?	1.2	295	#7	1.0	523
5	S	3.508	0.118	4.50	?	1.2	45.0			
Scaled		6.625	0.223	8.50	?	1.2	303	#7	1.0	523
GE24	S	6.625	0.280	9.00	54.2	0	210	#8	0	508

Notes on next page

Table X, Notes

(a) Except for the last li e, these are from Table 4, "Summary of Limit Load Tests on Elbows", of:

(1) "Evaluation of the Plastic Characteristics of Piping Products in Relation to ASME Code Criteria", NUREG/CR-0261, Rodabaugh and Moore, July 1978

All tests with -Mz moment (in-plane closing moment) are included. The number in ( ) is the reference number of Ref. (1). The last line is from the enclosed Fig. 7-28 of GE/EPRI Report, Vol. 2

(b) Elbow material: C = carbon steel, S = stainless steel

(c) Nominal dimensions of elbows. D = outside diameter, t = wall thickness, R = bend radius.

(d) Sy = yield strength of elbow material. ? indicates Sy not given in cited reference.

(e) p = internal pressure held constant in S-Tests

(f) For S-Tests other than Ref. (24)
M2 = moment as defined in enclosed Fig. X
For "S-Tests" of Ref. (24)
These were vibration tests; see page 22 of Ref. (1). They are more akin to D-Tests than S-Tests.
For other-than Ref. (24) tests, the maximum moment, Mm (see enclosed Fig. X), is close to M2 with two exceptions:

(23)1: M2 = 1.50 in-kip, Mm = 3.3 in-kip
(13)6: M2 = 0.184 in-kip, Mm = 0.313 in-kip

(g) Test # and internal pressure p from Table 2 of ETEC report

(h) From Jaquay, "Input to Bob Kennedy Mud Study", 7/21/97.

Table Y: Examples of use of "Calibrated: Eq. (d)

M't'l (a)	D-Test	D in	t in	R in	p psi	M in-kip (b)	Mud in-kip (c)
SS	#8	6.625	0.280	9	0	508	508
SS	#7	6.625	0.280	9	1000	558	523
SS	#6	6.625	0.280	9	1700	593	520
SS	#19	6.625	0.280	9	2500	633	633
SS	#37	6.625	0.134	9	0	154	72
SS	#3	6.625	0.134	9	400	194	162
SS	#30	6.625	0.134	9	400	194	115
SS	#31	6.625	0.134	9	400	194	192
CS	#4	6.625	0.280	9	1000	429	429
CS	#5	6.625	0.280	9	1700	474	534
CS	#13	6.625	0.280	6	1000	316	379
CS	#35	6.625	0.280	9	1700	474	470
CS	#41	6.625	0.280	9	1700	474	510
SS	---	24.00	0.375	36	0	5140	---
SS	---	24.00	0.375	36	500	8550	---
CS	---	24.00	0.375	36	0	3680	---
CS	---	24.00	0.375	36	500	8090	---

(a) SS = stainless steel, CS = carbon steel

(b) Moment per calibrated Eq. (d)

(c) From Jaquay, "Input to Bob Kennedy Mud Study", 7/21/97.

ECR to Jaquay
8/12/97

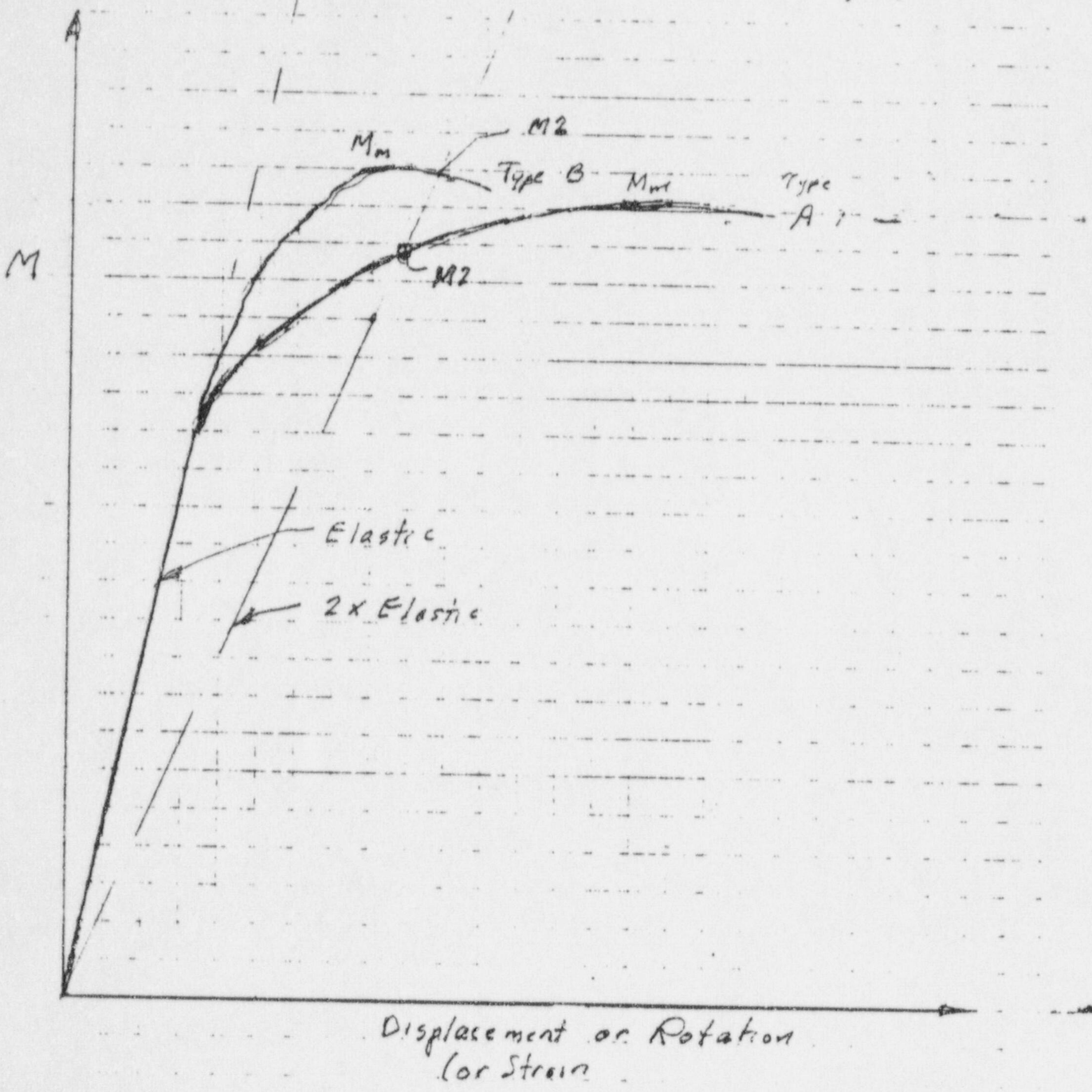

Fig X: Illustration of M2 and Mm
- Type A is usual for elbows with in-plane closing moment,
Type B can occur

ECR to Jaquay
8/12/97

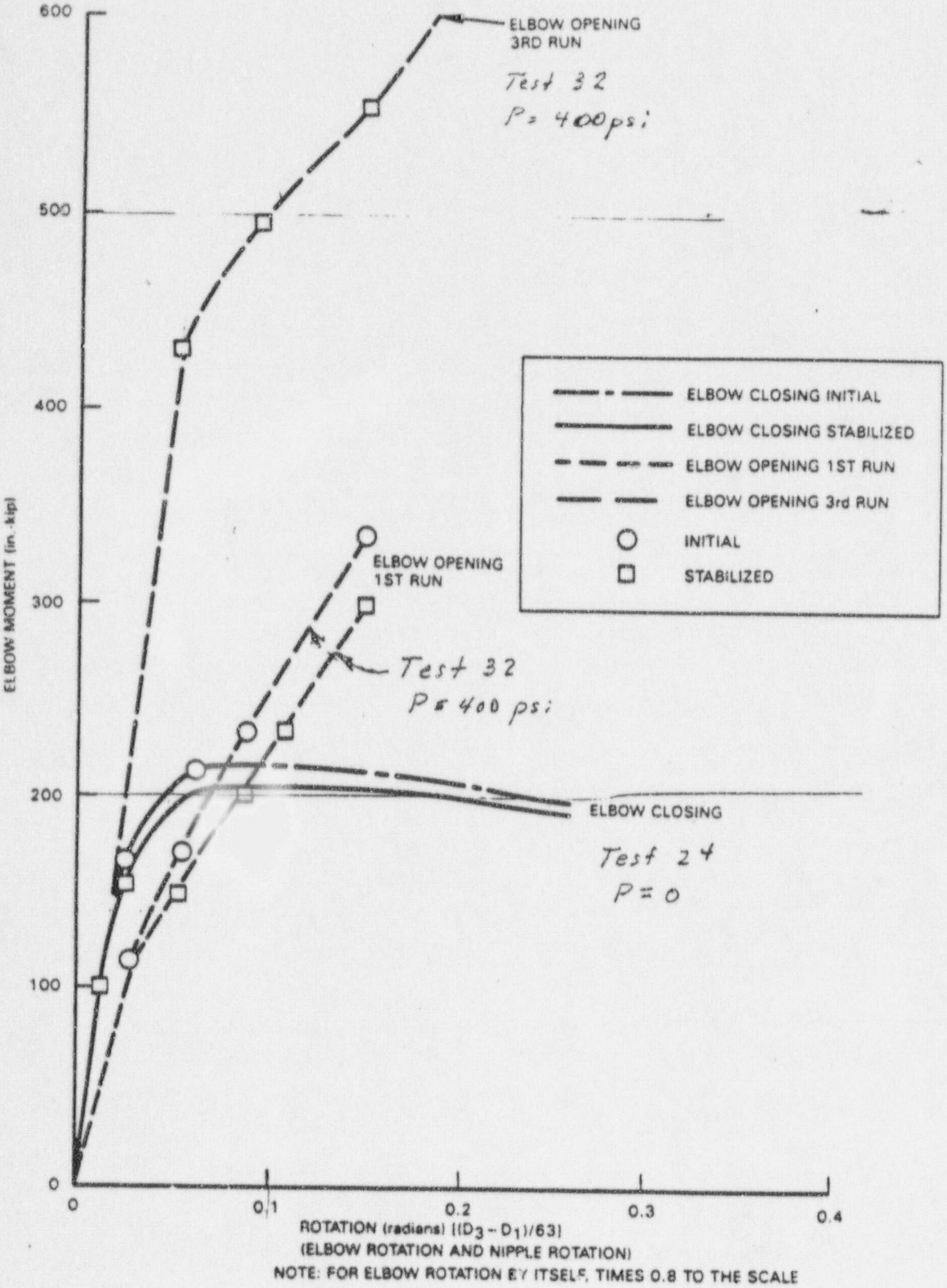

6 NPS, Sch. 40, 9" bend radius, SS, S_y = 54.2 ksi

Figure 7-28. Elbow Static Test, Moments Versus Rotation

E. C. Rodabaugh
7025 Scribner Way
Dublin, Ohio 43017
614-792-9142

July 28, 1997

Ken Jaquay
Energy Technology Engineering Center
P. O. Box 7930
Canoga Park, CA 91309-7930

Subject: "Straw Man" change in Code

Dear Ken:

(1) "Straw Man" Code Change

Enclosed is a marked-up copy of page 154 of the Code; it is all of NB-3656.

I deliberately kept the change very simple; e.g., I didn't put in the 3Sy limit that I would eventually like to see. Indeed, if I had my "druthers", I would replace 4.5Sm with 3Sy.

The change leaves a number of issues to be addressed. One major issue is an explanation of the behavior of GE/EPRI Test 37. Another issue is the question: Is the "Straw Man" change defensible for other-than-earthquake-caused reversing dynamic loads? If you don't have a current list of "SWG-SR Issues", I suggest you get it so that you can see what all other issues the "Straw Man" is not addressing.

(2) Limit Moment Alternative

Alternatively, the page 154 insert might read:

" ME shall not be taken as less than 1.273*(Do-t)^2*t*Sy "

(The Do/t <= 50, which is redundant for B-indices, becomes essential for the ME < Limit Moment.)

The reason why (Do-t) should be used is illustrated by the following NPS 6 examples:

Sch.	Do	t	Dm	Z=1.273*Dx^2*t = For Dx=Do	For Dx=Dm	Z(exact)
10	6.625	0.134	6.491	4.619	4.434	4.35
160	6.625	0.718	5.907	24.8	19.7	17.8

Assuming that Z = 1.273*Dm^2*t is an adequate approximation and that the limit of 4.5Sm can be replaced by 3Sy then with B2 = 2:

M = 1.178*Dm^2*t*Sy

As Bob Kennedy pointed out, this is essentially the same as the limit moment, M = 1.273*Dm^2*t*Sy.

(2) Relationship Between NB-3656(a) and (b)

The problem is that for components where the lower bound of B2 = 2 controls, such as straight pipe, some elbows, some tees, etc., NB-3656(a) permits higher moments for static loads than does NB-3656(b) for reversing dynamic loads.

A solution might be to modify NB-3656(a) so that it also has the lower bound limit of B2 = 2. For weight load, there probably be no objections. For other loadings such as water hammer and steady-state relief valve thrust, there might be strong objections.

Yours Very Truly,

Everett

E. C. Rodabaugh

Encl: Marked copy of page 154 of Code

File: ken797-2, Disk ETEC97

NB-3656 Consideration of Level D Service Limits

If the Design Specifications specify any Service Loading for which Level D Limits are designated [NCA-2142.2(b)(4)], the requirements of (a), (b), or (c) below shall apply.

(a) For Service Loadings for which Level D Service Limits are designated which do not include reversing dynamic loads or have reversing dynamic loads combined with nonreversing dynamic loads, the requirements of (1) and (2) below shall apply.

(1) The permissible pressure shall not exceed 2.0 times the pressure P_a calculated in accordance with Eq. (3) of NB-3641.1.

(2) The conditions of Eq. (9) of NB-3652 shall be met. The allowable stress to be used for this condition is 3.0 S_m, but not greater than 2.0 S_y.

(b) For piping fabricated from material designated P-No. 1 through P-No. 9 in Table 2A, Section II, Part D and limited to $D/t \leq 50$ if Level D Service Limits are designated which include reversing dynamic loads that are not required to be combined with nonreversing dynamic loads, the requirements of (1) through (5) below shall apply.

(1) The pressure occurring coincident with the earthquake or other reversing type loading shall not exceed the Design Pressure.

(2) The sustained stress due to weight loading shall not exceed the following:

$$B_2 \frac{D_O}{2I} M_W \leq 0.5\, S_m \qquad (x)$$

where

M_W = resultant moment due to weight effects (NB-3623)

(3) The stress due to weight and inertial loading due to reversing dynamic loads in combination with the Level D coincident pressure shall not exceed the following:

$$B_1 \frac{P_D D_O}{2t} + B_2 \frac{D_O}{2I} M_E \leq 4.5\, S_m \qquad (y)$$

B_2 in Eq. (y) is not less than 2.0.

where

M_E = the amplitude of the resultant moment due to the inertial loading from the earthquake, other reversing type dynamic events and weight. Earthquake and other reversing dynamic loads shall be computed from a linear elastic response spectrum analysis as defined in Appendix N-1226, except the spectrum peak broadening value Δ_{fj} in N-1226.3 shall not be less than 15% and, in place of the damping values for both large and small diameter piping systems in Table N-1230-1 for Operating Basis Earthquake and Safe Shutdown Earthquake, a value of 5 shall be used. The ground motion design input for generating the floor response spectrum to be used in the linear elastic analysis shall meet the requirements of Appendix N-1211(a) and N-1211(b). Moments and forces may be computed using a methodology other than prescribed above if the alternate methodology is demonstrated to produce results which envelope the prescribed methodology results. In the combination of loads, all directional moment components in the same direction shall be combined before determining the resultant moment. If the method of analysis is such that only magnitude without algebraic signs is obtained, the most conservative combination shall be assumed.

P_D = the pressure occurring coincident with the reversing dynamic load

(4) The range of the resultant moment M_{AM} and the amplitude of the longitudinal force F_{AM} resulting from the anchor motions due to earthquake and other reversing type dynamic loading shall not exceed the following:

$$C_2 \frac{M_{AM} D_O}{2I} < S_1$$

$$\frac{F_{AM}}{A_M} < S_2$$

where

A_M = cross–sectional area of metal in the piping component wall

$S_1 = 6S_m$

$S_2 = 1.0S_m$

(5) Piping displacements shall satisfy Design Specification limitations.

(c) As an alternative to NB-3656(a) and (b), the rules contained in Appendix F may be used in evaluating these service loadings independently of all other Design and Service Loadings.

Appendix III-D: L. Shipley Inputs

ARES
CORPORATION

COMMENTS ON THE DRAFT NUREG SEISMIC ANALYSIS OF PIPING

by
Larry Shipley
August 1997

I previously provided recommended editorial changes to the document and commented to Ken that I thought that the NUREG was well written and discussed the facts in a manner that was relatively easy to understand. Section 5 provides a clear summary of ETEC's concerns and recommendations.

General Comments

The independent evaluation and acceptance of the new code criteria for seismic design of piping systems has become one of an increasingly academic exercise. If the original component testing and code criteria development were subjected to this level of scrutiny, we would be designing piping like a pressure vessel today. It is important to understanding piping behavior and how the criteria is supported by the testing program, but it appears to be diverging from providing realistic criteria that a piping designer can use to qualify piping to the ASME code.

I agree fully with Bob Kennedy's recommendation and that we must develop a path forward, but have an additional recommendation that may be useful to move the effort off dead center.

It is difficult in today's environment to develop a bullet-proof criteria of such a sweeping magnitude that can be used on any piping system. However, it may be possible to approve the use of the criteria for a subset of piping systems by applying constraints on the use of the criteria. This would allow actual hands-on use of the criteria to see if there is any net benefit gained. Fragility of components, limitations imposed by small branch lines, deflection limitations, and other dynamic conditions may require the use of restraints, unrelated to seismic loading, that preclude a very flexible system design and high stresses. Only through the actual use of the criteria, even in a restricted form, will the industry and the NRC be able to assess the risk/benefit that it brings

Specific Comments

Section 5.1.1 One of the primary bases for the acceptability of the new rules is the concept that piping experiences a rachet-fatigue failure when exposed to reversing dynamic loads rather than failure based on a collapse mode, a concept on which much of the code criteria was previously based. However, the P-delta effects that were evident in a number of the tests resulted in piping failure mode that could be best described as incremental collapse. The concern is therefore voiced that the PFDR tests did not conclusively prove that a collapse failure mode can be ruled out of the evaluation of reversing dynamic loads.

The test configurations were apparently designed to provide the most rigorous set of loading possible to the component undergoing testing within the bounds of budget and the capability of the test equipment. In order to produce the moments of sufficient magnitude to induce failure in the test component, it was necessary to design test configurations such as those depicted in Figures 1 and 2. The weights used at the top of the riser were intended to simulate the effects of the first axial run after the elbow at the top of the riser. Although in the test the weight can induce P-delta effects, in an actual system the gravity weight of the horizontal axial run should be supported and in general will not have a significant contribution.

The use of any set of code rules presupposes that the engineer or designer has the intelligence, experience and common sense and is able to bring them to bear in an effort to layout and analyze a piping system that is within the bounds of good engineering practice.

Large displacements that have been observed in the near-field records in the first several cycles of large magnitude earthquakes present a somewhat different concern. The concern is clearly valid from an analytical point of view since displacements of up to 4 feet have been observed. However, viewing the matter from a slightly more pragmatic direction, it is highly unlikely that any nuclear power plant in this country or any other that is predisposed to use the ASME rules, is going to site a plant in close proximity to a major earthquake fault. Further, should the structure be able to withstand such a displacement, it would appear that the piping located within the building would "see" the displacement as an anchor movement and would be analyzed as such.

Section 5.1.5 The concern with pipe supports and the predicted loads generated from piping designed to relatively low frequencies is valid. However, it is one that is not likely to be resolved by providing a Code requirement that the loads generated by a linear elastic program be multiplied by a factor to account for non linear piping behavior. The use of a factor provides the designer with a false sense of security that if he/she only use the 1.x the systems and supports will be adequately designed. The primary issue may well rest with the ability of the pipe support/restraint to have sufficient ductility such that the support has the ability to deflect and transfer load if the piping load is in reality somewhat higher than calculated. The designer of the piping and supports will also have to be mindful of rod swing angles, and loads on equipment and structural steel but it should not be a foregone conclusion that the loads are always underpredicited.

Appendix III-E: E. Wais Inputs

SEISMIC ANALYSIS OF PIPING
PEER REVIEW INPUT

Edward A. Wais
Wais and Associates, Inc.

INTRODUCTION

In 1994, ASME Section III significantly revised the design rules related to nuclear power plant piping for seismic loads (as well as other "reversing dynamic" loads). These new rules were the result of an extensive industry effort involving several ASME Committees and other industry organizations (1). The Energy Technology engineering Center (ETEC) is supporting the US Nuclear Regulatory Commission (NRC) in evaluating the impact of these changes under the Seismic Analysis of Piping program. As part of this program, peer review input was requested.

SUMMARY

There have been several meetings with ETEC and the NRC to discuss the Seismic Analysis of Piping program's findings. Based upon this input and the various documentation regarding this effort, it is clear that that the basis for the new rules was incomplete.

ETEC, with support from staff from California Institute of Technology, has thoroughly investigated the majority of the significant issues which have been raised.

DISCUSSION

It should be noted, that in order to review various concerns regarding the new rules, ASME Section III has established a Special Working Group - Seismic Rules (SWG-SR). The SWG-SR reports to the Sub Group on Design and has identified 15 "Issue Categories" which are under review. "These Issue Categories" (2) are:

1. The 5% Strain Limit in NB-3200.
2. Basic Margin Definition.
3. Acceptable Level of Margin (Target Value)
4. Margin Calculations from Test Results (Data Reduction)
5. Section XI Issues
6. Limit for Combination of SAMS and Inertia Loads
7. Basis for Cycle Limits
8. Protection Against Collapse
9. Validity of Linear Elastic Analysis

10. Fatigue Equations vs. Primary stress Equations
11. Component Tests vs. System Tests
12. Limit higher Allowables to Building Filtered Loads
13. Code Compatibility Questions
14. Suggestions for Alternate Methods
15. Extensions to components/materials not tested.

Within these "Issue Categories", there are over 40 specific issues that have been identified.

It is important to note that the issues developed as part of the Seismic Analysis of Piping program were either previously included by the SWG-SR in this list or incorporated as they were identified. While the Seismic Analysis of Piping Project does not address all the issues listed by the SWG-SR, the "high priority" items were investigated.

The ETEC effort clearly provides a better understanding of the effects of various parameters than was previously available. While this effort may have resulted in different conclusions, it provides a basis for establishing rules with a complete justification. Items such as frequency effects are better understood and hence can be addressed.

In the process of developing the new rules, various organizations participated in developing margins for the new criteria as applied to the PFDR test program. The minimum margin (Test 36) was cited as 4.2 for the new rules. ETEC performed a margin evaluation which included adjustments for various considerations which reduced the calculated margin below an acceptable level. These considerations included: actual dimensions, actual material strengths, temperature effects, concurrent SAM loadings, etc. While one might argue with the method of evaluating any individual consideration, the overall conclusion is still that it has not been demonstrated that sufficient margin exists with the new rules.

In our last meeting with ETEC, the NRC and the Peer Review Group, held on July 15-16, 1997 at the NRC headquarters, Dr. Robert Kennedy suggested a revised criteria based on an "ultimate moment" approach. The suggestion was that this type of approach could result in margins such that piping systems did not control the High-Confidence-Low-Probability-of-Failure (HCLPF) of a nuclear plant. While, this approach is not without challenges, I believe that it is important to consider this type of approach. It has the advantage of potentially being able to resolve existing issues, and demonstrate adequate margin even within the methodology used by ETEC to evaluate overall margin.

References:

1. Chen, W.P. and Jaquay, K. R., *"Seismic Analysis of Piping, Vpll: Issue Identification,"* Energy Technology Engineering Center, 1997.

2. Letter from J. C. Minichiello to ASME Section III, SWG-Seismic Rules, *"Issues as Presented at the 1996 PVP Conference,"* July 25, 1996.

Appendix III-F: G. Wilkowski Inputs

Seismic Analysis of Piping Peer Review Group Report

Submitted by G. M. Wilkowski and R. J. Olson
Battelle-Columbus

CONCLUSIONS

From the various review meetings and written information supplied, we believe that the recent ASME seismic design code rules are in need of further validation before they are deemed acceptable. This statement is based on weaknesses in six technical areas, most of which are related to the EPRI/ANCO component tests that are the basis of the new seismic design rules. Some of these aspects may erode the safety margins that are thought to currently exist.

(1) Materials Considerations

The criteria are based on the tests conducted at ANCO on wrought stainless steel and low strength carbon steel pipe and components at room temperature. However, the criteria are said to be applicable to a large variety of materials (P1 to P8) at LWR temperatures. The concern here is that there may be materials where the margins experimentally determined from the limited component tests may not reach the desired levels. Materials with higher yield-to-ultimate strength ratios (i.e., lower strain hardening) or materials that may be less flaw tolerant at operating conditions may have lower margins than determined from the room temperature tests. Some specific materials that are of concern are:

- Low carbon steels at 300 to 600 F. These materials experience dynamic strain aging, also known as blue embrittlement. This causes changes in the ultimate strength, strain hardening and toughness of the material as a function of temperature and strain rate. For instance, the ANCO tests done on the ferritic components had yield-to-ultimate strengths of approximately 0.58 to 0.68 at room temperature. At higher strain rates and LWR temperatures, all of the ferritic steels tested to date in the NRC's International Piping Integrity Research Group programs (IPIRG-1 and IPIRG-2) have had slightly higher yield strengths, but much lower ultimate strengths. Typically, the ultimate strengths of ferritic base metals at 1 sec^{-1} to 10 sec^{-1} strain rates are lower by about 15 to 30 percent than at quasi-static rates. Thus, the yield-to-ultimate strengths can change from 0.45 at quasi-static rates to 0.77 at the 1 to 10 sec^{-1} strain rates. The change is even more significant for ferritic weld metals. Hence, ferritic steels at LWR temperatures and dynamic loading will have less strain hardening than ferritic steels at room temperature under dynamic loading.

- Other higher strength materials that have been used in ASME-designed nuclear power plants. Some additional examples are:
  - A106 Grade C,
  - cast stainless steel that has experienced thermal aging, and may be low in toughness at reactor start-up temperatures (i.e., 300 F), and
  - low alloy steel (i.e., A508) used in forgings for nozzles (i.e., surge line nozzles into cold leg piping) or pipe in German, Swiss, future Japanese PWR's, and perhaps the future European Pressurized Water Reactor (EPR).

- The decarbonized region that can occur in bimetallic welds. This would be a band of softer material bounded by higher strength material. Cyclic plasticity at the proposed design loads would concentrate in this lower strength region. Such welds are also hard to inspect.

(2) Effect of Code Acceptable Imperfections

In reviewing the test results at one of the meetings, it was stated that there were no observable imperfections that contributed to a component fracture other than one case of a stamp mark on an elbow. Thus, it appears that the effect of ASME Section XI Code allowable workmanship imperfections, see Tables IWB-3514-1 and -2, was never considered. Such imperfections would probably reduce the fatigue life of pipe components as shown in a 1995 PVP conference paper*. No work has been conducted in the EPRI Pipe and Fitting Dynamic Reliability program to make an assessment of workmanship flaws on the new seismic design rules.

In the case of piping with a flaw larger than the Code-acceptable workmanship standards in ASME Section XI, the pipe flaw evaluation standards in IWB-3640, IWB-3650, Appendix C, and Appendix H of Section XI and Code Case 494-2 do not allow flaws when the stresses are above $2.8S_m$ for Service Level C and D conditions. Hence, if a flaw larger than the workmanship standards occurs in service at a high stress location, then the only option is to replace the piping.

(3) Secondary Stress Criteria

The proposed criteria allows for primary stresses of up to $4.5S_m$. It also allows for secondary bending stresses of up to $6S_m$. In addition, there would also be thermal expansion stresses. The latest design code rules place no restriction on the combination of these stress components, i.e., $10.5S_m$ could be allowed for a combination of primary and secondary dynamic stresses plus the thermal expansion stresses.

Since the $4.5S_m$ criteria was experimentally based on the inertially-loaded component tests (no seismic anchor motion or thermal expansion stresses), and the ETEC pipe system tests were at room temperature with sleds moving in unison, there are no data on the effect of thermal expansion stresses or seismic anchor motion stresses. The technical basis for the secondary stress criterion seems to be missing.

In the IPIRG-1 program, we found that in pipe system fracture tests at 550 F with large flaws where the failure stresses in the uncracked pipe were below yield, the thermal expansion and SAM stresses contributed just as much to fracture as the inertial and pressure-induced stresses. This was true even for a crack in TP304 base metal. At higher failure loads for smaller flaws, we anticipate that the secondary stresses will be less effective in fracture, but are not sure how to handle that yet.

(4) Accuracy of Component Test Data Reduction

There are several aspects of the data reduction and analyses of the component tests that raise questions about the margins that were calculated. Some points are noted below and are being addressed in the ETEC reanalysis of the ANCO tests.

- The actual response spectrum from the tests should be used. To date there has been disagreement about using the input response spectrum versus a peak-broadened response spectrum. More fundamentally, the input versus the actual response-spectrum supplied by the sleds should be checked. Paul Chen showed some results suggesting the ANCO sled hydraulics were undersized and that the sled may have been stalling, hence, the actual

---

* Scott, P.M., and Wilkowski, G.M., "A Comparison of Recent Full-Scale Component Fatigue Data with ASME Section III Fatigue Design Curves," ASME PVP Vol. 306, pp 129-138, July 1995.

displacement-time history applied was not the same as the input. This results in a different actual response spectrum than the input or the peak-broadened input response spectrum. If this is true, then this is a very fundamental problem in the data reduction.

- The actual component strengths were well above the Section II Code minimums, i.e., the yield of the pipe in Test 18 is 1.53 times the Section II Part D minimum values. This was not accounted for in the analysis. Calculating an S_m based on actual properties rather than using the Code S_m values would normalize all the test articles as having material properties that just meet the Code minimum. We found this valuable in Code assessments of pipe fracture tests in Section XI. Doing this significantly reduced the scatter of the data in assessing Code procedures. The statistical material property variations can then be separately assessed.

  Several interesting aspects from the discussions at the information meeting relative to using the actual versus Code yield strengths were brought up. One of these aspects is that it was also noted that there is a limit on pressure since the pressure has a significant effect on the fatigue ratcheting behavior. However, the component tests with higher than Code minimum properties were tested with pressure levels using the Code limits. Hence, if the component tests were done with pressures corresponding to the actual properties, then the fatigue life may have been lower. Hence, a correction on the margins due to strength may not be a simple linear correction. As a result of this, the margins for piping components with properties near the Code minimum values is not known.

- The actual thickness of the component should have also been used rather than the Code nominal thicknesses. This has the same effect as not using the actual strength, and all the associated uncertainties as noted above.

- The stress intensification factor for the failure location in the component tests should be used. For instance in Experiment 3C, the failure was at a girth weld taper, not in the body of the tee.

(5) Fundamental Concerns of Seismic Time History Used

The response spectrum used came from current plant design criteria. It was used to develop a displacement-time history for conducting the experiments. Such displacement-time histories are generally designed with a motion enveloping function that ramps the response up to a strong motion phase of some duration and then ramps the response back down. The strong motion time used in the tests was 20 seconds. The question is, how fundamentally correct is this for assessing seismic damage? Is 20 seconds a reasonable time period? The Mexico City earthquake lasted almost 2 minutes, a 7.1 Richter Scale earthquake in the Philippines during the week of November 7, 1994 was reported to last 4 minutes, etc.,.

Bill Iwan raised a question about the Northridge Earthquake near-field motions being essentially a large step change in the displacement time history. I believe that the single, large-amplitude loading is less severe than large amplitude cyclic loading for pipe component damage.

Recently in the NRC's Second International Piping Integrity Research Group (IPIRG-2) program, it has been learned that for nonlinear problems, specific characteristics of the seismic time-history govern the "damage potential" for the excitation. Factors we believe to be important are; how the amplitude builds up prior to the first large-amplitude cycle, the number of large amplitude cycles within 90-percent of the largest amplitude cycle, and the stress ratio (ratio of the minimum to maximum stress) of the large-amplitude cycles. There are an infinite number of time histories that can be developed from a given response spectrum. However, as a result of the above factors, the propensity for causing damage can be very different for two supposedly "equal" spectrum-compatible excitations. This is relatively new information which suggests that consideration needs to be given to determine whether the time history used in the seismic tests is average, lower bound, or upper bound in causing material damage.

(6) Fundamental Aspects in Calculating Margins

The margins used in the new design criteria are based on accelerations not on stress. Our personal preference is to have the margins based on stress, since all other structural integrity rules in the ASME Code that we are familiar with use safety factors based on stress.

One difficulty with the proposed margin basis is that it is developed from a small computer code called REMS. The precise inner working of REMS is not well known and needs to be studied better.

The proposed design rules say that collapse will not be the failure mode, yet the indices developed for collapse avoidance are used. It would have been better to base the proposed changes on the fatigue based indices.

PART IV CONCLUSIONS AND RECOMMENDATIONS

where S_Y is the ASME Code specified yield stress.

This change has the advantage of retaining B_2 as an elastic stress indice. However, it has the disadvantage of introducing an additional code moment limit.

Alternate #2 also produces no change in the code moments and strength factors reported in Table 1 for the Elbow components. Table 3 also shows the revised M_{CODE} and F_S for the 12 Non-Elbow components based on Alternate #2. The yield stress S_Y used were:

S_Y = 30 ksi Stainless Steel
S_Y = 35 ksi Carbon Steel

2.3 Discussion of the Strength Factor F_S for the Proposed Alternates

With either the proposed Alternate #1 or #2, the statistical distribution of F_S shown in Table 3 for the Non-Elbow Components is sufficiently similar to that shown in Table 2 for the Elbow components so that the Elbow and Non-Elbow F_S distributions can be combined. The combined strength factor distribution becomes:

	Strength Factor Distribution	
	Alternate #1	Alternate #2
Median $F_{S_{50\%}}$	2.12	2.15
β_S	0.15	0.15
1% $F_{S_{1\%}}$	1.50	1.53

With either alternate the 1% NEP strength factor $F_{S_{1\%}}$ is estimated to be 1.5 which is sufficient to achieve the desired 1% NEP seismic capacity (code) margin $R_{CP_{1\%}}$ of 2.0 so long as $(F_{NL}F_{Red})_{CONS.} \geq 1.33$.

2.4 Check on Assumed Lognormal Distribution of Strength Factor Data

It remains to be shown whether the data is reasonably approximated as being lognormally distributed. This is best shown by ordering the data from low to high and plotting the natural logarithm of the seismic strength factor F_S versus the non-exceedance probability P_{NE} on cumulative normal probability paper, where P_{NE} is defined by:

$$P_{NE} = \frac{n}{N+1} \tag{9}$$

in which n is the ordered data number, and N is the total number of data. Since N = 24, the first ordered data is plotted at the 4% probability point, the second at 8%, etc., with the last at 96%. If the data is lognormally distributed, it will appear as a straight line on this plot. Figure 4 shows such a plot using the seismic strength factor data from Table 1 for the Elbow components (excluding Component 37) and from Table 3 Alternate #2 for the Non-Elbow components. A similar plot with identical conclusions results if Alternate #1 were used. This figure shows that the data can be reasonably approximated by a lognormal distribution at least between the 5% and 95% probability of failure range. The open question remains as to whether this lognormal distribution can be extrapolated down to the 1% probability of failure.

The problem is that the lognormal distribution extends down to a zero probability of failure at zero capacity. However, real capacity data achieves essentially a zero probability of failure at some lower bound capacity level significantly greater than zero. Therefore, most real data can generally be better represented by a truncated lognormal distribution in which the parameter $\left(F_S - F_{S_{min}}\right)$ is assumed to be lognormally distributed. The problem being how to establish the truncation level $F_{S_{min}}$ when only a limited amount of data is available. The shape of the lower tail of the data plotted on Figure 4 does not indicate any truncation level. In order to realistically estimate $F_{S_{min}}$ would require about 100 to 200 pieces of test data which is impractical. It is recommended that no truncation be assumed which leads to $F_{S_{min}} = 1.5$.

2.5 Elbow Component # 37

For Elbow Component #37, the Code Moment Capacity Eqn. (1) provides a strength factor F_S of only 1.0. For the 24 other tested components, this same Code Moment Capacity Eqn. (1) modified in accordance with either the proposed Alternate #1 or #2 provides a median strength factor $F_{S_{50\%}}$ of about 2.1 and a 1% NEP strength factor of about 1.5. As a result, it is necessary to understand the cause of Elbow Component #37 having an abnormally low ultimate dynamic moment capacity M_{UD}.

From conversations with E. Rodabaugh, I understand that except for Elbow Component #37 the ultimate dynamic moment capacity M_{UD} averages about two times the expected ultimate static moment capacity M_{US}. This increase is most likely due to some combination of:

a) strain rate increases in the inelastic range
b) cyclic strengthening as a result of prior nonlinear cycles

However, Elbow Component #37 does not show a similar increase. For Elbow Component #37, $M_{UD} \approx M_{US}$.

In many respects the dynamic testing of Elbow Component #37 was near the extreme range of tests conducted. Thus, there are a number of postulated reasons for the apparent lack of dynamic moment capacity increase for this component. The most likely causes are:

1. Elbow Component #37 had a low natural frequency f_N of 1.44 Hz and a low central frequency f_I for the input motion of 1.40 Hz. The only other component with similarly low frequencies was Elbow Component #30. For all other tested components the natural and input central frequencies were at least 2.5 times greater.

2. Both Elbow Components #30 and 37 had ratios of Weight Moment M_W to Code Moment M_{CODE} of 0.12. The only other Elbow with a significant ratio of Weight Moment to Code Moment was Component #35 for which this ratio was 0.086. However, Component #35 was a Sch. 40 Elbow, whereas Components #30 and 37 were Sch. 10 Elbows.

3. Elbow Components #37 and 8 were the only Elbows for which $\frac{PD}{2t}$ was less than about 10.0 ksi. These Elbows had zero pressure. In fact this zero pressure was the only difference between Elbow Component #37 and Elbow Component #30. Elbow Component #8 differed from Elbow Component #37 in that Elbow Component #8 was a Sch. 40 Elbow, had negligible weight moment, and approximately 5 times higher natural and input central frequencies.

4. Elbow Components #3, 30, 31, and 37 were the only Sch. 10 Elbows for which $D_O/t \approx 50$. All of the other Elbows were Sch. 40 for which $D_O/t \approx 24$ Elbow Component #30 had the next to lowest strength factor of 1.62. However, Elbow Components #3 and #37 had above average strength factors so that D_O/t does not seem to be the primary cause of the low M_{UD} for Elbow Component #37.

Elbow Components #30 and 37 were essentially identical and were subjected to essentially the same input. However, $\frac{PD}{2t} = 0$ for Component #37 and $\frac{PD}{2t} = 9.9$ ksi for Component #30. It is informative to compare the nonlinear moment-rotation hysteretic loops for Component #37 (see Figure 5) versus Component #30 (see Figure 6). For both components the weight moment stress:

$$\frac{B_2 M_W}{Z_N} \approx 0.5 S_M$$

This weight moment stress has the tendency to ratchet the elbow closed when subjected to a cyclic moment of approximately $M_{US} \approx 4.5 S_M (Z_N/B_2)$ as shown in Figure 5. Because of this one-way ratcheting, full reverse nonlinear opening cycles never developed. Therefore, cyclic strengthening did not occur and:

<u>Component #37</u>

$$M_{UD} \approx M_{US} \approx 4.5 S_M \left(\frac{Z_N}{B_2}\right)$$

However, the pressure stress $\frac{PD}{2t} \approx 0.5 S_M$ on Component #30 has the tendency to provide an opening effect on the Elbow which resists the tendency of the weight moment stress to ratchet the elbow closed. Thus, the full opening and closing hysteretic loop, shown in Figure 6 develop in Component #30 resulting in classic strengthening. Thus, for Component #30 M_{UD} is significantly greater than M_{US} and:

<u>Component #30</u>

$$M_{UD} \approx 7.3 S_M \left(\frac{Z_N}{B_2}\right)$$

My tentative opinion is that the strength factor F_S will reliably (less than 1% NEP) exceed 1.5 so long as:

<u>Elbows</u>

$$\frac{B_2 M_W}{Z_N} < \begin{cases} 0.4 S_M \\ \text{or} \\ 1.1\left(\frac{PD_0}{2t}\right) \\ \text{whichever greater} \end{cases} \qquad (10)$$

Neither Elbow Components #30 or 37 pass the first of these limits, whereas Elbow Component #35 barely passes this limit and all other tested Elbow easily pass.

Neither Elbow Components #8 or 37 pass the second limit, whereas Elbow Component #30 barely passes this limit. The combined result is that Elbow Component #37 fails to pass the limits of Eqn. (10) and Elbow Component #30 barely passes, whereas all other Elbows easily pass.

My tentative recommendation is that the increase to $S_A = 4.5S_M$ in the Code Moment Capacity Eqn. (1) not be permitted for Elbows which don't satisfy Eqn. (10). However, it would be preferable to have a better understanding of why Elbow Component #37 did not develop an ultimate dynamic moment capacity M_{UD} consistent with the other tested Elbows. To achieve such a better understanding may require additional cyclic (either static or dynamic) tests. Eqn. (10) is only a temporary stopgap measure.

3. Nonlinear Dynamic Behavior Factor For Component Tests

Ref. 2 presents a number of parametric study results which demonstrate how a Margin Factor (M_r/B_2) vary as a function of (1) the frequency ratio R_W of the component natural frequency f_n to the input motion central frequency f_I, (2) the breadth of the frequency content of the input motion, (3) model parameters, and (4) the assumed failure mode (for example, low cycle fatigue versus excessive nonlinear deformation failures). Figures 2 and 3 are examples of the Margin Factor information presented in Ref. 2. The PFDR input motion used in Ref. 2 is an example of narrow frequency input motion representative of floor motion at a high elevation of a moderately low damped stiff structure. The Reg. 1.60 input motion used in Ref. 2 is an example of a very broad frequency ground motion Therefore, these two motions tend to represent examples of the extremes on the breadth of frequency content in the input motion to which a piping component might be subjected.

The Margin Factor M_r used in Ref. 2 and the Seismic Capacity Margin R_{CP} used herein and in Ref. 3 are synonymous for component tests where the redundancy factor F_{Red} is 1.0. Therefore, the component nonlinear dynamic factor F_{NLC} for any situation studied in Ref. 2 is:

$$F_{NLC} = \frac{B_2}{F_S}\left(\frac{M_r}{B_2}\right) \tag{11}$$

where B_2 and F_S are from Table 1.

The parametric studies presented in Ref. 2 are for Components #14 and 40 for which:

Component	B_2/F_S
14	1.10
40	0.92

Thus, for these two components:

$$F_{NLC} \approx \left(\frac{M_r}{B_2}\right) \tag{12}$$

so that all of the figures in Ref. 2 of (M_r/B_2) versus R_W are approximately plots of F_{NLC}. Therefore, Ref. 2 provides an excellent basis for understanding F_{NLC}.

A study of the plots of (M_r/B_2) in Ref. 2 shows that F_{NLC} is highly variable and sensitive to the ratio R_W, the breadth of the input motion frequency content, and the postulated failure mode. Therefore, because of the possible variety of input motions to which the piping component might be subjected, it is impossible to establish any generic relationship between F_{NLC} and R_W. However, some reasonable but very broad bounds can be established.

The lowest F_{NLC} occur as R_W goes to zero for which:

$$\underline{\text{As } R_W \rightarrow 0}: \; F_{NLC} \approx 1.0 \tag{13}$$

However, if low R_W values are excluded:

$$\underline{R_W \geq 0.7} \;: \; F_{NLC} \approx 2.0 \text{ to } 8.0 \tag{14}$$

4. Estimating Generic $(F_{NL}F_{Red})_{CONS}$ for Piping Systems

Even at the component test level, a generic component nonlinear dynamic behavior factor F_{NLC} cannot be established even as a function of R_W. Only some reasonable but very broad bounds can be established. However even if F_{NLC} could be estimated, this estimate would only establish an unconservative upper bound on F_{NL} for a piping system. Many nonlinear dynamic analyses of multi-degree-of-freedom systems have demonstrated that the system nonlinear factor F_{NL} is generally less than the component factor F_{NLC}, i.e.:

$$F_{NL} \leq F_{NLC}$$

Therefore, in reality one can only realistically estimate F_{NL} for a piping system by a nonlinear analysis or a pseudo-linear analysis which approximates the increased effective flexibility of nonlinear components and uses increased effective damping.

However, again some reasonable bounds can be placed on F_{NL}. Within my experience, so long as the nonlinear behavior is reasonably spread throughout the system:

$$F_{NL} = F_K(F_{NLC} - 1.0) + 1.0$$
$$F_K \approx 0.5 \text{ to } 0.75 \qquad (15)$$

In addition, an actual piping system also has a redundancy factor F_{Red} due to redistribution. Again it would be necessary to perform either a nonlinear or pseudo-linear analysis of the actual piping system to accurately estimate this factor. For a uniform fixed-fixed beam subjected to uniform load, $F_{Red} = (16/12) = 1.33$. In general, for a piping system, I would expect:

$$F_{Red} \approx 1.2 \text{ to } 1.33 \qquad (16)$$

Considering the range of parameters defined by Eqns. (14) through (16), my judgment is that for typical piping systems:

<u>$R_W \geq 0.7$</u>

$$(F_{NL}F_{Red}) \approx 1.8 \text{ to } 8.3 \qquad (17)$$

and even for lower R_W piping systems:

$$(F_{NL}F_{Red}) \geq 1.33 \qquad (18)$$

Therefore, within my judgment, a reasonably conservative generic estimate of the product $(F_{NL}F_{Red})$ to cover a wide variety of piping systems and seismic inputs should lie in the range:

$$(F_{NL}F_{Red})_{CONS.} \approx 1.33 \text{ to } 1.8 \qquad (19)$$

and the resulting required 1% NEP strength factor $F_{S_{1\%}}$ from Eqn. (5) would be:

$(F_{NL}F_{Red})_{CONS.}$	$F_{S_{1\%}}$
1.33	1.5
1.5	1.33
1.8	1.1

In summary, the ultimate selection of $(F_{NL}F_{Red})_{CONS.}$ and thus required $F_{S_{1\%}}$ must be by judgment. Preferably the required $F_{S_{1\%}}$ should be established by consensus of a committee. I would be comfortable with and support any required $F_{S_{1\%}}$ value in the range of 1.1 to 1.5.

5. Conclusions

The ultimate moment M_{UD} achieved under dynamic cycles loading appears to be a stable and predictable parameter which is reliably reached prior to failure irrespective of whether the ultimate failure mode is low cycle fatigue or excessive deformation. Therefore, it is recommended that the Code Moment Capacity M_{CODE} be established based upon:

$$M_{CODE} = \frac{M_{UD_{1\%}}}{F_S} \tag{20}$$

where $M_{UD_{1\%}}$ is the 1% non exceedance probability (NEP) ultimate dynamic moment capacity and F_S is an appropriate strength factor of safety.

Based on Eqn. (5) and the information presented in Sections 3 and 4, it is recommended that the strength factor of safety F_S lie in the range of 1.1 to 1.5 in order to achieve an overall 1% NEP seismic capacity (code) margin $R_{CP_{1\%}}$ of about 2.0. The remainder of this capacity margin is accommodated by nonlinear dynamic behavior and redundancy benefits.

With the exception of Elbows which do not satisfy Eqn. (10) such as Component #37, Section 2 shows that the 1994 Addenda ASME Code Moment Capacity Eqn. (1) with an allowable stress S_A of $4.5S_M$ reliably achieves a strength factor of safety F_S of at least 1.5 for Elbows. However, Eqn. (1) does not reliably achieve an adequate F_S for Non-Elbow Components when $B_2 < 2.0$. Two alternates defined by Eqns. (7) and (8) are proposed to overcome this deficiency. With either alternate Eqn. (1) with $S_A = 4.5S_M$ reliably achieves a strength factor of safety F_S on M_{UD} of at least 1.5 for all tested components except Elbow Component # 37 which is excluded by Eqn. (10).

For most actual piping systems the Code Moment Capacity Eqn. (1) modified as recommended herein is expected to lead to a Seismic Capacity Margin R_{CP} much greater than 2.0. This Seismic Capacity Margin R_{CP} can be estimated from Eqn. (2). As shown in Section 2, the strength factor F_S is lognormally distributed with a median value $F_{S_{50\%}} = 2.12$ and a log. std. dev. β_S of 0.15. The product ($F_{NL}F_{Red}$) is highly variable and cannot reliably be estimated on a generic basis. However as noted in Eqn. (17), my judgment is that for typical piping systems ($F_{NL}F_{Red}$) lies in the range of 1.8 to 8.3. For illustrative purposes, let us assume for a typical piping system and seismic input that the median ($F_{NL}F_{Red}$) is 3.5 with a log. std. dev. β_{NLR} Of 0.40. This assumption is equivalent to assuming the 90% confidence bounds on ($F_{NL}F_{Red}$) are 1 8 to 6.8. The resulting Seismic Capacity Margin R_{CP} has the properties:

$$\begin{aligned}
\text{Median } R_{CP_{50\%}} &= 7.4 \\
\beta_{CP} &= 0.43 \\
1\% \text{ NEP } R_{CP_{1\%}} &= 2.7 \\
90\% \text{ Conf. Band } R_{CP_{5\%-95\%}} &= 3.7 \text{ to } 15.0
\end{aligned}$$

In this example, the resulting Seismic Capacity Margin R_{CP} is likely to be exceedingly and unnecessarily high. However, this margin is generically unreliable because ($F_{NL}F_{Red}$) is generically unreliable.

The only way I know of to avoid this problem that the average Seismic Capacity Margins are likely to be exceedingly and unnecessarily high would be to perform either nonlinear or pseudo-linear piping evaluations against a strain or inelastic rotation failure criteria in order to reasonably account for the nonlinear dynamic and redundancy benefits that exist for the specific situation being analyzed. Short of performing such analyses, I recommend living with the excessive conservatism which will be typically introduced by establishing the Code Moment capacity M_{CODE} from Eqn. (20) with an appropriately low F_S so as to avoid unconservatism for the odd case where ($F_{NL}F_{Red}$) is low.

References

1. Chen, W.P. and Jaquay, K.R. *"Seismic Analysis of Piping, Vol 1 : Issue Identification,"* Energy Technology Engineering Center, 1997

2. Huang, C.T. *"Seismic Analysis of Piping, Vol. 2 : Studies on Frequency Effects on Margins,"* Calif. Inst. Of Technology, 1997

3. Kennedy, R.P., *"Establishing the Required Seismic Margin for Piping Systems in Nuclear Power Plants,"* May 1995

4. Kennedy, R.P., *"Establishing Seismic Design Criteria to Achieve an Acceptable Seismic Margin,"* Proceedings of the Twenty-fourth Water Reactor Safety Information Meeting, NUREG/CP-0157, Vol. 1, pp. 221-224, U.S. NRC, October 1996

Table 1: Component Test Strength Factor F_S

Component	Mtl.	Z_N in^3	$\frac{PD}{2t}$ ksi	B_1	B_2	M_{CODE} kip-inch Eqn. (1)	M_{UD} kip-inch	F_S
Elbow								
3	SS	4.35	9.89	0	5.51	71	162	2.28
4	CS	8.50	11.83	0	3.27	234	429	1.83
5	CS	8.50	20.11	0	3.27	234	534	2.28
6	SS	8.50	20.11	0	3.27	234	520	2.22
7	SS	8.50	11.83	0	3.27	234	523	2.23
8	SS	8.50	0	0	3.27	234	508	2.17
13	CS	8.50	11.83	0	4.29	178	379	2.13
19	SS	8.50	29.58	0	3.27	234	633	2.71
30	SS	4.35	9.89	0	5.51	71	115	1.62
31	SS	4.35	9.89	0	5.51	71	192	2.71
35	CS	8.50	20.11	0	3.27	234	470	2.02
37	SS	4.35	0	0	5.51	71	72	1.01
41	CS	8.50	20.11	0	3.27	234	510	2.18
Non Elbow								
9	SS	8.50	20.11	0.5	1.0	679	629	0.93
10	SS	8.50	11.83	0.5	1.0	715	642	0.90
11	SS	4.35	9.89	0.5	1.0	370	369	1.00
12	SS	8.50	20.11	0.5	1.0	679	726	1.07
14	CS	8.50	20.11	0.5	1.0	679	617	0.91
15	SS	3.21	16.14	0.5	1.0	263	333	1.26
16	CS	3.21	16.14	0.5	1.0	263	385	1.46
34	CS	8.50	11.83	0.5	1.0	715	775	1.08
36	CS	8.50	20.11	0.5	1.0	679	700	1.03
38	SS	8.50	20.11	0.5	2.02	336	650	1.93
39	SS	8.50	0	0.5	2.02	379	629	1.66
40	SS	3.21	0	0.5	1.0	289	314	1.09

Table 2: Statistical Distribution of Component Strength Factors

	Elbow Tests* $B_2 > 3.0$			Non-Elbow Tests $B_2 = 1.0$		
	CS	SS	Combined	CS	SS	Combined
Number Tests	5	7	12	4	6	10
$F_{S_{50\%}}$	2.08	2.25	2.18	1.11	1.04	1.06
β_S	0.08	0.17	0.14	0.20	0.12	0.15
$F_{S_{1\%}}$			1.56			0.75

* Excludes Component #37

Table 3: Component Test Strength Factor F_S for Proposed Alternates

Non-Elbow Component	M_{CODE} (kip-inch) Alternate #1 Eqn. (7)	M_{CODE} (kip-inch) Alternate #2 Eqn. (8)	F_S Alternate #1	F_S Alternate #2
9	340	325	1.85	1.94
10	357	325	1.80	1.98
11	185	166	1.99	2.22
12	340	325	2.14	2.24
14	340	379	1.82	1.63
15	132	123	2.53	2.71
16	132	143	2.92	2.69
34	357	379	2.17	2.05
36	340	379	2.06	1.85
38	336	325	1.93	2.00
39	379	325	1.66	1.94
40	145	123	2.17	2.56
		$F_{S_{50\%}}$	2.06	2.13
		β_S	0.16	0.16
		$F_{S_{1\%}}$	1.43	1.48

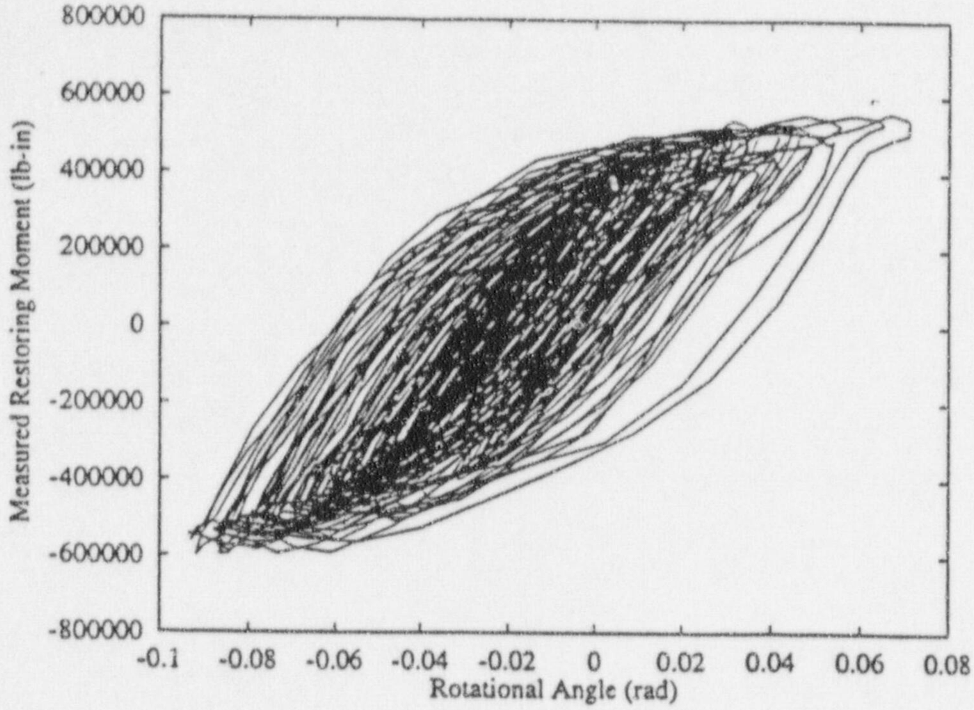

Figure 1: Measured hysteretic loops for ANCO Test 14, Run 6

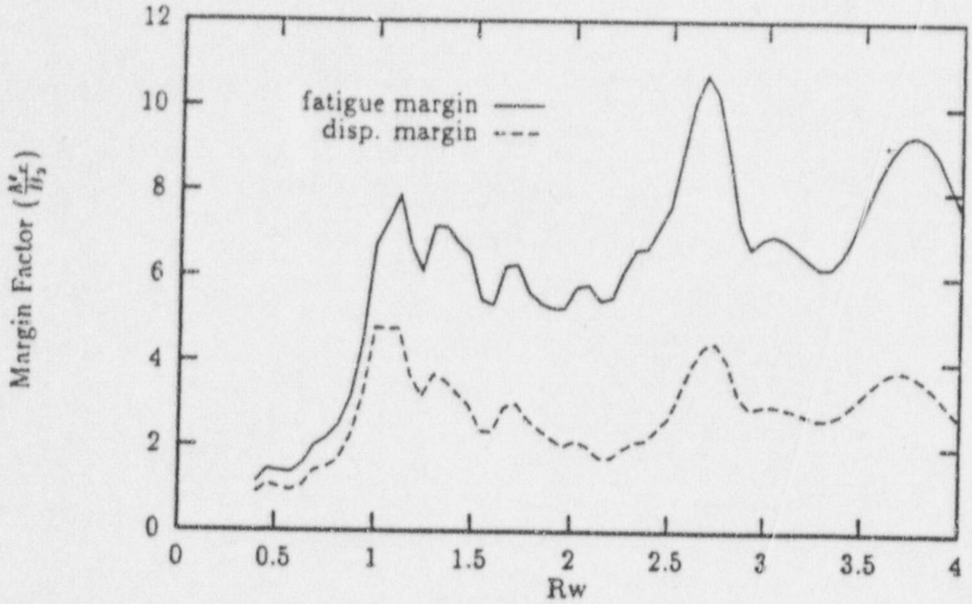

Figure 2: Component 14 Parametric Models, PFDR input; fatigue margin spectrum and displacement margin spectrum, αw = 0%, ς3 = 2.5% Sequential Method (From Ref. 2)

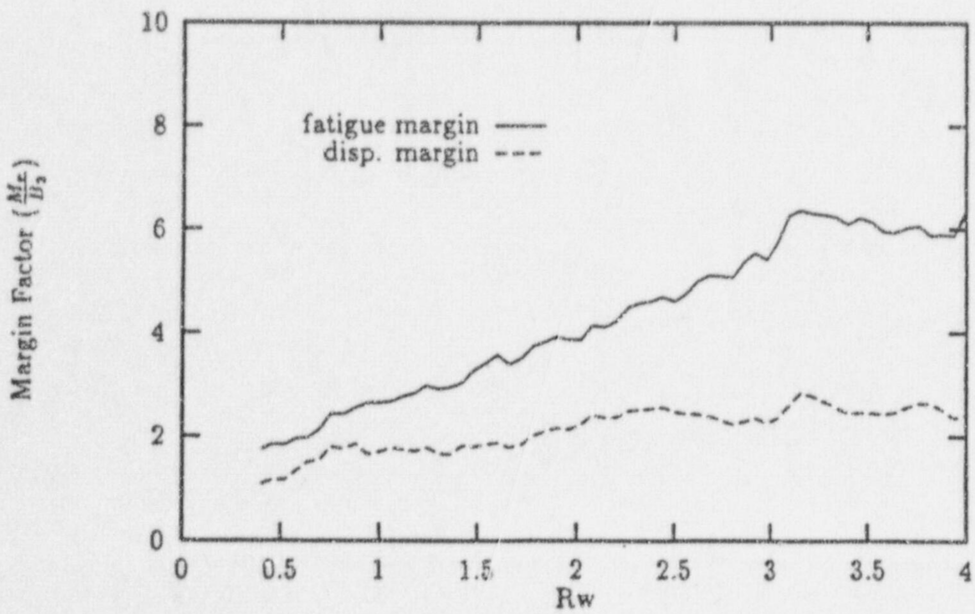

Figure 3: Component 14, Parametric Models, Reg. 1.60 input: fatigue margin spectrum and displacement margin spectrum, αw = 0%, ς3 = 2.5% Sequential Method (From Ref. 2)

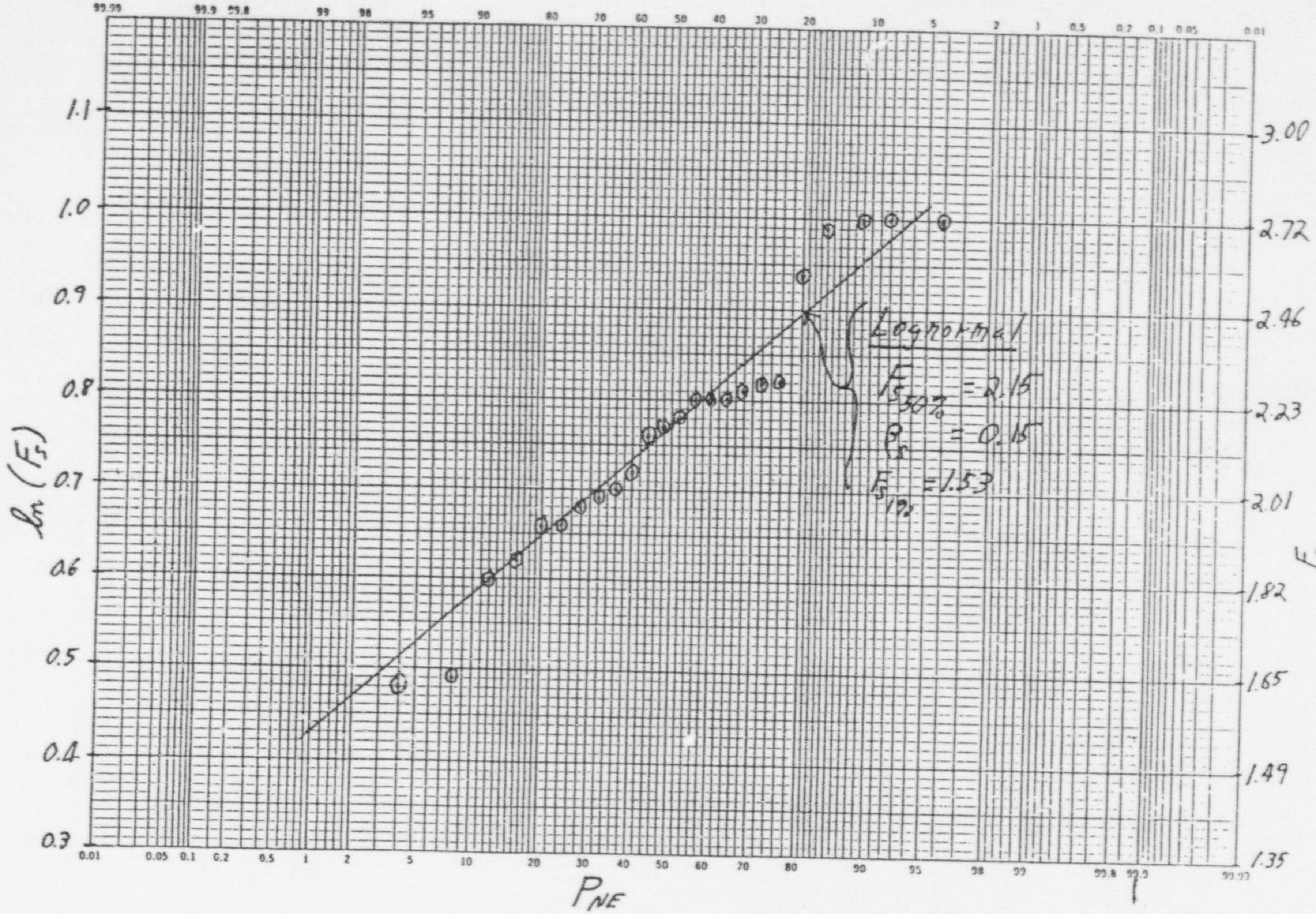

Figure 4: Cumulative Normal Probability of Log of Strength Factor

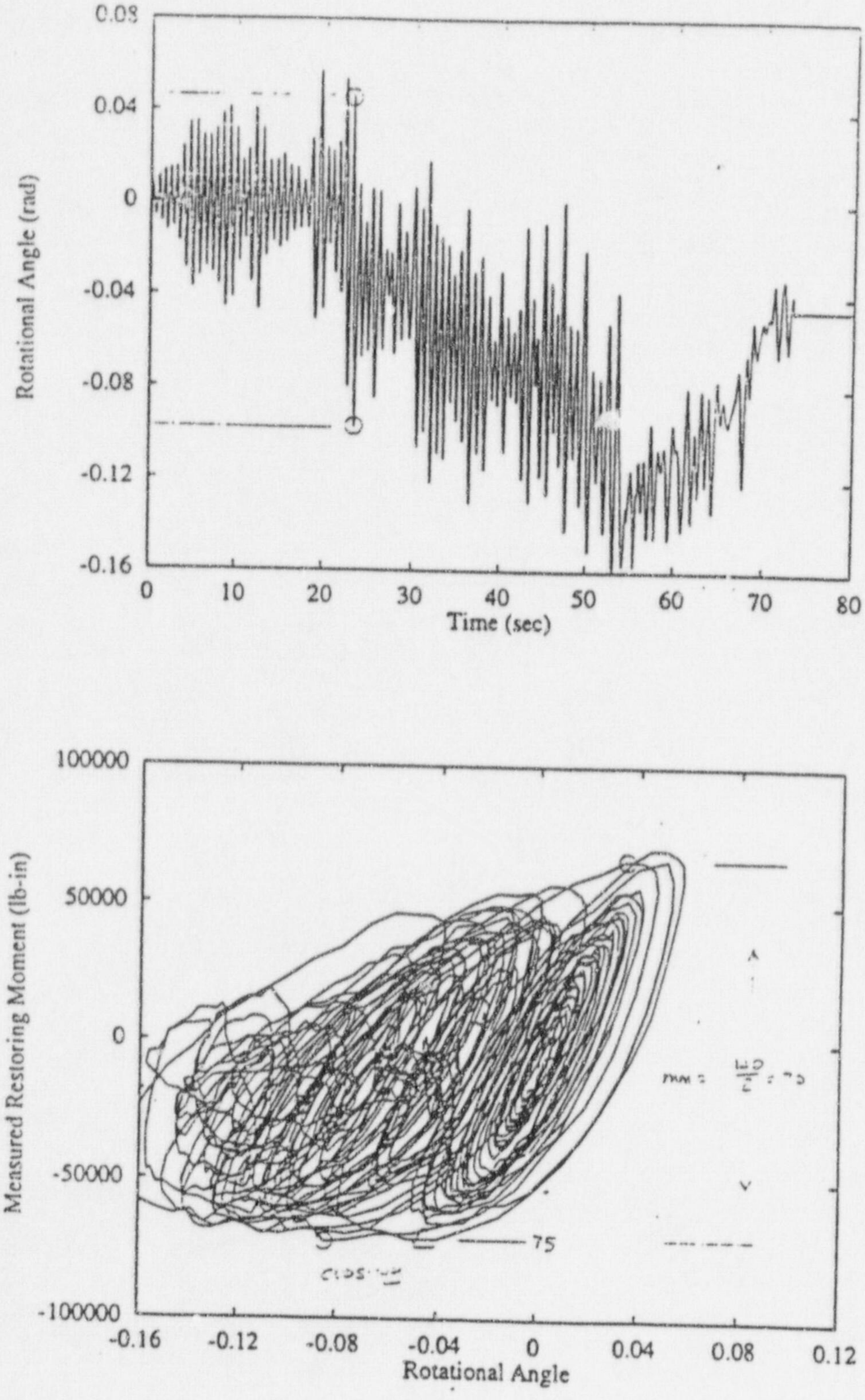

Figure 5: Response time history and hysteretic loops for ANCO Test 37 Run 5 (From Ref. 1)

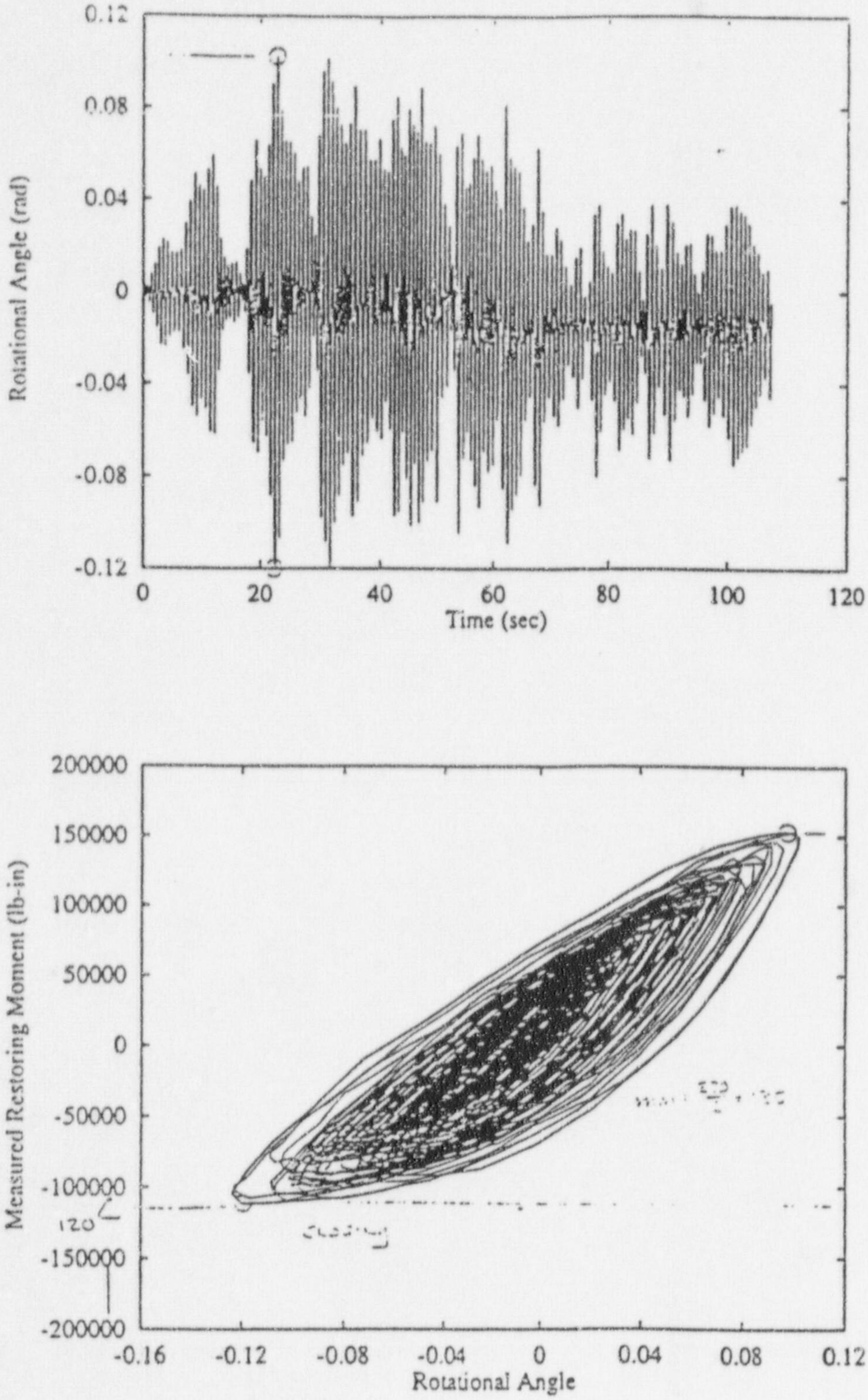

Figure 6: Response time history and hysteretic loops for ANCO Test 30 Run 6 (From Ref. 1)